CELL SIGNALING MEDIATING CRITICAL RADIATION RESPONSES

EDITED BY: Carsten Herskind and Mary Helen Barcellos-Hoff
PUBLISHED IN: Frontiers in Oncology and Frontiers in Cell and Development Biology

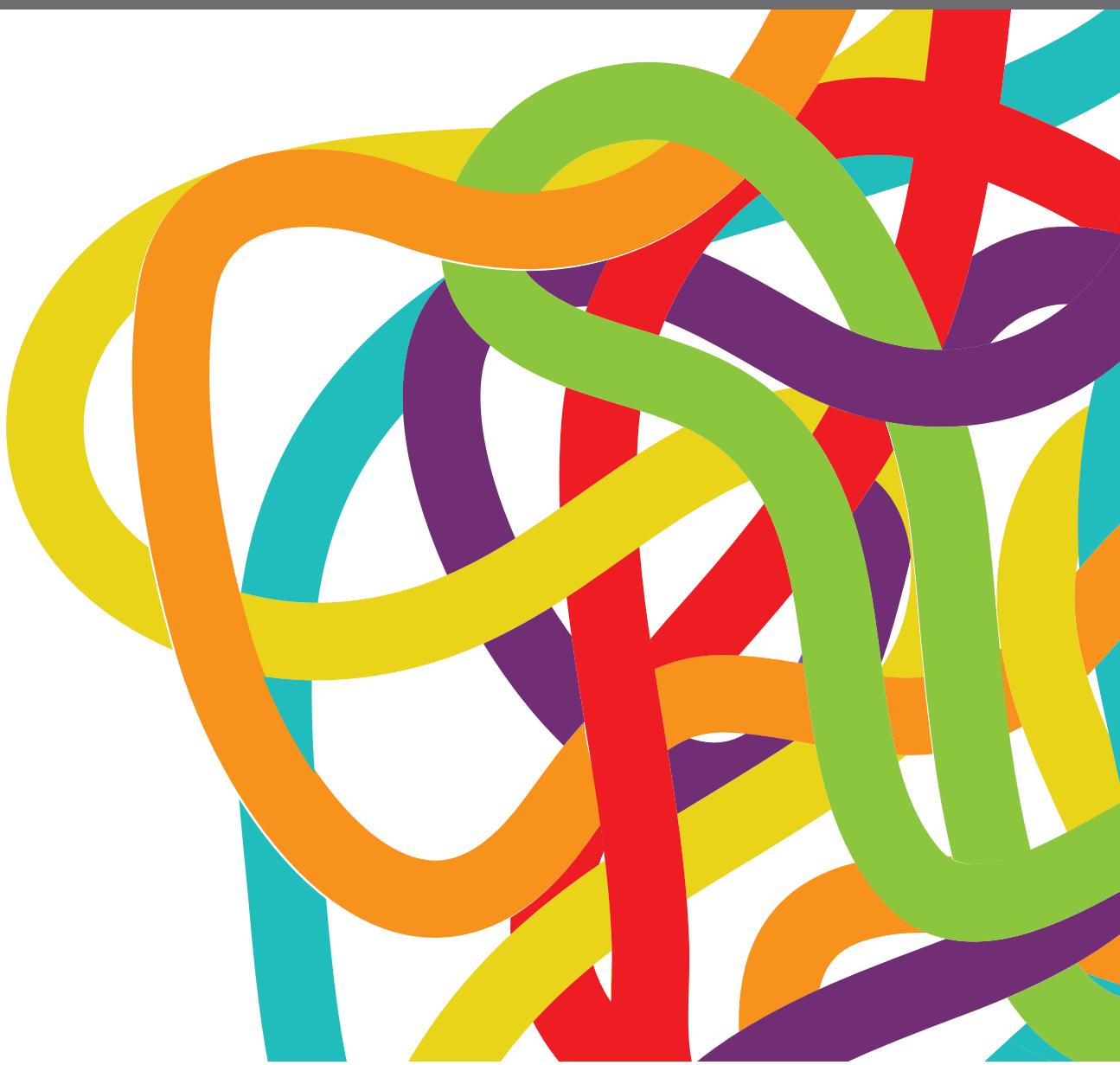

frontiers Research Topics

ISSN 1664-8714
ISBN 978-2-88966-979-0
DOI 10.3389/978-2-88966-979-0

About Frontiers

Frontiers is more than just an open-access publisher of scholarly articles: it is a pioneering approach to the world of academia, radically improving the way scholarly research is managed. The grand vision of Frontiers is a world where all people have an equal opportunity to seek, share and generate knowledge. Frontiers provides immediate and permanent online open access to all its publications, but this alone is not enough to realize our grand goals.

Frontiers Journal Series

The Frontiers Journal Series is a multi-tier and interdisciplinary set of open-access, online journals, promising a paradigm shift from the current review, selection and dissemination processes in academic publishing. All Frontiers journals are driven by researchers for researchers; therefore, they constitute a service to the scholarly community. At the same time, the Frontiers Journal Series operates on a revolutionary invention, the tiered publishing system, initially addressing specific communities of scholars, and gradually climbing up to broader public understanding, thus serving the interests of the lay society, too.

Dedication to Quality

Each Frontiers article is a landmark of the highest quality, thanks to genuinely collaborative interactions between authors and review editors, who include some of the world's best academicians. Research must be certified by peers before entering a stream of knowledge that may eventually reach the public - and shape society; therefore, Frontiers only applies the most rigorous and unbiased reviews.
Frontiers revolutionizes research publishing by freely delivering the most outstanding research, evaluated with no bias from both the academic and social point of view. By applying the most advanced information technologies, Frontiers is catapulting scholarly publishing into a new generation.

What are Frontiers Research Topics?

Frontiers Research Topics are very popular trademarks of the Frontiers Journals Series: they are collections of at least ten articles, all centered on a particular subject. With their unique mix of varied contributions from Original Research to Review Articles, Frontiers Research Topics unify the most influential researchers, the latest key findings and historical advances in a hot research area! Find out more on how to host your own Frontiers Research Topic or contribute to one as an author by contacting the Frontiers Editorial Office: frontiersin.org/about/contact

CELL SIGNALING MEDIATING CRITICAL RADIATION RESPONSES

Topic Editors:
Carsten Herskind, University of Heidelberg, Germany
Mary Helen Barcellos-Hoff, University of California, San Francisco, United States

Citation: Herskind, C., Barcellos-Hoff, M. H., eds. (2021). Cell Signaling Mediating Critical Radiation Responses. Lausanne: Frontiers Media SA.
doi: 10.3389/978-2-88966-979-0

Table of Contents

frontiers in Oncology

EDITORIAL
published: 10 May 2021
doi: 10.3389/fonc.2021.695355

Editorial: Cell Signaling Mediating Critical Radiation Responses

Carsten Herskind[1]* *and Mary Helen Barcellos-Hoff*[2]

[1] Department of Radiation Oncology, Universitätsmedizin Mannheim, Medical Faculty Mannheim, Heidelberg University, Mannheim, Germany, [2] Department of Radiation Oncology, University of California, San Francisco, San Francisco, CA, United States

Keywords: radiotherapy, radiation response, cell signaling, microenvironment, DNA repair, hypoxia, immunotherapy, fibrosis

Editorial on the Research Topic

Cell Signaling Mediating Critical Radiation Responses

Radiotherapy is an important loco-regional component of modern multimodal cancer therapy. Classically, radiobiology's 5 Rs: repair, repopulation, redistribution, reoxygenation, and radiosensitivity, as described by Steele et al. (1) have informed the use of radiotherapy. The past several decades have filled in molecular mechanism by which the radiation response of cells and tissues affect tumor control, expanding our knowledge of survival pathways beyond repair of radiation damage to DNA (2). In many cases, these pathways receive cues from extracellular signaling molecules *via* membrane-bound receptors (3). This emphasizes the importance of both intra- and extracellular signaling, and the interaction between different cell types in radiation-induced cell death as well as normal-tissue reaction after radiotherapy (4–6). The articles in the present Research Topic discuss recent progress and present original research on the contribution of cell signaling to radiation responses and radiation effects on cell signaling.

Residual double-strand breaks and complex DNA lesions are considered lethal and characteristic for ionizing radiation although typically some 98% are repaired by non-homologous end joining (NHEJ; all cell-cycle phases) or homologous recombination (HR, which is restricted to late S- and G2 phase). While the yield of single-strand breaks and base damage is much higher, these lesions contribute little to cell killing under normal circumstances as they are repaired with very high efficiency by the base excision repair (BER) system, although some single strand breaks in S-phase may be converted to double-strand break at replication forks. If HR is compromised (e.g. by *BRCA1* mutation), or overloaded, an error-prone backup mechanism, alternative end joining (alt-EJ) will repair the lesions. Liu et al. reviews the significant regulation of repair pathway choices by an extracellular cytokine, transforming growth factor (TGFβ), whose activity is a prominent signal in the irradiated tumor. TGFβ promotes HR and NHEJ but suppresses alt-EJ (7), and thus blocking TGFβ signaling increases radiosensitivity. An intracellular route to shifting repair competency is reviewed by Starcher et al. who describe the rationale for using quinone substrates to induce futile redox cycles leading to oxidative damage, BER hyperactivation, and depletion of NAD+ and ATP, which synergizes with ionizing radiation to radiosensitize human cancer cells at moderate doses. The study by Shukla et al. explores the synergy of combining the quinone derivative, β-lapachone with inhibition of a mitochondrial enzyme involved in folate metabolism.

Tumor hypoxia is well-recognize factor associated with resistance to radiotherapy and other therapies. The review by Sørensen and Horsman focuses on the hypoxia-inducible factor (HIF)

OPEN ACCESS

Edited and reviewed by:
Anatoly Dritschilo, Georgetown University, United States

***Correspondence:**
Carsten Herskind
carsten.herskind@medma.uni-heidelberg.de

Specialty section:
This article was submitted to Radiation Oncology, a section of the journal Frontiers in Oncology

Received: *14 April 2021*
Accepted: *21 April 2021*
Published: *10 May 2021*

Citation:
Herskind C and Barcellos-Hoff MH (2021) Editorial: Cell Signaling Mediating Critical Radiation Responses. Front. Oncol. 11:695355. doi: 10.3389/fonc.2021.695355

regulatory pathway, stress responses, and inflammatory pathways, and discusses the clinical applications of vascular modifiers and biomarkers. Extracellular signaling *via* transmembrane receptors can influence repair and survival pathways, and inhibition of EGFR is established in the clinic in combination with radiation therapy of head and neck, non-small cell lung and other cancers (8). Many cytokines, hormones and some growth factors activate the transcription factor STAT3 which is also involved in radioresistance as discussed by Wang et al. The study by Zhang et al. shows that a so far poorly characterized protein, FAM53A, influences vital cell functions related to the MAP kinase pathway in a p53-dependent manner and may be a candidate for targeted therapy in combination with DNA-damaging agents.

Radiotherapy is the canonical example of a DNA damage agent whose benefit is ascribed to cell kill in the irradiated field yet more than 15 years ago Formenti and Demaria showed that radiation could elicit systemic response in combinations with immunotherapy and formalized the concept by describing radiation as an '*in situ* vaccination' that can synergize with immunotherapy (9–11). Even though so-called 'abscopal' response, i.e., outside the irradiated field, are rare in the clinic, the idea of radiotherapy creating an 'in situ' vaccine has engendered significant interest given the remarkable successes of immune checkpoint blockade and other immunotherapy in many cancer patients. The study by Chen et al. on experimental hepatocarcinoma irradiated with different fractionation schemes found anti-tumor effects upon rechallenge with a reduction in immunosuppressing cells. Irradiation of the hepatocarcinoma inoculated on hind limbs triggered the antitumor immunity capable of suppressing the growth of subcutaneous tumors, accompanied with reduced myeloid derived suppressor cells in both blood and tumors. Radiotherapy can play a part in enhancing the response to immunotherapy by releasing damage-associated molecular pattern (DAMP) molecules that activate pattern recognition receptors (PRR, e.g. toll-like receptors, TLR), thereby acting as an immunological adjuvant (11). Domankevich et al. show that a PRR agonist synergizes with radiation from α-emitters in the treatment of experimental tumors.

In addition, complex signaling effects to and from the immune system beyond activation of immune cells are also beginning to be recognized. The study by Xia et al. describes how a small-molecule inhibitor of PD-L1 can radiosensitize glioblastoma cells by downregulating MiR-33a causing upregulation of PTEN, an endogenous suppressor of the AKT survival pathway. The clinical study by Minnaar et al. on mild hyperthermia in addition to chemoradiotherapy in cervical cancer patients found a marked increase in complete metabolic resolution in lymph nodes outside the irradiated field at six months.

The microenvironment of tumors and the surrounding stroma are key factors for both tumor control and normal tissue toxicities. Farias et al. review the evidence for the ability of mesenchymal stem cells and signaling *via* exosomes to mediate bystander (i.e., near-neighbor) and abscopal effects of radiotherapy. The study by Meyer et al. describes how host CD39 (part of the purinergic signaling pathway that responds to purine derivatives such as ATP and adenosine) has suppressive effects on the growth and radiosensitivity of Lewis lung tumors, which was abrogated in CD39 knockout mice and was associated with effects on the endothelial compartment. At the same time, CD39 deficiency enhanced radiation-induced lung fibrosis and osteopontin expression. Subcutaneous fibrosis after breast radiotherapy affects patients' quality of life and is an endpoint for risk prediction and mechanisms of radiation-induced fibrosis (12). Liu et al. review phosphatidic acid-mediated signaling from diacylglycerol kinase alpha and identify roles in T-cell activation, exosome production, and cell-cycle regulation as potential targets for interference. Finally, Herskind et al. analyzed genes expression profiles and genetic pathways associated with radiation-induced cell-cycle arrest and differentiation of fibroblasts *in vitro*. Notably, upregulated inflammatory pathways provide a potential link between fibrotic reaction and the immune system.

OUTLOOK

Therapeutic resistance is often intrinsic to the cancer cell, but signals generated between cells in the tumor microenvironment may ultimately determine response or resistance to radiotherapy, underscoring a gap that hampers cancer treatment optimization. Together, the papers in this Research Topic emphasize the importance of physiological context and intercellular communication within tumors and tissue as well as systemic signaling. Several provide a strong rationale for manipulating these signals that could enable optimization of radiotherapy.

AUTHOR CONTRIBUTIONS

All authors contributed to the article and approved the submitted version.

REFERENCES

1. Steel GG, Mcmillan TJ, Peacock JH. The 5Rs of radiobiology. *Int J Radiat Biol* (1989) 56:1045–8.
2. Maier P, Hartmann L, Wenz F, Herskind C. Cellular Pathways in Response to Ionizing Radiation and Their Targetability for Tumor Radiosensitization. *Int J Mol Sci* (2016) 17.
3. Bhattacharya P, Shetake NG, Pandey BN, Kumar A. Receptor Tyrosine Kinase Signaling in Cancer Radiotherapy and its Targeting for Tumor Radiosensitization. *Int J Radiat Biol* (2018) 94:628–44.
4. Wynn TA, Ramalingam TR. Mechanisms of Fibrosis: Therapeutic Translation for Fibrotic Disease. *Nat Med* (2012) 18:1028–40.
5. Citrin DE, Mitchell JB. Mechanisms of Normal Tissue Injury From Irradiation. *Semin Radiat Oncol* (2017) 27:316–24.
6. Rodriguez-Ruiz ME, Vitale I, Harringto KJ, Melero I, Galluzzi L. Immunological Impact of Cell Death Signaling Driven by Radiation on the Tumor Microenvironment. *Nat Immuno* (2020) 21:120–34.
7. Liu Q, Palomero L, Moore J, Guix I, Espin R, Aytes A, et al. Loss of TGFbeta Signaling Increases Alternative End-Joining DNA Repair That Sensitizes to Genotoxic Therapies Across Cancer Types. *Sci Transl Med* (2021) 13.

8. Cuneo KC, Nyati MK, Ray D, Lawrence TS. EGFR Targeted Therapies and Radiation: Optimizing Efficacy by Appropriate Drug Scheduling and Patient Selection. *Pharmacol Ther* (2015) 154:67–77.
9. Demaria S, Formenti SC. Sensors of Ionizing Radiation Effects on the Immunological Microenvironment of Cancer. *Int J Radiat Biol* (2007) 83:819–25.
10. Formenti SC, Demaria S. Systemic Effects of Local Radiotherapy. *Lancet Oncol* (2009) 10:718–26.
11. Demaria S, Formenti SC. Radiation as an Immunological Adjuvant: Current Evidence on Dose and Fractionation. *Front Oncol* (2012) 2:153.
12. Herskind C, Talbot CJ, Kerns SL, Veldwijk MR, Rosenstein BS, West CM. Radiogenomics: A Systems Biology Approach to Understanding Genetic Risk Factors for Radiotherapy Toxicity? *Cancer Lett* (2016) 382:95–109.

Conflict of Interest: The authors declare that the research was conducted in the absence of any commercial or financial relationships that could be construed as a potential conflict of interest.

frontiers in Oncology

REVIEW
published: 27 August 2019
doi: 10.3389/fonc.2019.00799

Misrepair in Context: TGFβ Regulation of DNA Repair

Qi Liu[1,2,3], *Kirsten Lopez*[4], *John Murnane*[1], *Timothy Humphrey*[4] *and Mary Helen Barcellos-Hoff*[1]*

[1] Department of Radiation Oncology, Helen Diller Family Comprehensive Cancer Center, University of California, San Francisco, San Francisco, CA, United States, [2] Institute of Biomedical Engineering, Peking University Shenzhen Graduate School, Shenzhen, China, [3] Shenzhen Bay Laboratory (SZBL), Shenzhen, China, [4] Department of Oncology, CRUK/MRC Oxford Institute for Radiation Oncology, University of Oxford, Oxford, United Kingdom

Repair of DNA damage protects genomic integrity, which is key to tissue functional integrity. In cancer, the type and fidelity of DNA damage response is the fundamental basis for clinical response to cytotoxic therapy. Here we consider the contribution of transforming growth factor-beta (TGFβ), a ubiquitous, pleotropic cytokine that is abundant in the tumor microenvironment, to therapeutic response. The action of TGFβ is best illustrated in head and neck squamous cell carcinoma (HNSCC). Survival of HNSCC patients with human papilloma virus (HPV) positive cancer is more than double compared to those with HPV-negative HNSCC. Notably, HPV infection profoundly impairs TGFβ signaling. HPV blockade of TGFβ signaling, or pharmaceutical TGFβ inhibition that phenocopies HPV infection, shifts cancer cells from error-free homologous-recombination DNA double-strand-break (DSB) repair to error-prone alternative end-joining (altEJ). Cells using altEJ are more sensitive to standard of care radiotherapy and cisplatin, and are sensitized to PARP inhibitors. Hence, HPV-positive HNSCC is an experiment of nature that provides a strong rationale for the use of TGFβ inhibitors for optimal therapeutic combinations that improve patient outcome.

Keywords: cancer, TGFβ, DNA repair, tumor microenvironment, genomic integrity, cytotoxic therapy, therapeutic response

OPEN ACCESS

Edited by:
Sergio Giannattasio, Consiglio Nazionale delle Ricerche, Istituto di Biomembrane, Bioenergetica e Biotecnologie Molecolari (IBIOM), Italy

Reviewed by:
Lukas Cermak, Institute of Molecular Genetics (ASCR), Czechia
Zhi-Xiang Xu, University of Alabama at Birmingham, United States

***Correspondence:**
Mary Helen Barcellos-Hoff
maryhelen.barcellos-hoff@ucsf.edu

Specialty section:
This article was submitted to Molecular and Cellular Oncology, a section of the journal Frontiers in Oncology

Received: *31 May 2019*
Accepted: *06 August 2019*
Published: *27 August 2019*

Citation:
Liu Q, Lopez K, Murnane J, Humphrey T and Barcellos-Hoff MH (2019) Misrepair in Context: TGFβ Regulation of DNA Repair. Front. Oncol. 9:799. doi: 10.3389/fonc.2019.00799

INTRODUCTION

DNA repair is executed by multiple pathways that must be coordinated to deal with different types of DNA damage, including oxidative damage, single strand breaks (SSB), and double strand breaks (DSB). Complex intracellular mechanisms have developed to ensure an appropriate DNA damage response (DDR). In cancer, gene mutations and altered cell signaling can give rise to dysregulated and aberrant DNA repair mechanisms that presumably contribute to genomic instability and mutational burden that are associated with cancer progression.

Cancer cells are actively involved in crosstalk with host cells of the tumor microenvironment (TME), which includes the vasculature, immune cells and stroma, constitutes a robust but skewed signaling network distinct from normal tissue. Though the TME is critical in shaping the biology of a tumor, the impact of context-related signaling on the tumor cell's DNA repair proficiency is poorly understood. This article reviews cell intrinsic execution of DSB repair proficiency and pathway competency to discuss DNA repair in the context of the TME.

We focus on transforming growth factor-beta (TGFβ), which is critically involved in extrinsic control of pathway competency in DSB repair. Recently, we determined that compromised TGFβ signaling caused by human papilloma virus (HPV) in head and neck squamous cell carcinoma (HNSCC) shifts DSB repair to error prone and inefficient alternative end-joining (altEJ). HPV is an experiment of nature that provides compelling evidence that signaling from TGFβ, and thus the TME, is critical for DNA repair execution and pathway choice. The insight gained from understanding of the mechanisms by which TGFβ signaling, DDR, and TME are functionally linked, paves the way to further exploit weakness in specific cancers and develop pertinent therapeutic strategies.

DSB REPAIR PATHWAYS

Tens of thousands of DNA lesions are produced in a cell's daily life as a result of endogenous metabolic activities such as DNA replication or reactive oxygen species (ROS), as well as exposure to exogenous agents like ultraviolet (UV) or ionizing radiation (1, 2). Of the many types of DNA damage, DSBs are among the most dangerous. Failure to repair DSBs may lead to mutations, genomic, and chromosomal rearrangements, or cell death. In order to maintain genomic integrity, two predominant DSB repair pathways have developed to deal with different types of lesions: classical non-homologous end-joining (c-NHEJ) and homologous recombination repair (HRR) [**Figure 1**; (3)]. In mammalian cells, c-NHEJ is the predominant DSB repair pathway that can efficiently rejoin most DSBs (4). Although c-NHEJ functions throughout the cell cycle, it is particularly critical in the G1 phase when the cell has yet to replicate its DNA (5, 6). C-NHEJ is initiated by the binding of the Ku70/Ku80 heterodimer to the ends of the DSB, which is then recognized with high affinity by the catalytic subunit of DNA-dependent protein kinase (DNA-PKcs), forming the DNA-PK complex (7). This enables the recruitment of nucleases, including Artemis, to trim any short overhangs that are present on the DSB ends (8), and polymerases, including Polμ, to fill in any gaps (9–11). The final ligation step involves a ligase complex comprised of DNA ligase IV, X-ray repair cross-complementing protein 4 (XRCC4), and XRCC4-like factor (XLF), which is responsible for bridging and ligating the two processed ends (12). Because DSB ends often require processing to remove damaged nucleotides to enable ligation, c-NHEJ is considered an error-prone form of repair that can lead to short insertions and/or deletions. However, growing evidence suggests the context under which c-NHEJ is used in DSB repair is a critical determinant of the repair outcome, i.e., error-prone or error-prevention (13, 14). Although it awaits further evidence, it has been speculated that orchestrated repair with c-NHEJ in normal cells prevents chromosome instability, but in cancer cells with dysregulated repair pathways, inappropriate implementation of c-NHEJ-dependent end joining of non-contiguous ends can cause genomic alterations and lead to chromosome instability (13, 14).

The repair of DSBs by HRR is a highly complex process that requires the generation of single-stranded 3′ overhangs at each end, after which the homologous sequence on the sister chromatid is used to accurately fill in the gaps and restore the original DNA sequence (15, 16). In the first step of HRR, the DSB ends are recognized by the MRN complex, which is composed of meiotic recombination 11 homolog A (MRE11), RAD50, and Nijmegen breakage syndrome 1 (NBS1). Once bound to the DSB, the MRN complex activates ataxia telangiectasia mutated (ATM), a serine-threonine kinase that initiates the DDR by phosphorylating a plethora of substrates, thus facilitating the recognition of the DSB and the activation of downstream repair

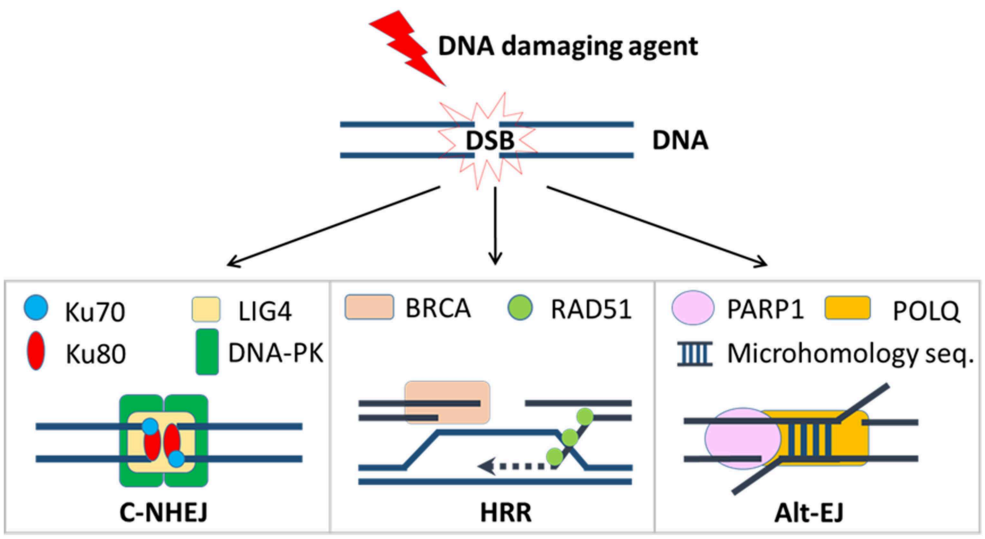

FIGURE 1 | DSB repair pathways. Once a DSB is induced by a DNA damaging agent, cancer cells will try to repair it by one of these three mechanisms. Critical repair proteins in each pathway are shown.

factors. In addition to its role in the MRN complex, MRE11 also associates with C-terminal binding protein interacting protein (CtIP), an endonuclease that allows for the removal of ∼100 nucleotides from the 3′ end of the DSB (17, 18).

Following the initial processing step by MRE11 and CtIP, more extensive resection is subsequently mediated by either the EXO1 exonuclease or a combination of the RECQ helicase (BLM or RECQL4) and the DNA2 exonuclease (19). The single-stranded DNA formed by these resection steps is very quickly coated with and stabilized by replication protein A (RPA), preventing them from being degraded or forming DNA hairpins (20). For the final phase of HRR, RPA is replaced with RAD51 to facilitate homology search, strand invasion into the sister chromatid, and initiation of DNA synthesis at the region of the DSB (21). This process requires several proteins known as recombination mediators, e.g., the tumor suppressor breast cancer 1, early onset 2 (BRCA2) (22, 23). Repair is then completed upon resolution of crossover junctions by resolvases (24). Because HRR requires a homologous template, it can only be used to repair DNA that has been replicated (i.e., during the S and G2 phases of the cell cycle).

A third mechanism for repair of DSBs is altEJ, which is also referred to as backup end joining, or microhomology-mediated end joining (25, 26). A comparison of repair strategies is depicted in **Figure 1**. AltEJ uses poly [ADP-ribose] polymerase 1 (PARP1) to tether broken DNA ends (27), DNA polymerase theta (Pol θ) coded by the *POLQ* gene to initiate DNA replication at sites within two single-stranded 3′ overhangs (28), and DNA ligase I (LIG1) or DNA ligase III (LIG3) to join the DNA ends (29). AltEJ commonly occurs at sites containing short complementary sequences, known as microhomology, that are exposed after end resection; this requirement for resection and minimal homology means that altEJ has low fidelity and therefore frequently results in small deletions, insertions, and gross chromosomal rearrangements (30, 31). Because its execution increases genomic instability, altEJ is believed to be more active in certain cancers (32).

Other DSB repair pathways, such as single-strand annealing (SSA), can result in large deletions during repair by annealing of longer (e.g., >100 nt) repeats following extensive end-resection. These are rarely used in mammalian cells and have been reviewed recently (24), and will not be discussed herein.

DSB REPAIR PATHWAY COMPETENCY IN CANCER

The mechanism by which DSB are repaired is determined by a variety of factors, although the outcome is ultimately determined by the presence or absence of end resection. The initial phase of c-NHEJ, i.e., binding of the Ku heterodimer to DSB ends, minimizes end resection to allow accurate end-joining. End processing and resection are therefore tightly regulated by Ku70/Ku80, along with WRN and 53BP1, which together protect DNA ends during the G1 phase when HRR cannot occur due to the absence of a sister chromatid. Resection is also normally limited to late S or G2 due to the cell-cycle dependent expression of CtIP and its activation by CDK1 or CDK2 (33, 34). Importantly, resection requires the repositioning of 53BP1 on DSB ends by BRCA1, and therefore the loss of BRCA1 inhibits HRR, which was demonstrated by the fact that a deficiency in 53BP1 rescues the defect in HRR caused by the absence of BRCA1 (35). Noordermeer et al. recently demonstrated that 53BP1 effector complex, shieldin, localizes to DSB to prioritize c-NHEJ repair (36). In BRCA1-deficient cells, loss of shieldin or its subunits can restore HRR and resistance to PARP inhibition (37).

AltEJ was initially believed to be a backup pathway for c-NHEJ and HRR (26). The Ku heterodimer has much higher affinity for DSB ends relative to PARP1; thus, c-NHEJ is highly favored over altEJ in most circumstances (38). A higher frequency of altEJ-mediated repair was observed after the depletion of HRR factors such as RPA, BRCA1, and BRCA2 (39), suggesting HRR is used with priority in normal settings. In addition, because both HRR and altEJ require an initial resection step at DSB ends, both pathways are inhibited by c-NHEJ factors. Conversely, end resection is sufficient to block repair by c-NHEJ, as Ku70/Ku80 has very low affinity for single stranded DNA (40). Notably, accumulating evidence suggests that altEJ also competes with HRR for the repair of DSB (28, 41). For example, by studying dysfunctional telomeres and accumulation of RAD51 at DSBs, Mateos-Gomez and co-authors found that the loss of a critical component in altEJ, Pol θ, increased HRR in mice (28). Similar findings have been reported in ovarian cancers: HRR was upregulated when Pol θ expression was inhibited, while Pol θ expression blocks RAD51-mediated HRR due to RAD51 binding motifs in Pol θ (41).

Cell cycle phase plays an important role in DSB repair pathway choice. In S and G2 phases, HRR is preferentially used to repair DSB due to the presence of CYREN, an inhibitor of c-NHEJ (42). AltEJ is largely inactive in normal cells, but in quickly dividing cancer cells, altEJ may be increased to handle the increased level of DNA damage and, as a result, generate more mutations as by-products. Although the cell cycle dependency of altEJ is not clear, it is possible that HRR-deficient cells use altEJ mainly in S or G2 phases, while c-NHEJ defects may increase altEJ in G1 phase. In addition, host cell type, chromosomal location, and epigenetic modification are also important factors for pathway competence at DSBs, which has been reviewed elsewhere (43).

EXPLOITING DNA REPAIR DEFICITS IN CANCER CELLS

Many DNA repair genes are tumor suppressors, and are frequently mutated during tumor progression. Loss of functions in some DNA repair genes increases compensating mechanisms of repair that may expose a targetable "Achilles heel." Synthetic lethality, which is defined as a cytotoxic response to the loss or inhibition of a gene or pathway that only happens in the presence of another specific genetic deficit, can specifically target cancer cells containing a defect in a DNA repair gene. The clinical application of synthetic lethality is best exemplified using PARP inhibitors in cells that have germ line or somatic mutations in *BRCA1* or *BRCA2* (44, 45). PARP inhibition results in the accumulation of single-strand breaks (SSB) that produce DSBs

upon collision with a DNA replication fork, which require HRR to repair. This is one mechanism by which BRCA1/2-deficient cancers are highly sensitized to PARP inhibition, although other functions of PARP may contribute as well. For example, PARP is directly involved in detoxifying endogenous ROS (46, 47), while BRCA1 down-regulates cellular levels of ROS (48). Thus, BRCA deficient cells may be more sensitive to increased cytotoxic ROS that result from PARP inhibition. Although the clinical benefits of PARP inhibition are clear in BRCA1/2-deficient cancers, tumors with HRR defects in the absence of BRCA gene mutations (i.e., BRCAness) are also responsive to PARP inhibition (49). Hence, mutation of genes that are directly or indirectly involved in HRR or the Fanconi anemia pathway, a DNA repair pathway that intersects HRR, can contribute to so-called BRCAness, i.e., tumors that behave as if *BRCA1* or *BRCA2* are mutated (49). Biomarkers to assess BRCAness, which include transcriptional signatures, genomic scars, or levels of Rad51 foci, are under intensive investigation (50–52).

SYNTHETIC LETHALITY BETWEEN ALTEJ AND OTHER DSB REPAIR PATHWAYS

Besides its key role in SSB repair, PARP1 is also a critical component of altEJ; thus, PARP inhibition can cause synthetic lethality in tumors that rely on altEJ (25). Other altEJ components are promising therapeutic targets for tumors that depend on this repair pathway. Indeed Pol θ -mediated end joining becomes critical when either HRR or c-NHEJ fails. A recent genetic screen reported that both Pol θ and another altEJ component, the structure-specific endonuclease FEN1, are synthetic lethal with BRCA2 (53). The potential synergy of HRR and altEJ is indicated by embryonic lethality of combined loss of *Brca1/Fancd2* and *Polq* in mice (28, 41). Depletion of Pol θ in human cancer cells deficient in HRR due to absence of BRCA1/2 increases chromosomal aberrations and impaired cell survival (28). Pol θ loss also increases HRR-impaired cells sensitivity to DNA-damage (41).

Moreover, there is growing evidence that defects in HRR can lead to increased dependence on altEJ for repair, particularly in the context of fork stalling during replication stress (26, 54). In addition to its relationship with HRR, altEJ may also be synthetic lethal with c-NHEJ. Combined deletion of *POLQ* and Ku70, as well as *POLQ* and *53BP1*, leads to markedly reduced cell proliferation and survival associated with excessive end resection and chromosomal aberrations (55). Notably, *POLQ* is highly expressed in a subset of cancer types (56, 57) and its expression is associated with poor prognosis (58, 59).

DNA REPAIR IN CONTEXT: THE TUMOR MICROENVIRONMENT

Cancer cells react to endogenous (e.g., replication stress) or exogenous (e.g., radiation, chemotherapy) DNA damage in the context of their TME. The TME plays an important role in determining cancer clinical behavior and progression, and can influence cancer cell response to therapy (60, 61). Components of the TME include cellular constituents of bone-marrow derived cells, fibroblasts and vessels, insoluble extracellular matrix, and soluble cytokines and chemokines (62). These TME components closely collaborate with cancer cells for development of a neoplastic phenotype. In this "team," frequent interactions and crosstalk in a complicated signaling network unite them as a whole. Better understanding of "tumor as a whole" could provide information about the optimal use of therapies, and improve the development of personalized therapy based on integrated features of a tumor derived from both cancer cells and TME composition.

The influence of TME conditions on DNA repair is complex. Although DNA repair is largely regulated through autonomous signaling cascades, tissue-wide stress responses from DNA damage may be networked among tumor cells, stromal cells, and other TME components. TME composition influences DNA repair efficiency by transmitting inter- and intra-cellular signals in a tissue-specific fashion. Many TME factors, which include cytokines, extracellular matrix, stromal cells, hypoxia, and inflammation, are known to modulate DNA repair efficiency (63–68).

Here we focus on TGFβ, a highly pleiotropic cytokine and a canonical tumor suppressor. Because TGFβ suppresses epithelial cell cycle progression, all carcinomas must escape TGFβ growth regulation (69). Notably, high TGFβ expression and signaling is associated with poor prognosis in multiple cancer types (52, 70) because TGFβ becomes a tumor promoter that is involved in tumor progression by modifying the TME, suppressing immune response, and promoting metastasis (71). Due to these critical functions and association with poor outcomes, TGFβ is an intriguing therapeutic target in clinical trials (72, 73).

TGFβ BIOLOGY

Understanding the biology of TGFβ is rooted in understanding when and where it is active. There are three mammalian TGFβ isoforms, each encode a polypeptide that is cleaved intracellularly to form a roughly 24 kD TGFβ that is non-covalently associated with an 80 kD dimer of its pre-pro peptide, called latency associated peptide (LAP). This complex, TGFβ and LAP, is secreted as the latent TGFβ complex and is often sequestered in forms bound to extracellular matrix. TGFβ canonical signaling is initiated upon the release of TGFβ ligand from its latent complex, and subsequent binding to the type II TGFβ receptor (TβRII), which causes recruitment and phosphorylation of type I receptor (TβRI). Activated TβRI kinase phosphorylates the carboxy-terminal serine residue of the mothers against DPP Homolog proteins SMAD2 or SMAD3, which induces oligomerization of SMAD2 or SMAD3 with SMAD4, and DNA binding of the complex to mediate transcriptional activation or repression of target genes. TGFβ also transduces signals through non-canonical signaling pathways, such as MAPK/ERK, PI3K/AKT, Rho/Rock. Activation of TGFβ is highly controlled in normal tissues. In cancers, TGFβ signaling is highly dysregulated (70, 74, 75). Defective TGFβ signaling, which can be caused by mutations

in *SMAD4* and *TGFBR2*, are frequent in certain types of cancer (52, 73).

Both cancer cells and stromal cells produce TGFβ that may, when activated, elicit paracrine or autocrine signaling to stimulate fibroblasts, endothelial cells and immune cells that further alter the TME. Moreover, TGFβ is a potent immunosuppressive cytokine involved in shaping TME by inhibiting the activation and function of T cells (76, 77), inducing immune suppressive myeloid cells (78), as well as by other multifaceted mechanisms (79–81). These complex interactions are just a few of TGFβ's roles in the TME.

An unexpected role for TGFβ, an intrinsically extracellular signal, is response to intracellular DNA damage. Glick et al. (82) was likely the first study to implicate TGFβ in the cellular response to DNA damage. They showed that *Tgfb1* null murine keratinocytes were highly genomically unstable, independent of G1 arrest and p53 function (82). Consistent with a role of TGFβ in maintaining genomic stability, Maxwell et al. (83) demonstrated more centrosome aberrations and aneuploidy in irradiated *Tgfb1*-null compared to TGFβ-competent keratinocytes. Notably, this effect is phenocopied by TGFβ inhibition in human epithelial cells (83). In a subsequent study, Glick and colleagues revealed a DNA repair deficit due to hypermethylated O(6)-methylguanine DNA methyltransferase (MGMT) that affected the DDR of *Tgfb1*-null keratinocytes (84). Similarly, Kirshner et al. (85) showed that inhibiting TGFβ signaling attenuates DDR by compromising the function of ATM, the DDR kinase involved in DSB recognition (85). Consequently, pharmaceutical inhibition of TβRI kinase or knockout of *Tgfb1* reduces ATM autophosphorylation and phosphorylation of its substrates, e.g., p53, Chk2, and Rad17, inhibits formation of radiation-induced γH2AX foci, and increases radiosensitivity (85). In support of this, Wiegman et al. (86) showed that exogenous TGFβ stimulates ATM and p53 phosphorylation in irradiated cells in a SMAD-independent fashion (86). Notably, TGFβ inhibition also reduces *LIG4* expression, which is required in c-NHEJ (87).

Nucleotide excision repair (NER) is a versatile DNA repair pathway that eliminates a wide variety of helix-distorting base lesions induced by environmental carcinogenic sources. UVB radiation downregulates E-cadherin, a cell adhesion protein, in mouse skin and skin tumors whereas inhibiting the TGFβ pathway in these cells increases the NER of UV-induced DNA damage (88). E-cadherin inhibition in keratinocytes suppresses NER through activating the TGF-β pathway and increasing *TGFβ1* mRNA levels. Interestingly, TGFβ is activated by ionizing radiation and in turn, promotes epithelial-mesenchymal transition characterized by loss of E-cadherin (89). Treatment of cells with exogenous TGFβ enhances NER of DNA damage formed by polycyclic aromatic hydrocarbons and UVC radiation independent of the cell cycle (90).

Consistent with role of TGFβ in DDR, the SMAD proteins, which are the critical transducers of TGFβ intracellular signaling, are involved in DSB repair. Both pSmad2 and Smad7 can co-localize with nuclear γH2AX foci at DSB, while pSmad2 foci formation is ATM dependent (91). Studies in *Smad4* conditional knockout mice confirmed that TGFβ is critical in maintaining genomic stability through regulation of genes in the Fanconi anemia/BRCA DNA repair pathway (92). SMAD4 suppresses a micro RNA, miR182, which inhibits FOXO3, which is required for ATM kinase activity (32, 52). MiR182 also suppresses BRCA1 expression (93, 94). Hence, TGFβ signaling through SMAD4 promotes HRR in part by suppressing miR182 (52). C-NHEJ is also partially compromised because LIG4 expression and ATM activity are reduced once TGFβ signaling is blocked (85, 87).

Although tumors must evade TGFβ growth control, at the time of clinical appearance, many tumors maintain signaling competency. Indeed, squamous cell carcinomas may take advantage of TGFβ signaling to maintain a sub-population of cells at a quiescent state for chemo-resistance (95). Moreover, the high TGFβ activity of TME could promote tumor-intrinsic resistance to cytotoxic agents due to its role in DNA damage recognition and repair. If so, pharmacological TGFβ blockade could sensitize certain tumors to radiation and other cytotoxic therapies. Exploration of brain, breast, and lung cancer pre-clinical models is consistent with this concept, since TGFβ inhibition radiosensitized 38 of 43 murine and human cancer cell lines *in vitro* (85, 96–98). Because TGFβ provides extrinsic control of several aspects of intracellular DNA repair pathway competency, one prediction is that tumors that are insensitive to TGFβ can be exploited by targeting their deficiency in DNA repair.

TGFβ SIGNALING REGULATES DNA REPAIR PATHWAY COMPETENCY

The contribution of TGFβ signaling as a barrier compromising therapeutic response to cytotoxic therapy is exemplified by HPV-positive (HPV+) HNSCC (52), which have much better (70%) survival at 5 years compared to HPV-negative (HPV-) cancers that attain only 30% survival, even when HNSCC location and stage are similar. The considerable difference in outcomes has stimulated significant interest based on the idea that the mechanism of sensitivity of HPV+ cancer to standard-of-care chemoradiation therapy, which could provide insights that can be therapeutically exploited to achieve better response in HPV- cancer.

Consistent with a cell-intrinsic effect, HPV+ cancer cell lines exhibit altered expression of DNA repair proteins (99) and increased sensitivity to cytotoxic therapy (100, 101). Most research has focused on oncogenic impairment of p53 and retinoblastoma (Rb) proteins by HPV E6 or E7, respectively. However, HPV proteins E5, E6, and E7 target both the type I and II TGFβ receptors and SMAD 2, 3, and 4, the transducers of ligand binding, for degradation (102, 103). We examined the impact of HPV on TGFβ signaling in HNSCC at multiple levels. Functionally, TGFβ induced phosphorylation of SMAD2 (pSMAD), indicative of signaling competency, is significantly reduced in HPV+ cell line, patient derived xenografts, and primary tumor explants, compared to HPV− specimens (52). Notably, HPV+ specimens in a HNSCC tumor array with 130 HPV− and 65 HPV+ samples exhibit less pSMAD compared to HPV− specimens. In addition, TCGA HPV+ tumors are

identified by low activity (243 HPV− vs. 36 HPV+ ones) of a TGFβ pathway signature, which contains 50 TGFβ-regulated genes that were derived from epithelial cells chronically stimulated or inhibited for the corresponding pathway.

Interestingly, Wang and colleagues engineered a conditional *Smad4* deletion in oral mucosa that gave rise to spontaneous HNSCC accompanied by high rates of genomic instability (92). Subsequent studies by this group showed that *Smad4* deletion leads to decreased Brca1 expression in mice and that loss of SMAD4 protein correlates with decreased BRCA1 and RAD51 proteins in human HNSCC. BRCA1 is crucial for HRR during S-phase/G2, acts upon the cell cycle machinery, and affects gene expression and cell fate decisions via chromatin remodeling and transcriptional activity (104). Wang and colleagues showed that BRCA1 is transcriptionally down-regulated by SMAD4-dependent CtPB1 (105). A second, more direct route by which TGFβ controls of BRCA1 is via TGFβ suppression of miR-182, which targets BRCA1 message stability and translation in mouse and human cells. Thus, pharmacologically or genetically compromised TGFβ increase levels of miR-182 and consequently suppress BRCA1 (94).

Consistent with our earlier studies in breast, lung and brain cancer cells (85, 96–98), HPV+ HNSCC cell lines were more sensitive to radiation than HPV− cell lines (52). Indeed, the degree of pSMAD response to TGFβ and cellular radiosensitivity are highly correlated. Radiation sensitivity reflects the cumulative damage and inherent capacity to repair the damage based on the cells ability to recognize DNA damage, assemble the repair machinery, and execute repair; abrogation of any of these components decreases cell survival. As noted above, BRCA1 is critical for HRR-mediated DNA repair. HRR requires RAD51 binding to 3′-single-stranded DNA overhangs from processed DSB and strand pairing; thus, the formation of RAD51 foci is evidence of HRR. Significantly, fewer RAD51 foci are formed in HPV- HNSCC cells and tumor specimens if TGFβ is pharmacologically blocked, which is not observed in HPV+ HNSCC cells.

A deficiency in HRR should increase the proportion of cells that are killed in response to PARPi. As predicted, TGFβ-unresponsive HPV+ cell lines are more sensitive to olaparib alone compared to TGFβ-responsive HPV- cancer cells, which were sensitized 4-fold by TGFβ inhibition (52).

Loss of effective HRR can activate altEJ, which competes with HRR for repair of DSBs in S-phase (41) and/or acts as backup repair when HRR or c-NHEJ are compromised (26). As mentioned earlier, altEJ requires PARP1 and Pol θ, the product of the *POLQ* gene (28). To evaluate altEJ, we established TGFβ-responsive cells with a reporter construct detecting altEJ events (106). As expected, a specific PARP1 inhibitor reduced altEJ events, while TGFβ inhibitors significantly increased altEJ events.

Thus, either pharmaceutical blockade of TGFβ signaling in HPV− cells or intrinsic-defects in TGFβ signaling in HPV+ cells shifts DSB repair to altEJ (**Figure 2**). This shift may result from decreased implementation of HRR and c-NHEJ, or may indicate an increase in altEJ competency. Notably, *BRCA1* heterozygous cells exhibit preferential use of altEJ (107), suggesting that the decrease in BRCA1 that occurs upon loss of TGFβ signaling phenocopies the genetic *BRCA1* loss. As c-NHEJ is also partially compromised because LIG4 expression and ATM activity are reduced (85, 87), cells with deficient TGFβ signaling may increase altEJ to compensate for a deficiency in both HRR and c-NHEJ.

TGFβ-unresponsive cells that depend on altEJ are still capable of rejoining most DSBs, which hinders the maximal cytotoxic response to DNA damage. As mentioned above, recent studies demonstrate that Pol θ is required in altEJ (28, 41). HRR-deficient ovarian and breast cancers exhibit increased *POLQ* expression, perhaps indicative of altEJ (41). Consistent with this, *POLQ* expression is increased in HPV+ vs. HPV− HNSCC TCGA (52). Notably, *POLQ* shRNA expressing HPV− cells treated with TGFβ inhibitors were more sensitive DNA damage, supporting the idea that Pol θ-mediated altEJ is increasingly used when TGFβ signaling is abrogated. These data suggest that combining altEJ inhibitors with pharmaceutical blockade of TGFβ signaling would induce synthetic lethality, thus creating a novel route that could boost the sensitivity of TGFβ-active tumors to therapies that involve DNA damage. Moreover, since altEJ is a backup mechanism that operates preferentially in cancer cells, inhibiting altEJ may pre-dominantly sensitize tumor cells and spare normal cells. Alternatively, one might select cancers that are defective in TGFβ to target drugs that interfere with altEJ, since these drugs will both improve the treatment effectiveness and the toxicity profile.

The importance of alt-EJ in TGFβ-deficient cells discovered in HNSCC raises several questions. We are following this lead to determine if the same mechanism is evident in other cancers in which TGFβ signaling is compromised. Almost all cervical cancers are HPV positive, which we would expect to show similar DDR choices as HNSCC. However, TGFβ signaling is compromised by various mechanisms in many cancers (108). Our analysis across the spectrum of cancers suggest that there is probably a generic mechanism (unpublished). We also find that the repair shift to altEJ in TGFβ-deficient cells occurs independent of miR-182. Further studies are necessary to decipher the underlying mechanisms.

Although most evidence supports TGFβ as a factor enforcing DNA-repair proficiency to protect against genomic instability, conflicting evidence about the role of TGFβ in DDR also exists (109–112). For example, Pal et al. reported that TGFβ hinders DSB repair in cancer stem cells by reducing HRR gene expression, which was proposed to heighten genetic diversity and adaptability of cancer stem cells (112). This subpopulation may regulate DDR differently, but it is interesting that in another study, glioblastoma cancer stem cells make 5-fold more TGFβ than bulk cultures (97). Considering that TGFβ is a pleotropic cytokine, the extensive technical and conditional differences in these studies may lead to a different conclusion.

For example, TGFβ signaling induces squamous cell carcinoma cancer stem cells quiescence, which would be expected to affect repair pathway competency in a manner that contributes to chemo-resistance (95). However, many cancer cells have escaped TGFβ cell growth control, as stated above. For example, in our HNSCC study, the cell cycle was not significantly changed upon TGFβ stimulation or inhibition of HNSCC cell

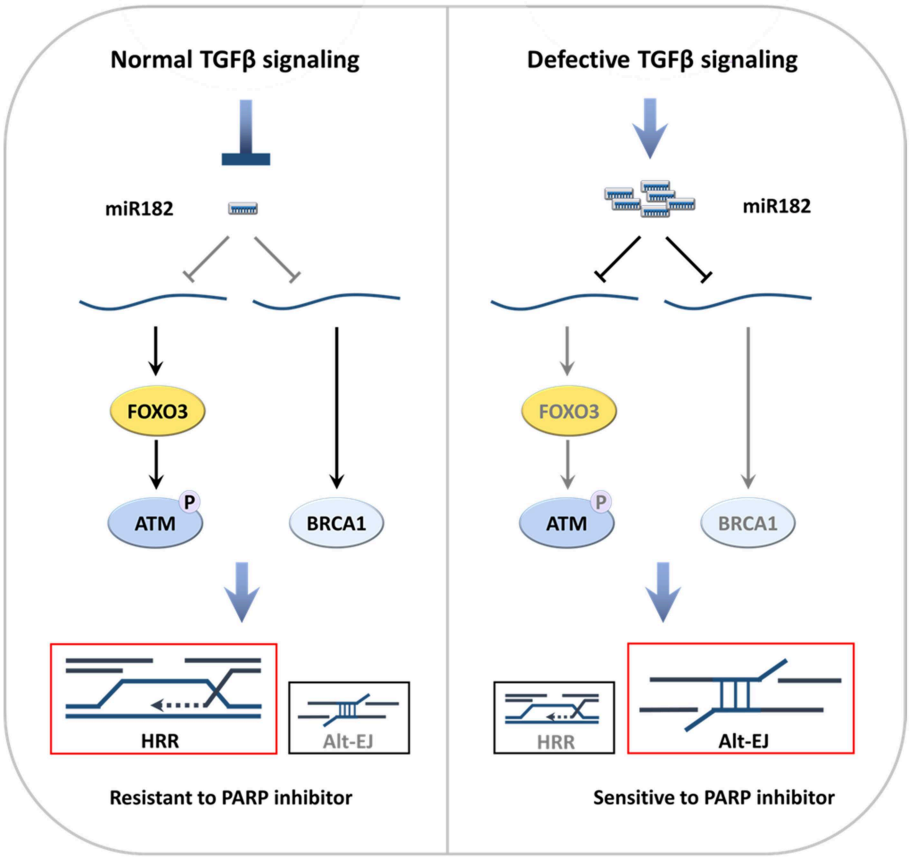

FIGURE 2 | Defective TGFβ signaling in HNSCC increases altEJ (52). **(A)** TGFβ signaling suppresses miR182, which suppresses expression of *BRCA1* and *FOXO3*. DNA damage elicits activates ATM autophosphorylation and its phosphorylation of BRCA1, which gives rise to use of HRR in S-phase. **(B)** In contrast, deficient TGFβ signaling, which can be caused by HPV infection, TGFβ receptor kinase inhibitors (TBRi) or *SMAD4* mutations (*SMAD4* mut), leads to increased miR182 that suppresses *BRCA1* and *FOXO3*. Loss of FOXO3 inhibits ATM auto-activation, which together with decreased BRCA1, impedes HRR. This is accompanied by increased altEJ.

lines (52), which indicates that TGFβ can regulate DNA repair pathway by mechanisms independent of cell cycle effects.

OUTLOOK

Intensive investigation of the TME has advanced our knowledge about the tumor as a whole, whereas in-depth analysis of DDR now provides mechanisms of DNA repair strategies and their implementation in cancer cells. How DDR is executed in different tumors is an area of growing complexity. The highly heterogeneous TME is a function of cancer cell genetics, epigenetics, host cell composition that result in complicated signaling networks. However, opportunities also lie in these challenges. DDR-related signaling pathways regulated by the TME components may contain biomarkers for cancer stratification, as well as molecular or cellular targets for drug development, which deserves significant investigation.

AUTHOR CONTRIBUTIONS

QL, JM, and MB-H wrote the review. TH and KL reviewed and revised the manuscript.

FUNDING

This research was supported by UCSF Department of Radiation Oncology funds to MB-H.

REFERENCES

1. Lindahl T, Barnes DE. Repair of endogenous DNA damage. *Cold Spring Harb Symp Quant Biol.* (2000) 65:127–33. doi: 10.1101/sqb.2000.65.127
2. Tubbs A, Nussenzweig A. Endogenous DNA damage as a source of genomic instability in cancer. *Cell.* (2017) 168:644–56. doi: 10.1016/j.cell.2017.01.002
3. Krejci L, Altmannova V, Spirek M, Zhao X. Homologous recombination and its regulation. *Nucleic Acids Res.* (2012) 40:5795–818. doi: 10.1093/nar/gks270

4. Beucher A, Birraux J, Tchouandong L, Barton O, Shibata A, Conrad S, et al. ATM and Artemis promote homologous recombination of radiation-induced DNA double-strand breaks in G2. *EMBO J.* (2009) 28:3413–27. doi: 10.1038/emboj.2009.276
5. Takata M, Sasaki MS, Sonoda E, Morrison C, Hashimoto M, Utsumi H, et al. Homologous recombination and non-homologous end-joining pathways of DNA double-strand break repair have overlapping roles in the maintenance of chromosomal integrity in vertebrate cells. *EMBO J.* (1998) 17:5497–508. doi: 10.1093/emboj/17.18.5497
6. Bozzella M, Seluanov A, Gorbunova V. DNA repair by nonhomologous end joining and homologous recombination during cell cycle in human cells AU - Mao, Zhiyong. *Cell Cycle.* (2008) 7:2902–6. doi: 10.4161/cc.7.18.6679
7. Meek K, Dang V, Lees-Miller SP. DNA-PK: the means to justify the ends? *Adv Immunol.* (2008) 99:33–58. doi: 10.1016/S0065-2776(08)00602-0
8. Stiff T, Walker SA, Cerosaletti K, Goodarzi AA, Petermann E, Concannon P, et al. ATR-dependent phosphorylation and activation of ATM in response to UV treatment or replication fork stalling. *Embo J.* (2006) 25:5775–82. doi: 10.1038/sj.emboj.7601446
9. Bebenek K, Pedersen LC, Kunkel TA. Structure-function studies of DNA polymerase lambda. *Biochemistry.* (2014) 53:2781–92. doi: 10.1021/bi4017236
10. Moon AF, Pryor JM, Ramsden DA, Kunkel TA, Bebenek K, Pedersen LC. Sustained active site rigidity during synthesis by human DNA polymerase mu. *Nat Struct Mol Biol.* (2014) 21:253–60. doi: 10.1038/nsmb.2766
11. Pryor JM, Conlin MP, Carvajal-Garcia J, Luedeman ME, Luthman AJ, Small GW, et al. Ribonucleotide incorporation enables repair of chromosome breaks by nonhomologous end joining. *Science.* (2018) 361:1126–9. doi: 10.1126/science.aat2477
12. Ahnesorg P, Smith P, Jackson SP. XLF interacts with the XRCC4-DNA ligase IV complex to promote DNA nonhomologous end-joining. *Cell.* (2006) 124:301–13. doi: 10.1016/j.cell.2005.12.031
13. Betermier M, Bertrand P, Lopez BS. Is non-homologous end-joining really an inherently error-prone process? *PLoS Genet.* (2014) 10:e1004086. doi: 10.1371/journal.pgen.1004086
14. Sishc BJ, Davis AJ. The role of the core non-homologous end joining factors in carcinogenesis and cancer. *Cancers.* (2017) 9:E81. doi: 10.3390/cancers9070081
15. Powell SN, Kachnic LA. Roles of BRCA1 and BRCA2 in homologous recombination, DNA replication fidelity and the cellular response to ionizing radiation. *Oncogene.* (2003) 22:5784–91. doi: 10.1038/sj.onc.1206678
16. Li X, Heyer WD. Homologous recombination in DNA repair and DNA damage tolerance. *Cell Res.* (2008) 18:99–113. doi: 10.1038/cr.2008.1
17. Sartori AA, Lukas C, Coates J, Mistrik M, Fu S, Bartek J, et al. Human CtIP promotes DNA end resection. *Nature.* (2007) 450:509–14. doi: 10.1038/nature06337
18. Zhu Z, Chung WH, Shim EY, Lee SE, Ira G. Sgs1 helicase and two nucleases Dna2 and Exo1 resect DNA double-strand break ends. *Cell.* (2008) 134:981–94. doi: 10.1016/j.cell.2008.08.037
19. Nimonkar AV, Genschel J, Kinoshita E, Polaczek P, Campbell JL, Wyman C, et al. BLM-DNA2-RPA-MRN and EXO1-BLM-RPA-MRN constitute two DNA end resection machineries for human DNA break repair. *Genes Dev.* (2011) 25:350–62. doi: 10.1101/gad.2003811
20. Chen H, Lisby M, Symington LS. RPA coordinates DNA end resection and prevents formation of DNA hairpins. *Mol Cell.* (2013) 50:589–600. doi: 10.1016/j.molcel.2013.04.032
21. Langberg CW, Hauer-Jensen M, Sung C-C, Kane CJM. Expression of fibrogenic cytokines in rat small intestine after fractionated irradiation. *Radiother Oncol.* (1994) 32:29–36. doi: 10.1016/0167-8140(94)90446-4
22. Yang H, Jeffrey PD, Miller J, Kinnucan E, Sun Y, Thoma NH, et al. BRCA2 function in DNA binding and recombination from a BRCA2-DSS1-ssDNA structure. *Science.* (2002) 297:1837–48. doi: 10.1126/science.297.5588.1837
23. Lord CJ, Ashworth A. PARP inhibitors: synthetic lethality in the clinic. *Science.* (2017) 355:1152–8. doi: 10.1126/science.aam7344
24. Jasin M, Rothstein R. Repair of strand breaks by homologous recombination. *Cold Spring Harb Perspect Biol.* (2013) 5:a012740. doi: 10.1101/cshperspect.a012740
25. Frit P, Barboule N, Yuan Y, Gomez D, Calsou P. Alternative end-joining pathway(s): bricolage at DNA breaks. *DNA Repair.* (2014) 17:81–97. doi: 10.1016/j.dnarep.2014.02.007
26. Iliakis G, Murmann T, Soni A. Alternative end-joining repair pathways are the ultimate backup for abrogated classical non-homologous end-joining and homologous recombination repair: Implications for the formation of chromosome translocations. *Mutat Res Genet Toxicol Environ Mutagen.* (2015) 793:166–75. doi: 10.1016/j.mrgentox.2015.07.001
27. Robert I, Dantzer F, Reina-San-Martin B. Parp1 facilitates alternative NHEJ, whereas Parp2 suppresses IgH/c-myc translocations during immunoglobulin class switch recombination. *J Exp Med.* (2009) 206:1047–56. doi: 10.1084/jem.20082468
28. Mateos-Gomez PA, Gong F, Nair N, Miller KM, Lazzerini-Denchi E, Sfeir A. Mammalian polymerase theta promotes alternative NHEJ and suppresses recombination. *Nature.* (2015) 518:254–7. doi: 10.1038/nature14157
29. Li X, Lu Y, Liang K, Pan T, Mendelsohn J, Fan Z. Requirement of hypoxia-inducible factor-1alpha down-regulation in mediating the antitumor activity of the anti-epidermal growth factor receptor monoclonal antibody cetuximab. *Mol Cancer Ther.* (2008) 7:1207–17. doi: 10.1158/1535-7163.MCT-07-2187
30. Ferguson DO, Sekiguchi JM, Chang S, Frank KM, Gao Y, Depinho RA, et al. The nonhomologous end-joining pathway of DNA repair is required for genomic stability and the suppression of translocations. *Proc Natl Acad Sci USA.* (2000) 97:6630–3. doi: 10.1073/pnas.110152897
31. Simsek D, Jasin M. Alternative end-joining is suppressed by the canonical NHEJ component Xrcc4-ligase IV during chromosomal translocation formation. *Nat Struct Mol Biol.* (2010) 17:410–6. doi: 10.1038/nsmb.1773
32. Tsai W-B, Chung YM, Takahashi Y, Xu Z, Hu MCT. Functional interaction between FOXO3a and ATM regulates DNA damage response. *Nat Cell Biol.* (2008) 10:460–7. doi: 10.1038/ncb1709
33. Yu X, Chen J. DNA damage-induced cell cycle checkpoint control requires CtIP, a phosphorylation-dependent binding partner of BRCA1 C-terminal domains. *Mol Cell Biol.* (2004) 24:9478–86. doi: 10.1128/MCB.24.21.9478-9486.2004
34. Chen L, Nievera CJ, Lee AY, Wu X. Cell cycle-dependent complex formation of BRCA1.CtIP.MRN is important for DNA double-strand break repair. *J Biol Chem.* (2008) 283:7713–20. doi: 10.1074/jbc.M710245200
35. Isono M, Niimi A, Oike T, Hagiwara Y, Sato H, Sekine R, et al. BRCA1 directs the repair pathway to homologous recombination by promoting 53BP1 dephosphorylation. *Cell Rep.* (2017) 18:520–32. doi: 10.1016/j.celrep.2016.12.042
36. Noordermeer SM, Adam S, Setiaputra D, Barazas M, Pettitt SJ, Ling AK, et al. The shieldin complex mediates 53BP1-dependent DNA repair. *Nature.* (2018) 560:117–21. doi: 10.1038/s41586-018-0340-7
37. Gupta R, Somyajit K, Narita T, Maskey E, Stanlie A, Kremer M, et al. DNA Repair network analysis reveals shieldin as a key regulator of NHEJ and PARP inhibitor sensitivity. *Cell.* (2018) 173:972–988.e923. doi: 10.1016/j.cell.2018.03.050
38. Paddock MN, Bauman AT, Higdon R, Kolker E, Takeda S, Scharenberg AM. Competition between PARP-1 and Ku70 control the decision between high-fidelity and mutagenic DNA repair. *DNA Repair.* (2011) 10:338–43. doi: 10.1016/j.dnarep.2010.12.005
39. Ahrabi S, Sarkar S, Pfister SX, Pirovano G, Higgins GS, Porter AC, et al. A role for human homologous recombination factors in suppressing microhomology-mediated end joining. *Nucleic Acids Res.* (2016) 44:5743–57. doi: 10.1093/nar/gkw326
40. Dynan WS, Yoo S. Interaction of Ku protein and DNA-dependent protein kinase catalytic subunit with nucleic acids. *Nucleic Acids Res.* (1998) 26:1551–9. doi: 10.1093/nar/26.7.1551
41. Ceccaldi R, Liu JC, Amunugama R, Hajdu I, Primack B, Petalcorin MI, et al. Homologous-recombination-deficient tumours are dependent on Poltheta-mediated repair. *Nature.* (2015) 518:258–62. doi: 10.1038/nature14184
42. Arnoult N, Correia A, Ma J, Merlo A, Garcia-Gomez S, Maric M, et al. Regulation of DNA repair pathway choice in S and G2 phases by the NHEJ inhibitor CYREN. *Nature.* (2017) 549:548–52. doi: 10.1038/nature24023
43. Kakarougkas A, Jeggo PA. DNA DSB repair pathway choice: an orchestrated handover mechanism. *Br J Radiol.* (2014) 87:20130685. doi: 10.1259/bjr.20130685

44. Bryant HE, Schultz N, Thomas HD, Parker KM, Flower D, Lopez E, et al. Specific killing of BRCA2-deficient tumours with inhibitors of poly(ADP-ribose) polymerase. *Nature.* (2005) 434:913–7. doi: 10.1038/nature 03443
45. Farmer H, Mccabe N, Lord CJ, Tutt AN, Johnson DA, Richardson TB, et al. Targeting the DNA repair defect in BRCA mutant cells as a therapeutic strategy. *Nature.* (2005) 434:917–21. doi: 10.1038/nature03445
46. Liu Q, Gheorghiu L, Drumm M, Clayman R, Eidelman A, Wszolek MF, et al. PARP-1 inhibition with or without ionizing radiation confers reactive oxygen species-mediated cytotoxicity preferentially to cancer cells with mutant TP53. *Oncogene.* (2018) 37:2793–805. doi: 10.1038/s41388-018-0130-6
47. Marcar L, Bardhan K, Gheorghiu L, Dinkelborg P, Pfaffle H, Liu Q, et al. Acquired resistance of EGFR-mutated lung cancer to tyrosine kinase inhibitor treatment promotes PARP inhibitor sensitivity. *Cell Rep.* (2019) 27:3422–32.e3424. doi: 10.1016/j.celrep.2019.05.058
48. Saha T, Rih JK, Rosen EM. BRCA1 down-regulates cellular levels of reactive oxygen species. *FEBS Lett.* (2009) 583:1535–43. doi: 10.1016/j.febslet.2009.04.005
49. Lord CJ, Ashworth A. BRCAness revisited. *Nat Rev Cancer.* (2016) 16:110–20. doi: 10.1038/nrc.2015.21
50. Willers H, Gheorghiu L, Liu Q, Efstathiou JA, Wirth LJ, Krause M, et al. DNA damage response assessments in human tumor samples provide functional biomarkers of radiosensitivity. *Semin Radiat Oncol.* (2015) 25:237–50. doi: 10.1016/j.semradonc.2015.05.007
51. Ganguly B, Dolfi SC, Rodriguez-Rodriguez L, Ganesan S, Hirshfield KM. Role of biomarkers in the development of PARP inhibitors. *Biomark Cancer.* (2016) 8:15–25. doi: 10.4137/BIC.S36679
52. Liu Q, Ma L, Jones T, Palomero L, Pujana MA, Martinez-Ruiz H, et al. Subjugation of TGFb signaling by human papilloma virus in head and neck squamous cell carcinoma shifts DNA repair from homologous recombination to alternative end joining. *Clin Cancer Res.* (2018) 24:6001–14. doi: 10.1158/1078-0432.CCR-18-1346
53. Mengwasser KE, Adeyemi RO, Leng Y, Choi MY, Clairmont C, D'andrea AD, et al. Genetic screens reveal FEN1 and APEX2 as BRCA2 synthetic lethal targets. *Mol Cell.* (2019) 73:885–99.e6. doi: 10.1016/j.molcel.2018.12.008
54. Garcia-Closas M, Couch FJ, Lindstrom S, Michailidou K, Schmidt MK, Brook MN, et al. (2013). Genome-wide association studies identify four ER negative-specific breast cancer risk loci. *Nat Genet.* 45:392–8. doi: 10.1038/ng.2561
55. Wyatt DW, Feng W, Conlin MP, Yousefzadeh MJ, Roberts SA, Mieczkowski P, et al. Essential roles for polymerase theta-mediated end joining in the repair of chromosome breaks. *Mol Cell.* (2016) 63:662–73. doi: 10.1016/j.molcel.2016.06.020
56. Kawamura K, Bahar R, Seimiya M, Chiyo M, Wada A, Okada S, et al. DNA polymerase theta is preferentially expressed in lymphoid tissues and upregulated in human cancers. *Int J Cancer.* (2004) 109:9–16. doi: 10.1002/ijc.11666
57. Lemee F, Bergoglio V, Fernandez-Vidal A, Machado-Silva A, Pillaire MJ, Bieth A, et al. DNA polymerase theta up-regulation is associated with poor survival in breast cancer, perturbs DNA replication, and promotes genetic instability. *Proc Natl Acad Sci USA.* (2010) 107:13390–5. doi: 10.1073/pnas.0910759107
58. Higgins GS, Harris AL, Prevo R, Helleday T, Mckenna WG, Buffa FM. Overexpression of POLQ confers a poor prognosis in early breast cancer patients. *Oncotarget.* (2010) 1:175–84. doi: 10.18632/oncotarget.124
59. Allera-Moreau C, Rouquette I, Lepage B, Oumouhou N, Walschaerts M, Leconte E, et al. DNA replication stress response involving PLK1, CDC6, POLQ, RAD51 and CLASPIN upregulation prognoses the outcome of early/mid-stage non-small cell lung cancer patients. *Oncogenesis.* (2012) 1:e30. doi: 10.1038/oncsis.2012.29
60. Chan N, Koch CJ, Bristow RG. Tumor hypoxia as a modifier of DNA strand break and cross-link repair. *Curr Mol Med.* (2009) 9:401–10. doi: 10.2174/156652409788167050
61. Sun Y, Campisi J, Higano C, Beer TM, Porter P, Coleman I, et al. Treatment-induced damage to the tumor microenvironment promotes prostate cancer therapy resistance through WNT16B. *Nat Med.* (2012) 18:1359–68. doi: 10.1038/nm.2890
62. Hanahan D, Coussens LM. Accessories to the crime: functions of cells recruited to the tumor microenvironment. *Cancer Cell.* (2012) 21:309–22. doi: 10.1016/j.ccr.2012.02.022
63. Kumareswaran R, Ludkovski O, Meng A, Sykes J, Pintilie M, Bristow RG. Chronic hypoxia compromises repair of DNA double-strand breaks to drive genetic instability. *J Cell Sci.* (2012) 125:189–99. doi: 10.1242/jcs.092262
64. Kidane D, Chae WJ, Czochor J, Eckert KA, Glazer PM, Bothwell AL, et al. Interplay between DNA repair and inflammation, and the link to cancer. *Crit Rev Biochem Mol Biol.* (2014) 49:116–39. doi: 10.3109/10409238.2013.875514
65. Geiger-Maor A, Guedj A, Even-Ram S, Smith Y, Galun E, Rachmilewitz J. Macrophages regulate the systemic response to DNA damage by a cell nonautonomous mechanism. *Cancer Res.* (2015) 75:2663–73. doi: 10.1158/0008-5472.CAN-14-3635
66. Scanlon SE, Glazer PM. Multifaceted control of DNA repair pathways by the hypoxic tumor microenvironment. *DNA Repair.* (2015) 32:180–9. doi: 10.1016/j.dnarep.2015.04.030
67. Centurione L, Aiello FB. DNA repair and cytokines: TGF-beta, IL-6, and thrombopoietin as different biomarkers of radioresistance. *Front Oncol.* (2016) 6:175. doi: 10.3389/fonc.2016.00175
68. Dickreuter E, Eke I, Krause M, Borgmann K, Van Vugt MA, Cordes N. Targeting of beta1 integrins impairs DNA repair for radiosensitization of head and neck cancer cells. *Oncogene.* (2016) 35:1353–62. doi: 10.1038/onc.2015.212
69. Derynck R, Akhurst RJ, Balmain A. TGF-b signaling in tumor suppression and cancer progression. *Nature Genet.* (2001) 29:117–29. doi: 10.1038/ng1001-117
70. Costanza B, Umelo IA, Bellier J, Castronovo V, Turtoi A. Stromal modulators of TGFβ in cancer. *J Clin Med.* (2017) 6:7. doi: 10.3390/jcm6010007
71. Akhurst RJ. TGFβ antagonists: why suppress a tumor suppressor? *J Clin Invest.* (2002) 109:1533–6. doi: 10.1172/JCI0215970
72. Akhurst RJ, Hata A. Targeting the TGFbeta signalling pathway in disease. *Nat Rev Drug Discov.* (2012) 11:790–11. doi: 10.1038/nrd3810
73. Neuzillet C, Tijeras-Raballand A, Cohen R, Cros J, Faivre S, Raymond E, et al. Targeting the TGFbeta pathway for cancer therapy. *Pharmacol Ther.* (2015) 147:22–31. doi: 10.1016/j.pharmthera.2014.11.001
74. Barcellos-Hoff MH. Latency and activation in the regulation of TGFβ. *J Mammary Gland Biol Neoplasia.* (1996) 3:353–63. doi: 10.1007/BF02017391
75. Jobling MF, Mott JD, Finnegan MT, Jurukovski V, Erickson AC, Walian PJ, et al. Isoform-specific activation of latent transforming growth factor beta (LTGFβ) by reactive oxygen species. *Radiat Res.* (2006) 166:839–48. doi: 10.1667/RR0695.1
76. Ghiringhelli F, Menard C, Terme M, Flament C, Taieb J, Chaput N, et al. $CD4^+CD25^+$ regulatory T cells inhibit natural killer cell functions in a transforming growth factor-beta-dependent manner. *J Exp Med.* (2005) 202:1075–85. doi: 10.1084/jem.20051511
77. Da Cunha AP, Wu HY, Rezende RM, Vandeventer T, Weiner HL. *In vivo* anti-LAP mAb enhances IL-17/IFN-γ responses and abrogates anti-CD3-induced oral tolerance. *Int Immunol.* (2015) 27:73–82. doi: 10.1093/intimm/dxu083
78. Gonzalez-Junca A, Driscoll KE, Pellicciotta I, Du S, Lo CH, Roy R, et al. Autocrine TGFβ is a survival factor for monocytes and drives immunosuppressive lineage commitment. *Cancer Immunol Res.* (2019) 7:306–20. doi: 10.1158/2326-6066.CIR-18-0310
79. Li Z, Zhang LJ, Zhang HR, Tian GF, Tian J, Mao XL, et al. Tumor-derived transforming growth factor-β is critical for tumor progression and evasion from immune surveillance. *Asian Pac J Cancer Prev.* (2014) 15:5181–6. doi: 10.7314/apjcp.2014.15.13.5181
80. Yang L, Moses HL. Transforming growth factor-β: tumor suppressor or promoter? are host immune cells the answer? *Cancer Res.* (2008) 68:9107–11. doi: 10.1158/0008-5472.CAN-08-2556
81. Wrzesinski SH, Wan YY, Flavell RA. Transforming growth factor-beta and the immune response: implications for anticancer therapy. *Clin Cancer Res.* (2007) 13:5262–70. doi: 10.1158/1078-0432.CCR-07-1157
82. Glick AB, Weinberg WC, Wu IH, Quan W, Yuspa SH. Transforming growth factor beta 1 suppresses genomic instability independent of a G1 arrest, p53, and Rb. *Cancer Res.* (1996) 56:3645–50.
83. Maxwell CA, Fleisch MC, Costes SV, Erickson AC, Boissiere A, Gupta R, et al. Targeted and nontargeted effects of ionizing radiation that impact genomic instability. *Cancer Res.* (2008) 68:8304–11. doi: 10.1158/0008-5472.CAN-08-1212

84. Yamada H, Vijayachandra K, Penner C, Glick A. Increased sensitivity of transforming growth factor (TGF) β1 null cells to alkylating agents reveals a novel link between TGFbeta signaling and O(6)-methylguanine methyltransferase promoter hypermethylation. *J Biol Chem.* (2001) 276:19052–8. doi: 10.1074/jbc.M100615200
85. Kirshner J, Jobling MF, Pajares MJ, Ravani SA, Glick AB, Lavin MJ, et al. Inhibition of transforming growth factor-beta1 signaling attenuates ataxia telangiectasia mutated activity in response to genotoxic stress. *Cancer Res.* (2006) 66:10861–9. doi: 10.1158/0008-5472.CAN-06-2565
86. Wiegman EM, Blaese MA, Loeffler H, Coppes RP, Rodemann HP. TGFbeta-1 dependent fast stimulation of ATM and p53 phosphorylation following exposure to ionizing radiation does not involve TGFβ-receptor I signalling. *Radiother Oncol.* (2007) 83:289–95. doi: 10.1016/j.radonc.2007.05.013
87. Kim MR, Lee J, An YS, Jin YB, Park IC, Chung E, et al. TGFβ1 protects cells from γ-IR by enhancing the activity of the NHEJ repair pathway. *Mol Cancer Res.* (2015) 13:319–29. doi: 10.1158/1541-7786.MCR-14-0098-T
88. Qiang L, Shah P, Barcellos-Hoff MH, He YY. TGF-β signaling links E-cadherin loss to suppression of nucleotide excision repair. *Oncogene.* (2016) 35:3293–302. doi: 10.1038/onc.2015.390
89. Andarawewa KL, Erickson AC, Chou WS, Costes SV, Gascard P, Mott JD, et al. Ionizing radiation predisposes nonmalignant human mammary epithelial cells to undergo transforming growth factor b induced epithelial to mesenchymal transition. *Cancer Res.* (2007) 67:8662–70. doi: 10.1158/0008-5472.CAN-07-1294
90. Zheng H, Jarvis IWH, Bottai M, Dreij K, Stenius U. TGF beta promotes repair of bulky DNA damage through increased ERCC1/XPF and ERCC1/XPA interaction. *Carcinogenesis.* (2019) 40:580–91. doi: 10.1093/carcin/bgy156
91. Wang M, Saha J, Hada M, Anderson JA, Pluth JM, O'neill P, et al. Novel smad proteins localize to IR-induced double-strand breaks: interplay between TGFβ and ATM pathways. *Nucleic Acids Res.* (2013) 41:933–42. doi: 10.1093/nar/gks1038
92. Bornstein S, White R, Malkoski S, Oka M, Han G, Cleaver T, et al. Smad4 loss in mice causes spontaneous head and neck cancer with increased genomic instability and inflammation. *J Clin Invest.* (2009) 119:3408–19. doi: 10.1172/JCI38854
93. Moskwa P, Buffa FM, Pan Y, Panchakshari R, Gottipati P, Muschel RJ, et al. miR-182-mediated downregulation of BRCA1 impacts DNA repair and sensitivity to PARP inhibitors. *Mol Cell.* (2011) 41:210–20. doi: 10.1016/j.molcel.2010.12.005
94. Martinez-Ruiz H, Illa-Bochaca I, Omene C, Hanniford D, Liu Q, Hernando E, et al. A TGFbeta-miR-182-BRCA1 axis controls the mammary differentiation hierarchy. *Sci Signal.* (2016) 9:ra118. doi: 10.1126/scisignal.aaf5402
95. Brown JA, Yonekubo Y, Hanson N, Sastre-Perona A, Basin A, Rytlewski JA, et al. TGF-β-induced quiescence mediates chemoresistance of tumor-propagating cells in squamous cell carcinoma. *Cell Stem Cell.* (2017) 21:650–64.e658. doi: 10.1016/j.stem.2017.10.001
96. Bouquet F, Pal A, Pilones KA, Demaria S, Hann B, Akhurst RJ, et al. TGFb1 inhibition increases the radiosensitivity of breast cancer cells *in vitro* and promotes tumor control by radiation *in vivo*. *Clin Cancer Res.* (2011) 17:6754–65. doi: 10.1158/1078-0432.CCR-11-0544
97. Hardee ME, Marciscano AE, Medina-Ramirez CM, Zagzag D, Narayana A, Lonning SM, et al. Resistance of glioblastoma-initiating cells to radiation mediated by the tumor microenvironment can be abolished by inhibiting transforming growth factor-beta. *Cancer Res.* (2012) 72:4119–29. doi: 10.1158/0008-5472.CAN-12-0546
98. Du S, Bouquet F, Lo C-H, Pellicciotta I, Bolourchi S, Parry R, et al. Attenuation of the DNA damage response by TGFβ inhibitors enhances radiation sensitivity of NSCLC cells *in vitro* and *in vivo*. *Int J Radiat Oncol Biol Phys.* (2014) 91:91–9. doi: 10.1016/j.ijrobp.2014.09.026
99. Weaver AN, Cooper TS, Rodriguez M, Trummell HQ, Bonner JA, Rosenthal EL, et al. DNA double strand break repair defect and sensitivity to poly ADP-ribose polymerase (PARP) inhibition in human papillomavirus 16-positive head and neck squamous cell carcinoma. *Oncotarget.* (2015) 6:26995–7007. doi: 10.18632/oncotarget.4863
100. Mirghani H, Amen F, Tao Y, Deutsch E, Levy A. Increased radiosensitivity of HPV-positive head and neck cancers: molecular basis and therapeutic perspectives. *Cancer Treat Rev.* (2015) 41:844–52. doi: 10.1016/j.ctrv.2015.10.001
101. Ziemann F, Arenz A, Preising S, Wittekindt C, Klussmann JP, Engenhart-Cabillic R, et al. Increased sensitivity of HPV-positive head and neck cancer cell lines to x-irradiation ± Cisplatin due to decreased expression of E6 and E7 oncoproteins and enhanced apoptosis. *Am J Cancer Res.* (2015) 5:1017–31.
102. Xu Q, Wang S, Xi L, Wu S, Chen G, Zhao Y, et al. Effects of human papillomavirus type 16 E7 protein on the growth of cervical carcinoma cells and immuno-escape through the TGF-beta1 signaling pathway. *Gynecol Oncol.* (2006) 101:132–9. doi: 10.1016/j.ygyno.2005.09.051
103. Perez-Plasencia C, Vazquez-Ortiz G, Lopez-Romero R, Pina-Sanchez P, Moreno J, Salcedo M. Genome wide expression analysis in HPV16 cervical cancer: identification of altered metabolic pathways. *Infect Agent Cancer.* (2007) 2:16. doi: 10.1186/1750-9378-2-16
104. Li ML, Greenberg RA. Links between genome integrity and BRCA1 tumor suppression. *Trends Biochem Sci.* (2012) 37:418–24. doi: 10.1016/j.tibs.2012.06.007
105. Deng Y, Deng H, Liu J, Han G, Malkoski S, Liu B, et al. Transcriptional down-regulation of Brca1 and E-cadherin by CtBP1 in breast cancer. *Mol Carcinog.* (2012) 51:500–7. doi: 10.1002/mc.20813
106. Bennardo N, Cheng A, Huang N, Stark JM. Alternative-NHEJ is a mechanistically distinct pathway of mammalian chromosome break repair. *PLoS Genet.* (2008) 4:e1000110. doi: 10.1371/journal.pgen.1000110
107. Bjorkman A, Qvist P, Du L, Bartish M, Zaravinos A, Georgiou K, et al. Aberrant recombination and repair during immunoglobulin class switching in BRCA1-deficient human B cells. *Proc Natl Acad Sci USA.* (2015) 112:2157–62. doi: 10.1073/pnas.1418947112
108. Korkut A, Zaidi S, Kanchi RS, Rao S, Gough NR, Schultz A, et al. A pan-cancer analysis reveals high-frequency genetic alterations in mediators of signaling by the TGF-β superfamily. *Cell Syst.* (2018) 7:422–37.e7. doi: 10.1016/j.cels.2018.08.010
109. Kanamoto T, Hellman U, Heldin CH, Souchelnytskyi S. Functional proteomics of transforming growth factor-β1-stimulated Mv1Lu epithelial cells: Rad51 as a target of TGFβ1-dependent regulation of DNA repair. *EMBO J.* (2002) 21:1219–30. doi: 10.1093/emboj/21.5.1219
110. Liu L, Zhou W, Cheng CT, Ren X, Somlo G, Fong MY, et al. TGFβ induces "BRCAness" and sensitivity to PARP inhibition in breast cancer by regulating DNA-repair genes. *Mol Cancer Res.* (2014) 12:1597–609. doi: 10.1158/1541-7786.MCR-14-0201
111. Zhang H, Kozono DE, O'connor KW, Vidal-Cardenas S, Rousseau A, Hamilton A, et al. TGF-β inhibition rescues hematopoietic stem cell defects and bone marrow failure in fanconi anemia. *Cell Stem Cell.* (2016) 18:668–81. doi: 10.1016/j.stem.2016.03.002
112. Pal D, Pertot A, Shirole NH, Yao Z, Anaparthy N, Garvin T, et al. TGF-beta reduces DNA ds-break repair mechanisms to heighten genetic diversity and adaptability of $CD44^{+}/CD24^{-}$ cancer cells. *Elife.* (2017) 6:21615. doi: 10.7554/eLife.21615

Conflict of Interest Statement: The authors declare that the research was conducted in the absence of any commercial or financial relationships that could be construed as a potential conflict of interest.

frontiers in Oncology

ORIGINAL RESEARCH
published: 14 November 2019
doi: 10.3389/fonc.2019.01244

FAM53A Affects Breast Cancer Cell Proliferation, Migration, and Invasion in a p53-Dependent Manner

*Jie Zhang, Mingfang Sun, Miaomiao Hao, Kexin Diao, Jian Wang, Shiping Li, Qixue Cao and Xiaoyi Mi**

Department of Pathology, College of Basic Medical Sciences, First Affiliated Hospital, China Medical University, Shenyang, China

Family with sequence similarity 53-member A (FAM53A) is an uncharacterized protein with a suspected but unclear role in tumorigenesis. In this study, we examined its role in breast cancer. Immunohistochemical staining of specimens from 199 cases of breast cancer demonstrated that FAM53A levels were negatively correlated with p53 status. In the p53 wild-type breast cancer cell line MCF-7, FAM53A overexpression inhibited cell migration, invasion, and proliferation, downregulated the expression of Snail, cyclin D1, RhoA, RhoC, and MMP9, and decreased mitogen-activated protein kinase kinase (MEK) and extracellular-signal regulated kinase (ERK) phosphorylation. Concurrently, it upregulated E-cadherin and p21 expression levels. Interestingly, opposite trends were observed in the p53-null breast cancer cell line MDA-MB-231. The MEK inhibitor PD98059 reduced the biological effects of FAM53A knockdown in MCF-7 cells and FAM53A overexpression in MDA-MB-231 cells, suggesting that FAM53A affects breast cancer through the MEK-ERK pathway. Silencing *TP53* in MCF-7 cells and stably expressing wild-type p53 in MDA-MB-231 cells confirmed that the effects of FAM53A signaling through the MEK/ERK pathway depended on the p53 status of the cells. These results suggest that FAM53A acts as a tumor suppressor in p53-positive breast cancer by modulating the MEK-ERK pathway, but may be a potential candidate for targeted anticancer therapies in p53-negative breast cancer.

Keywords: breast cancer, cell migration, epithelial-mesenchymal transition (EMT), invasion, metastasis, p53, extracellular-signal-regulated kinase (ERK)

OPEN ACCESS

Edited by:
Mary Helen Barcellos-Hoff, University of California, San Francisco, United States

Reviewed by:
Hanumantha Rao Madala, Harvard Medical School, United States
Ali Vaziri-Gohar, Case Western Reserve University, United States

****Correspondence:***
Xiaoyi Mi
xymi@cmu.edu.cn

Specialty section:
This article was submitted to Molecular and Cellular Oncology, a section of the journal Frontiers in Oncology

Received: *10 August 2019*
Accepted: *29 October 2019*
Published: *14 November 2019*

Citation:
Zhang J, Sun M, Hao M, Diao K, Wang J, Li S, Cao Q and Mi X (2019) FAM53A Affects Breast Cancer Cell Proliferation, Migration, and Invasion in a p53-Dependent Manner. Front. Oncol. 9:1244. doi: 10.3389/fonc.2019.01244

INTRODUCTION

The mitogen-activated protein kinase kinase (MEK)-extracellular-signal regulated kinase (ERK) pathway is an evolutionarily conserved signal transduction pathway of crucial importance in tumorigenesis. It is often aberrantly activated in malignant tumors, resulting in signal amplification during tumor invasion and metastasis (1, 2). Abnormal activation leads to loss of differentiation and apoptosis and increased proliferation and invasion, causing tumorigenesis and eventual metastasis (3–6). The MEK-ERK pathway is activated at the cell membrane by Ras, which activates Raf, starting a phosphorylation cascade that results in the sequential activation of MEK1/2 and ERK1/2 (7–12). ERK expression is significantly higher in breast cancer tissue than in benign hyperplastic breast tissue, and ERK phosphorylation is increased in severe atypical hyperplasia and breast cancer tissues compared with that in benign proliferating breast tissue, suggesting that abnormally

increased ERK activation plays an important role in the development of atypical hyperplasia into cancer, and can stimulate the proliferation of breast cancer cells (13). Phosphorylated ERK (p-ERK) enters the nucleus to phosphorylate specific transcription factors such as c-Myc and c-Jun (14). Decreased p-ERK reduces the expression of matrix metalloprotease (MMP)1 and MMP9, significantly inhibiting breast cancer invasiveness (14, 15). In breast cancer cells, ERK inactivation is accompanied by the inactivation of cyclin D1 and BCL2, leading to apoptosis (15).

Family sequence similarity (FAM) genes are families of uncharacterized genes of similar protein sequence. Several of these families have been linked to the development of tumors, including breast cancer, non-small cell lung cancer, lung adenocarcinoma, renal cell carcinoma, prostate cancer, colorectal cancer, and esophageal squamous cell carcinoma, where they are thought to play important roles in proliferation, apoptosis, migration, and invasion (16–23). FAM53 is a vertebrate-specific family of proteins that bind to transcriptional regulators of proliferation and neural tube development, encoded by three homologous genes: *FAM53A*, *FAM53B*, and *FAM53C* (24–27). FAM53A, also known as dorsal neural tube nuclear protein, is thought to play an important role in neurodevelopment by specifying the fate of dorsal cells within the neural tube (28, 29). Expression quantitative trait loci variants of *FAM53A* identified in *TP53*-based interaction analysis are associated with the use of therapeutic doxorubicin in breast cancer (27). In the triple-negative *TP53*-missense mutant breast cancer cell line MDA-MB-231, downregulation of FAM53A increased doxorubicin resistance. However, in the luminal B p53-truncated mutant line MDA-MB-361 and the luminal A p53-wild-type line MCF7, downregulation of FAM53A resulted in increased sensitivity to doxorubicin (27). The role of FAM53A in breast cancer is unclear, and its relevance to the clinical pathology of breast cancer has not been reported. In this study, we examined the expression and localization of FAM53A in breast cancer tissues and cell lines. We then altered FAM53A expression in two breast cancer cell lines to explore its effects on the cells and gain mechanistic insight into how FAM53A affects cancer.

EXPERIMENTAL PROCEDURES

Patients and Specimens

Primary tumor specimens were obtained from 199 patients diagnosed with invasive ductal carcinoma who underwent complete resection in the First Affiliated Hospital of China Medical University between 2011 and 2013. Patients whose tissue samples were used in this research provided written informed consent. This study was approved by the local institutional review board of China Medical University.

Cell Culture and Treatment

MCF-10A, MCF-7, T47D, MDA-MB-231, BT-474, and BT-549 cell lines were obtained from the Shanghai Cell Bank of the Chinese Academy of Sciences (Shanghai, China) and identified by short tandem repeat (STR) DNA analysis. The cells were cultured and frozen, and experiments were performed after 10 passages. MCF-10A cells were cultured in 1:1 Dulbecco's modified Eagle's medium (DMEM)/F12 (Gibco, Waltham, MA, USA) supplemented with 5% horse serum, 10 μg/mL insulin (Sigma-Aldrich Co, St. Louis, MO, USA), and 20 ng/mL epidermal growth factor (EGF). MDA-MB-231 cells were cultured in L15 (Gibco) supplemented with 10% fetal bovine serum (FBS). MCF7 and T47D cell lines were cultured in DMEM (Gibco) supplemented with 10% FBS. BT-474 and BT549 cells were cultured in Roswell Park Memorial Institute (RPMI)-1640 (Gibco) supplemented with 10% FBS. Cells were cultured in sterile culture flasks in a 5% CO_2 incubator at 37°C and subcultured every 2 days by trypsinization.

Immunohistochemistry

Surgically removed tumor specimens were fixed in 10% neutral formalin, embedded in paraffin, and continuously cut into 4-μm thick sections. The tissue slices were baked in an oven at 70°C for 2 h; then the sections were dewaxed in xylene, absolute ethanol, gradient alcohol, and distilled water, and boiled in 0.01 M citrate buffer (pH 6.0) at high temperature and high pressure for 2 min. Endogenous peroxidase activity was blocked with 0.3% hydrogen peroxide and sections were incubated with 5% normal goat serum for 30 min at 20°C to reduce non-specific binding. Tissue sections were then incubated with FAM53A antibody (1:100 dilution; see **Table S1** for information on antibodies used in the study) overnight at 4°C. The reaction was observed using an Elivision super HRP (mouse/rabbit) immunohistochemistry kit (Maixin-Bio, Shenzhen, China) and 3,3′-diaminobenzidine (DAB). The nuclei were counterstained with hematoxylin.

FAM53A expression levels were evaluated based on the percentage of positive cells (PP) and the staining intensity (SI) within the whole tissue section. FAM53A staining intensity was evaluated semi-quantitatively using the immune response score (IRS) and calculated as follows: IRS = PP × SI; where PP: 0, no dye; 1, 1–25%; 2, 26–50%; 3, 51–75%; and 4, 76–100%; and SI: 0, no staining; 1, weak staining; 2, medium staining; and 3, strong staining. The scores for each tumor sample were multiplied to give a final score of 0–9; tumor samples with scores >3 were classified as having high FAM53A expression, while samples with scores ≤ 3 were classified as having low FAM53A expression.

Plasmid Transfection, siRNA Interference, and Inhibitor Treatments

Transfection was performed using Xfect Transfection Reagent (Takara Bio USA, Mountain View, CA, USA) according to the manufacturer's instructions. The plasmids pCMV6-ddk-myc and pCMV6-ddk-myc-FAM53A were purchased from Origene (Rockville, MD, USA). One day before transfection, cells were plated in 2 mL of complete growth medium, aiming for 50–70% confluency at the time of transfection. Plasmid DNA (5 μg) was added to Xfect Reaction Buffer to a final volume of 100, and 1.5 μL Xfect Polymer was added. After a 10 min incubation at room temperature (15–25°C), the solution was added dropwise to the cell culture medium. Cells were incubated at 37°C for 4 h, then the medium was replaced with 2 mL of fresh complete growth medium and the cells were incubated at 37°C for 48 h. FAM53A (sc-88998) and non-targeted control (NC; sc-37007) siRNAs were

purchased from Santa Cruz Biotechnology (Dallas, TX, USA), and transfected into cells using HiPerFect Transfection Reagent (Qiagen, Hilden, Germany) according to the manufacturers' protocols. Cells were plated in 2 mL of complete growth medium, aiming for 30–50% confluence at the time of siRNA transfection. The next day, 37.5 ng of siRNA was added to 100 μL of serum-free culture medium, 3 μL of HiPerFect Transfection Reagent was added, and the solution was mixed by vortexing and incubated for 5–10 min at room temperature to allow the formation of transfection complexes. The complexes were then added to the cells, which were incubated for 48 h prior to analysis.

PD98059, a MEK inhibitor, was purchased from Selleck Chemicals (Houston, TX, USA). A stock solution was generated by dissolving PD98059 in dimethyl sulfoxide (DMSO). This solution was added to MCF-7 and MDA-MB-231 cells at final concentrations of 10 μM for 1 h and 25 μM for 2 h, respectively, prior to analysis.

Immunofluorescence

Breast cancer cells cultured in 24-well plates for 24 h were fixed in 2% paraformaldehyde for 15 min, blocked in 5% BSA for 2 h, and incubated with anti-FAM53A antibody (1:100) at 4°C overnight. Cells were then incubated with a tetramethylrhodamine-labeled secondary antibody at room temperature for 2 h in the dark; the nuclei were counterstained with 4′,6-diamidino-2-phenylindole. Images were captured using an Olympus FV1000 laser scanning confocal microscope (Olympus, Tokyo, Japan).

Western Blot Analysis

Cells and tumor tissues were lysed in lysis buffer (Thermo Fisher Scientific), and total protein was quantified using the Bradford method. Proteins (80 μg/lane) were separated by 10% SDS-PAGE and then transferred to polyvinylidene difluoride membranes (Millipore, Billerica, MA, USA). Membranes were incubated overnight at 4°C with the appropriate primary antibody (**Table S1**) and for 2 h at room temperature with horseradish peroxidase-labeled secondary antibody, then visualized with ECL (Thermo Fisher Scientific, Waltham, MA, USA) on a BioImaging System (UVP Inc., Upland, CA, USA). Protein levels were analyzed using the ImageJ software (National Institutes of Health, Bethesda, MD, USA), with glyceraldehyde 3-phosphate dehydrogenase (GAPDH) as a loading control.

Cell Proliferation and Colony Formation Assays

Cell viability was measured by the mitochondrial reduction of 3-[4,5-dimethylthiazole-2-yl]-2,5-diphenyltetrazolium bromide (MTT). Cells (3,000/well) were seeded in 96-well plates in medium containing 10% FBS and have used a separate blank (100 ml of fresh medium). MTT solution (10 μL/well) was added and samples were incubated for 4 h. Then, the medium was aspirated from each well, and the obtained MTT formazan was dissolved in 150 μL DMSO. Finally, the absorbance was measured at 490 nm using a microplate reader daily, and the OD value of the blank was subtracted from the absorbance at a given time. We calculated the relative ratio and plotted the cell curve.

For colony formation experiments, cells (1,000/dish) were seeded in 40-mm dishes and incubated for 10–15 days in medium containing 10% fetal calf serum, which was changed every 3 days. After incubation, the cells were washed with PBS and stained with hematoxylin, and the number of colonies with >50 cells were counted. At least three independent experimental replicates were performed.

Cell Migration and Invasion Assays

Cell migration and invasion experiments were performed using 24-well Transwell chambers (Costar, Cambridge, MA, USA) with a pore size of 8 μm. For the invasion assay, the upper chamber of the Transwell chamber was coated with 100 μL Matrigel (1:9 dilution; BD Biosciences); for cell migration assays, no Matrigel was added. Approximately 24 h after transfection, the cells were trypsinized, and 1×10^5 cells in 100 μL of medium supplemented with 2% FBS were transferred to the upper chamber. Medium supplemented with 10% FBS was added to the lower chamber as a chemoattractant. After 18 h of incubation, the chamber was removed and stained with hematoxylin, and cells that migrated through the chamber membrane were counted using an Olympus FV1000 laser-scanning confocal microscope (Olympus, Tokyo, Japan). At least three independent experimental replicates were performed.

Statistical Analysis

Correlations between FAM53A expression and clinicopathological features of breast cancer were analyzed using the chi-squared test. For experiments involving cells, differences between the control and experimental groups were compared by paired *t*-test. $P < 0.05$ was considered statistically significant.

RESULTS

FAM53A Expression in Breast Cancer Cells Is Associated With p53

We examined the localization of FAM53A in the breast cancer cell lines MCF-7, T47D, MDA-MB-231, and BT-549 and the non-malignant human mammary epithelial cell line MCF-10A by immunofluorescence and observed its presence in the cytoplasm and nucleus (**Figure 1A**). FAM53A was expressed at significantly lower levels in the p53-wild-type breast cancer cell line MCF-7 compared with the normal human mammary epithelial cell line MCF-10A, whereas in the p53-mutant breast cancer cell lines T47D, MDA-MB-231, BT-549, and BT-474, FAM53A was highly expressed, particularly in MDA-MB-231 cells (**Figure 1B**). We therefore selected MCF-7 and MDA-MB-231 cells for subsequent experiments. To investigate the association between FAM53A expression and clinicopathological features of breast cancer, we selected 199 breast cancer tissues for immunohistochemical staining. As shown in **Table 1**, FAM53A levels were negatively correlated with wild-type p53 ($P < 0.001$; **Figures 1C,D**), but had no significant correlation with age ($P = 0.781$); tumor size ($P = 0.110$); TNM stage ($P = 0.056$); lymph node metastasis ($P = 0.996$); or estrogen receptor, progesterone receptor, or human epidermal growth factor receptor 2 (HER-2) status ($P = 0.069$). Therefore, we next examined the effects of modulating FAM53A levels in the presence and absence of functional p53.

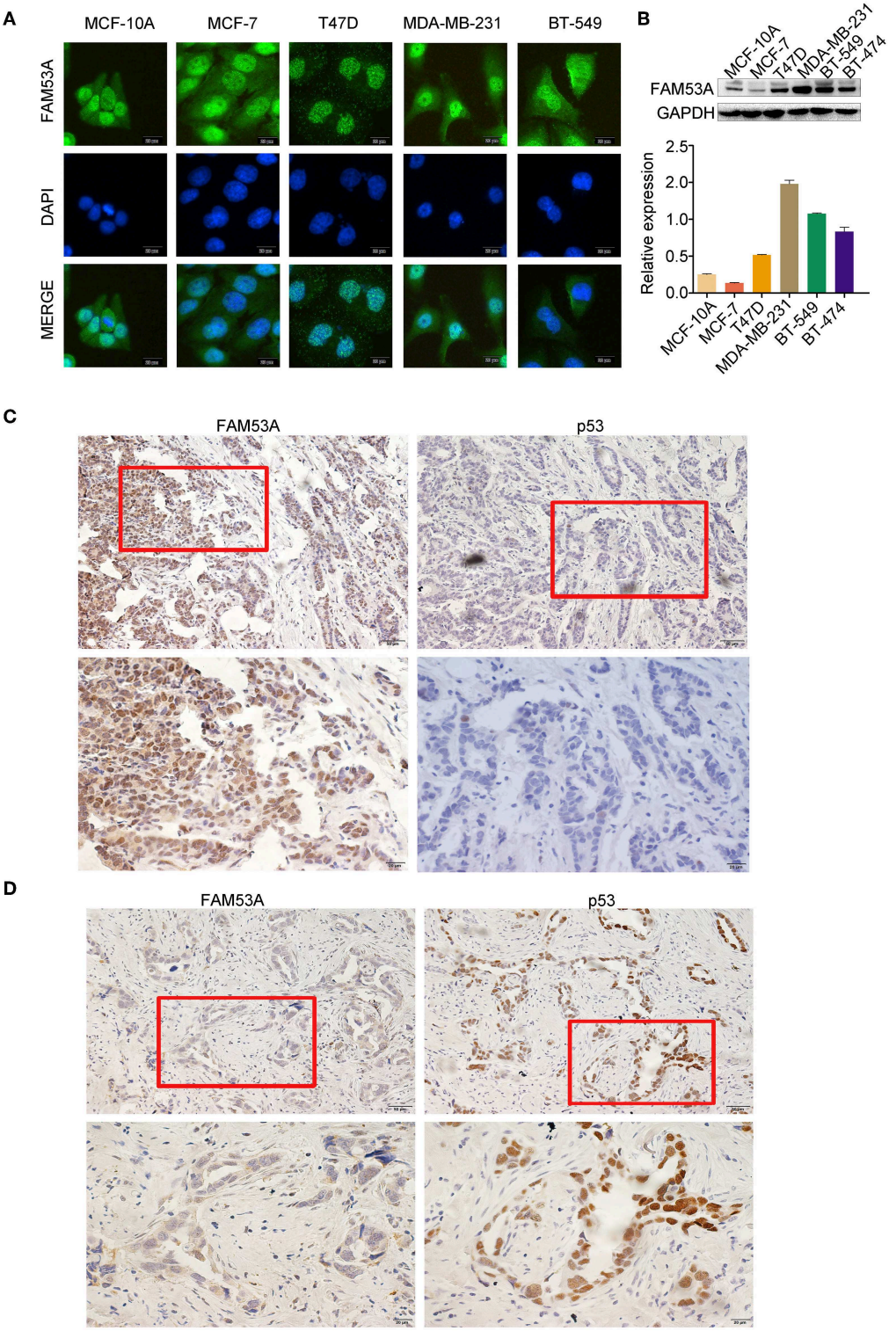

FIGURE 1 | FAM53A expression in breast cancer cell lines and tissues. **(A)** FAM53A expression in breast cancer cell lines was analyzed by immunofluorescence. **(B)** FAM53A protein levels in five breast cancer cell lines and a normal human mammary epithelial cell line (MCF-10A) were assessed by western blotting. **(C,D)** The relationship between FAM53A expression and p53 levels in breast cancer tissues was analyzed by immunohistochemistry.

TABLE 1 | Correlation between FAM53A expression and clinicopathological characteristics of invasive breast cancer.

Clinicopathological feature	*N*	FAM53A		*P*-value
		Positive	Negative	
All cases	199	70	129	
Age (years)				
≤50	105	36	69	0.781
>50	94	34	60	
Tumor size				
≤5.0 cm	92	27	65	0.110
>5.0 cm	107	43	64	
TNM stage				
I/II	109	32	77	0.056
III	90	38	52	
Lymph node metastasis				
Negative	119	42	77	0.996
Positive	80	28	52	
p53 status				
Negative	115	53	62	<0.001
Positive	84	17	67	
ER, PR, and HER-2 Status				
Non-TNBC	176	58	118	0.069
TNBC	23	12	11	

TNBC, triple-negative breast cancer; ER, estrogen receptor; PR, progesterone receptor.

FAM53A Inhibits Proliferation, Migration, and Invasion in the p53-Wild-Type Breast Cancer Cell Line MCF-7

To examine the effects of FAM53A expression on tumorigenesis-related processes in a wild-type p53 cell line, FAM53A was both overexpressed and depleted in MCF-7 cells (**Figure 2A**). When FAM53A was overexpressed, colony formation ability and proliferation were significantly decreased; accordingly, FAM53A depletion resulted in increased colony formation ability and proliferation (**Figures 2B,C**). We also performed western blot analysis to measure the levels of several proteins related to proliferation. When FAM53A was overexpressed, cyclin D1, cyclin-dependent kinase 4 (CDK4), and c-Myc expression was downregulated, while p21 expression was increased; FAM53A depletion resulted in the opposite effects on these proteins (**Figure 2D**). FAM53A overexpression inhibited the migration and invasion of MCF-7 cells, while FAM53A depletion promoted these processes (**Figure 2E**). Changes in FAM53A protein levels also affected the expression of proteins involved in cell migration and invasion, with decreased RhoA, RhoC, Rho kinase 1 (ROCK1), and MMP9 expression and increased RhoB expression after FAM53A overexpression. Expression of RhoA, RhoC, ROCK1, and MMP9 correspondingly increased after FAM53A depletion, along with decreased RhoB expression (**Figure 2F**). These results suggest that FAM53A inhibits proliferation, migration, and invasion in the presence of wild-type p53.

FAM53A Promotes Proliferation, Migration, and Invasion in the p53-Mutant Breast Cancer Cell Line MDA-MB-231

FAM53A overexpression and depletion was also performed in MDA-MB-231 cells (**Figure 3A**). In this cell line, overexpression of FAM53A increased colony formation ability and proliferation, while depletion had the opposite effects (**Figures 3B,C**). The expression of proteins important for proliferation showed opposite trends with FAM53A modulation to those observed in MCF-7 cells; namely, FAM53A overexpression increased cyclin D1, CDK4, and c-Myc levels, while decreasing p21 levels. The depletion of FAM53A expression resulted in decreased cyclin D1, CDK4, and c-Myc and increased p21 (**Figure 3D**). FAM53A overexpression promoted migration and invasion in MDA-MB-231 cells, while depletion inhibited these processes (**Figure 3E**). FAM53A overexpression increased RhoA, RhoC, ROCK1, and MMP9 expression and decreased RhoB expression, and the opposite trends were observed with FAM53A depletion (**Figure 3F**). Taken together, the above results indicate that FAM53A has opposing effects on proliferation, migration, and invasion of breast cancer cell lines with wild-type and mutated p53.

FAM53A Differentially Affects the Expression of Epithelial-Mesenchymal Transition (EMT)-Related Proteins

EMT has dramatic effects on tumor cell behavior, as it results in changes in cell polarity and the formation of tight junctions between cells, a gradual loss of adhesion leading to cell invasiveness and migration, and the expression of a large number of extracellular matrix components that affect proliferation, migration, and invasion. As the above experiments demonstrated that FAM53A affects the proliferation, migration, and invasion of breast cancer cell lines, we next explored whether FAM53A regulation is a potential inhibitory mechanism against EMT by examining the expression of EMT-related proteins after modulating FAM53A levels. FAM53A overexpression in MCF-7 cells increased ZO-1 and E-cadherin expression and decreased zinc finger E-box binding homeobox 1 (ZEB1), N-cadherin, and vimentin expression; depletion of FAM53A had the opposite effects on these proteins (**Figure 4A**). We also examined the expression of EMT-related proteins in MDA-MB-231 cells. FAM53A overexpression decreased the expression of ZO-1 and E-cadherin and increased the expression of ZEB1, N-cadherin, and vimentin, while FAM53A depletion had the opposite effects (**Figure 4B**).

FAM53A Regulates Breast Cancer Cells Through the MEK/ERK Signaling Pathway

We next sought to gain mechanistic insight into the effects of FAM53A on breast cancer cells. FAM53B, a homolog of FAM53A, is involved in the regulation of Wnt/β-catenin signaling and β-catenin nuclear localization (26). However, a Wnt/β-catenin signaling pathway-related protein assay found no significant changes upon modulation of FAM53A levels (**Figure S1**). The MEK/ERK signaling pathway is crucial for the proper regulation

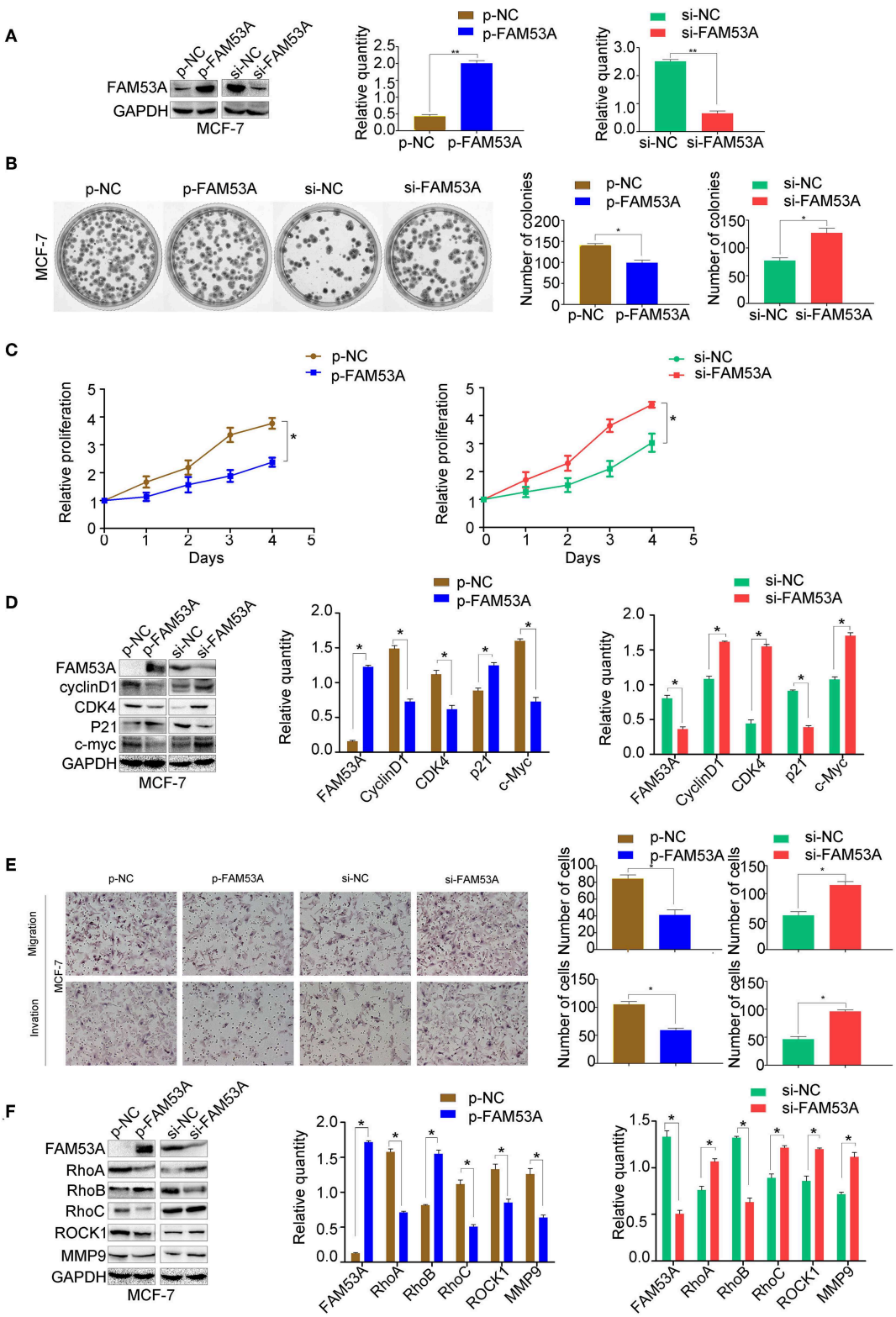

FIGURE 2 | FAM53A inhibits proliferation, migration, and invasion in p53-wild-type breast cancer cells. **(A)** MCF-7 cells were transfected with FAM53A-specific (si-FAM53A) or control (NC) siRNA, or with a FAM53A expression (p-FAM53A) or vehicle (p-NC) plasmid. Western blotting was performed to evaluate transfection and silencing efficiency. **(B)** Representative images and quantification of colony formation assays. **(C)** MTT assay results. **(D)** Expression changes in proliferation-related proteins. **(E)** Cell invasion and migration assays. **(F)** Expression of proteins associated with cell migration and invasion. For all panels, $^{*}P < 0.05$; $^{**}P < 0.01$.

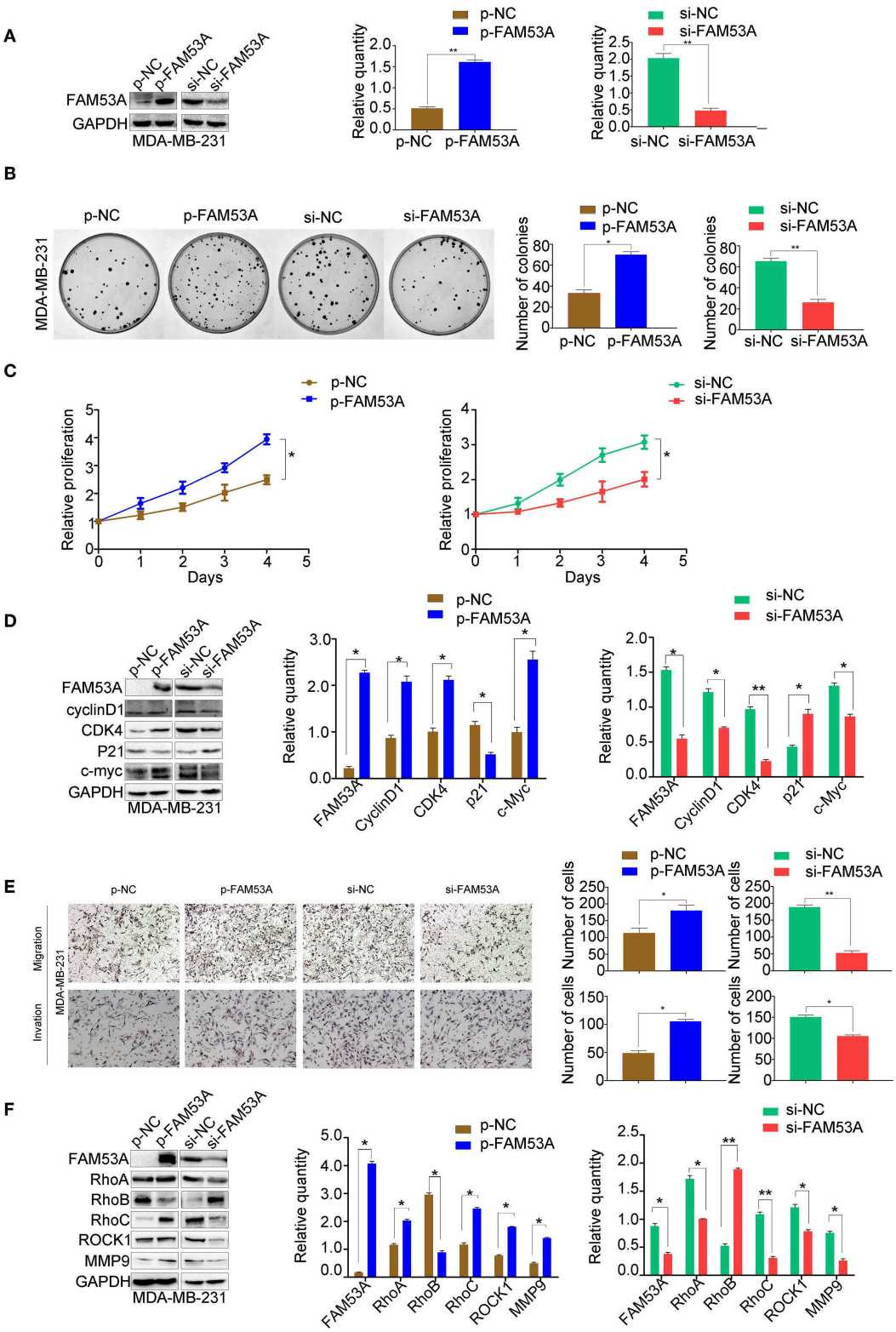

FIGURE 3 | FAM53A promotes proliferation, migration, and invasion in p53-mutant breast cancer cells. **(A)** MDA-MB-231 cells were transfected with FAM53A-specific (si-FAM53A) or control (NC) siRNA, or with a FAM53A expression (p-FAM53A) or vehicle (p-NC) plasmid. Western blotting was performed to evaluate transfection and silencing efficiency. **(B)** Representative images and quantification of colony formation assays. **(C)** MTT assay results. **(D)** Expression changes in proliferation-related proteins. **(E)** Cell invasion and migration assays. **(F)** Expression of proteins associated with cell migration and invasion. For all panels, $^{*}P < 0.05$; $^{**}P < 0.01$.

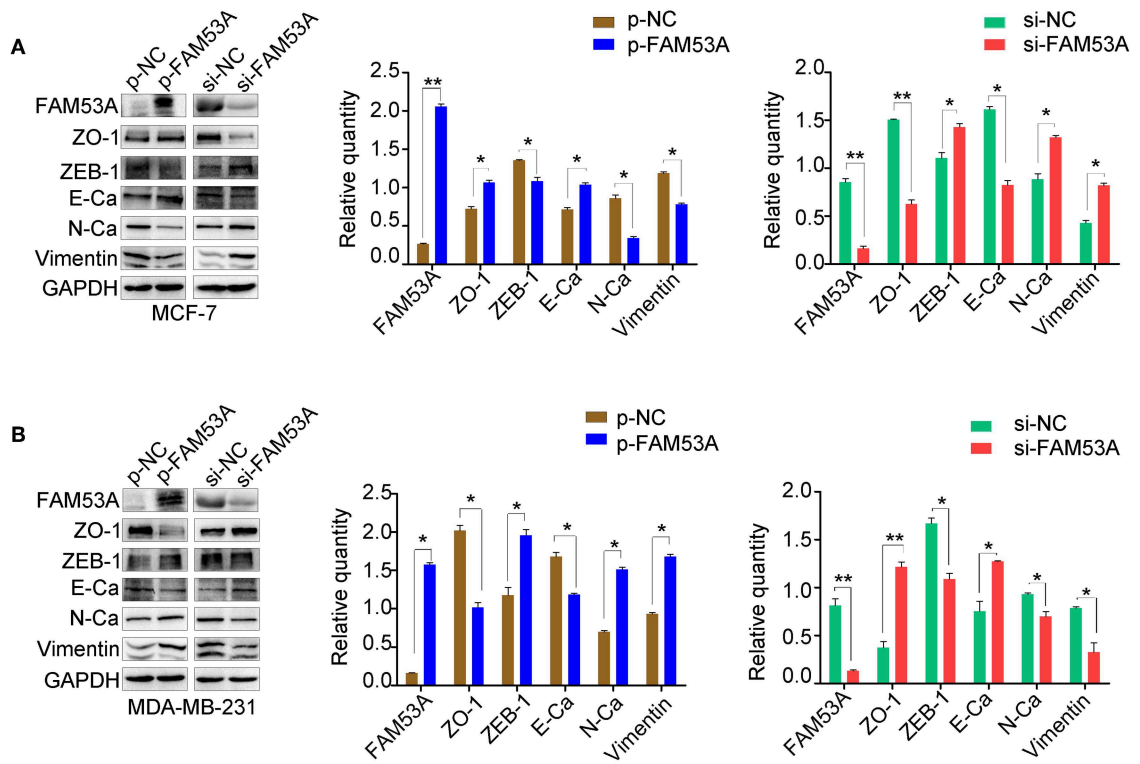

FIGURE 4 | FAM53A regulates the levels of EMT-related proteins. **(A,B)** Expression changes in EMT-related proteins in MCF-7 and MDA-MB-231 cells, respectively. E-Ca, E cadherin; N-Ca, N cadherin. *$P < 0.05$; **$P < 0.01$.

of proliferation, migration, and invasion, so we next examined the effects of FAM53A on MEK/ERK activation. In MCF-7 cells, FAM53A overexpression resulted in decreased p-MEK1/2 and p-ERK1/2, indicating decreased pathway activation. Conversely, FAM53A depletion significantly increased the phosphorylation of MEK1/2 and ERK1/2 (**Figure 5A**). Modulation of FAM53A levels had no effect on EGF receptor (EGFR), Ras, Raf, MEK1/2, or ERK1/2 levels, nor did it affect EGFR phosphorylation.

To confirm that FAM53A functions through the MEK/ERK signaling pathway, we employed the specific MEK/ERK pathway inhibitor PD98059. While FAM53A depletion significantly activated MEK/ERK signaling, PD98059 blocked this activation. PD98059 treatment also blocked the increased colony formation activity observed after FAM53A depletion, and rescued the increased migration and invasion, confirming that FAM53A regulates MCF-7 cells through the MEK/ERK signaling pathway (**Figures 5B,C**). We also examined the expression of proliferation- and EMT-related proteins with PD98059 treatment and found that MEK/ERK inhibition restored protein levels to those observed without FAM53A depletion (**Figure 5D**). These experiments demonstrate that FAM53A inhibits proliferation, migration, and invasion and negatively regulates the EMT in p53 wild-type breast cancer cells through the MEK/ERK pathway.

In MDA-MB-231 cells, MEK1/2 and ERK1/2 phosphorylation increased with FAM53A overexpression and decreased with its depletion, while EGFR, Ras, Raf, MEK, and ERK levels did not significantly change (**Figure 6A**). PD98059 rescued the increased colony formation caused by FAM53A overexpression, as well as the increased migration and invasion, confirming that the effects of FAM53A are mediated through MEK/ERK signaling in this cell line as well (**Figures 6B,C**). PD98059 also reversed the effects of FAM53A overexpression on the expression of proliferation- and EMT-related proteins (**Figure 6D**).

The Opposing Effects of FAM53A on MCF-7 and MDA-MB-231 Cells Depend on Their p53 Status

Interestingly, our results indicated that FAM53A has opposite effects on the MCF-7 and MDA-MB-231 cell lines. As the only positive correlation between FAM53A expression and the clinicopathological characteristics of invasive breast cancer was p53 status (**Table 1**), we next investigated whether the differential effects of FAM53A in these lines was due to the presence or absence of functional p53. An MCF-7 cell line with stable expression of a p53 shRNA was generated, which displayed decreased FAM53A expression compared with the parental line (**Figure 7A**). Depletion of p53 reversed the trends observed upon FAM53A depletion in the parental line, decreasing MEK/ERK activation (**Figure 7B**), colony formation (**Figure 7C**), and migration and invasion (**Figure 7D**).

Next, we constructed an MDA-MB-231 cell line stably expressing wild-type p53 (**Figure 7E**) and subjected it to

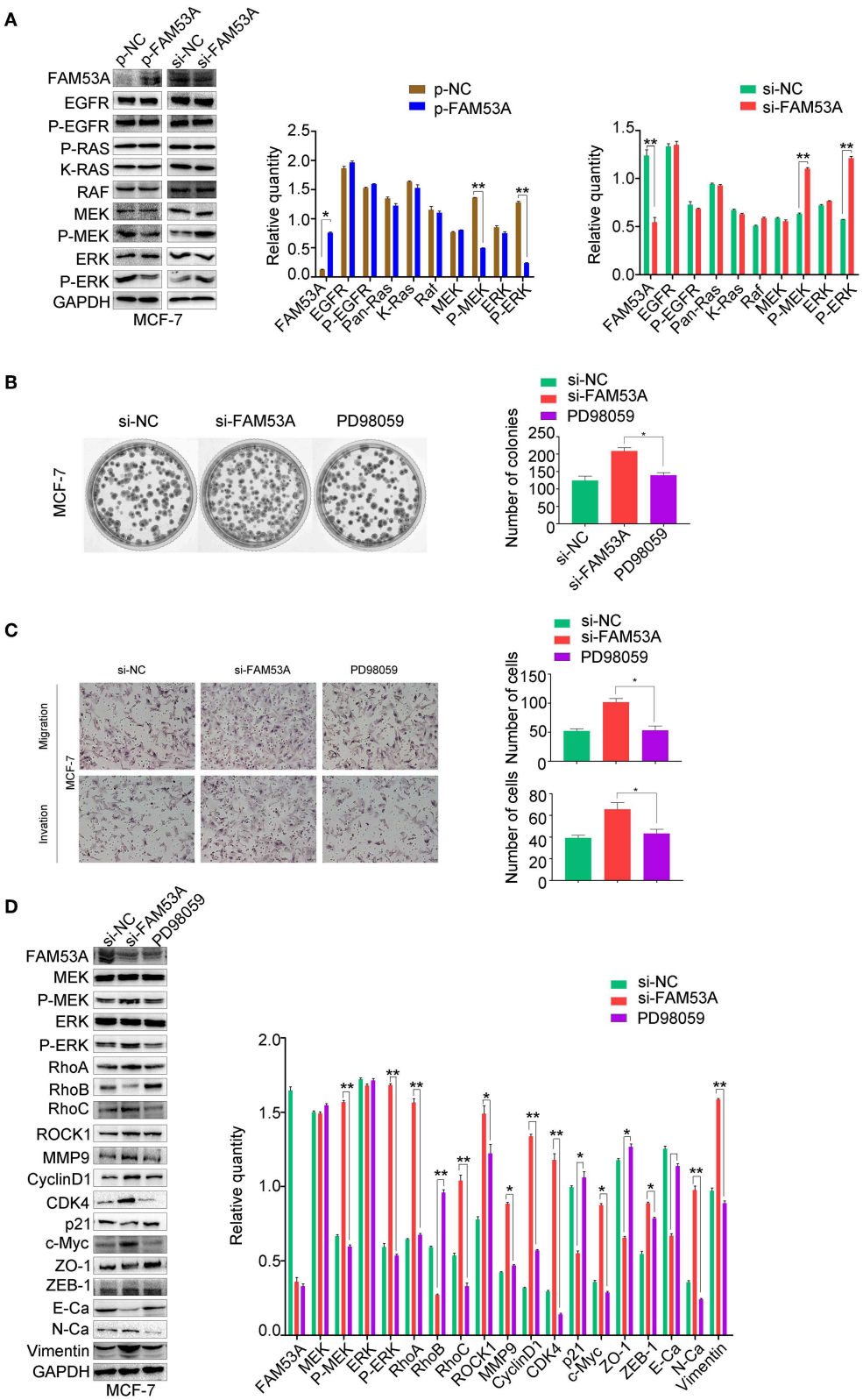

FIGURE 5 | FAM53A regulates MCF-7 cells via the MEK/ERK signaling pathway. MCF-7 cells transfected with control or FAM53A siRNA were treated with or without PD98059 and analyzed for **(A)** changes in the expression and activation of MEK/ERK signaling proteins, **(B)** colony formation ability, **(C)** migration and invasion, and **(D)** expression of proteins involved in cell proliferation, migration, and invasion. For all panels, $^{*}P < 0.05$; $^{**}P < 0.01$. E-Ca, E cadherin; N-Ca, N cadherin.

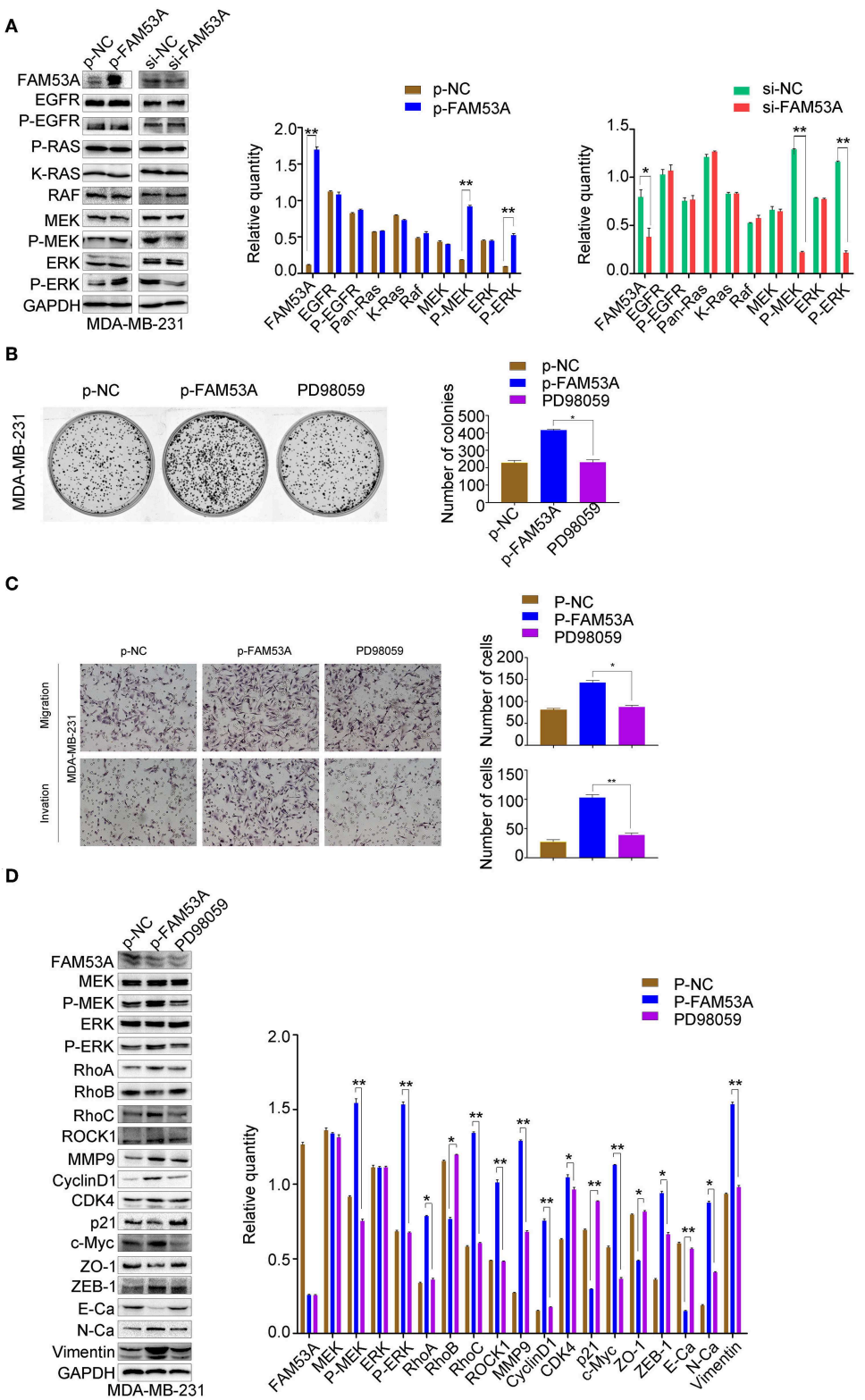

FIGURE 6 | FAM53A regulates MDA-MB-231 cells via the MEK/ERK signaling pathway. MDA-MB-231 cells were transfected with control or FAM53A overexpression plasmids, treated with or without PD98059, and analyzed for **(A)** changes in the expression and activation of MEK/ERK signaling proteins, **(B)** colony formation ability, **(C)** migration and invasion, and **(D)** expression of proteins involved in cell proliferation, migration, and invasion. For all panels, $^{*}P < 0.05$; $^{**}P < 0.01$. E-Ca, E cadherin; N-Ca, N cadherin.

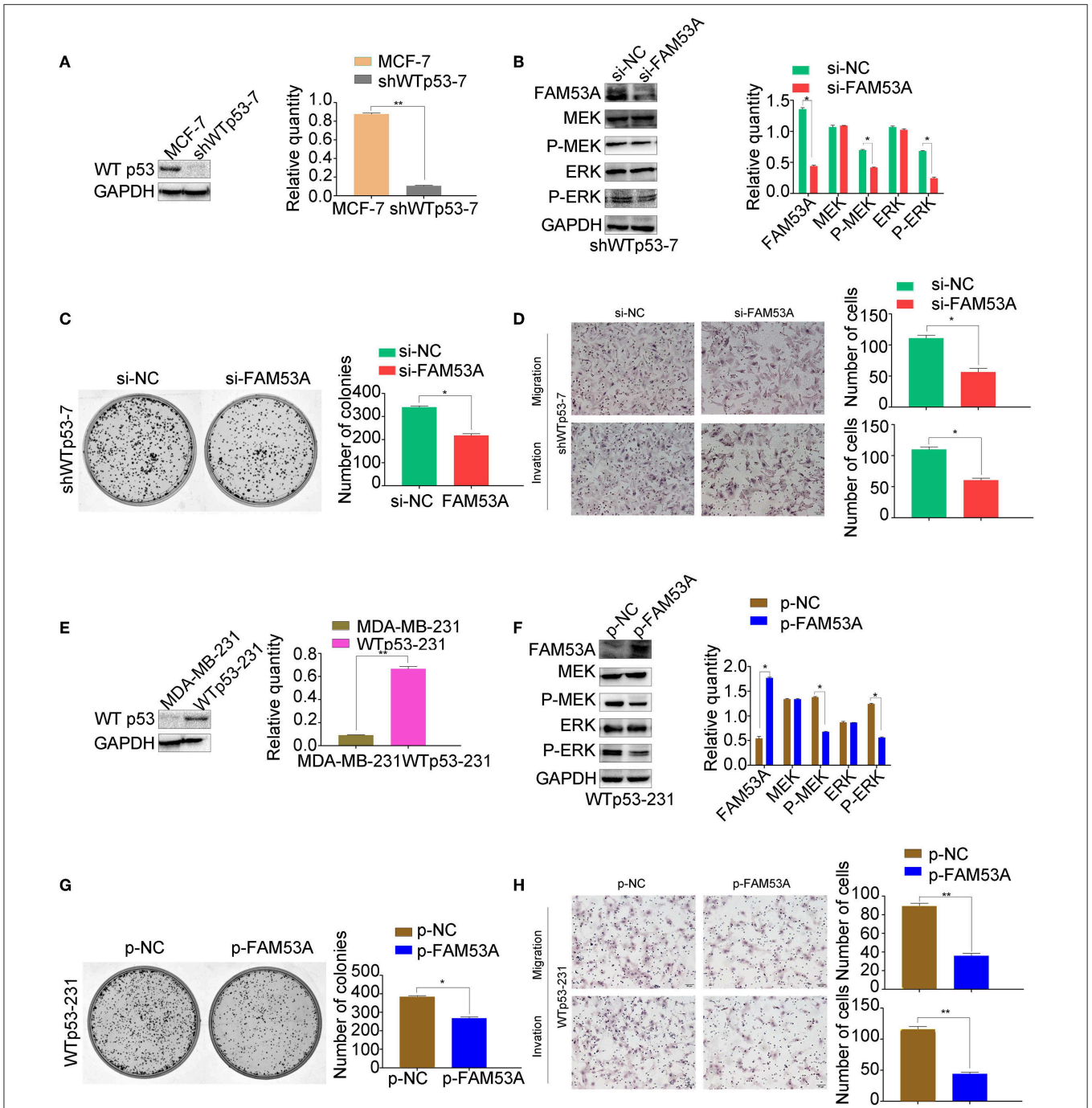

FIGURE 7 | The opposing effects of FAM53A on MCF-7 and MDA-MB-231 cells depend on their p53 status. **(A)** An MCF-7 cell line with stable depletion of wild-type p53 (shWTp53-7) was constructed and evaluated for **(B)** changes in the expression and activation of MEK/ERK signaling proteins, **(C)** colony formation ability, and **(D)** migration and invasion. **(E)** An MDA-MB-231 cell line stably expressing wild-type p53 (WTp53-231) was constructed, transfected with control or FAM53A overexpression plasmids, and evaluated for **(F)** changes in the expression and activation of MEK/ERK signaling proteins, **(G)** colony formation ability, and **(H)** migration and invasion. For all panels, $^{*}P < 0.05$; $^{**}P < 0.01$.

the same analysis. FAM53A overexpression in WTp53-231 cells inhibited MEK/ERK activation (**Figure 7F**), colony formation (**Figure 7G**), and migration and invasion (**Figure 7H**).

DISCUSSION

While FAM53A has yet to be directly linked to tumorigenesis, studies have shown that members of the FAM53 protein family

bind to transcriptional regulators that regulate cell proliferation, suggesting potential effects on cancer development. To the best of our knowledge, this is the first demonstration of the relevance of FAM53A expression in cancer. The results indicate that FAM53A levels are negatively correlated with wild-type p53, suggesting a link between the role of FAM53A in breast cancer and p53 status.

FAM53A was shown to affect the sensitivity of breast cancer cell lines to doxorubicin, with opposing effects on breast cancer cell lines with different p53 status (27). However, the effects of FAM53A on breast cancer cells and their related mechanisms were unknown. Our study demonstrates that overexpression of FAM53A reduces proliferation, migration, and invasion ability in the p53-wild-type breast cancer cell line MCF-7, but promoted these abilities in the p53-mutant line MDA-MB-231. We had also selected the p53-wild-type lung cancer cell line A549 and the p53-mutant breast cancer cell line SK-BR3, the results are consistent with the previous conclusions (**Figure S2**). Mechanistically, the results indicate that FAM53A affects cell proliferation by regulating the p21-cyclin D1-CDK4 signaling axis. In addition, FAM53A may affect the migration and invasion of breast cancer cells by regulating the expression of RhoA, RhoB, RhoC, ROCK1, and MMP9. Through these proteins, FAM53A could drastically affect the behavior of malignant cells.

EMT occurs during tumor invasion and metastasis and represents an important milestone in tumor progression. EMT is mainly characterized by loss of epithelial cell polarity, loss of adhesion between cells, and acquisition of mesenchymal cell characteristics, accompanied by enhanced migration ability (30, 31). Our results indicate that FAM53A affects several key proteins in EMT. Moreover, these effects were consistently opposite between the p53-positive and -negative cells.

Our result demonstrated that FAM53A inhibits MEK and ERK activity in p53 wild-type breast cancer cells, but activates these enzymes in p53-mutant cells. The use of PD98059 to antagonize ERK activation after FAM53A overexpression or depletion indicated that FAM53A affects breast cancer proliferation, migration, and invasion via the MEK/ERK signaling pathway. Further mapping of this pathway will allow more precise determination of the mechanism of FAM53A action.

As a key tumor suppressor gene involved in the regulation of the cell cycle, apoptosis, senescence, and DNA repair, somatic *TP53* mutations are estimated to occur in 20–30% of cancer cases, including breast cancer (31, 32). The prognosis of breast cancer is closely related to lymph node metastasis, which *TP53* mutations can be used clinically to predict (32). Importantly for breast cancer, *TP53* status may be associated with estrogen receptor (ER), HER-2, and Ki-67 status, with important synergistic or regulatory effects (33, 34). When *TP53* is mutated, normal regulation of these biomarkers is lost, promoting lymph node metastasis. The effects of FAM53A levels on the sensitivity of breast cancer to doxorubicin is correlated with p53 status (27), and our previous immunohistochemical staining demonstrated that FAM53A colocalizes with p53. In this study, FAM53A inhibited proliferation, migration, and invasion by inhibiting MEK/ERK signaling in p53 wild-type cells, while in p53 negative breast cancer cells, FAM53A activated MEK/ERK signaling, promoting these behaviors. This suggests that the role of FAM53A is reversed with loss of p53. We used immunoprecipitation experiments to test for protein-protein interaction between FAM53A and p53 and did not detect one (data not shown), suggesting an indirect regulatory link between FAM53A and p53. This relationship will require further exploration. It is important to note that in addition to their p53 status, MCF-7 and MDA-MB-231 cells differ in the expression of the ER, K-Ras, and other important cancer signaling proteins, and whether these factors affect the biological behavior of FAM53A in breast cancer remains to be determined.

Our understanding of the role of FAM53A in cancer tumorigenesis and progression is limited. Taken together, our study demonstrates for the first time that FAM53A affects the proliferation, migration, and invasion of breast cancer cells in a p53-dependent manner. These findings suggest that FAM53A has broad prospects in cancer research, particularly in P53 wild-type and P53 mutant breast cancer.

DATA AVAILABILITY STATEMENT

The raw data supporting the conclusions of this manuscript will be made available by the authors, without undue reservation, to any qualified researcher.

ETHICS STATEMENT

Patients whose tissue samples were used in this research provided written informed consent. This study was approved by the local institutional review board of China Medical University.

AUTHOR CONTRIBUTIONS

XM, MS, MH, KD, and JZ contributed conception and design of the study. JZ, MS, MH, JW, SL, and QC performed experiment and the statistical analysis. JZ and MS wrote the first draft of the manuscript. All authors contributed to manuscript revision, read, and approved the submitted version.

FUNDING

This work was supported by the National Natural Science Foundation of China (grant no. 81572615 to XM).

SUPPLEMENTARY MATERIAL

The Supplementary Material for this article can be found online at: https://www.frontiersin.org/articles/10.3389/fonc.2019.01244/full#supplementary-material

Table S1 | Antibodies used for western blotting.

Figure S1 | FAM53A does not regulate MCF-7 and MDA-MB-231 cells via the Wnt/β-catenin pathway. **(A)** In MCF-7 cells, up- or down-regulation of FAM53A levels did not significantly change β-catenin and glycogen synthase kinase 3β levels. **(B)** In MDA-MB-231 cells, changes in Wnt/β-catenin pathway-related proteins did not show any clear trends.

Figure S2 | FAM53A has the opposite effect on A549 and SK-BR3. In the p53-wild-type lung cancer cell line A549(ABC), FAM53A inhibits the ERK pathway and inhibits its proliferation, migration and invasion. While in the p53-mutant breast cancer cell line SK-BR3(ABC), FAM53A promotes the ERK pathway and promotes its proliferation migration and invasion.

REFERENCES

1. Lee JT Jr, McCubrey JA. The Raf/MEK/ERK signal transduction cascade as a target for chemotherapeutic intervention in leukemia. *Leukemia*. (2002) 16:486–507. doi: 10.1038/sj.leu.2402460
2. Boulton TG, Yancopoulos GD, Gregory JS, Slaughter C, Moomaw C, Hsu J, et al. An insulin-stimulated protein kinase similar to yeast kinases involved in cell cycle control. *Science*. (1990) 249:64–7. doi: 10.1126/science.2164259
3. Crews CM, Alessandrini A, Erikson RL. The primary structure of MEK, a protein kinase that phosphorylates the ERK gene product. *Science*. (1992) 258:478–80. doi: 10.1126/science.1411546
4. Kosako H, Gotoh Y, Matsuda S, Ishikawa M, Nishida E. Xenopus MAP kinase activator is a serine/threonine/tyrosine kinase activated by threonine phosphorylation. *EMBO J*. (1992) 11:2903–8. doi: 10.1002/j.1460-2075.1992.tb05359.x
5. Kyriakis JM, App H, Zhang XF, Banerjee P, Brautigan DL, Rapp UR, et al. Raf-1 activates MAP kinase-kinase. *Nature*. (1992) 358:417–21. doi: 10.1038/358417a0
6. Wang S, Liu Q, Zhang Y, Liu K, Yu P, Liu K, et al. Suppression of growth, migration and invasion of highly-metastatic human breast cancer cells by berbamine and its molecular mechanisms of action. *Mol Cancer*. (2009) 8:81. doi: 10.1186/1476-4598-8-81
7. Dhillon AS, Hagan S, Rath O, Kolch W. MAP kinase signalling pathways in cancer. *Oncogene*. (2007) 26:3279–90. doi: 10.1038/sj.onc.1210421
8. Bradham C, McClay DR. p38 MAPK in development and cancer. *Cell Cycle*. (2006) 5:824–8. doi: 10.4161/cc.5.8.2685
9. Chen J, Fujii K, Zhang L, Roberts T, Fu H. Raf-1 promotes cell survival by antagonizing apoptosis signal-regulating kinase 1 through a MEK-ERK independent mechanism. *Proc Natl Acad Sci USA*. (2001) 98:7783–8. doi: 10.1073/pnas.141224398
10. Roberts PJ, Der CJ. Targeting the Raf-MEK-ERK mitogen-activated protein kinase cascade for the treatment of cancer. *Oncogene*. (2007) 26:3291–310. doi: 10.1038/sj.onc.1210422
11. Sivaraman VS, Wang H, Nuovo GJ, Malbon CC. Hyperexpression of mitogen-activated protein kinase in human breast cancer. *J Clin Invest*. (1997) 99:1478–83. doi: 10.1172/JCI119309
12. Moreno-Aspitia A. Clinical overview of sorafenib in breast cancer. *Future Oncol*. (2010) 6:655–63. doi: 10.2217/fon.10.41
13. Steeb T, Wessely A, Ruzicka T, Heppt MV, Berking C. How to MEK the best of uveal melanoma: a systematic review on the efficacy and safety of MEK inhibitors in metastatic or unresectable uveal melanoma. *Eur J Cancer*. (2018) 103:41–51. doi: 10.1016/j.ejca.2018.08.005
14. Chiu LC, Kong CK, Ooi VE. The chlorophyllin-induced cell cycle arrest and apoptosis in human breast cancer MCF-7 cells is associated with ERK deactivation and Cyclin D1 depletion. *Int J Mol Med*. (2005) 16:735–40. doi: 10.3892/ijmm.16.4.735
15. Kanwar JR, Kamalapuram SK, Kanwar RK. Targeting survivin in cancer: the cell-signalling perspective. *Drug Discov Today*. (2011) 16:485–94. doi: 10.1016/j.drudis.2011.04.001
16. Bartel CA, Jackson MW. HER2-positive breast cancer cells expressing elevated FAM83A are sensitive to FAM83A loss. *PLoS ONE*. (2017) 12:e0176778. doi: 10.1371/journal.pone.0176778
17. Nakajima H, Koizumi K. Family with sequence similarity 107: a family of stress responsive small proteins with diverse functions in cancer and the nervous system (Review). *Biomed Rep*. (2014) 2:321–5. doi: 10.3892/br.2014.243
18. Yamaura T, Ezaki J, Okabe N, Takagi H, Ozaki Y, Inoue T, et al. Family with sequence similarity 83, member B is a predictor of poor prognosis and a potential therapeutic target for lung adenocarcinoma expressing wild-type epidermal growth factor receptor. *Oncol Lett*. (2018) 15:1549–58. doi: 10.3892/ol.2017.7517
19. Liu W, Wang S, Qian K, Zhang J, Zhang Z, Liu H. Expression of family with sequence similarity 172 member A and nucleotide-binding protein 1 is associated with the poor prognosis of colorectal carcinoma. *Oncol Lett*. (2017) 14:3587–93. doi: 10.3892/ol.2017.6585
20. Kobayashi T, Masaki T, Sugiyama M, Atomi Y, Furukawa Y, Nakamura Y. A gene encoding a family with sequence similarity 84, member A (FAM84A) enhanced migration of human colon cancer cells. *Int J Oncol*. (2006) 29:341–7. doi: 10.3892/ijo.29.2.341
21. Etokebe GE, Zienolddiny S, Kupanovac Z, Enersen M, Balen S, Flego V, et al. Association of the FAM46A gene VNTRs and BAG6 rs3117582 SNP with non small cell lung cancer (NSCLC) in Croatian and Norwegian populations. *PLoS ONE*. (2015) 10:e0122651. doi: 10.1371/journal.pone.0122651
22. Munoz IM, MacArtney T, Sanchez-Pulido L, Ponting CP, Rocha S, Rouse J. Family with sequence similarity 60A (FAM60A) protein is a cell cycle-fluctuating regulator of the SIN3-HDAC1 histone deacetylase complex. *J Biol Chem*. (2012) 287:32346–53. doi: 10.1074/jbc.M112.382499
23. Haque MH, Gopalan V, Chan KW, Shiddiky MJ, Smith RA, Lam AK. Identification of novel FAM134B (JK1) mutations in oesophageal squamous cell carcinoma. *Sci Rep*. (2016) 6:29173. doi: 10.1038/srep29173
24. Thermes V, Candal E, Alunni A, Serin G, Bourrat F, Joly JS. Medaka simplet (FAM53B) belongs to a family of novel vertebrate genes controlling cell proliferation. *Development*. (2006) 133:1881–90. doi: 10.1242/dev.02350
25. Panagopoulos I, Gorunova L, Torkildsen S, Tierens A, Heim S, Micci F. FAM53B truncation caused by t(10;19)(q26;q13) chromosome translocation in acute lymphoblastic leukemia. *Oncol Lett*. (2017) 13:2216–20. doi: 10.3892/ol.2017.5705
26. Kizil C, Kuchler B, Yan JJ, Ozhan G, Moro E, Argenton F, et al. Simplet/Fam53b is required for Wnt signal transduction by regulating beta-catenin nuclear localization. *Development*. (2014) 141:3529–39. doi: 10.1242/dev.108415
27. Fagerholm R, Khan S, Schmidt MK, Garcia-Closas M, Heikkila P, Saarela J, et al. TP53-based interaction analysis identifies cis-eQTL variants for TP53BP2, FBXO28, and FAM53A that associate with survival and treatment outcome in breast cancer. *Oncotarget*. (2017) 8:18381–98. doi: 10.18632/oncotarget.15110
28. Jun L, Balboni AL, Laitman JT, Bergemann AD. Isolation of DNTNP, which encodes a potential nuclear protein that is expressed in the developing, dorsal neural tube. *Dev Dyn*. (2002) 224:116–23. doi: 10.1002/dvdy.10090
29. Palumbo O, Palumbo P, Ferri E, Riviello FN, Cloroformio L, Carella M, et al. Report of a patient and further clinical and molecular characterization of interstitial 4p16.3 microduplication. *Mol Cytogenet*. (2015) 8:15. doi: 10.1186/s13039-015-0119-6
30. Suarez-Carmona M, Lesage J, Cataldo D, Gilles C. EMT and inflammation: inseparable actors of cancer progression. *Mol Oncol*. (2017) 11:805–23. doi: 10.1002/1878-0261.12095
31. Olivier M, Langerod A, Carrieri P, Bergh J, Klaar S, Eyfjord J, et al. The clinical value of somatic TP53 gene mutations in 1,794 patients with breast cancer. *Clin Cancer Res*. (2006) 12:1157–67. doi: 10.1158/1078-0432.CCR-05-1029
32. Hamroun D, Kato S, Ishioka C, Claustres M, Beroud C, Soussi T. The UMD TP53 database and website: update and revisions. *Human Mutat*. (2006) 27:14–20. doi: 10.1002/humu.20269
33. Ahn SG, Yoon CI, Lee JH, Lee HS, Park SE, Cha YJ, et al. Low PR in ER(+)/HER2(-) breast cancer: high rates of TP53 mutation and high SUV. *Endocr Relat Cancer*. (2018) 26:177–85. doi: 10.1530/ERC-18-0281
34. Wang L, Feng C, Ding G, Ding Q, Zhou Z, Jiang H, et al. Ki67 and TP53 expressions predict recurrence of non-muscle-invasive bladder cancer. *Tumour Biol*. (2014) 35:2989–95. doi: 10.1007/s13277-013-1384-9

Conflict of Interest: The authors declare that the research was conducted in the absence of any commercial or financial relationships that could be construed as a potential conflict of interest.

frontiers in Oncology

REVIEW
published: 08 January 2020
doi: 10.3389/fonc.2019.01381

Enhancing the Bystander and Abscopal Effects to Improve Radiotherapy Outcomes

Virgínea de Araújo Farias[1,2,3], *Isabel Tovar*[4], *Rosario del Moral*[4], *Francisco O'Valle*[1,2,3,5], *José Expósito*[4], *Francisco Javier Oliver*[2,3*] and *José Mariano Ruiz de Almodóvar*[1,2*]

[1] Centro de Investigación Biomédica, Instituto Universitario de Investigación en Biopatología y Medicina Regenerativa, PTS Granada, Granada, Spain, [2] CIBERONC (Instituto de Salud Carlos III), Granada, Spain, [3] Instituto de Parasitología y Biomedicina "López Neyra", Consejo Superior de Investigaciones Científicas, PTS Granada, Granada, Spain, [4] Complejo Hospitalario de Granada, Servicio Andaluz de Salud, PTS Granada, Granada, Spain, [5] Departamento de Anatomía Patológica, Facultad de Medicina, Universidad de Granada, PTS Granada, Granada, Spain

OPEN ACCESS

Edited by:
Carsten Herskind,
University of Heidelberg, Germany

Reviewed by:
Chandan Guha,
Albert Einstein College of Medicine, United States
Vinay Sharma,
University of the Witwatersrand, South Africa
Fiona Lyng,
Dublin Institute of Technology, Ireland

***Correspondence:**
Francisco Javier Oliver
joliver@ipb.csic.es
José Mariano Ruiz de Almodóvar
jmrdar@ugr.es

Specialty section:
This article was submitted to Radiation Oncology, a section of the journal Frontiers in Oncology

Received: 17 July 2019
Accepted: 22 November 2019
Published: 08 January 2020

Citation:
Farias VdA, Tovar I, del Moral R, O'Valle F, Expósito J, Oliver FJ and Ruiz de Almodóvar JM (2020) Enhancing the Bystander and Abscopal Effects to Improve Radiotherapy Outcomes. Front. Oncol. 9:1381. doi: 10.3389/fonc.2019.01381

In this paper, we summarize published articles and experiences related to the attempt to improve radiotherapy outcomes and, thus, to personalize the radiation treatment according to the individual characteristics of each patient. The evolution of ideas and the study of successively published data have led us to envisage new biophysical models for the interpretation of tumor and healthy normal tissue response to radiation. In the development of the model, we have shown that when mesenchymal stem cells (MSCs) and radiotherapy are administered simultaneously in experimental radiotherapy on xenotumors implanted in a murine model, the results of the treatment show the existence of a synergic mechanism that is able to enhance the local and systemic actions of the radiation both on the treated tumor and on its possible metastasis. We are convinced that, due to the physical hallmarks that characterize the neoplastic tissues, the physical–chemical tropism of MSCs, and the widespread functions of macromolecules, proteins, and exosomes released from activated MSCs, the combination of radiotherapy plus MSCs used intratumorally has the effect of counteracting the pro-tumorigenic and pro-metastatic signals that contribute to the growth, spread, and resistance of the tumor cells. Therefore, we have concluded that MSCs are appropriate for therapeutic use in a clinical trial for rectal cancer combined with radiotherapy, which we are going to start in the near future.

Keywords: experimental radiotherapy, cell loss, mesenchymal cells, bystander effect, abscopal effect, exosomes, mesenchymal cell enhancement ratio

INTRODUCTION

In clinical oncology, each patient is different. Therefore, the treatment should also be different; that is, each patient needs a specific treatment adjusted to their characteristics and the prognosis of the illness.

For most neoplastic diseases, the prognosis of the disease is a function of a small number of variables. Although the choice of these variables is supported by a broad medical consensus and it is assumed that each treatment is considered to be the most appropriate to achieve a cure, the number of therapeutic failures that result constitutes a medical problem of singular importance.

Currently the treatment of cancer patients is decided on the basis of the size of the tumor, the status of the loco-regional lymphatics, the presence or absence of distal disease, the histological type, and the general health state of the patient. Once the necessary values are known, the patients are classified (the staging) into well-defined clinical categories (1). This classification is so that the physician has a general approach to the prognosis of the illness suffered by the patient being treated, and that the treatment proposed is most appropriate and above all offers the patient the necessary information to decide and consent to how he/she wants to be treated.

Ionizing radiation is widely and effectively applied in oncology. However, due to dose limits, a complete tumor cure cannot be achieved for many tumors and localizations. Despite the advanced radiotherapy facilities and therapeutic methods that are currently available, high doses of radiation might still induce, fortunately only on rare occasions, early and late side effects of severe magnitude. Unacceptable normal tissue reactions persist as the limiting factor for administering a tumoricidal dose in radiotherapy. Moreover, the frequent presence of clinical and/or hide-metastatic foci in distal organs is beyond the range of the treatment and is a death threat for the patients. Therefore, research searching for progress in the control of metastatic disease is a target of major interest.

The previous paragraph reveals that both the study of the extension of the neoplasms and the prediction of the probabilities of tumor control or complications after therapy are based on techniques that are imperfect, imprecise, and insufficient. Indeed, when the results of therapy in groups of patients classified to be at the same stage are studied in the long term, a variability of response is found, which is impossible to predict (1–6).

The evolution of ideas and the study of successively published data have led us to imagine a new biophysical model for the interpretation of tumor response to radiation. In its development, we have shown that when human-umbilical cord mesenchymal stem cells (MSCs) and radiotherapy are administered simultaneously in experimental radiotherapy on xenotumors implanted in a murine model, the results of the treatment show the existence of a synergic mechanism that is able to enhance the local and systemic actions of the radiation both on the treated tumor and on its possible metastasis. We are convinced that due to the physical hallmarks that characterize the neoplastic tissues, the physical–chemical tropism of MSCs, and the widespread functions of macromolecules, proteins, and exosomes released from activated MSCs, the combination of radiotherapy plus MSCs used intratumorally has the effect of counteracting the protumorigenic and pro-metastatic signals that contribute to the growth, dissemination, and resistance of the tumor cells.

Therefore, we have concluded that the administration of MSC enhances the therapeutic effect of radiotherapy *in vivo* and does not produce toxic effects, indicating that they could be used as an adjuvant treatment for cancer, increasing the therapeutic effect of radiotherapy on the tumor as well as on possible tumor-metastatic foci.

The three objectives of this study are:

a. to propose a biophysics model that includes the classic radiobiological concepts together with the bystander and abscopal effects in a single picture.
b. to summarize results of our *in vivo* studies that demonstrate of the synergist effect of radiotherapy combined with mesenchymal cell therapy in the treatment of xenotumors.
c. to suggest that exosomes and proteins secreted by the activated-mesenchymal cells are responsible for the enhancement of radiotherapy action on the tumor, including the abscopal effect on tumor-metastatic foci.

THE ROLE OF RADIOBIOLOGY

The cellular consequences of direct radiation-induced DNA damage, producing lethal and potentially lethal damage to DNA, can be described by radiation cell survival models (7). Nevertheless, although we agree with Brown et al. (8), who suggested that, for the most part, the universally accepted radiobiology ideas of the 5 Rs (9) are enough to describe the clinical data and the isoeffect or tolerance calculations, we are convinced that the results obtained from the application of the LQ model (10, 11) in clinical studies through the calculation of biologically effective doses (BEDs) are absolutely correct, and that this model has also been successfully used, even with stereotactic radio-surgery (SRS), intraoperative radiotherapy (IORT), and stereotactic body radiotherapy (SBRT), although with the probable exception that, for some tumors in which high doses of irradiation may produce greater anti-tumor immunity (8), the role of the 5 Rs of radiotherapy is clearly different in these cases (12).

However, considering that the LQ model can explain neither the bystander effects (13–15), nor the variation of damage processing and tissue remodeling in the pathogenesis and severity of the of the late effects of radiation (16–18), nor the abscopal effects that can be intermediated principally by immune cells such as the T cells (19), it is clear that the models so far used to interpret the relationship between cell radiosensitivity and clinical radio-response are unable to explain all the effects of radiation in some circumstances and a more general radiobiological model appears to be mandatory (6, 20).

WE MUST UNDERSTAND THE WHOLE RESPONSE OF TUMOR AND NORMAL TISSUE TO RADIOTHERAPY

The happening of hyper-radiosensitivity at low radiotherapy doses (13) and the bystander effect (14–16) exemplifies that reactive molecular signaling and repair activity regulate the equilibrium of irradiated potential lethally damaged cells between radiation cell killing and cell survival, and this communication between irradiated and out-of-target cells can affect tumor cells, reducing their surviving fraction (17, 18).

Mounting data suggest that radiotherapy also recruits biological effectors away from the treatment field and has systemic effects (19, 20).

Consequently, in our view, non-target radiotherapy action could be thought as the complete immunological reaction of the tumor (21–25) and health tissues (6, 26) to the stress caused in the irradiated volume (27) that results in enhanced levels of DNA lesions (21), chromosomal aberrations (28), alterations in transcript levels and gene expression (29–32), and finally cell death (18, 33). The major question, however, is how to combine diverse information (clinical, imaging, and molecular data) in an algorithm to offer specific clinical information that precisely and significantly estimate patient outcomes as a function of potential therapeutic decisions (34).

We consider that neoplastic stem cell survival after radiation treatment be determined by (a) the effects of radiation-induced cellular damage (linear-quadratic model) and (b) the out-of-target bystander and abscopal interaction produced by free radicals, antigen–antibody interaction (19), and death receptor–ligand interaction (18, 35, 36).

The Biophysical Model

Assuming that the targeted action of radiation on the cell DNA and the non-targeted (bystander or abscopal) actions on cell survival are independent as has been proposed recently (37), our previously published model (35, 38) defines the final surviving fraction as the product of the surviving fraction produced by the targeted interaction of radiation with the tumor cells and the cell surviving fraction on tumors and metastatic foci through the short-range and long-range bystander effects that are promoted by the radiation treatment (18, 35).

Based on these concepts, we have described that, after radiation, cells in the therapeutic volume can be classified into four compartments (**Figure 1**) that we briefly update here:

Undamaged Cells (A)

Survival response of cells after each fraction of dose, which should be controlled with consecutive irradiation treatments.

Dead Cells (B)

This is the lethal-lesion compartment in Curtis's model (39) that arise from the targeted and non-targeted action of radiation on DNA, and from the bystander and abscopal immunological cell death promoted by the action of activated cells (38, 40) and death cells (35, 40–42) on other tumoral cells belonging to tumor process.

Activated Cells (C)

Cells that are either slightly damaged or have been able to restore their lesions to a level of residual damage compatible with survival. These cells might turn out to be an effective source of cytokines (38), macromolecules (43), exosomes (44, 45), reactive oxygen species (46), and reactive nitrogen species (18), and/or could suffer phenotypic changes to express hide-antigens in the tumors, which allow the triggering of the pro-immunogenic effects of radiotherapy on the tumors (19, 20, 47), with none of these possibilities being exclusive of the others, indeed all of them might affect the local and distal burden of tumor cells (48) and be the cause of the bystander and abscopal components of the radiation immunologically induced cell death on local and distal foci of the tumors (35).

As we will explain below, this compartment may be enlarged by human-umbilical cord MSC transplantation (38, 44, 49).

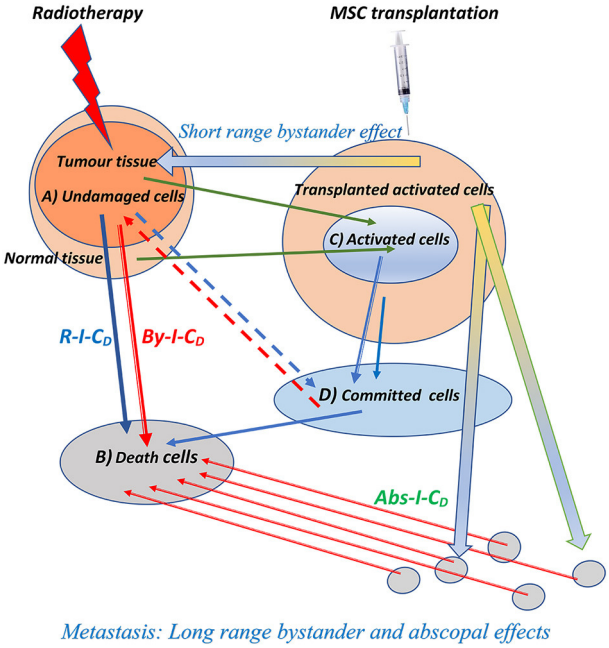

FIGURE 1 | Schematic representation of the biophysical model for direct, bystander, and abscopal actions of the radiotherapy and the enhancement produced by the addition of cellular therapy through mesenchymal cell transplantation simultaneously applied with radiation therapy. ***Rt-I-CD***, radiation-induced cell death on tumor cells; ***By-I-C$_D$***, short and long-range bystander-induced cell death on tumor cells; ***Abs-I-C$_D$***, abscopal-induced cell death on metastatic foci. The three types of induced cell death are enhanced by the combination of radiotherapy and cellular therapy, and the compartment of *activated cells* responsible for bystander and abscopal effects, labeled with (C) in the figure, may be enlarged by mesenchymal cell transplantation.

Committed Cells (D)

This compartment corresponds with the potentially lethal lesions in the LQ Equation (7, 39); cells in this compartment can flow back to compartments ***(A)*** or ***(B)*** through proper repair or binary misrepair.

Operational Terms

As operational purpose, we considered:

Short-Range Bystander Effect

It is generally accepted that the use of ionizing radiation to a treatment volume that contains the tumor causes effects that go beyond radiation-induced cell death (14), revealing intracellular transmission that implies the gap-junction intercellular connection and ends in cell death, enhanced amounts of DNA double-strand breaks, induction of

chromosomal aberrations, and/or alterations in transcript RNA levels and gene expression (50).

Long-Range Bystander Effects

Results obtained from "*in vivo*" irradiated tumors suggest that tumors may exert their influence far beyond its own microenvironment to spread peritumoral region and tissues far away from a tumor. The long-range bystander effect is generated by cytokines, macromolecules, and exosomes liberated into the extracellular space (38, 40, 44) that, through the lymphatic or vascular systems, might substantially alter conventional expectation in radiotherapy by yielding loco-regional positive effects (35).

Abscopal Effect

The abscopal effect is an anti-tumor radiation consequence seen in metastatic disease placed far away from the irradiated tissue. High-dose ablative radiotherapy results in release of debris of tumor cells containing molecules that may be immunogenic (51). Therefore, radiotherapy could imitate the effect of vaccination, as an unconventional method to present tumor antigens making cancer cells more receptive to T cell-mediated cytotoxicity (52). This effect could be associated first with the larger than usual effect of single doses by standard models (53), thus facilitating excellent local control rates, second to the unexpected abscopal effect. In this sense, new original associations of RT with immunotherapies have been designed to reverse tumor immune-related radioresistance (54), and the reactivation of the anti-tumor immune response can be considered as the 6th R of clinical radiobiology (36), opening an exciting field in patient treatment.

It is important to underline that unlike an increased reply concomitant with an escalation in radiation dose, the bystander reaction reaches a saturation level at comparatively low doses (18, 50).

The Mathematical Model

A key feature of bystander responses, as opposed to direct irradiation effects, is the dose–response relationship. Instead of a continuously increased response related with an increase in dose, the bystander response turns out to be saturated at low doses. This might indicate a receptor–ligand interaction, which we took as our original hypothesis (18), with the characteristic of being simultaneously dynamic and reversible. The same kinetic mechanism could be used to describe the antigen–antibody interaction.

Assuming the radiation and bystander consequences on tumor cell survival to be independent (38, 44), the whole response of the tumors and their metastatic foci to radiation therapy might be expressed as the product of the probability of radiation tumor cell death times the probability of cell death through bystander or abscopal effects (18, 37).

Data now indicate that, as well as these targeted DNA damage dependent effects, tumor cells and normal tissue-irradiated cells (activated cells) and immunological cell death also transmit signals to their adjacent cells (35). Here, we think that clonogenic cell survival $\boldsymbol{S}$ after radiation therapy depends together with the direct effects on DNA through radiation interaction $\boldsymbol{S_{RT}}$ and bystander and abscopal communication $\boldsymbol{\Pi\ S_{By}}$. Thinking that DNA damage caused by radiation and short- and long-ranged bystander effects on tumor cell survival are independent, the whole tumor response may be said as:

$$S = S_{RT} \cdot \prod_{i=1}^{n} S_{By(i)} \tag{1}$$

where the first term of the product of cell survival calculated using linear-quadratic model represents the pure RT action on the irradiated tumor and the second term, which begins with the Π symbol, is the product from $n = 1$ to $n = n$ of the cell death probabilities resulting from each one ($i = 1 \ldots i = n$) of the out-of-target cell death actions (bystander and abscopal effects) promoted for the combined treatment (RT + MSCs) that was used in our last papers. A set of these possibilities has been summarized here in the point section Activated Cells (C).

Following the same reasoning that we indicated in our previous paper (35), this entails that the chance of cell survival depends on both the direct radiation effect (the LQ model) and bystander effects, with these effects also being a phenomenon composed of long- and short-range bystander actions, whose importance, at least in experimental RT, may be estimated.

The final values of tumor cell survival (S) suggest that the lethal effects of radiation on tumor cells can be significantly enhanced by unanticipated interactions between live cells with the secretome of activated cells (14, 44) or with the molecules released after immunological cell death (42).

This model helps us to comprehend how anticancer treatment may have an additional and significant effect in that the radiation-activated MSC* cell response could be important for therapy to be successful due to the fact that the survival of tumor cells interconnecting with irradiated and activated cells is reduced.

THE LONG-RANGE BYSTANDER EFFECTS AND THE ABSCOPAL EFFECT OF RADIOTHERAPY

Anti-tumor consequences beyond the radiation field have been identified (43, 47, 55–61) and the regression of remote metastasis after tumor radiotherapy has been recently described in human melanoma skin cancer (48, 62, 63) and other tumor locations (64, 65).

Over recent years, the abscopal mechanism has been clarified by the effort of several investigators, including Formenti and Demaria (19, 20), who revealed that this activity was probably facilitated by the immune system leading to immunogenic cell death, a mechanism that implicates dendritic cells, T regulatory cells, and suppressor cells as key intermediaries. Radiation therapy sensitizes unresponsive tumors to the anti-neoplastic action of antibodies that target the inhibitory receptor CTLA-4 on T cells (66). Multiple studies have demonstrated that radiotherapy can increase the efficacy of anti-PD1 therapy by priming and recruiting more anti-tumor effector T cells (67, 68) and recently it has been suggested that the addition of immune checkpoint inhibition with local radiotherapy might increase

local and distant metastatic control and, in the end, the clinical results of disease control in patients with oligometastatic cancer (69). Moreover, the idea to generate an integrated clinical and molecular categorization of metastases along the spectrum of disease is very interesting, because this approach may perhaps influence the staging and treatment of patients with cancer diseases (70).

Golden and colleagues (42) were the first to prove that abscopal responses can be consistently identified in patients with confirmed solid metastatic cancer treated with radio- and immune-therapy. The combined treatment with and the granulocyte-macrophage colony-stimulating factor generated clear abscopal responses in certain patients with metastatic diseases, and this finding signifies a hopeful advance to establishing an *in situ* anti-tumor vaccine (71). Recently published results prove that radiotherapy in combination with the CTLA-4 blockade (72) or the PD1 blockade (68) produces systemic effects in patients with cancer. The early response in the TCR clonal dynamic detected in responders is coherent with a change and increase of the tumor-directed TCR repertoire provoked by radiation therapy and its study in representative cases means that increase of a huge amount of tumor-specific T cell clones in peripheral blood and their presence over time correlated well with the occurrence of abscopal outcomes (72). In spite of the growing number of clinical studies examining the ability of radiation to improve immunotherapy, clinical proof that it transforms cold tumors with little to no immune response into responsive ones remains elusive (66).

Nevertheless, it seems clear that reasonable combinations of immunotherapy with RT may dramatically change the model of care for many tumor types in the following decade (73).

MESENCHYMAL CELLS AS BIOLOGICAL RESPONSE MODIFIERS

It is generally recognized that MSCs can be found commonly in numerous tissues and are not limited to those of mesodermal origin, such as bone marrow, adipose, muscle, and bone (74). On the other hand, it has recently been revealed that *in vitro* differentiation of human MSCs is linked by an augmented sensitivity to apoptosis, which is in significant divergence to undifferentiated MSCs, which are moderately resistant to irradiation or temozolomide-induced DNA damage (75). We have demonstrated that MSCs are relatively sensitive to low-LET irradiation and very resistant to the bystander effect produced by the culture medium of irradiated cells (18).

Stem cell knowledge has also become the basic element in regenerative medicine (76, 77).

It is an exciting idea that inhibiting the mechanism that facilitates the bystander effect can give rise to therapeutic approaches that stimulate the radio-sensitivity of cells or protect healthy tissue against the damaging effects of ionizing radiation (78). Previous reports suggested a protective role for MSCs when combined with RT (79, 80). In effect, study on mesenchymal stem cell therapy for wounded and unhealthy tissues, involving the intestines, has been highly encouraging. Therapy with bone-marrow-derived or vascular-wall-derived MSCs protects the lung tissue from radiation-induced vascular damage and antagonizes the metastatic potential of circulating tumor cells to formerly irradiated lungs (81).

The use of human grade MSC is challenging and must fulfill EMA or FDA requirements to regulate autologous adult stem cells for therapeutic application. This has been widely summarized and discussed (82, 83) and we know that MSCs, commonly mentioned to as MSCs or mesenchymal stromal cells, are a varied population of cells that must be properly characterized. To clarify this controversial aspect, different papers have been published in the latest years (84–86) and contribute to the understanding of the composition of MSC-based products and provide the way to assess their *in vitro* and *in vivo* bioactivity.

Due to their properties, MSCs might be suitable as a therapeutic tool for handling radiation-induced normal tissue injury (84, 87). Numerous papers have demonstrated that administered either intraperitoneally or intravenously, MSCs effectively home onto primary tumors and their metastases (85, 86). Moreover, before supporting tissue repair functions, MSCs first organize the microenvironment by controlling inflammatory processes and releasing a variety of growth factors in reaction to the inflammation process (88). Due to their trophic, paracrine, and immunomodulatory functions, they may have the highest beneficial impact *in vivo* (89). However, the amount of MSCs that engraft into damaged tissues might not be enough to explain their robust protective effect.

The therapeutic efficacy of transplanted MSCs seems to be unconnected to the physical proximity of the transplanted cells to damaged tissue. Thus, we believe that the predominant mechanism by which MSCs contribute in tissue repair might be related to their paracrine activity, and in this way, it is also possible to think of the additional use of MSCs as an adjuvant to support and complement other therapeutic options as has recently been recently proposed (65, 90).

IS IT POSSIBLE TO WIDEN THE BYSTANDER AND ABSCOPAL RADIOTHERAPY EFFECTS?

MSCs have been studied for the treatment of cancers as they are able to home onto tumors and come to be incorporated into their stroma. Moreover, MSC homing is enhanced after radiotherapy (45). MSCs can both suppress or stimulate tumor progression (91–93). It has been described that the bioactivation of MSCs may be achieved by different treatments and the molecules secreted by the activated MSCs (MSCs*) could have an influence on a variety of immune cell lineages and establish a beneficial field (40).

We have recently shown that optimal bystander and abscopal effects can be obtained using MSCs plus RT administered on an experimental murine model with two xenotumors symmetrically placed in the upper region of both the rear legs, with only one of them being treated with radiotherapy (38, 44).

In a recently published article, the influence of MSC cell therapy on the progress of solid tumors using an orthotopic cancer model of human colorectal cancer cells has been studied, as well as in an immunocompetent rat model of colorectal carcinogenesis representative of human pathology (49). In their results, the authors show that MSC administration to immunocompetent rats treated topically with methylnitronitrosoguanidine (MNNG), a strong carcinogen, reduced the growth of the tumors and improved overall survival. In this experimental cancer model, the MSCs have strong action on colon cancer growth by altering the immune component of the tumor microenvironment. In an important concordance with our research (38, 44), when MSCs were administered after therapy of colorectal cancer (CRC) with fractionated irradiation, MSCs reduced tumor growth, extended animal survival, and reduced the presence of metastatic foci.

The MSCs also protected healthy tissue from radiation damage by rising the levels of growth factors, reducing fibrosis, and facilitating intestinal recovery (49).

Taking into account both the previous reports and our own experience and research on the extraordinary abilities of proliferation (94, 95), secretion (44, 96), and differentiation (95) of the umbilical cord mesenchymal cells that we have investigated (38, 44) and used in combination with radiotherapy in recent years, we have developed the following hypothesis:

> "Radiotherapy may not only be a successful local and regional treatment but also a novel systemic cancer therapy" (38).

To check this hypothesis, we used a set of human cancer cell lines implanted in NSG mice as xenotumors and MSCs obtained from human umbilical cord stroma. We have investigated the tumor response to direct irradiation (2Gy low-LET radiation fraction administered once a week for 5–6 weeks) and, in the non-irradiated contralateral tumor, the tumor sensitivity to the bystander effect.

In our experiments, mice with tumors larger than 60 mm^3 were treated with an intraperitoneal administration of 10^6 MSC once a week for 5–6 successive weeks (38, 44). The day after each cellular therapy, one of the four groups of mice was randomly chosen to have one of their tumors irradiated. Ionizing radiation was delivered by X-ray TUBE (YXLON, model Y, Tu 320-D03) as explained previously (38, 44). The treatment was repeated once a week for a total of 5–6 weeks. The other mice groups were treated with exclusively RT or exclusively MSC. The mice in the control group received no treatment (38, 44).

We have proved that tumor cell loss induced after treatment with radiotherapy enhances with the therapeutic combination of RT and MSCs, when compared to RT alone, in the three cell lines (A375, G361, and MCF7) used, and also that, through the bystander and abscopal effect, the therapeutic combination (RT + MSC) had a positive effect on the tumor-volume reduction of the contralateral, untreated tumor (**Table 1**). When the cell line used had metastatic potential, the combination (RT + MSC) produced a reduction in the microscopic number of metastasis in the internal organs of mice with A375 xenotumors (44). These results prove conclusively that the combination of MSC + RT produces a synergic, bystander, and abscopal effect.

In **Table 1**, notice the differences in the tumor volume doubling time values (T_D) corresponding to different cell lines treated with RT (from 7.60 to 17.60 days) and observe, also, the differences between the control and MSC+RT groups for each of the tumor cell lines implanted as xenotumors (from 22.5 to 38.9 days) and the gains derived from the addition of MSC to the RT treatment, measured as the mesenchymal cell enhancement ratio (MSC-ER), ranged between 1.60 and 2.00 and more than 3.00 for A375 in our last paper (44) designed to evaluate the anti-metastatic potential of MSCs combined with RT, when the tumor volume was followed only in the first 14 days.

It is important to analyze that the time-to-tumor growth to a volume of 2 ml reached an increase in time ranging between 12% for A375, the most aggressive cell line, and 117% for MCF7, the least aggressive. For details on the mathematical model used [see (38, 44)]. It is important to highlight that G361 and A375 are human melanoma cell lines, whereas MCF7 is a cell derived from a human breast cancer.

We define cell loss factor as $CL = 100 \cdot [1 - T_D(control)/T_D(\text{treatment})]$; in which T_D(treatment) is the volume doubling time in each of the treatment groups: MSC +RT and RT.

MSC-ER: the mesenchymal enhancement ratio is the ratio between the cell loss corresponding to the combined treatment divided by the cell loss corresponding to the treatment with radiotherapy alone.

CL: in the cell-loss factor, the following are included: (i) all the types of cell death, (ii) lengthening of the mean cell cycle duration produced by the treatment, and (iii) cells that have a null or limited growth potential due to misrepair of damage or because they have been involved in a differentiation process.

The abscopal effect has been estimated by the reduction of metastasis index that was 60% in the A375 cell line, with the difference between the control and RT + MSC groups being statistically significant ($P = 0.002$). In our experiments, A375 is the only cell line that has showed metastatic potential. It is very important to note that the amount of metastatic foci observed in the internal organs of the mice treated with MSC + RT was 60% fewer than in the mice treated with RT alone (44).

Moreover, in our last paper (44) (supplementary materials), we demonstrated that MSC, previously activated with 2 Gy low-LET radiation dose (MSC*) and used after tumor radiotherapy as adjuvant cellular therapy, retained a wide cytotoxic activity that affected the volume of the xenotumors treated, thus enhancing the therapeutic effect of radiotherapy in a similar level to that we have communicated previously (38, 44). Using these MSC*-activated cells, we found that when the tumors implanted in mice were first treated with radiotherapy and then treated immediately after the end of RT with infused intraperitonially MSC* activated, the tumors treated in this way significantly reduced their tumor growth rate compared with both control mice and mice treated with radiotherapy alone.

TABLE 1 | Characteristic growth kinetics parameters of the treatment of xenografts implanted in NSG mice on control and MSC + RT groups.

Parameter	Tumor cell line					
	G361		A375		MCF7	
	RT	MSC + RT	RT	MSC + RT	Control	MSC + RT
T_D (days)	11.5 (CI: 10.6–12.6)	22.5 (CI: 18.7–28.1)	7.6 (CI: 5.3–5.7)	8.5 (CI: 8.1–8.9)	17.6 (CI: 17.2–18.2)	38.9 (CI: 32.3–47.5)
CL (% days^{-1})	47.0	72.3	9.6	18.8	–	55.9
MSC-ER	1.6		2.0		Not calculated	
T-t-G (days)	60.8	91.1	32.8	36.6	195.0	422.3
Mx	No		Yes: 1.0±0.4	Yes: 0.4±0.1	No	
	% reduction Mx index: 60%; $P = 0.002$					

T_D, tumor volume doubling time (days); CL, cell loss factor in a treated tumor compared to a control tumor (%·days^{-1}); MSC-ER, radiotherapy mesenchymal cell enhancement ratio = (cell loss produced by the combination RT + MSC)/(cell loss produced by RT alone); T-t-G, time-to-tumor growth (days) to reach a volume of 2.0 ml; Mx, Metastasis index: % of decrease in the histological identification of microscopic metastasis in the MSC + RT group, compared to the control group; CI, confidence interval.

Accordingly, the results obtained in our study regarding the tumor doubling time (T_D) values were different among the groups, being longer for mice treated with RT + MSC* (8.46 days), compared with the control and RT groups (6.87 and 7.60 days, respectively).

Mesenchymal enhancement ratio (MSC-ER) is the ratio of tumor effect produced by the combination of radiotherapy plus MSCs therapy (RT + MSC*) divided by the tumor effect produced by exclusive radiotherapy. By means of doubling the time values, we have calculated the MSC*-ER values as the proportion of cell loss C_L (38) produced by RT + MSC* treatment, compared to the cell loss C_L produced by radiotherapy treatment alone and demonstrated that activated MSC* potentiated the radiotherapy effect when infused into tumor-bearing mice with a MSC*-ER of:

$$\text{MSC}^* - \text{ER} = \frac{\text{C}_\text{L}\ (\text{RT} + \text{MSC}^*\ \text{treatment})}{\text{C}_\text{L}\ (\text{RT treatment})} = \frac{18.\ 8\%}{9.6\%} = 1.95 \tag{2}$$

This result fits with previous results summarized in **Table 1** and proves that the combination (RT + MSC*) improves the therapeutic efficiency respect to RT alone (both in tumor and metastatic control) through enhancing short- and long-range bystander and abscopal effects. For more details on the mathematical model applied [see supplementary materials in (37)].

CELLULAR THERAPY WITH MSCS: A PROBLEM FOR ANTI-TUMOR THERAPY?

MSCs exist in many tissues and are recognized to actively be recruited to primary tumors and metastasis and also to other locations of normal tissue damaged, where they take part in wound repair. Tumors can be thought of as "wounds that never heal" and, in reply to signals from the neoplastic tissue, the MSCs can exhibit a marked tropism that might contribute to tumor growth promotion by several mechanisms that have been reviewed recently (97).

Tumors continuously recruit cells from the tumor microenvironment and become important elements of the tumor volume, interchanging proper signals that might acquire aggressive phenotypes of carcinoma cells and establish a complicated situation that concludes in metastasis (98). Recently, it has become apparent that tumor-associated MSCs have an effective role in tumor induction, promotion, growth, and metastasis (99), and although the tumor microenvironment is constituted of numerous cell types including tumor, stromal, endothelial, and immune cell populations, it appears clear that, under the influence of these cells, MSCs acquire different functional phenotypes that promote tumorigenesis (100), permitting the tumor to avoid immune clearance or impeding effectiveness through the acquisition of a chemotherapy and radiotherapy resistance mechanisms (101). On the other hand, it has been described that, in an inflammatory situation, resident tumor MSCs strikingly enhanced tumor growth by engaging monocytes/macrophages in comparison to bone marrow MSCs (102, 103) and exosomes present in the cancer cell secretome might be the principal agent able to modify the normal MSC cell phenotype toward a malignant one (104).

Nevertheless, it is still controversial whether this innate tropism of MSCs toward the tumors and metastatic foci is linked with cancer promotion or suppression (105), and it has been suggested that a better understanding of the interactions between cancerous cells and stromal components of tumor microenvironment is important to allow progress in the development of more specific and useful therapies in cancer (99, 100, 106).

EXOSOMES SECRETED FROM MSCS HAVE A TOTALLY DIFFERENT EFFECT FROM THE EXOSOMES RELEASED FROM TUMOR CELLS

Cancer cell-derived exosomes have been shown to participate in the key steps of the metastatic widening of a primary tumor, ranging from oncogenic reprogramming of malignant cells to the formation of pre-metastatic niches (107) and this

mechanism may be facilitated by RT under certain conditions (108, 109) or facilitated by released mir-939 in exosomes that, once internalized in endothelial cells, play a protumorigenic role for metastatic spread in association with triple-negative breast cancers (110).

By studying the exosomes and microvesicles released by tumor cells into the extracellular medium, we have been able understand that exosomes from tumor cells spread through the biological fluids and support tumor growth and metastasis formation (111, 112). There are several examples that confirm this hypothesis; for example, it is well-known that the process of cancer cell migration into the normal tissues and invasion-promoting effects may be due to cancer-cell-derived exosomes (113, 114). After release, the exosomes are taken up by neighboring or remote cells facilitating tumor progression and the miRNAs confined within the exosomes modify such processes as interfering with tumor immunity and the microenvironment, suggesting that exosomal miRNAs have a noteworthy role in regulating cancer progression (115).

Pancreatic ductal adenocarcinoma (PDAC) is an exceptionally aggressive tumor, characterized by a high metastatic potential, even at the point of diagnosis; in a recent paper (116), using proteomic studies, it has been shown that it is possible to identify the impact of exosomes on the Kuppfer cells in the liver, which may function to organize this organ for metastatic occupation. Recently, the exosome-mediated transfer of pyruvate kinase M2 (PKM2) from PCa cells into bone marrow stromal cells (BMSCs) has been identified as a new process through which primary tumor-derived exosomes stimulate premetastatic niche development (117).

Other published results (118) suggest that exosome-mediated discharge of tumor-suppressor miRNA is selected in tumor evolution as a mechanism to organize the activation of a metastatic cascade (119). The load of exosomes is given for the parental cells and the circumstances in which they deliver them, which implies that circulating miRNAs in exosomes have the ability to serve as prognostic and predictive biomarkers (120).

However, exosomes derived from MSCs play a completely different role, and previous reports have suggested a protective role for MSCs when combined with RT. Indeed, therapy with bone-marrow-derived MSCs or vascular-wall-derived MSCs protects the lung tissue from radiation-induced vascular dysfunction and antagonizes increased metastases of circulating tumor cells to previously irradiated lungs (81).

Exosomes produced by MSCs have been demonstrated to contain antiapoptotic miRNAs to improve epithelial and endothelial wound healing and angiogenesis, and to include growth factor receptor mRNAs, well-known to facilitate wound recovery and safeguard the intestines from experimental necrotizing enterocolitis (121). Results of the research on mesenchymal stem cell therapy for wounded and unhealthy tissues, including the intestines, have been highly promising (79, 80) and MSCs may be considered as a therapeutic tool to deal with radiation-induced tissue damage (87).

It is important to underline that the group of Chapel et al. (122) has initiated a phase 2 clinical trial (ClinicalTrials.gov Identifier: NCT02814864) for the treatment of severe adverse effects for patients receiving radiotherapy for prostate cancer and that this clinical trail is supported by numerous papers focused on the use of MSCs for alleviating the side effects on normal tissues after radiation therapy (123–125).

However, the biodistribution and the mechanism involved in the control of colateral side effects are not well-known, although there are also some reports directed to investigating this problem in more depth. But we do know that in an undamaged mouse, exogenous intravenously injected MSCs quickly accumulate within the lungs and are cleared from this site to other tissues, such as the liver, within days (126). Nevertheless, the quantity of MSCs that are uptaked for the injured tissues may not be sufficient to explain their strong protective effects.

Moreover, in a cancer rat model used to study the treatment of chemical-induced colorectal cancer (CRC) previously cited (49), it has been demonstrated that exogenous MSCs, although only briefly found in the colon tissue of treated animals, were able to alter the immune profile of the tissue microenvironment as far as 1 year after the last MSC administration, possibly due to polarization of resident MSCs and immune cells.

To sum up, it is generally accepted that MSC-derived microvesicles and exosomes have been proposed as a novel mechanism of cell-to-cell communication that permits the transmission of functional proteins or genetic material via mRNAs and microRNAs upon cell activation that may encourage a new approach for repairing acutely damaged organs by virtue of the exclusive MSC tropism for the injured tissue, as well as their paracrine action in nature and facilitated through the decrease of inflammation and enhancement of tissue repair (127).

On the other hand, our *in vitro* and *in vivo* results show that TRAIL and DKK3 are molecules delivered by mesenchymal cells that, as consequence of the cell treatment with 2 Gy low-LET gamma radiation, are released to the extracellular space where they can work as signaling molecules to yield tumor cell death (38, 44). The ability of MSCs to release TRAIL to culture medium that inhibits the growth of human cancer cells has recently been confirmed (128). Exosomes and microvesicles also appear in the extracellular medium of cell cultures that are quantitatively, qualitatively, and functionally different if they are removed from the MSC medium or from the activated MSC medium (44).

Together, all these results indicate that the administration of MSCs might be a safe and innovative therapeutic alternative to heal normal tissue after cancer radiotherapy (49).

ANNEXIN A1 AS A CANDIDATE FOR ENHANCING RADIOTHERAPY

When we examined the exosome load before and after the activation of MSCs with RT, we noticed statistically significant differences between the results of the proteomic analysis corresponding to the samples.

We have described that there are qualitative, quantitative, and functional variations among the proteins included in the exosomes found from MSCs and activated MSCs* (44). Thus, the comparison between cells studied in basal and in activated

states shows that whereas the amounts of very significant common GO terms and MSC GO terms are in concordance, the results produced a significant variability and number of pathways modified in MSCs* (44), and it demonstrates the intense metabolic change that these activated cell exosomes have suffered and the consequences after activation with radiation. Among the cluster representatives in MSCs*, we underline the leukocyte cell–cell adhesion, cell localization, and negative control of responses to activation and cell death. Several of these proteins are important elements of cell–cell or cell–matrix adhesion and include annexin and integrins. Among them, the presence of ANXA1 is very significant because it is always present in the exosomes secreted from MSCs* and constantly absent in MSCs.

We have verified these findings using quantitative mRNA-PCR to measure the mRNA of this molecule in MSCs and MSCs* and demonstrated that mRNA is dramatically induced in MSCs after irradiation, which supports the massive presence of ANXA1 in the exosomes released by MSCs* (44). Especially relevant is the presence of ANXA 1 in the exosomes from activated MSCs* and the absence of this protein in the conditioned medium separated from the non-irradiated MSCs.

During more than 30 years of research, annexins have been established as key elements in the control immune responses. The prototype member of this family, ANXA1, has been broadly accepted as an anti-inflammatory intermediary influencing migration and cellular reactions of various specialized cell types of the innate immune system (129). Nevertheless, it is now accepted that ANXA1 has extensive effects beyond the immune system with consequences in preserving homeostatic secretion, fetal development, the aging process, and development of several diseases such as cancer (130, 131).

Inflammation is a strongly controlled process, initiated after tissue damage or infection. If uncontrolled or unresolved, the inflammation itself can drive additional tissue destruction and cause persistent inflammatory disorders and autoimmunity with following deficiency of organ function. It is now clear that the control of inflammation is a functional process that appears during an acute inflammatory incident (132). Following cell activation and release, ANXA1 inhibits the accumulation of neutrophils in the tissue injured by numerous mechanisms; furthermore, ANXA1 promotes neutrophil apoptosis and takes actions on macrophages to stimulate the phagocytosis and the elimination of dead neutrophils (132, 133) and leads to the rapid restoration of tissue homeostasis. Inflammation outcome is regulated by numerous endogenous factors, involving fatty-acid-derived specialized pre-resolving mediators and protein, such as ANXA1 (134).

There is mounting evidence that ANXA1, and its mimetic peptides (135), may have a major function in mitigating ischemia–reperfusion injury-associated complications (136). Moreover, chronic inflammation in tumors is frequent and promotes tumor growth, progression, and metastatic spreading, as well as treatment resistance (137). Physical aberrancies of tumor vasculature comprise their chaotic organization, an enhanced interstitial pressure, an amplified solid stress, hypoxia, and a progressive contraction of solid tumors that are the physical barriers in tumors (138) and are inspiring new anti-cancer strategies aimed at targeting and normalizing the physical anomalies of these solid tumors (139).

On the other hand, the overexpression of this molecule has been reported in many cancers, although its clinical meaning is still controversial (140–142), which could be, in part, due to the localization of ANXA1 in the nuclear and cytoplasmic compartments, and also associated to the membrane (131). In fact, the expression level of ANXA1 is down-regulated in numerous types of cancer and is linked with metastasis, relapse, and poor prognosis (141, 143); ANXA1 is an endogenous inhibitor of NF-κB that may be stimulated in human cancer cells and in experimental mice models by powerful anti-inflammatory glucocorticoids and altered by non-steroidal anti-inflammatory drugs (143). In this context, ANXA1 has long been categorized as an anti-inflammatory molecule due to its influence over leukocyte-mediated immune responses (144).

Upon tissue damage, epithelial wound closure is a finely adjusted process detected in chronic inflammatory diseases related with non-healing wounds. In this process, ANXA1 is involved as a pre-resolving mediator (145). ANXA1 is a glucocorticoid-induced protein that is well-known to reproduce numerous anti-inflammatory effects of glucocorticoids and is implicated in the modulation of T-cell function and the adaptive immune response related to rheumatoid arthritis (146) and increasing data suggest that ANXA1, which act together with the formyl peptide receptor family, might have a major role in alleviating ischemia–reperfusion injury (136). ANXA1 interacts with p53 to co-regulate Bid expression and stimulate cell death after OGD/R via the caspase-3 pathway (147) and it has been described that ANXA1 is one of the molecules that is involved in p53-mediated radio-response and the abnormal expression of ANXA1 in nasopharyngeal carcinoma NPC might affect the apoptosis of tumor cells caused by ionizing radiation decreasing radiotherapeutic efficacy (148).

Recently, the function of ANXA1 in the therapy of acute radiation-induced lung injury has been analyzed and the mechanism of its action is investigated (149). The role of damage-associated molecular patterns in neuro-inflammation has been implicated in adverse neurological outcomes following lethal hemorrhagic shock and polytrauma. Data obtained in (150) provide new suggestion that appealing pro-resolving pharmacological approaches such as Annexin-A1 biomimetic peptides can effectively reduce neuro-inflammation and new data show a new multifaceted role for ANXA1 as a therapeutic and a prophylactic drug due to its capacity to stimulate endogenous pro-resolving, anti-thrombo-inflammatory circuits in cerebral ischemia–reperfusion injury (151). Finally, the chance of exploiting ANXA1 as a novel therapeutic molecule in diabetes and for treatment of microvascular disease has been announced (152).

CONCLUSIONS

Considering all the information summarized in this review, we are convinced that, due to (i) the physical hallmarks and

biological capabilities (153) that characterize neoplastic tissues, (ii) the physical–chemical tropism of MSCs (154), and (iii) the widespread functions of macromolecules, proteins, and exosomes, all these factors secreted by activated MSCs* are able to reduce pro-tumorigenic and pro-metastatic signals released by tumors that influence the progression, growth, spread, and drug resistance of tumor cells.

However, additional study is required to find the cause of tumor cells forsaking malign phenotypes of cancer cells and returning to their normal state.

We have recently shown that clinical grade umbilical cord MSCs can be expanded, cryogenically stored, and reconstituted after batch release, maintaining their immunophenotype, and show good viability and activation by irradiation. Our study indicates that no toxic effects are produced by MSCs or pre-irradiated MSC* inoculation. In addition, umbilical cord MSCs* have never been detected in any studied organ at 90 days, indicating that these cells will not be present for a long time in a treated patient (manuscript in preparation).

In an attempt to take our basic and regulatory research to clinical practice, we proceeded to apply for the registration of the patent P201500022 and title "*Activated stem cells and medical uses*," with the priority date of December 2014. Its international extension via PCT has the number PCT/ES2015/070951 (WO/2016/102735) and was published in June 2016.

Therefore, we conclude that umbilical cord mesenchymal cells combined with radiotherapy are adequate for therapeutic use in a clinical trial in patients with cancer due to the fact that increasing the therapeutic effect of radiotherapy on the tumors and possible metastatic foci improves the radiotherapy outcome.

AUTHOR CONTRIBUTIONS

JR and FO conceived and wrote the manuscript. VF performed most of the *in vitro* and *in vivo* experiments. FO'V performed immunohistochemistry. JE, RM, and IT critically revised the manuscript for important clinical observations. All the authors read and approved the final manuscript.

FUNDING

This work was supported by the Spanish Ministry of Economy and Competitiveness, MINECO: SAF201240011-C02-02 and SAF2015-70520-R to JR; CNPq, Conselho Nacional de Desenvolvimento Científico e Tecnológico—Brasil to VF; project of Excellence from the Andalusian Regional Government P12CTS-383 to FO; and the Spanish Ministry of Economy and Competitiveness SAF2012-40011-C02-01, SAF2015-70520-R, RTICC RD12/0036/0026, and CIBER Cáncer ISCIII CB16/12/00421 to FO, VF, and JR.

REFERENCES

1. Singletary SE, Allred C, Ashley P, Bassett LW, Berry D, Bland KI, et al. Staging system for breast cancer: revisions for the 6th edition of the AJCC cancer staging manual. *Surg Clin North Am*. (2003) 83:803–19. doi: 10.1016/S0039-6109(03)00034-3
2. West CM, McKay MJ, Holscher T, Baumann M, Stratford IJ, Bristow RG, et al. Molecular markers predicting radiotherapy response: report and recommendations from an International Atomic Energy Agency technical meeting. *Int J Radiat Oncol Biol Phys*. (2005) 62:1264–73. doi: 10.1016/j.ijrobp.2005.05.001
3. Robnett TJ, Machtay M, Vines EF, McKenna MG, Algazy KM, McKenna WG. Factors predicting severe radiation pneumonitis in patients receiving definitive chemoradiation for lung cancer. *Int J Radiat Oncol Biol Phys*. (2000) 48:89–94. doi: 10.1016/S0360-3016(00)00648-9
4. West CM, Elliott RM, Burnet NG. The genomics revolution and radiotherapy. *Clin Oncol*. (2007) 19:470–80. doi: 10.1016/j.clon.2007.02.016
5. Burnet NG, Johansen J, Turesson I, Nyman J, Peacock JH. Describing patients' normal tissue reactions: concerning the possibility of individualising radiotherapy dose prescriptions based on potential predictive assays of normal tissue radiosensitivity. Steering Committee of the BioMed2 European Union Concerted Action Programme on the development of predictive tests of normal tissue response to radiation therapy. *Int J Cancer*. (1998) 79:606–13. doi: 10.1002/(SICI)1097-0215(19981218)79:6<606::AID-IJC9>3.0.CO;2-Y
6. Lopez E, Guerrero R, Nunez MI, del Moral R, Villalobos M, Martinez-Galan J, et al. Early and late skin reactions to radiotherapy for breast cancer and their correlation with radiation-induced DNA damage in lymphocytes. *Breast Cancer Res*. (2005) 7:R690–8. doi: 10.1186/bcr1277
7. Peacock JH, de Almodovar MR, McMillan TJ, Steel GG. The nature of the initial slope of radiation cell survival curves. *BJR Suppl*. (1992) 24:57–60.
8. Brown JM, Carlson DJ, Brenner DJ. The tumor radiobiology of SRS and SBRT: are more than the 5 Rs involved? *Int J Radiat Oncol Biol Phys*. (2014) 88:254–62. doi: 10.1016/j.ijrobp.2013.07.022
9. Steel GG, McMillan TJ, Peacock JH. The 5Rs of radiobiology. *Int J Radiat Biol*. (1989) 56:1045–8. doi: 10.1080/09553008914552491
10. Fowler JF. The linear-quadratic formula and progress in fractionated radiotherapy. *Br J Radiol*. (1989) 62:679–94. doi: 10.1259/0007-1285-62-740-679
11. Fowler JF. 21 years of biologically effective dose. *Br J Radiol*. (2010) 83:554–68. doi: 10.1259/bjr/31372149
12. Herskind C, Ma L, Liu Q, Zhang B, Schneider F, Veldwijk MR, et al. Biology of high single doses of IORT: RBE, 5 R's, and other biological aspects. *Radiat Oncol*. (2017) 12:24. doi: 10.1186/s13014-016-0750-3
13. Marples B, Joiner MC. The response of Chinese hamster V79 cells to low radiation doses: evidence of enhanced sensitivity of the whole cell population. *Radiat Res*. (1993) 133:41–51. doi: 10.2307/3578255
14. Mothersill C, Seymour CB. Radiation-induced bystander effects–implications for cancer. *Nat Rev Cancer*. (2004) 4:158–64. doi: 10.1038/nrc1277
15. Mothersill CE, Moriarty MJ, Seymour CB. Radiotherapy and the potential exploitation of bystander effects. *Int J Radiat Oncol Biol Phys*. (2004) 58:575–9. doi: 10.1016/j.ijrobp.2003.09.038
16. Prise KM, Schettino G, Folkard M, Held KD. New insights on cell death from radiation exposure. *Lancet Oncol*. (2005) 6:520–8. doi: 10.1016/S1470-2045(05)70246-1
17. Marples B, Wouters BG, Joiner MC. An association between the radiation-induced arrest of G2-phase cells and low-dose hyper-radiosensitivity: a plausible underlying mechanism? *Radiat Res*. (2003) 160:38–45. doi: 10.1667/RR3013
18. Gomez-Millan J, Katz IS, Farias Vde A, Linares-Fernandez JL, Lopez-Penalver J, Ortiz-Ferron G, et al. The importance of bystander effects in radiation therapy in melanoma skin-cancer cells and umbilical-cord stromal stem cells. *Radiother Oncol*. (2012) 102:450–8. doi: 10.1016/j.radonc.2011.11.002

19. Formenti SC, Demaria S. Systemic effects of local radiotherapy. *Lancet Oncol*. (2009) 10:718–26. doi: 10.1016/S1470-2045(09)70082-8
20. Formenti SC, Demaria S. Radiation therapy to convert the tumor into an *in situ* vaccine. *Int J Radiat Oncol Biol Phys*. (2012) 84:879–80. doi: 10.1016/j.ijrobp.2012.06.020
21. Dickey JS, Redon CE, Nakamura AJ, Baird BJ, Sedelnikova OA, Bonner WM. H2AX: functional roles and potential applications. *Chromosoma*. (2009) 118:683–92. doi: 10.1007/s00412-009-0234-4
22. Azzam EI, de Toledo SM, Little JB. Expression of CONNEXIN43 is highly sensitive to ionizing radiation and other environmental stresses. *Cancer Res*. (2003) 63:7128–35.
23. Demaria S, Coleman CN, Formenti SC. Radiotherapy: changing the Game in Immunotherapy. *Trends Cancer*. (2016) 2:286–94. doi: 10.1016/j.trecan.2016.05.002
24. Demaria S, Golden EB, Formenti SC. Role of local radiation therapy in cancer immunotherapy. *JAMA Oncol*. (2015) 1:1325–32. doi: 10.1001/jamaoncol.2015.2756
25. Azzam EI, de Toledo SM, Little JB. Oxidative metabolism, gap junctions and the ionizing radiation-induced bystander effect. *Oncogene*. (2003) 22:7050–7. doi: 10.1038/sj.onc.1206961
26. Goodhead DT. New radiobiological, radiation risk and radiation protection paradigms. *Mutat Res*. (2010) 687:13–6. doi: 10.1016/j.mrfmmm.2010.01.006
27. López E, Núñez MI, Guerrero MR, del Moral R, de Dios Luna J, del Mar Rodríguez M, et al. Breast cancer acute radiotherapy morbidity evaluated by different scoring systems. *Breast Cancer Res Treat*. (2002) 73:127–34. doi: 10.1023/A:1015296607061
28. Little JB. Genomic instability and bystander effects: a historical perspective. *Oncogene*. (2003) 22:6978–87. doi: 10.1038/sj.onc.1206988
29. Barcellos-Hoff MH, Brooks AL. Extracellular signaling through the microenvironment: a hypothesis relating carcinogenesis, bystander effects, and genomic instability. *Radiat Res*. (2001) 156(5 Pt 2):618–27. doi: 10.1667/0033-7587(2001)156[0618:ESTTMA]2.0.CO;2
30. Burdak-Rothkamm S, Rothkamm K, Prise KM. ATM acts downstream of ATR in the DNA damage response signaling of bystander cells. *Cancer Res*. (2008) 68:7059–65. doi: 10.1158/0008-5472.CAN-08-0545
31. Ivanov VN, Zhou H, Ghandhi SA, Karasic TB, Yaghoubian B, Amundson SA, et al. Radiation-induced bystander signaling pathways in human fibroblasts: a role for interleukin-33 in the signal transmission. *Cell Signal*. (2010) 22:1076–87. doi: 10.1016/j.cellsig.2010.02.010
32. Luce A, Courtin A, Levalois C, Altmeyer-Morel S, Romeo PH, Chevillard S, et al. Death receptor pathways mediate targeted and non-targeted effects of ionizing radiations in breast cancer cells. *Carcinogenesis*. (2009) 30:432–9. doi: 10.1093/carcin/bgp008
33. Seymour CB, Mothersill C. Delayed expression of lethal mutations and genomic instability in the progeny of human epithelial cells that survived in a bystander-killing environment. *Radiat Oncol Investig*. (1997) 5:106–10. doi: 10.1002/(SICI)1520-6823(1997)5:3<106::AID-ROI4>3.0.CO;2-1
34. Lambin P, van Stiphout RG, Starmans MH, Rios-Velazquez E, Nalbantov G, Aerts HJ, et al. Predicting outcomes in radiation oncology–multifactorial decision support systems. *Nat Rev Clin Oncol*. (2013) 10:27–40. doi: 10.1038/nrclinonc.2012.196
35. Lara PC, Lopez-Penalver JJ, Farias Vde A, Ruiz-Ruiz MC, Oliver FJ, Ruiz de Almodovar JM. Direct and bystander radiation effects: a biophysical model and clinical perspectives. *Cancer Lett*. (2015) 356:5–16. doi: 10.1016/j.canlet.2013.09.006
36. Boustani J, Grapin M, Laurent PA, Apetoh L, Mirjolet C. The 6th R of radiobiology: reactivation of anti-tumor immune response. *Cancers*. (2019) 11:E860. doi: 10.3390/cancers11060860
37. Ebert MA, Suchowerska N, Jackson MA, McKenzie DR. A mathematical framework for separating the direct and bystander components of cellular radiation response. *Acta Oncol*. (2010) 49:1334–43. doi: 10.3109/0284186X.2010.487874
38. de Araujo Farias V, O'Valle F, Lerma BA, Ruiz de Almodovar C, Lopez-Penalver JJ, Nieto A, et al. Human mesenchymal stem cells enhance the systemic effects of radiotherapy. *Oncotarget*. (2015) 6:31164–80. doi: 10.18632/oncotarget.5216
39. Curtis SB. Lethal and potentially lethal lesions induced by radiation–a unified repair model. *Radiat Res*. (1986) 106:252–70. doi: 10.2307/3576798
40. Lee RH, Yoon N, Reneau JC, Prockop DJ. Preactivation of human MSCs with TNF-alpha enhances tumor-suppressive activity. *Cell Stem Cell*. (2012) 11:825–35. doi: 10.1016/j.stem.2012.10.001
41. Herskind C, Wenz F, Giordano FA. Immunotherapy combined with large fractions of radiotherapy: stereotactic radiosurgery for brain metastases-implications for intraoperative radiotherapy after resection. *Front Oncol*. (2017) 7:147. doi: 10.3389/fonc.2017.00147
42. Golden EB, Apetoh L. Radiotherapy and immunogenic cell death. *Semin Radiat Oncol*. (2015) 25:11–7. doi: 10.1016/j.semradonc.2014.07.005
43. Van der Meeren A, Monti P, Vandamme M, Squiban C, Wysocki J, Griffiths N. Abdominal radiation exposure elicits inflammatory responses and abscopal effects in the lungs of mice. *Radiat Res*. (2005) 163:144–52. doi: 10.1667/RR3293
44. de Araujo Farias V, O'Valle F, Serrano-Saenz S, Anderson P, Andres E, Lopez-Penalver J, et al. Exosomes derived from mesenchymal stem cells enhance radiotherapy-induced cell death in tumor and metastatic tumor foci. *Mol Cancer*. (2018) 17:122. doi: 10.1186/s12943-018-0867-0
45. Kim SM, Oh JH, Park SA, Ryu CH, Lim JY, Kim DS, et al. Irradiation enhances the tumor tropism and therapeutic potential of tumor necrosis factor-related apoptosis-inducing ligand-secreting human umbilical cord blood-derived mesenchymal stem cells in glioma therapy. *Stem Cells*. (2010) 28:2217–28. doi: 10.1002/stem.543
46. Manda G, Isvoranu G, Comanescu MV, Manea A, Debelec Butuner B, Korkmaz KS. The redox biology network in cancer pathophysiology and therapeutics. *Redox Biol*. (2015) 5:347–57. doi: 10.1016/j.redox.2015.06.014
47. Szeifert GT, Salmon I, Rorive S, Massager N, Devriendt D, Simon S, et al. Does gamma knife surgery stimulate cellular immune response to metastatic brain tumors? A histopathological and immunohistochemical study. *J Neurosurg*. (2005) 102(Suppl):180–4. doi: 10.3171/sup.2005.102.s_supplement.0180
48. Postow MA, Callahan MK, Barker CA, Yamada Y, Yuan J, Kitano S, et al. Immunologic correlates of the abscopal effect in a patient with melanoma. *N Engl J Med*. (2012) 366:925–31. doi: 10.1056/NEJMoa1112824
49. Francois S, Usunier B, Forgue-Lafitte ME, L'Homme B, Benderitter M, Douay L, et al. Mesenchymal stem cell administration attenuates colon cancer progression by modulating the immune component within the colorectal tumor microenvironment. *Stem Cells Transl Med*. (2019) 8:285–300. doi: 10.1002/sctm.18-0117
50. Prise KM, O'Sullivan JM. Radiation-induced bystander signalling in cancer therapy. *Nat Rev Cancer*. (2009) 9:351–60. doi: 10.1038/nrc2603
51. Nesslinger NJ, Sahota RA, Stone B, Johnson K, Chima N, King C, et al. Standard treatments induce antigen-specific immune responses in prostate cancer. *Clin Cancer Res*. (2007) 13:1493–502. doi: 10.1158/1078-0432.CCR-06-1772
52. Garnett CT, Palena C, Chakraborty M, Tsang KY, Schlom J, Hodge JW. Sublethal irradiation of human tumor cells modulates phenotype resulting in enhanced killing by cytotoxic T lymphocytes. *Cancer Res*. (2004) 64:7985–94. doi: 10.1158/0008-5472.CAN-04-1525
53. Chakraborty M, Abrams SI, Coleman CN, Camphausen K, Schlom J, Hodge JW. External beam radiation of tumors alters phenotype of tumor cells to render them susceptible to vaccine-mediated T-cell killing. *Cancer Res*. (2004) 64:4328–37. doi: 10.1158/0008-5472.CAN-04-0073
54. Formenti SC, Lee P, Adams S, Goldberg JD, Li X, Xie MW, et al. Focal irradiation and systemic TGFβ blockade in metastatic breast cancer. *Clin Cancer Res*. (2018) 24:2493–504. doi: 10.1158/1078-0432.CCR-17-3322
55. Ohba K, Omagari K, Nakamura T, Ikuno N, Saeki S, Matsuo I, et al. Abscopal regression of hepatocellular carcinoma after radiotherapy for bone metastasis. *Gut*. (1998) 43:575–7. doi: 10.1136/gut.43.4.575
56. Camphausen K, Moses MA, Menard C, Sproull M, Beecken WD, Folkman J, et al. Radiation abscopal antitumor effect is mediated through p53. *Cancer Res*. (2003) 63:1990–3. doi: 10.1016/S0360-3016(02)03449-1
57. Konoeda K. Therapeutic efficacy of pre-operative radiotherapy on breast carcinoma: in special reference to its abscopal effect on metastatic lymph-nodes. *Nihon Gan Chiryo Gakkai Shi*. (1990) 25:1204–14.
58. Nobler MP. The abscopal effect in malignant lymphoma and its relationship to lymphocyte circulation. *Radiology*. (1969) 93:410–2. doi: 10.1148/93.2.410

59. Petrovic N, Perovic J, Karanovic D, Todorovic L, Petrovic V. Abscopal effects of local fractionated X-irradiation of face and jaw region. *Strahlentherapie*. (1982) 158:40–2.
60. RaventosA. An abscopal effect of x-ray upon mouse spleen weight. *Radiat Res*. (1954) 1:381–7. doi: 10.2307/3570292
61. Rees GJ, Ross CM. Abscopal regression following radiotherapy for adenocarcinoma. *Br J Radiol*. (1983) 56:63–6. doi: 10.1259/0007-1285-56-661-63
62. Hiniker SM, Chen DS, Reddy S, Chang DT, Jones JC, Mollick JA, et al. A systemic complete response of metastatic melanoma to local radiation and immunotherapy. *Transl Oncol*. (2012) 5:404–7. doi: 10.1593/tlo.12280
63. Stamell EF, Wolchok JD, Gnjatic S, Lee NY, Brownell I. The abscopal effect associated with a systemic anti-melanoma immune response. *Int J Radiat Oncol Biol Phys*. (2013) 85:293–5. doi: 10.1016/j.ijrobp.2012.03.017
64. Ishiyama H, Teh BS, Ren H, Chiang S, Tann A, Blanco AI, et al. Spontaneous regression of thoracic metastases while progression of brain metastases after stereotactic radiosurgery and stereotactic body radiotherapy for metastatic renal cell carcinoma: abscopal effect prevented by the blood-brain barrier? *Clin Genitourin Cancer*. (2012) 10:196–8. doi: 10.1016/j.clgc.2012.01.004
65. Cotter SE, McBride SM, Yock TI. Proton radiotherapy for solid tumors of childhood. *Technol Cancer Res Treat*. (2012) 11:267–78. doi: 10.7785/tcrt.2012.500295
66. Demaria S, Pilones KA, Formenti SC, Dustin ML. Exploiting the stress response to radiation to sensitize poorly immunogenic tumors to anti-CTLA-4 treatment. *Oncoimmunology*. (2013) 2:e23127. doi: 10.4161/onci.23127
67. Herter-Sprie GS, Koyama S, Korideck H, Hai J, Deng J, Li YY, et al. Synergy of radiotherapy and PD-1 blockade in Kras-mutant lung cancer. *JCI Insight*. (2016) 1:e87415. doi: 10.1172/jci.insight.87415
68. Dovedi SJ, Cheadle EJ, Popple AL, Poon E, Morrow M, Stewart R, et al. Fractionated radiation therapy stimulates antitumor immunity mediated by both resident and infiltrating polyclonal T-cell populations when combined with PD-1 blockade. *Clin Cancer Res*. (2017) 23:5514–26. doi: 10.1158/1078-0432.CCR-16-1673
69. Pitroda SP, Chmura SJ, Weichselbaum RR. Integration of radiotherapy and immunotherapy for treatment of oligometastases. *Lancet Oncol*. (2019) 20:e434–42. doi: 10.1016/S1470-2045(19)30157-3
70. Pitroda SP, Weichselbaum RR. Integrated molecular and clinical staging defines the spectrum of metastatic cancer. *Nat Rev Clin Oncol*. (2019) 16:581–8. doi: 10.1038/s41571-019-0220-6
71. Golden EB, Chhabra A, Chachoua A, Adams S, Donach M, Fenton-Kerimian M, et al. Local radiotherapy and granulocyte-macrophage colony-stimulating factor to generate abscopal responses in patients with metastatic solid tumours: a proof-of-principle trial. *Lancet Oncol*. (2015) 16:795–803. doi: 10.1016/S1470-2045(15)00054-6
72. Formenti SC, Rudqvist NP, Golden E, Cooper B, Wennerberg E, Lhuillier C, et al. Radiotherapy induces responses of lung cancer to CTLA-4 blockade. *Nat Med*. (2018) 24:1845–51. doi: 10.1038/s41591-018-0232-2
73. Herrera FG, Bourhis J, Coukos G. Radiotherapy combination opportunities leveraging immunity for the next oncology practice. *CA Cancer J Clin*. (2017) 67:65–85. doi: 10.3322/caac.21358
74. Lai RC, Yeo RW, Lim SK. Mesenchymal stem cell exosomes. *Semin Cell Dev Biol*. (2015) 40:82–8. doi: 10.1016/j.semcdb.2015.03.001
75. Oliver L, Hue E, Sery Q, Lafargue A, Pecqueur C, Paris F, et al. Differentiation-related response to DNA breaks in human mesenchymal stem cells. *Stem Cells*. (2013) 31:800–7. doi: 10.1002/stem.1336
76. Matsuda S, Nakagawa Y, Kitagishi Y, Nakanishi A, Murai T. Reactive oxygen species, superoxide dimutases, and PTEN-p53-AKT-MDM2 signaling loop network in mesenchymal stem/stromal cells regulation. *Cells*. (2018) 7:36. doi: 10.3390/cells7050036
77. Perez-Estenaga I, Prosper F, Pelacho B. Allogeneic mesenchymal stem cells and biomaterials: the perfect match for cardiac repair? *Int J Mol Sci*. (2018) 19:3236. doi: 10.3390/ijms19103236
78. Decrock E, Hoorelbeke D, Ramadan R, Delvaeye T, De Bock M, Wang N, et al. Calcium, oxidative stress and connexin channels, a harmonious orchestra directing the response to radiotherapy treatment? *Biochim Biophys Acta Mol Cell Res*. (2017) 1864:1099–120. doi: 10.1016/j.bbamcr.2017.02.007
79. Chang PY, Qu YQ, Wang J, Dong LH. The potential of mesenchymal stem cells in the management of radiation enteropathy. *Cell Death Dis*. (2015) 6:e1840. doi: 10.1038/cddis.2015.189
80. Maziarz RT, Devos T, Bachier CR, Goldstein SC, Leis JF, Devine SM, et al. Single and multiple dose MultiStem (multipotent adult progenitor cell) therapy prophylaxis of acute graft-versus-host disease in myeloablative allogeneic hematopoietic cell transplantation: a phase 1 trial. *Biol Blood Marrow Transplant*. (2015) 21:720–8. doi: 10.1016/j.bbmt.2014.12.025
81. Klein D, Schmetter A, Imsak R, Wirsdorfer F, Unger K, Jastrow H, et al. Therapy with multipotent mesenchymal stromal cells protects lungs from radiation-induced injury and reduces the risk of lung metastasis. *Antioxid Redox Signal*. (2016) 24:53–69. doi: 10.1089/ars.2014.6183
82. Nicolay NH, Lopez Perez R, Saffrich R, Huber PE. Radio-resistant mesenchymal stem cells: mechanisms of resistance and potential implications for the clinic. *Oncotarget*. (2015) 6:19366–80. doi: 10.18632/oncotarget.4358
83. Lysaght T, Campbell AV. Regulating autologous adult stem cells: the FDA steps up. *Cell Stem Cell*. (2011) 9:393–6. doi: 10.1016/j.stem.2011.09.013
84. Bernardo ME, Cometa AM, Locatelli F. Mesenchymal stromal cells: a novel and effective strategy for facilitating engraftment and accelerating hematopoietic recovery after transplantation? *Bone Marrow Transplant*. (2012) 47:323–9. doi: 10.1038/bmt.2011.102
85. Loebinger MR, Janes SM. Stem cells as vectors for antitumour therapy. *Thorax*. (2010) 65:362–9. doi: 10.1136/thx.2009.128025
86. Loebinger MR, Sage EK, Davies D, Janes SM. TRAIL-expressing mesenchymal stem cells kill the putative cancer stem cell population. *Br J Cancer*. (2010) 103:1692–7. doi: 10.1038/sj.bjc.6605952
87. Nicolay NH, Liang Y, Lopez Perez R, Bostel T, Trinh T, Sisombath S, et al. Mesenchymal stem cells are resistant to carbon ion radiotherapy. *Oncotarget*. (2015) 6:2076–87. doi: 10.18632/oncotarget.2857
88. Skripcak T, Belka C, Bosch W, Brink C, Brunner T, Budach V, et al. Creating a data exchange strategy for radiotherapy research: towards federated databases and anonymised public datasets. *Radiother Oncol*. (2014) 113:303–9. doi: 10.1016/j.radonc.2014.10.001
89. Murphy MB, Moncivais K, Caplan AI. Mesenchymal stem cells: environmentally responsive therapeutics for regenerative medicine. *Exp Mol Med*. (2013) 45:e54. doi: 10.1038/emm.2013.94
90. Cotter SE, Dunn GP, Collins KM, Sahni D, Zukotynski KA, Hansen JL, et al. Abscopal effect in a patient with metastatic Merkel cell carcinoma following radiation therapy: potential role of induced antitumor immunity. *Arch Dermatol*. (2011) 147:870–2. doi: 10.1001/archdermatol.2011.176
91. Bergfeld SA, Blavier L, Declerck YA. Bone marrow-derived mesenchymal stromal cells promote survival and drug resistance in tumor cells. *Mol Cancer Ther*. (2014) 13:962–75. doi: 10.1158/1535-7163.MCT-13-0400
92. Yagi H, Kitagawa Y. The role of mesenchymal stem cells in cancer development. *Front Genet*. (2013) 4:261. doi: 10.3389/fgene.2013.00261
93. Green DR. Cell competition: pirates on the tangled bank. *Cell Stem Cell*. (2010) 6:287–8. doi: 10.1016/j.stem.2010.03.006
94. de Araújo Farias V, Linares-Fernandez JL, Penalver JL, Paya Colmenero JA, Ferron GO, Duran EL, et al. Human umbilical cord stromal stem cell express CD10 and exert contractile properties. *Placenta*. (2011) 32:86–95. doi: 10.1016/j.placenta.2010.11.003
95. López Peñalver JJ, de Araujo Farías V, López-Ramón MV, Tassi M, Oliver FJ, Moreno-Castilla C, et al. Activated carbon cloth as support for mesenchymal stem cell growth and differentiation to osteocyte. *Carbon*. (2009) 47:3574–7. doi: 10.1016/j.carbon.2009.08.016
96. de Araújo Farias V, Linares Fernández JL, Sirés-Campos J, López-Ramón MV, Moreno-Castilla C, Oliver FJ, et al. Growth and spontaneous differentiation of umbilical-cord stromal stem cells on activated carbon cloth. *J Mater Chem B*. (2013) 1:3359–68. doi: 10.1039/c3tb20305k
97. Rhee KJ, Lee JI, Eom YW. Mesenchymal stem cell-mediated effects of tumor support or suppression. *Int J Mol Sci*. (2015) 16:30015–33. doi: 10.3390/ijms161226215
98. Barcellos-de-Souza P, Comito G, Pons-Segura C, Taddei ML, Gori V, Becherucci V, et al. Mesenchymal stem cells are recruited and activated into carcinoma-associated fibroblasts by prostate cancer microenvironment-derived TGF-β1. *Stem Cells*. (2016) 34:2536–47. doi: 10.1002/stem.2412

99. Shi Y, Du L, Lin L, Wang Y. Tumour-associated mesenchymal stem/stromal cells: emerging therapeutic targets. *Nat Rev Drug Discov*. (2017) 16:35–52. doi: 10.1038/nrd.2016.193
100. O'Malley G, Heijltjes M, Houston AM, Rani S, Ritter T, Egan LJ, et al. Mesenchymal stromal cells (MSCs) and colorectal cancer: a troublesome twosome for the anti-tumour immune response? *Oncotarget*. (2016) 7:60752–74. doi: 10.18632/oncotarget.11354
101. Hass R, von der Ohe J, Ungefroren H. Potential role of MSC/cancer cell fusion and EMT for breast cancer stem cell formation. *Cancers*. (2019) 11:E1432. doi: 10.3390/cancers11101432
102. Li W, Ren G, Huang Y, Su J, Han Y, Li J, et al. Mesenchymal stem cells: a double-edged sword in regulating immune responses. *Cell Death Differ*. (2012) 19:1505–13. doi: 10.1038/cdd.2012.26
103. Ren G, Zhao X, Wang Y, Zhang X, Chen X, Xu C, et al. CCR2-dependent recruitment of macrophages by tumor-educated mesenchymal stromal cells promotes tumor development and is mimicked by TNFα. *Cell Stem Cell*. (2012) 11:812–24. doi: 10.1016/j.stem.2012.08.013
104. Chowdhury R, Webber JP, Gurney M, Mason MD, Tabi Z, Clayton A. Cancer exosomes trigger mesenchymal stem cell differentiation into pro-angiogenic and pro-invasive myofibroblasts. *Oncotarget*. (2015) 6:715–31. doi: 10.18632/oncotarget.2711
105. Vieira de Castro J, Gomes ED, Granja S, Anjo SI, Baltazar F, Manadas B, et al. Impact of mesenchymal stem cells' secretome on glioblastoma pathophysiology. *J Transl Med*. (2017) 15:200. doi: 10.1186/s12967-017-1303-8
106. Wu YL, Li HY, Zhao XP, Jiao JY, Tang DX, Yan LJ, et al. Mesenchymal stem cell-derived CCN2 promotes the proliferation, migration and invasion of human tongue squamous cell carcinoma cells. *Cancer Sci*. (2017) 108:897–909. doi: 10.1111/cas.13202
107. Lobb RJ, Lima LG, Moller A. Exosomes: key mediators of metastasis and pre-metastatic niche formation. *Semin Cell Dev Biol*. (2017) 67:3–10. doi: 10.1016/j.semcdb.2017.01.004
108. Shin JW, Son JY, Raghavendran HR, Chung WK, Kim HG, Park HJ, et al. High-dose ionizing radiation-induced hematotoxicity and metastasis in mice model. *Clin Exp Metast*. (2011) 28:803–10. doi: 10.1007/s10585-011-9411-y
109. Hamalukic M, Huelsenbeck J, Schad A, Wirtz S, Kaina B, Fritz G. Rac1-regulated endothelial radiation response stimulates extravasation and metastasis that can be blocked by HMG-CoA reductase inhibitors. *PLoS ONE*. (2011) 6:e26413. doi: 10.1371/journal.pone.0026413
110. Di Modica M, Regondi V, Sandri M, Iorio MV, Zanetti A, Tagliabue E, et al. Breast cancer-secreted miR-939 downregulates VE-cadherin and destroys the barrier function of endothelial monolayers. *Cancer Lett*. (2017) 384:94–100. doi: 10.1016/j.canlet.2016.09.013
111. Peinado H, Aleckovic M, Lavotshkin S, Matei I, Costa-Silva B, Moreno-Bueno G, et al. Melanoma exosomes educate bone marrow progenitor cells toward a pro-metastatic phenotype through MET. *Nat Med*. (2012) 18:883–91. doi: 10.1038/nm.2753
112. Hoshino A, Costa-Silva B, Shen TL, Rodrigues G, Hashimoto A, Tesic Mark M, et al. Tumour exosome integrins determine organotropic metastasis. *Nature*. (2015) 527:329–35. doi: 10.1038/nature15756
113. Weidle UH, Birzele F, Kollmorgen G, Ruger R. Long non-coding RNAs and their role in metastasis. *Cancer Genomics Proteomics*. (2017) 14:143–60. doi: 10.21873/cgp.20027
114. Weidle UH, Birzele F, Kollmorgen G, Ruger R. The multiple roles of exosomes in metastasis. *Cancer Genomics Proteomics*. (2017) 14:1–15. doi: 10.21873/cgp.20015
115. Sun Z, Shi K, Yang S, Liu J, Zhou Q, Wang G, et al. Effect of exosomal miRNA on cancer biology and clinical applications. *Mol Cancer*. (2018) 17:147. doi: 10.1186/s12943-018-0897-7
116. Le Large TYS, Bijlsma MF, Kazemier G, van Laarhoven HWM, Giovannetti E, Jimenez CR. Key biological processes driving metastatic spread of pancreatic cancer as identified by multi-omics studies. *Semin Cancer Biol*. (2017) 44:153–69. doi: 10.1016/j.semcancer.2017.03.008
117. Dai J, Escara-Wilke J, Keller JM, Jung Y, Taichman RS, Pienta KJ, et al. Primary prostate cancer educates bone stroma through exosomal pyruvate kinase M2 to promote bone metastasis. *J Exp Med*. (2019) 216:2883. doi: 10.1084/jem.20190158
118. Ostenfeld MS, Jeppesen DK, Laurberg JR, Boysen AT, Bramsen JB, Primdal-Bengtson B, et al. Cellular disposal of miR23b by RAB27-dependent exosome release is linked to acquisition of metastatic properties. *Cancer Res*. (2014) 74:5758–71. doi: 10.1158/0008-5472.CAN-13-3512
119. Baumgart S, Holters S, Ohlmann CH, Bohle R, Stockle M, Ostenfeld MS, et al. Exosomes of invasive urothelial carcinoma cells are characterized by a specific miRNA expression signature. *Oncotarget*. (2017) 8:58278–91. doi: 10.18632/oncotarget.17619
120. Schwarzenbach H. Clinical relevance of circulating, cell-free and exosomal microRNAs in plasma and serum of breast cancer patients. *Oncol Res Treat*. (2017) 40:423–9. doi: 10.1159/000478019
121. Rager TM, Olson JK, Zhou Y, Wang Y, Besner GE. Exosomes secreted from bone marrow-derived mesenchymal stem cells protect the intestines from experimental necrotizing enterocolitis. *J Pediatric Surg*. (2016) 51:942–7. doi: 10.1016/j.jpedsurg.2016.02.061
122. Chapel A, Mohty M. *Trial Evaluating the Efficacy of Systemic Mesenchymal Stromal Cell (MSC) Injections for the Treatment of Severe and Chronic Radiotherapy-induced Abdomino-pelvic Complications (Pelvic Radiation Disease, PRD) Refractory to Standard Therapy (PRISME)*. ClinicalTrials.gov Identifier: NCT02814864.
123. Moussa L, Pattappa G, Doix B, Benselama SL, Demarquay C, Benderitter M, et al. A biomaterial-assisted mesenchymal stromal cell therapy alleviates colonic radiation-induced damage. *Biomaterials*. (2017) 115:40–52. doi: 10.1016/j.biomaterials.2016.11.017
124. Bessout R, Demarquay C, Moussa L, Rene A, Doix B, Benderitter M, et al. TH17 predominant T-cell responses in radiation-induced bowel disease are modulated by treatment with adipose-derived mesenchymal stromal cells. *J Pathol*. (2015) 237:435–46. doi: 10.1002/path.4590
125. Van de Putte D, Demarquay C, Van Daele E, Moussa L, Vanhove C, Benderitter M, et al. Adipose-derived mesenchymal stromal cells improve the healing of colonic anastomoses following high dose of irradiation through anti-inflammatory and angiogenic processes. *Cell Transplant*. (2017) 26:1919–30. doi: 10.1177/0963689717721515
126. Leibacher J, Henschler R. Biodistribution, migration and homing of systemically applied mesenchymal stem/stromal cells. *Stem Cell Res Ther*. (2016) 7:7. doi: 10.1186/s13287-015-0271-2
127. Bateman ME, Strong AL, Gimble JM, Bunnell BA. Concise review: using fat to fight disease: a systematic review of nonhomologous adipose-derived stromal/stem cell therapies. *Stem Cells*. (2018) 36:1311–28. doi: 10.1002/stem.2847
128. Jung PY, Ryu H, Rhee KJ, Hwang S, Lee CG, Gwon SY, et al. Adipose tissue-derived mesenchymal stem cells cultured at high density express IFN-beta and TRAIL and suppress the growth of H460 human lung cancer cells. *Cancer Lett*. (2019) 440–441:202–10. doi: 10.1016/j.canlet.2018.10.017
129. Weyd H. More than just innate affairs - on the role of annexins in adaptive immunity. *Biol Chem*. (2016) 397:1017–29. doi: 10.1515/hsz-2016-0191
130. Guo C, Liu S, Sun MZ. Potential role of Anxa1 in cancer. *Future Oncol*. (2013) 9:1773–93. doi: 10.2217/fon.13.114
131. Boudhraa Z, Bouchon B, Viallard C, D'Incan M, Degoul F. Annexin A1 localization and its relevance to cancer. *Clin Sci*. (2016) 130:205–20. doi: 10.1042/CS20150415
132. Alessandri AL, Sousa LP, Lucas CD, Rossi AG, Pinho V, Teixeira MM. Resolution of inflammation: mechanisms and opportunity for drug development. *Pharmacol Ther*. (2013) 139:189–212. doi: 10.1016/j.pharmthera.2013.04.006
133. Soehnlein O, Lindbom L. Phagocyte partnership during the onset and resolution of inflammation. *Nat Rev Inmunol*. (2010) 10:427–39. doi: 10.1038/nri2779
134. Fredman G, Tabas I. Boosting inflammation resolution in atherosclerosis: the next frontier for therapy. *Am J Pathol*. (2017) 187:1211–21. doi: 10.1016/j.ajpath.2017.01.018
135. Fredman G, Spite M. Specialized pro-resolving mediators in cardiovascular diseases. *Mol Aspects Med*. (2017) 58:65–71. doi: 10.1016/j.mam.2017.02.003
136. Ansari J, Kaur G, Gavins FNE. Therapeutic potential of annexin A1 in ischemia reperfusion injury. *Int J Mol Sci*. (2018) 19:E1211. doi: 10.3390/ijms19041211

137. Shalapour S, Karin M. Immunity, inflammation, and cancer: an eternal fight between good and evil. *J Clin Invest*. (2015) 125:3347–55. doi: 10.1172/JCI80007
138. Ivey JW, Bonakdar M, Kanitkar A, Davalos RV, Verbridge SS. Improving cancer therapies by targeting the physical and chemical hallmarks of the tumor microenvironment. *Cancer Lett*. (2016) 380:330–9. doi: 10.1016/j.canlet.2015.12.019
139. Nicolas-Boluda A, Silva AKA, Fournel S, Gazeau F. Physical oncology: new targets for nanomedicine. *Biomaterials*. (2018) 150:87–99. doi: 10.1016/j.biomaterials.2017.10.014
140. Han GH, Lu KJ, Huang JX, Zhang LX, Dai SB, Dai CL. Association of serum annexin A1 with treatment response and prognosis in patients with esophageal squamous cell carcinoma. *J Cancer Res Ther*. (2018) 14(Supplement):S667–74. doi: 10.4103/0973-1482.187297
141. Raulf N, Lucarelli P, Thavaraj S, Brown S, Vicencio JM, Sauter T, et al. Annexin A1 regulates EGFR activity and alters EGFR-containing tumour-derived exosomes in head and neck cancers. *Eur J Cancer*. (2018) 102:52–68. doi: 10.1016/j.ejca.2018.07.123
142. Vidotto A, Polachini GM, de Paula-Silva M, Oliani SM, Henrique T, Lopez RVM, et al. Differentially expressed proteins in positive versus negative HNSCC lymph nodes. *BMC Med Genomics*. (2018) 11:73. doi: 10.1186/s12920-018-0382-6
143. Zhang Z, Huang L, Zhao W, Rigas B. Annexin 1 induced by anti-inflammatory drugs binds to NF-κB and inhibits its activation: anticancer effects *in vitro* and *in vivo*. *Cancer Res*. (2010) 70:2379–88. doi: 10.1158/0008-5472.CAN-09-4204
144. Sheikh MH, Solito E. Annexin A1: uncovering the many talents of an old protein. *Int J Mol Sci*. (2018) 19:E1045. doi: 10.3390/ijms19041045
145. Leoni G, Nusrat A. Annexin A1: shifting the balance towards resolution and repair. *Biol Chem*. (2016) 397:971–9. doi: 10.1515/hsz-2016-0180
146. Kao W, Gu R, Jia Y, Wei X, Fan H, Harris J, et al. A formyl peptide receptor agonist suppresses inflammation and bone damage in arthritis. *Br J Pharmacol*. (2014) 171:4087–96. doi: 10.1111/bph.12768
147. Li X, Zhao Y, Xia Q, Zheng L, Liu L, Zhao B, et al. Nuclear translocation of annexin 1 following oxygen-glucose deprivation-reperfusion induces apoptosis by regulating Bid expression via p53 binding. *Cell Death Dis*. (2016) 7:e2356. doi: 10.1038/cddis.2016.259
148. Zeng GQ, Cheng AL, Tang J, Li GQ, Li MX, Qu JQ, et al. Annexin A1: a new biomarker for predicting nasopharyngeal carcinoma response to radiotherapy. *Med Hypotheses*. (2013) 81:68–70. doi: 10.1016/j.mehy.2013.04.019
149. Han G, Lu K, Xu W, Zhang S, Huang J, Dai C, et al. Annexin A1-mediated inhibition of inflammatory cytokines may facilitate the resolution of inflammation in acute radiation-induced lung injury. *Oncol Lett*. (2019) 18:321–9. doi: 10.3892/ol.2019.10317
150. Ma Q, Zhang Z, Shim JK, Venkatraman TN, Lascola CD, Quinones QJ, et al. Annexin A1 bioactive peptide promotes resolution of neuroinflammation in a rat model of exsanguinating cardiac arrest treated by emergency preservation and resuscitation. *Front Neurosci*. (2019) 13:608. doi: 10.3389/fnins.2019.00608
151. Senchenkova EY, Ansari J, Becker F, Vital SA, Al-Yafeai Z, Sparkenbaugh EM, et al. Novel role for the AnxA1-Fpr2/ALX signaling axis as a key regulator of platelet function to promote resolution of inflammation. *Circulation*. (2019) 140:319–35. doi: 10.1161/CIRCULATIONAHA.118.039345
152. Purvis GSD, Solito E, Thiemermann C. Annexin-A1: therapeutic potential in microvascular disease. *Front Immunol*. (2019) 10:938. doi: 10.3389/fimmu.2019.00938
153. Hanahan D, Weinberg RA. Hallmarks of cancer: the next generation. *Cell*. (2011) 144:646–74. doi: 10.1016/j.cell.2011.02.013
154. Thomas JG, Parker Kerrigan BC, Hossain A, Gumin J, Shinojima N, Nwajei F, et al. Ionizing radiation augments glioma tropism of mesenchymal stem cells. *J Neurosurg*. (2018) 128:287–95. doi: 10.3171/2016.9.JNS16278

Conflict of Interest: The authors declare that the research was conducted in the absence of any commercial or financial relationships that could be construed as a potential conflict of interest.

frontiers in Oncology

ORIGINAL RESEARCH
published: 11 February 2020
doi: 10.3389/fonc.2020.00004

Hypofractionated Irradiation Suppressed the Off-Target Mouse Hepatocarcinoma Growth by Inhibiting Myeloid-Derived Suppressor Cell-Mediated Immune Suppression

Junying Chen[1,2†], Zeng Wang[1,2†], Yuxiong Ding[1,2], Fei Huang[1,2], Weikang Huang[1,2], Ruilong Lan[1,2], Ruiqing Chen[1,2], Bing Wu[1,2], Lengxi Fu[1,2], Yunhua Yang[3], Jun Liu[1,2], Jinsheng Hong[1,2], Weijian Zhang[1,2] and Lurong Zhang[4*]*

[1] First Affiliated Hospital of Fujian Medical University, Fuzhou, China, [2] Fujian Key Laboratory of Cancer Immunotherapy and Key Laboratory of Radiation Biology, Fujian Province Universities, Fuzhou, China, [3] Department of Otolaryngology, Fujian Provincial Geriatric Hospital, Fuzhou, China, [4] Fujian Medical University Cancer Hospital, Fujian Cancer Hospital, Fuzhou, China

Background: Stereotactic radiotherapy treats hepatocellular carcinoma (HCC) at different stages effectively and safely. Besides its direct killing of cancer cells, radiotherapy stimulates host immunity against hepatoma. However, the role of myeloid-derived suppressor cells (MDSCs) in on-target and off-target anti-HCC effects induced by hypofractionated irradiation (IR) is unclear.

Methods and Materials: Hepa1-6 and H22 allogeneic transplanted tumors on hind limbs of C57BL/6 and Institute of Cancer Research (ICR) mice, respectively, were irradiated with 0, 2.5, 4, 6, or 8 Gy/fraction until the total dose reached 40 Gy. The off-target effect induced by the IR was investigated by subsequently inoculating the same HCC cells subcutaneously on the abdomen. MDSCs in peripheral blood and tumor tissues were measured by flow cytometry or immunofluorescence microscopy analysis. IL-6, regulated on activation normal T cell expressed and secreted (RANTES), and granulocyte colony-stimulating factor (G-CSF) in irradiated mouse plasma and hepatoma cell cultures were measured with ELISA kits. Conditioned media (CM) from irradiated HCC cell cultures on bone marrow cell differentiation and MDSC proliferation were examined by co-culture and flow cytometry.

Results: Our study showed that the IR of primarily inoculated HCC on hind limbs created an "*in situ* tumor vaccine" and triggered the antitumor immunity. The immunity was capable of suppressing the growth of the same type of HCC subcutaneously implanted on the abdomen, accompanied with reduced MDSCs in both blood and tumors. The decreased MDSCs were associated with low plasma levels of IL-6, RANTES, and G-CSF. The cytokines IL-6 and RANTES in the CM were lower in the high single IR dose group than in the control groups, but G-CSF was higher.

OPEN ACCESS

Edited by:
Mary Helen Barcellos-Hoff, University of California, San Francisco, United States

Reviewed by:
Benjamin Frey, University of Erlangen Nuremberg, Germany
Michael Wayne Epperly, University of Pittsburgh, United States
Shisuo Du, Zhongshan Hospital, Fudan University, China

***Correspondence:**
Junying Chen
junyingchen01@163.com
Lurong Zhang
lz8506@163.com

†These authors have contributed equally to this work and share first authorship

Specialty section:
This article was submitted to Radiation Oncology, a section of the journal Frontiers in Oncology

Received: *14 June 2019*
Accepted: *06 January 2020*
Published: *11 February 2020*

Citation:
Chen J, Wang Z, Ding Y, Huang F, Huang W, Lan R, Chen R, Wu B, Fu L, Yang Y, Liu J, Hong J, Zhang W and Zhang L (2020) Hypofractionated Irradiation Suppressed the Off-Target Mouse Hepatocarcinoma Growth by Inhibiting Myeloid-Derived Suppressor Cell-Mediated Immune Suppression. Front. Oncol. 10:4. doi: 10.3389/fonc.2020.00004

The CM from high single-dose IR-Hepa1-6 cell culture reduced the differentiation of C57BL/6 mouse bone marrow cells into MDSCs, whereas CM from high single-dose IR-H22 cells reduced the proliferation of MDSCs, which might be due to the decreased p-STAT3 in bone marrow cells.

Conclusions: The hypofractionated IR on transplanted tumors at the primary location exerted a strong antitumor effect on the same tumor at a different location (off target). This abscopal effect is most likely through the reduction of MDSCs and decrease of IL-6, RANTES, and G-CSF.

Keywords: *in situ* tumor vaccine, high-dose low-fraction radiation, myeloid-derived suppressor cells, negative immune breaker, hepatocellular carcinoma

INTRODUCTION

Myeloid derived suppressor cells (MDSCs), a group of high-heterogeneity immune-negative regulating cells, have two subgroups: granulocytic MDSC (PMN-MDSC) and monocytic MDSC (M-MDSC) with their own functions (1). In pathological conditions (such as an infection and an autoimmune disease), overproduced inflammation molecules and overstimulated proliferation, and differentiation of immune cells could be restrained by MDSCs to keep the reaction under control and to balance immune response and host's homeostasis (2).

The traditional and new treatments are unsatisfactory for hepatocellular carcinoma (HCC) (3–5). Recently, stereotactic body radiotherapy (SBRT) has emerged as a preferred regimen for HCC owing to its effectiveness and safety (6, 7). Besides its direct killing of tumor cells, the irradiation (IR) also induces immune reactions that kill metastatic hepatoma tumor cells (8). Radiotherapy (RT) enhances the release of tumor-associated antigens (TAAs), creates damage-associated molecular patterns (DAMPs), and stimulates the immunomodulatory cell surface molecules, resulting in a manifestation "*in situ* vaccine" and antitumor immune response (9–11). The IR-targeted tumor could suppress the off-target tumors (tumors at locations away from the irradiated location) (12). This abscopal effect might relate to a fact that the IR turns on the body's antitumor immune response by up-regulating the tumor immunogenicity, which has been well summarized by Demaria and his colleagues (13, 14, 33). However, cellular, molecular, and immunological mechanisms of this off-target effect are not well-studied. Because MDSCs have a significant inhibitory effect on the immunity against malignancies during the development and progression, it is desired to understand the role of MDSCs in IR-induced on-target and off-target antitumor effects.

The alterations of MDSCs could be triggered by different IR regimens (15). IR induces the MDSCs, dendritic cells (DCs), macrophages, and other cells in the lymph nodes surrounding the tumor (16, 17), and affects the recruitment and redistribution of MDSCs in tumor (16, 18, 19). Crittenden et al. found that a total dose of 20 Gy (∼6 Gy × 3) given to 4T1- or Panc02 tumor-bearing mice could increase infiltrated MDSCs but decreased blood MDSCs significantly (20). Deng et al. reported that after a single-dose 12-Gy IR, the decreased MDSCs negatively correlated with the increased $CD8^+$ cells (21). IR also reduces MDSC levels, which requires high-dose ablative IR rather than multiple lower-dose treatments (22). Thus, MDSCs play an important role in the outcome of tumor RT (23). However, so far, there is no consensus about the best way of IR to fully utilize MDSCs in the RT owing to the lack of systematical comparison study of the IR effects on MDSCs.

We hypothesize that hypofractionated IR of primary tumor generated "*in situ* vaccine," which could suppress the off-IR-target tumor growth by reducing MDSCs in blood and tumor tissues. To prove this hypothesis, MDSCs in two IR HCC models and the consequent abscopal effects on off-target tumor growths were examined. In addition, MDSCs regulated inflammation molecules [granulocyte colony-stimulating factor (G-CSF), IL-6, and regulated on activation normal T cell expressed and secreted (RANTES)], and their effects on differentiation and proliferation of MDSCs were also explored.

MATERIALS AND METHODS

Cell Culture

Hepa1-6 cells [murine HCC, from American Type Culture Collection (ATCC), Manassas, USA] were cultured in Dulbecco's modified Eagle medium (DMEM); and H22 cells (murine HCC, from Bio-Rad Life Sciences Development Co., Ltd. Beijing, China) were cultured in Roswell Park Memorial Institute (RPMI) 1640 in 37°C in a humidified incubator with 5% CO_2. The media contained 10% fetal bovine serum (FBS) and 100 U/ml of penicillin and 100 μg/ml of streptomycin. The culture media, FBS, and antibiotics were purchases from Thermo Fisher Scientific (USA).

Animal Models

C57BL/6 and Institute of Cancer Research (ICR) mice (8-week-old pathogen-free female mice) were purchased from Slaccas Experimental Animal LLC (Shanghai, China). Hepa1-6 cells and H22 (1×10^6 cells/in 0.1 ml/site) were subcutaneously injected into hind limbs of C57BL/6 mice and ICR mice, respectively. Three days after the inoculation, the tumors were established as they were touchable (size about 2 mm^3). Each type of the tumor-bearing mice was randomly divided into five groups (Hepa1-6/C57BL/6, 6 mice/group; and H22/ICR, 8 mice/group)

for different IR doses/fractions (0, 2.5, 4, 6, or 8 Gy) with 40-Gy total dose. The IR schedule was as indicated in **Figure 1B**. Briefly, the mice were immobilized in a special device. The hind limbs bearing the HCC were stretched out, fixed on rear supporter as part of the device, placed on the 1-cm tissue equivalent compensator, and exposed to the IR (voltage, 6 MV; direction, 180°; dose rate, 5 Gy/min; irradiated volume, 36 cm × 4 cm; distance from source to skin, 100 cm) of linear accelerator (CL/1800, Varian Medical System Inc, USA).

The second tumor challenge of Hepa1-6 cells or H22 (1×10^6 cells/0.1 ml/site) was subcutaneously injected on the abdomen 3 days after the entire IR was completed.

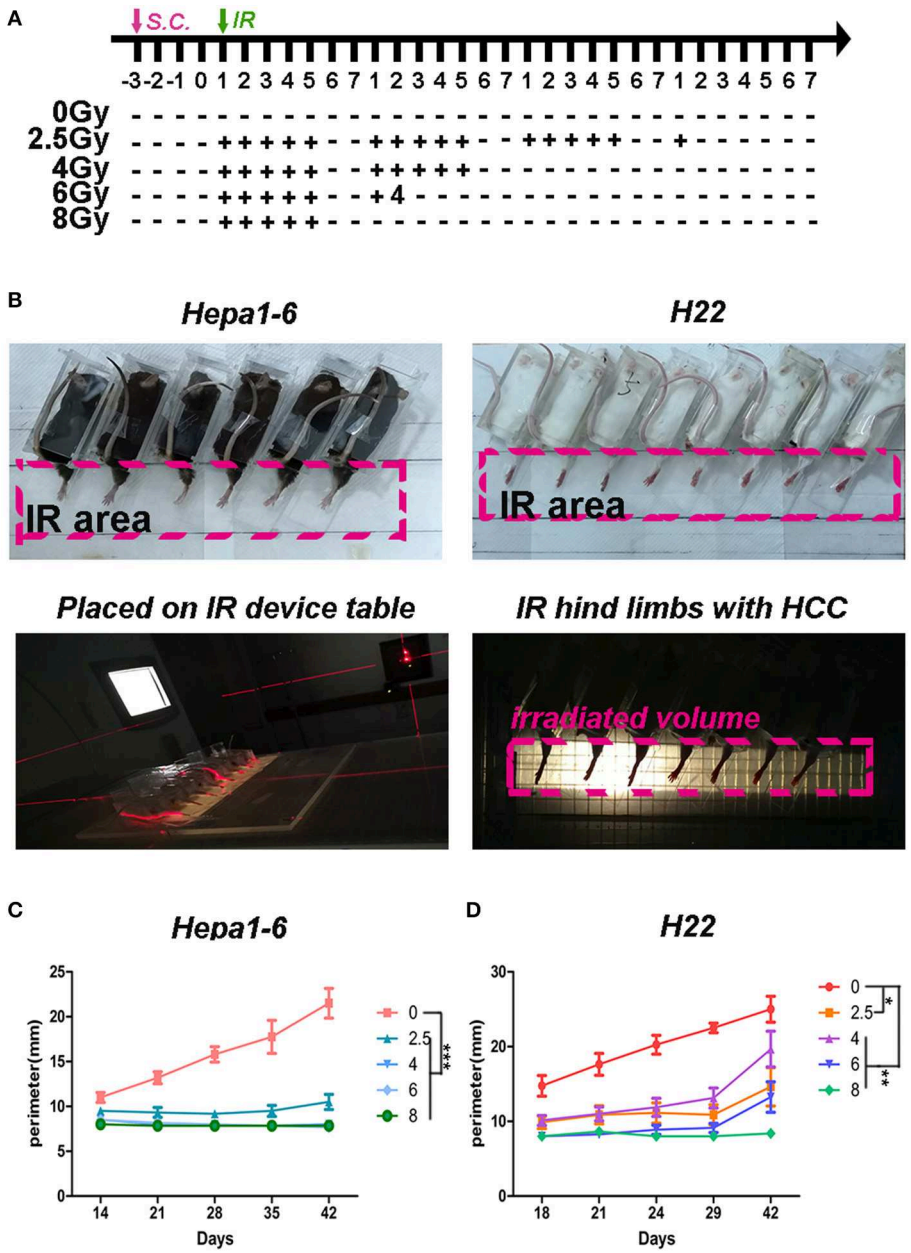

FIGURE 1 | Hypofraction irradiation (IR) significantly improved the local control of hepatocellular carcinoma (HCC) growth in mice. **(A)** Schedule of irradiation: after the Hepa1-6 or H22 allogeneic tumors in C57BL/6 or Institute of Cancer Research (ICR) mice were established, the IR was conducted with different doses (2.5, 4, 6, or 8 Gy) per fraction every day during weekdays until the total dose reached 40 Gy. The images of irradiation procedure of Hepa1-6/C57BL/6 and H22/ICR mouse models are shown **(B)**. The tumors in the hind limbs of mice were fixed in a special device and placed on the 1-cm tissue equivalent compensator and exposed to the IR (voltage, 6 MV; direction, 180°; dose rate, 5 Gy/min; irradiated volume, 36 × 4 cm; distance from source to skin, 100 cm) of linear accelerator (CL/1800, Varian Medical System Inc, USA). The tumor growth in hind limbs was measured by circumference ruler once a week for C57BL/6 mice or twice a week for ICR mice **(C,D)**. The differences of intra-groups were analyzed by one-way ANOVA test followed by Tukey's honestly significant difference (HSD) test in Kruskal–Wallis test. $^*p < 0.05$, $^{**}p < 0.01$, and $^{***}p < 0.0001$. ($n = 30$, 6 mice/group, 5 groups in Hepa1-6/C57BL/6 model; $n = 40$, 8 mice/group, 5 groups in the H22/ICR models).

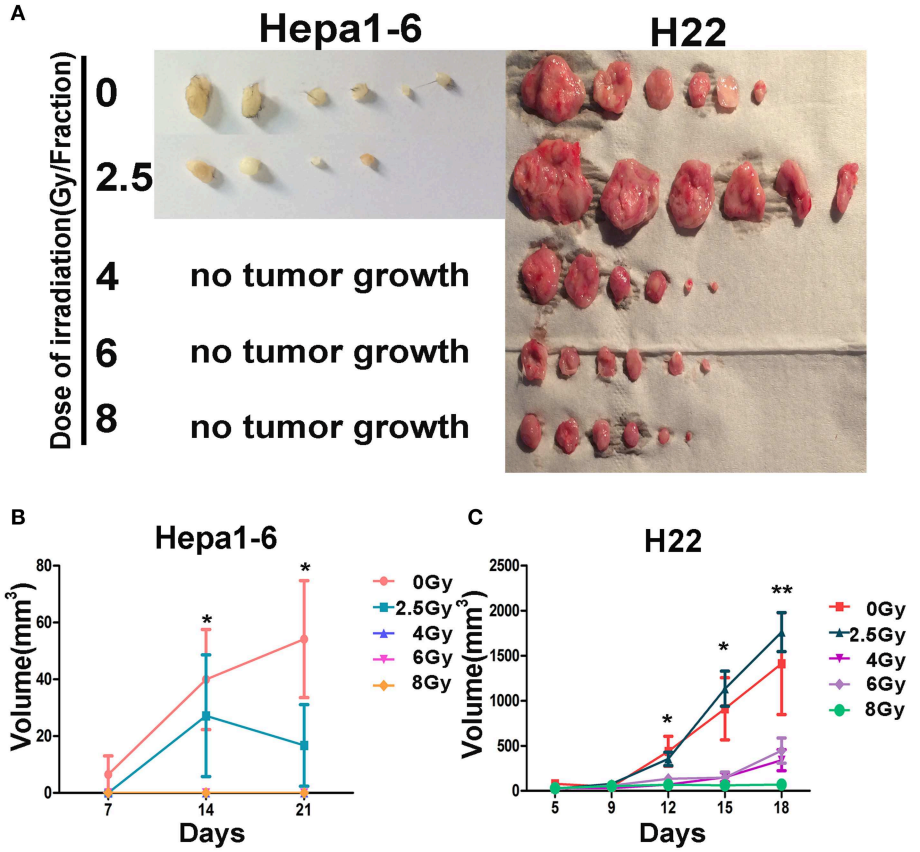

FIGURE 2 | Effectiveness of the on-target vaccine created by hypofraction irradiation (IR) on off-target tumors was dose dependent. The allogeneic tumors on mouse hind limbs underwent different IR doses/fraction to create *in situ* vaccines. The antitumor immunity elicited by *in situ* vaccines was evaluated by observing the growth of the second tumor challenge on abdomen in both Hepa1-6/C57BL/6 and H22/Institute of Cancer Research (ICR) models. The second tumor challenge volume was measured weekly for Hepa1-6/C57BL/6 models and twice a week for H22/ICR models; and the tumor were calculated as length × width^2/2. Results showed that all irradiated on-target tumors had an antitumor immunity effect on the second inoculated off-target tumors **(A)**, except for H22 tumors irradiated with 2.5 Gy/fraction, in which the off-target tumors grew bigger than controls. The antitumor immunity effect of the *in situ* vaccines on the second inoculated off-target tumors (abscopal effect) was dose per fraction dependent **(B,C)**. The higher the dose per fraction (>4 Gy) used, the stronger the antitumor immunity against the second tumor challenge developed. *$P < 0.05$, **$P < 0.01$.

The tumor volume of the hind limbs was evaluated by measuring with circumference ruler owing to the unclear tumor boundary. The volume of the second tumor challenge was measured with vernier caliper weekly for Hepa1-6/C57BL/6 models and twice a week for H22/ICR models; and the tumor volume was calculated as length × width^2/2.

All mice had *ad libitum* access to standard diet and water. The growth of subsequently inoculated tumors and animal well-being were closely monitored. All animal experiments were approved by Fujian Medical University Institutional Animal Ethical Committee (FJMU IACUC 2018-027).

Flow Cytometric Analysis for Blood Myeloid-Derived Suppressor Cells

Blood sample of mice was collected from the tail vein. After red blood cells were lysed with ACK lysis buffer (Sigma, USA), white blood cells (WBCs) were stained with fluorescein isothiocyanate (FITC)- or allophycocyanin-conjugated anti-mouse CD11b and phycoerythrin (PE)-conjugated anti-mouse Gr1 on ice for 45 min, and then the 7-aminoactinomycin (7AAD) (BioLegend, USA) was added for another 15 min. After being washed three times, the cells were analyzed by Accuri C6 flow cytometer (Becton Dickinson, USA). The negative 7AAD cells were gated for the live cells. Forward vs. side scatter (FSC vs. SSC) was used to gate the subpopulations of monocytes or neutrophils. It has been proved that the morphology of M-MDSCs ($CD11b^+Ly6G^-Ly6C^+$ or $CD11b^+Ly6G^-Ly6C^{hi}$) was mononuclear and that of PMN-MDSCs ($CD11b^+Ly6G^+Ly6C^-$ or $CD11b^+Ly6G^+Ly6C^{lo}$) was multinuclear (24). We used FSC/SSC-gated method to distinguish the mononuclear cells from granulocytes and to determine the MDSCs in the two groups by CD11b and Gr1 antibodies. The two groups of cells were stained with DAPI (BioLegend, USA) after being sorted by FACSAria™ (Becton Dickinson, USA). The nuclear morphology was observed using a fluorescence microscope (Olympus, Japan). In the FSC/SSC-gated mononuclear cells,

the $CD11b^+Gr1^+$ cells were recognized as M-MDSCs. In the FSC/SSC-gated granulocytes, the $CD11b^+Gr1^+$ cells were recognized as PMN-MDSCs. The percentage of $CD11b^+Gr\text{-}1^+$ MDSCs was calculated in gated monocytes or neutrophils using FlowJo7.6 software.

Immunofluorescence Analysis for Infiltrated Myeloid-Derived Suppressor Cells in Tumor Tissues

For infiltrated MDSCs in tumor tissues, tumor tissues from the mice were fixed in 10% neutralized formalin overnight and embedded in paraffin blocks [formalin fixed paraffin embedded (FFPE)]. FFPE slides that are 3–4 μm thick were cut from the blocks. The slides were deparaffinized with xylene, rehydrated with gradual alcohols, and incubated in 0.01 M of sodium citrate buffer (pH 6.0) in a 95°C water bath for 15 min for antigen retrieval. After being blocked with 5% FBS in 0.1% PBST (Triton X-100–PBS) for non-specific binding sites, the slides were incubated with FITC-conjugated anti-mouse CD11b and PE-conjugated anti-mouse Gr1 (BioLegend, USA) overnight at 4°C. For MDSC density, the $CD11b^+Gr1^+$ yellow area in random 0.42-mm^2 field within the tumors was measured and averaged. Images were acquired using a fluorescence microscope (Olympus, Japan). Quantification of fluorescent signals was performed using ImageJ software.

In vitro Radiation Response Assay

Hepa1-6 or H22 cells were seeded in 6-cm plates, each with 4×10^5 cells. After being cultured for 24 h, the cells were placed on the 1-cm tissue equivalent compensator and exposed to the IR (voltage, 6 MV; direction, 180°; dose rate, 5 Gy/min; irradiated volume, 10 cm × 10 cm; distance from source to skin, 100 cm) of linear accelerator (CL/1800, Varian Medical System Inc, USA) at different single doses (0, 2.5, 4, 6, or 8 Gy). At the indicated time points, the conditioned media (CM) were collected, and cell debris in CM was removed by centrifugation. The cells in the plates were washed with PBS, harvested, and frozen at −80°C for subsequent analyses.

In vitro Induction of Myeloid-Derived Suppressor Cells

Protein concentrations in the collected CM from the aforementioned irradiated Hepa1-6 or H22 cultures were determined by bicinchoninic acid (BCA) assay (Beyotime, China) and adjusted to the final concentration of 1 mg/ml. Bone marrow cells isolated from C57BL/6 or ICR mice were adjusted to the final density of 2.5×10^6/ml in culture media in the presence of 10 μg/ml of granulocyte-macrophage colony-stimulating factor (GM-CSF) (BioLegend, USA) or the CM from irradiated Hepa1-6 or H22 cells. Three days after the culture, the percentage of $CD11b^+Gr1^+$ MDSCs was measured with flow cytometry (FCM). The proliferation of MDSC was detected by 5,6-carboxyfluorescein diacetate (CFSE) staining.

Cytokine Assay

IL-6, G-CSF, and RANTES in the experimental mouse plasma and the CM collected from irradiated H22 or Hepa1-6 cells cultured *in vitro* were quantified using Mouse Cytokine ELISA Kit (MULTI SCIENCES, China) following the manufacturers' instructions.

Western Blot for p-P65 and p-STAT3

All steps for Western blot were consistent with the published literature (25). Briefly, the irradiated HCC cells were lysed with TNE buffer (10 mM of Tris-HCl, 150 mM of NaCl, 1 mM of EDTA, and 0.5% NP40, pH 7.5). Protein concentrations in the lysates were measured and adjusted to 2 mg/ml. The tumor cell lysates were mixed with 4 × loading buffer [40 mM of Tris-HCl, 200 mM of DTT, 4% sodium dodecyl sulfate (SDS), 40% glycerol, and 0.032% bromophenol blue, pH 8.0]. The mixtures were run on SDS–polyacrylamide gel electrophoresis (SDS-PAGE) gel with 4% stacking gel and 10% separating gel. After being run, separated proteins in the gels were then transferred to nitrocellulose membranes for standard Western blot assay. Target protein bands on the membranes were detected with specific antibodies and developed with Thermo Pierce ECL kit. The results were quantified on FluorChem E exposure device (ProteinSimple, USA).

Statistical Analysis

Quantitative data are presented as average ± standard deviation (SD) unless otherwise indicated. Statistical significance was determined with the one-way ANOVA test followed by Tukey's honestly significant difference (HSD) test with ranks for a multiple-group comparison. The correlation between *in situ* irradiated tumor sizes and the percentage of MDSCs in peripheral blood mononuclear cell (PBMC) of two HCC tumor-bearing models were determined with Pearson correlation with dose as control variate followed by statistical significance set to $p < 0.05$. A statistical analysis of the differences between groups was performed with GraphPad Prism 5.

RESULT

Hypofractionated Irradiation Improved the Local Control of Hepatocellular Carcinoma in Mice

To test what dose per fraction and how many fractions within the clinically used SBRT produce the best antitumor effect, a 40-Gy total ablative dose with different doses/fractions was tested in the two allogeneic HCC mouse models described in the *Materials and Methods*. The fractional radiation schedule is indicated in **Figure 1A**. The IR procedure and the quality control of the IR procedure are shown in **Figure 1B**. The IR suppression of the on-target tumor growth was dose dependent (**Figures 1C,D**). The higher the dose/low fraction used, the greater the suppression of the tumor growth obtained. In Hepa1-6/C57BL/6 model, higher than 4 Gy/fraction of hypofractionated IR (×10) could completely inhibit the tumor growth and 8 Gy/fraction of the hypofractionated IR (×5) completely suppressed tumor growth in the H22/ICR models for 42 days.

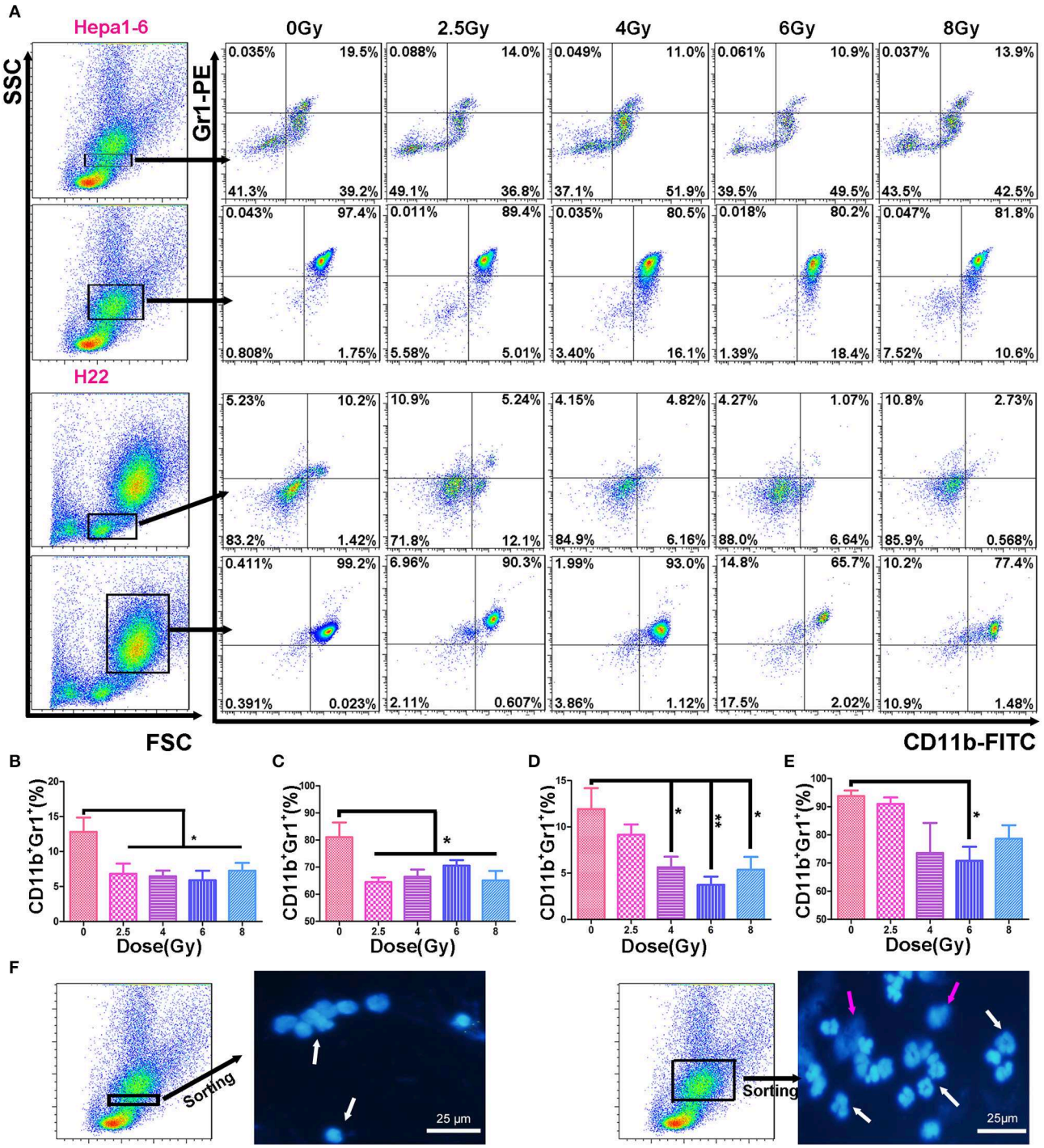

FIGURE 3 | Hypofraction irradiation (IR) reduced the percentage of myeloid-derived suppressor cells (MDSCs) in peripheral blood. On day 3 after a 40-Gy total IR, MDSCs ($CD11b^+Gr1^+$) in mouse peripheral blood were measured with flow cytometry (FCM) in both Hepa1-6/C57BL/6 and H22/Institute of Cancer Research (ICR) mouse models **(A)**. The percentages of MDSCs within monocyte population (the first and third rows of FCM charts, **A**) and granulocyte population (the second and fourth rows) in Hepa1-6/C57BL/6 (the first and second rows) and H22/ICR (the third and fourth rows) mouse models were compared among the groups with different doses of fractional IR. There were significant differences in monocyte-like MDSCs **(B,D)** and granulocyte-like MDSCs **(C,E)** between irradiated groups and unirradiated control group in both animal models [**(B, C)** from Hepa1-6/C57BL/6; **(D, E)** from H22/ICR mouse model] (*$p < 0.05$ and **$p < 0.01$). The nuclear morphological differences between the monocyte-gated MDSCs and granulocyte-gated MDSCs were sorted by flow cytometry and observed after DAPI staining. Images were acquired using a fluorescence microscope (Olympus, Japan). Magnification 400× white ↑ for target nuclear and red ↑ for impurities in the background **(F)**.

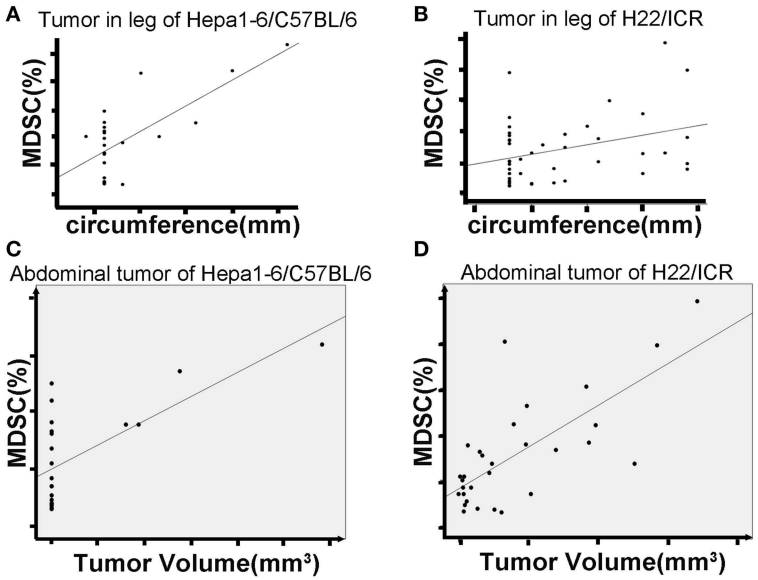

FIGURE 4 | Hypofraction irradiation (IR) reduced blood MDSCs, which was positively correlated with the growth of the tumors. The mice were subcutaneously injected with hepatocellular carcinoma (HCC) cells Hepa1-6 and H22 on one hind limb of each mouse. Three days after the inoculation, the inoculated site was irradiated according to the schedule in **Figure 1A**. The peripheral blood of the mice was collected from the tail vein. The growth of allogeneic tumors was closely monitored. MDSCs in the blood were measured by flow cytometry. Results showed that the size of on-target tumors is positively correlated with the percentage of MDSCs in total white blood cells (**A** for Hepa1-6 allogeneic tumor and **B** for H22 allogeneic tumor) [$r^2 = 0.716$, $p < 0.01$ in Hepa1-6/C57BL/6 model and $r^2 = 0.332$, $p = 0.032 < 0.05$ in H22/Institute of Cancer Research (ICR) models]. There was a positive correlation of blood MDSCs with off-target tumor growth (**C**, **D**, the Pearson $r^2 = 0.45$, $p = 0.041 < 0.05$ in Hepa1-6/C57BL/6 model; $r^2 = 0.529$, $p = 0.003 < 0.01$ in H22/ICR models).

Effects of Irradiation-Induced *in situ* Vaccine on the Growth of Off-Target Tumors

To test whether irradiated tumors formed by Hepa1-6 or H22 cells on one hind limb of each mouse could serve as "IR-induced *in situ* vaccine" and trigger an immune response to exert "abscopal effect," the same tumor cells were subsequently inoculated under the abdominal skin. Results showed that all irradiated on-target tumors had an antitumor immunity effect on the second inoculated off-target tumors (**Figure 2**), except for H22 tumors irradiated with 2.5 Gy/fraction, in which the off-target tumors grew bigger than controls. With the same 40-Gy total dose, the high dose and low fraction of 8 Gy × 5 groups had the strongest immune response and the best abscopal effect than had other low dose/fraction groups in both HCC-bearing mouse models.

Hypofractionated Irradiation Reduced Blood Myeloid-Derived Suppressor Cells, Which Was Positively Correlated With the Growth of the Tumors

The immunosuppressive tumor microenvironment has been believed to be not only one of the key factors stimulating tumor progression but also a strong obstacle for efficient tumor therapy (26). MDSCs as heterogeneous immunosuppressive cells develop and expend during the tumor progression (27). To determine the alteration of MDSCs in peripheral blood during the progression of allogeneic HCC tumors in mouse models, the double-stained ($CD11b^+Gr1^+$) MDSCs were measured in two populations: mononucleocytes and granulocytes with FCM (**Figure 3A**). Results showed that the IR decreased peripheral blood MDSCs in both animal models. There was a significant difference in the percentages of monocyte-like MDSCs (**Figures 3B,D**) and granulocyte-like MDSCs (**Figures 3C,E**) between irradiated groups and unirradiated control group. There was no significantly difference in the MDSC percentage among the irradiated groups with different doses/fraction in a C57BL/6 mouse model. There was a tendency that increasing dose/fraction radiation (except for 8 Gy/fraction) could increase its inhibitory effect on MDSCs in peripheral blood. At the high dose/fraction (≥4 Gy/fraction), the magnitude of MDSCs reduction was greater in C57BL/6 mice than in ICR mice.

Based on the size and nuclear density, the FSC/SSC analysis could further divide $CD11b^+Gr1^+$ MDSCs into monocyte MDSCs (M-MDSCs) *and* granulocyte-like MDSCs (G-MDSCs). Both subpopulations were reduced in mice with IR-treated tumors (**Figure 3**). The number of MDSCs in peripheral blood was positively correlated with the size of the on-target allogeneic tumors in both Hepa1-6/C57BL/6 (**Figure 4A**) and H22/ICR (**Figure 4B**, the Pearson $r^2 = 0.716$, $p < 0.01$ in Hepa1-6/C57BL/6 model; $r^2 = 0.332$, $p = 0.032 < 0.05$ in the H22/ICR models).

We also found a positive correlation of blood MDSCs with off-target tumor growth. That is, the higher the number of blood MDSCs, the faster the off-target tumors grew, indicating that MDSCs act as a positive promoter for the tumor growth (**Figures 4C,D**, the Pearson $r^2 = 0.45$, $p = 0.041 < 0.05$ in

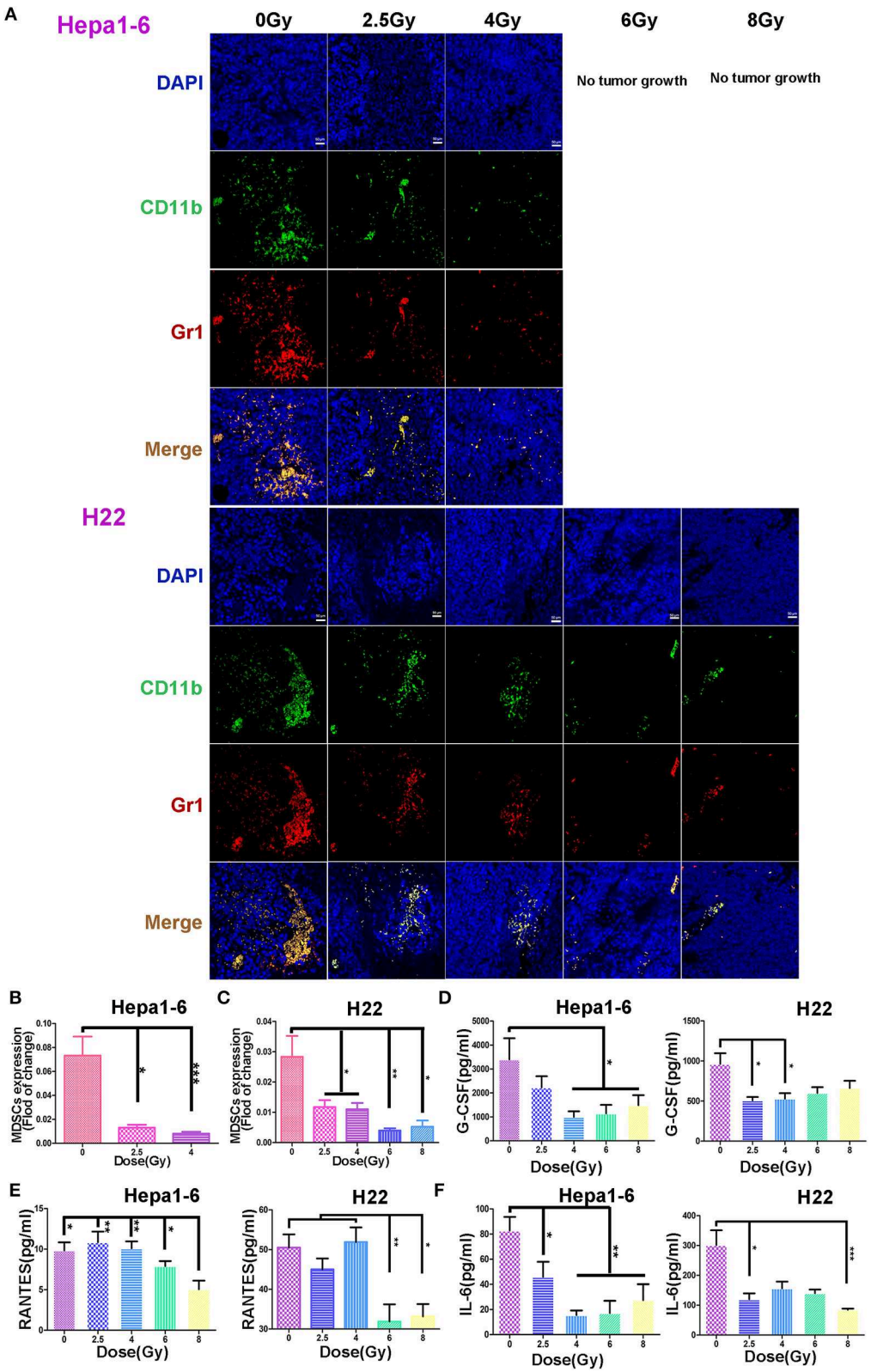

FIGURE 5 | Hypofraction irradiation (IR) reduced the tumor-infiltrating myeloid-derived suppressor cell (MDSC) and plasma granulocyte colony-stimulating factor (G-CSF), IL-6, and regulated on activation normal T cell expressed and secreted (RANTES). The infiltrated MDSCs in allogeneic tumors irradiated with different

(Continued)

FIGURE 5 | doses/fraction (2.5, 4, 6, or 8 Gy) and unirradiated tumors were stained with fluorescein isothiocyanate (FITC) anti-mouse CD11b antibody (green), phycoerythrin (PE) anti-mouse Gr1 antibody (red), and DAPI (blue). The infiltrated MDSCs ($CD11b^+Gr1^+$, yellow) decreased with the increase of radiation dose/fraction applied (**A**, magnification, 200×). The MDSCs in Hepa1-6 and H22 tumors irradiated with different IR doses/fraction were compared. Significant differences were found among the groups with different doses/fraction radiation and without radiation (**B** and **C**). Plasma G-CSF, IL-6, and RANTES in peripheral blood of the mice were quantitatively measured with ELISA kits in both Hepa1-6/C57BL/6 and H22/Institute of Cancer Research (ICR) models. Significant differences in these cytokines in the blood were found after IR with different doses/fraction **(D–F)**. $^*p < 0.05$, $^{**}p < 0.01$, and $^{***}p < 0.0001$.

Hepa1-6/C57BL/6 model; $r^2 = 0.529$, $p = 0.003 < 0.01$ in the H22/ICR models).

Hypofractionated Irradiation Reduced the Tumor-Infiltrating Myeloid-Derived Suppressor Cells

The infiltrated MDSCs in IR-on-target tumor tissues was examined under a fluorescence microscopy after being stained with FITC-labeled anti-mouse CD11b antibody and PE-labeled anti-mouse Gr1 antibody followed by DAPI counterstaining. **Figure 5A** shows that in non-IR control tumors, there was a large amount of infiltrated MDSCs. The MDSCs were significantly reduced in IR tumors. The higher the IR dose/fraction, the lower the tumor-infiltrating MDSCs, which was more obvious in Hepa1-6 tumors than in H22 tumors after 6 to 8 Gy of IR (**Figures 5A–C**). The reduction magnitude of infiltrated MDSCs was greater in C57BL/6 mice than in ICR mice. The difference in the infiltrated MDSCs in tumor tissues between unirradiated and irradiated with 2.5–4 Gy/fraction in Hepa1-6 C57BL/6 mice was less significant than in those irradiated with >4 Gy/fraction (**Figures 5A,C**).

Hypofractionated Irradiation Reduced the Plasma Cytokines and Chemokines

It is well-known that tumor and host cells in the tumor microenvironment produce the pro-inflammatory mediators that activate MDSCs (28, 29). To test if the alteration of MDSCs is related with IR-induced chemokines and cytokines, the plasma G-CSF, IL-6, and RANTES of each mouse were measured with Mouse Cytokine ELISA kits. The plasma IL-6 was decreased in all tumor IR groups (**Figure 5F**). The plasma G-CSF was also decreased in irradiated groups, especially in 4–8 Gy C57BL/6 and 2.5–4 Gy ICR groups, with statistical significance (**Figure 5D**). The plasma RANTES was decreased only in 6- and 8-Gy groups in two mouse models (**Figure 5E**). These results demonstrate that the IR could decrease the expression of MDSC-related stimulatory cytokines: IL-6, G-CSF, and RANTES.

Irradiation Caused Hepatocellular Carcinoma Necrosis, Which Was Related to the Activation of NF-κB and to the Alteration of Cytokine Production by Tumor Cells

It is well-known that tumor cell necrosis could be caused by TNF activation of NF-κB accompanied with tissue damage or inflammation (30, 31). To verify the biological response of HCC cells after different doses of IR, we monitored the phosphorylation change of NF-κB and the cytokine secretion from irradiated HCC. Results demonstrated that p-P65 was significantly elevated after IR in both Hepa1-6 and H22 cells (**Figure 6A**). The elevated p-P65 might relate to the decreased IL-6 and RANTES, whereas the increased G-CSF was significant in the 8-Gy group detected in the CM in both cell lines (**Figure 6B**).

Conditioned Media From High Single-Dose Irradiation Altered the Differentiation or Proliferation of Myeloid-Derived Suppressor Cells

To examine whether the cytokines in the IR-induced CM were correlated with the differentiation or proliferation of MDSC, CM of different single-dose IR-HCC were added to the cultures of bone marrow cells from C57BL/6 or ICR mice. **Figure 6C** shows that CM from high single-dose irradiated Hepa1-6 cells could significantly inhibit the differentiation of bone marrow cells into MDSCs, whereas CM of IR H22 cells did not affect the differentiation of MDSCs but inhibited the proliferation of MDSCs as evidenced by CFSE assay (**Figures 6C–E**).

We then tested the phosphorylation of STAT3 (p-STAT3) of bone marrow cells transformed into MDSCs *in vitro* triggered by CM from different IR doses of HCC with Western blot (**Figure 6F**). As expected, the p-STAT3 was significantly reduced in the MDSCs induced with CM from the high-dose irradiated H22 cultures, whereas the p-STAT3 was not changed in the cells treated with IR Hepa1-6 CM.

DISCUSSION

It has been reported that IR with different dose per fraction schemes could change the tumor immune microenvironment (32, 33) and create "*in situ* vaccine" to induce an effective abscopal effect on remote tumors (off target) (34, 35). This study, using two HCC mouse models, demonstrated that hypofractionated IR was more effective to create the abscopal effect with a high dose per fraction in the same 40-Gy total dose, that is, ≥4 Gy/fraction. The higher the dose/fraction of radiation, the better the inhibition of off-target tumor growth produced.

To reveal the cellular immunological mechanism of the abscopal effect, we focused on the alterations of IR-induced MDSCs (the negative immune breaker), by which hypofractionated IR exerted its off-target effect. It has been well-summarized that RT both promotes and inhibits MDSC function (36). In conventional fractionated IR, there is an increase in MDSCs in both clinical trials and animal models (19, 22). However, high-dose ablative IR reduced the level of MDSCs (22). We found the same results in two HCC tumor-bearing mouse models: (1) the higher the IR dose/fraction, the bigger the off-target effect (**Figure 2**); (2) the bigger the tumor, the higher the blood MDSCs (both G-MDSCs and M-MDSCs)

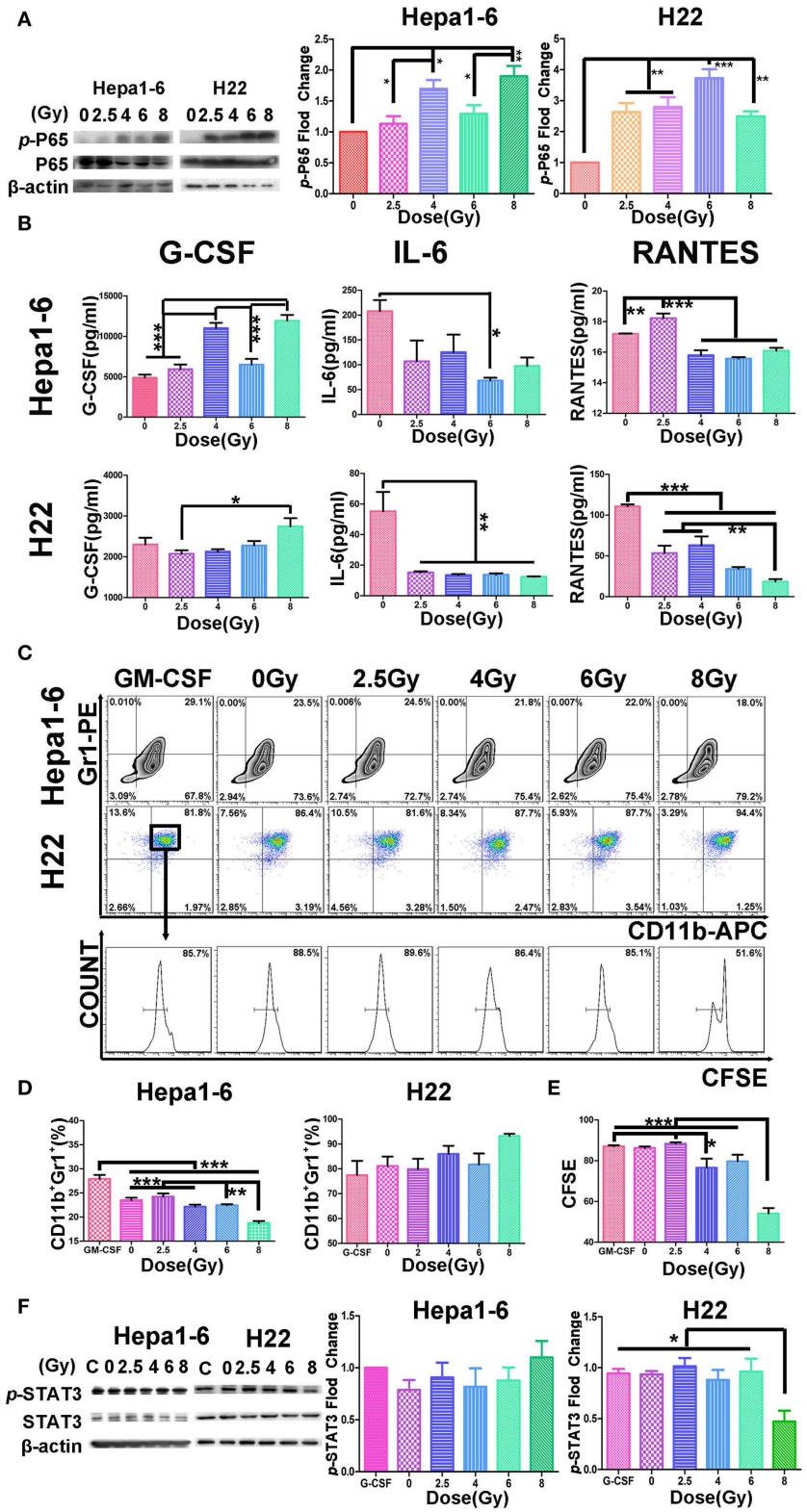

FIGURE 6 | Hypofraction irradiation (IR) increased p-P65, reduced the cytokine secretion from hepatocellular carcinoma (HCC), and inhibited the differentiation or proliferation of MDSCs. **(A)** The phosphorylated P65 increased in Hepa1-6 cells or H22 cells 1 h after IR with different doses of radiation detected by Western blot. **(B)** Two days after Hepa1-6 or H22 cells after IR with different doses (0, 2.5, 4, 6, or 8 Gy), conditioned media (CM) was harvested and the levels of granulocyte

(Continued)

FIGURE 6 | colony-stimulating factor (G-CSF), IL-6, and regulated on activation normal T cell expressed and secreted RANTES in CM were measured with ELISA kits. **(C–E)** The bone marrow cells were harvested from C57BL/6 or Institute of Cancer Research (ICR) mice and co-cultured with CM from Hepa1-6 or H22 cells irradiated with different single doses (0, 2.5, 4, 6, or 8 Gy). Three days later, the differentiation of the bone marrow cells into MDSCs or their proliferated was monitored by CD11b/Gr1 staining or 5,6-carboxyfluorescein diacetate (CFSE) assay. By comparing results from these assays, some differences were found among the different groups. $^{*}p < 0.05$; $^{**}p < 0.01$ except for the granulocyte-macrophage colony-stimulating factor (GM-CSF) concentration. **(F)** The phosphorylation of STAT3 was also detected by Western blotting; and the phosphorylated and unphosphorylated STAT3 bands on Western blots were scanned and their densities were compared. All cytological experiments were repeated three times. $^{***}P < 0.001$.

(**Figure 3**); (3) the higher IR dose, the less blood MDSCs (**Figure 4**) and infiltrated tumor MDSCs (**Figures 5A–C**) found. We also observed that the higher the IR sensitivity, the faster the reduction of tumor size (**Figure 1**) and MDSCs (**Figure 3**), and the better the suppression of remote (off-IR-target) tumor (**Figure 2**). Whether the speed of MDSCs reduction could be utilized as the sensitivity of tumors to IR remains to be further investigated.

Different methods have been used to detect the MDSC subpopulations in blood. Using Ly6G or Ly6C monoclonal antibodies to distinguish the M-MDSCs and PMN-MDSCs was a common method (1). The PMN-MDSCs ($CD11b^{+}Ly6G^{+}Ly6C^{-}$ or $CD11b^{+}Ly6G^{+}Ly6C^{lo}$) and M-MDSCs ($CD11b^{+}Ly6G^{-}Ly6C^{+}$ or $CD11b^{+}Ly6G^{-}Ly6C^{hi}$) (24) showed that the morphology of M-MDSCs was mononuclear and PMN-MDSCs was multinuclear. In this study, we used the FSC/SSC-gated method to distinguish the mononuclear cells and granulocytes and to determine the MDSCs in the two groups by CD11b and Gr1 antibodies. The two group cells were stained with DAPI after sorting by FACSAria^{TM}, and the nuclear morphology was observed using a fluorescence microscope. We proved that M-MDSCs were single nuclear cells and PMN-MDSCs were multinuclear cells (**Figure 3F**). In the FSC/SSC-gated mononuclear cells, the $CD11b^{+}Gr1^{+}$ cells were recognized as M-MDSCs; in the FSC/SSC-gated granulocytes, the $CD11b^{+}Gr1^{+}$ cells were recognized as PMN-MDSCs. The different functions of these two MDSC subpopulations in IR patients remain to be for further careful study.

To further reveal the molecular mechanism related to alterations of HCC with hypofractionated IR, we believe that the necrosis signal transduction should be changed. Therefore, the phosphorylation of key factor NF-κB of necrosis signal transduction was monitored. Consistent with others' report (30), we found that p-P65 was significantly elevated after IR in both Hepa1-6 and H22 cells (**Figure 6A**). The high dose IR of tumor cells also effectively reduced their production of IL-6 and RANTES (**Figure 6**). The phosphorylation of STAT3 was observed in MDSCs treated with H22 but not Hepa1-6 CM, indicating that the IR released NF-κB in H22 test system to reach the threshold of phosphorylation of STAT3, but not in Hepa1-6 test system. Tumor cell necrosis as triggered by TNF activation of NF-κB was also accompanied with inflammation (31). It might be a reason for G-CSF increase in CM of hypofractionated IR cells. It was reported that cytokines and chemokines, such as IL-6 and RANTES, produced by the tumor cells could promote the generation of MDSCs (37–39), which might explain that CM from high single-dose IR cells lead to less differentiation or proliferation of MDSCs (**Figure 6**). MDSCs are utilized by tumors to counteract the immune surveillance by suppressing antigen-presenting cells (APCs) such as DCs and macrophages (40), T cells (41), and NK cells (42). When MDSCs as the breaker of immune surveillance are reduced or removed, the APCs, T cells, and NK cells could better exert their effect on the recognition and killing of tumors, which could explain that the MDSCs were positively correlated with tumor size in our two mouse models (**Figure 4**). The advantage of the hypofractionated IR over surgery is that although surgery simply removes tumors, the "radiation surgery" also creates "*in situ* vaccine" to stimulate the antitumor immunity by removing the MDSC breaker of immune surveillance, a double benefit from IR.

The limitations of this study are as follows: (1) it is a mouse model study, and therefore, the conclusions need to be further confirmed by clinical research; (2) the reduction of MDSCs is one mechanism of the abscopal effect induced by hypofractionated IR, and more underlying mechanisms should be explored.

So far, it is clear that MDSCs, like PD-1, is a negative breaker of immune surveillance. Reduction or removal of MDSCs could be a new strategy for effective treatment of cancers. In fact, several agents have been found to reduce the proliferation of MDSCs or to target MDSCs' trafficking in mouse and human tumors, for example, the inhibitor of CXCR2 (43), the CXCR4 antagonist AMD3100 (44), and the chemotherapeutic drugs doxorubicin (45), sunitinib (tyrosine kinase inhibitor) (46), and Avastin (VEGF-specific monoclonal antibody) (47). Whether the combination of drugs inhibiting MDSC proliferation with hypofractionated IR could enhance the efficacy of antitumor and antimetastasis drugs needs to be studied.

CONCLUSION

The hypofractionated (4–8 Gy/fraction) IR exerts strong on-target and off-target antitumor effects *via* the reduction of MDSCs and its related IL-6, RANTES, and G-CSF. The alteration of MDSCs could be a potential target for effective RT.

DATA AVAILABILITY STATEMENT

All datasets generated for this study are included in the article/Supplementary Material.

ETHICS STATEMENT

This study was carried out in accordance with the recommendations of international guidelines and ethical standards. All animal experiments were approved by Fujian Medical University Institutional Animal Ethical Committee (FJMU IACUC 2018-027).

AUTHOR CONTRIBUTIONS

JC, LZ, and ZW conceived and designed the experiments. JC, ZW, YD, FH, WH, JL, BW, RL, RC, and LF performed the experiments. JC, JH, and YY analyzed the data. JC wrote the paper. JC, JH, WZ, and LZ revised the paper.

FUNDING

This study was supported in part by grants from Scientific Research Project of Education Department of Fujian Province (JAT170232); Fujian Medical University funds (0000-081919); and Science and Technology Program of Fujian Province (2018Y2003).

REFERENCES

1. Bronte V, Brandau S, Chen SH, Colombo MP, Frey AB, Greten TF, et al. Recommendations for myeloid-derived suppressor cell nomenclature and characterization standards. *Nat Commun.* (2016) 7:12150. doi: 10.1038/ncomms12150
2. Budhwar S, Verma P, Verma R, Rai S, Singh K. The yin and yang of myeloid derived suppressor cells. *Front Immunol.* (2018) 9:2776. doi: 10.3389/fimmu.2018.02776
3. Han K, Kim JH. Transarterial chemoembolization in hepatocellular carcinoma treatment: barcelona clinic liver cancer staging system. *World J Gastroenterl.* (2015) 21: 10327–35. doi: 10.3748/wjg.v21.i36.10327
4. Sakisaka M, Haruta M, Komohara Y, Umemoto S, Matsumura K, Ikeda T, et al. Therapy of primary and metastatic liver cancer by human iPS cell-derived myeloid cells producing interferon-β. *J Hepatobiliary Pancreat Sci.* (2017) 24:109–19. doi: 10.1002/jhbp.422
5. Omata M, Cheng AL, Kokudo N, Kudo, M, Lee JM, Jia J, et al. Asia-Pacific clinical practice guidelines on the management of hepatocellular carcinoma: a 2017update. *Hepatol Int.* (2017) 11:317–70. doi: 10.1007/s12072-017-9799-9
6. Lin TA, Lin JS, Wagner T, Pham N. Stereotactic body radiation therapy in primary hepatocellular carcinoma: current status and future directions. *J Gastrointest Oncol.* (2018) 9:858–70. doi: 10.21037/jgo.2018.06.01
7. Rim CH, Kim HJ, Seong J. Clinical feasibility and efficacy of stereotactic body radiotherapy for hepatocellular carcinoma: a systematic review and meta-analysis of observational studies. *Radiother Oncol.* (2019) 131:135–44. doi: 10.1016/j.radonc.2018.12.005
8. Jeong KY, Lee EJ, Kim SJ, Yang SH, Sung YC, Seong J. Irradiation-induced localization of IL-12-expressing mesenchymal stem cells to enhance the curative effect in murine metastatic hepatoma. *Int J Cancer.* (2015) 137:721–30. doi: 10.1002/ijc.29428
9. Yasmin-Karim S, Bruck PT, Moreau M, Kunjachan S, Chen GZ, Kumar R, et al. Radiation and local anti-CD40 generate an effective *in situ* vaccine in preclinical models of pancreatic cancer. *Front Immunol.* (2018) 9:2030. doi: 10.3389/fimmu.2018.02030
10. Kaur P, Asea A. Radiation-induced effects and the immune system in cancer. *Front Oncol.* (2012) 2:191. doi: 10.3389/fonc.2012.00191
11. Krysko DV, Garg AD, Kaczmarek A, Krysko O, Agostinis P, Vandenabeele P. Immunogenic cell death and DAMPs in cancer therapy. *Nat Rev Cancer.* (2012) 12:860–75. doi: 10.1038/nrc3380
12. Romano G, Marino IR. Abscopal effects observed in cancer radiation therapy and oncolytic virotherapy: an overview. *Drugs Today.* (2019) 55:117–30. doi: 10.1358/dot.2019.55.2.2903217
13. Muraro E, Furlan C, Avanzo M, Martorelli D, Comaro E, Rizzo A, et al. Local high-dose radiotherapy induces systemic immunomodulating effects of potential therapeutic relevance in oligometastatic breast cancer. *Front Immunol.* (2017) 8:1476. doi: 10.3389/fimmu.2017.01476
14. Rodríguez-Ruiz ME, Vanpouille-Box C, Melero I. Silvia chiara formenti and sandra demaria. Immunological mechanisms responsible for radiation-induced abscopal effect. *Trends Immunol.* (2018) 39:644–55. doi: 10.1016/j.it.2018.06.001
15. Solinas C, Porcu M, Hlavata Z, De Silva P, Puzzoni M, Willard-Gallo K, et al. Critical features and challenges associated with imaging in patients undergoing cancer immunotherapy. *Crit Rev Oncol Hematol.* (2017) 120:13–21. doi: 10.1016/j.critrevonc.2017.09.017
16. Lugade AA, Moran JP, Gerber SA, Rose RC, Frelinger JG, Lord EM. Local radiation therapy of B16 melanoma tumors increases the generation of tumor antigen-specific effector cells that traffic to the tumor. *J Immunol.* (2005) 174:7516–23. doi: 10.4049/jimmunol.174.12.7516
17. Lee Y, Auh SL, Wang Y, Burnette B, Wang Y, Meng Y, et al. Therapeutic effects of ablative radiation on local tumor require $CD8^+$ T cells: changing strategies for cancer treatment. *Blood.* (2009) 114:589–95. doi: 10.1182/blood-2009-02-206870
18. Vatner RE, Formenti SC. Myeloid-derived cells in tumors: effects of radiation. *Semin Radiat Oncol.* (2015) 25:18–27. doi: 10.1016/j.semradonc.2014.07.008
19. Xu J, Escamilla J, Mok S, David J, Priceman S, West B, et al. CSF1R signaling blockade stanches tumor-infiltrating myeloid cells and improves the efficacy of radiotherapy in prostate cancer. *Cancer Res.* (2013) 73:2782–94. doi: 10.1158/0008-5472.CAN-12-3981
20. Crittenden MR, Cottam B, Savage T, Nguyen C, Newell P, Gough MJ. Expression of NF-κB p50 in tumor stroma limits the control of tumors by radiation therapy. *PLoS ONE.* (2012) 7:e39295. doi: 10.1371/journal.pone.0039295
21. Deng L, Liang H, Burnette B, Beckett M, Darga T, Weichselbaum RR. Irradiation and anti-PD-L1 treatment synergistically promote antitumor immunity in mice. *J Clin Invest.* (2014) 124:687–95. doi: 10.1172/JCI67313
22. Lan J, Li R, Yin LM, Deng L, Gui J, Chen BQ, et al. Targeting myeloid-derived suppressor cells and programmed death ligand 1 confers therapeutic advantage of ablative hypofractionated radiation therapy compared with conventional fractionated radiation therapy. *Int J Radiat Oncol Biol Phys.* (2018) 101:74–87. doi: 10.1016/j.ijrobp.2018.01.071
23. Wang D, An G, Xie S, Yao Y, Feng G. The clinical and prognostic significance of $CD14^{(+)}HLA\text{-}DR^{(-/low)}$ myeloid-derived suppressor cells in hepatocellular carcinoma patients receiving radiotherapy. *Tumour Biol.* (2016) 37:10427–33. doi: 10.1007/s13277-016-4916-2
24. Bei Jia, Chenchen Zhao, Guoli Li, Yaxian Kong, Yaluan Ma, Qiuping Wang, et al. A Novel CD48-based analysis of sepsis-induced mouse myeloid-derived suppressor cell compartments. *Mediators Inflamm.* (2017) 2017:7521701. doi: 10.1155/2017/7521701
25. Huang F, Chen J, Lan R, Wang Z, Chen R, Lin J, et al. δ-Catenin peptide vaccines repress hepatocellular carcinoma growth via $CD8^+$ T cell activation. *Oncoimmunology.* (2018) 7:e1450713. doi: 10.1080/2162402X.2018.1450713
26. Lazăr DC, Avram MF, Romosan I, Cornianu M, Tăban S, Goldi? A. Prognostic significance of tumor immune microenvironment and immunotherapy: novel insights and future perspectives in gastric cancer. *World J Gastroenterol.* (2018) 24:3583–616. doi: 10.3748/wjg.v24.i32.3583
27. Kumar V, Patel S, Tcyganov E, Gabrilovich DI. The nature of myeloid-derived suppressor cells in the tumor microenvironment. *Trends Immunol.* (2016) 37:208–20. doi: 10.1016/j.it.2016.01.004
28. Parker KH, Beury DW, Ostrand-Rosenberg S. Myeloid-derived suppressor cells: critical cells driving immune suppression in the tumor microenvironment. *Adv Cancer Res.* (2015) 128:95–139. doi: 10.1016/bs.acr.2015.04.002
29. Clappaert EJ, Murgaski A, Van Damme H, Kiss M, Laoui D. Diamonds in the rough: harnessing tumor-associated myeloid cells for cancer therapy. *Front Immunol.* (2018) 9:2250. doi: 10.3389/fimmu.2018.02250
30. Wertz IE, O'Rourke KM, Zhou H, Eby M, Aravind L, Seshagiri S, et al. De-ubiquitination and ubiquitin ligase domains of A20 downregulate NF-kappaB signalling. *Nature.* (2004) 430:694–9. doi: 10.1038/nature02794
31. Vanden Berghe T, Linkermann A, Jouan-Lanhouet S, Walczak H, Vandenabeele P. Regulated necrosis: the expanding network of non-apoptotic cell death pathways. *Nat Rev Mol Cell Biol.* (2014) 15:135–47. doi: 10.1038/nrm3737

32. Mathieu G, Richard C, Limagne E, Boidot R, Morgand V, Bertaut A, et al. Optimized fractionated radiotherapy with anti-PD-L1 and anti-TIGIT: a promising new combination. *J ImmunoTher Cancer*. (2019) 7:160. doi: 10.1186/s40425-019-0634-9
33. Formenti SC, Demaria S. Systemic effects of local radiotherapy. *Lancet Oncol.* (2009) 10:718–26. doi: 10.1016/S1470-2045(09)70082-8
34. Marconi R, Strolin S, Bossi G, Strigari L. A meta-analysis of the abscopal effect in preclinical models: Is the biologically effective dose a relevant physical trigger? *PLoS ONE*. (2017) 12:e0171559. doi: 10.1371/journal.pone.0171559
35. McKelvey KJ, Hudson AL, Back M, Eade T, Diakos CI. Radiation, inflammation and the immune response in cancer. *Mamm Genome*. (2018) 29:843–65. doi: 10.1007/s00335-018-9777-0
36. Ostrand-Rosenberg S, Horn LA, and Ciavattone NG. Radiotherapy both promotes and inhibits myeloid-derived suppressor cell function: novel strategies for preventing the tumor-protective effects of radiotherapy. *Front. Oncol.* (2019) 9:215 doi: 10.3389/fonc.2019.00215
37. Ngwa W, Irabor OC, Schoenfeld JD, Hesser J, Demaria S, Formenti SC. Using immunotherapy to boost the abscopal effect. *Nat Rev Cancer*. (2018) 18:313–22. doi: 10.1038/nrc.2018.6
38. Zhang Y, Lv D, Kim HJ, Kurt RA, Bu W, Li Y, Ma X. A novel role of hematopoietic CCL5 in promoting triple-negative mammary tumor progression by regulating generation of myeloid-derived suppressor cells. *Cell Res.* (2013) 23:394–408. doi: 10.1038/cr.2012.178
39. Chen HM, Ma G, Gildener-Leapman N, Eisenstein S, Coakley BA, Ozao J, et al. Myeloid-derived suppressor cells as an immune parameter in patients with concurrent sunitinib and stereotactic body radiotherapy. *Clin Cancer Res.* (2015) 21:4073–85. doi: 10.1158/1078-0432.CCR-14-2742
40. Gabrilovich DI, Ostrand-Rosenberg S, Bronte V. Coordinated regulation of myeloid cells by tumours. *Nat Rev Immunol*. (2012) 12:253–68. doi: 10.1038/nri3175
41. Mazzoni A, Bronte V, Visintin A, Spitzer JH, Apolloni E, Serafini P, et al. Myeloid suppressor lines inhibit T cell responses by an NO-dependent mechanism. *J Immunol*. (2002) 168:689–95. doi: 10.4049/jimmunol.168.2.689
42. Li H, Han Y, Guo Q, Zhang M, Cao X. Cancer-expanded myeloid-derived suppressor cells induce anergy of NK cells through membrane-bound TGF-beta 1. *J Immunol*. (2009) 182:240–9. doi: 10.4049/jimmunol.182.1.240
43. Di Mitri D, Toso A, Chen JJ, Sarti M, Pinton S, Jost TR, et al. Tumour-infiltrating Gr-1^{+} myeloid cells antagonize senescence in cancer. *Nature*. (2014) 515:134–7. doi: 10.1038/nature13638
44. Benedicto A, Romayor I, Arteta B. CXCR4 receptor blockage reduces the contribution of tumor and stromal cells to the metastatic growth in the liver. *Oncol Rep*. (2018) 39:2022–30. doi: 10.3892/or.2018.6254
45. Alizadeh D, Trad M, Hanke NT, Larmonier CB, Janikashvili N, Bonnotte B, et al. Doxorubicin eliminates myeloid-derived suppressor cells and enhances the efficacy of adoptive T-cell transfer in breast cancer. *Cancer Res.* (2014) 74:104–18. doi: 10.1158/0008-5472.CAN-13-1545
46. van Hooren L, Georganaki M, Huang H, Mangsbo SM, Dimberg A. Sunitinib enhances the antitumor responses of agonistic CD40-antibody by reducing MDSCs and synergistically improving endothelial activation and T-cell recruitment. *Oncotarget*. (2016) 7:50277–89. doi: 10.18632/oncotarget.10364
47. Feng PH, Chen KY, Huang YC, Luo CS, Wu SM, Chen TT, et al. Bevacizumab reduces S100A9-positive mdscs linked to intracranial control in patients with EGFR-mutant lung adenocarcinoma. *J Thorac Oncol.* (2018) 13:958–67. doi: 10.1016/j.jtho.2018.03.032

Conflict of Interest: The authors declare that the research was conducted in the absence of any commercial or financial relationships that could be construed as a potential conflict of interest.

frontiers in Oncology

ORIGINAL RESEARCH
published: 24 March 2020
doi: 10.3389/fonc.2020.00376

Potentiation of the Abscopal Effect by Modulated Electro-Hyperthermia in Locally Advanced Cervical Cancer Patients

*Carrie Anne Minnaar[1], Jeffrey Allan Kotzen[2], Olusegun Akinwale Ayeni[3], Mboyo-Di-Tamba Vangu[3] and Ans Baeyens[1,4]**

[1] Radiobiology, Department of Radiation Sciences, University of the Witwatersrand, Johannesburg, South Africa, [2] Radiation Oncology, Wits Donald Gordon Medical Centre, Johannesburg, South Africa, [3] Nuclear Medicine, Department of Radiation Sciences, University of the Witwatersrand, Johannesburg, South Africa, [4] Radiobiology, Department of Human Structure and Repair, Ghent University, Ghent, Belgium

OPEN ACCESS

Edited by:
Mary Helen Barcellos-Hoff,
University of California, San Francisco,
United States

Reviewed by:
Aidan D. Meade,
Technological University
Dublin, Ireland
Peter B. Schiff,
New York University, United States

***Correspondence:**
Ans Baeyens
ans.baeyens@ugent.be;
ans.baeyens@wits.ac.za

Specialty section:
This article was submitted to
Radiation Oncology,
a section of the journal
Frontiers in Oncology

Received: 01 November 2019
Accepted: 04 March 2020
Published: 24 March 2020

Citation:
Minnaar CA, Kotzen JA, Ayeni OA,
Vangu M-D-T and Baeyens A (2020)
Potentiation of the Abscopal Effect by
Modulated Electro-Hyperthermia in
Locally Advanced Cervical Cancer
Patients. Front. Oncol. 10:376.
doi: 10.3389/fonc.2020.00376

Background: A Phase III randomized controlled trial investigating the addition of modulated electro-hyperthermia (mEHT) to chemoradiotherapy for locally advanced cervical cancer patients is being conducted in South Africa (Human Research Ethics Committee approval: M1704133; ClincialTrials.gov ID: NCT03332069). Two hundred and ten participants were randomized and 202 participants were eligible for six month local disease control evaluation. Screening ^{18}F-FDG PET/CT scans were conducted and repeated at six months post-treatment. Significant improvement in local control was reported in the mEHT group and complete metabolic resolution (CMR) of extra-pelvic disease was noted in some participants. We report on an analysis of the participants with CMR of disease inside and outside the radiation field.

Method: Participants were included in this analysis if nodes outside the treatment field (FDG-uptake SUV>2.5) were visualized on pre-treatment scans and if participants were evaluated by ^{18}F-FDG PET/CT scans at six months post-treatment.

Results: One hundred and eight participants (mEHT: HIV-positive $n = 25$, HIV-negative $n = 29$; Control Group: HIV-positive $n = 26$, HIV-negative $n = 28$) were eligible for analysis. There was a higher CMR of all disease inside and outside the radiation field in the mEHT Group: $n = 13$ [24.1%] than the control group: $n = 3$ [5.6%] (Chi squared, Fisher's exact: $p = 0.013$) with no significant difference in the extra-pelvic response to treatment between the HIV-positive and -negative participants of each group.

Conclusion: The CMR of disease outside the radiation field at six months post-treatment provides evidence of an abscopal effect which was significantly associated with the addition of mEHT to treatment protocols. This finding is important as the combined synergistic use of radiotherapy with mEHT could broaden the scope of radiotherapy to include systemic disease.

Keywords: modulated electro-hyperthermia, abscopal effect, radiotherapy, cervical cancer, immunomodulation

INTRODUCTION

The abscopal effect is a systemic response to ionizing radiation (IR) in which non-irradiated lesions respond after irradiation of the primary treatment site (1, 2). It is generally accepted that the abscopal effect is driven by underlying immune mechanisms which are activated by IR (2–4). One proposed mechanism is the immunogenic cell death (ICD) caused by IR (3) which requires the release of damage associated molecular patterns (DAMPs). These in turn activate dendritic cells and enhance antigen expression and presentation to the immune system. Ionizing radiation has also been shown to enhance the functioning of T-cells (4).

The frequency of reported abscopal effects in the literature is extremely low with only a handful of published cases per year (3, 4). In a review, Reynders et al. summarized 23 case reports, one retrospective study, and 13 pre-clinical papers, from the 1970s to 2014. Only one of these involved a primary squamous cell carcinoma of the cervix. The patient (age 69 years) was treated with external beam radiation (EBRT) and brachytherapy (BT) for locally advanced cervical cancer (LACC) and showed a complete response of the para-aortic nodes outside of the radiation field, as well as a complete response of the tumor, on the post-treatment Abdominal and Pelvic Computed Tomography (CT) and Pelvic Magnetic Resonance Imaging (MRI) scans (5). Reynders et al. concluded that the abscopal effect is based on anti-tumor immunity and was more common in immunogenic tumor types. Renal cell carcinoma had the most frequently reported cases of the abscopal effect followed by hepatocellular carcinoma. The abscopal effect was observed at all ages and with a variety of radiotherapy protocols. The preclinical data indicates that some immunomodulatory agents may have potential to act synergistically with IR to induce a systemic response (4) which may explain the increase in the number of reported abscopal effects with the combined treatment of immunotherapies and IR (6).

The addition of mild hyperthermia to local irradiation has shown to have immunomodulating effects which may result in enhanced tumor regression and an abscopal effect when combined with radiotherapy, as was seen in a liposarcoma patient treated with hyperthermia and radiotherapy (7). Hyperthermia may directly activate the immune cells present in the tumor and its microenvironment (8) and may further enhance the function of the dendritic cells (9).

Modulated electro-hyperthermia (mEHT) applies amplitude modulated radiofrequency (13.56 MHz), in a capacitive coupling set-up to target and heat malignant tissues, sensitizing them to treatments. The technique exploits the differences in impedance between the malignant and healthy tissue as well as impedance matching technology, to selectively deliver an energy to the malignant tissues. The energy deposition has the net effect of an increase in the thermal energy, and temperature. The biophysics are further described in detail in the literature (10–12). Preclinical research suggests that mEHT combined with immunotherapies is able to elicit an immune-mediated response (13) which may even extend to untreated tumors. Vancsik et al. showed that mEHT induced DAMPs in murine models was followed by an invasion of antigen presenting cells (APC) and T-cells at the site of the treated tumor and that when mEHT was administered combined with a T-cell stimulating agent, APC and T-cell invasion was also seen in the untreated tumors of the same murine model (14). In an *in vivo* study, mEHT combined with dendritic cell therapy elicited a response to untreated tumors in murine squamous cell carcinoma (SCCVII) models (15). Ionizing radiation has shown to increase the expression of immunogenic molecules such as calreticulin, on the surface of tumor cells and radiation-induced stress-response leads to the expression of heat shock protein70 (HSP70) on cell membranes. This Heat Shock Protein plays an important role in mounting an immune response at the site when released into the extracellular matrix (16). Yang et al. reported an increased release of the expressed HSP70 and increased levels of calreticulin after mEHT, compared to other heating methods (17).

The safety and heating efficacy of mEHT in cervical cancer patients has been demonstrated (18–20). Minnaar et al. (19) reported on local disease control in an ongoing randomized controlled trial investigating the effects of the addition of mEHT to chemoradiotherapy (CRT) protocols for the treatment of LACC. The trial was conducted in a resource-constrained setting and in high risk patients in South Africa. In the report, 202 participants were eligible for six month local disease-free survival (LDFS) and local disease control (LDC) (mEHT: $n = 101$; Control: $n = 101$), of which 171 [mEHT: $n = 88$ (87.1%); Control: $n = 83$ (82.2%)], were alive at six months post-treatment. Participants in the mEHT group had a higher LDC and complete metabolic response of the tumor (45% and 58%), than those in the Control Group (24% and 36%), ($p = 0.005$ and $p = 0.003$, respectively), and were significantly more likely to achieve six month LDFS (OR: 0.36, 95% CI: 0.19-0.69; $p = 0.002$) (19). During the LDC analysis, it was noted that some of the participants with extra-pelvic disease present on the pre-treatment Fluorodeoxyglucose (^{18}F-FDG) Positron Emission Tomography (PET) /CT scans showed a complete metabolic resolution (CMR) of disease outside the treatment field on the post-treatment ^{18}F-FDG PET/CT scans. An analysis of the subset of patients with extra-pelvic disease visualized on the pre-treatment ^{18}F-FDG PET/CT scans was subsequently planned. We present the results of this analysis with the aim of investigating the possibility of an abscopal effect induced by the addition of mEHT to CRT in these participants.

METHODS AND MATERIALS

A Randomized controlled trial by Minnaar et al. (19) is being conducted at the Charlotte Maxeke Johannesburg Academic Hospital, a public hospital in Johannesburg, South Africa, by the Radiation Sciences department of the University of the Witwatersrand. The trial was registered on the South African National Clinical Trials Register before recruitment was started (ID:3012) and approval from the Human Research Ethics Committee was obtained (M704133/M190295). The trial was registered at ClincialTrials.gov (NCT03332069). Enrolment began in January 2014 and was closed in November 2017.

Two hundred and ten participants were randomized to receive either CRT alone (Control Group) or combined with mEHT (mEHT Group). Randomization was conducted using the REDCap on-line computer generated random-sampling tool with stratification according to HIV status and accounting for age and FIGO stage. Physicians reporting on the ^{18}F-FDG PET/CT scans were blinded to treatment allocation and did not interact with the participants, eliminating the risk of biased reporting.

Eligibility

Eligibility criteria for the trial: Females with International Federation of Gynecology and Obstetrics (FIGO) (21) stages IIB to IIIB primary, treatment naïve, histologically confirmed squamous cell carcinoma of the cervix (staged based on clinical examination, chest radiography, and a pelvic ultrasound) eligible for CRT with radical intent; Signed informed consent; >18 years old; Eastern Cooperative Oncology Group (ECOG) score <2; Creatinine clearance >60 mL/min. Screening evaluations included full blood count, urea and creatinine levels, liver function, Human Immunodeficiency Virus (HIV) test; and a CD4 count if necessary. An ^{18}F-FDG PET/CT scan was performed on eligible participants prior to commencement of therapy, as a baseline study against which response to treatment could be measured. Participants with bilateral hydronephrosis, visceral metastases, or fistulas visualized on the ^{18}F-FDG PET/CT scan were excluded from the study. HIV-positive patients were included provided their CD4 count was above 200 cells/μL and/or they had been on antiretroviral therapy (ART) for more than six months.

Exclusion Criteria for the trial: Bilateral hydronephrosis; Second primary malignancy/prior malignancy treated in the preceding two years; vesicovaginal fistula or rectovaginal fistula that required a change in treatment protocols; Abnormal liver function tests; Pregnant or breast feeding; Prior hysterectomy; Cardiovascular disease (excluding controlled hypertension); Acute or life-threatening infections or medical conditions; Contraindications to any of the prescribed treatments.

At the time of this analysis all participants were a minimum of six months post-treatment and local disease control data at six months post-treatment was available for all participants (19). Participants were considered eligible for the sub-analysis presented in this report if: They met all the trial eligibility criteria; the pre-treatment ^{18}F-FDG PET/CT scan showed FDG-avid (SUV > 2.5) nodal disease outside of the pelvic treatment field; and the participants had a post-treatment ^{18}F-FDG PET/CT scan.

Data Management

Participant data was captured using REDCap (Research Electronic Data Capture), an online, secure web based application hosted by the University of the Witwatersrand.

Treatment

All participants were planned to receive 50Gy in 25 fractions EBRT to the whole pelvis and 24Gy in 3 fractions of high dose rate (HDR) BT (36Gy equivalent dose in 2Gy fractions for an alpha-beta ratio of 10; source used: Iridium-192) and two doses of cisplatin (80 mg/m2) administered 21 days apart (subject to the participant's fitness to receive cisplatin), as per institutional protocol. The goal of RT was for participants to receive a total dose of 86Gy equivalent by the combination of EBRT and BT. External beam radiation to the whole pelvis was delivered using a two dimensional four-field-box technique to include the tumor and pelvic nodes. Participants were simulated supine. The superior border of the Anterior-Posterior and Posterior-Anterior (AP-PA) field was mid-L5. The inferior border was either the inferior part of the ischial tuberosity or the lowest extension of the tumor with at least a 2 cm margin, whichever was lower. The lateral borders were 2 cm beyond the lateral margins of the bony pelvis. For the lateral fields, the superior and inferior borders were the same as for the AP-PA fields. The anterior border was the mid to anterior third of the symphysis pubis and the posterior border was S2–S3 to include the presacral nodes and possible tumor extension along the uterosacral ligament.

Modulate electro-hyperthermia (Model: EHY2000+; Manufacturer: Oncotherm GmbH, Troisdorf, Germany) was administered twice per week (maximum ten treatments), at a maximum power of 130 W, immediately before EBRT (maximum 30 min from completion of mEHT to completion of EBRT). Step-up heating protocols were adhered to and mEHT treatments were administered at least 48 h apart. A 30 cm diameter round electrode was used and treatment duration was 55 min at the final power output, with a minimum planned energy dose of 360 KJs. Details of the technique are described elsewhere in the literature (11, 19, 22).

Outcome Measures

Nodes with FDG-avid disease were grouped by region on the pre-treatment scans: Head and Neck; Thorax; Abdomen (including the upper pelvis outside of the radiation field); and Pelvis (within the radiation field). The standard uptake value (SUV) cut-off was considered to be 2.5 and evaluation of the ^{18}F-FDG PET/CT scans was based on PERSIST 1.0 Criteria. Tumor response was classified as Complete Metabolic Response (CMR); Partial Metabolic Response (PMR); Stable Metabolic Disease (SMD); Progressive Metabolic Disease (PMD) (23). On the follow-up scans each region was scored as: no change; resolved nodes; new nodes. Only the complete metabolic response of all disease (nodes outside of the radiation field, nodes inside the radiation field, and the tumor), as visualized on post-treatment ^{18}F-FDG PET/CT scans, was considered an indicator of the abscopal effect.

Statistics

The frequency of the observed abscopal effect was compared by group (mEHT or Control) and HIV status (positive or negative) using a Chi-squared frequency table. Paired *t*-test was used to compare the difference in means between groups and logistic regression was used to test prognostic factors. Two sided *p* values are reported and $p < 0.05$ were considered significant. STATA 13.0 Statistics software program (Stata Corporation, College Station, Texas, USA), was used to analyze the data.

Ethics

All procedures performed in studies involving human participants were in accordance with the ethical standards of the

institutional and/or national research committee (M120477 and M190295) and with the 1964 Helsinki declaration and its later amendments or comparable ethical standards.

RESULTS

Characteristics

Two hundred and ten participants were randomized for treatment, of which 146 [70%] had FDG-avid nodal disease visualized outside of the radiation field on the pre-treatment ^{18}F-FDG PET/CT scans (mEHT Group: $n = 68$ [64%]; Control Group: $n = 78$ [75%]). One hundred and eight of the participants with extra pelvic nodal disease survived six months post-treatment and were eligible for the post-treatment ^{18}F-FDG PET/CT scans (mEHT Group: $n = 54$ [79%]; Control Group: $n = 54$ [69%]) and were therefore included in this analysis. The characteristics, including treatment characteristics, of these 108 participants are listed in **Table 1**. The number of participants (grouped by treatment group and HIV status) with nodes visualized in each region on the pre-treatment ^{18}F-FDG PET/CT scans are shown **Figure 1**. The median number of weeks between the final RT treatment and the follow-up ^{18}F-FDG PET/CT scans was 26.3 in the mEHT Group (Q1: 25.3; Q3: 27.3) and 27 in the Control Group (Q1: 26; Q3: 29).

Abscopal Effect as Visualized on ^{18}F-FDG PET/CT

An abscopal response was only considered if all disease, including the primary tumor, nodes within the radiation field, and all nodes outside of the radiation field showed a complete metabolic response (SUV < 2.5) on the six month post-treatment ^{18}F-FDG PET/CT. Therefore all participants who had an abscopal effect also showed local disease control (a complete metabolic response of the tumor and nodes within the pelvic radiation field). The percentage of participants with complete resolution of all metabolically active disease on six month post-treatment ^{18}F-FDG PET/CT scans was higher in the mEHT group: $n = 13$ [24.1%] than in the control group: $n = 3$ [5.6%] (Chi-squared: $p = 0.013$). There was no significant difference in the response between the HIV-positive ($n = 51$) and -negative ($n = 57$) groups (HIV-positive: $n = 7$ [13%]; HIV-negative: $n = 9$ [16%]; Chi-squared: $p = 0.793$) with a close to even split in frequency of abscopal responses observed between the HIV-positive and -negative participants in each treatment group, as seen in **Figure 2**. In a multivariate analysis (confidence interval [CI] 95%) of age, cisplatin cycles, total radiation dose, and the number of days between the final radiation treatment and the follow-up ^{18}F-FDG PET/CT, none of the variables were indicators of an abscopal effect (Age: OR:1.01, $p = 0.692$, CI: 0.96-1.07; Cisplatin cycles: OR: 1.20; $p = 0.671$; CI: 0.51-2.83; Days to PET/CT: OR: 1.01; $p = 0.283$; CI: 0.99-1.07; Total RT: OR: 0.66; $p = 0.316$; CI: 0.30-1.47). In a univariate analysis, the CD4 count of participants was also not predictive of an abscopal effect (OR: 1.00, $p = 0.893$, CI: 0.997–1.003). In the participants in whom an abscopal effect was observed, the mean time between the final radiation and the follow-up ^{18}F-FDG PET/CT was 196 days (range 162–266).

TABLE 1 | Characteristics of participants eligible for analysis of the abscopal effect.

		mEHT 54	Control 54	
FIGO Staging	IIB	25 [46%]	22 [41%]	
	III	29 [54%]	32 [59%]	
Race	African	51 [94%]	52 [96%]	
	Caucasian	1 [2%]	0 [0%]	
	Other	2 [4%]	2 [4%]	
Age [years]	Mean	49.3	49.9	$p = 0.776$
	SD	9.98	9.99	
	Range	30–68	28–70	
BMI	Mean	28.7	27.0	$p = 0.127$
	SD	5.61	6.01	
	Range	18–44	15–39	
Total RT dose (EQD2)	Mean	85.7Gy	86Gy	$p = 0.251$
	SD	1.65	0	
	Range	74–86Gy	86Gy	
No of Cisplatin doses	Mean	1.37	1.25	$p = 0.321$
	SD	0.69	0.76	
	0 doses	5 [9%]	6 [11%]	
	1 dose	19 [35%]	20 [37%]	
	2 doses	30 [56%]	28 [52%]	
Days between final RT and PET/CT	Mean	188.2	193.4	$p = 0.242$
	SD	24.05	22.15	
	Range	54–310	155–266	
CD4 count [cells/μL]	Mean	552.9	543.9	$p = 0.089$
	SD	264.15	276.36	
	Range	194–1077	134–1524	
No of mEHT doses	Mean	9.54		
	SD	1.07		
	Range	4–10		
Average KJ administered during mEHT	Mean	382.6 KJ		
	SD	29.95		
	Range	259–427 KJ		

No significant differences in characteristics and treatment were seen between the two groups. mEHT, Modulated Electro-Hyperthermia; FIGO, Federation of Gynecology and Obstetrics; SD, Standard Deviation; BMI, Body Mass Index; RT, Radiation Therapy; PET/CT, Positron Emission Tomography / Computed Tomography; KJ, Kilojoules.

Follow up

One participant had visceral disease on the pre-treatment ^{18}F-FDG PET/CT scan: multiple lung nodules (highest SUV in the left lung of 6.03 and the right lung of 4.38) and a lesion in the T11 vertebra (SUV 9.71). This participant was in the mEHT group. The follow-up ^{18}F-FDG PET/CT scan showed no sign of metabolically active disease. This participant is 18 months post-treatment and is still disease free. Of the participants who

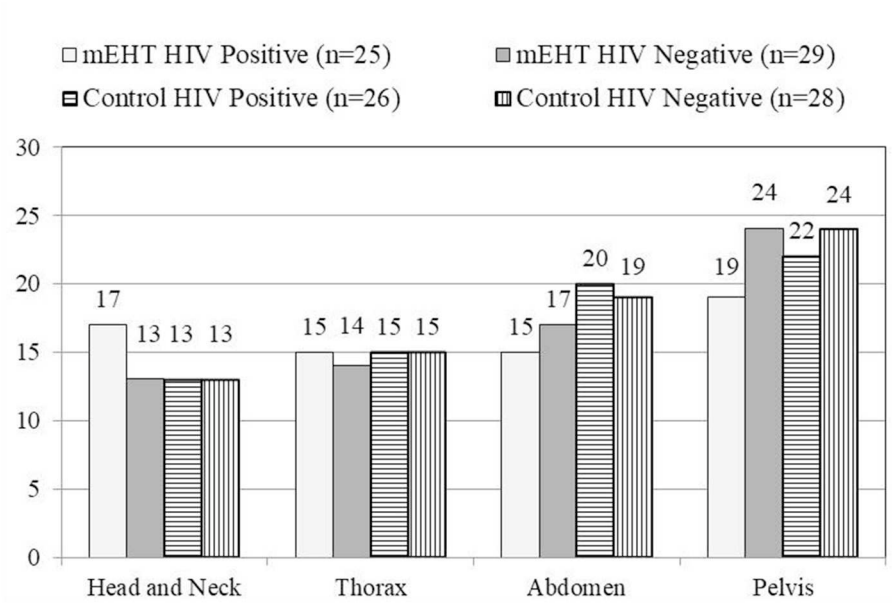

FIGURE 1 | Number of patients with nodes visualized by region. The number of participants with nodes visualized in each region is represented graphically, showing a similar pattern in all participants in each treatment group on the pretreatment ^{18}F-FDG PET/CT. mEHT, Modulated Electro-Hyperthermia; HIV, Human Immunodeficiency Virus.

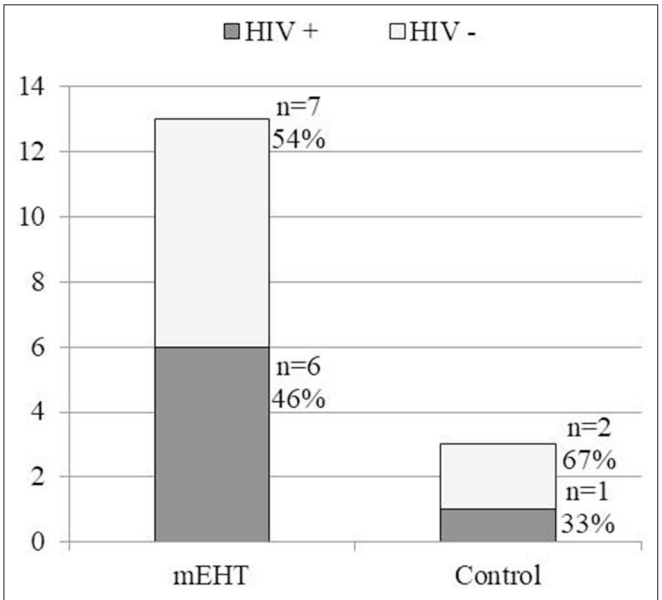

FIGURE 2 | Frequency of observed abscopal effect in HIV-positive and HIV-negative participants in each treatment group. A significant difference between the frequency of abscopal effect was noted between the mEHT Group (13 out of 54[24.1%]) and the Control Group (3 out of 54 [5.6%]) ($p = 0.013$). There was no significant difference in frequency of the observed abscopal between the HIV-positive and HIV-negative participants. mEHT, Modulated Electro-Hyperthermia; HIV, Human Immunodeficiency Virus.

showed an abscopal effect, seven out of 13 mEHT participants and two out of three control participants have reached 2 years post treatment and are still disease free. Two participants in the mEHT group and one in the Control group demised before reaching two years (cause of death: acute renal failure). Four participants in the mEHT group have not yet reached two years post treatment (two are 18 months and two are 12 months post-treatment), however they are still disease free. **Table 2** lists all the sites of FDG avid disease seen in the participants in whom an abscopal response was observed, the disease-free survival observed, the viral load, CD4 count, and the HIV status of the participants.

HIV Status

In order to rule out the effects of HIV on the visualization of nodes, the cases were reviewed with the intention of discarding cases which had nodes known to be visualized in HIV disease. HIV-positive participants with high viral load levels may have benign hypermetabolic foci visualized on ^{18}F-FDG PET/CT images, resulting in false positive interpretations of malignancy (24). Furthermore, Sathekge et al. showed that the CD4 count of HIV positive participants was inversely proportional to the FDG uptake in the nodes (25). During acute HIV infection FDG uptake increases in the head and neck lymph nodes, in mid stage of HIV infection hypermetabolism occurs in cervical, axillary, and inguinal lymph nodes, and an increased FDG uptake occurs in the colon, mesenteric, and ileocecal lymph nodes during late HIV disease (24). None of our participants were in acute (newly diagnosed) or late stage (no Acquired Immune Deficiency Syndrome-defining illnesses other than cervical carcinoma) of HIV infection. Four of the participants with an abscopal response showed increased FDG uptake in the axillary glands: one was HIV-negative and was therefore

TABLE 2 | Details of the extra-pelvic disease in participants with an *Abscopal Effect.

HIV status	Days to PET	No. ChT	Description of extra-pelvic disease on pre-treatment PET/CT	Survival
mEHT group				
Pos. (CD4: 863; VL:27)	211	2	Common carotid (SUV 7.5); Para tracheal (SUV 4.41); Axillary (SUV 5.59)	2YDFS
Pos. (CD4:194; VL:<20)	163	1	Bilat. Jugular. digastric (SUV Left: 2.62; Right: 3.34); Axillary (SUV 4.49); Pre- (SUV 2.75) and Sub-carinal (SUV 3.16); Retrocrural (SUV 3.47) Bilat. PA (SUV Left: 2.59; Right: 3.39)	OS: 335
Pos. (CD4: 905; VL:<20)	200	2	Jug. Digastric (SUV 2.6); Hilar (SUV 2.92)	2YDFS
Pos. (CD4: 845; VL: ND)	190	2	Bilateral supraclav. (SUV Right: 6.04; Left: 2.94)	2YDFS
Pos. (CD4: 456; VL: ND)	192	2	7 Bilat. cervical (highest SUV4.81); Axillary (SUV 4.24); Subcarinal (SUV 2.73); CI (SUV Right: 2.93; Left: 4.73)	2YDFS
Pos. (CD4: 284; VL:196)	182	2	Bilat. Jug. Digastric (SUV Right: 7.42; Left: 2.72); CI (SUV 3.89)	DF at 18 m
Neg.	185	1	Aorto-pulmonary (SUV 2.75)	2YDFS
Neg.	197	1	PA (SUV 4.73)	2YDFS
Neg.	185	2	Cervical (Level IIA SUV 5.67; Level IIB SUV 3.49)	2YDFS
Neg.	183	0	Bilat. axillary (SUV Left: 2.87; Right 2.98)	OS: 596
Neg.	193	2	Supraclav. (SUV 7.42); Paratracheal (SUV 20.38); Aorto-pulmonary (SUV 14.72); Bilat. hilar / Peribronchial (SUV Right 17.86, Left 13.47); Multiple Pulmonary nodules (SUV Right 6.03, Left 4.38); T11 (SUV 9.71)	DF at 18 m
Neg.	224	1	Coelic axis (SUV 7.93)	DF at 12 m
Neg.	189	2	Aorto-pulmonary (SUV 4.1); Pre-carinal (SUV 3.7)	DF at 12 m
Control				
Pos. (CD4: 564; VL: ND)	207	0	PA (SUV 3.35); CI (SUV 4.5 0.9)	OS: 483
Neg,	266	2	Aorto-pulmonary (SUV 2.79); PA (SUV 4.21)	2YDFS
Neg.	183	2	PA (SUV 4.81); Paravertebral (SUV 6.56)	2YDFS

**An abscopal response was considered if there was complete metabolic resolution of the extra-pelvic disease and pelvic disease, including the tumor and pelvic nodes, on the post-treatment ^{18}F-FDG PET/CT scans, with an SUV of <2.5. ChT, Chemotherapy; CI, Common Iliac; DF, Disease Free; HIV, Human Immunodeficiency Virus; mEHT, Modulated Electro-Hyperthermia; ND, Not Detectable; OS, Overall Survival; PA, Para aortic; SUV, Standard Uptake Value; YDFS, Years of Disease Free Survival; VL, Viral Load.*

still included, three were HIV-positive and all had increased FDG uptake in extra-pelvic nodes other than the axillary nodes. These three participants were therefore still included. Of the seven HIV-positive participants, one had increased FDG uptake in the inguinal nodes however several other extra-pelvic nodes were also visualized and the patient was included.

DISCUSSION

The CMR of disease outside the radiation field at six months post-treatment in our sample provides evidence of an abscopal effect. The frequency of the observed abscopal effect was significantly associated with the addition of mEHT. This finding is important as methods to enhance the abscopal effect could broaden the scope of ionizing radiation from a local treatment to a systemic and potentially curative modality for metastatic and systemic disease. The abscopal effect was seen equally in HIV-positive and -negative participants in the group treated with mEHT. This suggests that the potentiation of the systemic, immune-mediated response to IR was not inhibited by HIV-infection and could still be possible in such high risk patients.

Reynders et al. reported that the median time to achieve an abscopal response was five months, ranging from 1 to 24 months (4). In our study we assessed the abscopal effect as part of the disease response at six months, which corresponds to the findings by Reynders et al. In their review Reynders et al. report on patients who had received multiple fractions of radiotherapy followed by a reduction in size/metabolic activity of a non-irradiated lesion (partial response). In our report we present only participants who showed a complete metabolic response of all disease, including the primary tumor. This strengthens the probability of an abscopal response in our participants. Reynders et al. excluded papers in which systemic cytotoxic drugs were administered (4). We have included participants who were treated with cisplatin as a radiosensitiser, however the administration of cisplatin to participants in the mEHT Group and Control group was evenly matched suggesting that the difference between responses in the two groups was not the due to the cisplatin and is associated with the addition of mEHT. Furthermore cisplatin was not a predictor of an abscopal effect in our sample.

The rarity of the abscopal effect documented in the literature suggests that the abscopal effect alone is unlikely to impact clinical regimes and influence treatment choices (3). Considering their immune components, the combination of radiotherapy with immunotherapies and mEHT may provide an opportunity to boost abscopal response rates. Reynders et al. reported on four case reports of the abscopal effect using Ipilimumab (one in adenocarcinoma of the lung and three in melanoma patients), one using BCG-vaccination (adenocarcinoma of the lung) combined with IR, and one retrospective study in which 11 out of 21 melanoma patients treated with Ipilimumab followed by palliative radiotherapy showed an abscopal response (4). The increase in use of immunotherapies combined with IR has resulted in an increase in the reports of abscopal effects. At least ten trials have been registered on ClincialTrials.gov to investigate the effects, including the abscopal effect, of immunotherapies combined with IR. The lack of reliable biomarkers to predict and confirm the presence of an abscopal effect may impact

on the future optimization of protocols to induce an abscopal effect. An important future field of investigation is therefore the development of biomarkers which can reliably predict and quantify the presence of an abscopal effect.

Preclinical data on the synergistic effects of immunomodulating agents and mEHT with IR, as well as case reports, and the results of this study, provide strong support for the development of trials on the combined use of IR with mEHT and immunotherapies. Positive results in such trials would broaden the scope of ionizing radiation from local or palliative treatment to a potentially curative modality in metastatic and systemic disease.

DATA AVAILABILITY STATEMENT

The raw data supporting the conclusions of this article will be made available by the authors, without undue reservation, to any qualified researcher.

ETHICS STATEMENT

All procedures performed in studies involving human participants were in accordance with the ethical standards of the institutional and/or national research committee (Human Research Ethics Committee approval number: M120477) and with the 1964 Helsinki declaration and its later amendments or comparable ethical standards. Informed consent was obtained from all individual participants included in the study.

AUTHOR CONTRIBUTIONS

CM: conducted the research, gathered the data, statistical analysis, interpretation of results, and writing of the manuscript. JK: planning and prescribing of treatments, oversaw the treatment and follow-ups of trial participants, and reviewed manuscript. OA: reviewed ^{18}F-FDG PET/CT reports, reviewed manuscript. M-D-TV: oversaw all the ^{18}F-FDG PET/CT scans and related logistics, reviewed manuscript. AB: supervised data collection and data quality control, project planning, management of funding, and reviewed manuscript.

FUNDING

This study was funded National Research Foundation of South Africa (TP12082710852). ^{18}F-FDG was supplied at a discounted rate by Radioisotopes SOC Ltd. The hyperthermia device was supplied for the purpose of the study by Oncotherm GmbH. The funding sources did not play a role in study design, implementation, data collection, data analysis or in the development/review of the manuscript.

ACKNOWLEDGMENTS

The authors gratefully acknowledge the assistance of Dr. Mariza Tunmer (radiation oncologist) and Dr. Thanushree Naidoo (clinical oncologist) for the advice and support during the study and their input and comments on the manuscript.

REFERENCES

1. Wahl RL, Jacene H, Kasamon Y, Lodge MA. From RECIST to PERCIST: evolving considerations for PET response criteria in solid tumors. *J Nucl Med.* (2009) 50:122–51. doi: 10.2967/jnumed.108.057307
2. Brix N, Tiefenthaller A, Anders H, Belka C, Lauber K. Abscopal, immunological effects of radiotherapy: narrowing the gap between clinical and preclinical experiences. *Immunol Rev.* (2017) 280:249–79. doi: 10.1111/imr.12573
3. Hlavata Z, Solinas C, Scartozzi M. The abscopal effect in the era of cancer immunotherapy: a spontaneous synergism boosting anti-tumor immunity? *Target Oncol.* (2018) 13:113–23. doi: 10.1007/s11523-018-0556-3
4. Reynders K, Illidge T, Siva S, Chang JY, Ruysscher DDe. The abscopal effect of local radiotherapy: using immunotherapy to make a rare event clinically relevant. *Cancer Treat Rev.* (2018) 41:503–10. doi: 10.1016/j.ctrv.2015.03.011
5. Takaya M, Niibe Y, Tsunoda S, Jobo T, Imai M. Abscopal effect of radiation on toruliform para-aortic lymph node metastases of advanced uterine cervical carcinoma - a case report. *Antican Res.* (2007) 504:499–503. Available online at: http://ar.iiarjournals.org/content/27/1B/499.long
6. Ngwa W, Irabor OC, Schoenfeld JD, Hesser J, Formenti SC. Using immunotherapy to boost the abscopal effect. *Nat Rev Cancer.* (2018) 18:313–22. doi: 10.1038/nrc.2018.6
7. Datta NR, Ordóñez SG, Gaipl US, Paulides MM, Crezee H, Gellermann J, et al. Local hyperthermia combined with radiotherapy and- / or chemotherapy: recent advances and promises for the future. *Cancer Treat Rev.* (2015) 41:742–53. doi: 10.1016/j.ctrv.2015.05.009
8. Frey B, Weiss E-M, Rubner Y, Wunderlich R, Ott OJ, Sauer R, et al. Old and new facts about hyperthermia-induced modulations of the immune system. *Int J Hyper.* (2012) 28:528–42. doi: 10.3109/02656736.2012.677933
9. Knippertz I, Stein MF, Dörrie J, Schaft N, Müller I, Deinzer A, et al. Mild hyperthermia enhances human monocyte-derived dendritic cell functions and offers potential for applications in vaccination strategies. *Int J Hyper.* (2011) 27:591–603. doi: 10.3109/02656736.2011.589234
10. Fiorentini G, Szasz A. Hyperthermia today: electric energy, a new opportunity in cancer treatment. *J Cancer Res Ther.* (2006) 2:41–46. doi: 10.4103/0973-1482.25848
11. Szasz O, Szigeti GP, Szasz A. Connections between the specific absorption rate and the local temperature. *Open J Biophy.* (2016) 6:53–74. doi: 10.4236/ojbiphy.2016.63007
12. Szigeti GP, Szasz O, Hegyi G. Personalised dosing of hyperthermia. *J Cancer Diag.* (2016) 1:1–9. doi: 10.4172/2476-2253.1000107
13. Tsang Y, Huang C, Yang K, Chi MS, Chiang HC, Wang YS, et al. Improving immunological tumor microenvironment using electro-hyperthermia followed by dendritic cell immunotherapy. *Biomed Central Cancer.* (2015) 15:1–11. doi: 10.1186/s12885-015-1690-2
14. Vancsik T, Kovago C, Kiss E, Papp E, Forika G, Benyo Z. Modulated electro-hyperthermia induced loco-regional and systemic tumor destruction in colorectal cancer allografts. *J Cancer.* (2018) 9:41–53. doi: 10.7150/jca.21520
15. Qin W, Akutsu Y, Andocs G, Suganami A, Hu X, Yusup G. Modulated electro-hyperthermia enhances dendritic cell therapy through an abscopal effect in mice. *Oncol Rep.* (2014) 32:2373–9. doi: 10.3892/or.2014.3500
16. Frey B, Rückert M, Deloch L, Rühle PF, Derer A, Fietkau R, et al. Immunomodulation by ionizing radiation - impact for design of radio- -immunotherapies and for treatment of inflammatory diseases. *Immun Rev.* (2017) 280:231–48. doi: 10.1111/imr.12572
17. Yang K, Huang C, Chi M, Chiang H, Shan Y. *In vitro* comparison of conventional hyperthermia and modulated. *Oncotarget.* (2016) 7:84082–92. doi: 10.18632/oncotarget.11444

18. Lee S, Lee N, Cho D, Kim J. Treatment outcome analysis of chemotherapy combined with modulated electro-hyperthermia compared with chemotherapy alone for recurrent cervical cancer, following irradiation. *Oncol Lett*. (2017) 14:73–8. doi: 10.3892/ol.2017.6117
19. Minnaar CA, Kotzen JA, Ayeni AO, Naidoo T, Tunmer M, Sharma V, et al. The effect of modulated electro-hyperthermia on local disease control in HIV-positive and -negative cervical cancer women in South Africa : early results from a phase III randomised controlled trial. *PLoS ONE*. (2019) 14:e0217894. doi: 10.1371/journal.pone.0217894
20. Lee S-Y, Kim J-H, Han Y-H, CHo D-H. The effect of modulated electro-hyperthermia on temperature and blood flow in human cervical carcinoma. *Int J Hyper*. (2018) 34:953–60. doi: 10.1080/02656736.2018.1423709
21. Pecorelli S. Revised FIGO staging for carcinoma of the vulva, cervix, and endometrium. *Int J Gynecol Obst*. (2009) 105:103–104. doi: 10.1016/j.ijgo.2009.02.012
22. Szasz O, Szasz A. Heating, efficacy and dose of local hyperthermia. *Open J Biophys*. (2016) 6:10–8. doi: 10.4236/ojbiphy.2016.61002
23. Hyun JO, Lodge MA, Wahl RL. Practical PERCIST: a simplified guide to PET response criteria in solid tumors 1.0. *Radiology*. (2016) 280:576–84. doi: 10.1148/radiol.2016142043
24. Davison JM, Subhramaniam RM, Surasi DS, Cooley T, Mercier G, Peller PJ. FDG PET/CT in Patients With HIV. *Am J Radiol*. (2011) 197:284–94. doi: 10.2214/AJR.10.6332
25. Sathekge M, Maes A, Kgomo M, Van De WC. Fluorodeoxyglucose uptake by lymph nodes of HIV patients is inversely related to CD4 cell count. *Nuclear Med Commun*. (2010). 31:137–40. doi: 10.1097/MNM.0b013e3283331114

Conflict of Interest: The authors declare that the research was conducted in the absence of any commercial or financial relationships that could be construed as a potential conflict of interest.

frontiers in Oncology

REVIEW
published: 21 April 2020
doi: 10.3389/fonc.2020.00562

Tumor Hypoxia: Impact on Radiation Therapy and Molecular Pathways

Brita Singers Sørensen and Michael R. Horsman*

Experimental Clinical Oncology—Department of Oncology, Aarhus University Hospital, Aarhus, Denmark

Tumor hypoxia is a common feature of the microenvironment in solid tumors, primarily due to an inadequate, and heterogeneous vascular network. It is associated with resistance to radiotherapy and results in a poorer clinical outcome. The presence of hypoxia in tumors can be identified by various invasive and non-invasive techniques, and there are a number of approaches by which hypoxia can be modified to improve outcome. However, despite these factors and the ongoing extensive pre-clinical studies, the clinical focus on hypoxia is still to a large extent lacking. Hypoxia is a major cellular stress factor and affects a wide range of molecular pathways, and further understanding of the molecular processes involved may lead to greater clinical applicability of hypoxic modifiers. This review is a discussion of the characteristics of tumor hypoxia, hypoxia-related molecular pathways, and the role of hypoxia in treatment resistance. Understanding the molecular aspects of hypoxia will improve our ability to clinically monitor hypoxia and to predict and modify the therapeutic response.

Keywords: hypoxia, radiation response, gene regulation, intracellular signaling, hypoxia classifyer

OPEN ACCESS

Edited by:
Carsten Herskind,
University of Heidelberg, Germany

Reviewed by:
Chuan-Yuan Li,
Duke University Medical Center, United States
Heidi Lyng,
Oslo University Hospital, Norway

****Correspondence:***
Brita Singers Sørensen
bsin@oncology.au.dk

Specialty section:
This article was submitted to Radiation Oncology, a section of the journal Frontiers in Oncology

Received: *14 January 2020*
Accepted: *30 March 2020*
Published: *21 April 2020*

Citation:
Sørensen BS and Horsman MR (2020) Tumor Hypoxia: Impact on Radiation Therapy and Molecular Pathways. Front. Oncol. 10:562. doi: 10.3389/fonc.2020.00562

CHARACTERISTICS OF TUMOR HYPOXIA

Normal tissues require a regular supply of oxygen and nutrients to maintain viability, and a means for eliminating the waste products of metabolism (1, 2). These processes are achieved through a functional blood supply. Most solid tumors have the same metabolic requirements and to achieve this tumors initially utilize the blood supply of the host organ in which the tumor arises. Eventually that supply becomes inadequate in meeting the demands of the growing tumor mass (1, 2). To compensate, tumors develop their own functional vascular supply from the normal host vascular network by the process of angiogenesis (3, 4). However, despite the significance of this tumor neo-vasculature, the system formed is chaotic and primitive, suffering from numerous structural, and functional abnormalities (1, 2) (**Figure 1**). Consequently, it is actually unable to meet the metabolic demands of the developing tumor. Micro-regional areas are thus formed within the tumor that are characterized by glucose and energy deprivation, high lactate levels and extracellular acidity, and oxygen deficiency (1, 2).

The most extensively studied micro-environmental parameter is hypoxia. Hypoxia is a characteristic feature of most solid tumors and is generally defined as a state of reduced oxygenation that influences biological function (5). As such, it is usually considered as a single entity, which it most definitely is not. From histological data from patients with carcinoma of the bronchus, Thomlinson & Gray suggested that hypoxia could be present in tumors due to a diffusion limit of oxygen (6). Such hypoxia would be chronic in nature (**Figure 1**). Later it was proposed (7) and demonstrated (8) that a form of acute/transient hypoxia could occur, resulting from periodic fluctuations in blood flow (9) (**Figure 1**). This acute hypoxia can result from a complete shut-down in tumor blood flow thus causing ischemic hypoxia, or from a partial shut-down

sufficient to induce hypoxia by preventing red blood cell flow yet allowing plasma flow to continue to supply nutrients. The cause of chronic hypoxia can also be multi-factorial. Although the result of a diffusion limitation, the actual distance from the blood vessel can be highly variable due to several factors. These include the oxygen carrying capacity of the blood, which can be "normal" or reduced as in anemic patients or smokers and the ability of hemoglobin to release oxygen (10). It also involves the intravascular oxygen partial pressure gradient (from the arterial to the venous end of the micro-vessels), and the level of oxygen consumption by the tumor cells and the tumor growth fraction, both of which can vary within and between tumors (10). One also has to consider the degree of oxygenation, which can vary from reasonably well-oxygenated through intermediate levels of hypoxia to severely hypoxic (11).

HYPOXIA AND THE HYPOXIA-INDUCIBLE FACTOR (HIF) REGULATORY PATHWAY

Hypoxia is a major cellular stress factor and in response to this condition, cells undergo a wide range of molecular changes. A number of cellular pathways are affected, including increased glycolysis, decrease of cell proliferation, and enhancement processes involved in angiogenesis and erythropoiesis (**Figure 2**). The hypoxia-mediated intracellular signaling pathways are predominantly orchestrated by intracellular signaling, mainly under control by a family of transcription factors, the hypoxia inducible factors (HIFs) (12, 13). HIF upregulates target gene expression through binding at the hypoxia responsive elements (HREs) in the enhancer and promotor regions of the target genes (14). HIF binds to the DNA as a heterodimer consisting of a alpha (α) subunit (HIF-1α, HIF-2α, or HIF-3α) and a HIF-1β subunit (15). HIF-1β is constitutively expressed, while regulation of HIFα is controlled by tissue oxygenation status, through hydroxylation of two proline residues by prolyl hydroxylase domain proteins (PHD) 1-3 (16, 17) (**Figure 2**). Hydroxylation, occurring only in the presence of oxygen, promotes interaction with the von Hippel-Lindau tumor suppressor protein (pVHL), which targets HIFα for ubiquitination and subsequent proteasomal degradation (18, 19). At oxygen concentrations around 2% O_2 and below this hydroxylation is suppressed leading HIFα to not be degraded (20, 21), and form the active transcription complex with HIF-1β, which induce transcriptional upregulation of a broad range of target genes (22–24). The regulation of HIF-α is not only affected by PHD1-3, since a large plethora of kinases are also involved in the regulation, either directly, or indirectly (15). The major HIF complexes are comprised of HIF-1β, and one of either HIF-1α or HIF-2α, which constitutes the transcription factors referred to as HIF1 and HIF2 (25). HIF1 and HIF2 have structural similarities and identical DNA recognition motifs, but binds to different cell-specific sites across the genome (26, 27). HIF-3α has a structural difference, in that it lacks the C-terminal TAD, and as such is not able to induce the expression of hypoxia-inducible target genes to the same extent as HIF-1α and HIF-2α. HIF-3α competes with HIF-1α or HIF-2α to bind HIF-1β, and can thereby act as a suppressor of HIF-dependent gene expression (25, 28). The HIFs have been shown to influence a large range of cellular functions (**Figure 2**), such as angiogenesis, invasion and metastasis, apoptosis and autophagy, metabolism, intracellular acidosis, and tumor immunity.

HYPOXIA AND CELLULAR STRESS RESPONSES

Cancer cells adapt to hypoxia by a number of stress responses, mediated by the intracellular signaling aimed at facilitating the cells ability to cope with the microenvironment, and to alter the energy requirements as necessary. One of the stress responses is the unfolded protein response (UPR) activated in response to ER stress, endoplasmic reticulum stress, and leads to a downstream activation of adaptive mechanisms. ER stress is the result of an accumulation of unfolded or misfolded proteins, as oxygen depletion can interfere with protein folding (29, 30) Unlike HIF, which is activated at oxygen concentrations below 2%, UPR is activated at exposure to more severe hypoxia (<0.02% O_2) (31). The UPR is a complex of intracellular signaling pathways which are mediated by three independent ER transmembrane proteins: PKR-like ER kinase (PERK), Activating Transcription Factor 6 (ATF6) and inositol-requiring enzyme 1(IRE-1) (32). Exposure to severe hypoxia leads to a reduction in mRNA translation initiation and overall protein synthesis, through a activation of PERK which subsequently phosphorylates eIF2α (33) (**Figure 2**). Activated ATF6 and IRE-11 directly modulates transcriptional induction of UPR target genes. Activation of IRE-1 leads to expression of a panel of genes maintaining metabolic homeostasis and ER through activation of a transcription factor, spliced XBP1 (XBP1s) (34–36). ATF6 is cleaved in the Golgi apparatus, where after the active transcriptional form, ATF6f, translocate to the nucleus and induce transcription of the UPR target genes (29, 37, 38).

Translation of the majority of genes is inhibited under these conditions, but due to regulatory sequences in the 5′ untranslated regions, some gene transcripts are able to escape this inhibition, resulting in an alteration in differential protein expression during hypoxia due to the change in translational efficiency (33, 39).

UPR has been suggested to induce autophagy, an intracellular self-degradation process which can both induce or protect from cell death, through the PERK and BNIP3 pathways (40, 41). The impact of hypoxia on autophagy pathways in malignant cells, and the balance of autophagy in survival and death pathways under hypoxia has shown to be complex. It is susceptible to the genetic background of the cells, as well as the severity of the oxygen deprivation and of other tumor microenvironmental factors (40, 41).

The cellular response to hypoxia also affects the DNA Damage Response (DDR) at very low oxygen concentrations, which includes DNA replication arrest and rapid accumulation of replication stress (**Figure 2**). This is thought to be due to the enzyme responsible for nucleotide production, ribonucleotide

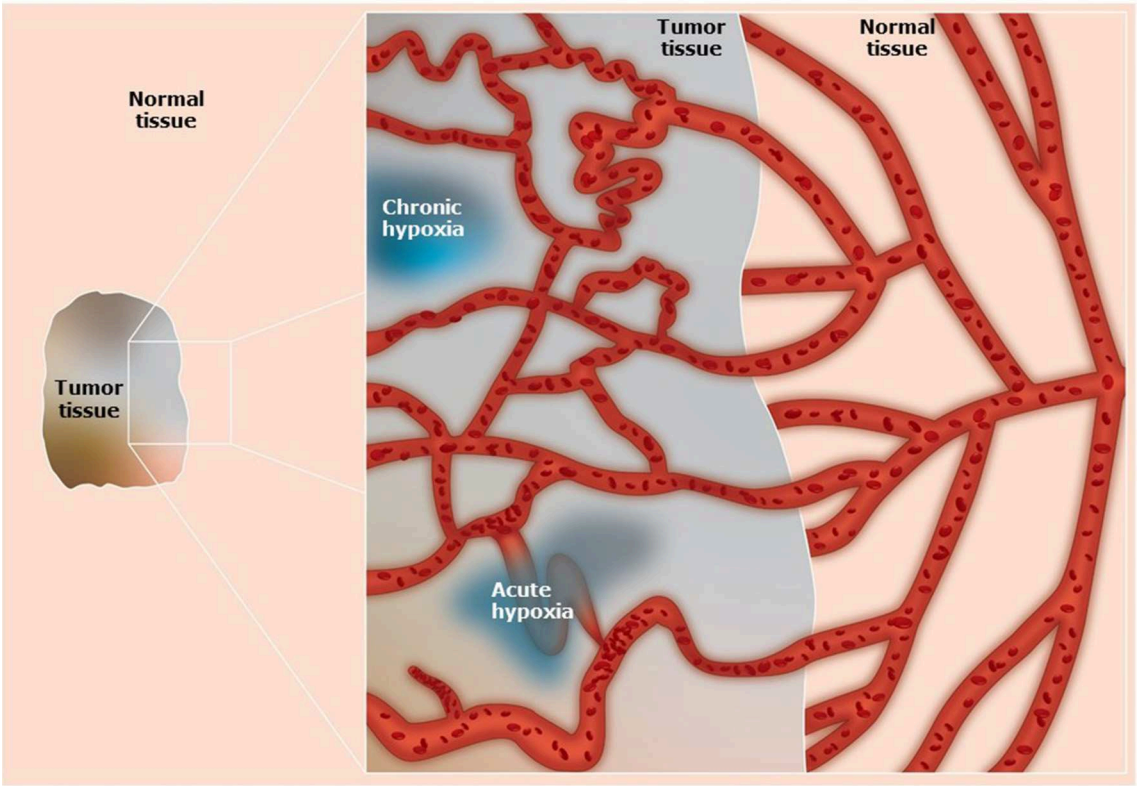

FIGURE 1 | Schematic illustration of the vascular networks in tumors and associated normal tissues. Compared to the well-organized blood supply of normal tissues, in tumors the system is primitive and chaotic. The tumor vascular supply shows abnormal vascular density, contour irregularities, enlarged vessels, vessels with blind ends, and transiently blocked vessels. In addition, there is a loss of hierarchy, a lack of regulatory control mechanisms, and the vessel walls can be structurally defective causing increased vascular permeability. These factors result in the development of diffusion limited chronic hypoxia and perfusion limited acute hypoxia.

reductase, being dependent on cellular oxygen for its function and, therefore, compromised in hypoxic conditions (32, 42). The DDR involves a complex collaboration between signaling pathways activated due to different types of DNA damaging stresses, and the hypoxia induced effects includes both ATR- and ATM-mediated signaling, despite the absence of detectable DNA damage. This results in cellular protection of the replication forks, minimizing the risk of further genomic instability (42–44). Activation of p53 is a consequence of the hypoxia induced DDR, by phosphorylation at a number of residues (45, 46).

The tumor microenvironment is characterized by factors other than tumor hypoxia, such as low pH. Lactic acid accumulation can cause acidosis in solid tumors. In order to compensate for reduced mitochondrial ATP, low oxygen concentrations leads to anaerobic energy production and the formation of lactic acid production, referred to as the Pasteur effect (47). Significant disparities in the temporal and spatial distribution of areas in tumors with low oxygenation level and high level of acidosis results from tumor cells maintaining a high rate of glycolysis even in the presence of oxygen, a which is referred to as aerobic glycolysis or the Warburg effect (48–50). The cellular response in terms of DNA repair and gene transcription and translation succeeding combination of low oxygen concentration and low extracellular pH in combination has shown to be very different compared to the response to either hypoxia or acidosis alone (51, 52). While both hypoxia and acidosis greatly effects the cellular response, simultaneous hypoxia and acidosis *in vitro* suppresses metabolic rate and protein synthesis to a greater extent than each of the factors on their own (53).

IMMUNE INFLAMMATORY PATHWAYS

Cancer immunotherapy has resulted in unprecedented improvements in outcome in patients with a spectrum of solid tumors, and has established itself as the fourth modality in cancer treatment. This is primarily the result of development of vaccines and agents targeting immune regulatory checkpoints, namely the cytotoxic T-lymphocyte-associated protein 4 (CTLA-4), or programmed death 1 (PD-1) and programmed death 1 ligand (PD-L1) (54). Despite positive results, many patients show little or no response to vaccines and checkpoint inhibitors (55). The immune response to tumors is a complex balance between antitumor mechanisms, where

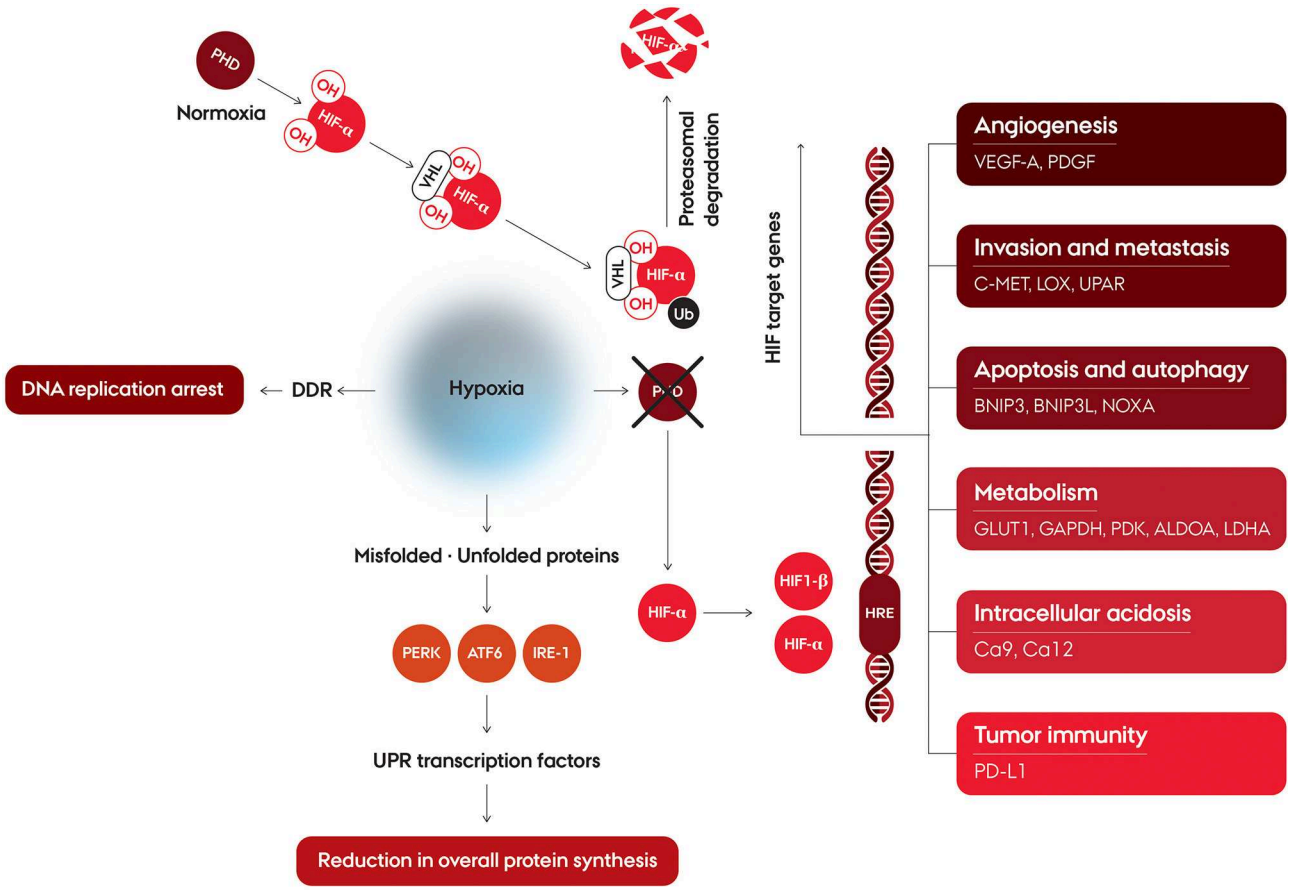

FIGURE 2 | Schematic illustration of cellular pathways affected by hypoxia. Hypoxia affects regulation of hypoxia-inducible factors and induction of HIF target. HIF is a heterodimer consisting of an alpha (α) subunit (HIF-1α, HIF-2α or HIF-3α) and a HIF-1β subunit. Under normoxic conditions, HIF-α is rapidly degraded due to hydroxylation by prolyl hydroxylase domain (PHD) protein. The proline-hydroxylated HIF-α interacts with the von Hippel-Lindau protein (VHL), which targets HIF-α for ubiquitination and degradation via the proteasome. Under hypoxia, HIF-α is stable, and forms the active transcription complex with HIF-1β. After translocation to the nucleus the HIF heterodimer binds at the hypoxia response element (HRE) of target genes thereby initiating the transcription of the HIF target genes. At severe hypoxia, the cellular response also affects the DNA Damage Response (DDR), which leads to DNA replication arrest. Exposure to very low oxygen concentrations also leads to an reduction in mRNA translation initiation and overall protein synthesis, through an activation of the Untranslated Protein Response (UPR).

infiltrating lymphocytes recognize tumor specific antigens on the surface of cancer cells and eliminate the cancer cells thereby decrease tumor growth, and the protumor inflammatory response, which increases immune tolerance, cell survival, and proliferation (56–58). There is evidence that radiation alone can induce an innate immune response, and recent studies have shown that the combination of radiotherapy with immunotherapy has the potential to be an effective treatment modality (59–61).

Hypoxia seems to play a significant role in influencing anti-cancer immune responses (62, 63). It promotes an immunosuppressive microenvironment by regulating the recruitment of T-cells, myeloid-derived suppressor cells (MDSCs), macrophages, and neutrophils (64, 65). In addition, hypoxia can have a negative effect on immunogenicity by altering the function of immune cells and/or increasing resistance of tumor cells to the cytolytic activity of immune effectors (66, 67). There is also evidence that hypoxia can influence immune checkpoints. A rapid and selective up-regulation of PD-L1 is induced by hypoxia on MDSCs, and significant increased expression of PD-L1 on macrophages, dendritic cells and tumor cells, all due to HIF1 binding directly to the HRE in the PD-L1 proximal promoter (68). Hypoxia has also been shown to regulate the CTLA-4 receptor, again potentially via HIF1 (69). Apart from direct immune suppressive effects, hypoxia can also indirectly affect immune response since it causes an increased accumulation of adenosine, drives the expression of vascular endothelial growth factor, and is associated with higher levels of lactate, all of which can inhibit anti-tumor immunity (62, 70). Interestingly, one pre-clinical study using a variety of tumor models showed that by allowing tumor-bearing mice to breathe high oxygen content gas (60% oxygen) rather than the normal 21% oxygen, resulted in an inhibition of tumor progression, a decrease in metastatic disease, and prolonged animal survival (67). This hyperoxia decreased tumor

hypoxia, increased pro-inflammatory cytokines, decreased the levels of immunosuppressive molecules, and weakened immunosuppression by regulatory T-cells.

Clearly, there is a need to investigate role of hypoxia on immune response and understand how modifiers of hypoxia influence that response. Non-invasive imaging may be helpful in this context. Substantial pre-clinical and clinical effort has been made in finding clinically relevant approaches that can non-invasively identify hypoxia in tumors (71). The techniques include positron emission tomography (PET), magnetic resonance imaging, and computed tomography. Using these techniques, especially the PET-based approaches, one not only identifies tumor hypoxia, but also shows its relationship to patient outcome following radiotherapy (71). More recently, a PET based approach has also been developed for non-invasively imaging immunotherapy. It involves radiolabeling various monoclonal antibodies with 89-Zirconium (^{89}Zr). Pre-clinically, these conjugates have included CD4 and CD8 antibodies (72), or an anti-PD-L1 antibody (73). Both approaches allowed for whole body visualization and evaluation of tumor response. Such approaches have even undergone clinical evaluation using ^{89}Zr-labeled atezolizumab, an antibody against PD-L1, and the images obtained in cancer patients was able to assess response to PD-L1 blockade (74). Combining PET-hypoxia markers with immunotherapy based PET markers should allow us to investigate the interaction between both parameters and how that influences patient outcome.

SIGNIFICANCE OF HYPOXIA FOR RADIATION RESPONSE

Estimates of tumor hypoxia obtained using electrodes, exogenous marker expression, or the upregulation of endogenous hypoxia-associated molecules, have not only demonstrated hypoxia to be a common feature of animal solid tumors, human tumor xenografts and human cancers (49, 75), but also a major negative factor influencing tumor radiation response. Pre-clinical studies in the early 1950s demonstrated that when the partial pressure of oxygen was reduced below about 20 mmHg at the time of irradiation cells became resistant to the radiation damage (76). When radiation is absorbed in biological material, highly reactive free radicals are produced either directly or indirectly in the target. These radicals are unstable and will react with oxygen to change the chemical composition of the target, ultimately causing damage. However, under hypoxic conditions the target can be chemically restored to its original form. Typically, under hypoxia one requires 2.5–3.0 fold higher radiation doses to induce the same level of damage as seen under normoxic conditions (77). The type of hypoxia (i.e., chronic or acute) is irrelevant for the initial radioprotection. However, while chronically hypoxic cells are generally also nutrient deprived, acutely hypoxic cells are hypoxic for only a short period (78) and as such are less likely to be nutrient deprived, and this could play a role in influencing the cells ability to repair the radiation damage, thus making acute hypoxia a more resistant factor.

Regardless of whether one type of hypoxia is more of a negative factor, there is good clinical evidence that hypoxia significantly impacts patient outcome following radiation therapy (71). Consequently, substantial effort has been made in the last 50 years to identify approaches that can overcome hypoxia-induced radiation resistance (1, 71). These have involved using agents that either increase oxygen delivery, radiosensitize the hypoxic cells, or preferentially kill them. Attempts have also been made to use dose painting, whereby the hypoxic areas are identified and the radiation dose to these areas is increased, or the use of high LET (linear energy transfer) radiation where hypoxia is less of an issue (79). However, despite the pre-clinical and even clinical demonstrations of the benefit of several of these approaches, only one approach has become established in routine clinical practice and that is the hypoxic cell radiosensitizer nimorazole, and only in head & neck squamous cell carcinoma and only in Denmark (80) and Norway (81).

VASCULAR TARGETING AGENTS AND HYPOXIA

A principal factor controlling the tumor microenvironment, and thus the degree of hypoxia, is its vascular supply. As a result, any treatment that modifies this tumor vascular supply can consequently change the level of hypoxia. One such group are the so-called vascular targeting agents (VTAs). These include angiogenesis inhibitors (AIs) that inhibit the development of the tumor neo-vasculature, and vascular disrupting agents (VDAs) that damage the already establish tumor vascular supply (82, 83).

With VDAs, the vascular damage induced causes a reduction in tumor blood flow and this increases the adverse microenvironmental conditions within tumors leading to substantial cell killing and subsequent increase in necrosis (82, 84, 85). The overall result is a reduction in tumor volume. AIs also inhibit tumor growth, but their effects on the tumor vascular supply and microenvironment are more complex and somewhat controversial. Some years ago it was suggested that rather than AIs simply stopping the angiogenesis process and thus decreasing vessel density they could also actually reduce or abolish the vascular abnormalities of the remaining vessels, causing vessel stabilization resulting in a more efficient vasculature similar to that seen in normal tissues. This stabilization process was termed "normalization" (86) and the more stable, organized vasculature that resulted would likely lead to a better delivery of oxygen and nutrients to the tumor, thus reducing the degree of tumor hypoxia. Numerous studies have since reported that treatment with a range of AIs can indeed give rise to an apparent decrease in tumor hypoxia (82, 84). The first study that demonstrated an improvement in oxygenation status that was associated with vessel normalization was that of Winkler and colleagues (87), using the anti-VEGF (vascular endothelial growth factor) monoclonal antibody DC101. Using a human glioblastoma xenograft grown orthotopically in the mouse brain they found that during treatment with DC101 there was a significant decrease in the level of binding of

the hypoxic marker, pimonidazole, and a similar increase in radiation sensitivity, an affect that was clearly associated with pericyte recruitment. They also found that when pericyte coverage was maximal there was an upregulation of human angiopoietin-1 (Ang-1) and Ephrin B2. Ang-1 is associated with pericyte recruitment and additional studies showed that an increased synthesis of Ang-1 mRNA resulted in an increased Ang-1 protein deposition close to its receptor Tie2 on the endothelial cells (87). Furthermore, when using a Tie2-blocking antibody or peptide to block Ang-1/Tie2 signaling, DC101 was unable to increase pericyte coverage of vessels. However, the reported improvements in oxygenation by AIs are not all due to vessel normalization. Using SU5416, an antagonist of the VEGF receptor, the increase in tumor oxygenation resulted from an inhibition of mitochondrial respiration, thereby decreasing hypoxia by increasing the oxygen diffusion distance (88).

Regardless of the mechanisms for these decreases in tumor hypoxia, the improved oxygenation in both these studies was somewhat transient and only lasted for a period of a few days despite the AI treatment being continued. This "narrow window" of improved oxygenation has also been seen with thalidomide (89, 90), a nucleolin antagonist (91), and bevacizumab (92–95), regardless of the technique used to monitor the changes in oxygenation/hypoxia. The transient nature of this effect would suggest that the timing of hypoxia measurement is critical. In fact, two studies reported both a decrease and increase in hypoxia depending on the time of measurement after treatment with either DC101 (96) or bevacizumab (95).

Although at least one clinical study suggested an apparent improvement in oxygenation with AI therapy (97), several pre-clinical studies reported no change in tumor oxygenation status despite the AIs causing a decrease in vascular density and blood perfusion (1, 98). More significantly, in the majority of reported pre-clinical studies these AI-induced anti-vascular effects actually led to an increase in hypoxia, in line with what one would expect (1, 82). It could be argued that these different effects on tumor oxygenation status could be the result of using different drugs, doses, scheduling, or the time of hypoxia assessment. However, it seems more likely that the effects are a tumor dependent phenomena. This is probably best illustrated using DC101, where one study showed that 2 days after treating animals with DC101 (3×40 mg/kg), U87 gliomas were significantly better oxygenated when measured using a hypoxic specific marker (87). Yet another study using the same drug, almost identical dose schedule (3×45 mg/kg), and similar hypoxic specific marker, found that 2 days after treatment, MCa4/MCa35 mammary carcinomas were significantly more hypoxic (99). This same controversy was seen in the limited clinical studies in which both a decrease (100) and an increase (101, 102) in tumor hypoxia have been reported. Such findings clearly argue against making sweeping statements about the effects of AIs on tumor hypoxia and that either measurements of the oxygenation status need to be routinely made when AIs are administered or that they be given in such a way as to avoid any negative influence on the conventional treatment with which they are combined.

MOLECULAR HYPOXIA BIOMARKERS

To take advantage of the cellular response to hypoxia, the use of expression levels of hypoxia induced genes as biomarkers for tumor hypoxia has been widely investigated. Initially, single genes such as HIF-1, Ca9, and Glut1 measured either at the protein level, with for example immunohistochemistry, or on the mRNA level with for instance qPCR, was used in a range of studies (103–106). The use of single gene expression markers for tumor hypoxia has often led to conflicting reports, due to the genes being influenced by factors other than hypoxia, such as extracellular pH or glucose concentrations (107, 108). Ca9 expression was one such factor proposed as a hypoxia marker in a number of studies, however other experimental studies clearly demonstrated that hypoxia and Ca9 expression did not exclusively correlate (109). Certain microRNAs (miRNAs) have also demonstrated to be inducible by hypoxia (110, 111), as for example hsa-mir-210 which has shown to be hypoxia related and to have prognostic significance in several tumor types, e.g., in cervical cancer (112), in breast cancer (113), and in bladder cancer (114).

Progresses in gene expression profiling have let to a higher level of understanding of the biology of hypoxia, and development of hypoxic signatures based on a number of genes rather than on single genes as biomarkers for tumor hypoxia (115–122). These have typically been developed by determining global gene expression levels by gene expression arrays, and identifying genes preferentially upregulated by hypoxia based on either *in vitro* or clinically derived gene expression data sets. There is no consensus to the optimal way to develop gene expression signatures, and the currently published hypoxia gene expression signatures are at different stages in respect to clinical usability and validation (123).

The Toustrup 15-gene-classifier was developed from a panel of genes, identified in an *in vitro* study in a panel of Head and Neck Squamous Cell Carcinoma (HNSCC) cell lines as upregulated by low oxygen concentration, independent of pH. It was developed in a training cohort of 58 HNSCC patients with the oxygenation status measured using an oxygen electrode. The classifier was validated in the DAHANCA 5 cohort, which is a Danish study where patients were randomized to receive either the previous mentioned hypoxic cell radiosensitizer nimorazole, or placebo, with radiotherapy. The classifier was in this cohort demonstrated to be both prognostic and have predictive impact for hypoxic modification (124). The 26-gene classifier by Eustace et al. (121), is another hypoxia signature in HNSCC. This signature is based on a metagene signature developed for patients with breast, lung and head and neck cancers. In the Dutch ARCON trial, which compared treatment with radiotherapy combined with carbogen and nicotinamide, two hypoxia modifying agents, compared to radiotherapy alone in patients with laryngeal cancer, the patients classified as "more hypoxic" according to the 26-gene classifier showed a significantly improved locoregional control in when treated with the modifying agents (123, 125).

Several studies have aimed at comparing the published gene signatures (126–129), but with the constraint that

common analyzing methods have been used, such as the two-class k-means clustering, and not the validated analysis method, which for some of the gene signatures include cutoff values.

To utilize the biological knowledge, studies have been focused on combining gene signatures for hypoxia with other factors known to affect cellular factors influencing the response to radiotherapy, such as markers for cancer stem cells (129), and for proliferation and DNA repair (119). Currently, for all signatures there is a need for a continued validation, both at the technical and clinical level (130, 131), especially to be able to advance from retrospective to prospective classification of the hypoxic status of patients and subsequently the assignment to hypoxia-modifying therapies in the clinic.

Tumor hypoxia mediates intercellular signaling through the regulation of many cytokines and angiogenic factors (CAF), and serum or plasma levels of hypoxia associated proteins have also been suggested as markers for hypoxia (132–134). One of the proteins which have been intensively studied is osteopontin (OPN). OPN has both *in vitro* and *in vivo* shown to be upregulated by hypoxia (108, 135), and clinical studies have found a high level of OPN to be associated with a poor prognosis, both in HNSCC (136, 137) and small cell lung cancer (138). The findings of a correlation of OPN levels and hypoxia is not consistent across studies (139), and it has been demonstrated that the measured level of OPN is sensitive to the choice of analysis platform (140). Nonetheless, hypoxia associated circulating proteins could add prognostic information on patient outcome.

CONCLUSION

In the age of targeted therapies, hypoxia has to be considered the ultimate target. Hypoxia exists in virtually all solid tumor types, it influences patient response to radio-, chemo-, and immune-therapy, and plays a major role in malignant progression. Its presence in tumors can be identified by various invasive and non-invasive techniques, and there are a number of approaches by which hypoxia can be modified to improve outcome. However, despite these factors and the ongoing extensive pre-clinical studies, the clinical focus on hypoxia is still to a large extent lacking. Molecular pathways are the fundamental background for the cellular response to hypoxia, and further understanding of the molecular processes involved may help overcome this limitation.

AUTHOR CONTRIBUTIONS

MH and BS formulated the topic of the review and drafted and approved the manuscript.

REFERENCES

1. Siemann DW, Horsman MR. Modulation of the tumor vasculature and oxygenation to improve therapy. *Pharmacol Ther.* (2015) 153:107–24. doi: 10.1016/j.pharmthera.2015.06.006
2. Horsman MR, Vaupel P. Pathophysiological basis for the formation of the tumor microenvironment. *Front Oncol.* (2016) 6:66. doi: 10.3389/fonc.2016.00066
3. Folkman J. How is blood vessel growth regulated in normal and neoplastic tissue? G.H.A. clowes memorial award lecture. *Cancer Res.* (1986) 46:467–73.
4. Bergers G, Benjamin LE. Tumorigenesis and the angiogenic switch. *Nat Rev Cancer.* (2003) 3:401–10. doi: 10.1038/nrc1093
5. Hockel M, Vaupel P. Tumor hypoxia: definitions and current clinical, biologic, and molecular aspects. *JNCI J Natl Cancer Inst.* (2001) 93:266–76. doi: 10.1093/jnci/93.4.266
6. Thomlinson RH, Gray LH. The histological structure of some human lung cancers and the possible implications for radiotherapy. *Br J Cancer.* (1955) 9:539–49. doi: 10.1038/bjc.1955.55
7. Brown JM. Evidence for acutely hypoxic cells in mouse tumours, and a possible mechanism of reoxygenation. *Br J Radiol.* (1979) 52:650–6. doi: 10.1259/0007-1285-52-620-650
8. Chaplin DJ, Olive PL, Durand RE. Intermittent blood flow in a murine tumor: radiobiological effects. *Cancer Res.* (1987) 47:597–601.
9. Kimura H, Braun RD, Ong ET, Hsu R, Secomb TW, Papahadjopoulos D, et al. Fluctuations in red cell flux in tumor microvessels can lead to transient hypoxia and reoxygenation in tumor parenchyma. *Cancer Res.* (1996) 56:5522–8.
10. Bayer C, Shi K, Astner ST, Maftei C-A, Vaupel P. Acute versus chronic hypoxia: why a simplified classification is simply not enough. *Int J Radiat Oncol.* (2011) 80:965–8. doi: 10.1016/j.ijrobp.2011.02.049
11. Wouters BG, Brown JM. Cells at intermediate oxygen levels can be more important than the "Hypoxic Fraction" in determining tumor response to fractionated radiotherapy. *Radiat Res.* (1997) 147:541. doi: 10.2307/3579620
12. Semenza GL. HIF-1: mediator of physiological and pathophysiological responses to hypoxia. *J Appl Physiol.* (2000) 88:1474–80. doi: 10.1152/jappl.2000.88.4.1474
13. Pugh CW, Ratcliffe PJ. New horizons in hypoxia signaling pathways. *Exp Cell Res.* (2017) 356:116–21. doi: 10.1016/j.yexcr.2017.03.008
14. Wang GL, Semenza GL. General involvement of hypoxia-inducible factor 1 in transcriptional response to hypoxia. *Proc Natl Acad Sci USA.* (1993) 90:4304–8. doi: 10.1073/pnas.90.9.4304
15. Kietzmann T, Mennerich D, Dimova EY. Hypoxia-Inducible Factors (HIFs) and phosphorylation: impact on stability, localization, and transactivity. *Front Cell Dev Biol.* (2016) 4:11. doi: 10.3389/fcell.2016.00011
16. Bruick R., McKnight SL. A conserved family of prolyl-4-hydroxylases that modify HIF. *Science.* (2001) 294:1337–40. doi: 10.1126/science.1066373
17. Epstein ACR, Gleadle JM, McNeill LA, Hewitson KS, O'Rourke J, Mole DR, et al. C. Elegans EGL-9 and mammalian homologs define a family of dioxygenases that regulate HIF by prolyl hydroxylation. *Cell.* (2001) 107:43–54. doi: 10.1016/S0092-8674(01)00507-4
18. Pugh CW, Ratcliffe PJ. The von Hippel–Lindau tumor suppressor, hypoxia-inducible factor-1 (HIF-1) degradation, and cancer pathogenesis. *Semin Cancer Biol.* (2003) 13:83–9. doi: 10.1016/S1044-579X(02)00103-7
19. Cockman ME, Masson N, Mole DR, Jaakkola P, Chang GW, Clifford SC, et al. Hypoxia inducible factor-α binding and ubiquitylation by the von Hippel-Lindau tumor suppressor protein. *J Biol Chem.* (2000) 275:25733–41. doi: 10.1074/jbc.M002740200
20. Bracken CP, Fedele AO, Linke S, Balrak W, Lisy K, Whitelaw ML, et al. Cell-specific regulation of hypoxia-inducible factor (HIF)-1alpha and HIF-2alpha stabilization and transactivation in a graded oxygen environment. *J Biol Chem.* (2006) 281:22575–85. doi: 10.1074/jbc.M600288200
21. Jiang BH, Semenza GL, Bauer C, Marti HH. Hypoxia-inducible factor 1 levels vary exponentially over a physiologically relevant range of O2 tension. *Am J Physiol.* (1996) 271:C1172–80. doi: 10.1152/ajpcell.1996.271.4.C1172

22. Jaakkola P, Mole DR, Tian YM, Wilson MI, Gielbert J, Gaskell SJ, et al. Targeting of HIF-alpha to the von Hippel-Lindau ubiquitylation complex by O2-regulated prolyl hydroxylation. *Science.* (2001) 292:468–72. doi: 10.1126/science.1059796
23. Ivan M, Kondo K, Yang H, Kim W, Valiando J, Ohh M, et al. HIFalpha targeted for VHL-mediated destruction by proline hydroxylation: implications for O2 sensing. *Science.* (2001) 292:464–8. doi: 10.1126/science.1059817
24. Maxwell PH, Wiesener MS, Chang G-W, Clifford SC, Vaux EC, Cockman ME, et al. The tumour suppressor protein VHL targets hypoxia-inducible factors for oxygen-dependent proteolysis. *Nature.* (1999) 399:271–5. doi: 10.1038/20459
25. Semenza GL. Hypoxia-inducible factors in physiology and medicine. *Cell.* (2012) 148:399–408. doi: 10.1016/j.cell.2012.01.021
26. Smythies JA, Sun M, Masson N, Salama R, Simpson PD, Murray E, et al. Inherent DNA-binding specificities of the HI-1α and HIF-2α transcription factors in chromatin. *EMBO Rep.* (2019) 20:e46401. doi: 10.15252/embr.201846401
27. Loboda A, Jozkowicz A, Dulak J. HIF-1 versus HIF-2 — Is one more important than the other? *Vascul Pharmacol.* (2012) 56:245–51. doi: 10.1016/j.vph.2012.02.006
28. Gu YZ, Moran SM, Hogenesch JB, Wartman L, Bradfield CA. Molecular characterization and chromosomal localization of a third alpha-class hypoxia inducible factor subunit, HIF3alpha. *Gene Expr.* (1998) 7:205–13.
29. Lee P, Chandel NS, Simon MC. Cellular adaptation to hypoxia through hypoxia inducible factors and beyond. *Nat Rev Mol Cell Biol.* (2020) doi: 10.1038/s41580-020-0227-y
30. Feldman DE, Chauhan V, Koong AC. The unfolded protein response: a novel component of the hypoxic stress response in tumors. *Mol Cancer Res.* (2005) 3:597–605. doi: 10.1158/1541-7786.MCR-05-0221
31. Koumenis C, Wouters BG. "Translating" Tumor Hypoxia: Unfolded Protein Response (UPR)-dependent and UPR-independent pathways. *Mol Cancer Res.* (2006). 4:423–36. doi: 10.1158/1541-7786.MCR-06-0150
32. Ron D, Walter P. Signal integration in the endoplasmic reticulum unfolded protein response. *Nat Rev Mol Cell Biol.* (2007) 8:519–29. doi: 10.1038/nrm2199
33. Koritzinsky M, Magagnin MG, van den Beucken T, Seigneuric R, Savelkouls K, Dostie J, et al. Gene expression during acute and prolonged hypoxia is regulated by distinct mechanisms of translational control. *EMBO J.* (2006) 25:1114–25. doi: 10.1038/sj.emboj.7600998
34. Xie H, Tang C-HA, Song JH, Mancuso A, Del Valle JR, Cao J, et al. IRE1α RNase–dependent lipid homeostasis promotes survival in Myc-transformed cancers. *J Clin Invest.* (2018) 128:1300–16. doi: 10.1172/JCI95864
35. Liu Y, Adachi M, Zhao S, Hareyama M, Koong AC, Luo D, et al. Preventing oxidative stress: a new role for XBP1. *Cell Death Differ.* (2009) 16:847–57. doi: 10.1038/cdd.2009.14
36. Chen X, Iliopoulos D, Zhang Q, Tang Q, Greenblatt MB, Hatziapostolou M, et al. XBP1 promotes triple-negative breast cancer by controlling the HIF1α pathway. *Nature.* (2014) 508:103–7. doi: 10.1038/nature13119
37. Haze K, Yoshida H, Yanagi H, Yura T, Mori K. Mammalian transcription factor ATF6 Is synthesized as a transmembrane protein and activated by proteolysis in response to endoplasmic reticulum stress. *Mol Biol Cell.* (1999) 10:3787–99. doi: 10.1091/mbc.10.11.3787
38. Yoshida H, Matsui T, Yamamoto A, Okada T, Mori K. XBP1 mRNA is induced by ATF6 and spliced by IRE1 in response to ER stress to produce a highly active transcription factor. *Cell.* (2001) 107:881–91. doi: 10.1016/S0092-8674(01)00611-0
39. Chipurupalli S, Kannan E, Tergaonkar V, D'Andrea R, Robinson N. Hypoxia induced ER stress response as an adaptive mechanism in Cancer. *Int J Mol Sci.* (2019) 20. doi: 10.3390/ijms20030749
40. Fang Y, Tan J, Zhang Q. Signaling pathways and mechanisms of hypoxia-induced autophagy in the animal cells. *Cell Biol Int.* (2015) 39:891–8. doi: 10.1002/cbin.10463
41. Mazure NM, Pouysségur J. Hypoxia-induced autophagy: cell death or cell survival? *Curr Opin Cell Biol.* (2010) 22:177–80. doi: 10.1016/j.ceb.2009.11.015
42. Olcina M, Lecane PS, Hammond EM. Targeting hypoxic cells through the DNA damage response. *Clin Cancer Res.* (2010) 16:5624–9. doi: 10.1158/1078-0432.CCR-10-0286
43. Ng N, Purshouse K, Foskolou IP, Olcina MM, Hammond EM. Challenges to DNA replication in hypoxic conditions. *FEBS J.* (2018) 285:1563–71. doi: 10.1111/febs.14377
44. Bristow RG, Hill RP. Hypoxia, DNA repair and genetic instability. *Nat Rev Cancer.* (2008) 8:180–92. doi: 10.1038/nrc2344
45. Green DR, Kroemer G. Cytoplasmic functions of the tumour suppressor p53. *Nature.* (2009) 458:1127–30. doi: 10.1038/nature07986
46. Riley T, Sontag E, Chen P, Levine A. Transcriptional control of human p53-regulated genes. *Nat Rev Mol Cell Biol.* (2008) 9:402–12. doi: 10.1038/nrm2395
47. Barnett JA. A history of research on yeasts 2: Louis Pasteur and his contemporaries, 1850-1880. *Yeast.* (2000) 16:755–71. doi: 10.1002/1097-0061(20000615)16:8<755::AID-YEA587>3.0.CO;2-4
48. Koppenol WH, Bounds PL, Dang C V. Otto Warburg's contributions to current concepts of cancer metabolism. *Nat Rev Cancer.* (2011) 11:325–37. doi: 10.1038/nrc3038
49. Vaupel P, Kallinowski F, Okunieff P. Blood flow, oxygen and nutrient supply, and metabolic microenvironment of human tumors: a review. *Cancer Res.* (1989) 49:6449–65.
50. Helmlinger G, Yuan F, Dellian M, Jain RK. Interstitial pH and pO2 gradients in solid tumors *in vivo:* high-resolution measurements reveal a lack of correlation. *NatMed.* (1997) 3:177–82. doi: 10.1038/nm0297-177
51. Sørensen BS, Toustrup K, Horsman MR, Overgaard J, Alsner J. Identifying pH independent hypoxia induced genes in human squamous cell carcinomas *in vitro*. *Acta Oncol.* (2010) 49:895–905. doi: 10.3109/02841861003614343
52. Chen JL, Lucas JE, Schroeder T, Mori S, Wu J, Nevins J, et al. The genomic analysis of lactic acidosis and acidosis response in human cancers. *PLoS Genet.* (2008) 4:e1000293. doi: 10.1371/journal.pgen.1000293
53. Sørensen BS, Busk M, Overgaard J, Horsman MR, Alsner J. Simultaneous hypoxia and low extracellular pH suppress overall metabolic rate and protein synthesis *in vitro*. *PLoS ONE.* (2015) 10:e0134955. doi: 10.1371/journal.pone.0134955
54. Drake CG, Lipson EJ, Brahmer JR. Breathing new life into immunotherapy: review of melanoma, lung and kidney cancer. *Nat Rev Clin Oncol.* (2014) 11:24–37. doi: 10.1038/nrclinonc.2013.208
55. Postow MA, Callahan MK, Wolchok JD. Immune checkpoint blockade in cancer therapy. *J Clin Oncol.* (2015) 33:1974–82. doi: 10.1200/JCO.2014.59.4358
56. Coussens LM, Werb Z. Inflammation and cancer. *Nature.* (2002) 420:860–7. doi: 10.1038/nature01322
57. Qu X, Tang Y, Hua S. Immunological approaches towards cancer and inflammation: a cross talk. *Front Immunol.* (2018) 9:563. doi: 10.3389/fimmu.2018.00563
58. Gonzalez H, Hagerling C, Werb Z. Roles of the immune system in cancer: from tumor initiation to metastatic progression. *Genes Dev.* (2018) 32:1267–84. doi: 10.1101/gad.314617.118
59. van Limbergen EJ, De Ruysscher DK, Olivo Pimentel V, Marcus D, Berbee M, Hoeben A, et al. Combining radiotherapy with immunotherapy: the past, the present and the future. *Br J Radiol.* (2017) 90:20170157. doi: 10.1259/bjr.20170157
60. Bernier J. Immuno-oncology: allying forces of radio- and immuno-therapy to enhance cancer cell killing. *Crit Rev Oncol Hematol.* (2016) 108:97–108. doi: 10.1016/j.critrevonc.2016.11.001
61. Durante M, Reppingen N, Held KD. Immunologically augmented cancer treatment using modern radiotherapy. *Trends Mol Med.* (2013) 19:565–82. doi: 10.1016/j.molmed.2013.05.007
62. Vaupel P, Multhoff G. Accomplices of the hypoxic tumor microenvironment compromising antitumor immunity: adenosine, lactate, acidosis, vascular endothelial growth factor, potassium ions, and phosphatidylserine. *Front Immunol.* (2017) 8:1–6. doi: 10.3389/fimmu.2017.01887
63. Multhoff G, Vaupel P. Hypoxia compromises anti-cancer immune responses. *Adv Exp Med Biol vol.* (2020) 1232:131–43. doi: 10.1007/978-3-030-34461-0_18
64. Rankin EB, Giaccia AJ. Hypoxic control of metastasis. *Science.* (2016) 352:175–80. doi: 10.1126/science.aaf4405

65. Triner D, Shah YM. Hypoxia-inducible factors: a central link between inflammation and cancer. *J Clin Invest.* (2016) 126:3689–98. doi: 10.1172/JCI84430
66. Barsoum IB, Koti M, Siemens DR, Graham CH. Mechanisms of hypoxia-mediated immune escape in cancer. *Cancer Res.* (2014) 74:7185–90. doi: 10.1158/0008-5472.CAN-14-2598
67. Hatfield SM, Kjaergaard J, Lukashev D, Schreiber TH, Belikoff B, Abbott R, et al. Immunological mechanisms of the antitumor effects of supplemental oxygenation. *Sci Transl Med.* (2015) 7:277ra30. doi: 10.1126/scitranslmed.aaa1260
68. Noman MZ, Desantis G, Janji B, Hasmim M, Karray S, Dessen P, et al. PD-L1 is a novel direct target of HIF-1α, and its blockade under hypoxia enhanced MDSC-mediated T cell activation. *J Exp Med.* (2014) 211:781–90. doi: 10.1084/jem.20131916
69. Petrova V, Annicchiarico-Petruzzelli M, Melino G, Amelio I. The hypoxic tumour microenvironment. *Oncogenesis.* (2018) 7:10. doi: 10.1038/s41389-017-0011-9
70. Vaupel P, Multhoff G. Fatal alliance of Hypoxia-/HIF-1α-driven microenvironmental traits promoting cancer progression. *Adv Exp Med Biol.* (2020) 1232:169–76. doi: 10.1007/978-3-030-34461-0_21
71. Horsman MR, Mortensen LS, Petersen JB, Busk M, Overgaard J. Imaging hypoxia to improve radiotherapy outcome. *Nat Rev Clin Oncol.* (2012) 9:674–87. doi: 10.1038/nrclinonc.2012.171
72. Kristensen LK, Fröhlich C, Christensen C, Melander MC, Poulsen TT, Galler GR, et al. CD4+ and CD8a+ PET imaging predicts response to novel PD-1 checkpoint inhibitor: studies of Sym021 in syngeneic mouse cancer models. *Theranostics.* (2019) 9:8221–38. doi: 10.7150/thno.37513
73. Christensen C, Kristensen LK, Alfsen MZ, Nielsen CH, Kjaer A. Quantitative PET imaging of PD-L1 expression in xenograft and syngeneic tumour models using a site-specifically labelled PD-L1 antibody. *Eur J Nucl Med Mol Imaging.* (2019) doi: 10.1158/1538-7445.AM2018-3030
74. Bensch F, van der Veen EL, Lub-de Hooge MN, Jorritsma-Smit A, Boellaard R, Kok IC, et al. 89Zr-atezolizumab imaging as a non-invasive approach to assess clinical response to PD-L1 blockade in cancer. *Nat Med.* (2018). 24:1852–8. doi: 10.1038/s41591-018-0255-8
75. Moulder JE, Rockwell S. Hypoxic fractions of solid tumors: experimental techniques, methods of analysis, and a survey of existing data. *Int J Radiat Oncol.* (1984) 10:695–712. doi: 10.1016/0360-3016(84)90301-8
76. Gray LH, Conger AD, Ebert M, Hornsey S, Scott OCA. The concentration of oxygen dissolved in tissues at the time of irradiation as a factor in radiotherapy. *Br J Radiol.* (1953) 26:638–48. doi: 10.1259/0007-1285-26-312-638
77. Horsman MR, Wouters BG, Joiner M, Overgaard J. The oxygen effect and fractionated radiotherapy. In: Joiner M, van der Kogel AJ, editors. *Basic Clinical Radiobiology 4th edit*. London: Hodder Arnold. (2009) p. 207–16. doi: 10.1201/b13224-16
78. Chaplin DJ, Trotter MJ. Chemical modifiers of tumour blood flow. In Vaupel P, Jain RK, editors. *Tumour blood supply Metabolism Microenvironment,* Stuttgart: Gustav Fischer. (1991) p. 65–85.
79. Bassler N, Toftegaard J, Lühr A, Sørensen BS, Scifoni E, Krämer M, et al. LET-painting increases tumour control probability in hypoxic tumours. *Acta Oncol.* (2014) 53:25–32. doi: 10.3109/0284186X.2013.832835
80. Overgaard J, Hansen HS, Overgaard M, Bastholt L, Berthelsen A, Specht L, et al. A randomized double-blind phase III study of nimorazole as a hypoxic radiosensitizer of primary radiotherapy in supraglottic larynx and pharynx carcinoma. results of the Danish Head and Neck Cancer Study (DAHANCA) protocol 5-85. *RadiotherOncol.* (1998) 46:135–46. doi: 10.1016/S0167-8140(97)00220-X
81. www.ous-research.no/hn/ n.d.
82. Horsman MR, Siemann DW. Pathophysiologic effects of vascular-targeting agents and the implications for combination with conventional therapies. *Cancer Res.* (2006) 66:11520–39. doi: 10.1158/0008-5472.CAN-06-2848
83. Siemann DW, Bibby MC, Dark GG, Dicker AP, Eskens FALM, Horsman MR, et al. Differentiation and definition of vascular-targeted therapies. *Clin Cancer Res.* (2005) 11:416–20.
84. Siemann DW, Chaplin DJ, Horsman MR. Realizing the potential of vascular targeted therapy: the rationale for combining vascular disrupting agents and anti-angiogenic agents to treat cancer. *Cancer Invest.* (2017) 35:519–34. doi: 10.1080/07357907.2017.1364745
85. Tozer GM, Kanthou C, Baguley BC. Disrupting tumour blood vessels. *Nat Rev Cancer.* (2005) 5:423–35. doi: 10.1038/nrc1628
86. Jain RK. Normalizing tumor vasculature with anti-angiogenic therapy: a new paradigm for combination therapy. *Nat Med.* (2001) 7:987–9. doi: 10.1038/nm0901-987
87. Winkler F, Kozin S V, Tong RT, Chae S-S, Booth MF, Garkavtsev I, et al. Kinetics of vascular normalization by VEGFR2 blockade governs brain tumor response to radiation: role of oxygenation, angiopoietin-1, and matrix metalloproteinases. *Cancer Cell.* (2004) 6:553–63. doi: 10.1016/S1535-6108(04)00305-8
88. Ansiaux R, Baudelet C, Jordan BF, Crokart N, Martinive P, DeWever J, et al. Mechanism of reoxygenation after antiangiogenic therapy using SU5416 and its importance for guiding combined antitumor therapy. *Cancer Res.* (2006) 66:9698–704. doi: 10.1158/0008-5472.CAN-06-1854
89. Segers J, Di Fazio V, Ansiaux R, Martinive P, Feron O, Wallemacq P, et al. Potentiation of cyclophosphamide chemotherapy using the anti-angiogenic drug thalidomide: importance of optimal scheduling to exploit the "normalization" window of the tumor vasculature. *Cancer Lett.* (2006) 244:129–35. doi: 10.1016/j.canlet.2005.12.017
90. Ansiaux R, Baudelet C, Jordan BF, Beghein N, Sonveaux P, De Wever J, et al. Thalidomide radiosensitizes tumors through early changes in the tumor microenvironment. *Clin Cancer Res.* (2005) 11:743–50.
91. Fogal V, Sugahara KN, Ruoslahti E, Christian S. Cell surface nucleolin antagonist causes endothelial cell apoptosis and normalization of tumor vasculature. *Angiogenesis.* (2009) 12:91–100. doi: 10.1007/s10456-009-9137-5
92. Vangestel C, Van de Wiele C, Mees G, Mertens K, Staelens S, Reutelingsperger C, et al. Single-photon emission computed tomographic imaging of the early time course of therapy-induced cell death using technetium 99m tricarbonyl His-annexin A5 in a colorectal cancer xenograft model. *Mol Imaging.* (2012) 11:135–47. doi: 10.2310/7290.2011.00034
93. Myers AL, Williams RF, Ng CY, Hartwich JE, Davidoff AM. Bevacizumab-induced tumor vessel remodeling in rhabdomyosarcoma xenografts increases the effectiveness of adjuvant ionizing radiation. *J Pediatr Surg.* (2010) 45:1080–5. doi: 10.1016/j.jpedsurg.2010.02.068
94. McGee MC, Hamner JB, Williams RF, Rosati SF, Sims TL, Ng CY, et al. Improved intratumoral oxygenation through vascular normalization increases glioma sensitivity to ionizing radiation. *Int J Radiat Oncol Biol Phys.* (2010) 76:1537–45. doi: 10.1016/j.ijrobp.2009.12.010
95. Dings RPM, Loren M, Heun H, McNiel E, Griffioen AW, Mayo KH, et al. Scheduling of radiation with angiogenesis inhibitors anginex and Avastin improves therapeutic outcome via vessel normalization. *Clin Cancer Res.* (2007) 13:3395–402. doi: 10.1158/1078-0432.CCR-06-2441
96. Hansen-Algenstaedt N, Stoll BR, Padera TP, Dolmans DE, Hicklin DJ, Fukumura D, et al. Tumor oxygenation in hormone-dependent tumors during vascular endothelial growth factor receptor-2 blockade, hormone ablation, and chemotherapy. *Cancer Res.* (2000) 60:4556–60.
97. Batchelor TT, Gerstner ER, Emblem KE, Duda DG, Kalpathy-Cramer J, Snuderl M, et al. Improved tumor oxygenation and survival in glioblastoma patients who show increased blood perfusion after cediranib and chemoradiation. *Proc Natl Acad Sci.* (2013) 110:19059–64. doi: 10.1073/pnas.1318022110
98. Vaupel P, Kallinowski F, Okunieff P. Blood flow, oxygen and nutrient supply, and metabolic microenvironment of human tumors: a review. *Cancer Res.* (1989) 49:6449–65.
99. Fenton BM, Paoni SF, Ding I. Pathophysiological effects of vascular endothelial growth factor receptor-2-blocking antibody plus fractionated radiotherapy on murine mammary tumors. *Cancer Res.* (2004) 64:5712–9. doi: 10.1158/0008-5472.CAN-04-0434
100. Hugonnet F, Fournier L, Medioni J, Smadja C, Hindie E, Huchet V, et al. Metastatic renal cell carcinoma: relationship between initial metastasis hypoxia, change after 1 month's sunitinib, and therapeutic response: an 18F-Fluoromisonidazole PET/CT Study. *J Nucl Med.* (2011) 52:1048–55. doi: 10.2967/jnumed.110.084517
101. Hattingen E, Jurcoane A, Bähr O, Rieger J, Magerkurth J, Anti S, et al. Bevacizumab impairs oxidative energy metabolism and shows

antitumoral effects in recurrent glioblastomas: a 31P/1H MRSI and quantitative magnetic resonance imaging study. *Neuro Oncol.* (2011) 13:1349–63. doi: 10.1093/neuonc/nor132
102. Milosevic MF, Townsley CA, Chaudary N, Clarke B, Pintilie M, Fan S, et al. Sorafenib increases tumor hypoxia in cervical cancer patients treated with radiation therapy: results of a phase 1 clinical study. *Int J Radiat Oncol Biol Phys.* (2016) 94:111–7. doi: 10.1016/j.ijrobp.2015.09.009
103. Olive PL, Aquino-Parsons C, MacPhail SH, Liao SY, Raleigh JA, Lerman MI, et al. Carbonic anhydrase 9 as an endogenous marker for hypoxic cells in cervical cancer. *Cancer Res.* (2001) 61:8924–9.
104. Giatromanolaki A, Koukourakis MI, Sivridis E, Pastorek J, Wykoff CC, Gatter KC, et al. Expression of hypoxia-inducible carbonic anhydrase-9 relates to angiogenic pathways and independently to poor outcome in non-small cell lung cancer. *Cancer Res.* (2001) 61:7992–8.
105. Airley RE, Loncaster J, Raleigh JA, Harris AL, Davidson SE, Hunter RD, et al. GLUT-1 and CAIX as intrinsic markers of hypoxia in carcinoma of the cervix: relationship to pimonidazole binding. *IntJ Cancer.* (2003) 104:85–91. doi: 10.1002/ijc.10904
106. Haugland HK, Vukovic V, Pintilie M, Fyles AW, Milosevic M, Hill RP, et al. Expression of hypoxia-inducible factor-1alpha in cervical carcinomas: correlation with tumor oxygenation. *Int J Radiat Oncol Biol Phys.* (2002) 53:854–61. doi: 10.1016/S0360-3016(02)02815-8
107. Sørensen BS, Hao J, Overgaard J, Vorum H, Honoré B, Alsner J, et al. Influence of oxygen concentration and pH on expression of hypoxia induced genes. *Radiother Oncol.* (2005) 76:187–93. doi: 10.1016/j.radonc.2005.06.037
108. Sørensen BS, Alsner J, Overgaard J, Horsman MR. Hypoxia induced expression of endogenous markers *in vitro* is highly influenced by pH. *Radiother Oncol.* (2007) 83:362–6. doi: 10.1016/j.radonc.2007.04.028
109. Troost EG, Bussink J, Kaanders JH, van EJ, Peters JP, Rijken PF, et al. Comparison of different methods of CAIX quantification in relation to hypoxia in three human head and neck tumor lines. *RadiotherOncol.* (2005) 76:194–9. doi: 10.1016/j.radonc.2005.06.031
110. Gee HE, Ivan C, Calin GA, Ivan M. HypoxamiRs and cancer: from biology to targeted therapy. *Antioxid Redox Signal.* (2014) 21:1220–38. doi: 10.1089/ars.2013.5639
111. Choudhry H, Harris AL, McIntyre A. The tumour hypoxia induced non-coding transcriptome. *Mol Aspects Med.* (2016) 47–48:35–53. doi: 10.1016/j.mam.2016.01.003
112. Nilsen A, Jonsson M, Aarnes E-K, Kristensen GB, Lyng H. Reference microRNAs for RT-qPCR assays in cervical cancer patients and their application to studies of HPV16 and hypoxia biomarkers. *Transl Oncol.* (2019) 12:576–84. doi: 10.1016/j.tranon.2018.12.010
113. Camps C, Buffa FM, Colella S, Moore J, Sotiriou C, Sheldon H, et al. Hsa-miR-210 is induced by hypoxia and is an independent prognostic factor in breast cancer. *Clin Cancer Res.* (2008) 14:1340–8. doi: 10.1158/1078-0432.CCR-07-1755
114. Irlam-Jones JJ, Eustace A, Denley H, Choudhury A, Harris AL, Hoskin PJ, et al. Expression of miR-210 in relation to other measures of hypoxia and prediction of benefit from hypoxia modification in patients with bladder cancer. *Br J Cancer.* (2016) 115:571–8. doi: 10.1038/bjc.2016.218
115. Toustrup K, Sørensen BS, Nordsmark M, Busk M, Wiuf C, Alsner J, et al. Development of a hypoxia gene expression classifier with predictive impact for hypoxic modification of radiotherapy in head and neck cancer. *Cancer Res.* (2011) 71:5923–31. doi: 10.1158/0008-5472.CAN-11-1182
116. Seigneuric R, Starmans MHW, Fung G, Krishnapuram B, Nuyten DSA, van Erk A, et al. Impact of supervised gene signatures of early hypoxia on patient survival. *Radiother Oncol.* (2007) 83:374–82. doi: 10.1016/j.radonc.2007.05.002
117. Winter SC, Buffa FM, Silva P, Miller C, Valentine HR, Turley H, et al. Relation of a hypoxia metagene derived from head and neck cancer to prognosis of multiple cancers. *Cancer Res.* (2007) 67:3441–9. doi: 10.1158/0008-5472.CAN-06-3322
118. Buffa FM, Harris AL, West CM, Miller CJ. Large meta-analysis of multiple cancers reveals a common, compact and highly prognostic hypoxia metagene. *Br J Cancer.* (2010) 102:428–35. doi: 10.1038/sj.bjc.6605450
119. Ragnum HB, Vlatkovic L, Lie AK, Axcrona K, Julin CH, Frikstad KM, et al. The tumour hypoxia marker pimonidazole reflects a transcriptional programme associated with aggressive prostate cancer. *Br J Cancer.* (2015) 112:382–90. doi: 10.1038/bjc.2014.604
120. Yang L, Roberts D, Takhar M, Erho N, Bibby BAS, Thiruthaneeswaran N, et al. Development and validation of a 28-gene hypoxia-related prognostic signature for localized prostate cancer. *EBioMedicine.* (2018) 31:182–9. doi: 10.1016/j.ebiom.2018.04.019
121. Eustace A, Mani N, Span PN, Irlam JJ, Taylor J, Betts GNJ, et al. A 26-gene hypoxia signature predicts benefit from hypoxia-modifying therapy in laryngeal cancer but not bladder cancer. *Clin Cancer Res.* (2013) 19:4879–88. doi: 10.1158/1078-0432.CCR-13-0542
122. Fjeldbo CS, Julin CH, Lando M, Forsberg MF, Aarnes E-K, Alsner J, et al. Integrative analysis of DCE-MRI and gene expression profiles in construction of a gene classifier for assessment of hypoxia-related risk of chemoradiotherapy failure in cervical cancer. *Clin Cancer Res.* (2016) 22:4067–76. doi: 10.1158/1078-0432.CCR-15-2322
123. Harris BHLHL, Barberis A, West CMLML, Buffa FMM. Gene expression signatures as biomarkers of tumour hypoxia. *Clin Oncol.* (2015) 27:547–60. doi: 10.1016/j.clon.2015.07.004
124. Toustrup K, Sørensen BS, Alsner J, Overgaard J. Hypoxia gene expression signatures as prognostic and predictive markers in head and neck radiotherapy. *Semin Radiat Oncol.* (2012) 22:119–27. doi: 10.1016/j.semradonc.2011.12.006
125. Janssens GO, Rademakers SE, Terhaard CH, Doornaert PA, Bijl HP, van den Ende P, et al. Accelerated radiotherapy with carbogen and nicotinamide for laryngeal cancer: results of a phase III randomized trial. *J Clin Oncol.* (2012) 30:1777–83. doi: 10.1200/JCO.2011.35.9315
126. Bhandari V, Hoey C, Liu LY, Lalonde E, Ray J, Livingstone J, et al. Molecular landmarks of tumor hypoxia across cancer types. *Nat Genet.* (2019) 51:308–18. doi: 10.1038/s41588-018-0318-2
127. van der Heijden M, de Jong MC, Verhagen CVM, de Roest RH, Sanduleanu S, Hoebers F, et al. Acute hypoxia profile is a stronger prognostic factor than chronic hypoxia in advanced stage head and neck cancer patients. *Cancers.* (2019) 11:583. doi: 10.3390/cancers11040583
128. Tawk B, Schwager C, Deffaa O, Dyckhoff G, Warta R, Linge A, et al. Comparative analysis of transcriptomics based hypoxia signatures in head- and neck squamous cell carcinoma. *Radiother Oncol.* (2016) 118:350–8. doi: 10.1016/j.radonc.2015.11.027
129. Linge A, Löck S, Gudziol V, Nowak A, Lohaus F, von Neubeck C, et al. Low cancer stem cell marker expression and low hypoxia identify good prognosis subgroups in HPV(–) HNSCC after postoperative radiochemotherapy: a multicenter study of the DKTK-ROG. *Clin Cancer Res.* (2016) 22:2639–49. doi: 10.1158/1078-0432.CCR-15-1990
130. Betts GNJ, Eustace A, Patiar S, Valentine HR, Irlam J, Ramachandran A, et al. Prospective technical validation and assessment of intra-tumour heterogeneity of a low density array hypoxia gene profile in head and neck squamous cell carcinoma. *Eur J Cancer.* (2013) 49:156–65. doi: 10.1016/j.ejca.2012.07.028
131. Toustrup K, Sørensen BS, Metwally MAH, Tramm T, Mortensen LS, Overgaard J, et al. Validation of a 15-gene hypoxia classifier in head and neck cancer for prospective use in clinical trials. *Acta Oncol.* (2016) 55:1091–8. doi: 10.3109/0284186X.2016.1167959
132. Byers LA, Holsinger FC, Kies MS, William WN, El-Naggar AK, Lee JJ, et al. Serum signature of hypoxia-regulated factors is associated with progression after induction therapy in head and neck squamous cell cancer. *Mol Cancer Ther.* (2010) 9:1755–63. doi: 10.1158/1535-7163.MCT-09-1047
133. Brøndum L, Sørensen BS, Eriksen JG, Mortensen LS, Lønbro S, Overgaard J, et al. An evaluation of multiplex bead-based analysis of cytokines and soluble proteins in archived lithium heparin plasma, EDTA plasma and serum samples. *Scand J Clin Lab Invest.* (2016) 76:601–11. doi: 10.1080/00365513.2016.1230882
134. Ock C-Y, Nam A-R, Bang J-H, Kim T-Y, Lee K-H, Han S-W, et al. Signature of cytokines and angiogenic factors (CAFs) defines a clinically distinct subgroup of gastric cancer. *Gastric Cancer.* (2017) 20:164–74. doi: 10.1007/s10120-015-0583-z
135. Lukacova S, Khalil AA, Overgaard J, Alsner J, Horsman MR. Relationship between radiobiological hypoxia in a C3H mouse mammary carcinoma and osteopontin levels in mouse serum. *IntJRadiatBiol.* (2005) 81:937–44. doi: 10.1080/09553000600567616

136. Overgaard J, Eriksen JG, Nordsmark M, Alsner J, Horsman MR. Plasma osteopontin, hypoxia, and response to the hypoxia sensitiser nimorazole in radiotherapy of head and neck cancer: results from the DAHANCA 5 randomised double-blind placebo-controlled trial. *Lancet Oncol.* (2005) 6:757–64. doi: 10.1016/S1470-2045(05)70292-8
137. Petrik D, Lavori PW, Cao H, Zhu Y, Wong P, Christofferson E, et al. Plasma osteopontin is an independent prognostic marker for head and neck cancers. *J Clin Oncol.* (2006) 24:5291–7. doi: 10.1200/JCO.2006.06.8627
138. Carvalho S, Troost EGC, Bons J, Menheere P, Lambin P, Oberije C. Prognostic value of blood-biomarkers related to hypoxia, inflammation, immune response and tumour load in non-small cell lung cancer – A survival model with external validation. *Radiother Oncol.* (2016) 119:487–94. doi: 10.1016/j.radonc.2016.04.024
139. Hui EP, Sung FL, Yu BKH, Wong CSC, Ma BBY, Lin X, et al. Plasma osteopontin, hypoxia, and response to radiotherapy in nasopharyngeal cancer. *Clin Cancer Res.* (2008) 14:7080–7. doi: 10.1158/1078-0432.CCR-08-0364
140. Vordermark D, Said HM, Katzer A, Kuhnt T, Hänsgen G, Dunst J, et al. Plasma osteopontin levels in patients with head and neck cancer and cervix cancer are critically dependent on the choice of ELISA system. *BMC Cancer.* (2006) 6:207. doi: 10.1186/1471-2407-6-207

Conflict of Interest: BS was a co-inventor on a patent on a method (gene expression profile) for determining clinically relevant hypoxia in cancer (WO2012146259 A1) that is owned by Aarhus University, Aarhus, Denmark.

The remaining author declares that the research was conducted in the absence of any commercial or financial relationships that could be construed as a potential conflict of interest.

frontiers in Oncology

REVIEW
published: 12 May 2020
doi: 10.3389/fonc.2020.00737

Diacylglycerol Kinase Alpha in Radiation-Induced Fibrosis: Potential as a Predictive Marker or Therapeutic Target

*Chun-Shan Liu, Peter Schmezer and Odilia Popanda**

Division of Cancer Epigenomics, German Cancer Research Center (DKFZ), Heidelberg, Germany

Radiotherapy is an efficient tool in cancer treatment, but it brings along the risk of side effects such as fibrosis in the irradiated healthy tissue thus limiting tumor control and impairing quality of life of cancer survivors. Knowledge on radiation-related fibrosis risk and therapeutic options is still limited and requires further research. Recent studies demonstrated that epigenetic regulation of diacylglycerol kinase alpha (DGKA) is associated with radiation-induced fibrosis. However, the specific mechanisms are still unknown. In this review, we scrutinized the role of DGKA in the radiation response and in further cellular functions to show the potential of DGKA as a predictive marker or a novel target in fibrosis treatment. DGKA was reported to participate in immune response, lipid signaling, exosome production, and migration as well as cell proliferation, all processes which are suggested to be critical steps in fibrogenesis. Most of these functions are based on the conversion of diacylglycerol (DAG) to phosphatidic acid (PA) at plasma membranes, but DGKA might have also other, yet not well-known functions in the nucleus. Current evidence summarized here underlines that DGKA activation may play a central role in fibrosis formation post-irradiation and shows a potential of direct DGKA inhibitors or epigenetic modulators to attenuate pro-fibrotic reactions, thus providing novel therapeutic choices.

Keywords: radiotherapy, late adverse effects, fibrosis, lipid signaling, diacylglycerol, phosphatidic acid

OPEN ACCESS

Edited by:
Mary Helen Barcellos-Hoff, University of California, San Francisco, United States

Reviewed by:
Hyuk-Jin Cha, Seoul National University, South Korea
Gianluca Baldanzi, Università Piemonte Orientale, Italy
Elena Rainero, University of Sheffield, United Kingdom

****Correspondence:***
Odilia Popanda
o.popanda@dkfz-heidelberg.de

Specialty section:
This article was submitted to Radiation Oncology, a section of the journal Frontiers in Oncology

Received: *07 February 2020*
Accepted: *17 April 2020*
Published: *12 May 2020*

Citation:
Liu C-S, Schmezer P and Popanda O (2020) Diacylglycerol Kinase Alpha in Radiation-Induced Fibrosis: Potential as a Predictive Marker or Therapeutic Target. Front. Oncol. 10:737. doi: 10.3389/fonc.2020.00737

INTRODUCTION

Radiotherapy is a valuable part of cancer treatment; more than 50% of all cancer patients receive radiation therapy at some point during their treatment for curative or palliative purposes (1, 2). Ionizing radiation (IR) is given to kill tumor cells but radiation also targets the surrounding normal tissue resulting in tissue damage (radiation injury) and development of adverse side effects (3). Within hours to weeks after radiation, an acute tissue response occurs but late adverse effects may appear even after months or years post-therapy. Early radiation effects include DNA damage, cell cycle arrest and cell death which will lead to cell loss, endothelial and tissue damage and inflammation. During this stage of tissue destruction, chemokines, and cytokines are emitted to activate a wound healing response. Fibroblast to myofibroblast trans-differentiation, extracellular matrix (ECM) production and angiogenesis occur, resulting in cell proliferation and tissue regeneration. Once tissue repair is completed, the inflammatory response is resolved, activated myofibroblasts are deactivated by cellular senescence or cell death and the damaged area should

turn back to a normal tissue phenotype (4). However, in a considerable number of irradiated patients, the wound healing response after radiation is maintained for longer leading to scars, tissue indurations and contractions, fibrosis, and in some cases, organ failure. Thus, side effects might strongly affect quality of life of cancer survivors and can even be a deadly threat. Some examples revealing the clinical relevance of radiation-induced fibrosis should shortly be mentioned here.

Regarding the lung, radiotherapy of the thorax is strongly limited by radiation-induced early side effects in the organ like acute radiation pneumonitis which even may cause interruption or premature termination of therapy (5–8). Over a period of 1–2 years post-treatment, radiation-induced alterations in the lung may lead to destruction of lung architecture or deletion of specific lung cells like alveolar cells involved in oxygen exchange. Together with the accumulation of fibrotic tissue forming a "scar," these alterations may cause dyspnea, oxygen starvation, and even organ failure and dead (9). Such severe late side effects occur in about 5–20% of patients, and despite considerable technical efforts in targeting specifically the tumor, they are limiting the applicable dose in lung or esophageal cancer even at the cost of tumor control.

Also in head and neck cancer patients, radiation-induced fibrosis can occur. In a Belgian study, 68% of cancer patients treated with radiotherapy showed mild-to-severe neck fibrosis with an increasing risk for this side effect with every year after therapy (10). In these patients, again, fibrotic side effects can be rather harmful according to the affected site, for example they strongly affect oral mucosae and swallowing and thus adequate food intake.

Chronic fibrosis is also frequently identified in breast cancer patients. About 21% of breast cancer patients developed fibrosis 8 years after they obtained an intra-operative boost radiotherapy (11). In these patients, fibrosis can result in cosmetic changes of the breast but also severe and harmful endurations and limited mobility. Overall, these examples show that tissue fibrosis is a severe side effect of radiotherapy strongly affecting therapy success but also quality of life in cancer survivors.

In general, the molecular mechanisms leading to radiation-induced fibrosis are expected to be similar to those of other fibrotic diseases in the liver, kidney, lung, or heart. Radiation causes the initial tissue injury by directly damaging DNA and by generating reactive oxygen or nitrogen species (ROS or RNS) which will react with DNA but also with other cellular components like membranes and lipids (12). Besides escaping to senescence, the damaged cells can undergo cell death and represent a severe tissue damage which triggers the wound healing response. They may cause inflammation and release of inflammatory chemokines and cytokines which activate neutrophils, lymphocytes, and monocytes as well as endothelial cells and resident macrophages, stromal fibroblasts, and further mesenchymal cells (13, 14). As in other fibrotic processes, the secretion of tumor growth factor beta (TGF-β) or platelet-derived growth factor (PDGF) promotes the development of myofibroblasts expressing alpha-smooth muscle actin (α-SMA) and producing excess ECM proteins like collagens with an increased stability of ECM. Enrichment of ECM and myofibroblasts results in manifestation of indurations and limited tissue functions.

Although many of the released cytokines like TGF-β, IL-6 and IL-10 are well-known pro-fibrotic triggers leading to myofibroblast activation (15), the steps resulting in the elongation or even perpetuation of wound healing processes are mostly unknown.

Further cellular components, the phospholipids, are reported to be involved in radiation-induced fibrogenesis. In primary human dermal fibroblasts, phospholipids such as phosphatidylcholine (PC) and phosphatidylethanolamine (PE) are increased after gamma-irradiation (16). A further bioactive phospholipid, lysophosphatidic acid (LPA) is synthesized from PC and is suggested to be a pro-fibrotic factor in radiation-induced fibrosis (17, 18). Another LPA precursor is phosphatidic acid (PA) which is converted from diacylglycerol (DAG) by diacylglycerokinases (DGKs). Increased PA levels trigger the generation of LPA which is involved in many chronic inflammatory diseases including idiopathic pulmonary fibrosis and liver fibrosis (19, 20). In irradiated mice as well as in cell cultures, supplementation with LPA reduced irradiation-induced apoptosis (21). LPA functions include stimulation of cell proliferation, activation of pro-fibrotic responses and anti-apoptotic mechanisms by LPA receptor-mediated extracellular signal-regulated kinase (ERK) activation (18). Thus, targeting LPA with antibodies or antagonists against its receptor LPAR could make it a valuable target for novel therapeutic anti-fibrotic approaches. Hence, a LPA type 2 receptor antagonist, octadecenyl thiophosphate (OTP), could attenuate irradiation-induced apoptosis and activate anti-apoptotic ERK signaling which both are leading to increased cell survival (21).

During fibroblast transactivation, epigenetic mechanisms are involved in activating the appropriate transcriptional reprogramming in the affected cells (22). Epigenetic variation might predispose patients for developing a prolonged tissue response. Changes in post-translational histone marks and miRNAs have been described (23, 24). Epigenetic changes during such reprogramming processes can be reverted not only by intrinsic mechanisms but also by epigenetic drugs. Thus, this might offer possibilities to attenuate fibrotic processes and alleviate reconstitution of normal tissue characteristics. Epigenetic therapies might be helpful substitutions to current treatment options for radiation-induced fibrosis. These include small molecules and even stem cells and target the different specific steps of fibrogenesis, however only some of them are in clinical use (9, 25, 26). Examples are antioxidants and radical scavengers which are applied to protect the irradiated normal tissue from damage through radiolysis of water and other cellular components (25). Especially drugs already approved for clinical application for other purposes like hesperidin, rutin, or melatonin could easily be included in therapeutic schedules [for a recent summary, see (25)]. Currently, amifostine acting as a radical scavenger is the only FDA-approved cytoprotective drug used in head and neck cancer patients. Its use for lung protection shows ambiguous results (5). Further treatments include anti-inflammatory drugs like glucocorticosteroids to

repress the immune response activated in the damaged tissue (27). Molecular therapies targeting pro-fibrotic players like the fibrosis driver TGF-β or the connective tissue growth factor (CTGF) are promising but still in preclinical testing (26, 28, 29). Further approaches are using mesenchymal stem cells (MSCs) for tissue regeneration (9). In preclinical models, MSCs not only replace damaged lung epithelial cells but also promote tissue repair through the secretion of anti-inflammatory and anti-fibrotic factors. They can even be genetically modified, e.g., by over-expression of the radical scavenging enzyme superoxide dismutase, to improve their radioprotective potential. First clinical trials in patients with idiopathic pulmonary fibrosis are encouraging. There are however strong concerns about the safety of such a therapy. Therefore, further investigations to identify novel molecular targets for radioprotective and antifibrotic treatments are urgently needed to improve personalized radiotherapy.

DIACYLGLYCEROL KINASE ALPHA (DGKA) AS A POTENTIAL CANDIDATE IN RADIATION-INDUCED FIBROSIS

A cohort of breast cancer patients undergoing intraoperative radiotherapy were observed for occurrence of adverse side effects with a median follow-up time of 4.9 years (range 2.0–5.5) (30). For each patient, skin fibroblasts were cultivated. DNA methylation patterns were determined from patients who did or did not develop radiation-induced fibrosis using Illumina 450K arrays (31). A number of differentially methylated sites was identified, among them an intragenic enhancer in the *DGKA* gene. Low methylation at this site was associated with moderate to severe fibrosis (LENT-SOMA grade 2–3) and high methylation with mild to no reaction (31, 32). A more detailed analysis revealed that the radiation-inducible transcription factor EGR1 was able to bind to the differentially methylated region thereby inducing DGKA expression in fibroblasts which then expressed enhanced levels of the pro-fibrotic ECM proteins collagen and fibronectin. DGKA is involved in lipid signaling, cell migration and cell growth (33). It is expressed in normal T cells, spleen and skin as well as in cancer cells but it was not yet described in the context of fibrosis. Several inhibitors are known for this protein making it an attractive target in the fight against fibrosis. To further boost studies of DGKA and fibrosis development, the known characteristics of DGKA are summarized in the following.

DIACYLGLYCEROL KINASES, FUNCTION, AND STRUCTURE

DGKA is part of a family of mammalian diacylglycerol kinases (DGKs) which includes 10 isoforms grouped into five subtypes. DGKs convert diacylglycerol (DAG) to phosphatidic acid (PA), which both are lipids with important and far-reaching signaling properties [**Figure 1**; (33–37)]. Thus, DGKs terminate DAG-regulated signals and activate PA-regulated ones. These two lipids are generated at the membrane and act as hot spots to localize and activate numerous signaling cascades (38, 39). In mammals, on the one hand, DGKs act as negative modulators of classical protein kinase C (cPKC; PKCα, β, and γ) and novel PKC isoforms (nPKC; PKCδ, ε, η, and θ), protein kinase D (PKD), and guanyl nucleotide-releasing protein for Ras (RasGRP) (40, 41). On the other hand, DGKs-induced PA promotes the activation of mammalian target of rapamycin (mTOR), atypical PKC (aPKC, PKCζ, and PKCι/κ), and phosphatidylinositol-4-phosphate 5-kinase (PIP5K) (42).

All DGKs contain at least two cysteine-rich C1 like domains and a highly conserved catalytic domain (43). The C1 domains in DGKs originally contribute to DAG-dependent binding to the membrane. The catalytic domain is a common domain in all DGKs with a highly conserved motif "ϕϕϕGGDGT" (ϕ indicates any hydrophobic residue) that involves ATP binding (44). Each DGK subtype contains accessory regulatory motifs in its primary sequence that might divert their function, regulation and localization. There are numerous reviews on DGKs (34, 43, 45–48) but here we are focusing on DGKA which belongs to type I DGKs that specifically contain a Ca^{2+}-dependent regulatory domain at its N-terminus including a recoverin-like domain (RVH) and two EF-hand motifs.

CELLULAR MECHANISMS TO MODULATE DGKA RNA EXPRESSION

DGKA levels differ considerably in various tissues. Transcripts are enriched in lymphoid tissues especially lymph nodes, tonsils and spleen, as well as in skin, esophagus, duodenum and small intestine (**Figure 2A**). Expression is low in primary melanocytes, hepatocytes, and neurons (49–51) and in the corresponding tissues like liver, brain, kidney, heart and skeletal muscle, suggesting tissue-specific functions of the protein. This is confirmed by the evaluation of immunohistochemistry images of DGKA protein in human tissue sections (**Figure 2B**). They show heterogeneous amounts of DGKA in the different cell types constituting the various tissues. In contrast, *DGKA* expression is strongly increased in tumors like melanoma, hepatocarcinoma, and glioblastoma as detected by RNA quantification or immunohistochemistry (49–51). In tumors, high DGKA expression was reported to be associated with cell growth and activation of Ras, mTOR, or HIF1-α signaling pathways and poor survival (50, 51). In gastric cancer, however, DGKA expression was found to be modulated by lipid metabolism and high DGKA levels were related with good survival (52). These observations show that DGKA levels can affect many cellular functions depending on tissue or cell type. Comprehensive expression patterns in tumor cells reveal that the interplay with tumor-type specific activated signaling pathways might control DGKA function. Therefore, DGKA was postulated to be a critical signaling node in malignant transformation (51).

At the molecular level, several mechanisms of *DGKA* regulation have been observed, although which mechanism is active in which cell type is not completely understood. *DGKA* is located on chromosome 12 encoding several isoforms (**Figure 3**). Transcription is controlled by at least two functional units,

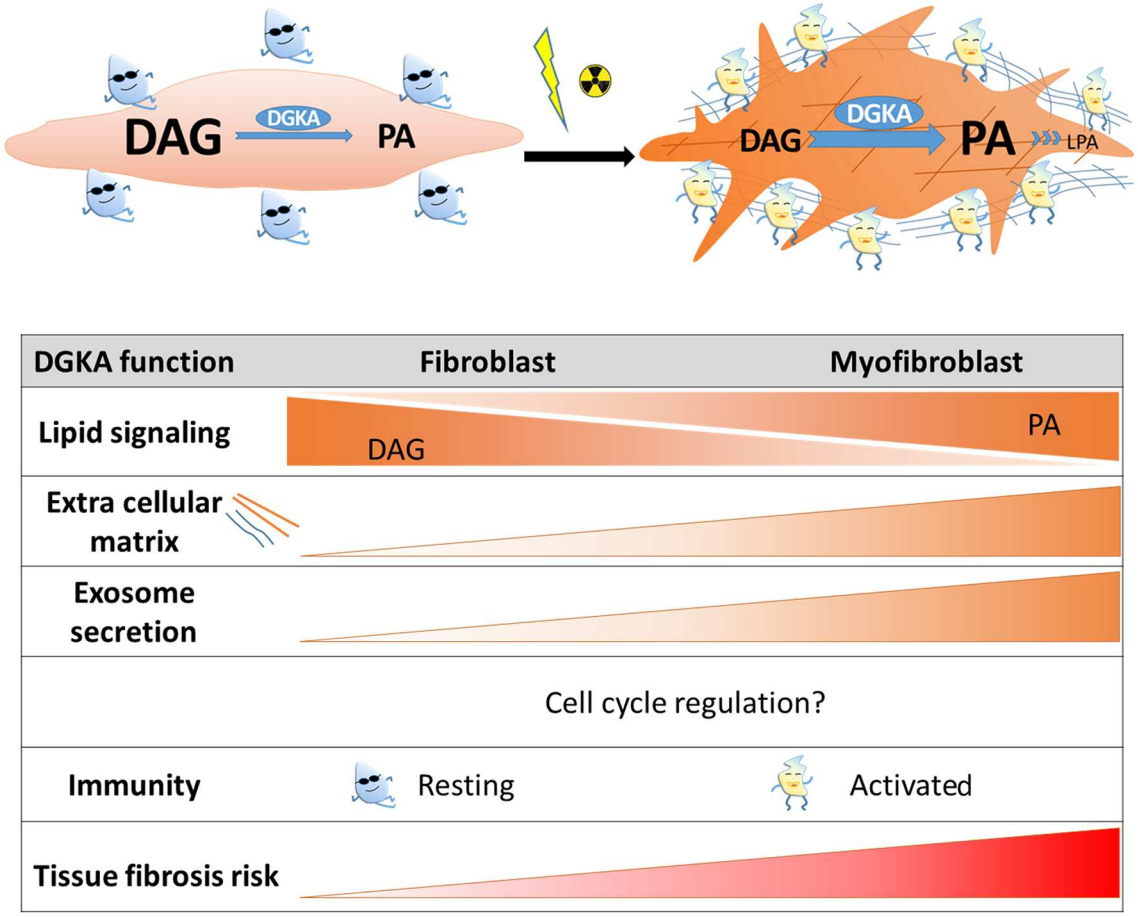

FIGURE 1 | Scheme of DGKA functions contributing to radiation-induced fibrosis. Induction of DGKA by ionizing irradiation or other extracellular stimuli activates several functions in cells like DAG to PA conversion, lipid signaling, exosome secretion, and production of extracellular matrix proteins. According to cell type, these functions might regulate trans-differentiation to myofibroblasts, activation of immune cells, or pro-fibrotic processes. Interaction of these activated cell types is required for tissue regeneration after irradiation, however, persistence of activated cell states and increased extracellular matrix production will contribute to fibrosis.

a promoter region 5′-upstream of the transcription start site and an intragenic enhancer located in intron 1 which can interact with the promoter as shown by chromatin conformation capture experiments (31). Moreover, differential methylation of the enhancer site modulated induction of *DGKA* expression after irradiation of fibroblasts. Low *DGKA* methylation resulted in increased *DGKA* expression after irradiation and was associated with the development of radiation-induced fibrosis (31). In the patient fibroblasts used in this study, the differential methylation which modulates *DGKA* expression after irradiation was already present before treatment of cells. A methylation change after irradiation or upregulation of DNA methyltransferase 1 (DNMT1) was not observed (31). Therefore, differential *DGKA* methylation seems to indicate a stable predisposition of patients for radiation-induced fibrosis. Nevertheless, radiation by itself could change DNA methylation patterns. Although reports on overall changes causing hyper- or hypomethylation are rather contradictory, specific DNA methylation changes have repeatedly been found (55, 56) suggesting an epigenetic reprogramming after irradiation which might affect cell fate and therapy outcome.

DGKA expression was up-regulated by exposure to DNA damaging treatments like γ-irradiation (31, 57), UV-exposure or treatment with cytostatic drugs and under hypoxic conditions [summarized in (58)]. Up-regulation was attenuated by silencing or mutating p53 in the investigated cell models suggesting that DGKA-related functions might be part of the comprehensive p53-mediated cellular damage response, as for example after radiotherapy (59). Furthermore, *DGKA* expression was strongly regulated in different tissues and cell types by activating signaling cascades like those of Src, HIF1-α, mTOR, and Ras/ERK (see below) and by binding of pathway-specific transcription factors (TFs). An example in the mouse is the forkhead box O (FoxO) TF in T cells linking the T cell receptor (TCR) activity to DGKA abundance via PI3K activity (60) or the TF Egr2 regulating T cell anergy (61). Regarding the function of the enhancer region, *DGKA* expression was stimulated by binding of the radiation-inducible transcription factor EGR1 (31).

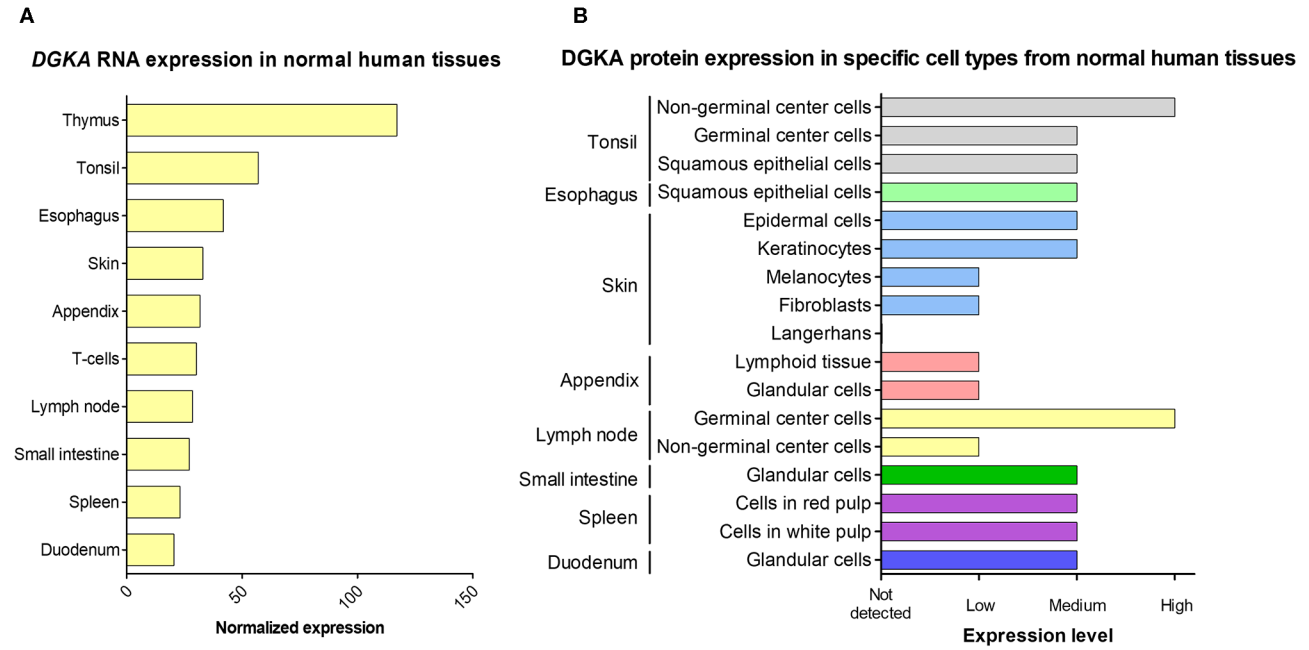

FIGURE 2 | DGKA expression in normal human tissues. **(A)** The 10 tissues with the highest *DGKA* RNA expression are shown. Data are derived from a consensus dataset in the Human Protein Atlas (HPA) which combines data from three comprehensive databases (HPA, GTEx, and FANTOM5). **(B)** DGKA protein expression measured by immunohistochemistry in cell types present in the tissue with the highest RNA expression shown in **(A)**. Protein data for thymus and T cells were not included in the HPA protein database. For details of protein expression, normalization and quantification, see website (https://www.proteinatlas.org/ENSG00000065357-DGKA/tissue).

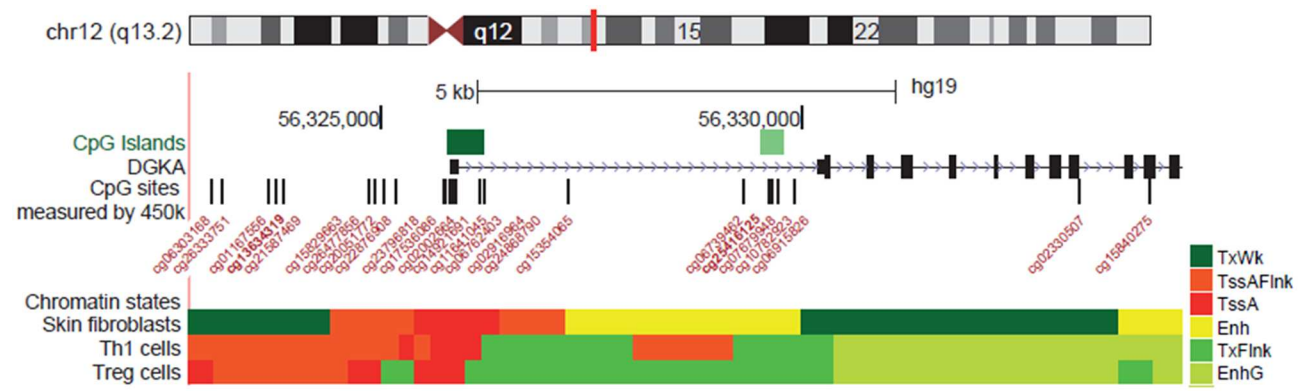

FIGURE 3 | Regulation of DGKA expression by DNA methylation. Location of *DGKA* on chromosome 12 and transcriptional regulation as shown in the UCSC Browser, hg19 assembly [http://genome.ucsc.edu/; (53)]. Regulatory elements are indicated by CpG islands and chromatin states (Encode ChromHMM) characterizing transcription start site (TssA, TssAFlnk, TXFlnk) and enhancer (Enh) in human skin fibroblasts (54). CpG probes (Illumina 450K BeadChipArray) located in the *DGKA* promotor area are indicated.

Small RNAs were also involved in the control of *DGKA* transcripts. Overexpression of miRNA-297 was shown to be cytotoxic to glioblastoma cells but not to normal astrocytes (62). *DGKA* was the most prominent target of this miRNA. Further evidence comes from the observation that DGKA, when upregulated by hypoxia and its mediator, the heterogeneous nuclear ribonucleoprotein L (HNRNPL), was able to buffer the cytotoxic effects of increased miRNA-297 expression.

Importantly, DGKA controls TF abundance and signaling pathways by itself through the conversion of DAG to PA and regulation of the downstream signaling (33) thus inducing an auto-regulatory loop for a well-balanced equilibrium between these pathways. These findings underpin the importance of maintaining an adequate DGKA level in cells for their proper functioning as it was shown when describing the role of DGKA during T cell differentiation. Similar to the growth stimulation

in tumor cells, it is conceivable that differences in DGKA levels affect the cellular amounts of DAG and PA and might contribute to fibroblast activation and migration during wound healing and to the perpetuation of myofibroblast activation in a pro-fibrotic situation.

DGKA-MEDIATED SIGNALING AND LIPID METABOLISM

The DGK family is involved in lipid metabolism specifically in the conversion of DAG to PA. Both are important intermediates involved in phospholipid metabolism, and they serve as second messengers at the plasma membrane. The DAG/PA ratio is important to maintain cellular homeostasis, and the dysregulation of cellular phospholipids has been implicated in several disorders. For example, radiation-induced free lipid accumulation impairs the normal cellular metabolism via induction of lipoprotein lipase and fatty acid binding protein 4 (FABP4). At the same time, triacylglycerol is also increased resulting in steatosis, progression to inflammation, and fibrosis (19, 63).

Overexpressed or activated DGKA results in the generation of PA and activates PA-mediated signaling (**Figure 4**). This includes mTOR, atypical PKC (aPKC)-RhoGDI, Rab11 family interacting protein 1 (Rab11-FIP1), and phosphatidylinositol-4-phosphate 5-kinase (PIP5K) signaling which can lead to fibrosis formation or tumor cell invasion and migration (42, 64–67). In contrast, downregulation or inhibition of DGKA results in the accumulation of DAG, which functions as a second messenger by binding to C1 domain containing proteins. This binding triggers multiple signaling pathways including RasGRP, classical and novel PKC and PKD, which contribute to T cell anergy and an insulin secretory defect (33, 35, 68).

Biochemical inhibition or silencing of DGKA was reported to reduce HIF-1α and mTOR signaling by limiting PA in glioblastoma cells (51). In addition, the cyclic adenosine monophosphate (cAMP) level was observed to be significantly increased in these cells which resulted in downregulation of *MTOR* transcription. Downregulation of DGKA and its downstream targets HIF-1α and mTOR resulted in suppression of tumor cell migration and survival. Rescue experiments with mTOR or HIF-1α restored cell viability. Remarkably, the cytotoxic activity of DGKA attenuation was observed in tumor cells but not in normal cells (51, 69). The authors suggested a unique DGKA–PA–posphodiesterase–cAMP–mTOR transcription pathway which would be active besides the lipid signaling DGKA function. Similarly, Chen et al. found a stimulation of the PTEN pathway and the oncogenic Akt/NF-κB activity via cAMP in esophageal squamous cell carcinoma cells (70) suggesting that, in this way, DGKA might promote cell growth and cancer progression. Both observations were found to be specifically active in malignant cells and make DGKA an exciting target in cancer therapy. These studies further support a unique role of DGKA in cell growth as this activity was independent of the kinase activity. Other DGKs were not reported to be able to substitute the DGKA function in this process (51, 70). In L6 myotubes overexpressing the human insulin receptor, DGK inhibition resulted in DAG accumulation, PKCα activation at the plasma membrane, and reduced glucose-induced insulin receptor activation (71). Interestingly, DGKA knockdown or inhibition induces a stronger cytotoxicity in cancer cells than in normal cells (69), underlining again that the amount of DGKA might determine its cellular effects. In addition, this observation supports DGKA as a potential therapeutic target for cancer and fibrosis treatment.

DAG and PA are not only acting as second messengers but are also involved in phospholipid metabolism. For example, downregulation of DGKs results in the accumulation of DAG which can cause metabolic disorders because DAG is a precursor for triglycerides and phospholipids such as phosphatidylcholine (PC) and phosphatidylethanolamine (PE) (20). Increased PA levels, in contrast, trigger the generation of lysophosphatidic acid, a lipid involved in many chronic inflammatory diseases including idiopathic pulmonary fibrosis and liver fibrosis (19). Conversion of DAG to PA by DGKs is a demanding task as shown by more than 50 structurally different DAG and PA species in mammals (34). DAG consists of a glycerol backbone which is linked to a saturated and an unsaturated fatty acid which vary in chain length and composition according to the cellular turnover of various phosphatidylinositol (PI) species. Specific DGKs are reported to convert different DAGs (72). For DGKA, this process might be cell type specific as the spectrum of DAG species converted in AKI melanoma cells is not identical to the one observed in normal human dermal fibroblasts (31, 34). However, different methods were used for quantification in both cell types.

Finally, it is likely that ionizing radiation which is inducing highly reactive ROS in cells may alter the composition of the DAG spectrum mainly by reacting with the unsaturated part of DAG and PA. This substrate change will cause at least an intermediate imbalance in the DAG to PA ratio with all the possible changes in cellular functions as already described.

RADIATION-INDUCED IMMUNE RESPONSE AND DGKA-MEDIATED T CELL ACTIVATION

Radiotherapy has been used for decades to eliminate local tumor growth, while different radiation dosage and fractionation also lead to various degrees of injury in surrounding normal tissue because of the induced immune responses (73). Thus, DGKA, as regulated by IR, may be involved in IR-induced immune response through mediating T cell activation.

During the initial phase of radiation exposure, DNA damage, ROS induction and cell death trigger the release of pro-inflammatory cytokines (e.g., IL-1, IL-6, IL-10, TGF-β, TNF-α, and IFN-γ) and activate immune response (6, 74, 75). The induction time of pro-inflammatory cytokine secretion can vary from minutes to hours (initial phase) up to days and weeks (early acute inflammatory phase) depending on the radiation dosage and fractionation (15). Lymphocytes and macrophages infiltrate

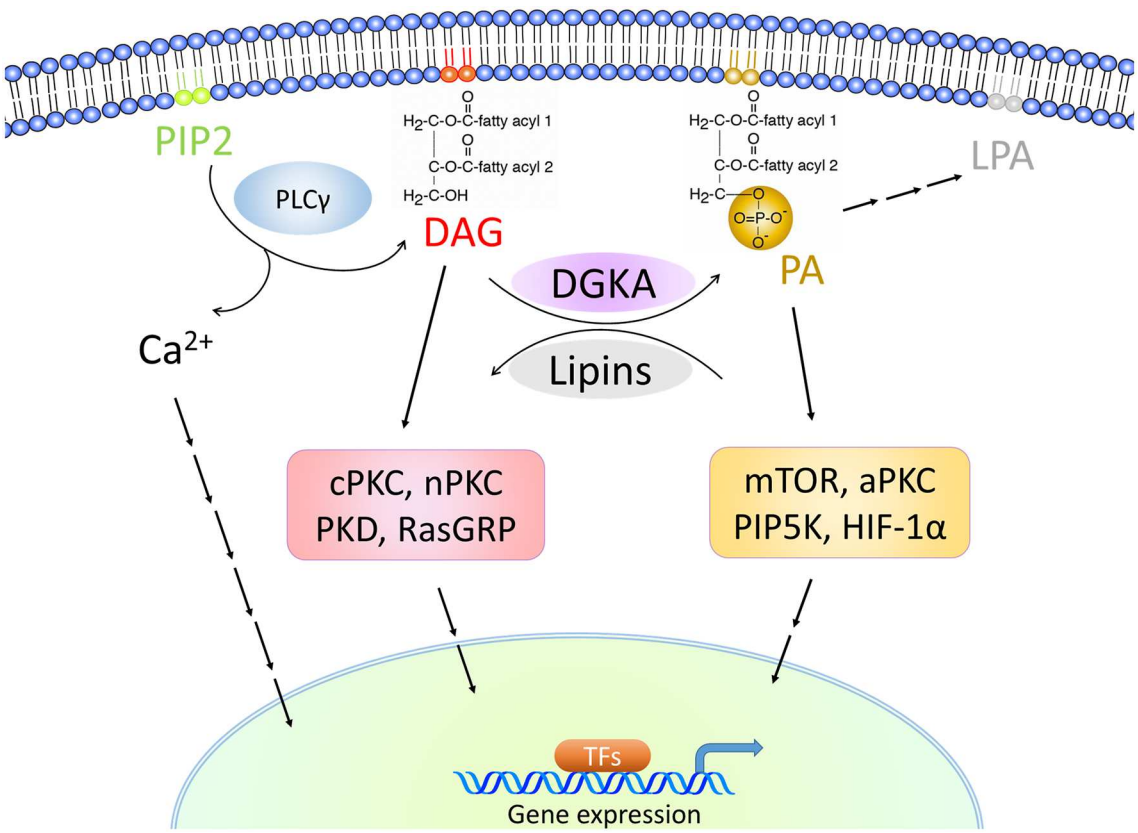

FIGURE 4 | DGKA-associated signaling cascades. DGKA controls the conversion of DAG to PA, two membrane-associated lipid messengers. High DAG levels activate classical PKCs (cPKC) with PKCα, β and γ, novel PKCs (nPKC) with PKCδ, ε, η, and θ, PKD and RasGRP signaling. High PA levels activate mTOR, atypical PKCs (aPKC) with PKCζ and PKCι/κ, PIP5K, and HIF-1α. The stimulated signaling cascades induce transcription in the nucleus by triggering pathway-specific transcription factors (TFs).

into the injured tissue and induce inflammasome formation. Type I T helper cells (Th1), Th17, and macrophages (M1) are activated and contribute to inflammation around the damaged area. In the late acute inflammatory phase, anti-inflammatory cells including Th2 and regulatory T cells (Treg) are induced to suppress pro-inflammatory responses. Th2 releases cytokines including IL-3, IL-4, and IL-10 around the injured tissue and triggers fibroblast-to-myofibroblast differentiation along with the accumulation of M2 macrophages (76). During this stage, TGF-β stimulates the generation of Tregs which further produce TGF-β and IL-10 thus contributing to tissue repair and a pro-fibrotic action (77). These alterations continue even throughout the chronic phase of radiation-induced fibrosis. Moreover, radiation-induced accumulation of lipid products such as free fatty acids, triglycerides and DAGs activate the infiltration of macrophages into the damaged tissue and further induce chronic inflammation (7).

Several reviews indicate that DGKs, especially DGKA and DGKZ, play an important role in T cell activation via termination of DAG signaling (42, 78–80), but here we focus on the role of DGKA. In general, T cell activation requires two signals: the first consists of the interaction of the T cell receptor (TCR) with foreign antigens bound to the major histocompatibility complex (MHC) on the surface of antigen-presenting cells (APC). This initial signal is responsible for the generation of two phospholipase PLC-γ-mediated cleavage products, inositol triphosphate (IP3) and DAG. The two second messengers promote the signaling cascades of both the Ca^{2+}-mediated nuclear factor of activated T cells (NFAT) and the Ras/ERK pathway (81). DGKA participates in this step as follows. During initial TCR signaling, Ca^{2+} generated by PLC-γ promotes a conformational change of DGKA leading to the activation of its membrane-binding domain, and subsequently to its rapid translocation and binding to the plasma membrane. Membrane-bound DGKA (activated DGKA) metabolizes DAG to PA. However, a further signal is necessary to complete T cell activation. Co-stimulatory molecules such as CD28, which interact with CD80 on the surface of APC, are essential to fully activate T cells. During this step, PKCθ is involved in activating NF-κB-mediated IL-2 synthesis (6). The co-stimulatory signals balance the catalytic DGKA activity which is still located at the plasma membrane to avoid that DAG levels become insufficient to activate downstream signaling such as IL-2 secretion. Therefore, over-activated DGKA would result in T cell

anergy. Co-stimulatory signals and IL-2 also trigger PI3K/AKT activation to further suppress FoxO-dependent *DGKA* mRNA expression finally creating a feed-back loop limiting DGKA levels and signal intensity (33, 78). Thus, DGKA acts as an immunological checkpoint to control the activities of T and NK cells (82, 83). A recent study further showed that a lack of DGKA reduced inflammation markers like IL-1β expression in white adipose tissue in mice which were fed with a short-term high-fat diet (84). This suggests that DGKA may be involved in the early immune response also in other tissues.

As a part of the immune response after irradiation, T and NK cells were shown to be activated and to gain the ability to kill tumor cells after radiotherapy; however, tumors seem to be protected from this cytotoxic activity (85). In renal clear cell carcinoma, for example, the activity of tumor-infiltrating NK cells was inhibited by strong expression of DGKA and insufficient ERK pathway activity. Inhibition of DGKA or reactivation of the ERK pathway reconstituted the anti-tumor activity of T and NK cells (86). This was also observed in other tumors where inhibition of DGKA and other DGKs restored pro-apoptotic signaling in normal T and NK cells against tumor (83, 87–90). This suggests that DGKA inhibition might be an interesting strategy for tumor therapy. If however, DGKA inhibition results in a similar T and NK cell activation by irradiation in the normal tissue, an increase in tissue damage might be observed which would increase therapeutic side effects. Remarkably, cell toxicity of DGKA inhibitors was found to be lower in normal cells (51, 69) making this possibility less probable. In the irradiated healthy tissue, it is therefore assumed that immune cells are infiltrating the damaged tissue, and together with fibroblasts and endothelial cells, induce tissue regeneration. DGKA has been shown to be activated in irradiated fibroblasts of patients with high fibrosis risk (31). This response has not yet been investigated in T cells or in irradiated tissues but it would be interesting to analyze DGKA under both conditions. This would show how the different cell types are interacting during wound healing and whether induced DGKA levels sustainably disturb the DAG balance and induce a prolonged wound healing response which might be pro-fibrotic.

DGKA REGULATES EXOSOME PRODUCTION WHICH CAN ACTIVATE PRO-FIBROTIC FUNCTIONS

Regeneration of normal tissue after irradiation requires cooperation of multiple cell types like immune cells, fibroblasts or mesenchymal stem cells which are attracted to the injured tissue site and activated for their specific function in the wound. When the wound is closed, attracted cells and induced processes have to be shut down to avoid accumulation of excessive ECM, scars, and on a long-term basis, fibrosis. It is evident that such a process needs multiple intercellular communications. One way could be mediated by membrane trafficking related processes like the release of multivesicular bodies or secretion of exosomes (47, 91). Exosomes can transport signaling peptides, proteins or miRNAs depending on cell type and regulated function. They are excreted or internalized by various cell types like stem cells, fibroblasts or lymphocytes (92). These exosome-mediated processes are by far not completely understood but there are some examples that underline the importance of exosomes in fibrogenesis. Exosomes derived from mesenchymal stem cells were reported to activate fibroblast migration and proliferation and to regulate collagen synthesis during wound healing (92, 93).

DAGs were suggested to belong to the lipids that contribute to exosome production in T lymphocytes (94–96). In T cells, exosomes mainly transport Fas ligand which mediates cytotoxicity and Fas-induced cell death in the targeted area. Membrane-bound DKGA is an essential regulator of the membrane-related process of exosome production as it controls the formation and polarization of mature multivesicular bodies as precursors of exosomes (94). DGKA might drive similar exosome-mediated effects in other cell types. An example is shown in H1299 tumor cells expressing a gain of function p53 mutant (mutp53; R270H; p53R172H). ECM production and the orthogonal branching of collagen, one of the hallmarks of fibrosis, could be substantially impeded by pharmaceutically inhibiting DGKA in these cells (97). In fact, this process was strongly controlled by DGKA-mediated exosome production. A further analysis in mice with mutp53-driven pancreatic cancer revealed this orthogonal ECM characteristic even in the lungs of the animals where it preceded metastasis indicating a potential role of DGKA in ECM production via exosomes (97).

Migration of different cell types to the wound and their perpetuated activation is required for fibrosis to occur. In tumor cells harboring gain-of-function p53 mutations, DGKA increases cell migration and invasion capability. In this process, membrane-bound DGKA generates increased PA levels, thus recruiting β1 integrin trafficking and MMP9 secretion to promote cytoskeleton reorganization for protrusion elongation, lamellipodia formation, membrane ruffling, migration, and spreading through the atypical aPKC/Rab-coupling protein (RCP) mediated signaling in epithelial cells (65–67). In mouse embryonic fibroblasts (MEFs), PA-Rac1-mediated cytoskeleton reorganization was mainly promoted by DGKZ or DGKG not by DGKA (98, 99). However, DGKA expression in MEFs is relatively low compared to human fibroblasts, so further investigations on DGKA and cell migration in human fibroblasts is needed.

DGKA inhibition or silencing reduce the migration-related membrane processes and finally attenuate migration. Although detection of these processes depends mainly on expression of the mutated p53 protein, data reveal that membrane-bound DGKA is involved in this process, and in a similar way, might participate in wound healing and pro-fibrotic events.

In this context, it should be mentioned that increased collagen production was measured as a pro-fibrotic endpoint in fibroblasts. This was depending on DGKA protein abundance and activity in fibroblasts after γ-irradiation (31). Whether this *in vitro* process was accomplished by membrane processes resulting in vesicles or exosomes formation as summarized by Stephens (100) was not analyzed, however increased collagen synthesis and secretion was associated with an increase of mRNA transcription and protein synthesis. This observation underpins the multiple functions DGKA might have depending on the intracellular location of the protein and the abundance in different cell types.

NUCLEAR LOCALIZATION OF DGKA AND CELL CYCLE REGULATION

There is evidence that several DGK family members are not only present in the cytosol and cellular membranes but also in the cell nucleus [**Table 1**; (112, 113)]. This led to the assumption that there might be a role for DGKs in cell cycle regulation. DGKA nuclear localization was observed in specific cell types such as the human natural killer cell line YT, the mouse lymphocyte cell line CTLL-2 (102) or in rat thymocytes and T-cell-enriched peripheral lymphocytes (103). Furthermore, DGKA was observed to shuttle between the nucleus and the cytoplasm, e.g., Baldanzi et al. showed that upon stimulation of human T lymphocytes, DGKA can exit from the nucleus which is associated with a rapid negative regulation of its enzymatic activity (104). In contrast, serum starvation in the mouse embryo fibroblast cell line NIH/3T3 led to the transport of DGKA from the cytoplasm into the nucleus, a process which could be reversed by serum restoration (105).

DGKA is distinctly expressed in different tumor cell types while their normal tissue counterparts are often devoid of its expression; this suggests that it is able to enhance tumor cell proliferation. DGKA is highly expressed in various human hepatocellular carcinoma cell lines (50). Here, the authors observed a significantly enhanced cell proliferation upon overexpression of DGKA. Furthermore, immunohistochemical analyses in tissue samples from patients with hepatocellular carcinoma revealed an association of high DGKA expression and high expression of the cellular proliferation marker Ki-67. DGKA was also strongly expressed in the nuclei of human K562 leukemia cells and was shown to be involved in both changes of the RB phosphorylation status and in the progression of the cell cycle through the G1/S checkpoint (101). These authors used synchronized cells to demonstrate cell cycle phase-dependent

TABLE 1 | DGKA function according to cellular localization.

Cellular Compartment	Function	Species	Cell line (cell type)	References
Nucleus	Cell cycle regulation	Human	K562 (myelogenous leukemia)	(101)
	Proliferation	Human	YT (natural killer cell)	(102)
		Mouse	CTLL-2 (T lymphocytes)	(102)
	Lymphocyte activation	Rat	Primary thymocytes	(103)
	nr[a]	Human	Jurkat (T cell leukemia)	(104)
		Mouse	NIH/3T3 (embryonic fibroblasts)	(105)
Cytosol	T cell activation	Human	Jurkat (T cell leukemia)	(104–107)
		Rat	Primary thymocytes	(103)
	Lipid metabolism, signaling	Swine	Primary vascular smooth muscle cells	(68, 106, 107)
		Human	Jurkat (T cell leukemia)	(68, 108)
		Rat	L6 (skeletal myoblasts)	(71, 108)
	nr[a]	Mouse	NIH/3T3 (embryonic fibroblasts)	(105)
		Rat	Primary thymocytes	(103)
Membrane	T cell activation	Human	Jurkat (T cell leukemia)	(104, 106–110)
		Mouse	Primary T cells	(111)
	Lipid metabolism, signaling	Swine	Primary vascular smooth muscle cells	(68)
		Mouse	CTLL-2 (T lymphocytes)	(72)
		Mouse	BaF/3 (pro-B cells)	(72)
		Dog	MDCK (kidney epithelial cells)	(67)
		Rat	L6 (skeletal myoblasts)	(71)
	Exosome maturation	Human	Jurkat (T cell leukemia)	(94)
	Migration	Human	H1299 (lung carcinoma)	(65)
	Matrix invasion	Human	MDA-MB-231 (breast cancer cells)	(66)
	Multivesicular body secretion	Human	Jurkat (T cell leukemia)	(95)
		Human	Raji B (B lymphocytes)	
Total cell	Cell proliferation, signaling	Human	HuH7, PLC/PRF/5, HLE, and Hep3B (hepatocellular carcinoma)	(50)

[a] *nr, not reported.*

DGKA expression, and they applied DGK inhibitors resulting in down-regulation of cell growth and accumulation of cells into G0/G1 phase. Yanagisawa et al. observed DGKA expression in several human melanoma cell lines while normal epidermal melanocytes did not express this protein (49). In addition, they revealed DGKA as a negative regulator of TNF-α-induced apoptosis in these tumor cells. Further evidence for an anti-apoptotic and proliferation-enhancing activity of DGKA in cancer cells derived from different cancer entities is reported using selective inhibitors of DGKA (51, 69, 114).

All in all, the above-mentioned studies demonstrate that DGKA (i) is present in the nucleus of different cell types, (ii) is involved in cell cycle regulation, and (iii) has cell-type specificity functions based on its expression levels. Although there is a lack of data on DGKA and cell cycle regulation in fibrosis, it is conceivable that DGKA might play a role in transactivation of resident fibroblasts to replicating active myofibroblasts, the activity of which has to be maintained in fibrotic tissues.

TARGETING OF DGKA BY SMALL COMPOUNDS

To interfere with the manifold cellular functions of DGKs, compounds were designed to suppress DGK activity. So far, the compounds R59022 and R59949 are described to show a higher selectivity toward type I DGKs including DGKA by binding to the catalytic domain (115). Ritanserin, a serotonin receptor antagonist, and a chemical fragment of it, RF001, were identified to attenuate DGKA function e.g., by increasing the DGKA affinity toward ATP *in vitro* (116, 117). Especially RF001 shows strong effects because it targets both the catalytic domain and the C1 domains of DGKA (117). Most recently, a novel compound, AMB639752, has been identified based on its structural analogy to Ritanserin, R59022 and R59949 (118). The drug shows high specificity for DGKA but does not have the associated activity against the serotonin receptor like the parental drugs. A further compound, CU-3, functions as a competitive ATP inhibitor, but it is unclear why CU-3 has high selectivity for type I DGKs (114). In contrast, a recent study showed that DGKA can be activated when treated with KU-8 (119). Several authors describe that the growth of glioblastoma and other cancers can be impeded with DGKA inhibitors in cell cultures and in xenografts (51, 114, 120). Also AMB639752 is impeding cell migration of MCF7 tumor cells (121). DGKA inhibitors, therefore, offer not only a promising way to manipulate DGKA activity for therapeutic purposes in tumor cells but they might also be helpful to confine a perpetuated wound healing response leading to fibrosis. The current drugs, however, show poor pharmacokinetic data in mice and have considerable off-target effects like targeting the serotonin receptor (116). Still, novel drug screening strategies as those described by Velnati et al. (121) give promise that these limitations can be overcome.

Additional attractive candidates to modulate DGKA levels are epigenetic drugs as they can alter or even reverse aberrant gene expression. Gene expression is organized on different layers by epigenetic mechanisms, especially by DNA methylation and histone modifications (22). As most epigenetic marks in differentiated cells are highly stable and serve as an epigenomic memory (122), a protective epigenomic layout, once established by an epigenetic treatment, could be maintained throughout numerous rounds of cellular replication in fibroblasts (123). As a proof-of-concept for epigenetic therapy, Zeybel et al. (124) halted CCl_4-induced liver fibrosis progression in mice with the histone methyltransferase inhibitor 3-deazaneplanocin A (DZNep). DZNep also inhibited myofibroblast transactivation *in vitro* (124). In a fibroblast model for radiation-induced fibrosis (31), BET-bromodomain inhibitors (JQ1 and PFI-1) suppressed induction of *DGKA* in bleomycin-treated fibroblasts, reduced histone H3 lysine 27 acetylation (H3K27ac) at the *DGKA* enhancer and repressed collagen marker gene expression (125). Here, BET-bromodomain inhibitors altered the epigenetic landscape of fibroblasts, counteracting pro-fibrotic transcriptional events. Of course, the use of epigenetic drugs to alter pro-fibrotic signaling requires further experimental proof, but there is sufficient evidence (126) that altering the chromatin state at the *DGKA* locus could be a valuable therapeutic approach in fibrosis prevention and might lead to long-lasting, stable protection against radiation-induced fibrogenesis.

A further promising therapeutic approach could be a co-treatment of both disturbed DGKA levels and downstream signaling. In a tentative approach, co-treatment with the DGK inhibitor R59949 and the protein kinase C alpha inhibitor Gö6976 attenuated cell growth and *COL1A1* transcription in primary human fibroblasts, indicating great potential to synergistically treat fibrosis development (31). It should however be mentioned here that all anti-fibrotic treatments targeting DGKA either directly or by changing its expression might be demanding, as in case of drug-induced DAG/PA imbalance, other DGK isoforms expressed in cells or further signaling pathways might step in to take over the function of DGKA.

CONCLUSIONS

Radiotherapy is a highly efficient tool for cancer treatment but the risk of side effects especially radiation-induced fibrosis may considerably restrain therapy outcome by either reducing tumor control or the overall quality of life *post*-therapy. Therefore, how to prevent fibrosis still requires more detailed studies. Recently, growing evidence indicates that DGKA is a central node regulating numerous cellular functions like immune response, lipid signaling, exosome production and migration as well as cell proliferation by maintaining an adequate DAG to PA balance at cell membranes but also by potential, yet unknown functions in the nucleus. In addition, DGKA expression is inducible by irradiation. Even though the mechanisms of how DGKA contributes, after irradiation of cells, to the pro-fibrotic processes of myofibroblast transactivation and production of ECM are still not fully elucidated, there is strong evidence that DGKA is activated after irradiation and that it has many competences to play a central function in fibrosis development when disturbed by irradiation. Inhibitors

that target DGKA function and protein levels either by direct interaction with the protein, by addressing its epigenetic control or by modulating DAG-dependent signaling might therefore offer novel therapeutic avenues to prevent or attenuate radiotherapy-induced fibrosis.

AUTHOR CONTRIBUTIONS

All authors were involved in literature search, drafting the manuscript and designing the figures, developed the concept and aim of the review, and approved the final manuscript.

FUNDING

This work was supported by the Deutsche Krebshilfe, Grant No. 70112734.

ACKNOWLEDGMENTS

We thank Carsten Herskind and Marlon R. Veldwijk for critically reading the manuscript and helpful suggestions. We are grateful to Clarissa Gerhäuser for supportive discussions and graphical assistance.

REFERENCES

1. Thompson MK, Poortmans P, Chalmers AJ, Faivre-Finn C, Hall E, Huddart RA, et al. Practice-changing radiation therapy trials for the treatment of cancer: where are we 150 years after the birth of Marie Curie? *Br J Cancer.* (2018) 119:389–407. doi: 10.1038/s41416-018-0201-z
2. De Ruysscher D, Niedermann G, Burnet NG, Siva S, Lee AWM, Hegi-Johnson F. Radiotherapy toxicity. *Nat Rev Dis Primers.* (2019) 5:13. doi: 10.1038/s41572-019-0064-5
3. Pavlopoulou A, Bagos PG, Koutsandrea V, Georgakilas AG. Molecular determinants of radiosensitivity in normal and tumor tissue: a bioinformatic approach. *Cancer Lett.* (2017) 403:37–47. doi: 10.1016/j.canlet.2017.05.023
4. Schafer MJ, Haak AJ, Tschumperlin DJ, LeBrasseur NK. Targeting senescent cells in fibrosis: pathology, paradox, and practical considerations. *Curr Rheumatol Rep.* (2018) 20:3. doi: 10.1007/s11926-018-0712-x
5. Jain V, Berman AT. Radiation pneumonitis: old problem, new tricks. *Cancers.* (2018) 10:222. doi: 10.3390/cancers10070222
6. Wirsdorfer F, Jendrossek V. The role of lymphocytes in radiotherapy-induced adverse late effects in the lung. *Front Immunol.* (2016) 7:591. doi: 10.3389/fimmu.2016.00591
7. Gowda SSN, Raviraj R, Nagarajan D, Zhao W. Radiation-induced lung injury: impact on macrophage dysregulation and lipid alteration - a review. *Immunopharmacol Immunotoxicol.* (2019) 41:370–9. doi: 10.1080/08923973.2018.1533025
8. Giuranno L, Ient J, De Ruysscher D, Vooijs MA. Radiation-induced lung injury (RILI). *Front Oncol.* (2019) 9:877. doi: 10.3389/fonc.2019.00877
9. Zanoni M, Cortesi M, Zamagni A, Tesei A. The role of mesenchymal stem cells in radiation-induced lung fibrosis. *Int J Mol Sci.* (2019) 20:3876. doi: 10.3390/ijms20163876
10. Baudelet M, Van den Steen L, Tomassen P, Bonte K, Deron P, Huvenne W, et al. Very late xerostomia, dysphagia, and neck fibrosis after head and neck radiotherapy. *Head Neck.* (2019) 41:3594–603. doi: 10.1002/hed.25880
11. Pez M, Keller A, Welzel G, Abo-Madyan Y, Ehmann M, Tuschy B, et al. Long-term outcome after intraoperative radiotherapy as a boost in breast cancer. *Strahlenther Onkol.* (2019) 196:349–55. doi: 10.1007/s00066-019-01525-7
12. Straub JM, New J, Hamilton CD, Lominska C, Shnayder Y, Thomas SM. Radiation-induced fibrosis: mechanisms and implications for therapy. *J Cancer Res Clin Oncol.* (2015) 141:1985–94. doi: 10.1007/s00432-015-1974-6
13. Ramachandran P, Dobie R, Wilson-Kanamori JR, Dora EF, Henderson BEP, Luu NT, et al. Resolving the fibrotic niche of human liver cirrhosis at single-cell level. *Nature.* (2019) 575:512–8. doi: 10.1038/s41586-019-1631-3
14. Weiskirchen R, Weiskirchen S, Tacke F. Recent advances in understanding liver fibrosis: bridging basic science and individualized treatment concepts. *F1000Res.* (2018) 7:F1000. doi: 10.12688/f1000research.14841.1
15. Ejaz A, Greenberger JS, Rubin PJ. Understanding the mechanism of radiation induced fibrosis and therapy options. *Pharmacol Ther.* (2019) 204:107399. doi: 10.1016/j.pharmthera.2019.107399
16. Kwon YK, Ha IJ, Bae HW, Jang WG, Yun HJ, Kim SR, et al. Dose-dependent metabolic alterations in human cells exposed to gamma irradiation. *PLoS ONE.* (2014) 9:e113573. doi: 10.1371/journal.pone.0113573
17. Xu Y, Wang D, Wang Z. Lipid generation and signaling in ovarian cancer. *Cancer Treat Res.* (2009) 149:241–67. doi: 10.1007/978-0-387-98094-2_12
18. Rancoule C, Espenel S, Trone JC, Langrand-Escure J, Vallard A, Rehailia-Blanchard A, et al. Lysophosphatidic acid (LPA) as a pro-fibrotic and pro-oncogenic factor: a pivotal target to improve the radiotherapy therapeutic index. *Oncotarget.* (2017) 8:43543–54. doi: 10.18632/oncotarget.16672
19. Magkrioti C, Galaris A, Kanellopoulou P, Stylianaki EA, Kaffe E, Aidinis V. Autotaxin and chronic inflammatory diseases. *J Autoimmun.* (2019) 104:102327. doi: 10.1016/j.jaut.2019.102327
20. Itani SI, Ruderman NB, Schmieder F, Boden G. Lipid-induced insulin resistance in human muscle is associated with changes in diacylglycerol, protein kinase C, and IkappaB-alpha. *Diabetes.* (2002) 51:2005–11. doi: 10.2337/diabetes.51.7.2005
21. Deng W, Shuyu E, Tsukahara R, Valentine WJ, Durgam G, Gududuru V, et al. The lysophosphatidic acid type 2 receptor is required for protection against radiation-induced intestinal injury. *Gastroenterology.* (2007) 132:1834–51. doi: 10.1053/j.gastro.2007.03.038
22. Weigel C, Schmezer P, Plass C, Popanda O. Epigenetics in radiation-induced fibrosis. *Oncogene.* (2015) 34:2145–55. doi: 10.1038/onc.2014.145
23. Ghosh K, O'Neil K, Capell BC. Histone modifiers: dynamic regulators of the cutaneous transcriptome. *J Dermatol Sci.* (2018) 89:226–32. doi: 10.1016/j.jdermsci.2017.12.006
24. Mori R, Tanaka K, Shimokawa I. Identification and functional analysis of inflammation-related miRNAs in skin wound repair. *Dev Growth Differ.* (2018) 60:306–15. doi: 10.1111/dgd.12542
25. Lu L, Sun C, Su Q, Wang Y, Li J, Guo Z, et al. Radiation-induced lung injury: latest molecular developments, therapeutic approaches, and clinical guidance. *Clin Exp Med.* (2019) 19:417–26. doi: 10.1007/s10238-019-00571-w
26. Wang B, Wei J, Meng L, Wang H, Qu C, Chen X, et al. Advances in pathogenic mechanisms and management of radiation-induced fibrosis. *Biomed Pharmacother.* (2020) 121:109560. doi: 10.1016/j.biopha.2019.109560
27. Wang LP, Wang YW, Wang BZ, Sun GM, Wang XY, Xu JL. Expression of interleukin-17A in lung tissues of irradiated mice and the influence of dexamethasone. *Sci World J.* (2014) 2014:251067. doi: 10.1155/2014/251067
28. Bickelhaupt S, Erbel C, Timke C, Wirkner U, Dadrich M, Flechsig P, et al. Effects of CTGF blockade on attenuation and reversal of radiation-induced pulmonary fibrosis. *J Natl Cancer Inst.* (2017) 109:djw339. doi: 10.1093/jnci/djw339
29. Luangmonkong T, Suriguga S, Bigaeva E, Boersema M, Oosterhuis D, de Jong KP, et al. Evaluating the antifibrotic potency of galunisertib in a human ex vivo model of liver fibrosis. *Br J Pharmacol.* (2017) 174:3107–3117. doi: 10.1111/bph.13945
30. Sperk E, Welzel G, Keller A, Kraus-Tiefenbacher U, Gerhardt A, Sutterlin M, et al. Late radiation toxicity after intraoperative radiotherapy (IORT) for breast cancer: results from the randomized phase III trial TARGIT A. *Breast Cancer Res Treat.* (2012) 135:253–60. doi: 10.1007/s10549-012-2168-4
31. Weigel C, Veldwijk MR, Oakes CC, Seibold P, Slynko A, Liesenfeld DB, et al. Epigenetic regulation of diacylglycerol kinase alpha promotes radiation-induced fibrosis. *Nat Commun.* (2016) 7:10893. doi: 10.1038/ncomms10893

32. LENT SOMA scales for all anatomic sites. *Int J Radiat Oncol Biol Phys.* (1995). 31:1049–91. doi: 10.1016/0360-3016(95)90159-0
33. Merida I, Arranz-Nicolas J, Torres-Ayuso P, Avila-Flores A. Diacylglycerol kinase malfunction in human disease and the search for specific inhibitors. *Handb Exp Pharmacol.* (2020) 259:133–62. doi: 10.1007/164_2019_221
34. Sakane F, Mizuno S, Takahashi D, Sakai H. Where do substrates of diacylglycerol kinases come from? Diacylglycerol kinases utilize diacylglycerol species supplied from phosphatidylinositol turnover-independent pathways. *Adv Biol Regul.* (2018) 67:101–8. doi: 10.1016/j.jbior.2017.09.003
35. Massart J, Zierath JR. Role of diacylglycerol kinases in glucose and energy homeostasis. *Trends Endocrinol Metab.* (2019) 30:603–17. doi: 10.1016/j.tem.2019.06.003
36. Merida I, Arranz-Nicolas J, Rodriguez-Rodriguez C, Avila-Flores A. Diacylglycerol kinase control of protein kinase C. *Biochem J.* (2019) 476:1205–19. doi: 10.1042/BCJ20180620
37. Purow B. Molecular pathways: targeting diacylglycerol kinase alpha in cancer. *Clin Cancer Res.* (2015) 21:5008–12. doi: 10.1158/1078-0432.CCR-15-0413
38. Stace CL, Ktistakis NT. Phosphatidic acid- and phosphatidylserine-binding proteins. *Biochim Biophys Acta.* (2006) 1761:913–26. doi: 10.1016/j.bbalip.2006.03.006
39. Almena M, Merida I. Shaping up the membrane: diacylglycerol coordinates spatial orientation of signaling. *Trends Biochem Sci.* (2011) 36:593–603. doi: 10.1016/j.tibs.2011.06.005
40. Topham MK, Prescott SM. Diacylglycerol kinase zeta regulates Ras activation by a novel mechanism. *J Cell Biol.* (2001) 152:1135–43. doi: 10.1083/jcb.152.6.1135
41. Carrasco S, Merida I. Diacylglycerol, when simplicity becomes complex. *Trends Biochem Sci.* (2007) 32:27–36. doi: 10.1016/j.tibs.2006.11.004
42. Chen SS, Hu Z, Zhong XP. Diacylglycerol kinases in T cell tolerance and effector function. *Front Cell Dev Biol.* (2016) 4:130. doi: 10.3389/fcell.2016.00130
43. Merida I, Avila-Flores A, Merino E. Diacylglycerol kinases: at the hub of cell signalling. *Biochem J.* (2008) 409:1–18. doi: 10.1042/BJ20071040
44. Labesse G, Douguet D, Assairi L, Gilles AM. Diacylglyceride kinases, sphingosine kinases and NAD kinases: distant relatives of 6-phosphofructokinases. *Trends Biochem Sci.* (2002) 27:273–5. doi: 10.1016/s0968-0004(02)02093-5
45. Shulga YV, Topham MK, Epand RM. Regulation and functions of diacylglycerol kinases. *Chem Rev.* (2011) 111:6186–208. doi: 10.1021/cr1004106
46. Shirai Y, Saito N. Diacylglycerol kinase as a possible therapeutic target for neuronal diseases. *J Biomed Sci.* (2014) 21:28. doi: 10.1186/1423-0127-21-28
47. Xie S, Naslavsky N, Caplan S. Diacylglycerol kinases in membrane trafficking. *Cell Logist.* (2015) 5:e1078431. doi: 10.1080/21592799.2015.1078431
48. Ma Q, Gabelli SB, Raben DM. Diacylglycerol kinases: relationship to other lipid kinases. *Adv Biol Regul.* (2019) 71:104–110. doi: 10.1016/j.jbior.2018.09.014
49. Yanagisawa K, Yasuda S, Kai M, Imai S, Yamada K, Yamashita T, et al. Diacylglycerol kinase alpha suppresses tumor necrosis factor-alpha-induced apoptosis of human melanoma cells through NF-kappaB activation. *Biochim Biophys Acta.* (2007) 1771:462–74. doi: 10.1016/j.bbalip.2006.12.008
50. Takeishi K, Taketomi A, Shirabe K, Toshima T, Motomura T, Ikegami T, et al. Diacylglycerol kinase alpha enhances hepatocellular carcinoma progression by activation of Ras-Raf-MEK-ERK pathway. *J Hepatol.* (2012) 57:77–83. doi: 10.1016/j.jhep.2012.02.026
51. Dominguez CL, Floyd DH, Xiao A, Mullins GR, Kefas BA, Xin W, et al. Diacylglycerol kinase alpha is a critical signaling node and novel therapeutic target in glioblastoma and other cancers. *Cancer Discov.* (2013) 3:782–97. doi: 10.1158/2159-8290.CD-12-0215
52. Kong Y, Zheng Y, Jia Y, Li P, Wang Y. Decreased LIPF expression is correlated with DGKA and predicts poor outcome of gastric cancer. *Oncol Rep.* (2016) 36:1852–60. doi: 10.3892/or.2016.4989
53. Kent WJ, Sugnet CW, Furey TS, Roskin KM, Pringle TH, Zahler AM, et al. The human genome browser at UCSC. *Genome Res.* (2002) 12:996–1006. doi: 10.1101/gr.229102
54. Rosenbloom KR, Sloan CA, Malladi VS, Dreszer TR, Learned K, Kirkup VM, et al. ENCODE data in the UCSC genome browser: year 5 update. *Nucleic Acids Res.* (2013) 41:D56–63. doi: 10.1093/nar/gks1172
55. Kuhmann C, Weichenhan D, Rehli M, Plass C, Schmezer P, Popanda O. DNA methylation changes in cells regrowing after fractioned ionizing radiation. *Radiother Oncol.* (2011) 101:116–21. doi: 10.1016/j.radonc.2011.05.048
56. Zielske SP. Epigenetic DNA methylation in radiation biology: on the field or on the sidelines? *J Cell Biochem.* (2015) 116:212–7. doi: 10.1002/jcb.24959
57. Heinloth AN, Shackelford RE, Innes CL, Bennett L, Li L, Amin RP, et al. Identification of distinct and common gene expression changes after oxidative stress and gamma and ultraviolet radiation. *Mol Carcinog.* (2003) 37:65–82. doi: 10.1002/mc.10122
58. Merida I, Avila-Flores A, Garcia J, Merino E, Almena M, Torres-Ayuso P. Diacylglycerol kinase alpha, from negative modulation of T cell activation to control of cancer progression. *Adv Enzyme Regul.* (2009) 49:174–88. doi: 10.1016/j.advenzreg.2009.01.003
59. Kerley-Hamilton JS, Pike AM, Li N, DiRenzo J, Spinella MJ. A p53-dominant transcriptional response to cisplatin in testicular germ cell tumor-derived human embryonal carcinoma. *Oncogene.* (2005) 24:6090–100. doi: 10.1038/sj.onc.1208755
60. Martinez-Moreno M, Garcia-Lievana J, Soutar D, Torres-Ayuso P, Andrada E, Zhong XP, et al. FoxO-dependent regulation of diacylglycerol kinase alpha gene expression. *Mol Cell Biol.* (2012) 32:4168–80. doi: 10.1128/MCB.00654-12
61. Zheng Y, Zha Y, Driessens G, Locke F, Gajewski TF. Transcriptional regulator early growth response gene 2 (Egr2) is required for T cell anergy *in vitro* and *in vivo*. *J Exp Med.* (2012) 209:2157–63. doi: 10.1084/jem.20120342
62. Kefas B, Floyd DH, Comeau L, Frisbee A, Dominguez C, Dipierro CG, et al. A miR-297/hypoxia/DGK-alpha axis regulating glioblastoma survival. *Neuro Oncol.* (2013) 15:1652–63. doi: 10.1093/neuonc/not118
63. Gorden DL, Ivanova PT, Myers DS, McIntyre JO, VanSaun MN, Wright JK, et al. Increased diacylglycerols characterize hepatic lipid changes in progression of human nonalcoholic fatty liver disease; comparison to a murine model. *PLoS ONE.* (2011) 6:e22775. doi: 10.1371/journal.pone.0022775
64. Shende P, Xu L, Morandi C, Pentassuglia L, Heim P, Lebboukh S, et al. Cardiac mTOR complex 2 preserves ventricular function in pressure-overload hypertrophy. *Cardiovasc Res.* (2016) 109:103–14. doi: 10.1093/cvr/cvv252
65. Rainero E, Caswell PT, Muller PA, Grindlay J, McCaffrey MW, Zhang Q, et al. Diacylglycerol kinase alpha controls RCP-dependent integrin trafficking to promote invasive migration. *J Cell Biol.* (2012) 196:277–95. doi: 10.1083/jcb.201109112
66. Rainero E, Cianflone C, Porporato PE, Chianale F, Malacarne V, Bettio V, et al. The diacylglycerol kinase alpha/atypical PKC/beta1 integrin pathway in SDF-1alpha mammary carcinoma invasiveness. *PLoS ONE.* (2014) 9:e97144. doi: 10.1371/journal.pone.0097144
67. Chianale F, Rainero E, Cianflone C, Bettio V, Pighini A, Porporato PE, et al. Diacylglycerol kinase alpha mediates HGF-induced Rac activation membrane ruffling by regulating atypical PKC RhoGDI. *Proc Natl Acad Sci USA.* (2010) 107:4182–7. doi: 10.1073/pnas.0908326107
68. Du X, Jiang Y, Qian W, Lu X, Walsh JP. Fatty acids inhibit growth-factor-induced diacylglycerol kinase alpha activation in vascular smooth-muscle cells. *Biochem J.* (2001) 357(Pt 1):275–82. doi: 10.1042/0264-6021:3570275
69. Yamaki A, Akiyama R, Murakami C, Takao S, Murakami Y, Mizuno S, et al. Diacylglycerol kinase alpha-selective inhibitors induce apoptosis and reduce viability of melanoma and several other cancer cell lines. *J Cell Biochem.* (2019) 120:10043–56. doi: 10.1002/jcb.28288
70. Chen J, Zhang W, Wang Y, Zhao D, Wu M, Fan J, et al. The diacylglycerol kinase alpha (DGα)/Akt/NF-κB feedforward loop promotes esophageal squamous cell carcinoma (ESCC) progression via FAK-dependent and FAK-independent manner. *Oncogene.* (2019) 38:2533–50. doi: 10.1038/s41388-018-0604-6
71. Miele C, Paturzo F, Teperino R, Sakane F, Fiory F, Oriente F, et al. Glucose regulates diacylglycerol intracellular levels and protein kinase C activity by modulating diacylglycerol kinase subcellular localization. *J Biol Chem.* (2007) 282:31835–43. doi: 10.1074/jbc.M702481200

72. Cipres A, Carrasco S, Merino E, Diaz E, Krishna UM, Falck JR, et al. Regulation of diacylglycerol kinase alpha by phosphoinositide 3-kinase lipid products. *J Biol Chem.* (2003) 278:35629–35. doi: 10.1074/jbc.M305635200
73. Herskind C, Wenz F, Giordano FA. Immunotherapy combined with large fractions of radiotherapy: stereotactic radiosurgery for brain metastases-implications for intraoperative radiotherapy after resection. *Front Oncol.* (2017) 7:147. doi: 10.3389/fonc.2017.00147
74. McBride WH, Chiang CS, Olson JL, Wang CC, Hong JH, Pajonk F, et al. A sense of danger from radiation. *Radiat Res.* (2004) 162:1–19. doi: 10.1667/rr3196
75. Najafi M, Motevaseli E, Shirazi A, Geraily G, Rezaeyan A, Norouzi F, et al. Mechanisms of inflammatory responses to radiation and normal tissues toxicity: clinical implications. *Int J Radiat Biol.* (2018) 94:335–56. doi: 10.1080/09553002.2018.1440092
76. Ding NH, Li JJ, Sun LQ. Molecular mechanisms and treatment of radiation-induced lung fibrosis. *Curr Drug Targets.* (2013) 14:1347–56. doi: 10.2174/13894501113149990198
77. Das A, Sinha M, Datta S, Abas M, Chaffee S, Sen CK, et al. Monocyte and macrophage plasticity in tissue repair and regeneration. *Am J Pathol.* (2015) 185:2596–606. doi: 10.1016/j.ajpath.2015.06.001
78. Merida I, Andrada E, Gharbi SI, Avila-Flores A. Redundant and specialized roles for diacylglycerol kinases alpha and zeta in the control of T cell functions. *Sci Signal.* (2015) 8:re6. doi: 10.1126/scisignal.aaa0974
79. Joshi RP, Koretzky GA. Diacylglycerol kinases: regulated controllers of T cell activation, function, and development. *Int J Mol Sci.* (2013) 14:6649–73. doi: 10.3390/ijms14046649
80. Zhong XP, Guo R, Zhou H, Liu C, Wan CK. Diacylglycerol kinases in immune cell function and self-tolerance. *Immunol Rev.* (2008) 224:249–64. doi: 10.1111/j.1600-065X.2008.00647.x
81. Krishna S, Zhong XP. Regulation of lipid signaling by diacylglycerol kinases during T cell development and function. *Front Immunol.* (2013) 4:178. doi: 10.3389/fimmu.2013.00178
82. Sadreddini S, Baradaran B, Aghebati-Maleki A, Sadreddini S, Shanehbandi D, Fotouhi A, et al. Immune checkpoint blockade opens a new way to cancer immunotherapy. *J Cell Physiol.* (2019) 234:8541–8549. doi: 10.1002/jcp.27816
83. Noessner E. DGK-alpha: a checkpoint in cancer-mediated immuno-inhibition and target for immunotherapy. *Front Cell Dev Biol.* (2017) 5:16. doi: 10.3389/fcell.2017.00016
84. Nascimento EBM, Manneras-Holm L, Chibalin AV, Bjornholm M, Zierath JR. Diacylglycerol kinase alpha deficiency alters inflammation markers in adipose tissue in response to a high-fat diet. *J Lipid Res.* (2018) 59:273–282. doi: 10.1194/jlr.M079517
85. Abbas AK, Lichtman AH, Pillai S, Baker DL, Baker A. *Cellular and Molecular Immunology*. 9th ed. Philadelphia, PA. Elsevier (2018). p. 565.
86. Prinz PU, Mendler AN, Brech D, Masouris I, Oberneder R, Noessner E. NK-cell dysfunction in human renal carcinoma reveals diacylglycerol kinase as key regulator and target for therapeutic intervention. *Int J Cancer.* (2014) 135:1832–41. doi: 10.1002/ijc.28837
87. Riese MJ, Wang LC, Moon EK, Joshi RP, Ranganathan A, June CH, et al. Enhanced effector responses in activated CD8+ T cells deficient in diacylglycerol kinases. *Cancer Res.* (2013) 73:3566–77. doi: 10.1158/0008-5472.CAN-12-3874
88. Riese MJ, Moon EK, Johnson BD, Albelda SM. Diacylglycerol kinases (DGKs): novel targets for improving T cell activity in cancer. *Front Cell Dev Biol.* (2016) 4:108. doi: 10.3389/fcell.2016.00108
89. Riese MJ, Grewal J, Das J, Zou T, Patil V, Chakraborty AK, et al. Decreased diacylglycerol metabolism enhances ERK activation and augments CD8+ T cell functional responses. *J Biol Chem.* (2011) 286:5254–65. doi: 10.1074/jbc.M110.171884
90. Ruffo E, Malacarne V, Larsen SE, Das R, Patrussi L, Wulfing C, et al. Inhibition of diacylglycerol kinase alpha restores restimulation-induced cell death and reduces immunopathology in XLP-1. *Sci Transl Med.* (2016) 8:321ra7. doi: 10.1126/scitranslmed.aad1565
91. Colletti M, Galardi A, De Santis M, Guidelli GM, Di Giannatale A, Di Luigi L, et al. Exosomes in systemic sclerosis: messengers between immune. *Vascular and Fibrotic Components*? *Int J Mol Sci.* (2019) 20:4337. doi: 10.3390/ijms20184337
92. Hu L, Wang J, Zhou X, Xiong Z, Zhao J, Yu R, et al. Exosomes derived from human adipose mensenchymal stem cells accelerates cutaneous wound healing via optimizing the characteristics of fibroblasts. *Sci Rep.* (2016) 6:32993. doi: 10.1038/srep32993
93. Zhang J, Guan J, Niu X, Hu G, Guo S, Li Q, et al. Exosomes released from human induced pluripotent stem cells-derived MSCs facilitate cutaneous wound healing by promoting collagen synthesis and angiogenesis. *J Transl Med.* (2015) 13:49. doi: 10.1186/s12967-015-0417-0
94. Alonso R, Mazzeo C, Rodriguez MC, Marsh M, Fraile-Ramos A, Calvo V, et al. Diacylglycerol kinase alpha regulates the formation and polarisation of mature multivesicular bodies involved in the secretion of Fas ligand-containing exosomes in T lymphocytes. *Cell Death Differ.* (2011) 18:1161–73. doi: 10.1038/cdd.2010.184
95. Mazzeo C, Calvo V, Alonso R, Merida I, Izquierdo M. Protein kinase D1/2 is involved in the maturation of multivesicular bodies and secretion of exosomes in T and B lymphocytes. *Cell Death Differ.* (2016) 23:99–109. doi: 10.1038/cdd.2015.72
96. Alonso R, Rodriguez MC, Pindado J, Merino E, Merida I, Izquierdo M. Diacylglycerol kinase alpha regulates the secretion of lethal exosomes bearing Fas ligand during activation-induced cell death of T lymphocytes. *J Biol Chem.* (2005) 280:28439–50. doi: 10.1074/jbc.M501112200
97. Novo D, Heath N, Mitchell L, Caligiuri G, MacFarlane A, Reijmer D, et al. Mutant p53s generate pro-invasive niches by influencing exosome podocalyxin levels. *Nat Commun.* (2018) 9:5069. doi: 10.1038/s41467-018-07339-y
98. Abramovici H, Mojtabaie P, Parks RJ, Zhong XP, Koretzky GA, Topham MK, et al. Diacylglycerol kinase zeta regulates actin cytoskeleton reorganization through dissociation of Rac1 from RhoGDI. *Mol Biol Cell.* (2009) 20:2049–59. doi: 10.1091/mbc.E07-12-1248
99. Tsushima S, Kai M, Yamada K, Imai S, Houkin K, Kanoh H, et al. Diacylglycerol kinase gamma serves as an upstream suppressor of Rac1 and lamellipodium formation. *J Biol Chem.* (2004) 279:28603–13. doi: 10.1074/jbc.M314031200
100. Stephens DJ. Cell biology: collagen secretion explained. *Nature.* (2012) 482:474–5. doi: 10.1038/482474a
101. Poli A, Fiume R, Baldanzi G, Capello D, Ratti S, Gesi M, et al. Nuclear localization of diacylglycerol kinase alpha in K562 cells is involved in cell cycle progression. *J Cell Physiol.* (2017) 232:2550–7. doi: 10.1002/jcp.25642
102. Flores I, Casaseca T, Martinez AC, Kanoh H, Merida I. Phosphatidic acid generation through interleukin 2 (IL-2)-induced alpha-diacylglycerol kinase activation is an essential step in IL-2-mediated lymphocyte proliferation. *J Biol Chem.* (1996) 271:10334–40. doi: 10.1074/jbc.271.17.10334
103. Wada I, Kai M, Imai S, Sakane F, Kanoh H. Translocation of diacylglycerol kinase alpha to the nuclear matrix of rat thymocytes and peripheral T-lymphocytes. *FEBS Lett.* (1996) 393:48–52. doi: 10.1016/0014-5793(96)00857-5
104. Baldanzi G, Pighini A, Bettio V, Rainero E, Traini S, Chianale F, et al. SAP-mediated inhibition of diacylglycerol kinase alpha regulates TCR-induced diacylglycerol signaling. *J Immunol.* (2011) 187:5941–51. doi: 10.4049/jimmunol.1002476
105. Matsubara T, Ikeda M, Kiso Y, Sakuma M, Yoshino K, Sakane F, et al. c-Abl tyrosine kinase regulates serum-induced nuclear export of diacylglycerol kinase alpha by phosphorylation at Tyr-218. *J Biol Chem.* (2012) 287:5507–17. doi: 10.1074/jbc.M111.296897
106. Sanjuan MA, Jones DR, Izquierdo M, Merida I. Role of diacylglycerol kinase alpha in the attenuation of receptor signaling. *J Cell Biol.* (2001) 153:207–20. doi: 10.1083/jcb.153.1.207
107. Sanjuan MA, Pradet-Balade B, Jones DR, Martinez AC, Stone JC, Garcia-Sanz JA, et al. T cell activation *in vivo* targets diacylglycerol kinase alpha to the membrane: a novel mechanism for Ras attenuation. *J Immunol.* (2003) 170:2877–83. doi: 10.4049/jimmunol.170.6.2877
108. Arranz-Nicolas J, Ogando J, Soutar D, Arcos-Perez R, Meraviglia-Crivelli D, Manes S, et al. Diacylglycerol kinase alpha inactivation is an integral component of the costimulatory pathway that amplifies TCR signals. *Cancer Immunol Immunother.* (2018) 67:965–80. doi: 10.1007/s00262-018-2154-8
109. Merino E, Sanjuan MA, Moraga I, Cipres A, Merida I. Role of the diacylglycerol kinase alpha-conserved domains in

membrane targeting in intact T cells. *J Biol Chem.* (2007) 282:35396–404. doi: 10.1074/jbc.M702085200
110. Merino E, Avila-Flores A, Shirai Y, Moraga I, Saito N, Merida I. Lck-dependent tyrosine phosphorylation of diacylglycerol kinase alpha regulates its membrane association in T cells. *J Immunol.* (2008) 180:5805–15. doi: 10.4049/jimmunol.180.9.5805
111. Chauveau A, Le Floc'h A, Bantilan NS, Koretzky GA, Huse M. Diacylglycerol kinase alpha establishes T cell polarity by shaping diacylglycerol accumulation at the immunological synapse. *Sci Signal.* (2014) 7:ra82. doi: 10.1126/scisignal.2005287
112. Raben DM, Tu-Sekine B. Nuclear diacylglycerol kinases: regulation and roles. *Front Biosci.* (2008) 13:590–7. doi: 10.2741/2704
113. Ratti S, Ramazzotti G, Faenza I, Fiume R, Mongiorgi S, Billi AM, et al. Nuclear inositide signaling and cell cycle. *Adv Biol Regul.* (2018) 67:1–6. doi: 10.1016/j.jbior.2017.10.008
114. Liu K, Kunii N, Sakuma M, Yamaki A, Mizuno S, Sato M, et al. A novel diacylglycerol kinase alpha-selective inhibitor, CU-3, induces cancer cell apoptosis and enhances immune response. *J Lipid Res.* (2016) 57:368–79. doi: 10.1194/jlr.M062794
115. Jiang Y, Sakane F, Kanoh H, Walsh JP. Selectivity of the diacylglycerol kinase inhibitor 3-[2-(4-[bis-(4-fluorophenyl)methylene]-1-piperidinyl)ethyl]-2, 3-dihydro-2-thioxo-4(1H)quinazolinone (R59949) among diacylglycerol kinase subtypes. *Biochem Pharmacol.* (2000) 59:763–72. doi: 10.1016/s0006-2952(99)00395-0
116. Boroda S, Niccum M, Raje V, Purow BW, Harris TE. Dual activities of ritanserin and R59022 as DGα inhibitors and serotonin receptor antagonists. *Biochem Pharmacol.* (2017) 123:29–39. doi: 10.1016/j.bcp.2016.10.011
117. Franks CE, Campbell ST, Purow BW, Harris TE, Hsu KL. The ligand binding landscape of diacylglycerol kinases. *Cell Chem Biol.* (2017) 24:870–80.e5. doi: 10.1016/j.chembiol.2017.06.007
118. Velnati S, Ruffo E, Massarotti A, Talmon M, Varma KSS, Gesu A, et al. Identification of a novel DGKalpha inhibitor for XLP-1 therapy by virtual screening. *Eur J Med Chem.* (2019) 164:378–90. doi: 10.1016/j.ejmech.2018.12.061
119. Hayashi D, Tsumagari R, Liu K, Ueda S, Yamanoue M, Sakane F, et al. Screening of subtype-specific activators and inhibitors for diacylglycerol kinase. *J Biochem.* (2019) 165:517–22. doi: 10.1093/jb/mvz008
120. Olmez I, Love S, Xiao A, Manigat L, Randolph P, McKenna BD, et al. Targeting the mesenchymal subtype in glioblastoma and other cancers via inhibition of diacylglycerol kinase alpha. *Neuro Oncol.* (2018) 20:192–202. doi: 10.1093/neuonc/nox119
121. Velnati S, Massarotti A, Antona A, Talmon M, Fresu LG, Galetto AS, et al. Structure activity relationship studies on Amb639752: toward the identification of a common pharmacophoric structure for DGα inhibitors. *J Enzyme Inhib Med Chem.* (2020) 35:96–108. doi: 10.1080/14756366.2019.1684911
122. Ostuni R, Piccolo V, Barozzi I, Polletti S, Termanini A, Bonifacio S, et al. Latent enhancers activated by stimulation in differentiated cells. *Cell.* (2013) 152:157–71. doi: 10.1016/j.cell.2012.12.018
123. Zeybel M, Hardy T, Wong YK, Mathers JC, Fox CR, Gackowska A, et al. Multigenerational epigenetic adaptation of the hepatic wound-healing response. *Nat Med.* (2012) 18:1369–77. doi: 10.1038/nm.2893
124. Zeybel M, Luli S, Sabater L, Hardy T, Oakley F, Leslie J, et al. A proof-of-concept for epigenetic therapy of tissue fibrosis: inhibition of liver fibrosis progression by 3-deazaneplanocin A. *Mol Ther.* (2017) 25:218–31. doi: 10.1016/j.ymthe.2016.10.004
125. Valinciute G, Weigel C, Veldwijk MR, Oakes CC, Herskind C, Wenz F, et al. BET-bromodomain inhibitors modulate epigenetic patterns at the diacylglycerol kinase alpha enhancer associated with radiation-induced fibrosis. *Radiother Oncol.* (2017) 125:168–74. doi: 10.1016/j.radonc.2017.08.028
126. Duong TE, Hagood JS. Epigenetic regulation of myofibroblast phenotypes in fibrosis. *Curr Pathobiol Rep.* (2018) 6:79–96. doi: 10.1007/s40139-018-0155-0

Conflict of Interest: The authors declare that the research was conducted in the absence of any commercial or financial relationships that could be construed as a potential conflict of interest.

frontiers in Oncology

ORIGINAL RESEARCH
published: 27 May 2020
doi: 10.3389/fonc.2020.00821

PD-L1 Inhibitor Regulates the miR-33a-5p/PTEN Signaling Pathway and Can Be Targeted to Sensitize Glioblastomas to Radiation

Wenzheng Xia[1†], *Jin Zhu*[1†], *Yinda Tang*[1†], *Xueyi Wang*[1], *Xiangyu Wei*[1], *Xuan Zheng*[1], *Meng Hou*[2*] and *Shiting Li*[1*]

[1] Department of Neurosurgery, Xinhua Hospital Affiliated to Shanghai Jiaotong University School of Medicine, Shanghai, China, [2] Department of Radiation Oncology, First Affiliated Hospital, Wenzhou Medical University, Wenzhou, China

OPEN ACCESS

Edited by:
Mary Helen Barcellos-Hoff, University of California, San Francisco, United States

Reviewed by:
Alessandra Cataldo, Istituto Nazionale dei Tumori (IRCCS), Italy
Priyanka Gupta, University of Alabama at Birmingham, United States

***Correspondence:**
Meng Hou
244517813@qq.com
Shiting Li
lishiting@xinhuamed.com.cn

[†]These authors have contributed equally to this work

Specialty section:
This article was submitted to Molecular and Cellular Oncology, a section of the journal Frontiers in Oncology

Received: 27 November 2019
Accepted: 27 April 2020
Published: 27 May 2020

Citation:
Xia W, Zhu J, Tang Y, Wang X, Wei X, Zheng X, Hou M and Li S (2020) PD-L1 Inhibitor Regulates the miR-33a-5p/PTEN Signaling Pathway and Can Be Targeted to Sensitize Glioblastomas to Radiation. Front. Oncol. 10:821. doi: 10.3389/fonc.2020.00821

Glioblastoma (GBM) is the most common and lethal brain tumor in adults. Ionizing radiation (IR) is a standard treatment for GBM patients and results in DNA damage. However, the clinical efficacy of IR is limited due to therapeutic resistance. The programmed death ligand 1 (PD-L1) blockade has a shown the potential to increase the efficacy of radiotherapy by inhibiting DNA damage and repair responses. The miR-33a-5p is an essential microRNA that promotes GBM growth and self-renewal. In this study, we investigated whether a PD-L1 inhibitor (a small molecule inhibitor) exerted radio-sensitive effects to impart an anti-tumor function in GBM cells by modulating miR-33a-5p. U87 MG cells and U251 cells were pretreated with PD-L1 inhibitor. The PD-L1 inhibitor-induced radio-sensitivity in these cells was assessed by assaying cellular apoptosis, clonogenic survival assays, and migration. TargetScan and luciferase assay showed that miR-33a-5p targeted the phosphatase and tensin homolog (PTEN) 3′ untranslated region. The expression level of PTEN was measured by western blotting, and was also silenced using small interfering RNAs. The levels of DNA damage following radiation was measured by the presence of γ-H_2AX foci, cell cycle, and the mRNA of the DNA damage-related genes, BRCA1, NBS1, RAD50, and MRE11. Our results demonstrated that the PD-L1 inhibitor significantly decreased the expression of the target gene, miR-33a-5p. In addition, pretreatment of U87 MG and U251 cells with the PD-L1 inhibitor increased radio-sensitivity, as indicated by increased apoptosis, while decreased survival and migration of GBM cells. Mir-33a-5p overexpression or silencing PTEN in U87 MG and U251 cells significantly attenuated PD-L1 radiosensitive effect. Additionally, PD-L1 inhibitor treatment suppressed the expression of the DNA damage response-related genes, BRCA1, NBS1, RAD50, and MRE11. Our results demonstrated a novel role for the PD-L1 inhibitor in inducing radio- sensitivity in GBM cells, where inhibiting miR-33a-5p, leading to PTEN activated, and inducing DNA damage was crucial for antitumor immunotherapies to treat GBM.

Keywords: glioblastoma, programmed death ligand 1 (PD-L1) blockade, radio-sensitization, miR-33a-5p/PTEN signaling pathway, DNA damage response

INTRODUCTION

Glioblastomas (GBM) are one of the most treatment-resistant tumors, often recurring after chemotherapy and radiation treatment (1). Amount of effort has been taken to identify therapeutics that radio-sensitize GBMs because most patients will receive radiation treatment (2). However, it's difficult to identify such radiosensitive chemotherapeutic agents because GBMs exhibit redundant pro-growth and pro-survival pathways, leading to chemotherapy resistance (3). To overcome such resistance, it's needed to devise therapeutic strategies targeting such redundant treatment-resistant pathways to increase the radiosensitivity of GBMs.

Programmed death ligand 1 (PD-L1)regulates the immune system by binding the programmed cell death protein 1 (PD-1) receptor as an immune checkpoint protein (4, 5). By combining with PD-1 on immune cells, PD-L1 helps tumor cells escape from the immune system and survive (6). Therefore, abrogation of the PD-1 and PD-L1 interaction has acted as an effective therapeutic strategy to enhance antitumor immunity across multiple malignancies. The immune checkpoint blockade has shown a therapeutic effect in immunosuppressive GBMs (7). With respect to radiosensitization in colorectal carcinoma and breast cancer cell lines, knockdown of PD-L1 sensitizes cells to radiotherapy (8). Although the impact of the PD-L1 blockade on radiosensitization has been suggested in GBM, its role has yet to be fully elucidated.

MicroRNAs (miRNAs) are a series of small, noncoding RNA molecules, typically about 18–22 nucleotides in length in the mature form (9). miRNAs negatively regulate gene expression at the post-transcriptional level by inhibiting mRNA translation and/or promoting mRNA degradation (10). In recent years, abundant miRNAs have been found to be deregulated in many types of cancer: some function as tumor suppressors and others as tumor promoters (11). The miR-33a-5p is located on chromosome 22, and its high expression is related with the poor prognosis of GBM patients (12). miR-33a-5p influences the radiation resistance-associated pathway protein, STAT3, leading to radiation resistance in GBM cells. Importantly, miR-33a-5p is also an essential component of the PTEN regulatory network (13).

PTEN is a critical inhibitor of cell proliferation, viability, and migration in GBMs (14, 15). Following the treatment of cells with PD-1 inhibitors (e.g., pembrolizumab), genomic and transcriptomic analyses revealed a significant accumulation of PTEN mutations, leading to an immunotherapeutic response in GBMs (16). Thus, in the present study, we sought to reveal whether the PD-L1 inhibitor could influence the radiosensitivity of GBM cells by modulating the miR-33a-5p/PTEN pathway.

Genetic alterations involved in GBM progression or recurrence have close relationships with DNA damage response (DDR) (17). DDR contributes to malignancy by regulating diverse cellular functions, including cell metabolism, proliferation and programmed cell death (18). Importantly, the DDR induces chemo- or radio-resistance in GBM (19). Thus, targeting the DDR could promote the growth-suppressive effects of radiation (20). Immune checkpoint blockade using a PD-L1 antagonist targeted the DDR and induced radiosensitization in tumor cells (8). Thus, direct pharmacological targeting of PD-L1 is an attractive approach for sensitizing GBMs to radiation.

Here, we suggested that immune checkpoint blockade using the PD-L1 inhibitor was a potent therapy for GBM radio-sensitization. Furthermore, we showed that the PD-L1 inhibitor induced radiosensitization by modulating the miR-33a-5p/PTEN pathway. Thus, we propose that the immune checkpoint blockade is a promising treatment strategy for GBM radiosensitization.

MATERIALS AND METHODS

Cell Culture and Treatment

The U87 MG human glioblastoma cell line and U251 cells were obtained from the American Type Culture Collection (ATCC). They were cultured in Dulbecco's modified Eagle's medium (DMEM) supplemented with 10% fetal bovine serum and 1% antibiotic-antimycotic solution at 37°C with 5% CO_2. Experiments were performed with cells grown to 70% confluency.

For the PD-L1 blockade, cells were fed media containing 4 mg/mL PD-L1 inhibitor (Abcam, ab230369) and incubated at 37°C, as previously described (21).

Ionizing Radiation

Cells were placed in a cesium-137 source irradiator. Cells were irradiated using a single dose of 10 Gy, as previously reported (22).

TABLE 1 | Primer sequences.

Genes	Sequences
miR-33a-5p	F: 5′ - GATCCTCAGTGCATTGTAGTTGC–3′
	R: 5′ - CTCTGTCTCTCGTCTTGTTGGTAT-3′
U6	F: 5′- GCTTCGGCAGCACATATACTAAAAT–3′
	R: 5′- CGCTTCACGAATTTGCGTGTCA-3′
PTEN	F: 5′ - GCAGAAAGACTTGAAGGCGTA–3′
	R: 5′ - AGCTGTGGTGGGTTATGGTC–3′
BRCA1	F: 5′ - GGCTATCCTCTCAGAGTGACATTT–3′
	R: 5′ - GCTTTATCAGGTTATGTTGCATGGT–3′
NBS1	F: 5′ - TTGGTTGCATGCTCTTCTTG–3′
	R: 5′ - GGCTGCTTCTTGGACTCAAC–3′
RAD50	F: 5 ′-CTTGGATATGCGAGGACGA–3′
	R: 5′ - CCAGAAGCTGGAAGTTACGC–3′
MRE11	F: 5 ′- GCCTTCCCGAAATGTCACTA–3′
	R: 5′ - TTCAAAATCAACCCCTTTCG–3′
GAPDH	F: 5′- AGGAGCGAGACCCCACTAAC–3′
	R: 5′- GATGACCCTTTTGGCTCCA-3′
siRNA-PTEN	5′-AAAGAGATCGTTAGCAGAA–3′
siRNA-NT	5′-ACACGTCCGAACATACTAC–3′
miR-33a-5p mimic	GUGCAUUGUAGUUGCAUUGCA
miR-NC mimic	TTCTCCGAACGTGTCACGT

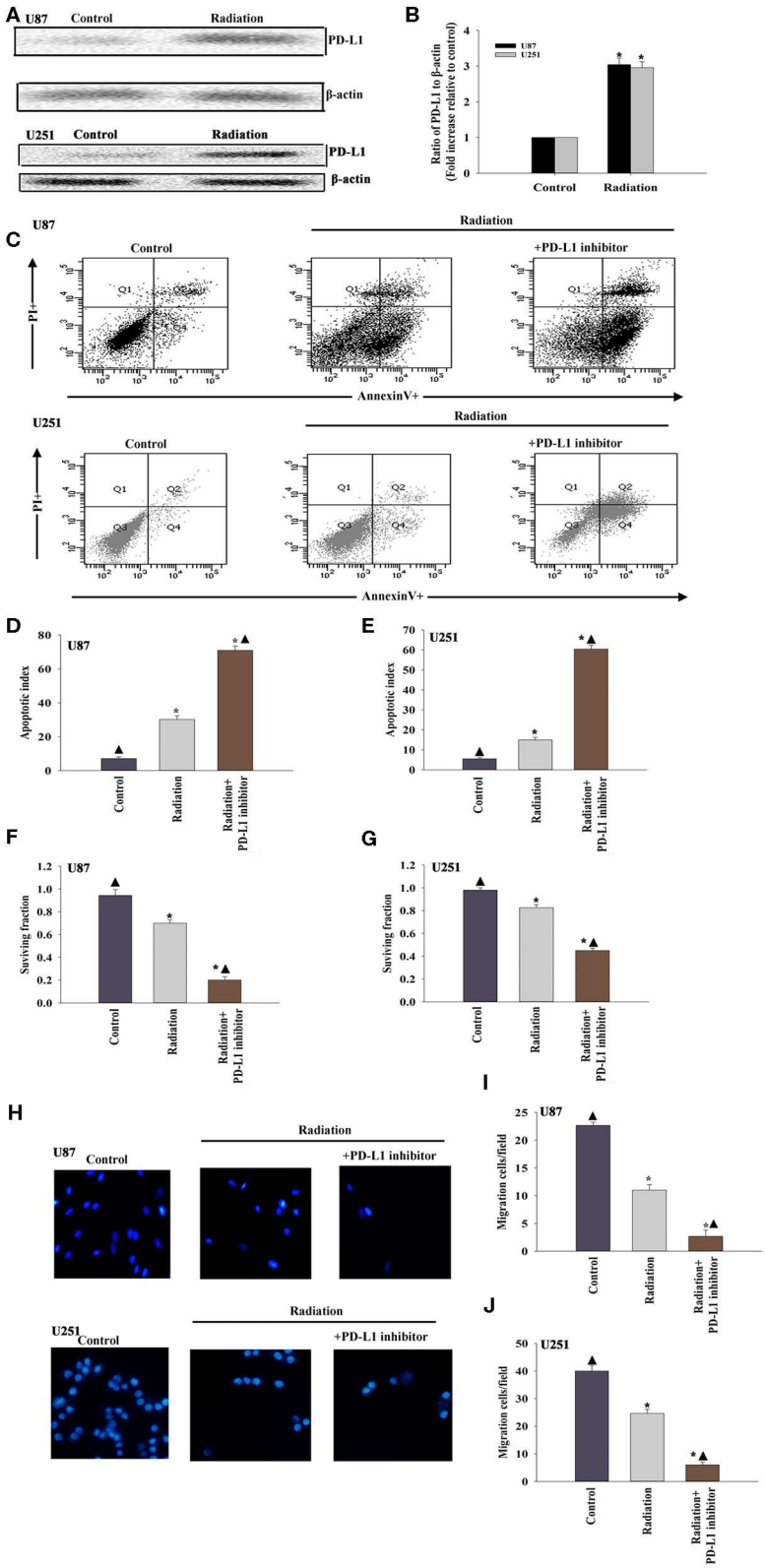

FIGURE 1 | The immune checkpoint inhibitor sensitizes GBM to radiotherapy. **(A,B)** Representative images of western blots of PD-L1 and β-actin in radiated or untreated U87 MG cells and U251 cells. Fold changes were normalized to β-actin. Each column represents the mean ± SD from three independent experiments;

(Continued)

FIGURE 1 | *$P < 0.05$, vs. Control. U87 MG cells and U251 cells were subjected to radiation, with or without PD-L1-inhibitor treatment. Untreated U87 MG cells and U251 cells were used as the control separately. **(C)** Representative distributions of PI and Annexin V staining from FACScan flow cytometric analyses of apoptotic cells. **(D,E)** Percentage of apoptotic cells in above conditions. **(F,G)** Colony formation was presented as a bar graph in the U87 MG cells and U251 cells. **(H)** Fluorescence microscope images of the migrated U87 MG cells and U251 cells. **(I,J)** Data are presented as the number of migrated cells. Each column represents the mean ± SD from three independent experiments; *$P < 0.05$, vs. Control; ▲$P < 0.05$, vs. Radiation.

Western Blot Analysis

Cells were harvested using RIPA buffer (Sigma-Aldrich). Proteins were separated on 10% SDS-PAGE gels and transferred to polyvinylidene difluoride membranes. The membranes were incubated overnight with the following primary antibodies: anti-PD-L1 (ab205921,1:500), anti-PTEN (ab32199, 1:750), anti-gamma H_2AX (ab2893, 1:500), and anti-β-actin (ab8227, 1:1000). Following incubation, membranes were washed, incubated for 1 h with appropriate secondary antibodies conjugated to horseradish peroxidase, and developed using chemiluminescent substrates. The stained protein bands were visualized using a Bio-Rad ChemiDoc XRS instrument, and quantified and analyzed using the Quantity One software.

Flow Cytometric Analysis of Apoptosis

The extent of apoptotic cell death was assayed using the Annexin V-FITC Apoptosis Detection Kit, according to the manufacturer's instructions. Briefly, cells were harvested and washed in ice-cold phosphate-buffered saline (PBS), resuspended in 300 μL of binding buffer and incubated with 5 μL of Annexin V-FITC solution for 30 min at 4°C in the dark. This was followed by incubation with 5 μL of propidium iodide (PI) for 5 min. The samples were immediately analyzed by bivariate flow cytometry on the BD FACSCanto II instrument, equipped with Cell Quest software (BD). Approximately 1-5 × 10^5 cells were analyzed in each sample (23).

Colony Formation Assay

A colony formation (clonogenic) assay was used in order to determine cell survival. Briefly, remaining U87 MG cells and U251 cells after indicated treatments were trypsinized and plated into 6-well plates. The density of per well is 1,500 cells. Colonies were allowed to grow (∼9–10 days). Fixed cells were then stained with a 0.5% (v/v) crystal violet (Sigma-Aldrich) solution. Only colonies consisting of ≥50 cells were counted as previously described (24).

Transwell Migration Assay

DAPI labeled U87 MG cells and U251 cells were plated in the upper compartment of 0.8 μm Transwell chambers. After 6–8 h migration to the underside of the top chamber, a fluorescence microscope was applied to evaluate the migration of the fluorescently-labeled U87 MG cells and U251 cells. Each experiment was performed in triplicate.

Microarray

Cells were immediately lysed in 500 μl TRIzol reagent (ThermoFisher Scientific) and stored at −80°C before purification using a standard phenol-chloroform extraction protocol with the RNAqueous Micro Kit (ThermoFisher Scientific). The transcriptome was analyzed using an Affymetrix human microarray (ThermoFisher Scientific) and normalized based on quantiles.

Quantitative Reverse-Transcription Polymerase Chain Reaction (qRT-PCR)

Total RNA from clonal cells was isolated using RNeasy spin columns (Qiagen), per the manufacturer's protocol. For reverse-transcription reactions, first-strand cDNA was synthesized using Superscript reverse transcriptase (Invitrogen), per the manufacturer's protocol. TaqMan probes (Applied Biosystems) were used to estimate the level of gene expression of miR-33a-5p, PTEN, BRCA1, NBS1, RAD50, and MRE11. *GAPDH* and *U6* were used as housekeeping genes (25). The primer sets (Invitrogen) used are listed in **Table 1**.

Luciferase Reporter Assay

The 3′-UTR of PTEN was synthesized, annealed, and inserted into the SacI and HindIII sites of the pMIR-reporter luciferase vector (Ambion), downstream of the luciferase stop codon. To induce mutagenesis, the sequences complementary to the binding sites of miR-33a-5p in the 3′-UTR of PTEN (gguuuUGCUACUCUAAUGCAu) were replaced by gguuuUGCUACUCUUUACGUu. The constructs were validated by sequencing. U87 MG cells and U251 cells were seeded into a 24-well plate to perform the luciferase assay. After overnight culture, cells were co-transfected with the wild-type or mutated plasmid, and equal amounts of the miR-33a-5p mimic or the miR- negative control mimic (miR-NC mimic). Luciferase assays were performed using the Dual Luciferase Reporter Assay System (Promega) 24 h after transfection.

The miR-33a-5p Overexpression

Before transfection with the miR-33a-5p mimic and negative control (NC) mimic, U87 MG cells and U251 cells were seeded into 6-well plates at a density of 1 × 10^5 cells per well, and incubated for 12 h. For the overexpression of miR-33a-5p, cells were transfected with the miR-33a-5p mimic or the NC mimic (Invitrogen, Carlsbad, CA, USA) using the X-treme transfection reagent (Roche Applied Science, Penzberg, Germany), according to the manufacturer's protocol. Forty-eight hours after transfection, cells were harvested for further analysis. The transfection efficiency was analyzed by qRT-PCR.

Small Interfering (si) RNA Transfection

The siRNAs were applied to knock down PTEN expression in U87 MG cells and U251 cells. A non-targeting siRNA was used as a negative control (Invitrogen). The target sequences were as follows: PTEN: 5′-AAAGAGATCGTTAGCAGAA-3′;

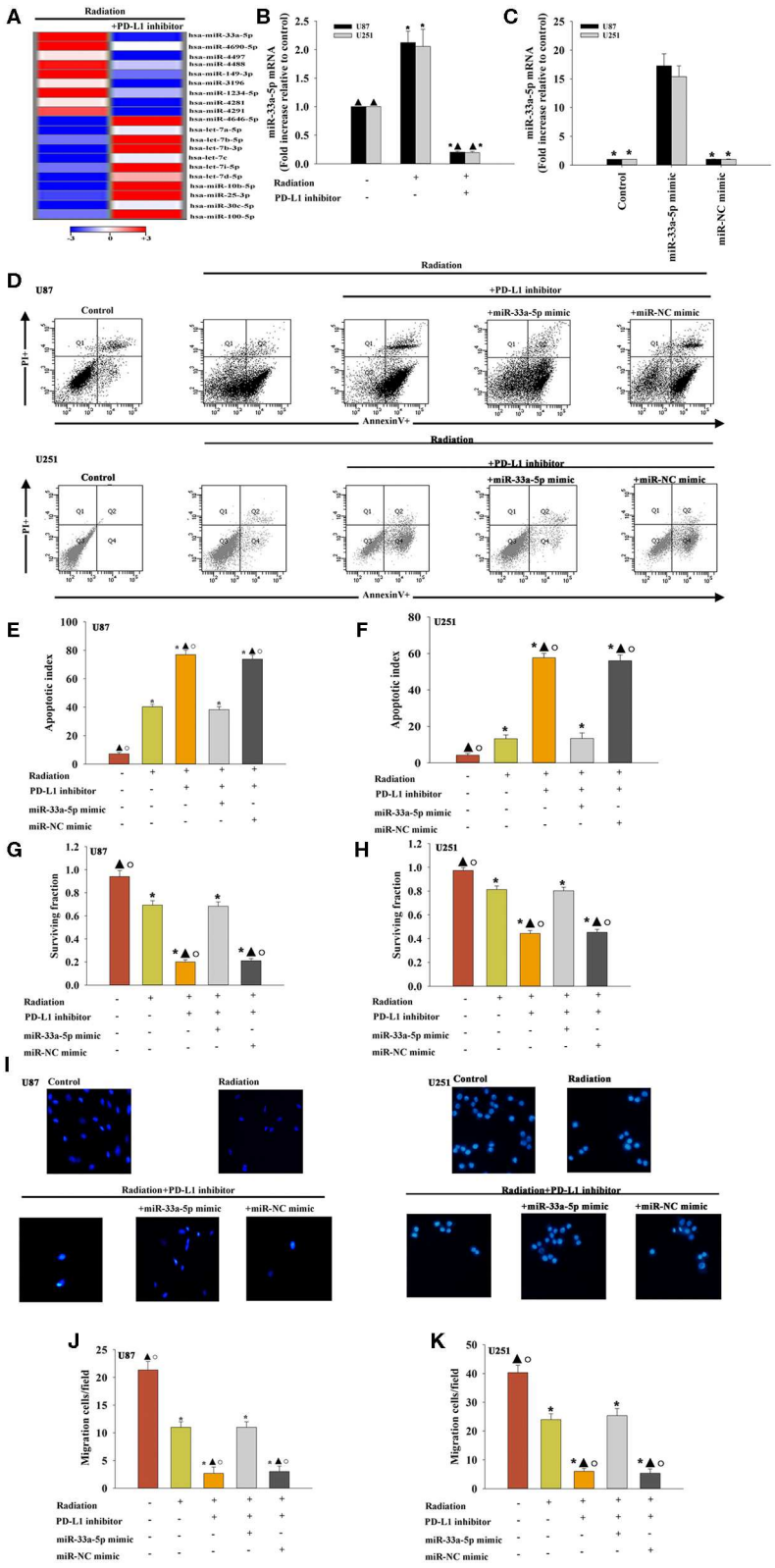

FIGURE 2 | Effect of the PD-L1 inhibitor on miRNA expression in glioma cells. **(A)** Heat map of miRNAs differentially regulated by the PD-L1 inhibitor in radiated U87 MG cells. "Red" indicates up-regulation, and "blue" indicates down-regulation. **(B)** RT-qPCR validation of the differentially regulated miRNAs in U87 MG cells and

(Continued)

FIGURE 2 | U251 cells treated with radiation, with or without PD-L1 inhibitor pre-treatment. Untreated U87 MG cells and U251 cells were used as the control separately. *$P < 0.05$, vs. Control; ▲$P < 0.05$, vs. Radiation. U87 MG cells and U251 cells were transfected with a mimic control or the miR-33a-5p mimic, treated with the PD-L1 inhibitor, and subjected to radiation. In parallel, U87 MG cells and U251 cells, treated or untreated with the PD-L1 inhibitor were radiated. Un-treated U87 MG cells and U251 cells were used as the control separately. **(C)** The transfection efficiency was analyzed by qRT-PCR; *$P < 0.05$, vs. the miR-33a-5p mimic. **(D)** Representative distributions of PI and Annexin V staining from FACScan flow cytometric analyses of apoptotic cells. **(E,F)** Apoptotic cells in the above conditions. **(G,H)** Colony formation was presented as a bar graph in the U87 MG cells and U251 cells. **(I)** Fluorescence microscope images of the migrated U87 MG cells and U251 cells. **(J,K)** Data are presented as the number of migrated cells. Each column represents the mean ± SD from three independent experiments; *$P < 0.05$, vs. Control; ▲$P < 0.05$, vs. Radiation; ◦$P < 0.05$, vs. Radiation + PD-L1 inhibitor + miR-33a-5p mimic.

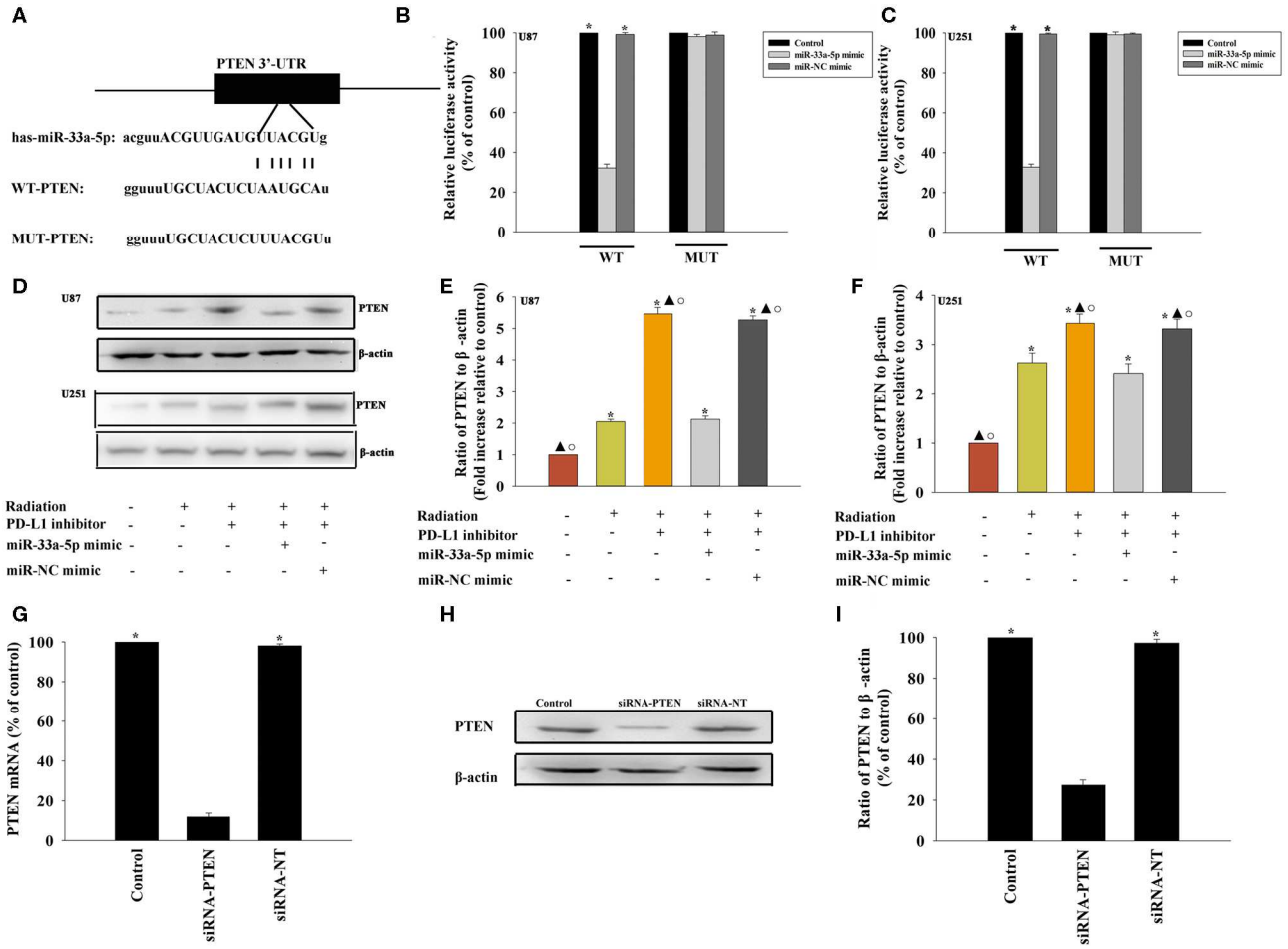

FIGURE 3 | PTEN is a direct target of miR-33a-5p. **(A)** The predicted binding sites between miR-33a-5p and the PTEN 3′-UTR. **(B,C)** A dual luciferase assay was performed in U87 MG cells and U251 cells after co-transfection with PTEN 3′-UTR wild type (WT) or mutant (MUT) plasmids, miR-33a-5p mimics, and miR-NC mimic. *$P < 0.05$, vs. the miR-33a-5p mimic in the WT group; **(D–F)** western blot analysis of PTEN and β-actin protein levels in follow cells; U87 MG cells and U251 cells were transfected with a mimic control or the miR-33a-5p mimic, treated with the PD-L1 inhibitor, and subjected to radiation. In parallel, U87 MG cells and U251 cells, treated or untreated with the PD-L1 inhibitor were radiated. Untreated U87 MG cells and U251 cells were used as the control separately. *$P < 0.05$, vs. Control; ▲$P < 0.05$, vs. Radiation; ◦$P < 0.05$, vs. Radiation + PD-L1 inhibitor + miR-33a-5p mimic. **(G–I)** U87 MG cells were transfected with siRNA-PTEN, or with siRNA-NT as a control. siRNA-mediated transfection efficiency was determined by qRT-PCR **(G)** and western blotting **(H,I)**. Each column represents the mean ± SD from three independent experiments; *$P < 0.05$, vs. siRNA-PTEN.

and Control: 5′-ACACGTCCGAACATACTAC-3′. Transfection efficiency was detected by qRT-PCR and western blotting.

Immunofluorescence

Briefly, cells were fixed by 3% paraformaldehyde and then permeabilized with 0.5% Triton X-100. Cells were then blocked by 5% goat serum, followed by incubation with primary antibodies. Cells were then incubated with fluorescent secondary antibodies and DAPI to stain the targeted proteins and the nucleus, respectively (8). The cells were then analyzed by fluorescence microscopy.

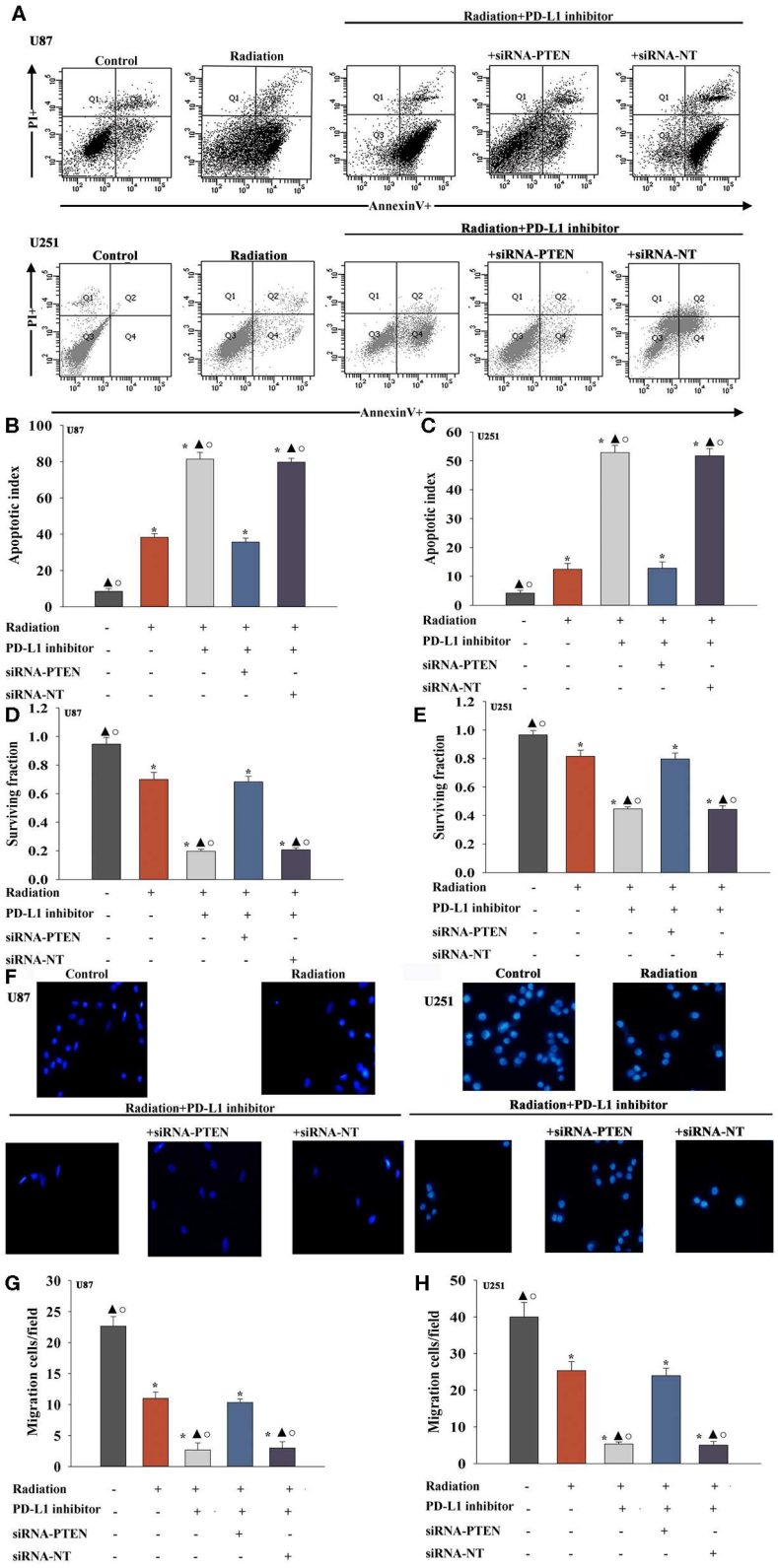

FIGURE 4 | PD-L1 inhibitor confers radio-sensitization by targeting PTEN. U87 MG cells and U251 cells were transfected with siRNA against PTEN, or with siRNA-NT as a control, followed by treatment with the PD-L1 inhibitor and radiation. In parallel experiments, U87 MG and U251 cells were treated with radiation alone, or treated

(Continued)

FIGURE 4 | with the PD-L1 inhibitor in the presence of radiation. U87 MG and U251 cells under normal culture conditions were used as the control separately. **(A)** Representative distributions of PI and Annexin V staining from FACScan flow cytometric analyses of apoptotic cells. **(B,C)** Apoptotic cells in the above conditions. **(D,E)** Colony formation was presented as a bar graph in the U87 MG cells and U251 cells. **(F)** Fluorescence microscope images of the migrated U87 MG cells and U251 cells. **(G,H)** Data are presented as the number of migrated cells. Each column represents the mean ± SD from three independent experiments; $^{*}P < 0.05$, vs. Control; $^{\blacktriangle}P < 0.05$, vs. Radiation; $^{\circ}P < 0.05$, vs. Radiation + PD-L1 inhibitor + siRNA-PTEN.

Cell Cycle Assay

Further, 70% cold anhydrous ethanol was applied to fix the cells. Then, the cells were treated with propidium iodide (PI) (Sigma, St. Louise, MO, USA) and RNase A. A flow cytometer equipped with Cell Quest software was used to detect the cell cycle distribution.

Statistical Analysis

Data were expressed as the mean ± standard deviation (SD). Differences among groups were tested by one-way analysis of variance, and comparisons between two groups were evaluated by the Student's *t*-test, using the SPSS package v19.0 (SPSS Inc., Chicago, IL, USA). A *P*-value of <0.05 was considered statistically significant.

RESULTS

The Immune Checkpoint Inhibitor Sensitizes Gliomas to Radiotherapy

To determine whether the PD-L1 inhibitor would radiosensitize U87 MG cells and U251 cells, we first examined the expression of PD-L1 in the U87 MG cells and U251 cells under radiotherapy conditions. The results suggested that radiation induced PD-L1 expression (**Figures 1A,B**). We then administered the PD-L1 inhibitor two hours before radiation treatment and found that U87 MG cells and U251 cells were sensitized, as indicated by increased apoptosis (**Figures 1C–E**) and decreased cellular survival (**Figures 1F,G**). Cellular migration of the U87 MG cells and U251 cells was also inhibited by PD-L1 inhibitor (**Figures 1H–J**).

Effect of the PD-L1 Inhibitor on miRNA Expression of Glioma Cells

To examine the effect of miRNAs in the PD-L1 inhibitor-induced sensitization to radiotherapy, miRNA microarray probes were used. We found that the expression of specific miRNAs in–PD-L1 inhibitor treated before radiated U87 MG cells was significantly altered when compared with that in only radiated cells. Among them, miR-33a-5p was significantly downregulated in the PD-L1 inhibitor group, and therefore, we selected the down-regulated miR-33a-5p and verified the expression level using real-time PCR. The results showed that radiation induced increasing expression of miR-33a-5p, compared to the untreated cells. While, PD-L1 inhibitor decreased the expression of the miR-33a-5p (**Figures 2A,B**).

To determine the role of miR-33a-5p in PD-L1 inhibitor-induced radio-sensitization, U87 MG cells and U251 cells were transfected with the miR-33a-5p mimic (**Figure 2C**), and the negative control before treatment with the PD-L1 inhibitor. Compared to the radiation only group, treatment with the PD-L1 inhibitor induced more cellular apoptosis, while the overexpression of miR-33a-5p significantly inhibited apoptosis (**Figures 2D–F**). PD-L1 inhibitor treatment reduced the U87 MG cells and U251 cells surviving fraction compared to the radiation-only group; however, the overexpression of miR-33a-5p promoted the survival of U87 MG cells and U251 cells (**Figures 2G,H**). Transfection with the miR-33a-5p mimic dramatically promoted cell migration as well (**Figures 2I–K**). No apparent changes in the control miR-mimic were detected.

PTEN Is a Direct Target of miR-33a-5p

To further explore the molecular action of miR-33a-5p in GBM tissues, we searched for potential miR-33a-5p targets using TargetScan. Bioinformatics databases were used to check the potential targets. PTEN is considered to be a putative target of miR-33a-5p (**Figure 3A**). Thus, GBM cells were co-transfected with a wild-type PTEN-luciferase reporter vector, together with the miR-33a-5p mimic or the miR-NC mimic, and tested luciferase activity. miR-33a-5p-transfected cells showed a remarkable reduction of luciferase activities from the PTEN reporter in U87 MG cells and U251 cells (**Figures 3B,C**). At meanwhile, compared with the mutated 3′-UTR, the luciferase activities of the cells transfected with the wild-type 3′-UTR showed significant reductions (**Figures 3B,C**). Next, western blot analyses were performed to evaluate PTEN protein expression. We found that the expression of PTEN was downregulated in the radiation group, while it was increased following treatment with the PD-L1 inhibitor. Overexpression of miR-33a-5p reversed the inducement of PD-L1 inhibitor (**Figures 3D–F**).

The PD-L1 Inhibitor Confers Radiosensitization by Targeting PTEN

A previous study demonstrated that PTEN mediated the DNA damage response to radiosensitize high-grade gliomas (26). To assess whether the downregulation of PTEN reversed the PD-L1 inhibitor-mediated radio-sensitization, we used siRNA-PTEN to down regulate PTEN expression (**Figures 3G–I**). To test whether the PD-L1 inhibitor and PTEN have a role in cell apoptosis following radiation, we performed FACS analysis to determine the rates of cell apoptosis. The combined treatment of the PD-L1 inhibitor + radiation significantly increased cell apoptosis, compared to that observed following radiation only. As expected, the silencing of PTEN partially abolished the effect caused by PD-L1 inhibitor + radiation treatment (**Figures 4A–C**). Similarly, we also found that silencing PTEN partially reversed the inhibition of survival that was induced by the PD-L1 inhibitor + radiation treatment (**Figures 4D,E**). Our results also showed that PTEN silencing reversed the inhibition of U87 MG cells and U251 cells migration that was induced by the PD-L1 inhibitor (**Figures 4F–H**).

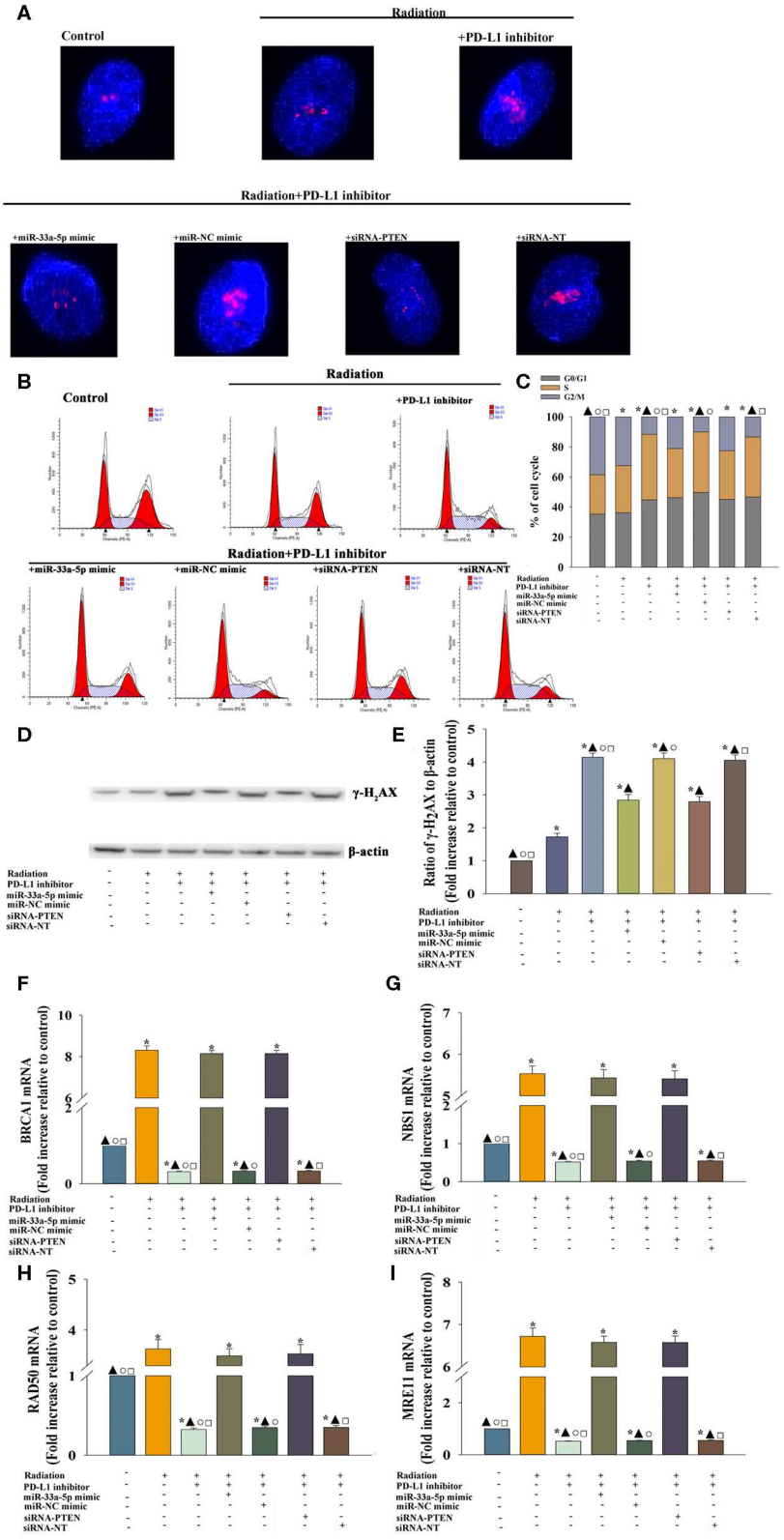

FIGURE 5 | PD-L1 inhibitor-induced DNA damage and the reduced DNA damage response to take radiosensitization effect. U87 MG cells were transfected with siRNA against PTEN, or with siRNA-NT as a control, the miR-33a-5p mimic, or the miR-mimic control. Following transfection, cells were treated with the PD-L1

(Continued)

FIGURE 5 | inhibitor in the presence of radiation. In parallel experiments, U87 MG were treated with radiation, or the PD-L1 inhibitor in the presence of radiation. U87 MG cells under normal culture conditions were used as the control. **(A)** The formation and resolution of γ-H_2AX foci were assessed using immunofluorescence. **(B,C)** Cell cycle distribution was analyzed. **(D,E)** Western blot analysis of γ-H_2AX and β-actin protein levels. **(F–I)** qRT-PCR analysis of BRCA1 **(F)**; NBS1 **(G)**; RAD50 **(H)**; and MRE11 **(I)**. $^{*}P < 0.05$, vs. Control; $^{\blacktriangle}P < 0.05$, vs. Radiation; $^{\circ}P < 0.05$, vs. Radiation + PD-L1 inhibitor + miR-33a-5p mimic. $^{\square}P < 0.05$, vs. Radiation + PD-L1 inhibitor + siRNA-PTEN.

The PD-L1 Inhibitor Induced DNA Damage and Reduced the DNA Damage Response to Take Radio-Sensitization Effect

We evaluated whether DNA repair could be impaired in cells treated with the PD-L1 inhibitor. Immunofluorescence was used to examine the kinetics of radiation-induced γ-H_2AX foci following PD-L1 inhibitor treatment, which are indication of DNA double-strand breaks (**Figure 5A**). After PD-L1 inhibitor treatment, cells had higher basal levels of γ-H_2AX, trapping in S-phase (**Figures 5B,C**), which was likely the result of the decreased repair of spontaneous DNA damage. PD-L1 inhibitor +radiation also increased the expression of γ-H_2AX, compared with radiation alone (**Figures 5D,E**). However, either miR-33a-5p overexpression or silencing PTEN, could abolished the inducement of DNA damage by PD-L1 inhibitor (**Figures 5A–E**).

Then we searched to explore mechanistic insight into how the PD-L1 inhibitor affected the DDR. Thus, we assessed whether the important DDR pathway genes was affected by the PD-L1 inhibitor in U87 MG cells. We found that the expression of the DDR-related genes, BRCA1 (**Figure 5F**), NBS1 (**Figure 5G**), RAD50 (**Figure 5H**), and MRE11 (**Figure 5I**) were decreased following treatment with the PD-L1 inhibitor + radiation, compared to the levels of expression observed following radiation only. Additionally, there was a particularly reversed effect of DDR in the miR-33a-5p-overexpression or PTEN-silencing groups (**Figures 5F–I**).

DISCUSSION

GBM is the most common malignant primary central nervous system (CNS) tumor in adults, and is resistant to current therapies (27). Current evidence points toward the existence of a small fraction of tumor cells in the bulk tumor that also exhibit radio-resistant properties (28). Glioblastoma has been extensively studied as a paradigm for cancer-associated immunosuppression (29). Mount of immunosuppressive factors were existed on the glioma cell surface (30, 31). Importantly, PD-L1 was upregulated in the GBM microenvironment; thus, protecting GBM from T-cell killing (29). Our results revealed that GBM cells expressed PD-L1, and that radiation induced PD-L1 expression beyond that observed without radiation. H1A is a PD-L1 antibody that destabilizes PD-L1 by disrupting its binding with the PD-L1 stabilizer. Such destabilization results in greater PD-L1 degradation through the lysosome and sensitivity to radiotherapy is increased (8). Our results suggested that the inhibition of PD-L1, using a small molecular inhibitor, increased radio-sensitivity, which was indicated by increased apoptosis, decreased survive, and impaired migration in U87 MG cells and U251 cells.

In this study, our group is the first to report that the PD-L1 inhibitor repressed miR-33a-5p activity. We also demonstrated that the PD-L1 inhibitor was able to induce the expression of the PTEN by inhibiting miR-33a-5p, and further confer radiosensitization in GBM cells. To maintain the primary biological features of those cells, including stemness, self-renewal, and tumor initiation *in vivo*, the higher level of miR-33a-5p expression in GBM is required (32). Extensive research has been performed to demonstrate the important roles of miR-33a-5p in GBM initiation, progression, and recurrence associated with resistance to radiotherapy (14). Our results showed that radiation induced miR-33a-5p expression, which led to radiation resistance, while reversed by PD-L1 inhibitor. After delivering the PD-L1 inhibitor, we observed an upregulation of the miR-33a-5p target, PTEN. It has been reported that the loss of PTEN promotes gliomagenesis (33) and GBM radiation resistance (34). Similarly, PTEN silencing abolished the PD-L1 inhibitor-induced radiosensitization.

The inhibition of DNA repair was required to overcome radio-resistance (35). Thus, we found that the PD-L1 inhibitor was effective at radiosensitizing U87 MG cells by inhibiting the DDR. Other reports have confirmed the radiosensitizing potential associated with inhibiting the DDR at the pre-clinical level (36, 37). As report, the DDR recently has been confirmed to promote the radiation-induced upregulation of PD-L1 in tumor cells, increased exhaustion of CD8+ T cell induced by radiation, to achieve a greater pro-tumor response (38). Given the well-characterized GBM related immunosuppressive tumor microenvironment, treatment with PD-L1 inhibitors may present important weapons against this disease, such as targeting the DDR in GBM cells following radiation therapy (39, 40). The increasing number of γ-H2AX foci in the S-phase fraction commonly occurred in the DNA damage process (41). Similarly, our results showed that radiation induced the DDR in the U87 MG cells, while the PD-L1 inhibitor impaired the DDR, accompanied with increasing γ-H2AX foci and GBM cells trapping the S-phase; thus, leading to radiation sensitization.

In conclusion, the present study showed that the PD-L1 inhibitor induced radiation sensitization in U87 MG cells and U251 cells by directly targeting miR-33a-5p, activating the PTEN signaling pathway, and inhibiting the DDR process. These findings provide new insights into the understanding of the molecular mechanisms by which PD-L1 inhibitors mediate radiation sensitization in GBM.

DATA AVAILABILITY STATEMENT

The original contributions presented in the study are publicly available. This data can be found here: ArrayExpress (https://www.ebi.ac.uk/arrayexpress/) accession E-MTAB-9007.

AUTHOR CONTRIBUTIONS

WX, JZ, and YT made substantial contributions to the acquisition, analysis and interpretation of data. XWa, XWe, and XZ were the major contributors in writing the manuscript. MH and SL were involved in conception and design, revising it critically for important intellectual content. All authors read and approved the final manuscript.

FUNDING

This study was supported by the national natural science foundation of China (grant no. 81671205 to SL; grant no. 81974186 to SL; grant no.81600278 to WX), the Program from Shanghai Committee of Science and technology (grant no. 18XD1402700 to SL) and the Foundation for Interdisciplinary Research of Shanghai JiaoTong University (grant no. YG2017MS68 to JZ).

REFERENCES

1. Reifenberger G, Wirsching HG, Knobbe-Thomsen CB, Weller M. Advances in the molecular genetics of gliomas - implications for classification and therapy. *Nat Rev.* (2017) 14:434–52. doi: 10.1038/nrclinonc.2016.204
2. Brandsma D, Stalpers L, Taal W, Sminia P, van den Bent. MJ Clinical features, mechanisms, and management of pseudoprogression in malignant gliomas. *Lancet.* (2008) 9:453–61. doi: 10.1016/S1470-2045(08)70125-6
3. Van Meir EG, Hadjipanayis CG, Norden AD, Shu HK, Wen PY, Olson JJ. Exciting new advances in neuro-oncology: the avenue to a cure for malignant glioma. *Cancer J Clin.* (2010) 60:166–93. doi: 10.3322/caac.20069
4. Chen L, Han X. Anti-PD-1/PD-L1 therapy of human cancer: past, present, and future. *J Clin Invest.* (2015) 125:3384–91. doi: 10.1172/JCI80011
5. Chen DS, Irving BA, Hodi FS. Molecular pathways: next-generation immunotherapy–inhibiting programmed death-ligand 1 and programmed death-1. *Clin Cancer Res.* (2012) 18:6580–7. doi: 10.1158/1078-0432.CCR-12-1362
6. He J, Hu Y, Hu M, Li B. Development of PD-1/PD-L1 pathway in tumor immune microenvironment and treatment for non-small cell lung cancer. *Sci Rep.* (2015) 5:13110. doi: 10.1038/srep13110
7. Saha D, Martuza RL, Rabkin SD. Macrophage polarization contributes to glioblastoma eradication by combination immunovirotherapy and immune checkpoint blockade. *Cancer Cell.* (2017) 32:253–67.e5. doi: 10.1016/j.ccell.2017.07.006
8. Tu X, Qin B, Zhang Y, Zhang C, Kahila M, Nowsheen S, et al. PD-L1 (B7-H1) competes with the RNA exosome to regulate the dna damage response and can be targeted to sensitize to radiation or chemotherapy. *Molecular Cell.* (2019) 74:1215–26.e4. doi: 10.1016/j.molcel.2019.04.005
9. Bushati N, Cohen SM. microRNA functions. *Ann Rev Cell Dev Biol.* (2007) 23:175–205. doi: 10.1146/annurev.cellbio.23.090506.123406
10. Baek D, Villen J, Shin C, Camargo FD, Gygi SP, Bartel DP. The impact of microRNAs on protein output. *Nature.* (2008) 455:64–71. doi: 10.1038/nature07242
11. Farazi TA, Spitzer JI, Morozov P, Tuschl T. miRNAs in human cancer. *J Pathol.* (2011) 223:102–15. doi: 10.1002/path.2806
12. Chang M, Qiao L, Li B, Wang J, Zhang G, Shi W, et al. Suppression of SIRT6 by miR-33a facilitates tumor growth of glioma through apoptosis and oxidative stress resistance. *Oncol Rep.* (2017) 38:1251–58. doi: 10.3892/or.2017.5780
13. Wang H, Sun T, Hu J, Zhang R, Rao Y, Wang S, et al. miR-33a promotes glioma-initiating cell self-renewal via PKA and NOTCH pathways. *J Clin Invest.* (2014) 124:4489–502. doi: 10.1172/JCI 75284
14. Sumazin P, Yang X, Chiu HS, Chung WJ, Iyer A, Llobet-Navas D, et al. An extensive microRNA-mediated network of RNA-RNA interactions regulates established oncogenic pathways in glioblastoma. *Cell.* (2011) 147:370–81. doi: 10.1016/j.cell.2011.09.041
15. Gu Y, Cai R, Zhang C, Xue Y, Pan Y, Wang J, et al. miR-132-3p boosts caveolae-mediated transcellular transport in glioma endothelial cells by targeting PTEN/PI3K/PKB/Src/Cav-1 signaling pathway. *FASEB J.* (2019) 33:441–54. doi: 10.1096/fj.201800095RR
16. Zhao J, Chen AX, Gartrell RD, Silverman AM, Aparicio L, Chu T, et al. Immune and genomic correlates of response to anti-PD-1 immunotherapy in glioblastoma. *Nat Med.* (2019) 25:462–9. doi: 10.1038/s41591-019-0349-y
17. Bai H, Harmanci AS, Erson-Omay EZ, Li J, Coskun S, Simon M, et al. Integrated genomic characterization of IDH1-mutant glioma malignant progression. *Nature Genet.* (2016) 48:59–66. doi: 10.1038/ng.3457
18. Dang CV. MYC on the path to cancer. *Cell.* (2012) 149:22–35. doi: 10.1016/j.cell.2012.03.003
19. Goellner EM, Grimme B, Brown AR, Lin YC, Wang XH, Sugrue KF, et al. Overcoming temozolomide resistance in glioblastoma via dual inhibition of NAD+ biosynthesis and base excision repair. *Cancer Res.* (2011) 71:2308–17. doi: 10.1158/0008-5472.CAN-10-3213
20. Akamandisa MP, Nie K, Nahta R, Hambardzumyan D, Castellino RC. Inhibition of mutant PPM1D enhances DNA damage response and growth suppressive effects of ionizing radiation in diffuse intrinsic pontine glioma. *Neuro-Oncol.* (2019) 21:786–99. doi: 10.1093/neuonc/noz053
21. Wang J, Hu C, Wang J, Shen Y, Bao Q, He F, et al. Checkpoint blockade in combination with doxorubicin augments tumor cell apoptosis in osteosarcoma. *J Immunother.* (2019) 42:321–30. doi: 10.1097/CJI.0000000000000281
22. Lau J, Ilkhanizadeh S, Wang S, Miroshnikova YA, Salvatierra NA, Wong RA, et al. STAT3 Blockade Inhibits Radiation-Induced Malignant Progression in Glioma. *Cancer Res.* (2015) 75:4302–11. doi: 10.1158/0008-5472.CAN-14-3331
23. Xia W, Zhuang L, Hou M. Role of lincRNAp21 in the protective effect of macrophage inhibition factor against hypoxia/serum deprivationinduced apoptosis in mesenchymal stem cells. *Int J Mol Med.* (2018) 42:2175–84. doi: 10.3892/ijmm.2018.3767
24. Harder BG, Peng S, Sereduk CP, Sodoma AM, Kitange GJ, Loftus JC, et al. Inhibition of phosphatidylinositol 3-kinase by PX-866 suppresses temozolomide-induced autophagy and promotes apoptosis in glioblastoma cells. *Mol Med.* (2019) 25:49. doi: 10.1186/s10020-019-0116-z
25. Palanichamy K, Patel D, Jacob JR, Litzenberg KT, Gordon N, Acus K, et al. Lack of constitutively active DNA repair sensitizes glioblastomas to Akt inhibition and induces synthetic lethality with radiation treatment in a p53-dependent manner. *Mol Cancer Ther.* (2018) 17:336–46. doi: 10.1158/1535-7163.MCT-17-0429
26. Pal S, Kozono D, Yang X, Fendler W, Fitts W, Ni J, et al. Dual HDAC and PI3K inhibition abrogates NFkappaB- and FOXM1-mediated DNA damage response to radiosensitize pediatric high-grade gliomas. *Cancer Res.* (2018) 78:4007–21. doi: 10.1158/0008-5472.CAN-17-3691
27. Furnari FB, Fenton T, Bachoo RM, Mukasa A, Stommel JM, Stegh A, et al. Malignant astrocytic glioma: genetics, biology, and paths to treatment. *Gen Dev.* (2007) 21:2683–710. doi: 10.1101/gad.1596707
28. Chen J, McKay RM, Parada LF. Malignant glioma: lessons from genomics, mouse models, stem cells. *Cell.* (2012) 149:36–47. doi: 10.1016/j.cell.2012.03.009
29. Nduom EK, Weller M, Heimberger AB. Immunosuppressive mechanisms in glioblastoma. *Neuro-Oncology.* (2015) 7:vii9-vii14. doi: 10.1093/neuonc/nov151
30. Badie B, Schartner J, Prabakaran S, Paul J, Vorpahl J. Expression of Fas ligand by microglia: possible role in glioma immune evasion. *J Neuroimmunol.* (2001) 120:19–24. doi: 10.1016/S0165-5728(01)00361-7
31. Wischhusen J, Jung G, Radovanovic I, Beier C, Steinbach JP, Rimner A, et al. Identification of CD70-mediated apoptosis of immune effector cells as

a novel immune escape pathway of human glioblastoma. *Cancer research.* (2002) 62:2592–9.
32. Chen R, Nishimura MC, Bumbaca SM, Kharbanda S, Forrest WF, Kasman IM, et al. A hierarchy of self-renewing tumor-initiating cell types in glioblastoma. *Cancer Cell.* (2010) 17:362–75. doi: 10.1016/j.ccr.2009.12.049
33. Shin CH, Robinson JP, Sonnen JA, Welker AE, Yu DX, VanBrocklin MW, et al. HBEGF promotes gliomagenesis in the context of Ink4a/Arf and Pten loss. *Oncogene.* (2017) 36:4610–8. doi: 10.1038/onc.2017.83
34. Miyahara H, Yadavilli S, Natsumeda M, Rubens JA, Rodgers L, Kambhampati M, et al. The dual mTOR kinase inhibitor TAK228 inhibits tumorigenicity and enhances radiosensitization in diffuse intrinsic pontine glioma. *Cancer letters.* (2017) 400:110–6. doi: 10.1016/j.canlet.2017.04.019
35. Ahmed SU, Carruthers R, Gilmour L, Yildirim S, Watts C, Chalmers AJ. Selective inhibition of parallel DNA damage response pathways optimizes radiosensitization of glioblastoma stem-like cells. *Cancer Res.* (2015) 75:4416–28. doi: 10.1158/0008-5472.CAN-14-3790
36. Biddlestone-Thorpe L, Sajjad M, Rosenberg E, Beckta JM, Valerie NC, Tokarz M, et al. ATM kinase inhibition preferentially sensitizes p53-mutant glioma to ionizing radiation. *Clin Cancer Res.* (2013) 19:3189–200. doi: 10.1158/1078-0432.CCR-12-3408
37. Venere M, Hamerlik P, Wu Q, Rasmussen RD, Song LA, Vasanji A, et al. Therapeutic targeting of constitutive PARP activation compromises stem cell phenotype and survival of glioblastoma-initiating cells. *Cell Death Differe.* (2014) 21:258–69. doi: 10.1038/cdd.2013.136
38. Morgan MA, Canman CE. Replication stress: an achilles' heel of glioma cancer stem-like cells. *Cancer Rese.* (2018) 78:6713–16. doi: 10.1158/0008-5472.CAN-18-2439
39. Woroniecka KI, Rhodin KE, Chongsathidkiet P, Keith KA, Fecci PE. T-cell dysfunction in glioblastoma: applying a new framework. *Clin Cancer Res.* (2018) 24:3792–802. doi: 10.1158/1078-0432.CCR-18-0047
40. Woroniecka K, Chongsathidkiet P, Rhodin K, Kemeny H, Dechant C, Farber SH, et al. T-cell exhaustion signatures vary with tumor type and are severe in glioblastoma. *Clin Cancer Res.* (2018) 24:4175–86. doi: 10.1158/1078-0432.CCR-17-1846
41. Ewald B, Sampath D, Plunkett W. H2AX phosphorylation marks gemcitabine-induced stalled replication forks and their collapse upon S-phase checkpoint abrogation. *Mol Cancer Ther.* (2007) 6:1239–48. doi: 10.1158/1535-7163.MCT-06-0633

Conflict of Interest: The authors declare that the research was conducted in the absence of any commercial or financial relationships that could be construed as a potential conflict of interest.

frontiers in Oncology

MINI REVIEW
published: 07 July 2020
doi: 10.3389/fonc.2020.01120

STAT3 Contributes to Radioresistance in Cancer

Xuehai Wang[1], *Xin Zhang*[2,3], *Chen Qiu*[4] *and Ning Yang*[2,3]*

[1] Department of Otolaryngology, Weihai Municipal Hospital, Shandong University, Weihai, China, [2] Department of Neurosurgery, Qilu Hospital of Shandong University and Institute of Brain and Brain-Inspired Science, Shandong University, Jinan, China, [3] Shandong Key Laboratory of Brain Function Remodeling, Jinan, China, [4] Department of Radiation Oncology, Qilu Hospital of Shandong University, Jinan, China

Radiotherapy has been used in the clinic for more than one century and it is recognized as one of the main methods in the treatment of malignant tumors. Signal Transducers and Activators of Transcription 3 (STAT3) is reported to be upregulated in many tumor types, and it is believed to be involved in the tumorigenesis, development and malignant behaviors of tumors. Previous studies also found that STAT3 contributes to chemo-resistance of various tumor types. Recently, many studies reported that STAT3 is involved in the response of tumor cells to radiotherapy. But until now, the role of the STAT3 in radioresistance has not been systematically demonstrated. In this study, we will review the radioresistance induced by STAT3 and relative solutions will be discussed.

Keywords: STAT3, apoptosis, aggressive behaviors, cancer cell stemness, reactive oxygen species

OPEN ACCESS

Edited by:
Carsten Herskind,
University of Heidelberg, Germany

Reviewed by:
James William Jacobberger,
Case Western Reserve University, United States
Franz Rödel,
University Hospital Frankfurt, Germany

***Correspondence:**
Ning Yang
yangning@sdu.edu.cn

Specialty section:
This article was submitted to Radiation Oncology, a section of the journal Frontiers in Oncology

Received: *06 February 2020*
Accepted: *04 June 2020*
Published: *07 July 2020*

Citation:
Wang X, Zhang X, Qiu C and Yang N (2020) STAT3 Contributes to Radioresistance in Cancer. Front. Oncol. 10:1120. doi: 10.3389/fonc.2020.01120

INTRODUCTION

With the development of technology and our understanding of tumors, there are multiple methods for the treatment of tumors, such as surgical resection, chemotherapy, radiotherapy and immunotherapy. Among all these approaches to treatment, radiotherapy is one of the most cost-effective methods for the treatment of various cancers. Since its introduction into the clinic, radiotherapy has existed for more than one century, which shows that its efficiency is well-approved (1). But for some tumor types, radiotherapy doesn't work so well. Until now, we have recognized that after irradiation treatment, tumor cells develop complicated mechanisms, like DNA repair, cell cycle arrest, and autophagy, to protect themselves so as to survive (2–4). As a result, most tumor cells will develop radioresistance, which leads to the failure of radiotherapy. Although many methods have been used to overcome radioresistance, their efficiency is not as what we have expected (5, 6). Thus, more research is needed to help us have a better understanding of radioresistance.

Signal Transducers and Activators of Transcription 3 (STAT3), one of the most important intracellular transcription factors, is reported to be constitutively activated in most tumor types (7, 8). Many cytokines, hormones and growth factors are involved in the activation of STAT3, among which canonical Janus kinase (JAK) is the most studied (9). STAT3 plays an important role in cell proliferation, and is also involved in anti-apoptosis process (9). Besides, STAT3 also promotes angiogenesis, invasiveness and immunosuppression in cancer (10–12). All these functions are related to STAT3's role in controlling gene transcription. Previously, STAT3 was recognized as a direct transcription factor. For example, STAT3 regulates pro-survival gene expression to increase apoptotic resistance in cancer. But more and more recent studies discover that STAT3 also regulates gene expression through DNA methylation and chromatin modulation (9).

Previously, STAT3 is reported to be involved in chemo-resistance and this is well-reviewed by Tan et al. (13). Recently, more and more studies showed that STAT3 contributed to radioresistance. Huang et al. showed that sorafenib and its derivative could increase the anti-tumor effect of radiotherapy by inhibiting STAT3 (14, 15). Lau et al. found that blocking STAT3 could inhibit radiation-induced malignant progression, such as increased migration and invasion (16). These studies have shown that STAT3 is not only involved in tumorigenesis and tumor development, but also leads to chemo- and radio-resistance. Here, we mainly review the role of STAT3 in mediating radioresistance from points of apoptosis, aggressive behaviors, DNA damage repair, cancer stem cells. And novel modalities to reverse the failure of radiotherapy will be discussed.

INHIBITING STAT3 INCREASED RADIATION-INDUCED APOPTOSIS

Apoptosis is essential for the maintenance of normal physiological functions in normal cells. But anti-apoptosis process could be induced in tumor cells after chemo- or radio-therapy, so as to help them survive (17).

The B cell lymphoma-2 (BCL-2) family of proteins are important among all the factors that are involved in regulating programmed cell death or apoptosis (18). BCL-2 family of proteins are mainly mitochondria localized and involved in the release of cytochrome C, an essential mediator of apoptosis (19, 20). They possess BH 1–4 domains and have the function of maintaining mitochondrial integrity. STAT3 is involved in tumorigenesis by activating anti-apoptotic proteins, like surviving (17, 21). Conversely, inhibiting STAT3 increases apoptosis (22, 23). Besides, a study found that heat shock protein 70 (Hsp70) has anti-apoptosis effect by preventing JNK-induced phosphorylation and inhibiting BCL-2 and BCL-XL, so as to maintain the stability of mitochondria (24). STAT3 can affect the Hsp70 promoter and increases its expression in cancer cells, mediating the upregulation of antiapoptotic proteins (25). As a result, we assume that inhibiting STAT3 could decrease the expression of antiapoptotic proteins, leading to apoptosis.

Until now, there are a large number of studies showing that inhibiting STAT3 increases radiosensitivity in numerous tumor types (14, 15, 26–31), which are summarized in **Table 1**.

Studies showed that STAT3 is one of the most important regulators of survivin (33, 34). Survivin, a member of the inhibitor of apoptosis protein (IAP) family and one of the most important anti-apoptotic proteins, is found highly expressed in various cancer types, making it a potential anticancer target (35, 36).

Several studies found that inhibiting survivin could enhance radiosensitivity in various tumor types. Grdina et al. found that the expression of survivin upregulated after irradiation treatment and increased survivin promoted cell survival, while knocking down survivin with siRNA abrogated this adaptive response (37). Iwasa et al. showed that YM155, an inhibitor of survivin, enhanced radiosensitivity in non-small cell lung cancer cell lines (38). Qin et al. showed that YM155 increases radiosensitivity in esophageal squamous cell carcinoma by the inhibiting cell cycle checkpoint and homologous recombination repair (32).

TABLE 1 | A summary of pre-clinical studies in which STAT3-targeted compounds are used to enhance the radiosensitivity of malignant tumors by inducing apoptosis.

Compounds/ Genes	Cancer type	Mechanisms	References
Sorafenib	Hepatocellular carcinoma	Inhibiting STAT3	(14)
SC-59	Hepatocellular carcinoma	Inhibiting SHP-1/STAT3 pathway	(15)
Dovitinib	Hepatocellular Carcinoma	Inhibiting SHP-1/STAT3 pathway	(26)
GRIM-19	Gastric cancer cells	Suppressing accumulation of STAT3	(27)
Stattic	Head and neck squamous cell carcinoma	Inhibiting STAT3	(28)
Casticin	Human renal clear cell carcinoma, neck squamous cell carcinoma	Inhibiting IL-6/STAT3 pathway	(29)
Zoledronic acid	Human pancreatic cancer cells	Inhibiting STAT3/NF-kappa B pathway	(30)
YM155	Glioma	Inhibiting STAT3/survivin pathway	(32)

GRIM-19, genes associated retinoid–IFN induced mortality-19. SHP-1, Src-homology phosphatase type-1.

But these studies didn't demonstrate whether the radiosensitive effect of YM155 is STAT3-dependent. Our recent study found that YM155 decreased the activity of STAT3 and increased the radiosensitivity of glioblastoma, one of the most radioresistant tumor types. This might provide some clues for the role of STAT3/survivin pathway in the radioresistance of various neoplasms (31). Further studies are warranted to clarify the direct interaction between STAT3 and survivin after irradiation treatment.

INHIBITING STAT3 DECREASED RADIATION-INDUCED AGGRESSIVE BEHAVIORS

Although irradiation kills cancers, we have to recognize that it can also induce carcinogenesis. The carcinogenic potential of ionizing radiations could be traced back to 1902 and more radiation-induced (RI) neoplasia have been observed (39, 40). Over the last 45 years, 296 cases of radiation-induced brain tumors have been reported.

Except for RT tumors, more and more studies discovered that radiation might enhance malignant progression, like aggressive migration and invasion in cancer cells (16, 41–45). This will induce more extensive spread of tumor cells, which is a contributing factor to tumor relapse and recurrence (46, 47).

TABLE 2 | A summary of genes involved in irradiation-induced invasion of various cancers.

Genes	Cancer type	Mechanisms	References
MMP2	Glioma; Esophageal squamous cell carcinoma	Degrading extracellular matrix components	(42, 54, 55)
SDF-1	Murine astrocytoma tumor	Through macrophage mobilization and tumor revascularization	(56)
MRCK	Glioma; Squamous cell carcinoma; Skin cancer	By targeting MLC and MYPT1; By disturbing a network of communicating glioma cell protrusions	(57–60)
MMP9	Glioma	Degrading extracellular matrix components	(61)

MLC, myosin light chain proteins. MRCK, myotonic dystrophy kinase-related CDC42-binding kinase. MMP: matrix metalloproteinase. MYPTI, myosin phosphatase targeting subunit 1. SDF-1: stromal cell-derived factor-1.

Among all the mechanisms that explaining radiation-induced migration and invasion, epithelial–mesenchymal transition (EMT) accounting for the most. In the process of EMT, epithelial characteristics will be downregulated and mesenchymal characteristics will be gained in epithelial cells. This phenomena were reported by Elizabeth Hay in the early 1980s (48). Cancer cells underwent EMT will acquire elevated capabilities to invade and disseminate to distant sites, which increases its malignance.

Previous studies showed that among all signaling pathways that are involved in EMT, STAT3 is one of the most important (49–51). Many studies found that irradiation actually promoted EMT process (43, 52, 53). Lau et al. found that blocking STAT3 decreased radiation-induced malignant behaviors in glioma (16). Our previous study showed that YM155 not only decreased DNA damage repair, but also decreased radiation-induced invasion and reversed EMT by inhibiting STAT3, which was a promising radiosensitizer in the treatment of cancer (31). But whether it has the same effect in other tumor types is still unknown.

Except for EMT process, there are other mechanisms to explain for the increased invasive ability induced by irradiation (42, 54–61), which are summarized in **Table 2**. But whether they have relationships with STAT3 is still unknown.

Yu et al. showed that irradiated breast cancer cells could promote the invasion of non-irradiated tumor cells and angiogenesis through IL-6/STAT3 signaling (62). This might explain that STAT3 plays a role in radiation-induced bystander effect (RIBE) (63). RIBE happens when irradiated cells affect non-irradiated cells through gap junctional intercellular communication (GJIC) or the release of soluble factors (64). Results induced by RIBE are still unclear. Some studies found decreased survival in unirradiated cells, whereas others observed that RIBE helped irradiated cells survive (65).

Duan et al. showed that irradiation of normal brain before tumor cell implantation contributed to aggressive tumor growth, which suggested a brain tumor microenvironment-induced, tumor-extrinsic effect (66). Tumor microenvironment (TM) is mainly composed of epithelial cells, stromal cells, extracellular matrix (ECM) components or immune cells (67). The concept of TM can be traced back to 1889, when Paget put forward the concept, "seed and soil" (68). The role of TM in tumorigenesis and development is attracting more and more attention. Studies also found that TM contributed to chemo- or radio-resistance (67, 69, 70).

Recent studies also verified the important role of STAT3 in tumor microenvironment. A study by Chang et al. concluded that IL-6/JAK/STAT3 pathways played a key role in regulating the tumor microenvironment that promoted growth, invasion, and metastasis (71). Deng et al. reported that sphingosine-1-phosphate receptor type 1 (S1PR1)-STAT3 signaling was activated in pre-metastatic sites, contributing to the formation of pre-metastatic niche (72). Bohrer et al. found that upregulation of the fibroblast growth factor receptor (FGFR)-STAT3 signaling in breast cancer cells led to a hyaluronan-rich microenvironment, which helped tumor progression (73).

STAT3 also established an immunosuppressive microenvironment to promote the growth and metastasis breast cancer (74). All these studies showed that STAT3 played an important role in tumor microenvironment-induced aggressive behaviors, which made STAT3 a promising target in the radiorensitization of cancers. A study by Gao et al. showed that myeloid cell-specific inhibition of Toll-like receptor 9 (TLR9)/STAT3 signaling enhanced the antitumor effect of irradiation (75). More studies are warranted in the future to verify whether targeting STAT3 is efficient in inhibiting irradiation-induced malignant behaviors of cancers.

STAT3 IS INVOLVED IN DNA DAMAGE REPAIR

Ionizing radiation damages DNA mainly in two ways, by direct and indirect action. Direct action occurs by ionization in the DNA molecule itself. On the other hand, ionization of water produces reactive oxygen species (ROS) and reactive nitrogen species (RNS), and these free radical species (in particular the OH radical) damage DNA by indirect action (31). The efficacy of radiotherapy is mainly determined by DNA damage. However, radioresistance can be induced after repeat radiotherapy treatment. Among all the cellular processes that are involved in the development of radioresistance, DNA damage repair is one of the most important factors (76).

When DNA damage occurs, a series of sequential reactions are induced to maintain the consistency and integrity of genetic material. These reactions are called DNA damage repair (77). Among all the pathways that are involved in DNA damage repair, ataxia-telangiectasia mutated (ATM)- check-point kinase 2 (Chk2) and ATM and Rad3-related (ATR)- check-point kinase 1 (Chk1) signaling pathways are the best studied. ATM and ATR are recognized as the central components of the DNA damage response (78, 79). When DNA double strand breaks (DSBs) occur, ATM is upregulated and activates the phosphorylation of important proteins like check-point kinase 2 (Chk2), p53, and BRCA1 (80, 81). ATR initiates the late phosphorylation of p53 and check-point kinase 1 (Chk1) (82, 83). Details can be seen in the review by Zhang et al. (84).

There are various types of DNA damage, like base damage, deletion, insertion, exon skipping, single strand breaks and double strand breaks (DSBs). Among them, DSBs are the

most lethal. There are mainly two mechanism in repairing DSBs, non-homologous end joining (NHEJ) and homologous recombination (HR). In the process of NHEJ, ligation occurs regardless of whether the ends come from the same chromosome. As a result, mistakes might occur. On the other hand, HR uses the information that is usually from the sister chromatid to repair damaged DNA. So, HR has a higher accuracy in repairing DNA (76).

Recently, more and more studies showed that STAT3 was involved in DNA damage repair. STAT3 was reported to be involved in the regulation of breast cancer susceptibility gene 1 (BRCA1), an important factor in DNA damage repair, especially HR (85, 86). Barry et al. showed that knocking down STAT3 impaired the efficiency of damage repair by downregulating the ATM-Chk2 and ATR-Chk1 pathways (87). Essential meiotic endonuclease 1 homolog 1 (Eme1), a key endonuclease involved in DNA repair, was reported to be the downstream of STAT3 (88–90).Chen et al. showed that silencing Jumonji domain-containing protein 2B (JMJD2B) activated DNA damage by the suppression of STAT3 signaling (91). All these studies suggested that STAT3 was part of DNA damage repair mechanisms. But it is still insufficient to conclude that STAT3 is directly participating in DNA damage repair. What's more, these studies are not enough to show that it is ubiquitous for STAT3 to be involved in DNA damage repair. Studies like knocking down STAT3 to test the efficiency of HR or NHEJ are needed in the future.

STAT3 CONTRIBUTES TO ROS DEPLETION IN CANCER STEM CELLS

Cancer stem cells (CSCs) are a group of cells with characteristics of self-renewing, multipotent, and tumor-initiating. Recently more and more studies showed that most malignant cancer cells were derived from CSCs (92, 93). CSCs have high expression of anti-apoptotic proteins and ATP-binding cassette (ABC) pump, and all these contribute to its chemo- or radio-resistant feature (94–96). Many studies showed that STAT3 was one of the most important factors in maintaining the phenotype of CSCs (97–99). Besides, STAT3 also suppressed differentiation-related genes (100). In the aspect of radiotherapy, recent studies found that STAT3 and CCS were closely connected in contributing to radioresistance. Lee et al. found that STAT3 was involved in enhancing cancer stemness and radioresistant properties (101). Shi et al. showed that ibrutinib, a Bruton's tyrosine kinase (BTK) inhibitor, could impair radioresistance by inactivating STAT3 in glioma stem cells (102). A study by Park et al. showed that JAK2/STAT3/ cyclin D2 (CCND2) pathway promoted colorectal cancer stem cell persistence and radioresistance (103). Gao et al. found that lemonin, a triterpenoid compound, enhanced radiosensitivity by attenuating Stat3-induced cell stemness (104). Many studies have been done to find out the underlying mechanisms of CSCs in radioresistance. A review by Skvortsova et al. showed that the ability of DNA damage repair was enhanced in CSCs, so as to help them defend against ROS (105). Arnold found that radiation expanded cancer stem cell populations and can induce stemness in nonstem cells in a STAT3-dependent manner (106). Since ionizing radiation causes cell death by DNA damage, here we mainly focus on how CSCs respond to DNA damage. Until now, little is known about the DNA repair mechanisms in CSCs. But more and more attention has been paid to the role of ROS in CSC survival and radiation resistance (107).

High ROS levels affect many aspects of tumor biology and one of the most important roles is that it induces DNA damage and genomic instability (108). Normally, single strand breaks (SSBs) are the main DNA damage type after ROS treatment and can be repaired through nucleotide or base excision repair (NER/BER) (109). But the accumulation of SSBs can lead to stalling of the replication fork or error in replication, which ultimately induces more lethal DNA damage type, DSBs. A study showed that CSCs possess lower concentrations of ROS than do non-stem cancer cells (96). Studies also found that inhibiting ROS scavenging machinery could enhance radiosensitivity in CSCs (110, 111). Lu et al. found that niclosamide, an inhibitor of STAT3, increased the radiosensitivity in triple negative breast cancer (TNBC) cells via triggering the production of ROS (112). Their study showed that inhibiting STAT3 and increasing ROS led to radiosensitivity. But they didn't illustrate enough evidence to prove the relationship between STAT3 and ROS in DNA damage repair.

Intracellular ROS is mainly produced by the mitochondria, and another source is NADPH oxidases (NOXs) (113). Initially, mitochondria ROS production is unwanted by cells. Recently, more and more studies found that STAT3 was actively involved in regulating the activity of mitochondria. Lapp et al. found that activating STAT3 decreased mitochondrial ROS production by upregulating the expression of uncoupling protein 2 (UCP2) (114). Meier et al. showed that phosphorylation of Ser^{727} in STAT3 recruited mitochondrially localized STAT3 (115). But phospho-$Stat3Y^{705}$ is not responsible for the STAT3 mitochondrial translocation (115–117). What's more, a recent study by Cheng et al. found that selectively inhibiting mitochondrial STAT3 could provide a promising target for chemotherapy (118). As a result, we assume that mitochondrial STAT3 may be a potential target in enhancing the radioresensitizing effect of cancer cells. More studies are warranted in the future.

CONCLUSION

Persistent activation of STAT3 in various tumor types makes STAT3 a specific and promising target in anticancer treatment. Inhibiting STAT3 by STAT3 dominant negative molecules, decoy oligonucleotides, and peptidomimetics is proven efficient in numerous preclinical studies.

STAT3 is well-known for its roles in tumor initiation and development. Besides, STAT3 also leads to chemo- or radio-resistance. In this review, we mainly focused on the role of STAT3 in response to radiotherapy, and the underlying mechanisms including but not limited to apoptosis, aggressive behaviors, DNA damage repair, cancer stem cells were discussed (**Supplementary Figure 1**). Except for the mechanisms we have discussed above, there are still other explanations for STAT3's role in radioresistance. Hypoxia is also a well-known factor that contributes to radioresistance in many tumor types. Hypoxia induces the production of ROS by mitochondrial electron transport chain. It also activates Hypoxia inducible factors

(HIFs), important factors which will induce malignant behaviors and proliferation of tumor cells under hypoxia. Mitochondrial ROS stabilizes HIF1 and HIF2 by inhibiting prolyl hydroxylases (PHDs) (119, 120). Studies showed that NSC74859 and stattic, two inhibitors of STAT3, enhanced radiosensitivity by inhibiting hypoxia- and radiation-induced STAT3 activation in esophageal cancer (121, 122).

On the other hand, we have to realize that STAT3 has many other functions except for disease formation and progression, like cardioprotection, liver protection, and obesity (123–126). As a result, targeting STAT3 may have many side effects. For example, strong inhibitors of STAT3 could cause fatigue, diarrhea, infection, and periphery nervous system toxicities (127).

Although the inhibitors of STAT3 have been studied and proven to be efficient in preclinic for 20 years, they showed poor anti-tumor effect in clinical trials (17). Recently, drug repurposing, a method based on the theory that established drugs may have many other mechanisms except for their well-known indications, has gained increased attention (128). Drug repurposing has advantages such as highly approved safety, avoiding laborious and expensive drug development processes. As a result, testing FDA-approved drugs may help us find potential inhibitors of STAT3 and promote its quick translation into clinic to treat human cancers. In conclusion, the role of STAT3 in the radio-response of cancer has been paid more and more attention to. STAT3 is becoming a promising target in the radiosensitization of cancer.

AUTHOR CONTRIBUTIONS

XW, XZ, and NY contributed to conception and manuscript writing. XW and CQ searched the literature. NY supervised the whole writing work. All authors have read and approved the final manuscript.

FUNDING

This work was supported by the National Natural Science Foundation of China (Grant Nos. 81702475, 81803045, 81903126), Medical Science Technology Development Program of Shandong Province (2018WS103), and The Jinan Science and Technology Bureau of Shandong Province (201704083).

SUPPLEMENTARY MATERIAL

The Supplementary Material for this article can be found online at: https://www.frontiersin.org/articles/10.3389/fonc.2020.01120/full#supplementary-material

Supplementary Figure 1 | Radioresistance caused by signaling pathways related to STAT3. Radiation induced anti-apoptosis is mediated by STAT3-HSP70-BCL2 family members pathways. After radiation treatment, STAT3 promoted aggressive behaviors in tumor cells through epithelial–mesenchymal transition (EMT), radiation-induced bystander effect (RIBE) and tumor microenvironment (TM). STAT3 contributes to DNA damage repair through ATM-Chk2 and ATR-Chk1 pathways. Cancer stemness and reactive oxygen species (ROS) depletion are also involved in STAT3-induced radioresistance.

REFERENCES

1. Zhang X, Wang J, Li X, Wang D. Lysosomes contribute to radioresistance in cancer. *Cancer Lett.* (2018) 439:39–46. doi: 10.1016/j.canlet.2018.08.029
2. Pilie PG, Tang C, Mills GB, Yap TA. State-of-the-art strategies for targeting the DNA damage response in cancer. *Nat Rev Clin Oncol.* (2018) 16:81–104. doi: 10.1038/s41571-018-0114-z
3. Branzei D, Foiani M. Regulation of DNA repair throughout the cell cycle. *Nat Rev Mol Cell Biol.* (2008) 9:297–308. doi: 10.1038/nrm2351
4. Czarny P, Pawlowska E, Bialkowska-Warzecha J, Kaarniranta K, Blasiak J. Autophagy in DNA damage response. *Int J Mol Sci.* (2015) 16:2641–62. doi: 10.3390/ijms16022641
5. Nelson DF, Diener-West M, Horton J, Chang CH, Schoenfeld D, Nelson JS. Combined modality approach to treatment of malignant gliomas–re-evaluation of RTOG 7401/ECOG 1374 with long-term follow-up: a joint study of the Radiation Therapy Oncology Group and the Eastern Cooperative Oncology Group. *NCI Monogr.* (1988) 279–84.
6. Chan JL, Lee SW, Fraass BA, Normolle DP, Greenberg HS, Junck LR, et al. Survival and failure patterns of high-grade gliomas after three-dimensional conformal radiotherapy. *J Clin Oncol.* (2002) 20:1635–42. doi: 10.1200/JCO.2002.20.6.1635
7. Furtek SL, Backos DS, Matheson CJ, Reigan P. Strategies and approaches of targeting STAT3 for cancer treatment. *ACS Chem Biol.* (2016) 11:308–18. doi: 10.1021/acschembio.5b00945
8. Banerjee K, Resat H. Constitutive activation of STAT3 in breast cancer cells: a review. *Int J Cancer.* (2016) 138:2570–8. doi: 10.1002/ijc.29923
9. Yu H, Lee H, Herrmann A, Buettner R, Jove R. Revisiting STAT3 signalling in cancer: new and unexpected biological functions. *Nat Rev Cancer.* (2014) 14:736–46. doi: 10.1038/nrc3818
10. Bournazou E, Bromberg J. Targeting the tumor microenvironment: JAK-STAT3 signaling. *Jak Stat.* (2013) 2:e23828. doi: 10.4161/jkst.23828
11. Yu H, Pardoll D, Jove R. STATs in cancer inflammation and immunity: a leading role for STAT3. *Nat Rev Cancer.* (2009) 9:798–809. doi: 10.1038/nrc2734
12. Yu H, Jove R. The STATs of cancer–new molecular targets come of age. *Nat Rev Cancer.* (2004) 4:97–105. doi: 10.1038/nrc1275
13. Tan FH, Putoczki TL, Stylli SS, Luwor RB. The role of STAT3 signaling in mediating tumor resistance to cancer therapy. *Curr Drug Targets.* (2014) 15:1341–53. doi: 10.2174/1389450115666141120104146
14. Huang CY, Lin CS, Tai WT, Hsieh CY, Shiau CW, Cheng AL, et al. Sorafenib enhances radiation-induced apoptosis in hepatocellular carcinoma by inhibiting STAT3. *Int J Rad Oncol Biol Phys.* (2013) 86:456–62. doi: 10.1016/j.ijrobp.2013.01.025
15. Huang CY, Tai WT, Hsieh CY, Hsu WM, Lai YJ, Chen LJ, et al. A sorafenib derivative and novel SHP-1 agonist, SC-59, acts synergistically with radiotherapy in hepatocellular carcinoma cells through inhibition of STAT3. *Cancer Lett.* (2014) 349:136–43. doi: 10.1016/j.canlet.2014.04.006
16. Lau J, Ilkhanizadeh S, Wang S, Miroshnikova YA, Salvatierra NA, Wong RA, et al. STAT3 blockade inhibits radiation-induced malignant progression in Glioma. *Cancer Res.* (2015) 75:4302–11. doi: 10.1158/0008-5472.CAN-14-3331
17. Siveen KS, Sikka S, Surana R, Dai X, Zhang J, Kumar AP, et al. Targeting the STAT3 signaling pathway in cancer: role of synthetic and natural inhibitors. *Biochim Biophys Acta.* (2014) 1845:136–54. doi: 10.1016/j.bbcan.2013.12.005
18. Chipuk JE, Moldoveanu T, Llambi F, Parsons MJ, Green DR. The BCL-2 family reunion. *Mol Cell.* (2010) 37:299–310. doi: 10.1016/j.molcel.2010.01.025
19. Krajewski S, Tanaka S, Takayama S, Schibler MJ, Fenton W, Reed JC. Investigation of the subcellular distribution of the bcl-2 oncoprotein: residence in the nuclear envelope, endoplasmic reticulum, and outer mitochondrial membranes. *Cancer Res.* (1993) 53:4701–14.

20. Opferman JT, Kothari A. Anti-apoptotic BCL-2 family members in development. *Cell Death Differ.* (2018) 25:37–45. doi: 10.1038/cdd.2017.170
21. Fukada T, Hibi M, Yamanaka Y, Takahashi-Tezuka M, Fujitani Y, Yamaguchi T, et al. Two signals are necessary for cell proliferation induced by a cytokine receptor gp130: involvement of STAT3 in anti-apoptosis. *Immunity.* (1996) 5:449–60. doi: 10.1016/S1074-7613(00)80501-4
22. Epling-Burnette PK, Liu JH, Catlett-Falcone R, Turkson J, Oshiro M, Kothapalli R, et al. Inhibition of STAT3 signaling leads to apoptosis of leukemic large granular lymphocytes and decreased Mcl-1 expression. *J Clin Invest.* (2001) 107:351–62. doi: 10.1172/JCI9940
23. Daino H, Matsumura I, Takada K, Odajima J, Tanaka H, Ueda S, et al. Induction of apoptosis by extracellular ubiquitin in human hematopoietic cells: possible involvement of STAT3 degradation by proteasome pathway in interleukin 6-dependent hematopoietic cells. *Blood.* (2000) 95:2577–85. doi: 10.1182/blood.V95.8.2577.008k17_2577_2585
24. Zorzi E, Bonvini P. Inducible hsp70 in the regulation of cancer cell survival: analysis of chaperone induction, expression and activity. *Cancers.* (2011) 3:3921–56. doi: 10.3390/cancers3043921
25. Whitesell L, Lindquist S. Inhibiting the transcription factor HSF1 as an anticancer strategy. *Expert Opin Ther.* (2009) 13:469–78. doi: 10.1517/14728220902832697
26. Huang CY, Tai WT, Wu SY, Shih CT, Chen MH, Tsai MH, et al. Dovitinib acts as a novel radiosensitizer in hepatocellular carcinoma by targeting SHP-1/STAT3 signaling. *Int J Rad Oncol Biol Phys.* (2016) 95:761–71. doi: 10.1016/j.ijrobp.2016.01.016
27. Bu X, Zhao C, Wang W, Zhang N. GRIM-19 inhibits the STAT3 signaling pathway and sensitizes gastric cancer cells to radiation. *Gene.* (2013) 512:198–205. doi: 10.1016/j.gene.2012.10.057
28. Adachi M, Cui C, Dodge CT, Bhayani MK, Lai SY. Targeting STAT3 inhibits growth and enhances radiosensitivity in head and neck squamous cell carcinoma. *Oral Oncol.* (2012) 48:1220–6. doi: 10.1016/j.oraloncology.2012.06.006
29. Lee JH, Kim C, Ko JH, Jung YY, Jung SH, Kim E, et al. Casticin inhibits growth and enhances ionizing radiation-induced apoptosis through the suppression of STAT3 signaling cascade. *J Cell Biochem.* (2019) 120:9787–98. doi: 10.1002/jcb.28259
30. You Y, Wang Q, Li H, Ma Y, Deng Y, Ye Z, et al. Zoledronic acid exhibits radio-sensitizing activity in human pancreatic cancer cells via inactivation of STAT3/NF-kappaB signaling. *Onco Targets Ther.* (2019) 12:4323–30. doi: 10.2147/OTT.S202516
31. Zhang X, Wang X, Xu R, Ji J, Xu Y, Han M, et al. YM155 decreases radiation-induced invasion and reverses epithelial-mesenchymal transition by targeting STAT3 in glioblastoma. *J Transl Med.* (2018) 16:79. doi: 10.1186/s12967-018-1451-5
32. Qin Q, Cheng H, Lu J, Zhan L, Zheng J, Cai J, et al. Small-molecule survivin inhibitor YM155 enhances radiosensitization in esophageal squamous cell carcinoma by the abrogation of G2 checkpoint and suppression of homologous recombination repair. *J Hematol Oncol.* (2014) 7:62. doi: 10.1186/s13045-014-0062-8
33. Sehara Y, Sawicka K, Hwang JY, Latuszek-Barrantes A, Etgen AM, Zukin RS. Survivin Is a transcriptional target of STAT3 critical to estradiol neuroprotection in global ischemia. *J Neurosci.* (2013) 33:12364–74. doi: 10.1523/JNEUROSCI.1852-13.2013
34. Chuang YF, Huang SW, Hsu YF, Yu MC, Ou G, Huang WJ, et al. WMJ-8-B, a novel hydroxamate derivative, induces MDA-MB-231 breast cancer cell death via the SHP-1-STAT3-survivin cascade. *Br J Pharmacol.* (2017) 174:2941–61. doi: 10.1111/bph.13929
35. Rauch A, Hennig D, Schafer C, Wirth M, Marx C, Heinzel T, et al. Survivin and YM155: how faithful is the liaison? *Biochim Biophys Acta.* (2014) 1845:202–20. doi: 10.1016/j.bbcan.2014.01.003
36. Chen X, Duan N, Zhang C, Zhang W. Survivin and tumorigenesis: molecular mechanisms and therapeutic strategies. *J Cancer.* (2016) 7:314–23. doi: 10.7150/jca.13332
37. Grdina DJ, Murley JS, Miller RC, Mauceri HJ, Sutton HG, Li JJ, et al. A survivin-associated adaptive response in radiation therapy. *Cancer Res.* (2013) 73:4418–28. doi: 10.1158/0008-5472.CAN-12-4640
38. Iwasa T, Okamoto I, Suzuki M, Nakahara T, Yamanaka K, Hatashita E, et al. Radiosensitizing effect of YM155, a novel small-molecule survivin suppressant, in non-small cell lung cancer cell lines. *Clin Cancer Res.* (2008) 14:6496–504. doi: 10.1158/1078-0432.CCR-08-0468
39. Giannini L, Incandela F, Fiore M, Gronchi A, Stacchiotti S, Sangalli C, et al. Radiation-induced sarcoma of the head and neck: a review of the literature. *Front Oncol.* (2018) 8:449. doi: 10.3389/fonc.2018.00449
40. Wang Y, Song S, Su X, Wu J, Dai Z, Cui D, et al. Radiation-induced glioblastoma with rhabdoid characteristics following treatment for medulloblastoma: a case report and review of the literature. *Mol Clin Oncol.* (2018) 9:415–8. doi: 10.3892/mco.2018.1703
41. Kegelman TP, Wu B, Das SK, Talukdar S, Beckta JM, Hu B, et al. Inhibition of radiation-induced glioblastoma invasion by genetic and pharmacological targeting of MDA-9/Syntenin. *Proc Natl Acad Sci USA.* (2017) 114:370–5. doi: 10.1073/pnas.1616100114
42. Park CM, Park MJ, Kwak HJ, Lee HC, Kim MS, Lee SH, et al. Ionizing radiation enhances matrix metalloproteinase-2 secretion and invasion of glioma cells through Src/epidermal growth factor receptor-mediated p38/Akt and phosphatidylinositol 3-kinase/Akt signaling pathways. *Cancer Res.* (2006) 66:8511–9. doi: 10.1158/0008-5472.CAN-05-4340
43. Cui YH, Suh Y, Lee HJ, Yoo KC, Uddin N, Jeong YJ, et al. Radiation promotes invasiveness of non-small-cell lung cancer cells through granulocyte-colony-stimulating factor. *Oncogene.* (2015) 34:5372–82. doi: 10.1038/onc.2014.466
44. Wild-Bode C, Weller M, Rimner A, Dichgans J, Wick W. Sublethal irradiation promotes migration and invasiveness of glioma cells: implications for radiotherapy of human glioblastoma. *Cancer Res.* (2001) 61:2744–50.
45. Jung CH, Kim EM, Song JY, Park JK, Um HD. Mitochondrial superoxide dismutase 2 mediates gamma-irradiation-induced cancer cell invasion. *Exp Mol Med.* (2019) 51:1–10. doi: 10.1038/s12276-019-0207-5
46. Vehlow A, Cordes N. Invasion as target for therapy of glioblastoma multiforme. *Biochim Biophys Acta.* (2013) 1836:236–44. doi: 10.1016/j.bbcan.2013.07.001
47. Fiveash JB, Spencer SA. Role of radiation therapy and radiosurgery in glioblastoma multiforme. *Cancer J.* (2003) 9:222–9. doi: 10.1097/00130404-200305000-00010
48. Hay ED. An overview of epithelio-mesenchymal transformation. *Acta Anat.* (1995) 154:8–20. doi: 10.1159/000147748
49. Yadav A, Kumar B, Datta J, Teknos TN, Kumar P. IL-6 promotes head and neck tumor metastasis by inducing epithelial-mesenchymal transition via the JAK-STAT3-SNAIL signaling pathway. *Mol Cancer Res.* (2011) 9:1658–67. doi: 10.1158/1541-7786.MCR-11-0271
50. Rokavec M, Oner MG, Li H, Jackstadt R, Jiang L, Lodygin D, et al. IL-6R/STAT3/miR-34a feedback loop promotes EMT-mediated colorectal cancer invasion and metastasis. *J Clin Invest.* (2014) 124:1853–67. doi: 10.1172/JCI73531
51. Lamouille S, Xu J, Derynck R. Molecular mechanisms of epithelial-mesenchymal transition. *Nat Rev Mol Cell Biol.* (2014) 15:178–96. doi: 10.1038/nrm3758
52. Zhou YC, Liu JY, Li J, Zhang J, Xu YQ, Zhang HW, et al. Ionizing radiation promotes migration and invasion of cancer cells through transforming growth factor-beta-mediated epithelial-mesenchymal transition. *Int J Rad Oncol Biol Phys.* (2011) 81:1530–7. doi: 10.1016/j.ijrobp.2011.06.1956
53. Liu W, Huang YJ, Liu C, Yang YY, Liu H, Cui JG, et al. Inhibition of TBK1 attenuates radiation-induced epithelial-mesenchymal transition of A549 human lung cancer cells via activation of GSK-3beta and repression of ZEB1. *Lab Invest.* (2014) 94:362–70. doi: 10.1038/labinvest.2013.153
54. Xuan X, Li S, Lou X, Zheng X, Li Y, Wang F, et al. Stat3 promotes invasion of esophageal squamous cell carcinoma through up-regulation of MMP2. *Mol Biol Rep.* (2015) 42:907–15. doi: 10.1007/s11033-014-3828-8
55. Desmarais G, Charest G, Therriault H, Shi M, Fortin D, Bujold R, et al. Infiltration of F98 glioma cells in Fischer rat brain is temporary stimulated by radiation. *Int J Rad Biol.* (2016) 92:444–50. doi: 10.1080/09553002.2016.1175682
56. Wang SC, Yu CF, Hong JH, Tsai CS, Chiang CS. Radiation therapy-induced tumor invasiveness is associated with SDF-1-regulated macrophage mobilization and vasculogenesis. *PLoS ONE.* (2013) 8:e69182. doi: 10.1371/journal.pone.0069182
57. Birch JL, Strathdee K, Gilmour L, Vallatos A, McDonald L, Kouzeli A, et al. A novel small-molecule inhibitor of MRCK prevents

radiation-driven invasion in glioblastoma. *Cancer Res.* (2018) 78:6509–22. doi: 10.1158/0008-5472.CAN-18-1697
58. Unbekandt M, Croft DR, Crighton D, Mezna M, McArthur D, McConnell P, et al. A novel small-molecule MRCK inhibitor blocks cancer cell invasion. *Cell Commun Signal.* (2014) 12:54. doi: 10.1186/s12964-014-0054-x
59. Unbekandt M, Olson MF. The actin-myosin regulatory MRCK kinases: regulation, biological functions and associations with human cancer. *J Mol Med.* (2014) 92:217–25. doi: 10.1007/s00109-014-1133-6
60. Unbekandt M, Belshaw S, Bower J, Clarke M, Cordes J, Crighton D, et al. Discovery of potent and selective MRCK inhibitors with therapeutic effect on skin cancer. *Cancer Res.* (2018) 78:2096–114. doi: 10.1158/0008-5472.CAN-17-2870
61. Zhou W, Yu X, Sun S, Zhang X, Yang W, Zhang J, et al. Increased expression of MMP-2 and MMP-9 indicates poor prognosis in glioma recurrence. *Biomed Pharmacother.* (2019) 118:109369. doi: 10.1016/j.biopha.2019.109369
62. Yu YC, Yang PM, Chuah QY, Huang YH, Peng CW, Lee YJ, et al. Radiation-induced senescence in securin-deficient cancer cells promotes cell invasion involving the IL-6/STAT3 and PDGF-BB/PDGFR pathways. *Sci Rep.* (2013) 3:1675. doi: 10.1038/srep01675
63. Peng Y, Zhang M, Zheng L, Liang Q, Li H, Chen JT, et al. Cysteine protease cathepsin B mediates radiation-induced bystander effects. *Nature.* (2017) 547:458–62. doi: 10.1038/nature23284
64. Prise KM, O'Sullivan JM. Radiation-induced bystander signalling in cancer therapy. *Nat Rev Cancer.* (2009) 9:351–60. doi: 10.1038/nrc2603
65. Rzeszowska-Wolny J, Przybyszewski WM, Widel M. Ionizing radiation-induced bystander effects, potential targets for modulation of radiotherapy. *Eur J Pharmacol.* (2009) 625:156–64. doi: 10.1016/j.ejphar.2009.07.028
66. Duan C, Yang R, Yuan L, Engelbach JA, Tsien CI, Rich KM, et al. Late effects of radiation prime the brain microenvironment for accelerated tumor growth. *Int J Rad Oncol Biol Phys.* (2018) 103:190–4. doi: 10.1016/j.ijrobp.2018.08.033
67. Casey SC, Vaccari M, Al-Mulla F, Al-Temaimi R, Amedei A, Barcellos-Hoff MH, et al. The effect of environmental chemicals on the tumor microenvironment. *Carcinogenesis.* (2015) 36(Suppl. 1):S160–83. doi: 10.1093/carcin/bgv035
68. Paget S. The distribution of secondary growths in cancer of the breast. 1889. *Cancer Metastasis Rev.* (1989) 8:98–101.
69. Fidoamore A, Cristiano L, Antonosante A, d'Angelo M, Di Giacomo E, Astarita C, et al. Glioblastoma stem cells microenvironment: the paracrine roles of the niche in drug and radioresistance. *Stem Cells Int.* (2016) 2016:6809105. doi: 10.1155/2016/6809105
70. Zhang X, Ding K, Wang J, Li X, Zhao P. Chemoresistance caused by the microenvironment of glioblastoma and the corresponding solutions. *Biomed Pharmacother.* (2018) 109:39–46. doi: 10.1016/j.biopha.2018.10.063
71. Chang Q, Bournazou E, Sansone P, Berishaj M, Gao SP, Daly L, et al. The IL-6/JAK/Stat3 feed-forward loop drives tumorigenesis and metastasis. *Neoplasia.* (2013) 15:848–62. doi: 10.1593/neo.13706
72. Deng J, Liu Y, Lee H, Herrmann A, Zhang W, Zhang C, et al. S1PR1-STAT3 signaling is crucial for myeloid cell colonization at future metastatic sites. *Cancer Cell.* (2012) 21:642–54. doi: 10.1016/j.ccr.2012.03.039
73. Bohrer LR, Chuntova P, Bade LK, Beadnell TC, Leon RP, Brady NJ, et al. Activation of the FGFR-STAT3 pathway in breast cancer cells induces a hyaluronan-rich microenvironment that licenses tumor formation. *Cancer Res.* (2014) 74:374–86. doi: 10.1158/0008-5472.CAN-13-2469
74. Jones LM, Broz ML, Ranger JJ, Ozcelik J, Ahn R, Zuo D, et al. STAT3 establishes an immunosuppressive microenvironment during the early stages of breast carcinogenesis to promote tumor growth and metastasis. *Cancer Res.* (2016) 76:1416–28. doi: 10.1158/0008-5472.CAN-15-2770
75. Gao C, Kozlowska A, Nechaev S, Li H, Zhang Q, Hossain DM, et al. TLR9 signaling in the tumor microenvironment initiates cancer recurrence after radiotherapy. *Cancer Res.* (2013) 73:7211–21. doi: 10.1158/0008-5472.CAN-13-1314
76. Zhang X, Xu R, Zhang C, Xu Y, Han M, Huang B, et al. Trifluoperazine, a novel autophagy inhibitor, increases radiosensitivity in glioblastoma by impairing homologous recombination. *J Exp Clin Cancer Res.* (2017) 36:118. doi: 10.1186/s13046-017-0588-z
77. Campillo-Marcos I, Lazo PA. Olaparib and ionizing radiation trigger a cooperative DNA-damage repair response that is impaired by depletion of the VRK1 chromatin kinase. *J Exp Clin Cancer Res.* (2019) 38:203. doi: 10.1186/s13046-019-1204-1
78. Jiang M, Zhao L, Gamez M, Imperiale MJ. Roles of ATM and ATR-mediated DNA damage responses during lytic BK polyomavirus infection. *PLoS Pathog.* (2012) 8:e1002898. doi: 10.1371/journal.ppat.1002898
79. Yan S, Sorrell M, Berman Z. Functional interplay between ATM/ATR-mediated DNA damage response and DNA repair pathways in oxidative stress. *Cell Mol Life Sci.* (2014) 71:3951–67. doi: 10.1007/s00018-014-1666-4
80. Zhou BB, Elledge SJ. The DNA damage response: putting checkpoints in perspective. *Nature.* (2000) 408:433–9. doi: 10.1038/35044005
81. Zhang J, Willers H, Feng Z, Ghosh JC, Kim S, Weaver DT, et al. Chk2 phosphorylation of BRCA1 regulates DNA double-strand break repair. *Mol Cell Biol.* (2004) 24:708–18. doi: 10.1128/MCB.24.2.708-718.2004
82. Liu Q, Guntuku S, Cui XS, Matsuoka S, Cortez D, Tamai K, et al. Chk1 is an essential kinase that is regulated by Atr and required for the G(2)/M DNA damage checkpoint. *Genes Dev.* (2000) 14:1448–59. doi: 10.1101/gad.14.12.1448
83. Zhao H, Piwnica-Worms H. ATR-mediated checkpoint pathways regulate phosphorylation and activation of human Chk1. *Mol Cell Biol.* (2001) 21:4129–39. doi: 10.1128/MCB.21.13.4129-4139.2001
84. Zhang D, Tang B, Xie X, Xiao YF, Yang SM, Zhang JW. The interplay between DNA repair and autophagy in cancer therapy. *Cancer Biol Therapy.* (2015) 16:1005–13. doi: 10.1080/15384047.2015.1046022
85. Gao B, Shen X, Kunos G, Meng Q, Goldberg ID, Rosen EM, et al. Constitutive activation of JAK-STAT3 signaling by BRCA1 in human prostate cancer cells. *FEBS Lett.* (2001) 488:179–84. doi: 10.1016/S0014-5793(00)02430-3
86. Xu F, Li X, Yan L, Yuan N, Fang Y, Cao Y, et al. Autophagy promotes the repair of radiation-induced DNA damage in bone marrow hematopoietic cells via enhanced STAT3 signaling. *Rad Res.* (2017) 187:382–96. doi: 10.1667/RR14640.1
87. Barry SP, Townsend PA, Knight RA, Scarabelli TM, Latchman DS, Stephanou A. STAT3 modulates the DNA damage response pathway. *Int J Exp Pathol.* (2010) 91:506–14. doi: 10.1111/j.1365-2613.2010.00734.x
88. Vigneron A, Gamelin E, Coqueret O. The EGFR-STAT3 oncogenic pathway up-regulates the Eme1 endonuclease to reduce DNA damage after topoisomerase I inhibition. *Cancer Res.* (2008) 68:815–25. doi: 10.1158/0008-5472.CAN-07-5115
89. Weinandy A, Piroth MD, Goswami A, Nolte K, Sellhaus B, Gerardo-Nava J, et al. Cetuximab induces eme1-mediated DNA repair: a novel mechanism for cetuximab resistance. *Neoplasia.* (2014) 16:207–20. doi: 10.1016/j.neo.2014.03.004
90. Courapied S, Sellier H, de Carne Trecesson S, Vigneron A, Bernard AC, Gamelin E, et al. The cdk5 kinase regulates the STAT3 transcription factor to prevent DNA damage upon topoisomerase I inhibition. *J Biol Chem.* (2010) 285:26765–78. doi: 10.1074/jbc.M109.092304
91. Chen L, Fu L, Kong X, Xu J, Wang Z, Ma X, et al. Jumonji domain-containing protein 2B silencing induces DNA damage response via STAT3 pathway in colorectal cancer. *British J Cancer.* (2014) 110:1014–26. doi: 10.1038/bjc.2013.808
92. Pattabiraman DR, Weinberg RA. Tackling the cancer stem cells - what challenges do they pose? *Nat Rev Drug Discov.* (2014) 13:497–512. doi: 10.1038/nrd4253
93. Chen J, Li Y, Yu TS, McKay RM, Burns DK, Kernie SG, et al. A restricted cell population propagates glioblastoma growth after chemotherapy. *Nature.* (2012) 488:522–6. doi: 10.1038/nature11287
94. Eyler CE, Rich JN. Survival of the fittest: cancer stem cells in therapeutic resistance and angiogenesis. *J Clin Oncol.* (2008) 26:2839–45. doi: 10.1200/JCO.2007.15.1829
95. Li X, Lewis MT, Huang J, Gutierrez C, Osborne CK, Wu MF, et al. Intrinsic resistance of tumorigenic breast cancer cells to chemotherapy. *J Natl Cancer Inst.* (2008) 100:672–9. doi: 10.1093/jnci/djn123
96. Diehn M, Cho RW, Lobo NA, Kalisky T, Dorie MJ, Kulp AN, et al. Association of reactive oxygen species levels and radioresistance in cancer stem cells. *Nature.* (2009) 458:780–3. doi: 10.1038/nature07733

97. Marotta LL, Almendro V, Marusyk A, Shipitsin M, Schemme J, Walker SR, et al. The JAK2/STAT3 signaling pathway is required for growth of CD44(+)CD24(-) stem cell-like breast cancer cells in human tumors. *J Clin Invest.* (2011) 121:2723–35. doi: 10.1172/JCI44745
98. Schroeder A, Herrmann A, Cherryholmes G, Kowolik C, Buettner R, Pal S, et al. Loss of androgen receptor expression promotes a stem-like cell phenotype in prostate cancer through STAT3 signaling. *Cancer Res.* (2014) 74:1227–37. doi: 10.1158/0008-5472.CAN-13-0594
99. Sherry MM, Reeves A, Wu JK, Cochran BH. STAT3 is required for proliferation and maintenance of multipotency in glioblastoma stem cells. *Stem Cells.* (2009) 27:2383–92. doi: 10.1002/stem.185
100. Carro MS, Lim WK, Alvarez MJ, Bollo RJ, Zhao X, Snyder EY, et al. The transcriptional network for mesenchymal transformation of brain tumours. *Nature.* (2010) 463:318–25. doi: 10.1038/nature08712
101. Lee JH, Choi SI, Kim RK, Cho EW, Kim IG. Tescalcin/c-Src/IGF1Rbeta-mediated STAT3 activation enhances cancer stemness and radioresistant properties through ALDH1. *Sci Rep.* (2018) 8:10711. doi: 10.1038/s41598-018-29142-x
102. Shi Y, Guryanova OA, Zhou W, Liu C, Huang Z, Fang X, et al. Ibrutinib inactivates BMX-STAT3 in glioma stem cells to impair malignant growth and radioresistance. *Sci Transl Med.* (2018) 10:eaah6816. doi: 10.1126/scitranslmed.aah6816
103. Park SY, Lee CJ, Choi JH, Kim JH, Kim JW, Kim JY, et al. The JAK2/STAT3/CCND2 Axis promotes colorectal Cancer stem cell persistence and radioresistance. *J Exp Clin Cancer Res.* (2019) 38:399. doi: 10.1186/s13046-019-1405-7
104. Gao L, Sang JZ, Cao H. Limonin enhances the radiosensitivity of nasopharyngeal carcinoma cells via attenuating Stat3-induced cell stemness. *Biomed Pharmacother.* (2019) 118:109366. doi: 10.1016/j.biopha.2019.109366
105. Skvortsova I, Debbage P, Kumar V, Skvortsov S. Radiation resistance: cancer stem cells (CSCs) and their enigmatic pro-survival signaling. *Semin Cancer Biol.* (2015) 35:39–44. doi: 10.1016/j.semcancer.2015.09.009
106. Arnold KM, Opdenaker LM, Flynn NJ, Appeah DK, Sims-Mourtada J. Radiation induces an inflammatory response that results in STAT3-dependent changes in cellular plasticity and radioresistance of breast cancer stem-like cells. *Int J Radiat Biol.* (2020) 96:434–47. doi: 10.1080/09553002.2020.1705423
107. Ogawa K, Yoshioka Y, Isohashi F, Seo Y, Yoshida K, Yamazaki H. Radiotherapy targeting cancer stem cells: current views and future perspectives. *AntiCancer Res.* (2013) 33:747–54.
108. Turgeon MO, Perry NJS, Poulogiannis G. DNA damage, repair, and cancer metabolism. *Front Oncol.* (2018) 8:15. doi: 10.3389/fonc.2018.00015
109. Lindahl T. Instability and decay of the primary structure of DNA. *Nature.* (1993) 362:709–15. doi: 10.1038/362709a0
110. Sappington DR, Siegel ER, Hiatt G, Desai A, Penney RB, Jamshidi-Parsian A, et al. Glutamine drives glutathione synthesis and contributes to radiation sensitivity of A549 and H460 lung cancer cell lines. *Biochim Biophys Acta.* (2016) 1860:836–43. doi: 10.1016/j.bbagen.2016.01.021
111. Xiang L, Xie G, Liu C, Zhou J, Chen J, Yu S, et al. Knockdown of glutaminase 2 expression decreases glutathione, NADH, and sensitizes cervical cancer to ionizing radiation. *Biochim Biophys Acta.* (2013) 1833:2996–3005. doi: 10.1016/j.bbamcr.2013.08.003
112. Lu L, Dong J, Wang L, Xia Q, Zhang D, Kim H, et al. Activation of STAT3 and Bcl-2 and reduction of reactive oxygen species (ROS) promote radioresistance in breast cancer and overcome of radioresistance with niclosamide. *Oncogene.* (2018) 37:5292–304. doi: 10.1038/s41388-018-0340-y
113. Dan Dunn J, Alvarez LA, Zhang X, Soldati T. Reactive oxygen species and mitochondria: a nexus of cellular homeostasis. *Redox Biol.* (2015) 6:472–85. doi: 10.1016/j.redox.2015.09.005
114. Lapp DW, Zhang SS, Barnstable CJ. Stat3 mediates LIF-induced protection of astrocytes against toxic ROS by upregulating the UPC2 mRNA pool. *Glia.* (2014) 62:159–70. doi: 10.1002/glia.22594
115. Meier JA, Hyun M, Cantwell M, Raza A, Mertens C, Raje V, et al. Stress-induced dynamic regulation of mitochondrial STAT3 and its association with cyclophilin D reduce mitochondrial ROS production. *Sci Signal.* (2017) 10:eaag2588. doi: 10.1126/scisignal.aag2588
116. Gough DJ, Corlett A, Schlessinger K, Wegrzyn J, Larner AC, Levy DE. Mitochondrial STAT3 supports Ras-dependent oncogenic transformation. *Science.* (2009) 324:1713–6. doi: 10.1126/science.1171721
117. Wagner EF, Nebreda AR. Signal integration by JNK and p38 MAPK pathways in cancer development. *Nat Rev Cancer.* (2009) 9:537–49. doi: 10.1038/nrc2694
118. Cheng X, Peuckert C, Wolfl S. Essential role of mitochondrial Stat3 in p38(MAPK) mediated apoptosis under oxidative stress. *Sci Rep.* (2017) 7:15388. doi: 10.1038/s41598-017-15342-4
119. Chandel NS, McClintock DS, Feliciano CE, Wood TM, Melendez JA, Rodriguez AM, et al. Reactive oxygen species generated at mitochondrial complex III stabilize hypoxia-inducible factor-1alpha during hypoxia: a mechanism of O2 sensing. *J Biol Chem.* (2000) 275:25130–8. doi: 10.1074/jbc.M001914200
120. Chae YC, Vaira V, Caino MC, Tang HY, Seo JH, Kossenkov AV, et al. Mitochondrial Akt regulation of hypoxic tumor reprogramming. *Cancer Cell.* (2016) 30:257–72. doi: 10.1016/j.ccell.2016.07.004
121. Zhang C, Yang X, Zhang Q, Guo Q, He J, Qin Q, et al. STAT3 inhibitor NSC74859 radiosensitizes esophageal cancer via the downregulation of HIF-1alpha. *Tumour Biol.* (2014) 35:9793–9. doi: 10.1007/s13277-014-2207-3
122. Zhang Q, Zhang C, He J, Guo Q, Hu D, Yang X, et al. STAT3 inhibitor stattic enhances radiosensitivity in esophageal squamous cell carcinoma. *Tumour Biol.* (2015) 36:2135–42. doi: 10.1007/s13277-014-2823-y
123. Boengler K, Hilfiker-Kleiner D, Drexler H, Heusch G, Schulz R. The myocardial JAK/STAT pathway: from protection to failure. *Pharmacol Ther.* (2008) 120:172–85. doi: 10.1016/j.pharmthera.2008.08.002
124. Obana M, Maeda M, Takeda K, Hayama A, Mohri T, Yamashita T, et al. Therapeutic activation of signal transducer and activator of transcription 3 by interleukin-11 ameliorates cardiac fibrosis after myocardial infarction. *Circulation.* (2010) 121:684–91. doi: 10.1161/CIRCULATIONAHA.109.893677
125. Mair M, Zollner G, Schneller D, Musteanu M, Fickert P, Gumhold J, et al. Signal transducer and activator of transcription 3 protects from liver injury and fibrosis in a mouse model of sclerosing cholangitis. *Gastroenterology.* (2010) 138:2499–508. doi: 10.1053/j.gastro.2010.02.049
126. Wang P, Yang FJ, Du H, Guan YF, Xu TY, Xu XW, et al. Involvement of leptin receptor long isoform (LepRb)-STAT3 signaling pathway in brain fat mass- and obesity-associated (FTO) downregulation during energy restriction. *Mol Med.* (2011) 17:523–32. doi: 10.2119/molmed.2010.000134
127. Beebe JD, Liu JY, Zhang JT. Two decades of research in discovery of anticancer drugs targeting STAT3, how close are we? *Pharmacol Ther.* (2018) 191:74–91. doi: 10.1016/j.pharmthera.2018.06.006
128. Strittmatter SM. Overcoming drug development bottlenecks with repurposing: old drugs learn new tricks. *Nat Med.* (2014) 20:590–1. doi: 10.1038/nm.3595

Conflict of Interest: The authors declare that the research was conducted in the absence of any commercial or financial relationships that could be construed as a potential conflict of interest.

frontiers in Oncology

ORIGINAL RESEARCH
published: 17 July 2020
doi: 10.3389/fonc.2020.00990

RIG-1-Like Receptor Activation Synergizes With Intratumoral Alpha Radiation to Induce Pancreatic Tumor Rejection, Triple-Negative Breast Metastases Clearance, and Antitumor Immune Memory in Mice

*Vered Domankevich[1,2], Margalit Efrati[1,2], Michael Schmidt[2,3], Eran Glikson[1,4], Fairuz Mansour[1], Amit Shai[2], Adi Cohen[1], Yael Zilberstein[5], Elad Flaisher[2], Razvan Galalae[6,7], Itzhak Kelson[3] and Yona Keisari[1]**

[1] Department of Clinical Microbiology and Immunology, Sackler Faculty of Medicine, Tel Aviv University, Tel Aviv-Yafo, Israel, [2] Alpha Tau Medical, Tel Aviv-Yafo, Israel, [3] Sackler Faculty of Exact Sciences, School of Physics and Astronomy, Tel Aviv University, Tel Aviv-Yafo, Israel, [4] Department of Otolaryngology, Head and Neck Surgery, Sheba Medical Center, Tel HaShomer, Israel, [5] Sackler Cellular and Molecular Imaging Center, Sackler Faculty of Medicine, Tel Aviv University, Tel Aviv-Yafo, Israel, [6] MedAustron, Wiener Neustadt, Austria, [7] Medical Faculty, Christian-Albrechts University, Kiel, Germany

OPEN ACCESS

Edited by:
Carsten Herskind,
University of Heidelberg, Germany

Reviewed by:
Gabi Niedermann,
University of Freiburg, Germany
Zhenkun Lou,
Mayo Clinic, United States

***Correspondence:**
Yona Keisari
ykeisari@tauex.tau.ac.il

Specialty section:
This article was submitted to Radiation Oncology, a section of the journal Frontiers in Oncology

Received: 20 February 2020
Accepted: 19 May 2020
Published: 17 July 2020

Citation:
Domankevich V, Efrati M, Schmidt M, Glikson E, Mansour F, Shai A, Cohen A, Zilberstein Y, Flaisher E, Galalae R, Kelson I and Keisari Y (2020) RIG-1-Like Receptor Activation Synergizes With Intratumoral Alpha Radiation to Induce Pancreatic Tumor Rejection, Triple-Negative Breast Metastases Clearance, and Antitumor Immune Memory in Mice. Front. Oncol. 10:990. doi: 10.3389/fonc.2020.00990

Diffusing alpha-emitting radiation therapy (DaRT) employs intratumoral Ra-224-coated seeds that efficiently destroy solid tumors by slowly releasing alpha-emitting atoms inside the tumor. In immunogenic tumor models, DaRT was shown to activate systemic antitumor immunity. Agonists of the membrane-bound toll-like receptors (TLRs) enhanced these effects and led to tumor rejection. Here, we examined the combination of DaRT with agents that activate a different type of pattern recognition receptors, the cytoplasmatic RIG1-like receptors (RLRs). In response to cytoplasmatic viral dsRNA, RLRs activate an antiviral immune response that includes the elevation of antigen presentation. Thus, it was postulated that in low-immunogenic tumor models, RLR activation in tumor cells prior to the induction of their death by DaRT will be superior compared to TLR activation. Intratumoral cytoplasmatic delivery of the dsRNA mimic polyIC by polyethylenimine (PEI), was used to activate RLR, while polyIC without PEI was used to activate TLR. PolyIC(PEI) prior to DaRT synergistically retarded 4T1 triple-negative breast tumors and metastasis development more efficiently than polyIC and rejected panc02 pancreatic tumors in some of the treated mice. Splenocytes from treated mice, adoptively transferred to naive mice in combination with 4T1 tumor cells, delayed tumor development compared to naïve splenocytes. Low-dose cyclophosphamide, known to reduce T regulatory cell number, enhanced the effect of DaRT and polyIC(PEI) and led to high long-term survival rates under neoadjuvant settings, which confirmed metastasis clearance. The epigenetic drug decitabine, known to activate RLR in low doses, was given intraperitoneally prior to DaRT and caused tumor growth retardation, similar to local polyIC(PEI). The systemic and/or local administration of RLR activators was also tested in the squamous cell carcinoma (SCC) tumor model

SQ2, in which a delay in tumor re-challenge development was demonstrated. We conclude that RIG-I-like activation prior to intratumoral alpha radiation may serve as a potent combination technique to reduce both tumor growth and the spread of distant metastases in low-immunogenic and metastatic tumor models.

Keywords: PolyIC, polyethylenimine, decitabine, radiotherapy, immunotherapy, alpha radiation, triple-negative, breast carcinoma

INTRODUCTION

The destruction of the live tumor inside the host (namely, tumor ablation) releases tumor antigens to the tumor microenvironment and stimulates the activation of systemic and specific antitumor immune responses. Accordingly, tumor ablation can be considered as a form of "*in situ* vaccination" against tumor cells (1–4). Consequently, tumor ablation treatments may achieve two important goals simultaneously: [1] the destruction of the primary tumor and [2] the activation of antitumor immune responses against residual and distant tumor cells. This contrasts with surgical tumor resection, which achieves the first goal yet may suppress the second (5–7).

A unique radiotherapeutic tumor ablation technique utilizing the diffusion of alpha emitting atoms inside the tumor (diffusing alpha-emitters radiation therapy, referred to as DaRT henceforth) was shown to efficiently destroy a wide range of solid tumors, while sparing the adjacent tissues. This technique utilizes Radium (^{224}Ra)-loaded stainless-steel wires or tubes (DaRT seeds) that release daughter atoms inside the tumor to a range of several millimeters (8–14). DaRT was shown to activate systemic immune memory when used as a monotherapy (15, 16). When combined with immunoadjuvants and inhibitors of immune suppressive cells, DaRT led to long-term rejection of immunogenic tumors in mice, whereas the same immunomodulatory treatment with a non-radioactive seed mostly led to tumor recurrence (17, 18). Long-term rejection of tumors was correlated with a specific immune memory against tumor antigens (18), suggesting that cell death by alpha radiation activates tumor antigen recognition at the ablation site. This agrees with reports showing that the cell response to radiation includes the elevation of damage-associated molecular patterns (DAMPs) (19), MHC class I expression (20), and interferon responses (21) that may contribute to antigen presentation, cross presentation, APC activation, and recruitment of effector T lymphocytes (22).

Another type of *in situ* vaccination employs the activation of cytoplasmatic viral sensors such as RIG-I-like receptors (RLRs). RLRs (e.g., RIG-I and MDA5) sense cytoplasmatic viral dsRNA as part of a conserved defense mechanism of the innate immune system (22–24). Upon activation, these sensors promote antigen presentation, a type-1 interferon response, pyroptosis, DAMPs secretion, and immunogenic cell death (25). Recently, RLR activation was found to boost the efficiency of anticancer vaccines and to be critical for responsiveness to immune checkpoint blockade (26, 27).

One way to activate RLRs is to deliver a dsRNA viral mimic, such as polyIC, directly into the cytoplasm of the cell, while bypassing endosomal recognition via toll-like receptors, such as TLR3 (28). This is done using a delivery agent, such as the cationic polymer polyethylenimine (PEI), which masks the viral dsRNA until it reaches the cytoplasm, where it is released and recognized (29, 30). PolyIC cytoplasmic delivery was previously tested as a targeted therapy (26, 31), a systemic therapy (32, 33), and a local therapy (34). However, the effects of this treatment on distant metastases or in combination with radiotherapy have not been well-investigated. Interestingly, hallmarks of immunogenic cell death were observed in tumor cells following treatment with polyIC complexed with PEI, including the elevation of MHC class I expression. However, identical concentrations of polyIC (a TLR3 agonist) without PEI failed to elevate MHC class I expression (3), suggesting that the RLR pathway is superior to the TLR pathway with regard to antigen presentation on tumor cells following activation.

Another way to stimulate RLRs is by using DNA methyltransferase (DNMT) inhibitors such as decitabine (35). DNMT inhibitors can stimulate endogenous retroviruses that are sensed by RLRs (36–38) or inhibit the methylation of RLR genes promoters (35). RLR activation by both cytoplasmatic delivery of dsRNA (34) and DNMT inhibitors (39–41) was shown to upregulate MHC class I and to potentiate interferon and cytotoxic T lymphocyte responses.

Both alpha radiation-based ablation (16) and RLR activation (34) were shown to induce local tumor cell killing and a systemic antitumor response. It was shown that radiation-mediated antitumor immunity requires a cytosolic DNA-sensing pathway, such as the stimulator of interferon genes (STING) pathway (42). The fact that DNA-sensing and RNA-sensing function via different pathways may increase the potential to achieve a synergy between DaRT and RLR activation.

The current study investigated a novel approach to combine alpha radiation-based ablation and RLR activation in low-immunogenic and metastatic tumor models, such as the triple negative breast cancer (TNBC) mouse model 4T1, the pancreatic carcinoma tumor model Panc02, and the squamous cell carcinoma (SCC) tumor model, SQ2. Aggressive tumors such as TNBC and pancreatic cancer demonstrate low immunogenicity, which correlates with low responsiveness to immunotherapy and is mainly determined by tumor antigenicity and antigen presentation efficiency (43). MHC class I molecules on the surface of tumor cells were identified as critical for the enhancement of immunotherapy effectiveness (44). In support of this, it was recently demonstrated that antigens presented in the context of MHC class I, pulled down from tumor cell lysate, can serve as an artificial antigen presenting cell and induce potent and specific effector CD8+ T cell responses against tumor cells (45). In the current study, RLR activation was used long

enough prior to the induction of cell death by alpha radiation to allow the potential enhancement of antigen presentation on tumor cells, which may be crucial for achieving antigen-specific antitumor immunity in low-immunogenic tumors. The effect of the treatment on tumor development and on metastatic load was investigated by probing lung metastases at a late timepoint. In addition, long-term survival after local treatment and tumor resection was used to confirm clearance of metastases. Immune memory was investigated by employing the Winn and challenge assays. Finally, the treatment was combined with systemic immunomodulation.

MATERIALS AND METHODS

Animals

All animal experiments were carried out in accordance with the government and institution guidelines and regulations (Ethics approval IDs 01-18-030, 01-19-039, 01-19-081) and with the National Institutes of Health guide for the care and use of Laboratory animals (NIH Publications No. 8023, revised 1978). BALB/c and C57BL/6 female mice (∼20 g, 10 weeks old) were obtained from Envigo (Jerusalem, Israel) and were kept in the animal facility of Tel Aviv University. All surgical and invasive procedures were performed under anesthesia using ketamine (100 mg/kg, Bremer Pharma, Germany) and xylazine hydrochloride (10 mg/kg, Eurovet Animal Health B.V., Bladel, Netherlands) solution in PBS. Intraperitoneal inoculation was given 10 min before starting the treatment.

Tumor Cell Lines

All cell lines were incubated in a humid incubator at a temperature of 37°C and 5% CO_2. M-cherry-labeled 4T1 mammary adenocarcinoma tumor cells (kindly provided by Prof. Satchi-Fainaro, Faculty of Medicine, Tel Aviv University, Tel Aviv, Israel) were grown in RPMI-1640 containing L-glutamine, supplemented with 10% fetal calf serum, penicillin (100 U/ml), streptomycin (100 μg/ml), nystatin (12.5 U/ml), sodium pyruvate (1 mM), and HEPES buffer 1 M (Biological Industries, Kibbutz Beit Haemek, Israel). Panc02 murine pancreatic carcinoma (kindly provided by Dr. Hollingsworth, Eppley Institute, Nebraska University Medical Center, USA) were grown in Dulbecco's modified eagle medium (DMEM) supplemented with 10% fetal calf serum, penicillin (100 U/ml), streptomycin (100 μg/ml), nystatin (12.5 U/ml), sodium pyruvate (1 mM), and MEM Non-Essential Amino Acids (Biological Industries, Kibbutz Beit Haemek, Israel). SQ2 murine squamous cell carcinoma (kindly provided by Dr. Gad Lavie from the Sheba Medical Center, Tel HaShomer, Israel) were grown in Dulbecco's modified eagle medium (DMEM) supplemented with 10% fetal calf serum, penicillin (100 U/ml), streptomycin (100 μg/ml), and nystatin (12.5 U/ml) (Biological Industries, Kibbutz Beit Haemek, Israel).

Tumor Cell Inoculation

$4T1^{MCherry}$, SQ2, and panc02 tumor cells were inoculated in doses of 2.5×10^5, 5×10^5, and 6×10^5, respectively. Mice were inoculated intracutaneously into the right (unless stated otherwise) low lateral side of the back in 0.05 mL Hanks' balanced salt solution (HBSS, Biological Industries, Kibbutz Beit Haemek, Israel).

Drug Preparations

According to previous studies, high-molecular-weight (HMW) polyIC induced stronger immune activation than low-molecular-weight (LMW) polyIC (46) and was therefore chosen to be delivered into tumor cells in the current study. PolyIC HMW VacciGrade™ (InvivoGen, USA) was prepared in aliquots according to manufacturer instructions and kept at −20°C. At the day of treatment, polyIC was mixed with *in vivo*-jetPEI® (Polyplus, France) according to manufacturer instructions. Briefly, polyIC and PEI were diluted in 5% glucose solution and incubated at a ratio of N:P = 6 for 15 min at room temperature. PolyIC was intratumorally injected to the tumor 72 and 24 h prior to DaRT insertion. 5% glucose served as vehicle unless mentioned otherwise. Cyclophosphamide (Sigma C0768, Israel) was prepared at the indicated concentrations in saline solution. CP was administrated i.p. in the dose of 100 mg/kg 24 h prior to polyIC. Decitabine (Tocris, UK) was prepared in PBS. Decitabine was administrated i.p. in the dose of 1 mg/kg daily for 4 consecutive days prior to DaRT insertion.

^{224}Ra-Loaded Seed Preparation and Insertion

Stainless steel (316 LVM) 0.7-mm-diameter tubes in the length of 6.5 mm (unless mentioned otherwise) were loaded with ^{224}Ra atoms, following an electrostatic collection process similar to that described in (12). To prevent radium detachment from the surface, the seeds were coated, in this study, with a 250-nm (nanometer) polymeric layer (Nusil, med2-4213 model). The ^{220}Rn desorption probability (the probability that a ^{220}Rn atom is emitted from the seed following a decay of ^{224}Ra) was 45% (unless mentioned otherwise). The ^{224}Ra activity in kBq is indicated for each experiment in the Results section. Seeds, either loaded with ^{224}Ra or inert, were placed near the tip of a 19-gauge needle, which is attached to an insertion applicator. The radioactive and inert seeds were inserted into the tumor under anesthesia.

In vivo Tumor Measurements

Local tumor growth was determined by measuring 3 mutually orthogonal tumor dimensions 2–3 times per week, according to the following formula: Tumor volume = $\pi/6 \times$ Diameter 1 $\times$ Diameter 2$\times$ Height. Daily survival monitoring was performed and recorded.

Tumor and Metastasis Imaging and Analysis

CRI Maestro™ (Cambridge Research and Instrumentation, USA) was used to measure M-Cherry signal. Multispectral image cubes were acquired through a 550–800-nm spectral range in 10-nm steps using an excitation (595 nm longpass) and emission (645 nm longpass) filter set, under exposure time of 2,000 ms. Autofluorescence signals were eliminated by spectral analysis and linear unmixing algorithm of the CRI-Maestro software. Computed tomography (CT) scan was performed

using the TomoScope Synergy microCT scanner (CT imaging, Erlangen, Germany) under anesthesia. Data was acquired using 360° individual projection collected every 1° to complete one rotation around the animal, with X-ray tube voltage of 40 kV. Cross-sectional images (DICOM format) were generated using TomoScope image reconstruction software (CT imaging, Germany) and were analyzed using "RadiAnt" software.

Histology

For histological H&E staining, lungs were washed in PBS and fixed in a 4% formaldehyde solution (Bio-Lab, Jerusalem, Israel) for at least 24 h. The preserved specimens were processed in ethanol and xylene and then embedded in paraffin. Six-μm sections were then stained with hematoxylin (Sigma, Rehovot, Israel) and eosin (Surgipath, Richmond, VA, USA).

Winn Assay

Spleens were harvested, immersed in PBS, ground with the flat end of a syringe, and passed through a cell strainer. Cells were washed in RPMI/HBSS and centrifuged at 394 × g for 7 min. The supernatant was removed, and cells were resuspended and pooled. Red blood cells were lysed, and cells were washed in HBSS. Cells were then mixed with tumor cells in the indicated ratio and immediately injected in a volume of 0.15 ml.

Statistical Analysis

The difference between the mean values of two groups was determined by two-sided Student's T-test on the last day of the experiment, unless mentioned otherwise. The difference in the proportion of an event between two groups was determined by χ^2 test. Differences in the survival period between two groups were determined by log-rank test. $p < 0.05$ was considered as significant difference between groups.

RESULTS

Intratumoral polyIC^{PEI} and DaRT Synergistically Inhibit the Development of 4T1 Solid Tumors and Metastases

A previous study done in the immunogenic tumor model CT26 has shown that combining DaRT with TLR agonists led to long-term tumor rejection, which was not observed when DaRT was used alone (18). Here, it was investigated whether in the low-immunogenic tumor model 4T1 using RLR activation in combination with DaRT is superior to TLR activation, and whether this combination is synergistic in terms of long-term local and systemic retardation of tumor development. To answer these questions, intratumoral administration of the dsRNA viral mimic, polyIC, was used in two forms, as follows. Either complexed with the delivery polymer PEI (polyIC^{PEI}) to enable the cytoplasmatic delivery of polyIC and the activation of the RIG-1 receptor MDA5 (47) or "Naked" polyIC (polyIC^{naked}), which agonizes the toll-like receptor TLR3 (48).

Mice bearing 4T1 tumors were treated by an intratumoral injection of 20 μg/40 μl polyIC^{PEI}, polyIC^{naked}, or PBS followed by the insertion of a single DaRT seed (length = 8 mm, activity =70 kBq) or a non-radioactive (inert) seed. Twenty-nine days after treatment started, lungs were scanned by computed tomography (CT). The experiment was terminated 37–38 days following tumor cell inoculation, and lungs were imaged for M-Cherry fluorescent signal (**Figures 1A,B**).

The results indicated that DaRT combined with polyIC^{PEI} significantly retarded tumor growth ($p_{t-test} < 0.05$) compared to all other groups (**Figures 1C–E**). The percent reduction in tumor volume compared to inert+vehicle control was calculated for each treatment (according to the following formula: [(mean tumor volume at day 29 in the treatment group)/(mean tumor volume at day 29 of control group)−1] × 100). The cytoplasmatic delivery of polyIC treatment on its own reduced tumor size by 26% compared to inert+vehicle (control). Alpha radiation treatment on its own reduced tumor size by up to about 34% compared to control. The combination of alpha radiotherapy and cytoplasmatic delivery of the viral mimic polyIC reduced the tumor size by 82%, demonstrating a synergistic effect between the treatments. Treatment with DaRT+polyIC^{naked} significantly retarded tumor growth compared to DaRT alone or inert+vehicle control (**Figures 1C,E**). However, the treatment was significantly less effective compared to DaRT combined with polyIC^{PEI}.

Analysis of lung metastases by CT scan or M-Cherry fluorescence imaging (see Methods, **Figure 2A**) revealed that 37 days after tumor inoculation, the percent of animals bearing lung metastases was significantly smaller in the polyIC^{PEI}+DaRT group (23%) compared to DaRT alone (77%) or inert+vehicle control (75%), p (χ^2 test) < 0.05 (**Figure 2B**). DaRT+polyIC^{naked} also reduced metastatic burden, as demonstrated by total M-Cherry signal in the lungs (**Figure 2C**). However, a higher number of mice treated with DaRT+polyIC^{naked} were positive for metastases than those treated with DaRT+polyIC^{PEI} (55% compared with 23%). Histology sections of lungs correlated with the findings obtained by M-Cherry and CT (**Figure 2D**).

Treatment With Intratumoral polyIC^{PEI} Prior to DaRT Caused Rejection of Panc02 Solid Tumors

The robustness of this treatment was tested by applying it to another aggressive and metastatic tumor model, the pancreatic tumor cell line Panc02. Mice bearing Panc02 tumors were treated with polyIC^{PEI} (25 μg/50 μl), followed by the insertion of a DaRT seed (75 kBq). On the seed insertion day, average tumor volume was ∼35 mm^3.

DaRT+polyIC^{PEI} significantly retarded tumor growth compared with DaRT (12-fold change on day 24 post-DaRT) (**Figure 3A**). Moreover, the treatment caused tumor rejection in 42.9% (3 out of 7) of the animals for up to 38 days following DaRT upper panel (**Figure 3B**). At this timepoint, one tumor recurred and 2 out of 7 mice remained tumor-free and survived from this timepoint on, with no signs of illness. Tumors that were not rejected developed more slowly in the DaRT+polyIC^{PEI} group relative to the DaRT group (**Figures 3C,D**).

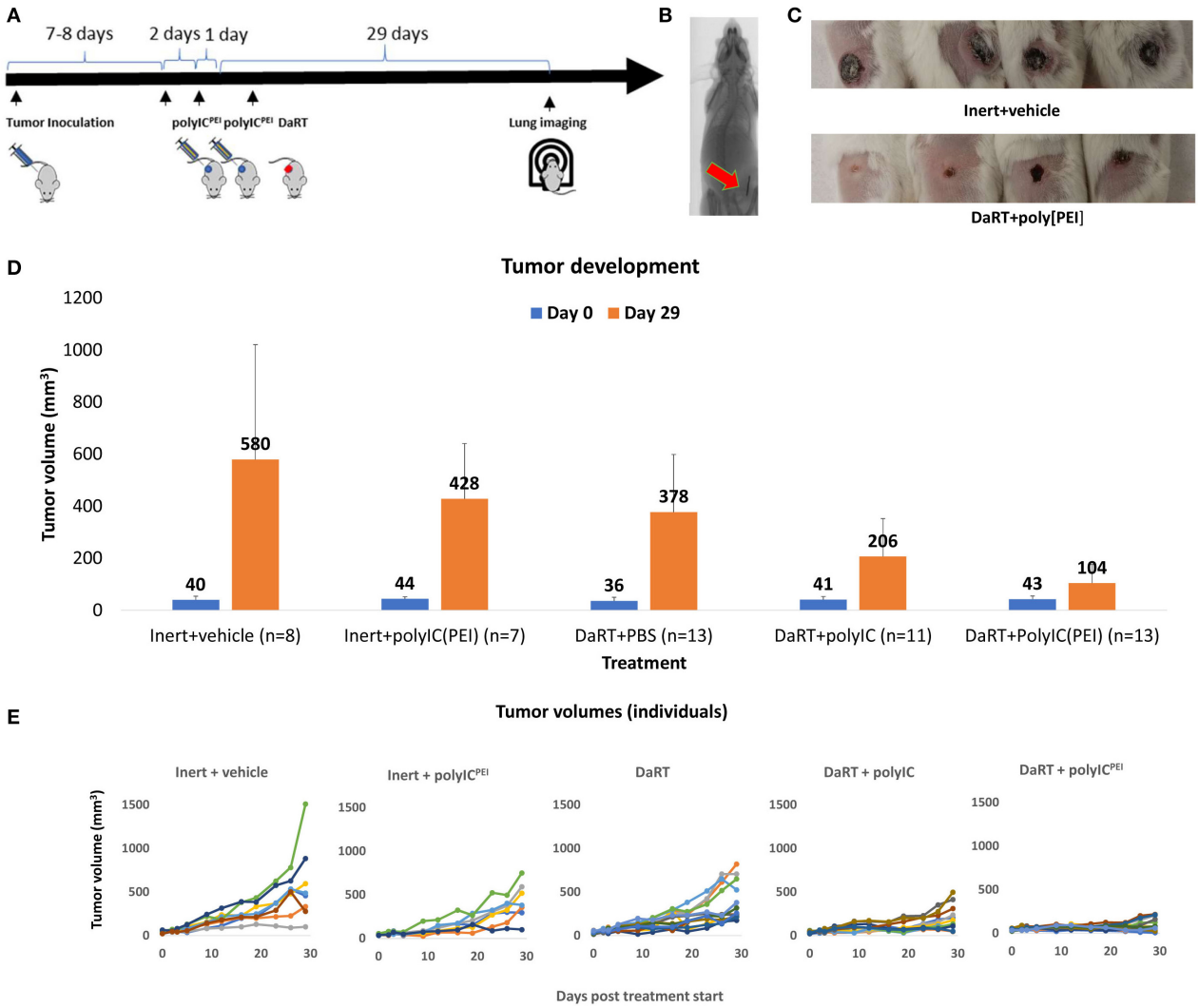

FIGURE 1 | Primary tumor growth following treatment with DaRT+polyIC^{PEI}. 4T1-bearing mice (40 mm^3) were treated intratumorally with polyIC^{PEI} (20 μg/40 μl) or polyIC^{naked} (20 μg/40 μl) or vehicle, 72 and 24 h prior to the insertion of a single DaRT seed (length = 8 mm, activity = 70 kBq) or an inert seed (for 29 days). **(A)** Schematic representation of the treatment protocol. **(B)** CT image of a DaRT seed inside the tumor. **(C)** Representative primary tumors 29 days after tumor cell inoculation. **(D)** Mean tumor volumes ± SEM on the day of treatment start (0) and on the day of experiment termination (29). $p_{t-test} < 0.005$ for DaRT+ polyIC^{PEI} vs. control; $p_{t-test} < 0.0005$ for DaRT+ polyIC^{PEI} vs. DaRT alone; $p_{t-test} < 0.0005$ for DaRT+ polyIC^{PEI} vs. polyIC^{PEI} alone; $p_{t-test} < 0.05$ for DaRT+ polyIC^{PEI} vs. DaRT+polyIC^{naked}. **(E)** Individual tumor growth curves for each treatment, up to 29 days from treatment start. Each line represents an individual mouse. The results are based on cumulative data from two different experiments.

Splenocytes From Mice Pretreated With Intratumoral polyIC^{PEI} and DaRT Inhibit 4T1 Tumor Development When Adoptively Transferred to Naïve Mice

The results above showed that even though polyIC^{PEI}+DaRT therapy was administrated locally, at the primary tumor site only, it led to both long-term tumor growth retardation and clearance of distant metastases. The Winn assay was employed to investigate whether the treatment activated a long-term systemic immune memory against tumor antigens. In this *in vivo* cytotoxic test, splenocytes from treated mice or from naïve mice are adoptively transferred to naïve mice in combination with tumor cells, and tumor development is monitored.

Mice (n = 16) bearing 4T1 tumors (30 mm^3) were treated with polyIC^{PEI}+DaRT (as depicted in **Figure 1A**). Residual tumors were resected 24 days following tumor cell inoculation (at a time in which metastases were already present in the lungs), and animals were observed for long-term survival (namely, metastases-related death). Mice surviving for 9 months after tumor inoculation were considered as cured, and their splenocytes were used for an adoptive cell transfer assay

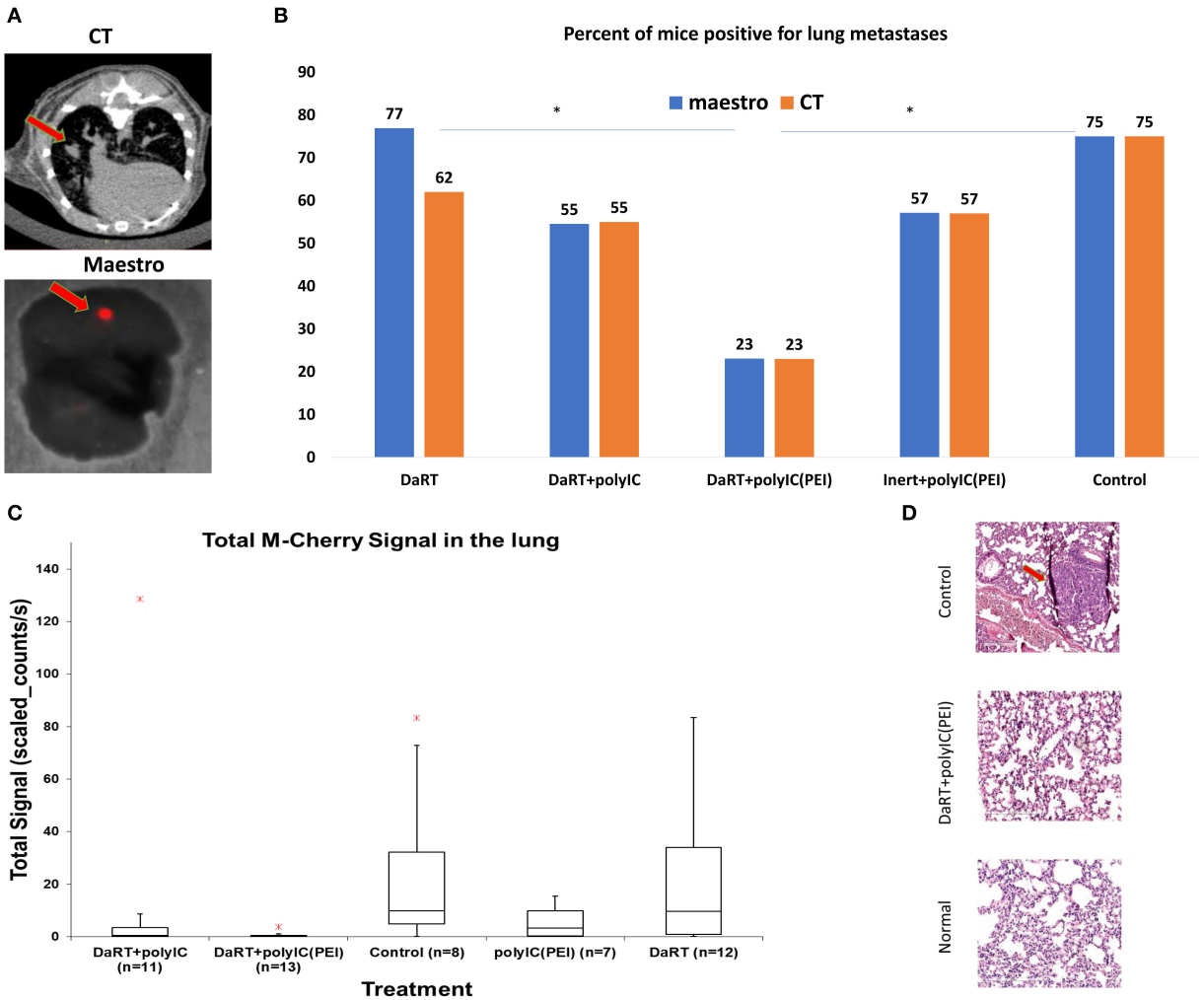

FIGURE 2 | Lung metastases following treatment with DaRT+polyIC^{PEI}. 4T1^{MCherry}-bearing mice were treated intratumorally with polyIC^{PEI}, polyIC^{naked}, or vehicle, prior the insertion of a single DaRT seed or an inert seed (see **Figure 1A**). Lungs were imaged by CT and fluorescence imaging using Maestro, 37 days following tumor cell inoculation. **(A)** Illustrative pictures of metastases as imaged by CT scan or M-Cherry fluorescence imaging. **(B)** Percent of mice that were positive for lung metastases according to CT scan and M-Cherry fluorescence imaging. **(C)** Box plot of M-cherry total signal in the lungs. Red cross denotes an outlier (the graph does not include a DaRT outlier with the value of 362 counts/s). **(D)** Representative histology sections of a normal lung, a lung of a 4T1-bearing mouse treated with DaRT+polyIC^{PEI}, and a lung of a 4T1-bearing mouse treated with inert+vehicle. The results are based on cumulative data from two different experiments.

(Winn assay). Autopsy of non-surviving mice confirmed lung metastases in all animals (except one animal which had an inflamed lung without visible metastases). Lymphocytes from the spleens of cured mice ($n = 4$) were harvested, pooled, mixed with 2.5×10^5 4T1 tumor cells in a ratio of 100:1 (splenocytes: tumor cells), and inoculated into naïve mice. Splenocytes of naïve mice ($n = 4$) served as control (**Figure 4A**).

Splenocytes of treated mice significantly retarded tumor development compared to splenocytes of naïve mice (**Figure 4B**). A significant reduction in tumor size lasted for 19 days after co-inoculation with tumor cells (52% reduction was evident 14 days after co-inoculation, $p_{t-test} = 0.002$: 42 ± 8 and 87 ± 8 mm^3 for immune vs. naïve splenocytes, respectively), demonstrating that the treatment induced a long-term antitumor immune memory that is efficient even 9 months following the initial tumor cell inoculation.

Systemic Low-Dose Cyclophosphamide Combined With Intratumoral polyIC^{PEI} Synergizes With DaRT in Preventing Lung Metastases-Related Death

Next, it was investigated whether systemic immunomodulation could further augment tumor growth retardation caused by polyIC^{PEI}+DaRT treatment or prolong mouse survival by preventing metastasis-related death. To reduce the number of T regulatory cells (Tregs), a previously proven treatment regimen

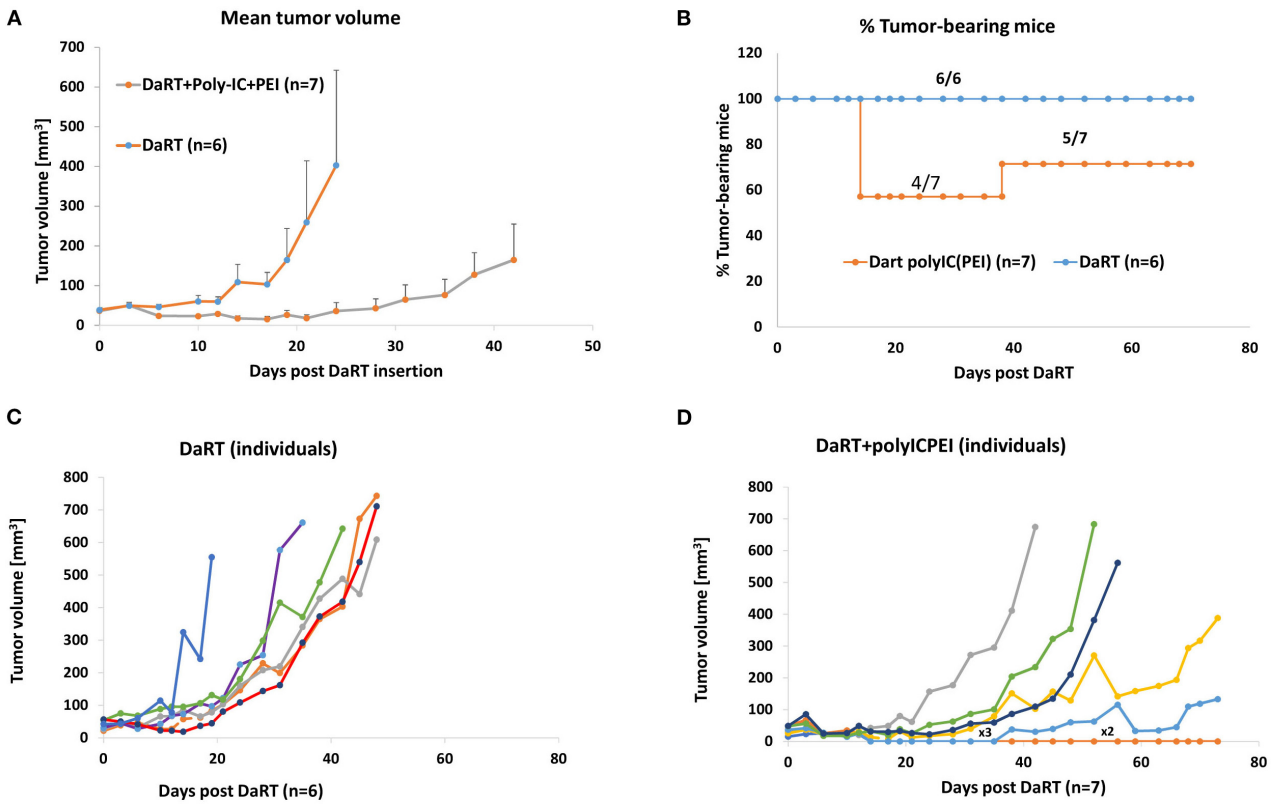

FIGURE 3 | DaRT+polyIC^{PEI} treatment rejected Panc02 tumors. Panc02-bearing mice were treated with an intratumoral injection of polyIC^{PEI} (25 μg /50 μl) 72 and 24 h prior DaRT seed insertion (activity=75 kBq). **(A)** Tumor volume ± SEM. **(B)** The percent of tumor-bearing mice. **(C,D)** Individual tumor development of mice treated with DaRT+polyIC^{PEI} (left) or DaRT+vehicle (right). Each line represents an individual mouse. "x3" denotes a line representing three individuals; "x2" denotes a line representing two individuals.

of low-dose CP was employed (49). 4T1-bearing mice were treated with CP 1 day before the first polyIC^{PEI} injection (30 μg/60 μl), which is 4 days prior to DaRT insertion (activity = 65 kBq), at a time in which tumor size was ∼24 mm^3. DaRT+polyIC^{PEI}+vehicle served as a control. Tumor development was followed for 14 days after DaRT insertion, and the tumors were resected thereafter (**Figure 5A**). In order to examine the effect of the treatments on lung metastases in the above treated animals, monitoring was done for metastases-related death for ∼6 months post DaRT, and animal death and the presence of lung metastases were recorded.

Adding CP to DaRT+polyIC^{PEI} treatment significantly reduced tumor volume on the day of tumor resection (47 ± 5, 29 ± 3 mm^3, $p_{t-test} < 0.05$). The manual measurements of tumor dimensions by a caliper were corroborated with M-cherry fluorescence imaging of the resected tumors. This analysis confirmed that total M-cherry signal and the tumor area (according to M-Cherry fluorescence) where smaller in the polyIC^{PEI}+DaRT+CP group compared to the polyIC^{PEI}+DaRT group (83 ± 23 vs. 693 ± 280 scaled counts/s, $p_{t-test} = 0.051$; 65 ± 14 vs. 163 ± 20 mm^2, $p_{t-test}t < 0.005$, respectively).

Adding CP to polyIC^{PEI}+DaRT treatment extended the survival period relative to treatment with polyIC^{PEI}+DaRT without CP. During the 143 days post DaRT insertion, 100% of the animals treated with polyIC^{PEI}+DaRT+CP were still alive, at the same timepoint only 71% of the mice treated with polyIC^{PEI}+DaRT survived. Nonetheless, the difference between the groups according to log-rank test was not significant and at the end of the experiment identical survival rates (71.4%) were observed in both groups.

Next, an additional experiment was conducted to explore the contribution of DaRT alone (85 kBq) or immunotherapy alone by CP+polyIC^{PEI} (30 μg/60 μl i.t.) relative to the combined treatment. PolyIC^{PEI}+CP+inert seed or DaRT+vehicle significantly retarded tumor development compared to inert+vehicle control (p_{t-test} <0.05, on the day of resection) (**Figures 5B,C**). The combined treatment using DaRT+polyIC^{PEI}+CP was significantly more effective than all other treatments (**Figure 5C**). Ten days post DaRT, for example, tumor volume in the control (inert+vehicle) group was 2.5-fold higher than DaRT only group (DaRT+vehicle), and 3.1-fold higher than that in the immunotherapy-only group (polyIC^{PEI}+CP+inert). On that same day, the control group was 6.2-fold higher than the combination treatment (DaRT+polyIC^{PEI}+CP), which is more than the expected additive effect (5.6-fold).

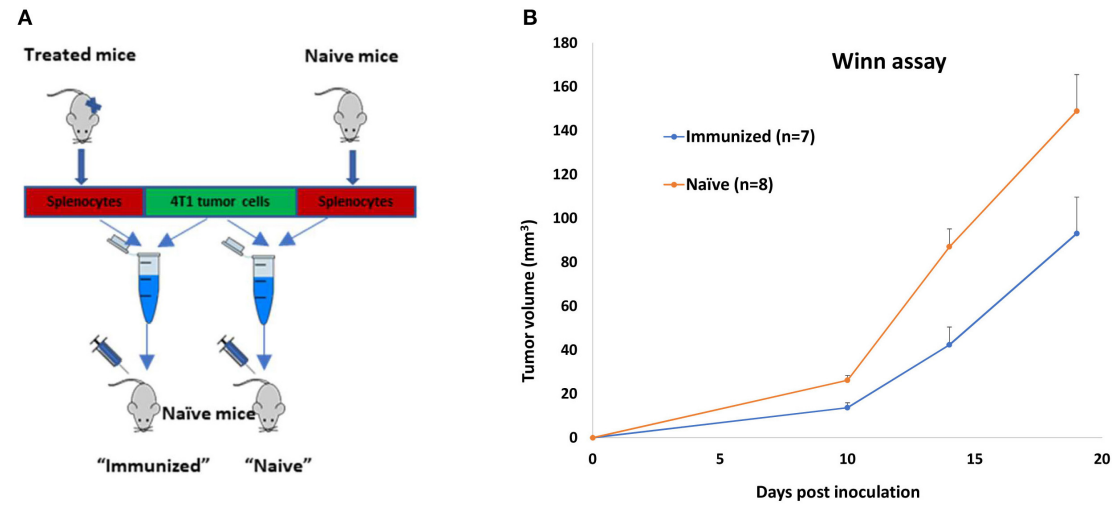

FIGURE 4 | Long-term immune memory in 4T1-bearing mice treated by polyICPEI+DaRT and surgery. 4T1-bearing mice ($n = 16$) were treated by intratumoral 20 μg/40 μl polyIC^{PEI} or vehicle 72 and 24 h prior the insertion of a single DaRT seed (7 mm, 80 kBq). Twenty-four days after tumor cell inoculation, tumors were resected. Mice surviving 9 months after initial tumor cell inoculation ($n = 4$) or naïve mice ($n = 4$) were sacrificed, and their splenocytes were pooled and mixed with 4T1 tumor cells in the ratio of 100:1 (splenocytes: tumor cells). The combined suspension was inoculated into naïve mice. **(A)** Winn assay scheme. **(B)** Mean tumor volume ± SEM, $p_{t-test} < 0.05$ for immunized vs. naïve groups.

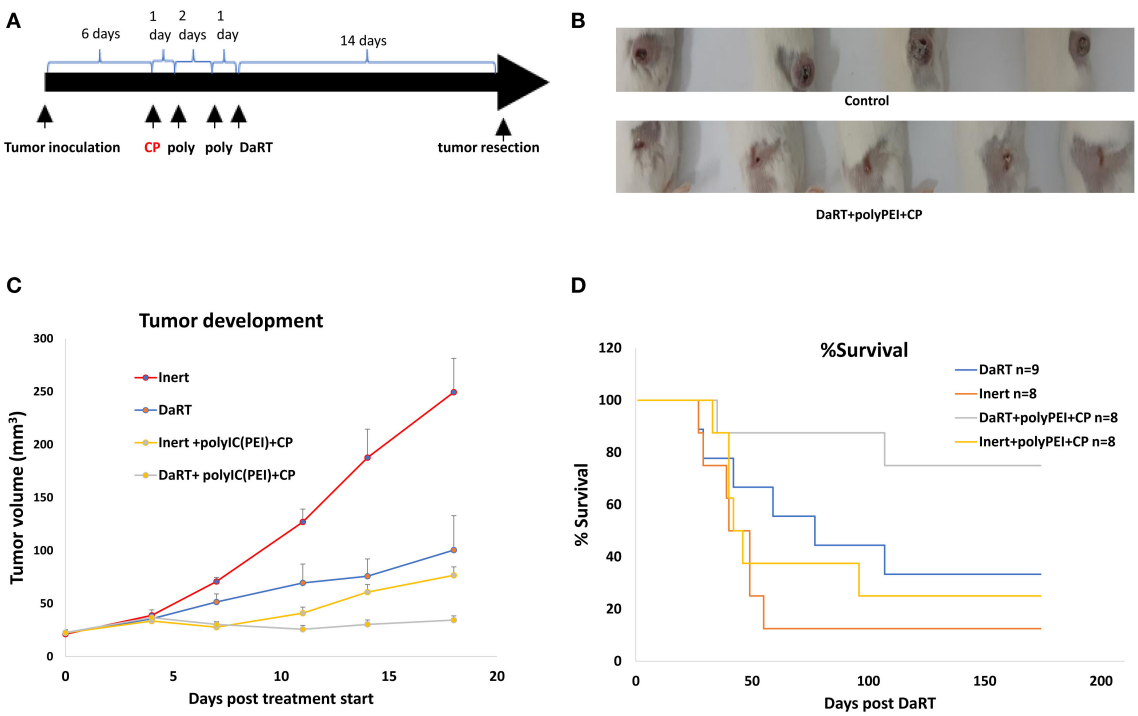

FIGURE 5 | The effect of systemic low-dose CP in combination with local polyIC^{PEI}+DaRT on tumor development and metastasis-related death. **(A)** Schematic representation of the treatments with low-dose cyclophosphamide combined with DaRT+polyIC^{PEI} and tumor resection. **(B)** Representative tumors on the day of tumor resection. **(C)** Mice were treated with CP (100 mg/kg, i.p.) combined with polyIC^{PEI} (30 μg/60 μl i.t.) + DaRT (activity = 85 kBq). Presented are tumor volume ± SEM. $P_{t-test} < 0.05$ for DaRT+polyIC^{PEI}+CP compared all other treatments. **(D)** Kaplan–Meier survival curves of tumor-resected mice following treatment. $P_{log-ranktest} < 0.01$; <0.05, for DaRT+ polyIC^{PEI}+CP vs. inert+vehicle control or polyIC^{PEI}+CP, respectively.

At the end of the follow-up period, 75% (6/8) of the mice treated with DaRT+polyIC^{PEI}+CP survived, whereas lower survival rates were obtained by DaRT+vehicle (33%, 3/9), inert+polyIC^{PEI}+CP (25%, 2/8), or inert+vehicle (12%, 1/8) treatments (**Figure 5D**). Autopsies of non-surviving animals confirmed metastasis-related death. The effect of DaRT+polyIC^{PEI}+CP was significant compared to inert+vehicle ($p_{log-rank\ test} < 0.01$) and compared to

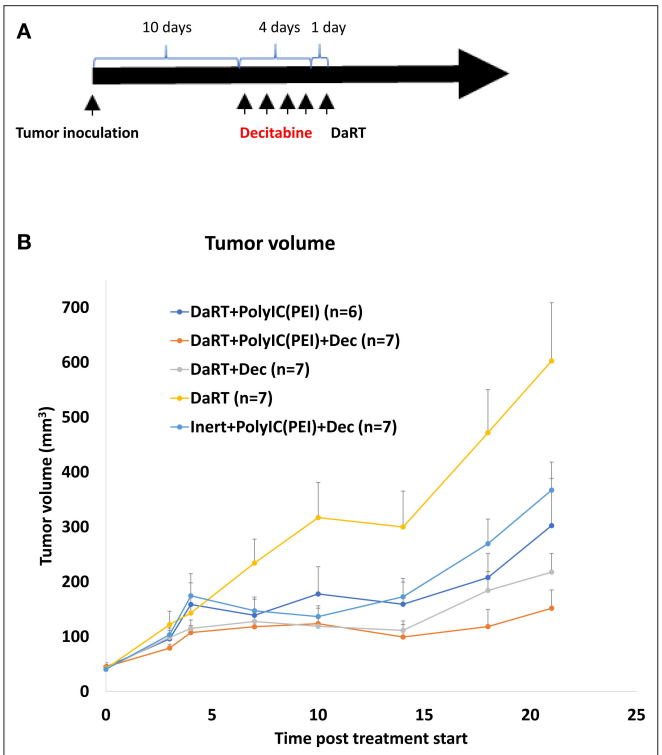

FIGURE 6 | Effect of DaRT combined with decitabine and/or polyIC^{PEI} on 4T1 tumor development. Mice bearing 4T1 tumors (40 mm^3) were treated with a DaRT seed (75 kBq) in combination with decitabine (1 mg/kg i.p. for 4 consecutive days prior to DaRT) and/or polyIC^{PEI} (30 μg/60 μl, 72 h prior to DaRT and 50 μg/100 μl polyIC^{PEI}, 24 h prior DaRT). **(A)** Schematic representation of the treatment by decitabine. **(B)** Presented are the tumor volumes ± SEM.

inert+polyIC^{PEI}+CP ($p_{\log-rank\ test}$ <0.05), but not compared to DaRT alone ($p_{\log-rank\ test}$ =0.081).

Systemic Low-Dose Decitabine Combined With DaRT Retarded the Growth of 4T1 Tumors

It was then investigated whether systemic low-dose administration of the epigenetic drug decitabine (37), which is known to activate RLR, will strengthen tumor growth retardation induced by DaRT, similar to locally administered polyIC^{PEI}. This question is of special therapeutic importance, because decitabine can be administrated systematically to patients.

Mice bearing 4T1 tumors (40 mm^3) were treated with polyIC^{PEI} (30 μg/60 μl 72 h prior to DaRT and 50 μg/100 μl 24 h prior to DaRT) and/or decitabine (1 mg/kg i.p. daily for 4 consecutive days) prior to the insertion of a DaRT seed (activity = 75 kBq) (**Figure 6A**).

DaRT combined with decitabine significantly reduced tumor size by 64% compared to DaRT alone, similar to the 50% reduction achieved by DaRT+polyIC^{PEI} (**Figure 6B**). DaRT combined with both decitabine and polyIC^{PEI} achieved the strongest effect (75% reduction compared with DaRT alone, p_{t-test} = 0.001), yet it was only marginally better than DaRT with each stimulator alone. In addition, it was demonstrated that DaRT+decitabine+polyIC^{PEI} was significantly stronger (2.5-fold) compared to the same treatment with a non-radioactive seed (**Figure 6B**). These results were confirmed in an additional experiment in which mice were bearing larger tumors (85 mm^3 at the day of treatment start). Tumor volume determined at the same timepoint for inert or DaRT, combined with polyIC^{PEI} and decitabine, was 194 ± 25 vs. 115 ± 16 mm^3, respectively, p_{t-test} < 0.05).

DaRT Combined With Systemic Low-Dose Decitabine or Intratumoral polyIC^{PEI} Inhibited the Growth of SQ2 Solid Tumors and Induced Antitumor Immune Response Against Tumor Cell Re-challenge

To further test the robustness of these treatment regimens, including their ability to induce an antitumor systemic immune memory, a tumor model of squamous cell carcinoma (SCC), SQ2, was investigated. SCC was the first type of tumor for which DaRT was tested in human patients (50). SQ2-bearing mice were treated with DaRT (85 kBq) combined with polyIC^{PEI} (25 μg /50 μl), decitabine, or both. Residual tumors were resected 24 days after DaRT, and mice were subjected to tumor re-challenge of the same number of cells (5 × 10^5 tumor cells), 22 days after tumor resection.

DaRT combined with polyIC^{PEI}, decitabine, or both significantly retarded tumor development compared to DaRT alone. DaRT+decitabine significantly retarded tumor development similar to DaRT+polyIC^{PEI}, leading to a ∼65% reduction in tumor size compared to DaRT+vehicle treatment, for up to 27 days from treatment initiation. In this tumor model, the combination of DaRT+polyIC^{PEI}+decitabine provided the best results with 92% reduction (20-fold change) compared to DaRT alone and was significantly superior to both DaRT+decitabine or DaRT+polyIC^{PEI} (**Figure 7A**). DaRT combined with polyIC^{PEI}, decitabine, or both preserved the ability to induce long-term immune memory, as demonstrated by a significant reduction (∼80%) in tumor size after re-challenge, compared to naïve mice inoculated with the same number of tumor cells (**Figure 7B**).

DISCUSSION

In the present study, we examined the possible synergy between the activation of cytoplasmatic dsRNA sensors and tumor ablation by intratumoral diffusion of alpha emitting atoms, both at the local and systemic levels. Treatment with DaRT in combination with cytoplasmatic delivery of polyIC synergistically retarded the development of mouse TNBC tumors and demonstrated rejection of mouse pancreatic tumors. Although the treatment was administrated locally, it also reduced the metastatic load in the lungs and induced a long-term systemic antitumor immune response. Low-dose CP, which was previously shown to reduce the number of Tregs (49), enhanced the tumor control achieved by the local treatment and led to high long-term survival rates that confirmed the reduction in metastatic load.

DaRT-related antitumor immunity (16) was previously attributed to the *in situ* dispersion of tumor antigens, processed

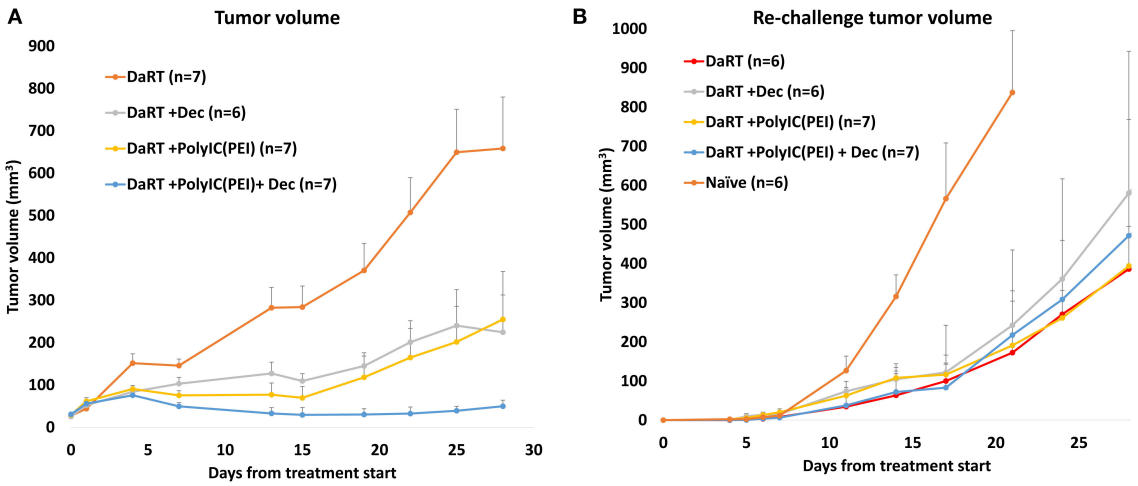

FIGURE 7 | Tumor control and long-term immune memory following treatment with DaRT, decitabine, polyIC^{PEI}, or both, in SQ2 tumor model. **(A)** SQ2-bearing mice (30 mm^3 on first decitabine dose day) were treated with decitabine (1 mg/kg i.p. daily for 4 consecutive days prior to the DaRT) and/or an intratumoral injection of polyIC^{PEI} (25 μg/50 μl 72 and 24 h prior to DaRT). A DaRT (activity=85 kBq) seed was inserted into the tumor 24 h later. Presented are the tumor volumes ± SEM. $P_{t-test} < 0.05$ for all treatments vs. DaRT and for DaRT+decitabine+polyIC^{PEI} vs. DaRT+decitabine. **(B)** Residual tumors were resected 24 days after DaRT and mice were subjected to tumor re-challenge of 5×10^5 tumor cells 21 days after tumor resection. Presented are the tumor volumes ± SEM of the re-challenged tumors. Significant difference was observed for all groups vs. naïve mice ($P_{t-test} < 0.05$, on day 17). *On day 17 one mouse from the DaRT+decitabine+polyIC^{PEI} group died from unknown reason and was not included in the mean tumor volume calculation from this time point on.

by APCs (4). Addition of TLR agonists (16–18) that activate APCs enhanced DaRT's effect. In the current study, combining DaRT with polyIC, complexed with the delivery reagent PEI (PolyIC^{PEI}), led to more robust solid tumor control and greater clearance of metastases relative to the same treatment with polyIC only (a TLR3 agonist by itself). This finding suggests that polyIC^{PEI} may exhibit a dual effect, both augmenting antigen presentation by tumor cells (via RLR) and antigen presentation by dendritic cells (via TLR).

The use of DaRT after polyIC^{PEI} may consequently lead to the release of DAPMs after DNA damage, pathogen-associated molecular patterns (PAMPs) from radiation killed cells containing dsRNA, and a massive amount of tumor antigens in the context of MHC class I. This may support important processes such as cross-presentation and cross-dressing (51). In addition, the potential elevation of MHC class I on tumor cells by PolyIC^{PEI} (34) prior to cell death by DaRT may increase the probability to present yet non-presented tumor antigens in the context of MHC class I. Thus, it can be speculated that PolyIC^{PEI}-treated, and alpha-radiation-killed, tumor cells may release such MHC class I-antigen complexes, which can be picked up by DCs that in turn present them to CD8+ T cells and help to expand the number of clones recognizing tumor antigens.

In this study, it was shown that DaRT combined with different types of agents known to activate RLR achieved robust antitumor effects in three tumor models. Low-dose decitabine resulted in tumor retardation, similar to polyIC^{PEI}. In the SCC tumor model, adding decitabine, polyIC^{PEI}, or both reduces tumor size compared to DaRT, yet in the challenge assay, the addition of RLR activation did not affect the power of the long-term immune response relative to DaRT alone (**Figure 7B**). This may be due to the relatively high number of tumor cells used in the assay. Another possibility is that cells inoculated in the challenge assay were not subjected to a treatment that elevates antigen presentation before inoculation. Namely, antigens that were potentially unmasked by RLR activation *in situ* were not presented by the tumor cells inoculated in the challenge assay, since they were not exposed to the RLR activator and no elevation of MHC class I was induced. Further study is needed to clarify these mechanisms.

The synergy between DaRT and RLR activation can be attributed to additional non-immune-related potential mechanisms. For example, the cellular response to a viral attack may promote transcription related to programmed cell death (52), and thus when DNA damage is induced by alpha radiation, the cellular stress response is already biased to favor cellular death over DNA repair. Indeed, RLR activation by cytoplasmatic delivery of polyIC was found to sensitize tumor cells to ionizing radiation also *in vitro* (53). In the case of decitabine, sensitization to alpha radiation may also be due to chromatin de-condensation (54).

In its first-in-human clinical trial, DaRT was used to treat SCC patients. All patients responded to DaRT, with almost 80% showing complete responses with minor adverse effects (50). In one case, evidence suggests the possible induction of an abscopal effect (55). The treatment regimens presented here efficiently affected both the tumor and distant metastases and extended long-term survival. Low-dose cyclophosphamide, previously found to reduce the number of Tregs, demonstrated the potential of immunomodulating therapies used in clinical practice (56) to further enhance these effects. Taken together, the results presented here may suggest future directions for improved therapeutic protocols for treating patients with metastatic cancer.

DATA AVAILABILITY STATEMENT

The datasets generated for this study are available on request to the corresponding author.

ETHICS STATEMENT

The animal study was reviewed and approved by Tel Aviv University ethics committee.

AUTHOR CONTRIBUTIONS

VD: conceptualization, formal analysis, investigation, methodology, project administration, resources, supervision, validation, visualization, writing—original draft, and writing—review & editing. ME and MS: investigation, methodology, and resources. EG: formal analysis, investigation, visualization, and writing—original draft. FM, AS, AC, and EF: investigation. YZ: investigation and resources. RG: conceptualization and writing—review & editing. IK: conceptualization, funding acquisition, methodology, supervision, and writing—review & editing. YK: conceptualization, funding acquisition, methodology, project administration, supervision, validation, visualization, writing—original draft, and writing—review & editing. All authors contributed to the article and approved the submitted version.

FUNDING

This study was partially funded by a grant from the Israel Innovation Authority.

ACKNOWLEDGMENTS

We thank the staff of the animal facility at the Tel University Medical School, headed by Dr. Michael Harlev, for their assistance and support.

REFERENCES

1. Den Brok MH, Sutmuller RP, Van Der Voort R, Bennink EJ, Figdor CG, Ruers TJ, et al. In situ tumor ablation creates an antigen source for the generation of antitumor immunity. *Cancer Res.* (2004) 64:4024–9. doi: 10.1158/0008-5472.CAN-03-3949
2. Pierce RH, Campbell JS, Pai SI, Brody JD, Kohrt HE. In-situ tumor vaccination: bringing the fight to the tumor. *Hum Vaccin Immunother.* (2015) 11:1901–9. doi: 10.1080/21645515.2015.1049779
3. Aznar MA, Tinari N, Rullan AJ, Sanchez-Paulete AR, Rodriguez-Ruiz ME, Melero I. Intratumoral delivery of immunotherapy-act locally, think globally. *J Immunol.* (2017) 198:31–9. doi: 10.4049/jimmunol.1601145
4. Keisari Y. Tumor abolition and antitumor immunostimulation by physico-chemical tumor ablation. *Front Biosci.* (2017) 22:310–47. doi: 10.2741/4487
5. Tohme S, Simmons RL, Tsung A. Surgery for cancer: a trigger for metastases. *Cancer Res.* (2017) 77:1548–52. doi: 10.1158/0008-5472.CAN-16-1536
6. Ben-Eliyahu S, Golan T. Harnessing the perioperative period to improve long-term cancer outcomes. *J Natl Cancer Inst.* (2018) 110:1137–8. doi: 10.1093/jnci/djy055
7. Chen Z, Zhang P, Xu Y, Yan J, Liu Z, Lau WB, et al. Surgical stress and cancer progression: the twisted tango. *Mol Cancer.* (2019) 18:132. doi: 10.1186/s12943-019-1058-3
8. Arazi L, Cooks T, Schmidt M, Keisari Y, Kelson I. Treatment of solid tumors by interstitial release of recoiling short-lived alpha emitters. *Phys Med Biol.* (2007) 52:5025–42. doi: 10.1088/0031-9155/52/16/021
9. Cooks T, Arazi L, Schmidt M, Marshak G, Kelson I, Keisari Y. Growth retardation and destruction of experimental squamous cell carcinoma by interstitial radioactive wires releasing diffusing alpha-emitting atoms. *Int J Cancer.* (2008) 122:1657–64. doi: 10.1002/ijc.23268
10. Cooks T, Arazi L, Efrati M, Schmidt M, Marshak G, Kelson I, et al. Interstitial wires releasing diffusing alpha emitters combined with chemotherapy improved local tumor control and survival in squamous cell carcinoma-bearing mice. *Cancer.* (2009) 115:1791–801. doi: 10.1002/cncr.24191
11. Cooks T, Schmidt M, Bittan H, Lazarov E, Arazi L, Kelson I, et al. Local control of lung derived tumors by diffusing alpha-emitting atoms released from intratumoral wires loaded with radium-224. *Int J Radiat Oncol Biol Phys.* (2009) 74:966–73. doi: 10.1016/j.ijrobp.2009.02.063
12. Arazi L, Cooks T, Schmidt M, Keisari Y, Kelson I. The treatment of solid tumors by alpha emitters released from (224)Ra-loaded sources-internal dosimetry analysis. *Phys Med Biol.* (2010) 55:1203–18. doi: 10.1088/0031-9155/55/4/020
13. Cooks T, Tal M, Raab S, Efrati M, Reitkopf S, Lazarov E, et al. Intratumoral 224Ra-loaded wires spread alpha-emitters inside solid human tumors in athymic mice achieving tumor control. *Anticancer Res.* (2012) 32:5315–21.
14. Horev-Drori G, Cooks T, Bittan H, Lazarov E, Schmidt M, Arazi L, et al. Local control of experimental malignant pancreatic tumors by treatment with a combination of chemotherapy and intratumoral 224radium-loaded wires releasing alpha-emitting atoms. *Transl Res.* (2012) 159:32–41. doi: 10.1016/j.trsl.2011.08.009
15. Keisari Y, Hochman I, Confino H, Korenstein R, Kelson I. Activation of local and systemic anti-tumor immune responses by ablation of solid tumors with intratumoral electrochemical or alpha radiation treatments. *Cancer Immunol Immunother.* (2014) 63:1–9. doi: 10.1007/s00262-013-1462-2
16. Confino H, Hochman I, Efrati M, Schmidt M, Umansky V, Kelson I, et al. Tumor ablation by intratumoral Ra-224-loaded wires induces anti-tumor immunity against experimental metastatic tumors. *Cancer Immunol Immunother.* (2015) 64:191–9. doi: 10.1007/s00262-014-1626-8
17. Confino H, Schmidt M, Efrati M, Hochman I, Umansky V, Kelson I, et al. Inhibition of mouse breast adenocarcinoma growth by ablation with intratumoral alpha-irradiation combined with inhibitors of immunosuppression and CpG. *Cancer Immunol Immunother.* (2016) 65:1149–58. doi: 10.1007/s00262-016-1878-6
18. Domankevich V, Cohen A, Efrati M, Schmidt M, Rammensee HG, Nair SS, et al. Combining alpha radiation-based brachytherapy with immunomodulators promotes complete tumor regression in mice via tumor-specific long-term immune response. *Cancer Immunol Immunother.* (2019) 68:1949–58. doi: 10.1007/s00262-019-02418-5
19. Iyer SP, Hunt CR, Pandita TK. Cross Talk between Radiation and Immunotherapy: The Twain Shall Meet. *Radiat Res.* (2018) 189:219–24. doi: 10.1667/RR14941.1
20. Reits EA, Hodge JW, Herberts CA, Groothuis TA, Chakraborty M, Wansley EK, et al. Radiation modulates the peptide repertoire, enhances MHC class I expression, and induces successful antitumor immunotherapy. *J Exp Med.* (2006) 203:1259–71. doi: 10.1084/jem.20052494
21. Lim JY, Gerber SA, Murphy SP, Lord EM. Type I interferons induced by radiation therapy mediate recruitment and effector function of CD8(+) T cells. *Cancer Immunol Immunother.* (2014) 63:259–71. doi: 10.1007/s00262-013-1506-7
22. Lhuillier C, Rudqvist NP, Elemento O, Formenti SC, Demaria S. Radiation therapy and anti-tumor immunity: exposing immunogenic mutations to the immune system. *Genome Med.* (2019) 11:40. doi: 10.1186/s13073-019-0653-7
23. Reikine S, Nguyen JB, Modis Y. Pattern Recognition and Signaling Mechanisms of RIG-I and MDA5. *Front Immunol.* (2014) 5:342. doi: 10.3389/fimmu.2014.00342
24. Brisse M, Ly H. Comparative Structure and Function Analysis of the RIG-I-Like Receptors: RIG-I and MDA5. *Front Immunol.* (2019) 10:1586. doi: 10.3389/fimmu.2019.01586

25. Elion DL, Cook RS. Harnessing RIG-I and intrinsic immunity in the tumor microenvironment for therapeutic cancer treatment. *Oncotarget*. (2018) 9:29007–17. doi: 10.18632/oncotarget.25626
26. Heidegger S, Kreppel D, Bscheider M, Stritzke F, Nedelko T, Wintges A, et al. RIG-I activating immunostimulatory RNA boosts the efficacy of anticancer vaccines and synergizes with immune checkpoint blockade. *EBioMedicine*. (2019) 41:146–55. doi: 10.1016/j.ebiom.2019.02.056
27. Heidegger S, Wintges A, Stritzke F, Bek S, Steiger K, Koenig PA, et al. RIG-I activation is critical for responsiveness to checkpoint blockade. *Sci Immunol*. (2019) 4:eaau8943. doi: 10.1126/sciimmunol.aau8943
28. Chattopadhyay S, Sen GC. dsRNA-activation of TLR3 and RLR signaling: gene induction-dependent and independent effects. *J Interferon Cytokine Res*. (2014) 34:427–36. doi: 10.1089/jir.2014.0034
29. Bhoopathi P, Quinn BA, Gui Q, Shen XN, Grossman SR, Das SK, et al. Pancreatic cancer-specific cell death induced in vivo by cytoplasmic-delivered polyinosine-polycytidylic acid. *Cancer Res*. (2014) 74:6224–35. doi: 10.1158/0008-5472.CAN-14-0819
30. Duewell P, Steger A, Lohr H, Bourhis H, Hoelz H, Kirchleitner SV, et al. RIG-I-like helicases induce immunogenic cell death of pancreatic cancer cells and sensitize tumors toward killing by CD8(+) T cells. *Cell Death Differ*. (2014) 21:1825–37. doi: 10.1038/cdd.2014.96
31. Levitzki A, Klein S. My journey from tyrosine phosphorylation inhibitors to targeted immune therapy as strategies to combat cancer. *Proc Natl Acad Sci USA*. (2019) 116:11579–86. doi: 10.1073/pnas.1816012116
32. Besch R, Poeck H, Hohenauer T, Senft D, Hacker G, Berking C, et al. Proapoptotic signaling induced by RIG-I and MDA-5 results in type I interferon-independent apoptosis in human melanoma cells. *J Clin Invest*. (2009) 119:2399–411. doi: 10.1172/JCI37155
33. Duewell P, Beller E, Kirchleitner SV, Adunka T, Bourhis H, Siveke J, et al. Targeted activation of melanoma differentiation-associated protein 5 (MDA5) for immunotherapy of pancreatic carcinoma. *Oncoimmunology*. (2015) 4:e1029698. doi: 10.1080/2162402X.2015.1029698
34. Aznar MA, Planelles L, Perez-Olivares M, Molina C, Garasa S, Etxeberria I, et al. Immunotherapeutic effects of intratumoral nanoplexed poly I:C. *J Immunother Cancer*. (2019) 7:116. doi: 10.1186/s40425-019-0568-2
35. Gonzalez-Cao M, Karachaliou N, Santarpia M, Viteri S, Meyerhans A, Rosell R. Activation of viral defense signaling in cancer. *Ther Adv Med Oncol*. (2018) 10:1758835918793105. doi: 10.1177/1758835918793105
36. Chiappinelli KB, Strissel PL, Desrichard A, Li H, Henke C, Akman B, et al. Inhibiting DNA Methylation Causes an Interferon Response in Cancer via dsRNA Including Endogenous Retroviruses. *Cell*. (2015) 162:974–86. doi: 10.1016/j.cell.2015.07.011
37. Roulois D, Loo Yau H, Singhania R, Wang Y, Danesh A, Shen SY, et al. DNA-demethylating agents target colorectal cancer cells by inducing viral mimicry by endogenous transcripts. *Cell*. (2015) 162:961–73. doi: 10.1016/j.cell.2015.07.056
38. Daskalakis M, Brocks D, Sheng YH, Islam MS, Ressnerova A, Assenov Y, et al. Reactivation of endogenous retroviral elements via treatment with DNMT- and HDAC-inhibitors. *Cell Cycle*. (2018) 17:811–22. doi: 10.1080/15384101.2018.1442623
39. Adair SJ, Hogan KT. Treatment of ovarian cancer cell lines with 5-aza-2'-deoxycytidine upregulates the expression of cancer-testis antigens and class I major histocompatibility complex-encoded molecules. *Cancer Immunol Immunother*. (2009) 58:589–601. doi: 10.1007/s00262-008-0582-6
40. Stone ML, Chiappinelli KB, Li H, Murphy LM, Travers ME, Topper MJ, et al. Epigenetic therapy activates type I interferon signaling in murine ovarian cancer to reduce immunosuppression and tumor burden. *Proc Natl Acad Sci USA*. (2017) 114:E10981–E10990. doi: 10.1073/pnas.1712514114
41. Luo N, Nixon MJ, Gonzalez-Ericsson PI, Sanchez V, Opalenik SR, Li H, et al. DNA methyltransferase inhibition upregulates MHC-I to potentiate cytotoxic T lymphocyte responses in breast cancer. *Nat Commun*. (2018) 9:248. doi: 10.1038/s41467-017-02630-w
42. Deng L, Liang H, Xu M, Yang X, Burnette B, Arina A, et al. STING-dependent cytosolic dna sensing promotes radiation-induced type i interferon-dependent antitumor immunity in immunogenic tumors. *Immunity*. (2014) 41:843–52. doi: 10.1016/j.immuni.2014.10.019
43. Wang S, He Z, Wang X, Li H, Liu XS. Antigen presentation and tumor immunogenicity in cancer immunotherapy response prediction. *Elife*. (2019) 8:e03401. doi: 10.7554/eLife.49020.036
44. Garrido F, Aptsiauri N, Doorduijn EM, Garcia Lora AM, Van Hall T. The urgent need to recover MHC class I in cancers for effective immunotherapy. *Curr Opin Immunol*. (2016) 39:44–51. doi: 10.1016/j.coi.2015.12.007
45. Su Q, Igyarto BZ. One-step artificial antigen presenting cell-based vaccines induce potent effector CD8 T cell responses. *Sci Rep*. (2019) 9:18949. doi: 10.1038/s41598-019-55286-5
46. Zhou Y, Guo M, Wang X, Li J, Wang Y, Ye L, et al. TLR3 activation efficiency by high or low molecular mass poly I:C. *Innate Immun*. (2013) 19:184–92. doi: 10.1177/1753425912459975
47. Alonso-Curbelo D, Soengas MS. Self-killing of melanoma cells by cytosolic delivery of dsRNA: wiring innate immunity for a coordinated mobilization of endosomes, autophagosomes and the apoptotic machinery in tumor cells. *Autophagy*. (2010) 6:148–50. doi: 10.4161/auto.6.1.10464
48. Bianchi F, Pretto S, Tagliabue E, Balsari A, Sfondrini L. Exploiting poly(I:C) to induce cancer cell apoptosis. *Cancer Biol Ther*. (2017) 18:747–56. doi: 10.1080/15384047.2017.1373220
49. Hughes E, Scurr M, Campbell E, Jones E, Godkin A, Gallimore A. T-cell modulation by cyclophosphamide for tumour therapy. *Immunology*. (2018) 154:62–8. doi: 10.1111/imm.12913
50. Popovtzer A, Rosenfeld E, Mizrachi A, Bellia SR, Ben-Hur R, Feliciani G, et al. Initial safety and tumor control results from a "first-in-human" multicenter prospective trial evaluating a novel alpha-emitting radionuclide for the treatment of locally advanced recurrent squamous cell carcinomas of the skin and head and neck. *Int J Radiat Oncol Biol Phys*. (2019) 106:571–78. doi: 10.1016/j.ijrobp.2019.10.048
51. Nakayama M. Antigen presentation by MHC-dressed cells. *Front Immunol*. (2014) 5:672. doi: 10.3389/fimmu.2014.00672
52. Barber GN. Host defense, viruses and apoptosis. *Cell Death Differ*. (2001) 8:113–26. doi: 10.1038/sj.cdd.4400823
53. Yoshino H, Iwabuchi M, Kazama Y, Furukawa M, Kashiwakura I. Effects of retinoic acid-inducible gene-I-like receptors activations and ionizing radiation cotreatment on cytotoxicity against human non-small cell lung cancer in vitro. *Oncol Lett*. (2018) 15:4697–705. doi: 10.3892/ol.2018.7867
54. Poplineau M, Doliwa C, Schnekenburger M, Antonicelli F, Diederich M, Trussardi-Regnier A, et al. Epigenetically induced changes in nuclear textural patterns and gelatinase expression in human fibrosarcoma cells. *Cell Prolif*. (2013) 46:127–36. doi: 10.1111/cpr.12021
55. Bellia SR, Feliciani G, Duca MD, Monti M, Turri V, Sarnelli A, et al. Clinical evidence of abscopal effect in cutaneous squamous cell carcinoma treated with diffusing alpha emitters radiation therapy: a case report. *J Contemp Brachytherapy*. (2019) 11:449–57. doi: 10.5114/jcb.2019.88138
56. Scurr M, Pembroke T, Bloom A, Roberts D, Thomson A, Smart K, et al. Low-Dose Cyclophosphamide Induces Antitumor T-Cell Responses, which Associate with Survival in Metastatic Colorectal Cancer. *Clin Cancer Res*. (2017) 23:6771–80. doi: 10.1158/1078-0432.CCR-17-0895

Conflict of Interest: YK and IK serve as consultants for Alpha Tau Medical LTD. Tel Aviv, Israel. VD, ME, MS, EF, and AS are employees of Alpha Tau Medical LTD. Tel Aviv, Israel. YK, IK, VD, ME, and MS hold stock options in Alpha Tau Medical LTD. Tel Aviv, Israel. YK, IK, and VD are the inventors of a patent application submitted by Alpha Tau Medical LTD, which is related to the results of the current study.

The remaining authors declare that the research was conducted in the absence of any commercial or financial relationships that could be construed as a potential conflict of interest.

frontiers in Oncology

REVIEW
published: 19 August 2020
doi: 10.3389/fonc.2020.01575

Targeting Base Excision Repair in Cancer: NQO1-Bioactivatable Drugs Improve Tumor Selectivity and Reduce Treatment Toxicity Through Radiosensitization of Human Cancer

Colton L. Starcher[1], S. Louise Pay[1], Naveen Singh[1], I-Ju Yeh[1], Snehal B. Bhandare[1], Xiaolin Su[1], Xiumei Huang[2], Erik A. Bey[1], Edward A. Motea[1]* and David A. Boothman[1†]*

[1] Department of Biochemistry and Molecular Biology, IU Simon Cancer Center, Indiana University School of Medicine, Indianapolis, IN, United States, [2] Department of Radiation Oncology, IU Simon Cancer Center, Indiana University School of Medicine, Indianapolis, IN, United States

Ionizing radiation (IR) creates lethal DNA damage that can effectively kill tumor cells. However, the high dose required for a therapeutic outcome also damages healthy tissue. Thus, a therapeutic strategy with predictive biomarkers to enhance the beneficial effects of IR allowing a dose reduction without losing efficacy is highly desirable. NAD(P)H:quinone oxidoreductase 1 (NQO1) is overexpressed in the majority of recalcitrant solid tumors in comparison with normal tissue. Studies have shown that NQO1 can bioactivate certain quinone molecules (e.g., ortho-naphthoquinone and β-lapachone) to induce a futile redox cycle leading to the formation of oxidative DNA damage, hyperactivation of poly(ADP-ribose) polymerase 1 (PARP1), and catastrophic depletion of NAD^+ and ATP, which culminates in cellular lethality via NAD^+-Keresis. However, NQO1-bioactivatable drugs induce methemoglobinemia and hemolytic anemia at high doses. To circumvent this, NQO1-bioactivatable agents have been shown to synergize with PARP1 inhibitors, pyrimidine radiosensitizers, and IR. This therapeutic strategy allows for a reduction in the dose of the combined agents to decrease unwanted side effects by increasing tumor selectivity. In this review, we discuss the mechanisms of radiosensitization between NQO1-bioactivatable drugs and IR with a focus on the involvement of base excision repair (BER). This combination therapeutic strategy presents a unique tumor-selective and minimally toxic approach for targeting solid tumors that overexpress NQO1.

Keywords: NQO1, PARP1 hyperactivation, ionizing radiation, base excision repair, double-strand break repair, synergy, β-lapachone, abasic sites

OPEN ACCESS

Edited by:
Carsten Herskind, University of Heidelberg, Germany

Reviewed by:
Aidan D. Meade, Technological University Dublin, Ireland
Bernd Kaina, Johannes Gutenberg University Mainz, Germany

***Correspondence:**
Erik A. Bey
beye@iu.edu
Edward A. Motea
eamotea@iu.edu

†Deceased

Specialty section:
This article was submitted to Radiation Oncology, a section of the journal Frontiers in Oncology

Received: *19 February 2020*
Accepted: *21 July 2020*
Published: *19 August 2020*

Citation:
Starcher CL, Pay SL, Singh N, Yeh I-J, Bhandare SB, Su X, Huang X, Bey EA, Motea EA and Boothman DA (2020) Targeting Base Excision Repair in Cancer: NQO1-Bioactivatable Drugs Improve Tumor Selectivity and Reduce Treatment Toxicity Through Radiosensitization of Human Cancer. Front. Oncol. 10:1575. doi: 10.3389/fonc.2020.01575

Abbreviations: 53BP1, tumor suppressor p53 binding protein 1; 8-oxoG, 8-Oxoguanine; AP site, apurinic/apyrimidinic site; APE1, apurinic/apyrimidinic endonuclease 1; APE2, apurinic/apyrimidinic endonuclease 2; ATP, adenosine triphosphate; BAPTA-AM, (1,2-bis(o-aminophenoxy)ethane-N,N,N',N'-tetraacetic acid); BER, base excision repair; CtIP Complex, complex involved with MRN and BRCA as a scaffold; DIC, dicoumarol; DNA pol β, DNA polymerase beta; DNA-PKcs, DNA dependent protein kinase, catalytic subunit; DSB, double-strand break; ER, endoplasmic reticulum; gH2AX, H2A histone family member X (phosphorylated Serine 139); Gy, gray of ionizing radiation; HAN, head and neck cancer; IR, ionizing radiation; Ku70/Ku80, XRCC5/XRCC6; MeOX, methoxyamine; MRN, complex of Mre11, Rad50, and Nbs1 involved in end processing; NAD^+, nicotinamide adenine dinucleotide; NAMPT, nicotinamide phosphoribosyltransferase; NER, nucleotide excision repair; NHEJ, non-homologous end-joining; NQO1, NAD(P)H:quinone oxidoreductase 1; NSCLC, non-small cell lung cancer; OGG1, 8-Oxoguanine DNA glycosylase 1; PARylation, poly-ADP-ribosylation; PDAC, pancreatic ductal adenocarcinoma; ROS, reactive oxygen species; RPA, replication protein A; SSB, single-strand break; ssDNA, single-strand DNA; TNBC, triple-negative breast cancer; XRCC1, X-ray repair cross-complementing protein 1; XRCC4, X-ray repair cross-complementing protein 4.

INTRODUCTION

Ionizing radiation induces high levels of single-strand DNA breaks (SSBs), double-strand DNA breaks (DSBs), and oxidized bases via ROS production and DNA–protein cross-links that activate almost all DNA repair pathways (1, 2). Although effective, the toxicity of IR to healthy tissue at a therapeutic dose presents a significant limitation in the clinic (3–5). IR activates the BER pathway, in which DNA glycosylases (e.g., OGG1) create abasic sites and SSBs for base excision and replacement (6). If these SSBs persist, are replicated through, or are within three base pairs of each other, they are converted to DSBs. The presence of one unrepaired DSB has been reported to be lethal (7, 8). Thus, combining IR with an agent that also promotes a significant increase in DNA damage through modified bases and deleterious DSBs preferentially in tumors may effectively reduce the necessary dose of IR in a clinical setting to lessen toxicity to healthy tissues and improve patient outcomes. The use of a tumor-selective drug for this purpose is an attractive possibility.

NAD(P)H:quinone oxidoreductase 1 (NQO1, also called DT-diaphorase) is a phase II two-electron redox enzyme that is highly overexpressed in most solid tumor types compared with most healthy tissues, as shown through studies by Siegel and Ross (9, 10). Ortho-napthoquinones are a unique class of quinone molecules that, unlike other quinones that are conjugated to glutathione and excreted from the cell, are bioactivated specifically by NQO1 to undergo a two-step back-reaction with oxygen (11). In this futile cycle, NQO1 continuously metabolizes the drugs and then reverts them to the parent compound (12). This process causes rapid accumulation of ROS such as superoxide radical and hydrogen peroxide (H_2O_2) that permeate the cell and nuclear membrane to cause significant numbers of oxidized bases and SSBs, which consequently lead to the formation of lethal DSBs. Poly(ADP-ribose) polymerase-1 (PARP1) is hyperactivated by this DNA damage, which rapidly depletes NAD^+ and ATP, causing metabolic catastrophe and cell death via programmed necrosis (termed NAD^+-Keresis) (13).

Base excision repair is the main repair pathway involved in activating PARP1 during the repair of SSBs and oxidized bases (14). Depleting BER enzymes, such as XRCC1, and modification of apurinic/apyridinic (AP) sites with methoxyamine (MeOX) synergizes with NQO1-bioactivatable drugs, promoting increased DSBs and rapid cell death (15). NQO1-bioactivatable drugs have long been known to synergize with halogenated pyrimidine radiosensitizers (16). More recently, synergy between PARP inhibitors (17) and IR (18, 19) has been shown. The use of NQO1-bioactivatable drugs, therefore, may be a clinically viable approach to reduce the toxicity of IR associated with high doses and also to improve the tumor selectivity of treatment. In this review, we discuss the mechanisms of radiosensitization between low doses of NQO1-bioactivatable drugs and IR—with a focus on the BER repair pathway and PARP1 hyperactivation—and present a case for combination treatment with NQO1-bioactivatable drugs and IR in the clinic.

NQO1-BIOACTIVATABLE DRUGS INDUCE A SPECIFIC FORM OF PROGRAMMED NECROSIS (NAD^+-KERESIS)

β-Lapachone (β-lap/ARQ761 in clinical form) is an NQO1-bioactivatable drug derived from lapachone (20), with known antimicrobial (21) and anticancer activity as a single agent (22). The futile redox cycling of β-lap by NQO1 (11) produces ROS-induced DNA damage (**Figure 1A**), which ultimately leads to cell death via metabolic and bioenergetic catastrophe caused by NAD^+ and ATP depletion following PARP1 hyperactivation (23). Boothman and colleagues have shown that within 5 min of β-lap treatment, there is a significant calcium flux from the ER to the cytosol (24). Calcium flux from the ER is necessary to activate calpain protease (24) and hyperactivate PARP1; however, the mechanistic role of calcium in PARP1 hyperactivation has yet to be firmly established (25). Within 30 min, the NAD^+ molecules that are produced during the futile redox cycling of β-lap by NQO1 are rapidly exhausted by hyperactivated PARP1 during the repair of ROS-induced DNA damage and SSBs (17). Depletion of NAD^+ consequently depletes ATP and induces a specific type of programmed necrosis, termed NAD^+-Keresis (26). Expression of catalase can spare cellular lethality by neutralizing the effects of hydrogen peroxide (H_2O_2) produced by β-lap (an NQO1-bioactivatable agent), confirming the role of ROS formation in toxicity (27). Inhibition of NQO1 activity with a small-molecule inhibitor (e.g., Dicoumarol) or genetically knocking out NQO1 eliminates β-lap lethality, showing the selectivity of β-lap-induced cell death to NQO1-expressing cells (17, 23). Calcium release from the ER can be blocked with the calcium chelator, BAPTA-AM, which prevents PARP1 hyperactivation and spares cancer cells from lethality, further highlighting the role of PARP1 in β-lap-induced cell death (25). When NAD^+ production is inhibited genetically by depleting NAMPT or pharmacologically with NAMPT inhibitors (e.g., FK866) (26) prior to β-lap treatment in NQO1-overexpressing cancer cells, a synergistic cell death due to compromised NAD^+ production following PARP hyperactivation highlights the critical role of catastrophic NAD^+ depletion in NAD^+-Keresis (**Figure 1A**) (26).

TRAPPING PARP1 ON DNA SYNERGIZES WITH NQO1-BIOACTIVATABLE DRUGS

There are 17 known PARP proteins (28) that share a common catalytic domain but exhibit differential roles in DNA repair, chromatin structure and modification, transcription, and cell death. PARP proteins catalyze the transfer of one or more ADP-ribose units to substrate proteins through a process known as mono- or poly(ADP) ribosylation, respectively (29). Of particular importance to the NQO1-bioactivatable drug field is PARP1, which is required for both BER and NER to recruit and activate SSB repair proteins (30). In BER, PARP1 forms a critical complex with DNA ligase III, XRCC1, and DNA pol β (30).

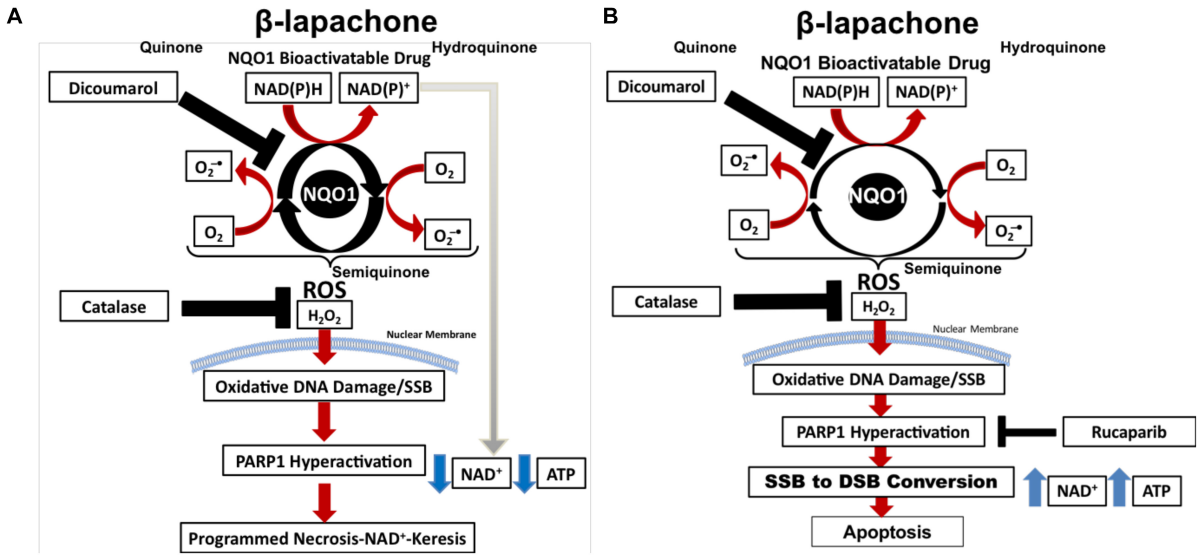

FIGURE 1 | PARP inhibitors switch cell death to apoptosis from programmed necrosis. **(A)** NOQ1 bioactivatable drug β-lap mediates a futile redox cycle with NQO1 detoxifying enzyme, creating a large pool of NAD^+ and hydrogen peroxide. Hydrogen peroxide formation leads to the formation of oxidized bases and SSBs that induces PARP1 hyperactivation. PARP1 utilizes NAD^+ for activity, which depletes NAD^+ and ATP, resulting in NAD^+-Keresis. **(B)** Addition of PARP inhibitor prevents PARP1 hyperactivation and spares ATP and NAD^+. Cellular processes can then recycle NAD^+ back to NAD(P)H, which power more turns of the futile cycle creating even more oxidized bases and SSBs. PARP1 inhibition results in SSB-to-DSB conversion and death by apoptosis.

In BRCA1/2-deficient breast and ovarian cancers—which are deficient in homologous recombination (HR) to repair DSBs—PARP1 inhibitors are an effective therapeutic strategy targeting repair of SSBs and BER (31). PARP trapping agents (e.g., talazoparib, rucaparib, and olaparib) are the most effective PARP1-targeting drugs, which trap PARP1/2 on the DNA by binding at the active site, preventing its interaction with NAD^+ and therefore preventing dissociation via the auto-PARylation domain (32). PARP trapping prevents the recruitment of proteins needed to complete BER, leaving unrepaired SSBs that are then converted to lethal DSBs upon collision with the replication and transcription machineries (31, 32).

Recently, we reported that PARP-trapping agents Rucaparib and Talazoparib synergize with β-lap in NQO1+ lung, pancreatic, and TNBC cell lines and *in vivo* models of NSCLC (17). Sublethal β-lap doses showed significant synergy with non-toxic doses of PARP inhibitor Rucaparib in multiple cancer types, and up to 60 different NSCLC cell lines (17). Synergy occurred regardless of oncogenic and tumor-repressor mutations and was entirely NQO1-dependent in all cell types (17), according to the gold standard combinatorial index obtained using the Chou and Talalay method (**Figure 1B**) (33).

Mechanistically, the addition of non-toxic doses of PARP inhibitor (e.g., Rucaparib) to sublethal β-lap doses prevents the loss of NAD^+ and ATP (17). No PARylation of PARP1 occurred in this instance; however, DSBs significantly increased, indicating a β-lap-mediated SSB-to-DSB conversion (17). NAD^+ and ATP sparing allows for more oxygen consumption during the futile redox cycling of NQO1-bioactivatable agents, increasing the formation of oxidized bases and unrepaired SSBs (17). This process overwhelms the DNA damage response and repair (17). ATP is then used to initiate caspase-dependent apoptosis, which is in contrast with the NAD^+-Keresis observed with β-lap monotherapy (17). PARP inhibitors, therefore, enhance DNA damage caused by NQO1-bioactivatable drugs and switch cell death from programmed necrosis to apoptosis (17). This is significant as necrosis may cause inflammation and lead to complications, whereas apoptosis does not. Combining β-lap with PARP1 inhibitors, therefore, reduces the toxicity of the drug in addition to enhancing its mechanism of action, making it more attractive for clinical application.

BER IS THE MAJOR DNA REPAIR PATHWAY INVOLVED IN THE NQO1-BIOACTIVATABLE DRUG MECHANISM OF ACTION

Base excision repair resolves non-distorting DNA lesions resulting from alkylation, oxidation, depurine/pyrimidination, and deamination, which can be drug-induced or occur from exposure to environmental toxins. There are two types of BER: short patch that repairs a single damaged base and long patch that repairs up to three damaged bases (34). The typical mammalian BER pathway occurs as follows: DNA glycosylases detect damaged bases and cleave the glycosidic bond holding the damaged base to the DNA backbone, creating an apurinic/apyridinic site (AP site). AP sites are cleaved by AP endonucleases (APE1/APE2), allowing DNA pol β to fill the site with the appropriate base

(35, 36). Mechanistically, APE1 provides a significant portion of the endonuclease activity, while APE2 provides some endonuclease activity and a large portion of exonuclease activity (34). Both APE1 and APE2 provide proofreading capabilities for pol β to reduce error rates (37). DNA ligase then seals up this stretch of DNA to finalize the DNA repair (35).

Hydrogen peroxide induced by β-lap permeates the nucleus and oxidizes nucleotides, particularly guanine bases (e.g., 8-oxo-guanine or 8-oxoG) (15). Oxidized guanine (8-oxoG) formed during treatment with β-lap recruits DNA glycosylase OGG1, which, combined with APE1/2, produces a SSB that activates PARP1 during BER (15). OGG1 recognizes the oxidized lesion, cleaves at the 3′ end, and removes the lesion, in a reaction that is catalyzed by ATP (38). It has been shown that silencing OGG1 prevents 8-oxoG recognition and increases the overall amount of 8-oxoG incorporated into DNA (32). This prevents PARP1 hyperactivation, thus abrogating NAD^+/ATP loss and β-lap-mediated lethality (15). This is an important finding and a potential route of resistance in the clinic to NQO1-bioactivatable drugs.

Silencing the key BER protein, XRCC1, synergizes with NQO1-bioactivatable drugs in PDAC cell lines, further indicating that BER inactivation plays a critical role in β-lap toxicity (15). XRCC1 is a scaffolding protein required for clearing oxidized bases (39). PARylated-PARP1 bound to SSBs recruits XRCC1 through the BRCT 1 domain and forms a complex consisting of XRCC1 (40), DNA pol β (41), DNA Ligase IIIα (42), and APE1 (43). Without XRCC1, DNA base lesions and SSBs cannot be repaired. In addition to mediating synthetic lethality, XRCC1 knockdown also depletes NAD^+ levels at a higher rate than with β-lap alone (15). XRCC1 knockdown is currently known to be embryonic lethal and essential for mouse development (44). NQO1-bioactivatable drug synergy with BER deficiencies in PDAC cells indicates a potential for these drugs to be beneficial in targeting pancreatic cancer.

Silencing OGG1 spared β-lap-mediated lethality in PDAC, compared with XRCC1 knockdown (15). It is thought that knockdown of OGG1 glycosylase protects PDAC cells from death because BER is not activated if the scanning glycosylase is non-functional. This suggests an important role for different proteins in BER with regard to solid tumors. Alteration of expression or mutation of different proteins in the BER pathway can either sensitize or protect cancer cells from NQO1-bioactivatable drug-mediated lethality.

Methoxyamine is an AP site modifier (**Figure 2**) used to sensitize temozolomide-resistant glioblastoma (45) and ovarian cancer (46). MeOX modification of AP sites prevents their degradation, thus mitigating sodium hydroxide-mediated hydrolysis of the DNA backbone, preventing AP site cleavage, blocking AP endonuclease action, and preventing BER, resulting in cell death (47). MeOX synergizes with β-lap, increasing the number and persistence of AP sites, PARylation, and DSBs in PDAC. This is specific to β-lap, as co-treatment with NQO1-inhibitor dicoumarol abrogates AP site formation. β-lap and MeOX were also shown to synergize and ultimately reduce tumor volume in 33% of PDAC murine xenografts (15).

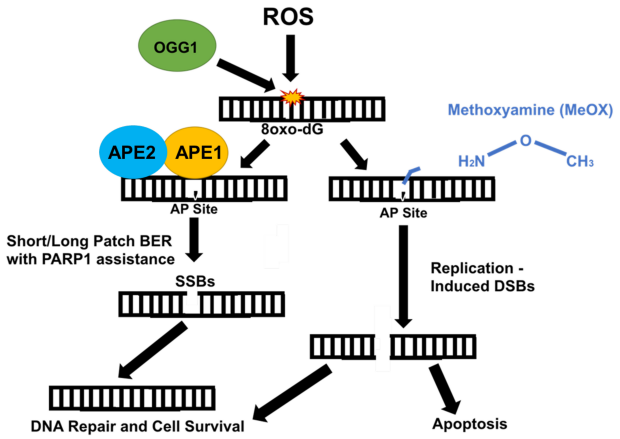

FIGURE 2 | Methoxyamine permanently modifies AP sites and prevents their repair by BER. Reactive oxygen species (ROS) modify guanine bases in DNA, which are recognized and cut by type II DNA glycosylase, OGG1, creating an AP site. Due to OGG1 activity as a type II glycosylase, OGG1 is capable of cleaving the AP site directly. However, under normal circumstances, APE1/APE2 come in and cut, cleaving the AP site, which is repaired either through short patch or long patch BER via PARP1 and XRCC1 scaffold protein that recruit appropriate proteins (i.e., Pol β) necessary for repair. APE1/APE2 both provide proofreading for pol-β to prevent errors in repair (37). APE1 provides most of the endonuclease activity compared with APE2, which provides some endonuclease activity and a large amount of exonuclease activity (36). Methoxyamine permanently modifies the AP site preventing PARP1 and other necessary proteins from accessing and fixing SSBs. These SSBs are converted to DSBs and result in cell death.

DOUBLE-STRAND BREAK AND BER PLAY A CRITICAL ROLE IN TUMOR RESPONSE TO IR

Ionizing radiation is one of the most common and effective methods for treating solid tumors in cancer patients. IR damages DNA directly by causing ionization in DNA itself or indirectly by ionizing the surrounding water resulting in aqueous free radicals that can react with DNA. Inducing significant DNA damage by IR over several treatments results in cancer cell death; however, there are significant drawbacks to this approach, including limitations on the number of IR dose a person can receive in a lifetime, costs, the need for special diets, and serious side effects arising from healthy tissue damage (48). IR produces 1000 SSBs, 40 DSBs, 700 altered thymine bases, 700 8-oxoG base alterations, and 150 DNA–protein cross-links per gray (Gy) (49, 50). The resistance of cancer cells is considered to be determined by the efficacy of DSB repair (51, 52).

Ionizing radiation-induced DSBs activate DSB repair via NHEJ and HR (**Figure 3A**). NHEJ occurs in all phases of the cell cycle (53), which is a quick and easy way to fix massive levels of dsDNA breaks, and is utilized for V(D)J recombination for the human immune system (52). During this process, Ku70 and Ku80 heterodimers bind the end of the double-stranded DNA breaks and form a complex to protect and recruit DNA-PKcs (54) to the site of the damage. XRCC4 binds to the Ku dimers through Ku70 mediating the attachment of other proteins necessary to fix

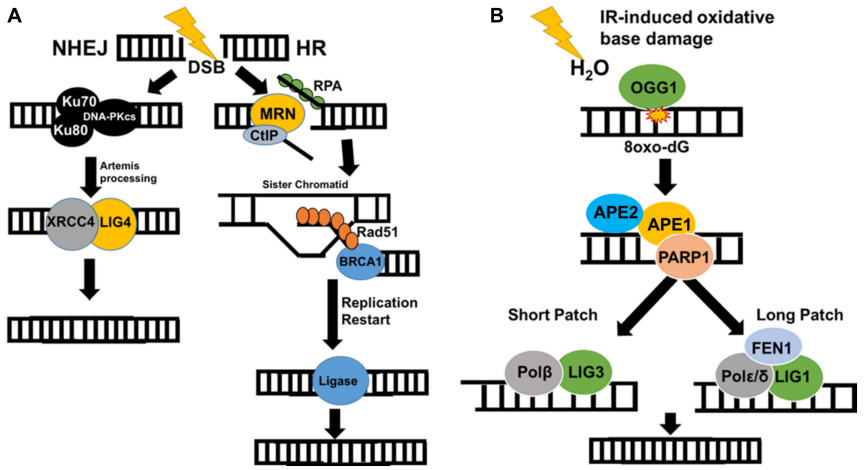

FIGURE 3 | Ionizing radiation induces a wide variety of DNA damage. **(A)** IR causes dsDNA breaks that are repaired by HR (in S/G2 phase) or NHEJ (all phases of cell cycle). In HR, the RPA complex and BRC proteins form a scaffold complex with the sister chromatid and use it as a template to correct damage without error. NHEJ utilizes the KU70/80/DNA-PKc complex to quickly combine and ligate double-strand breaks. **(B)** IR-mediated radiolysis of water leads to ROS formation, which then creates base damage through oxidation. BER then repairs these lesions through the use of a type II DNA glycosylase (OGG1), AP endonuclease (APE1/APE2), PARP1, DNA polymerase, and ligase. This occurs through either short patch or long patch BER.

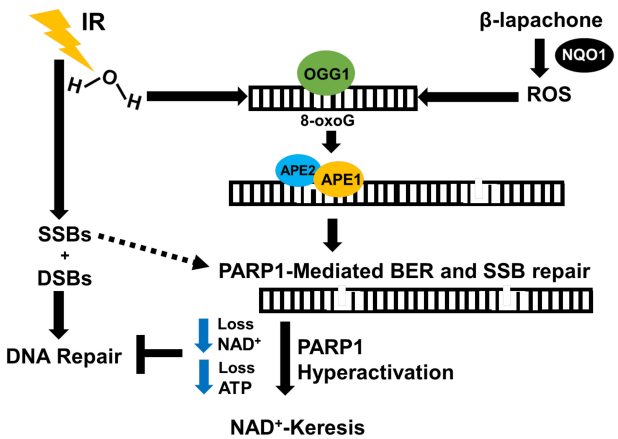

FIGURE 4 | Proposed mechanism of IR and β-lap radiosensitization. NSCLC tumors contain high levels of NQO1 compared to normal tissues. In the presence of NQO1, β-lap causes ROS-induced oxidative base DNA damage, which eventually leads to the formation of SSBs that activate PARP1. IR induces massive SSBs through contact with DNA and oxidized bases due to water radiolysis that require PARP1 and BER to resolve. This combination therapy pushes cumulative amount of DNA damage high enough that overwhelms and hyperactivates PARP1 during DNA damage response and repair, leading to programmed necrosis. Thus, NQO1 may be used as a predictive biomarker for selective targeting of NQO1-overexpressing cancers with low-dose IR in combination with NQO1-bioactivatable agents as radiosensitizers.

the damage (e.g., PNKP, APLF, and XLF) (55). Artemis trims the complex ends (56) of the DSBs for efficient ligation of DNA ends by DNA Ligase IV/XRCC4 complex (**Figure 3A**) (57) to complete the repair of DSB.

Homologous recombination occurs specifically in the S/G2 phase of the cell cycle and uses the sister chromatid as a template to complete repair of DSBs. HR is known as an error-free repair and minimizes the chances of mutations of functional genes (58). After IR creates a DSB, the MRN complex (Mre11-Rad50-Nbs1) will bind to the ends of the breaks and recruits the CtIP complex exonuclease to create free ends that can be modified (59). Single-stranded DNA-binding protein (hSSB1) and RPA bind the free single-stranded DNA after resection to prevent the degradation, improper hybridization, or combination of DNA ends (60). These proteins then bind to BRCA scaffold proteins (44) that load Rad51 proteins, which are responsible for creating a Holliday Junction to align homologous sequences with the sister chromatid strand (**Figure 3A**) (61). Rad51 is then released from the RPA complex (62); DNA is synthesized and then ligated by DNA Ligase I (63). Up-regulation of HR or NHEJ can lead to IR resistance and neoplastic growth.

A significant portion of DNA lesions created by IR is through a water-mediated radiolysis reaction (64). Radiolysis of water causes significant ROS production including extremely reactive hydroxyl (•OH) radicals close to DNA resulting in damage that is primarily repaired by BER (**Figure 3B**) (65). BER may result in DSBs being formed by replication through lesions. If multiple oxidized lesions are within 3 base pairs of each other and BER enzymes cut these lesions out, this will result in the formation of DSBs (65). In addition, mutations in bacterial BER proteins have been known to confer resistance to IR up to 250 Gy, suggesting that BER is necessary for sensitization of IR (65).

SUBLETHAL DOSES OF β-LAP RADIOSENSITIZE NSCLC CELLS TO LOW-DOSE RADIATION THERAPY

In A549 and H1650 NSCLC cell lines, a sublethal dose of β-lap causes significant sensitization to low-dose radiation therapy,

leading to a remarkable increase in cell death. Monotherapy with sublethal β-lap induces minimal DSBs, and low-dose radiation monotherapy induces characteristic increase in DSBs followed by efficient repair (18). Combination therapy with low doses of β-lap and radiation therapy, however, promotes rapid and sustained 53BP1 and gamma-H2AX foci formation that is consistent with DSB formation and compromised DSB repair (18). In NQO1+ NSCLC luciferase murine models, β-lap and IR combination therapy reduces tumor volume and increases survival up to 70% in comparison with either agents alone. Tumor tissues from mice treated with IR and β-lap demonstrated enhanced PAR and gamma-H2AX (pS139-H2AX, surrogate marker for DSBs) level compared with monotherapy, as well as decreased NAD^+ and ATP levels (18). Normal tissues, which generally overexpress catalase and lack NQO1, were unaffected by co-treatment. The BER pathway may play a crucial role in this sensitization since β-lap treatment engages BER and PARP hyperactivation, and IR also activates BER. Mechanistically, we hypothesize that the combination of IR and β-lap treatment creates cumulative clusters of oxidative DNA damage and SSBs that result in severe PARP1 hyperactivation (inactive form of PARP1), which compromises BER and SSB repair. SSBs that are unrepaired are eventually converted to lethal unrepaired DSBs due to the lack of NAD^+ and ATP molecules available to activate the efficient repair of SSBs and DSBs (**Figure 4**). Since most solid tumors overexpress NQO1, combining low-dose radiation with a sublethal concentration of β-lap may enhance tumor-selective and targeted killing and improve patient safety by lowering the overall doses of both agents. Using NQO1 as a predictive biomarker, this combination treatment strategy may reduce the impact of treatment on a patient's lifetime exposure to IR, may cut the costs associated with cancer treatment, and potentially reduce the amount of time needed for therapeutic response.

OUTLOOK/FUTURE

Further work is required to fully determine the critical role of BER in IR and β-lap combination therapy. We have previously shown that loss of specific BER factors potentiates the lethality of an NQO1-bioactivatable agent, β-lap, selectively in NQO1-overexpressing solid tumors. In fact, inhibition of PARP1—a critical factor involved in DNA damage response and repair of modified DNA bases and SSBs—prior to treatment with NQO1-bioactivatable drug causes a synergistic cancer cell death. Thus, we hypothesize that PARP1-mediated BER and SSB repair are the main DNA repair pathways that are activated by β-lap, which promotes severe PARP1 hyperactivation and subsequent lethality at high doses. PARP inhibitors in combination with IR *and* NQO1-bioactivatable drugs may further enhance synergy seen previously (6); however, three-drug combinations are currently rare. Overall, combining low-dose radiation therapy with NQO1-bioactivatable drugs may be a viable, less toxic, and more tumor-selective strategy for treatment of various solid tumors that overexpress a predictive biomarker, NQO1.

AUTHOR CONTRIBUTIONS

DB, prior to his death, directed the review's thematic points regarding the synergistic value of IR or PARP inhibitors in combination with NQO1-bioactivatable therapies in the treatment of various NQO1-positive cancers. Following DB's death, CS (DB's graduate student), EB, EM, and XH (DB's previous postdoctoral fellows, now faculty at IU School of Medicine) worked to write, edit, and review the manuscript. CS and EM took the lead in writing and made all the figures. EB, XH, NS, SB, SP, I-JY, and XS contributed to the editing of the review article. All authors contributed to the article and approved the submitted version.

FUNDING

This work was supported in part by NIH/NCI R01 CA210489 and NIH/NCI R01 CA224493. The content of the article is solely the responsibility of the authors and does not necessarily represent the official views of the funders.

ACKNOWLEDGMENTS

This review article is dedicated to the memory of our mentor, DB, who contributed significantly to the studies on the mechanism of action of NQO1-bioactivatable drugs. He will be greatly missed.

REFERENCES

1. Nickoloff JA, Boss MK, Allen CP, LaRue SM. Translational research in radiation-induced DNA damage signaling and repair. *Transl Cancer Res.* (2017) 6:S875–91.
2. Toulany M. Targeting DNA double-strand break repair pathways to improve radiotherapy response. *Genes (Basel).* (2019) 10:25. doi: 10.3390/genes10010025
3. Barnett GC, West CM, Dunning AM, Elliott RM, Coles CE, Pharoah PD, et al. Normal tissue reactions to radiotherapy: towards tailoring treatment dose by genotype. *Nat Rev Cancer.* (2009) 9:134–42. doi: 10.1038/nrc2587
4. Ryan JL. Ionizing radiation: the good, the bad, and the ugly. *J Invest Dermatol.* (2012) 132:985–93. doi: 10.1038/jid.2011.411
5. Hubenak JR, Zhang Q, Branch CD, Kronowitz SJ. Mechanisms of injury to normal tissue after radiotherapy: a review. *Plast Reconstr Surg.* (2014) 133:49–56e. doi: 10.1097/01.prs.0000440818.23647.0b
6. Pachkowski BF, Tano K, Afonin V, Elder RH, Takeda S, Watanabe M, et al. Cells deficient in PARP-1 show an accelerated accumulation of DNA single strand breaks, but not AP sites, over the PARP-1-proficient cells exposed to MMS. *Mutat Res.* (2009) 671:93–9. doi: 10.1016/j.mrfmmm.2009.09.006
7. Khanna KK, Jackson SP. DNA double-strand breaks: signaling, repair and the cancer connection. *Nat Genet.* (2001) 27:247–54. doi: 10.1038/85798
8. Frankenberg-Schwager M, Frankenberg D, Harbich R. Potentially lethal damage, sublethal damage and DNA double strand breaks. *Radiat Protect Dosimetry.* (1985) 13:171–4. doi: 10.1093/oxfordjournals.rpd.a079571
9. Siegel D, Ross D. Immunodetection of NAD(P)H:quinone oxidoreductase 1 (NQO1) in human tissues. *Free Radic Biol Med.* (2000) 29:246–53.

10. Ross D, Siegel D. Functions of NQO1 in cellular protection and CoQ10 metabolism and its potential role as a redox sensitive molecular switch. *Front Physiol.* (2017) 8:595.
11. Pink JJ, Planchon SM, Tagliarino C, Varnes ME, Siegel D, Boothman DA. NAD(P)H:Quinone oxidoreductase activity is the principal determinant of beta-lapachone cytotoxicity. *J Biol Chem.* (2000) 275:5416–24. doi: 10.1074/jbc.275.8.5416
12. Silvers MA, Deja S, Singh N, Egnatchik RA, Sudderth J, Luo X, et al. The NQO1 bioactivatable drug, beta-lapachone, alters the redox state of NQO1+ pancreatic cancer cells, causing perturbation in central carbon metabolism. *J Biol Chem.* (2017) 292:18203–16. doi: 10.1074/jbc.m117.813923
13. Morales J, Li L, Fattah FJ, Dong Y, Bey EA, Patel M, et al. Review of poly (ADP-ribose) polymerase (PARP) mechanisms of action and rationale for targeting in cancer and other diseases. *Crit Rev Eukaryot Gene Expr.* (2014) 24:15–28. doi: 10.1615/critreveukaryotgeneexpr.2013006875
14. Reynolds P, Cooper S, Lomax M, O'Neill P. Disruption of PARP1 function inhibits base excision repair of a sub-set of DNA lesions. *Nucleic Acids Res.* (2015) 43:4028–38. doi: 10.1093/nar/gkv250
15. Chakrabarti G, Silvers MA, Ilcheva M, Liu Y, Moore ZR, Luo X, et al. Tumor-selective use of DNA base excision repair inhibition in pancreatic cancer using the NQO1 bioactivatable drug, beta-lapachone. *Sci Rep.* (2015) 5: 17066.
16. Boothman DA, Greer S, Pardee AB. Potentiation of halogenated pyrimidine radiosensitizers in human carcinoma cells by beta-lapachone (3,4-dihydro-2,2-dimethyl-2H-naphtho[1,2-b]pyran- 5,6-dione), a novel DNA repair inhibitor. *Cancer Res.* (1987) 47:5361–6.
17. Huang X, Motea EA, Moore ZR, Yao J, Dong Y, Chakrabarti G, et al. Leveraging an NQO1 bioactivatable drug for tumor-selective use of poly(ADP-ribose) polymerase inhibitors. *Cancer Cell.* (2016) 30:940–52.
18. Motea EA, Huang X, Singh N, Kilgore JA, Williams NS, Xie X-J, et al. NQO1-dependent, tumor-selective radiosensitization of non-small cell lung cancers. *Clin Cancer Res.* (2019) 25:2601–9. doi: 10.1158/1078-0432.ccr-18-2560
19. Park HJ, Ahn KJ, Ahn SD, Choi E, Lee SW, Williams B, et al. Susceptibility of cancer cells to beta-lapachone is enhanced by ionizing radiation. *Int J Radiat Oncol Biol Phys.* (2005) 61:212–9. doi: 10.1016/j.ijrobp.2004.09.018
20. Reinicke KE, Bey EA, Bentle MS, Pink JJ, Ingalls ST, Hoppel CL, et al. Development of β-lapachone prodrugs for therapy against human cancer cells with elevated NAD(P)H:quinone oxidoreductase 1 levels. *Clin Cancer Res.* (2005) 11:3055–64. doi: 10.1158/1078-0432.ccr-04-2185
21. Cruz FS, Docampo R, Boveris A. Generation of superoxide anions and hydrogen peroxide from beta-lapachone in bacteria. *Antimicrob Agents Chemother.* (1978) 14:630–3. doi: 10.1128/aac.14.4.630
22. Ough M, Lewis A, Bey EA, Gao J, Ritchie JM, Bornmann W, et al. Efficacy of beta-lapachone in pancreatic cancer treatment: exploiting the novel, therapeutic target NQO1. *Cancer Biol Ther.* (2005) 4:95–102.
23. Bey EA, Bentle MS, Reinicke KE, Dong Y, Yang CR, Girard L, et al. An NQO1- and PARP-1-mediated cell death pathway induced in non-small-cell lung cancer cells by beta-lapachone. *Proc Natl Acad Sci USA.* (2007) 104:11832–7. doi: 10.1073/pnas.0702176104
24. Tagliarino C, Pink JJ, Dubyak GR, Nieminen AL, Boothman DA. Calcium is a key signaling molecule in beta-lapachone-mediated cell death. *J Biol Chem.* (2001) 276:19150–9. doi: 10.1074/jbc.m100730200
25. Bentle MS, Reinicke KE, Bey EA, Spitz DR, Boothman DA. Calcium-dependent modulation of poly(ADP-ribose) polymerase-1 alters cellular metabolism and DNA repair. *J Biol Chem.* (2006) 281:33684–96. doi: 10.1074/jbc.m603678200
26. Moore Z, Chakrabarti G, Luo X, Ali A, Hu Z, Fattah FJ, et al. NAMPT inhibition sensitizes pancreatic adenocarcinoma cells to tumor-selective, PAR-independent metabolic catastrophe and cell death induced by beta-lapachone. *Cell Death Dis.* (2015) 6:e1599. doi: 10.1038/cddis.2014.564
27. Bey EA, Reinicke KE, Srougi MC, Varnes M, Anderson VE, Pink JJ, et al. Catalase abrogates beta-lapachone-induced PARP1 hyperactivation-directed programmed necrosis in NQO1-positive breast cancers. *Mol Cancer Ther.* (2013) 12:2110–20. doi: 10.1158/1535-7163.mct-12-0962
28. Ame JC, Spenlehauer C, De Murcia G. The PARP superfamily. *Bioessays.* (2004) 26:882–93. doi: 10.1002/bies.20085
29. D'Amours D, Desnoyers S, D'Silva I, Poirier GG. Poly(ADP-ribosyl)ation reactions in the regulation of nuclear functions. *Biochem J.* (1999) 342(Pt 2):249–68. doi: 10.1042/bj3420249
30. Caldecott KW, Aoufouchi S, Johnson P, Shall S. XRCC1 polypeptide interacts with DNA polymerase beta and possibly poly (ADP-ribose) polymerase, and DNA ligase III is a novel molecular 'nick-sensor' in vitro. *Nucleic Acids Res.* (1996) 24:4387–94. doi: 10.1093/nar/24.22.4387
31. Farmer H, McCabe N, Lord CJ, Tutt AN, Johnson DA, Richardson TB, et al. Targeting the DNA repair defect in BRCA mutant cells as a therapeutic strategy. *Nature.* (2005) 434:917–21. doi: 10.1038/nature03445
32. Pommier Y, O'Connor MJ, de Bono J. Laying a trap to kill cancer cells: PARP inhibitors and their mechanisms of action. *Sci Trans Med.* (2016) 8:362s317.
33. Chou TC, Talalay P. Quantitative analysis of dose-effect relationships: the combined effects of multiple drugs or enzyme inhibitors. *Adv Enzyme Regul.* (1984) 22:27–55. doi: 10.1016/0065-2571(84)90007-4
34. Robertson AB, Klungland A, Rognes T, Leiros I. DNA repair in mammalian cells: base excision repair: the long and short of it. *Cell Mol Life Sci.* (2009) 66:981–93.
35. Wallace SS. Base excision repair: a critical player in many games. *DNA Repair (Amst).* (2014) 19:14–26. doi: 10.1016/j.dnarep.2014.03.030
36. Wallace BD, Berman Z, Mueller GA, Lin Y, Chang T, Andres SN, et al. APE2 Zf-GRF facilitates 3'-5' resection of DNA damage following oxidative stress. *Proc Natl Acad Sci USA.* (2017) 114:304–9. doi: 10.1073/pnas.1610011114
37. Burkovics P, Szukacsov V, Unk I, Haracska L. Human Ape2 protein has a 3'-5' exonuclease activity that acts preferentially on mismatched base pairs. *Nucleic Acids Res.* (2006) 34:2508–15. doi: 10.1093/nar/gkl259
38. Boiteux S, Coste F, Castaing B. Repair of 8-oxo-7,8-dihydroguanine in prokaryotic and eukaryotic cells: properties and biological roles of the Fpg and OGG1 DNA N-glycosylases. *Free Radical Biol Med.* (2017) 107:179–201. doi: 10.1016/j.freeradbiomed.2016.11.042
39. El-Khamisy SF, Masutani M, Suzuki H, Caldecott KW. A requirement for PARP-1 for the assembly or stability of XRCC1 nuclear foci at sites of oxidative DNA damage. *Nucleic Acids Res.* (2003) 31:5526–33. doi: 10.1093/nar/gkg761
40. Masson M, Niedergang C, Schreiber V, Muller S, Menissier-de Murcia J, de Murcia G. XRCC1 is specifically associated with poly(ADP-ribose) polymerase and negatively regulates its activity following DNA damage. *Mol Cell Biol.* (1998) 18:3563–71. doi: 10.1128/mcb.18.6.3563
41. Kubota Y, Nash RA, Klungland A, Schar P, Barnes DE, Lindahl T. Reconstitution of DNA base excision-repair with purified human proteins: interaction between DNA polymerase beta and the XRCC1 protein. *Embo J.* (1996) 15:6662–70. doi: 10.1002/j.1460-2075.1996.tb01056.x
42. Mackey ZB, Ramos W, Levin DS, Walter CA, McCarrey JR, Tomkinson AE. An alternative splicing event which occurs in mouse pachytene spermatocytes generates a form of DNA ligase III with distinct biochemical properties that may function in meiotic recombination. *Mol Cell Biol.* (1997) 17:989–98. doi: 10.1128/mcb.17.2.989
43. Vidal AE, Boiteux S, Hickson ID, Radicella JP. XRCC1 coordinates the initial and late stages of DNA abasic site repair through protein-protein interactions. *Embo J.* (2001) 20:6530–9. doi: 10.1093/emboj/20.22.6530
44. Tebbs RS, Flannery ML, Meneses JJ, Hartmann A, Tucker JD, Thompson LH, et al. Requirement for the Xrcc1 DNA base excision repair gene during early mouse development. *Dev Biol.* (1999) 208:513–29. doi: 10.1006/dbio.1999.9232
45. Montaldi AP, Sakamoto-Hojo ET. Methoxyamine sensitizes the resistant glioblastoma T98G cell line to the alkylating agent temozolomide. *Clin Exp Med.* (2013) 13:279–88. doi: 10.1007/s10238-012-0201-x
46. Fishel ML, He Y, Smith ML, Kelley MR. Manipulation of base excision repair to sensitize ovarian cancer cells to alkylating agent temozolomide. *Clin Cancer Res.* (2007) 13:260–7. doi: 10.1158/1078-0432.ccr-06-1920
47. Liuzzi M, Talpaert-Borle M. A new approach to the study of the base-excision repair pathway using methoxyamine. *J Biol Chem.* (1985) 260:5252–8.
48. National Cancer Institute. *Cancer.Gov: Radiation Therapy to Treat Cancer*. (Vol. 4). New York, NY: National Cancer Institute (2019).
49. Aparicio T, Baer R, Gautier J. DNA double-strand break repair pathway choice and cancer. *DNA Repair (Amst).* (2014) 19:169–75. doi: 10.1016/j.dnarep.2014.03.014
50. Ward JF. DNA damage produced by ionizing radiation in mammalian cells: identities, mechanisms of formation, and reparability. In: Cohn WE, Moldave

K editors. *Progress in Nucleic Acid Research and Molecular Biology*. (Vol. 35), Cambridge, MA: Academic Press (1988). p. 95–125.
51. Mladenov E, Magin S, Soni A, Iliakis G. DNA double-strand break repair as determinant of cellular radiosensitivity to killing and target in radiation therapy. *Front Oncol.* (2013) 3:113.
52. Borrego-Soto G, Ortiz-Lopez R, Rojas-Martinez A. Ionizing radiation-induced DNA injury and damage detection in patients with breast cancer. *Genet Mol Biol.* (2015) 38:420–32. doi: 10.1590/s1415-475738420150019
53. Deckbar D, Jeggo PA, Lobrich M. Understanding the limitations of radiation-induced cell cycle checkpoints. *Crit Rev Biochem Mol Biol.* (2011) 46:271–83. doi: 10.3109/10409238.2011.575764
54. Williams GJ, Hammel M, Radhakrishnan SK, Ramsden D, Lees-Miller SP, Tainer JA. Structural insights into NHEJ: building up an integrated picture of the dynamic DSB repair super complex, one component and interaction at a time. *DNA Repair (Amst).* (2014) 17:110–20. doi: 10.1016/j.dnarep.2014.02.009
55. Ochi T, Wu Q, Blundell TL. The spatial organization of non-homologous end joining: from bridging to end joining. *DNA Repair (Amst).* (2014) 17:98–109. doi: 10.1016/j.dnarep.2014.02.010
56. Roberts SA, Strande N, Burkhalter MD, Strom C, Havener JM, Hasty P, et al. Ku is a 5'-dRP/AP lyase that excises nucleotide damage near broken ends. *Nature.* (2010) 464:1214–7. doi: 10.1038/nature08926
57. Gu J, Lu H, Tippin B, Shimazaki N, Goodman MF, Lieber MR. XRCC4:DNA ligase IV can ligate incompatible DNA ends and can ligate across gaps. *Embo J.* (2007) 26:1010–23. doi: 10.1038/sj.emboj.7601559
58. Krejci L, Altmannova V, Spirek M, Zhao X. Homologous recombination and its regulation. *Nucleic Acids Res.* (2012) 40:5795–818.
59. Limbo O, Chahwan C, Yamada Y, de Bruin RAM, Wittenberg C, Russell P. Ctp1 is a cell-cycle-regulated protein that functions with Mre11 complex to control double-strand break repair by homologous recombination. *Molecular Cell.* (2007) 28:134–46. doi: 10.1016/j.molcel.2007.09.009
60. West SC. Molecular views of recombination proteins and their control. *Nat Rev Mol Cell Biol.* (2003) 4:435–45. doi: 10.1038/nrm1127
61. Masson JY, Tarsounas MC, Stasiak AZ, Stasiak A, Shah R, McIlwraith MJ, et al. Identification and purification of two distinct complexes containing the five RAD51 paralogs. *Genes Dev.* (2001) 15:3296–307. doi: 10.1101/gad.947001
62. Constantinou A, Chen X-B, McGowan CH, West SC. Holliday junction resolution in human cells: two junction endonucleases with distinct substrate specificities. *EMBO J.* (2002) 21:5577–85. doi: 10.1093/emboj/cdf554
63. Matos J, West SC. Holliday junction resolution: regulation in space and time. *DNA Repair (Amst).* (2014) 19:176–81. doi: 10.1016/j.dnarep.2014.03.013
64. Ward JF. Biochemistry of DNA lesions. *Radiat Res Suppl.* (1985) 8:S103–11.
65. Blaisdell JO, Wallace SS. Abortive base-excision repair of radiation-induced clustered DNA lesions in *Escherichia coli*. *Proc Natl Acad Sci USA.* (2001) 98:7426–30. doi: 10.1073/pnas.131077798

Conflict of Interest: The authors declare that the research was conducted in the absence of any commercial or financial relationships that could be construed as a potential conflict of interest.

frontiers in Oncology

ORIGINAL RESEARCH
published: 22 October 2020
doi: 10.3389/fonc.2020.554883

Host CD39 Deficiency Affects Radiation-Induced Tumor Growth Delay and Aggravates Radiation-Induced Normal Tissue Toxicity

*Alina V. Meyer[1], Diana Klein[1], Simone de Leve[1], Klaudia Szymonowicz[1], Martin Stuschke[2], Simon C. Robson[3], Verena Jendrossek[1] and Florian Wirsdörfer[1]**

[1] Medical School, Institute of Cell Biology (Cancer Research), University of Duisburg-Essen, Essen, Germany, [2] Department of Radiotherapy, University Hospital Essen, Essen, Germany, [3] Departments of Medicine and Anesthesia, Beth Israel Deaconess Medical Center, Harvard Medical School, Harvard University, Boston, MA, United States

OPEN ACCESS

Edited by:
Mary Helen Barcellos-Hoff, University of California, San Francisco, United States

Reviewed by:
Erik Wennerberg, Weill Cornell Medicine, United States
Raphael A. Nemenoff, University of Colorado Denver, United States
Gennady G. Yegutkin, University of Turku, Finland

***Correspondence:**
Florian Wirsdörfer
florian.wirsdoerfer@uk-essen.de

Specialty section:
This article was submitted to Radiation Oncology, a section of the journal Frontiers in Oncology

Received: *23 April 2020*
Accepted: *10 September 2020*
Published: *22 October 2020*

Citation:
Meyer AV, Klein D, de Leve S, Szymonowicz K, Stuschke M, Robson SC, Jendrossek V and Wirsdörfer F (2020) Host CD39 Deficiency Affects Radiation-Induced Tumor Growth Delay and Aggravates Radiation-Induced Normal Tissue Toxicity. Front. Oncol. 10:554883. doi: 10.3389/fonc.2020.554883

The ectonucleoside triphosphate diphosphohydrolase (CD39)/5′ ectonuclotidase (CD73)-dependent purinergic pathway emerges as promising cancer target. Yet, except for own previous work revealing a pathogenic role of CD73 and adenosine in radiation-induced lung fibrosis, the role of purinergic signaling for radiotherapy outcome remained elusive. Here we used C57BL/6 wild-type (WT), CD39 knockout ($CD39^{-/-}$), and CD73 knockout ($CD73^{-/-}$) mice and hind-leg tumors of syngeneic murine Lewis lung carcinoma cells (LLC1) to elucidate how host purinergic signaling shapes the growth of LLC1 tumors to a single high-dose irradiation with 10 Gy *in vivo*. In complementary *in vitro* experiments, we examined the radiation response of LLC1 cells in combination with exogenously added ATP or adenosine, the proinflammatory and anti-inflammatory arms of purinergic signaling. Finally, we analyzed the impact of genetic loss of CD39 on pathophysiologic lung changes associated with lung fibrosis induced by a single-dose whole-thorax irradiation (WTI) with 15 Gy. Loss of CD73 in the tumor host did neither significantly affect tumor growth nor the radiation response of the CD39/CD73-negative LLC1 tumors. In contrast, LLC1 tumors exhibited a tendency to grow faster in $CD39^{-/-}$ mice compared to WT mice. Even more important, tumors grown in the CD39-deficient background displayed a significantly reduced tumor growth delay upon irradiation when compared to irradiated tumors grown on WT mice. CD39 deficiency caused only subtle differences in the immune compartment of irradiated LLC1 tumors compared to WT mice. Instead, we could associate the tumor growth and radioresistance-promoting effects of host CD39 deficiency to alterations in the tumor endothelial compartment. Importantly, genetic deficiency of CD39 also augmented the expression level of fibrosis-associated osteopontin in irradiated normal lungs and exacerbated radiation-induced lung fibrosis at 25 weeks after irradiation. We conclude that genetic loss of host CD39 alters the tumor microenvironment, particularly the tumor microvasculature, and thereby promotes

growth and radioresistance of murine LLC1 tumors. In the normal tissue loss of host, CD39 exacerbates radiation-induced adverse late effects. The suggested beneficial roles of host CD39 on the therapeutic ratio of radiotherapy suggest that therapeutic strategies targeting CD39 in combination with radiotherapy have to be considered with caution.

Keywords: ionizing radiation, purinergic signaling, CD73, cancer, ATP

INTRODUCTION

Radiotherapy (RT) alone or in combination with surgery and chemotherapy is a central component of curative or palliative treatment for many cancer patients. For example, patients suffering from advanced non–small cell lung cancer (NSCLC) receive standard treatment with fractionated RT to the thoracic region or concurrent platinum-based radiochemotherapy (RCT), yielding local control rates of 40–66% (1–3). Yet, intratumoral heterogeneity and high intrinsic or acquired radioresistance can lead to relapse, whereas a pronounced radiosensitivity of coirradiated normal lung tissue causes adverse effects in sensitive patients, thereby limiting the application of curative RT doses and therapy intensification efforts of RT or RCT (3, 4). Instead tolerable radiation doses are often linked to suboptimal tumor control, despite accepting side effects that decrease quality of life (2, 3, 5). Current efforts to improve RT outcome therefore aim at combining highly conformal RT with molecularly tailored treatments to increase efficacy of tumor cell killing or reduce adverse effects to normal tissues, respectively. Based on exciting findings about RT-induced support of local and systemic antitumor immunity particularly in combination with immunotherapy (6–11), further clinical trials evaluate the use of combining RT or RCT with immune checkpoint inhibitors (ICIs); yet despite encouraging results and durable responses obtained, for example, in NSCLC patients, only a fraction of patients respond to multimodal therapies with RCT and inhibitors of the PD-1/PD-L1 immune checkpoint, or patients develop resistance (12, 13). Because RT-induced immune effects can also contribute to radiation-induced adverse effects (14–16), sensitive patients may even suffer from more pronounced radiotoxicity or fear new immune-related adverse effects upon such multimodal combinatorial treatments (13, 17–19). A better understanding of the mechanisms underlying resistance to RT/ICI and of immune-associated adverse effects is required for the design of effective combinatorial treatments that are suited to overcome these limitations. For improving the therapeutic gain of RT, such combinatorial treatments will ideally sensitize the tumor cells only, or at least more substantially than the coirradiated normal tissues or prevent or reduce acute and late toxicities to normal tissues without protecting the tumor.

Herein, the purinergic pathway emerges as promising immune checkpoint for improving antitumor immune responses and the efficacy of immunotherapy in cancer patients, including lung cancer (20–24). The canonical adenosinergic pathway is an evolutionary conserved signaling system that converts extracellular proinflammatory ATP, a potent danger signal, into immunosuppressive adenosine (Ado) through the concerted action of ectonucleoside triphosphate diphosphohydrolase (CD39) and ecto-5′-nucleotidase (CD73), thus functioning as an "immune checkpoint" (25). CD39 and CD73 are expressed by immunosuppressive immune cell types, particularly regulatory T cells (Tregs) and regulatory B cells and mesenchymal stem cells, and are important to their immunosuppressive actions (25–27). Furthermore, CD39 and CD73 are expressed on other immune cells, for example, neutrophils, monocytes, macrophages, and dendritic cells, as well as on human alveolar and bronchial epithelial cells, fibroblasts and the vascular endothelium, and contribute in regulating their phenotypes (28, 29) and functions in various physiological processes with potential pathophysiological function, e.g., angiogenesis and vasculogenesis, barrier function, leukocyte transmigration, wound healing, and potentially cell death (30–32). Intriguingly, solid human tumors coopt the physiological functions of CD39 and CD73 to support tumor growth–promoting neovascularization, tumor metastasis, and tumor immune escape by various mechanisms (25, 33–38). In fact, CD39 and CD73 are expressed on various tumor cells supporting high extracellular Ado levels in the adverse microenvironment of solid tumors, particularly in the context of hypoxia (39). CD39 is overexpressed in lung cancer, and inhibition of CD39 on tumor cells alleviated their immunosuppressive activity (40). Furthermore, CD39 expression identified exhaustion of tumor-infiltrating $CD8^+$ T cells in tumor regions of the lung (41). CD73 is also expressed on lung cancer cells, as well as on tumor-promoting mesenchymal stromal cells and myeloid-derived suppressor cells in tumor tissue from NSCLC patients, and has been identified as a prognostic factor for poor overall survival and recurrence-free NSCLC survival (42–44).

Thus, modulating CD39, CD73, and/or Ado in the tumor microenvironment (TME) is considered as attractive novel therapeutic strategy to limit tumor progression and improve antitumor immune responses (20, 45–47). Although up-regulation of CD39 and CD73 in circulating immune cells of cancer patients upon RCT has been reported (48), the role of the CD39/CD73 immune checkpoint for the tumor response to RT has not yet been investigated in detail. We hypothesized that activation of purinergic signaling may not only contribute to an immunosuppressive environment in NSCLC patients but also dampen RT-induced antitumor immune responses. Even more important, own previous work on the pathogenic role of CD73 in radiation-induced lung fibrosis in mice (49, 50) suggests that pharmacologic strategies inhibiting CD73-dependent accumulation of Ado might be suited to improve the therapeutic ratio of RT by influencing both tumor-promoting and fibrosis-promoting effects of CD73/Ado signaling

in irradiated tumor and normal tissues. Yet, the role of CD39 in radiation-induced lung fibrosis had not yet been investigated.

The previously described canonical pathway produces Ado through the metabolism of ATP toward AMP through the action of CD39. Among the extracellular nucleotides that can highly increase and become catabolized under pathologic conditions is also the extracellular nicotinamide adenine dinucleotide (NAD^+) in addition to ATP (51, 52). In this non-canonical pathway, extracellular NAD^+ is metabolized into ADP ribose (ADPR) via the cyclic ADPR hydrolase (CD38). The product is further converted to AMP via the action of ectonucleotide pyrophosphatase/phosphodiesterase family member 1 (ENPP1 or CD203a/PC-1) (53–56). Moreover, CD203a is capable to hydrolyze ATP, NAD^+, and ADPR directly to produce AMP, but CD203a has a (significantly) lower affinity to ATP (57, 58). Both described adenosinergic pathways are able to produce AMP that converges to CD73, where it is degraded to Ado. Thus, both the canonical and non-canonical pathway can exert functions in pathological settings.

Cancer and fibrosis are both complex multistep processes that are tightly integrated with deregulated immune defense. Because various cell types involved in the underlying wound healing and tissue repair mechanisms respond to both ATP and Ado (32), we were interested to further elucidate how host purinergic signaling, especially the canonical pathway, shapes radiation responses in tumor and normal lung tissues and to shed light on potential context-dependent actions of the purinergic signaling under malignant vs. benign conditions. Here, we used mice with genetic deficiency of CD39 and CD73 to explore the impact of CD39 and CD73 in the tumor host on radiation-induced tumor growth delay in the syngeneic LLC1 murine lung cancer model and the consequences of CD39 deficiency for radiation-induced lung fibrosis. A better understanding of the mechanisms underlying the beneficial and adverse effects of purinergic signaling in tumor and normal tissue responses to RT will allow us to define rational strategies for exploiting the CD39/CD73 immune checkpoint to improve RT outcome.

MATERIALS AND METHODS

Cells

The murine Lewis lung carcinoma cell line LLC1 was purchased from ATCC (Manassas, VA, USA) and was cultured in Dulbecco modified eagle medium (DMEM) with 10% fetal calf serum (FCS).

Mice

Eight- to twelve-week-old C57BL/6 [wild-type (WT) controls], CD39-deficient ($CD39^{-/-}$; C57BL/6 background) (59) and CD73-deficient mice ($CD73^{-/-}$; C57BL/6 background; kindly provided from Dr. Linda F. Thompson, Oklahoma Medical Research Foundation, Oklahoma City, OK, USA) (30) were bred and kept under specific pathogen-free conditions in the Laboratory Animal Facilities of the University Hospital in Essen. Mixed genders of each mice strain were used. All protocols were approved by the universities' animal protection boards in conjunction with the legal authority (LANUV Düsseldorf) according to German animal welfare regulations and by the Committee on the Ethics of Animal Experiments of the responsible authorities [Landesamt für Natur, Umwelt und Verbraucherschutz (LANUV), Regierungspräsidium Düsseldorf Az.84-02.04.2015.A518 and 84-02.04.2014.A351].

Thorax Irradiation

Mice were anesthetized with 2% isoflurane, placed in holders and irradiated either with a single dose of 0 (sham control) or 15 Gy over their whole thorax [whole-thorax irradiation (WTI)] using a Cobalt-60 source (Phillips, Hamburg, Germany; 0.5 Gy/min) as described previously (60). This setup for WTI with the Cobalt-60 source using a single dose of 15 Gy induces a moderate fibrosis in C57BL/6 mice (49).

Mouse Tumor Model

Mouse syngeneic tumors were generated by subcutaneous injection of 0.5×10^6 LLC1 cells into the hindlimb of mice (total volume 50 μL) as previously described for prostate cancer (61, 62). As predefined single-dose irradiation for LLC1 hind-leg tumors from the literature (63–65), a dose of 10 Gy was confirmed for the growth retardation of LLC1 hind-leg tumors (set up experiments) and replicated to study potential additional effects of genetic modification or drug treatment. Animals of each experimental group received a single subcutaneous injection. For radiation (tumor volume: ∼ 100 mm^3), mice were anesthetized (2% isoflurane), and tumors were exposed to a single dose of 10 Gy ± 5% in 5-mm tissue depth (∼1.53 Gy/min, 300 kV, filter: 0.5 mm Cu, 10 mA, focus distance: 60 cm) using a collimated beam with an XStrahl RS 320 cabinet irradiator (XStrahl Limited, Camberly, Surrey, Great Britain).

Tissue Preparation for Paraffin Sections

Lungs and tumors were fixed in 4% Paraformaldehyde (PFA) in phosphate-buffered saline (PBS), pH 7.2, and placed in embedding cassettes. After dehydration in 70% ethanol, PFA-fixed tumors were processed using automated standard procedures and subsequent embedding in paraffin. Six-micrometer tissue sections were obtained with a Leica microtome and mounted on coated microscope slides.

Immunohistochemistry and Histology

Paraffin-embedded tissue sections were hydrated using a descending alcohol series, incubated for 10 min in H_2O_2 and for 10 min in target retrieval solution (95°C) and further incubated for 30 min with blocking solution (2% goat serum/PBS). Permeabilized sections were incubated with primary antibodies overnight at 4°C. Antigen was detected with a peroxidase-conjugated secondary antibody and DAB staining (Dako, Agilent, Santa Clara, USA). Nuclei were counterstained using hematoxylin. Tissue sections were stained with hematoxylin and eosin and Masson Goldner trichrome (Carl Roth, Karlsruhe, Germany) as previously described (49, 66).

Immunofluorescence

Immunofluorescence staining of paraffin-embedded lung tissue was performed using the Mouse on Mouse (M.O.M.™) Immunodetection Kit BASIC (Vector Laboratories) according to

the manufacturer's instructions. Tissue sections were incubated with anti-CD34 (MEC 14.7; Santa Cruz Biotechnology, Dallas, TX, USA) antibody ON at 4°C. Anti-CD34 was detected using a secondary anti–mouse Alexa Fluor® 488 antibody (Invitrogen, Thermo Fisher Scientific, Waltham, MA, USA). Slides were further stained with DAPI.

Semiquantitative Analysis of Lung Tissue Using Orbit Image Analysis

Osteopontin (OPN) and transforming growth factor β (TGF-β) (R&D Systems, Bio-Techne GmbH, Wiesbaden-Nordenstedt, Germany) stained lung tissue slides were photographed using a 25-fold magnification, and pictures were analyzed for positively stained areas in the lung tissue using the Software Orbit Image Analysis version 2.65 [Idorsia Pharmaceuticals Ltd., (67)]. Positively defined areas were calculated as percentage of the whole tissue lung section.

Semiquantitative Analysis of the Tumor Proliferative Activity

DAB quantification of slides stained for proliferation cell nuclear antigen (PCNA) (GeneTex Inc., Irvine, USA) and counterstained with hematoxylin was performed by semiquantitative analyses. Ten random, non-overlapping fields (magnification, ×200) of tumor tissue from each specimen were photographed, and pictures were automated single cell counted for DAB using the "Fiji" version of ImageJ from http://fiji.sc (68). The following adjustments for automatic counting were used: Color Deconvolution DAB, threshold 150, particle size 150–6,000, Circularity 0.14–1.00. From all fields, the mean counts were averaged to yield the final score for each specimen.

Fibrosis Scoring

Lung sections were stained with hematoxylin and eosin (H&E) or Masson Goldner trichrome (MT) (Carl Roth) and scored by four individuals blinded to the genotype and treatment group. Ten random, non-overlapping fields (magnification, ×200) of lung parenchyma from each specimen were photographed, and lung fibrosis was scored using a 0–8-point *Ashcroft* scale (69). The mean scores for each observer were averaged to yield the final score for each specimen.

Tumor-Infiltrating Immune Cell Phenotyping

Tumors were cut into pieces, and the tissue was sequentially passed with DMEM medium through a 70-μm cell strainer and subsequently centrifuged by 1,500 rpm for 7 min. Total tumor cells were then rinsed with an erythrocyte lysis buffer (containing 0.15 M NH_4Cl, 10 mM $KHCO_3$, and 0.5 M EDTA), passed through a 30-μm cell strainer, and washed with DMEM medium and 10% FCS for subsequent phenotyping. Isolated cells were stained with fixable viability dye eFluor780 to identify living cells and anti–mouse CD45 PacificBlue (30-F11) for total leukocytes, respectively. Within tumor-infiltrating leukocytes, populations were further characterized for Ly6C, Ly6G, CD11b, CD11c, CD3, CD4, and CD8. Antibodies were obtained from BD Biosciences (Heidelberg, Germany), BioLegend (Fell, Germany), or eBioscience (Frankfurt, Germany). Analyses were performed on an LSRII using FACS DIVA Software version 8.0.1 (BD Biosciences, Germany).

Irradiation of Cell Cultures

Radiation with a dose of 0, 5, and 10 Gy was performed using the ISOVOLT-320 X-ray machine (Seifert–Pantak, East Haven, CT) at 320 keV, 10 mA, dose rate about 3 Gy/min with a 1.65-mm aluminum filter, and a distance of about 500 mm to the object being irradiated (61).

Treatment of Cells

For the flow cytometry analysis of the LLC1 cell line, cells were incubated with ATP used at a final concentration of 1,000 μg/mL and Ado at a final concentration of 2,000 μg/mL (both purchased from Sigma–Aldrich Chemie GmbH, Steinheim, Germany). These concentrations were chosen according to *in vitro* investigations for determination of the half maximal inhibitory concentration (IC_{50}) using the crystal violet assay data at 72 h after treatment (70).

Flow Cytometry Analysis of Cell Cultures

The mitochondrial membrane potential ($\Delta\Psi m$) was analyzed using the $\Delta\Psi m$-specific dye tetra-methyl-rhodamine ethyl ester (TMRE; Molecular Probes, Thermo Fisher Scientific, Grand Island, NY, USA). Cells were stained for 30 min in PBS containing 25 nM TMRE. For quantification of apoptotic DNA fragmentation (sub-G1 population), cells were incubated for 15–30 min with a staining solution containing 0.1% (wt/vol) sodium citrate, 50 μg/mL Propidium iodide (PI), and 0.05% (vol/vol) Triton X-100 (vol/vol) (61, 62). For quantification of expression of surface markers, cell lines were further fluorochrome-labeled with antibodies against CD73, CD39, P2X7R (Biolegend), AdoRA1 (Bioss Antibodies, Woburn, USA), AdoRA2A (Santa Cruz, Heidelberg, Germany), AdoRA2B (Bioss Antibodies), and AdoRA3 (Abcore, Ramona, USA). The specificity of all antibodies has been tested using primary murine total lung cells. The specificity of anti-CD73, anti-CD39, anti-AdoRA2A, and anti-AdoRA2B had been additionally tested using cells from the respective knockout mice (CD39, CD73, A2AR, A2BR) as a control. Cells were subsequently analyzed by flow cytometry using Cellquest Pro (FACS Calibur; Becton Dickinson, Heidelberg, Germany).

Real-Time Reverse Transcription Polymerase Chain Reaction

RNA was isolated using RNeasy Mini Kit (74,106; Qiagen, Hilden, Germany) according to the manufacturer's instruction. Total RNA (1 μg) was used for reverse transcription with Superscript™-II reverse transcriptase (Qiagen) using oligo-dT primers according to the manufacturer's instructions; 0.5 μL of obtained cDNA was used for polymerase chain reaction (PCR) reaction as previously described (71). Analysis was carried out using the oligonucleotide primers (bActin_fw CCAGAGCAAGAGAGGTATCC, bActin_bw

CTGTGGTGGTGAAGCTGTAG; VE-Cad_fw CAG CAC TTC AGG CAA AAA CA, VE-Cad_bw ATTCGGAAGAATTG GCCTCT; VEGFR2_fw ATGACAGCCAGACAGACAGT; VEGFR2_bw GGTGTCTGTGTCATCTGAGT, VCAM_fwAA GGCAGGCTGTAAAAGAATTG, VCAM_bw ATTCCAGA ATCTTCCATCCTCA, CD38_fw ACAAGAGAAGAC TACGCCCCAC, CD38_bw CACACCACCTGAGATCAT CAGC, ENPP1_fw AGAACAGGACCACAGTGGGAAG, ENPP1_bw TAACAGGGGAAAGGGCAAGGAG) as previously described (72, 73).

Statistics

Statistical analyses were performed using Prism 7.0e (GraphPad, La Jolla, CA, USA). Student two-tailed unpaired *t*-tests were used to compare differences between two groups. One-way analysis of variance (ANOVA) followed by Tukey multiple comparison tests were used to compare more than two groups. Two-way ANOVA with *post hoc* Tukey, Bonferroni, or Newman–Keuls multiple comparison tests were used to compare groups split on two independent variables. Statistical significance was set at $P < 0.05$.

RESULTS

Loss of Host CD39 Abrogates Radiation-Induced Tumor Growth Delay, Whereas Loss of CD73 Had No Effect

First, we aimed to explore the role of CD39 and CD73 in the tumor host for tumor growth and response to therapeutic irradiation using Lewis lung carcinoma (LLC1) cells, a syngeneic C57BL/6 tumor model. LLC1 tumor cells were subcutaneously implanted onto the hind-leg of C57BL/6 WT mice, CD39-deficient mice ($CD39^{-/-}$), or CD73-deficient mice ($CD73^{-/-}$) (**Figures 1**, **2**). When the tumors reached a volume of 50–100 mm^3 (after 5–7 days), tumors of each mouse strain were irradiated with 0 Gy (sham control) or 10 Gy, and tumor growth was followed up until tumors reached a critical size of 1,000 mm^3 (**Figure 1A**).

Characterization of purinergic signaling in the tumor cells revealed that LLC1 cells uncovered a CD39 gene expression that was not altered by irradiation (data not shown), but cell surface staining revealed that the LLC1 cells did neither express CD39, CD73, nor the ATP receptor P2X7R (**Figure 1B**), nor did irradiation with 5 or 10 Gy induce an expression of

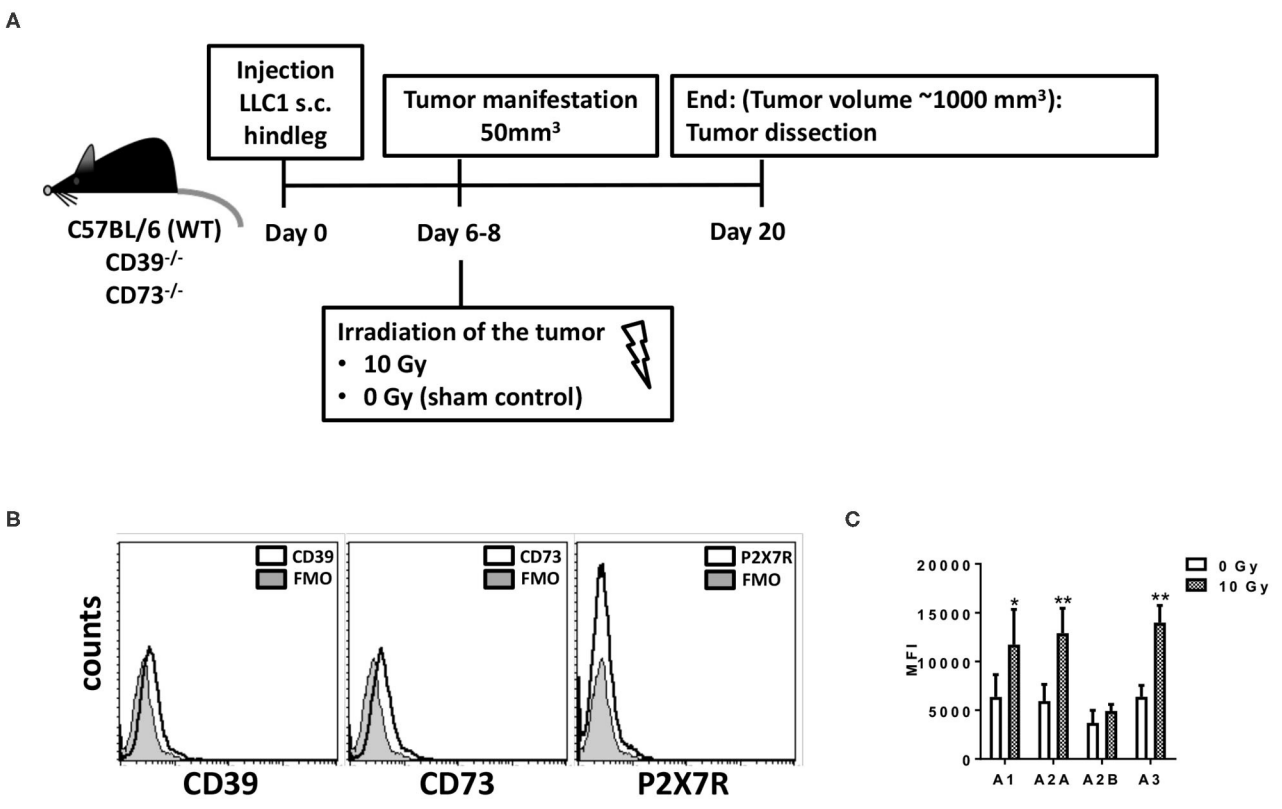

FIGURE 1 | LLC1 murine lung cancer cells are deficient for CD39, CD73, and P2X7 but express the four Ado receptors. For *in vivo* experiments mouse syngeneic tumors were generated by subcutaneous injection of 0.5×10^6 LLC1 cells into the hindlimb of C57BL/6 (WT), $CD73^{-/-}$, and $CD39^{-/-}$ mice. On days 6–8 after tumor manifestation, tumors were irradiated with 0 Gy (sham) or 10 Gy. Tumors were dissected at day 20 or when the tumor volume reached 1,000 mm^3. **(A)** Schematic depiction of the experimental setup. **(B,C)** LLC1 cells were stained against **(B)** CD39, CD73, P2X7R; FMO = fluorescence minus one) or **(C)** AdoR- A1, A2A, A2B, and A3 and were further analyzed by flow cytometry (data show means ± SD; $^*P \leq 0.05$, $^{**}P \leq 0.01$ by one-way ANOVA followed by *post hoc* Newman–Keuls test).

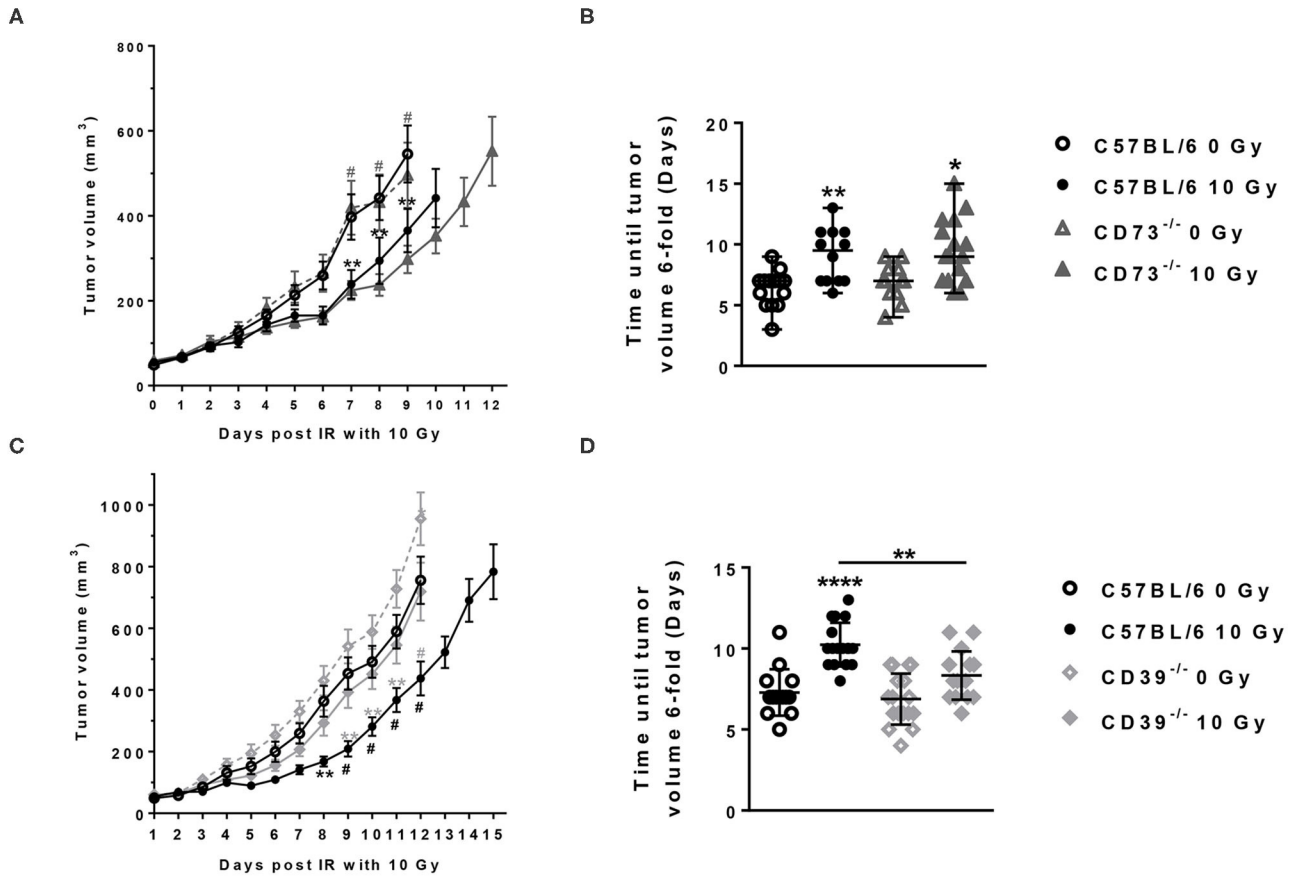

FIGURE 2 | Host CD39 deficiency accelerates LLC1 tumor growth and reduces radiation-induced tumor growth delay. LLC1 tumor cells (0.5×10^6 cells each) were subcutaneously transplanted onto the hindlimb of C57BL/6 wild-type (circles) CD73-knockout [knockout ($^{-/-}$), triangles] and CD39$^{-/-}$ (diamonds) mice. Hind-leg single-dose irradiation with 0 or 10 Gy was conducted at the timepoint of tumor manifestation (~100 mm^3). LLC1 tumor volume in mm^3 in respective experimental groups was determined at indicated time points using a sliding caliper (A/C). Growth delay was calculated as time (days) until the 6-fold tumor volume was reached (B/D). Shown are means ± SEM, $^*P \leq 0.05$, $^{**}P \leq 0.01$, $^{\#,****}P \leq 0.0001$ analyzed by two-way ANOVA followed by a *post hoc* Tukey test, *n* **(A)** = 15/17/17/15; *n* **(B)** = 17/15/13/16; n **(C)** = 16/14/13/16, *n* **(D)** = 13/14/15/15. In **(A,C)**, significant results between the animal of the same groups are marked with asterisks (0 and 10 Gy) and between the strains (C57BL/6 10 Gy and CD73$^{-/-}$ or CD39$^{-/-}$ 10 Gy) with hashtags.

these markers (data not shown). However, LLC1 cells expressed all four AdoR, namely, AdoRA1, AdoRA2A, AdoRA2B, and AdoRA3, and except AdoRA2B, the expression levels of the AdoR further increased upon irradiation (**Figure 1C** and **Supplementary Figure 1**). Thus, the LLC1 cells were an optimal tool to investigate the role of CD39 and CD73 in the tumor–host on tumor growth and RT response.

No differences in growth were detected between tumors growing on the unirradiated C57BL/6 and CD73$^{-/-}$ mice between the day of irradiation and the end of the experiment (**Figures 2A,B**). As expected, exposure to a single dose of 10 Gy induced a significant growth delay of the LLC1 tumors in the irradiated C57BL/6, as well as in the irradiated CD73$^{-/-}$ mice, compared to their unirradiated controls resulting in a difference in tumor volume of 180.2 ± 47.75 mm^3 in WT and 210.2 ± 47.63 mm^3 in CD73$^{-/-}$ mice at day 9 after irradiation (**Figures 2A,B**). Although there was a trend for a slight increase in growth retardation of irradiated LLC1 tumors grown on CD73-deficient background compared to WT mice, the differences in radiation-induced tumor growth delay between the LLC1 tumors grown in the C57BL/6 and CD73$^{-/-}$ mice did not reach statistical significance (**Figures 2A,B**).

In contrast, tumors tended to grow faster on the CD39-deficient mice than on WT mice (**Figure 2C**). The follow-up of the tumor growth demonstrated that without irradiation tumors grown on CD39$^{-/-}$ mice reached a certain tumor volume at an earlier time point than tumors grown on WT mice, yielding a significant difference of ~200 mm^3 between WT and CD39$^{-/-}$ mice at day 12 (**Figure 2C**). Exposure of the LLC1 tumors to a single irradiation with 10 Gy significantly delayed LLC1 tumor growth in both backgrounds (**Figures 2C,D**). Herein, average differences in tumor volumes of ~200 ± 100 mm^3 between irradiated tumors and sham controls were obtained at days 8–12 in tumors grown on WT mice and were thus comparable to the growth delay values obtained in the experiments with WT and CD73$^{-/-}$ mice described above (**Figures 2A,B**). In

contrast, irradiated tumors grown on CD39$^{-/-}$ mice showed a significantly reduced growth delay in comparison to the values observed in irradiated tumors from WT mice (**Figures 2C,D**). The time until the tumors reached a 6-fold volume upon irradiation was significantly shorter (by 2 days) for tumors growing on CD39$^{-/-}$ mice compared to irradiated tumors on WT mice, indicating a radioresistance promoting effect of CD39 deficiency in the tumor host (**Figure 2D**). These differences were not due to differences in tumor volume at the time of irradiation (data not shown).

ATP and Ado have been described to impact the survival of cancer cells (74–76). In complementary *in vitro* investigations, we therefore aimed to explore if high ATP or Ado levels would impact cancer cell survival. Therefore, we determined the effects of exogenously added extracellular ATP and Ado in combination with irradiation on short-term cell survival (**Figure 3**). In untreated cells, irradiation induced a dose-dependent increase in cells with low mitochondrial potential (**Figure 3A**), in the sub-G1 population (**Figure 3B**), and in PI-positive cells (**Figure 3C**) 48 h after irradiation, which is indicative for the induction of apoptosis and total cell death, respectively. Similar results were obtained when ATP was added to the culture medium 1 h before irradiation up to a concentration of 1 mg/mL. Despite a trend to single-drug toxicity of exogenously added ATP on LLC1 cells, high ATP levels in the culture medium did not alter the toxic effects of irradiation with 5 or 10 Gy in these cells (**Figures 3A–C**). In contrast, very high extracellular Ado concentrations (2 mg/mL) were highly toxic to the LLC1 cells, as indicated by the significant increase in the fraction of LLC1 cells with a low mitochondrial potential, in the sub-G1 population, and of PI-positive cells (**Figures 3A–C**). Yet, neither a further increase in toxicity nor a protective effect of high Ado levels in the culture medium was observed in LLC1 cells in combination with irradiation (**Figures 3A–C**).

CD39 Deficiency in the Tumor Host Did Not Significantly Alter Radiation-Induced Tumor Immune Responses

As ATP and Ado are well-known potent immunomodulators, we next investigated a potential contribution of differences in infiltrating immune cells within LLC1 tumors to the observed effects by quantification and phenotypic characterization of immune cell subsets using flow cytometry. To study an initial irradiation-induced immune infiltration, tumors were harvested 3 days after irradiation with 0 Gy (sham controls) or 10 Gy and subjected to immune cell analysis (**Figure 4**). Irradiation of LLC1 tumors grown on WT mice induced a significant increase in the percentage of CD45^{+} leukocytes in the tumor tissue at 3 days after irradiation (**Figure 4A**). In contrast to WT mice, unirradiated LLC1 tumors grown on CD39$^{-/-}$ or CD73$^{-/-}$ mice already had higher percentages of CD45^{+} leukocytes. While exposure to a single dose with 10 Gy did not significantly increase the number of CD45^{+} leukocytes in LLC1 tumors grown on CD39$^{-/-}$ mice, there was a significantly higher leukocyte number detected in irradiated tumors growing on CD73$^{-/-}$ mice compared to tumors grown on WT mice (**Figure 4A**).

Furthermore, no significant differences were detected for different immune cell subsets, in unirradiated LLC1 tumors growing on either WT, CD39$^{-/-}$, or CD73$^{-/-}$ mice, including neutrophils, monocytic cells, dendritic cells, and cytotoxic T lymphocytes (**Figures 4B–F**). Moreover, exposure to irradiation did not increase the infiltration either of CD11b^{+} myeloid cells (**Figure 4B**) or of CD11c^{hi} dendritic cells (**Figure 4C**) into LLC1 tumors at day 3 after irradiation in the three different mouse strains. In contrast, a significant increase in the percentage of infiltrating Ly6G^{-} Ly6C^{+} monocytic cells and a significant decrease in the percentage of Ly6G^{+} Ly6C^{-} neutrophils among tumor-infiltrating CD45^{+} immune cells were detected in irradiated tumors from WT and CD73$^{-/-}$ mice (**Figures 4D,E**). Instead, radiation-induced changes in the myeloid compartment of tumors grown on CD39$^{-/-}$ mice were not statistically significant (**Figures 4D,E**). Interestingly, exposure of LLC1 tumors to a single dose of 10 Gy induced a significantly increased percentage of CD8^{+} cytotoxic T cells in tumors grown on CD73$^{-/-}$ mice (**Figure 4F**), whereas no difference in the percentage of cytotoxic T cells was observed in irradiated tumors grown on WT and CD39$^{-/-}$ mice (**Figure 4F**).

Taken together, irradiation of LLC1 tumors with a single dose of 10 Gy induced a significant increase in immune cell infiltration when grown on WT (monocytic cells) and CD73$^{-/-}$ mice (monocytic cells, CD8^{+} T cells) but not when grown

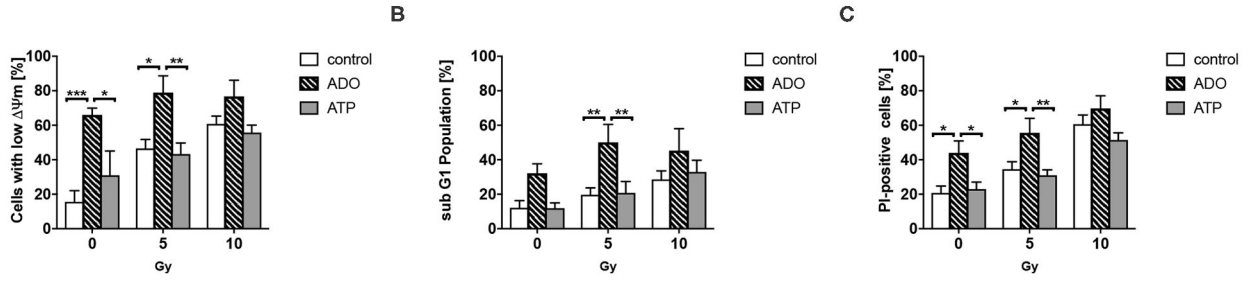

FIGURE 3 | Effects of extracellular ATP and Ado on LLC1 tumor cells *in vitro*. LLC1 cells were incubated with ATP (2 mg/mL) or Ado (1 mg/mL) 1 h prior to 0-, 5-, or 10-Gy irradiation. Forty-eight hours later, cells were stained with TMRE or PI and further analyzed with flow cytometry to investigate the **(A)** mitochondrial potential ($\Delta\Psi$m), **(B)** the sub-G1 fraction (apoptosis), and **(C)** PI-positive cells (cell death). Data show means ± SEM; $^{*}P \leq 0.05$, $^{**}P \leq 0.01$, $^{***}P \leq 0.001$ by two-way ANOVA followed by *post hoc* Tukey test.

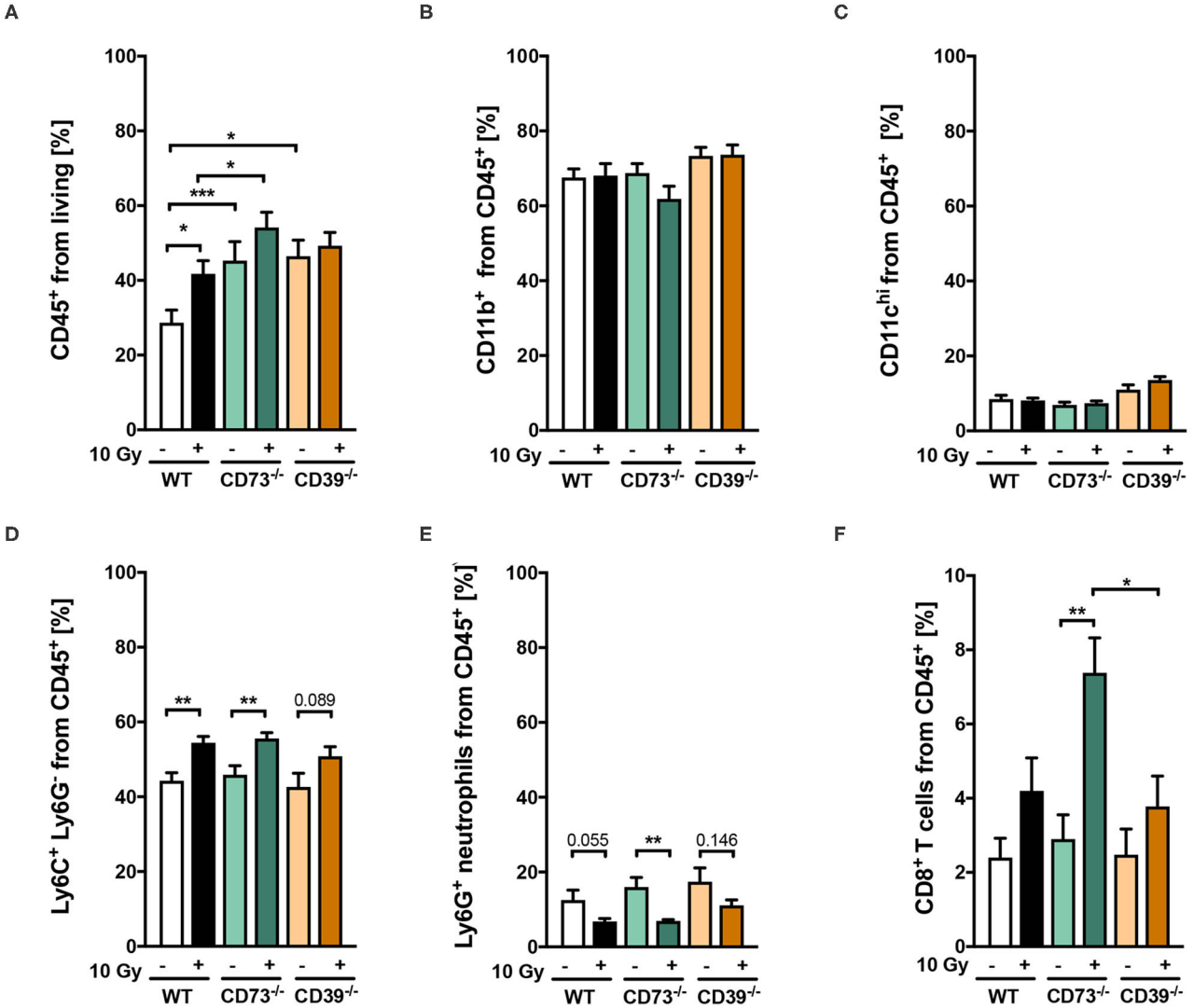

FIGURE 4 | (A–F) Host CD39 deficiency causes only subtle changes in radiation-induced tumor immune cell infiltration. LLC1 tumor cells (0.5×10^6 cells each) were subcutaneously transplanted onto the hindlimb of C57BL/6 wild-type (white/black) CD73-knockout ($CD73^{-/-}$; green, triangles) and CD39-knockout mice ($CD39^{-/-}$; orange circles) mice. Hind-leg single-dose irradiation with 0 or 10 Gy was conducted at the timepoint of tumor manifestation. Three days after irradiation, tumors were dissected, and single-cell suspensions were generated. Tumor-infiltrating leukocytes were analyzed via flow cytometry. Shown in bar diagrams are the percentages of diverse immune cell populations. Shown are means ± SEM, $^*P \leq 0.05$, $^{**}P \leq 0.01$, $^{***}P \leq 0.001$, analyzed by one-way ANOVA followed by a *post hoc* Tukey test, $n = (13/14)$ (C57BL/6), (9/9) ($CD73^{-/-}$), (10/9) ($CD39^{-/-}$).

on $CD39^{-/-}$ mice. However, because the basal infiltration of $CD45^+$ immune cells was significantly higher when LLC1 tumors grew on $CD39^{-/-}$ mice when compared to WT mice, we assumed that the subtle differences in the observed immunological parameters upon irradiation might have potential tumor promoting effects, because infiltrating myeloid cells are the majority of immune cells.

To elucidate if the non-canonical adenosinergic pathway might have an impact on a radiation-induced tumor response and immunomodulation, we analyzed the expression of CD38 and CD203a/PC-1 in LLC1 tumors grown on WT, $CD39^{-/-}$, and $CD73^{-/-}$ mice. As shown in **Supplementary Figure 2A**, quantitative reverse transcriptase (qRT)–PCR analysis revealed a CD38 mRNA expression in LLC1 cells that further increased after irradiation. However, we could not detect any CD203a mRNA expression in LLC1 cells before and after irradiation. We further performed IHC staining from paraffin-embedded tumor tissue sections from LLC1 hind-leg tumors grown on WT mice for CD38 and CD203a protein expression. Surprisingly as shown in **Supplementary Figure 2B**, LLC1 tumors itself did not express CD38 or CD203a protein, nor were there any obvious CD38/CD203a positive immune or stroma cells. Moreover, irradiation did not alter the expression, nor did the different tumor hosts (WT, $CD39^{-/-}$, and $CD73^{-/-}$) have an effect on

the expression of both receptors (data not shown). Our anti-CD38 staining from the liver tissue as positive control revealed the specificity of this antibody (**Supplementary Figure 2B**, right panel). Identical results were obtained from LLC1 tumors grown on CD39$^{-/-}$ and CD73$^{-/-}$ mice (data not shown). Nevertheless, because our data clearly demonstrate that CD203a is not expressed on gene and protein level, we hypothesize that independent of a potential CD38 expression, the adenosinergic non-canonical pathway cannot function in the tumor to produce AMP to fuel CD73.

Host CD39 Deficiency Caused a Reduced Regressive Phenotype of Irradiated Tumors

Because CD39 is also important to the function of stromal cells, e.g., fibroblasts, mesenchymal stem cells, and vascular cells, we aimed to explore a potential contribution of an altered function of stromal cells in CD39$^{-/-}$ mice to the observed differences in the radiation response of tumors grown CD39$^{-/-}$ mice vs. WT and CD73$^{-/-}$ mice. Therefore, we performed a detailed histological analysis of the respective tumor sections using H&E and MT staining (**Figure 5**).

All control (0 Gy) tumors isolated from the different mouse strains were generally characterized by a densely packed epithelial cell structure, and no obvious histological differences could be detected between tumors grown on WT, CD73$^{-/-}$, or CD39$^{-/-}$ mice (**Figure 5A**, upper panels). As expected, exposure to ionizing radiation (IR) induced regressive tissue alterations, as visualized by the reduced packaging of tumor cells, increased areas of necrosis and of connective tissue structures, and an altered morphology of the cell nuclei (violet staining), respectively (**Figure 5A**, lower panels). Of note, while tumors from WT mice and CD73$^{-/-}$ mice seemed to be similarly affected following IR, less regression and thus more remaining tumor cells became visible in tumors grown on CD39$^{-/-}$ background, indicating a reduced degree of tissue damage (**Figure 5A**, right panel). Additional Masson trichrome (MT)

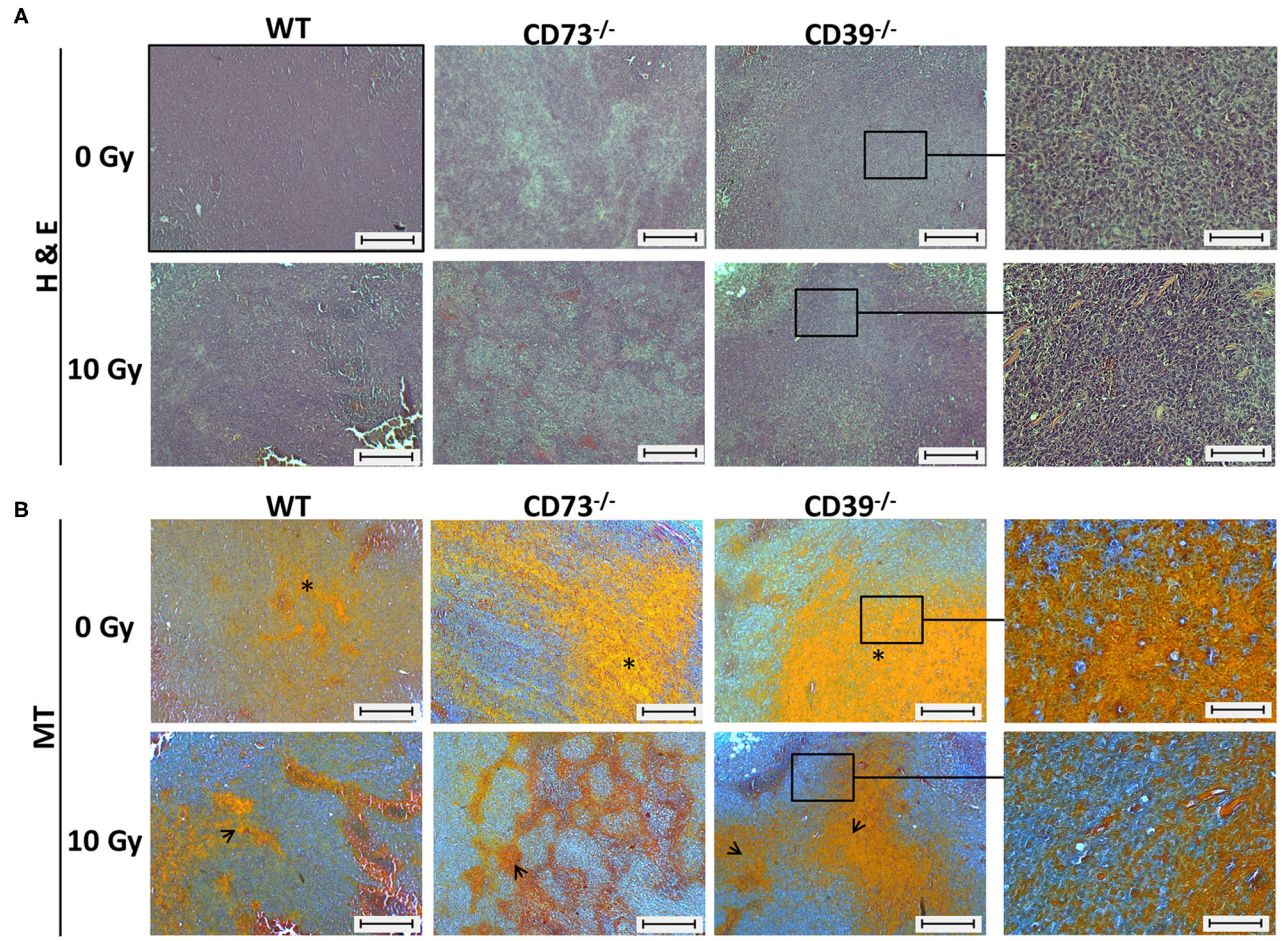

FIGURE 5 | Host CD39 deficiency causes a reduced regressive phenotype of irradiated tumors. LC1 tumor cells (0.5 × 10^6 cells each) were subcutaneously transplanted onto the hindlimb of C57BL/6 wild-type and CD39- and CD73-deficient [knockout ($^{-/-}$)] mice. Hind-leg single-dose irradiation with 0 or 10 Gy was conducted at the timepoint of tumor manifestation. Mice were sacrificed at the timepoint of maximal tumor volume (1,000 mm^3). **(A)** Hematoxylin-eosin (H&E) or **(B)** Masson Goldner trichrome (MT) staining of paraffin-embedded LLC1 tumor tissue, scale bar 100 μm. Magnified pictures (400-fold) highlight special structures. n = 15/17 (C57BL/6), 17/13 (CD39$^{-/-}$), 7/13 (CD73$^{-/-}$). Asterisks and open arrows indicate areas of a higher degree of epithelial structures (orange colored).

staining confirmed a higher degree of epithelial structures (orange colored) in tumors of CD39$^{-/-}$ mice, which might be indicative for an altered tumor cell proliferation state (**Figure 5B**).

So far, our data revealed that LLC1 grown on a CD39-deficient mouse grew faster and were less sensitive to the growth-limiting effects of RT. For further histological evaluation of the tumor tissue sections, and to specify if LLC1 tumors grown on CD39$^{-/-}$ mice have altered levels viable tumor cells and necrosis after irradiation, we investigated the proliferative activity in the tumors by immunohistological staining of the PCNA (**Figure 6**). In the respective unirradiated conditions (**Figure 6A**, upper panel), proliferating cells were found in all tumors independent of the mouse strain. Even in irradiated tumors (10–14 days after irradiation), strong PCNA immunoreactivities were detected in tumors isolated from all three mouse strains (**Figure 6A**, lower panel). Quantification of the PCNA^{+} tumor cells using an automatic DAB-positive (brown) cell counting procedure (semiquantitative analysis) revealed that in unirradiated tumors grown on CD73$^{-/-}$ and CD39$^{-/-}$ mice, significantly more PCNA^{+} cells were present than in tumors grown on WT mice (**Figure 6B**). Even more important, tumors grown on CD39$^{-/-}$ mice had significantly more PCNA^{+} cells than tumors grown on WT mice and showed no impairment in their proliferative activity after a single high-dose irradiation with 10 Gy. In line with the results obtained from the histological analyses, our findings indicate that irradiation causes less tissue damage and necrosis in tumors grown on CD39$^{-/-}$ mice when compared to tumors grown on WT or CD73-deficient mice. Thus, the loss of CD39 in the tumor host did not result in more pronounced tissue damage and inflammation upon a single high-dose irradiation with 10 Gy but instead in a more pronounced proliferation.

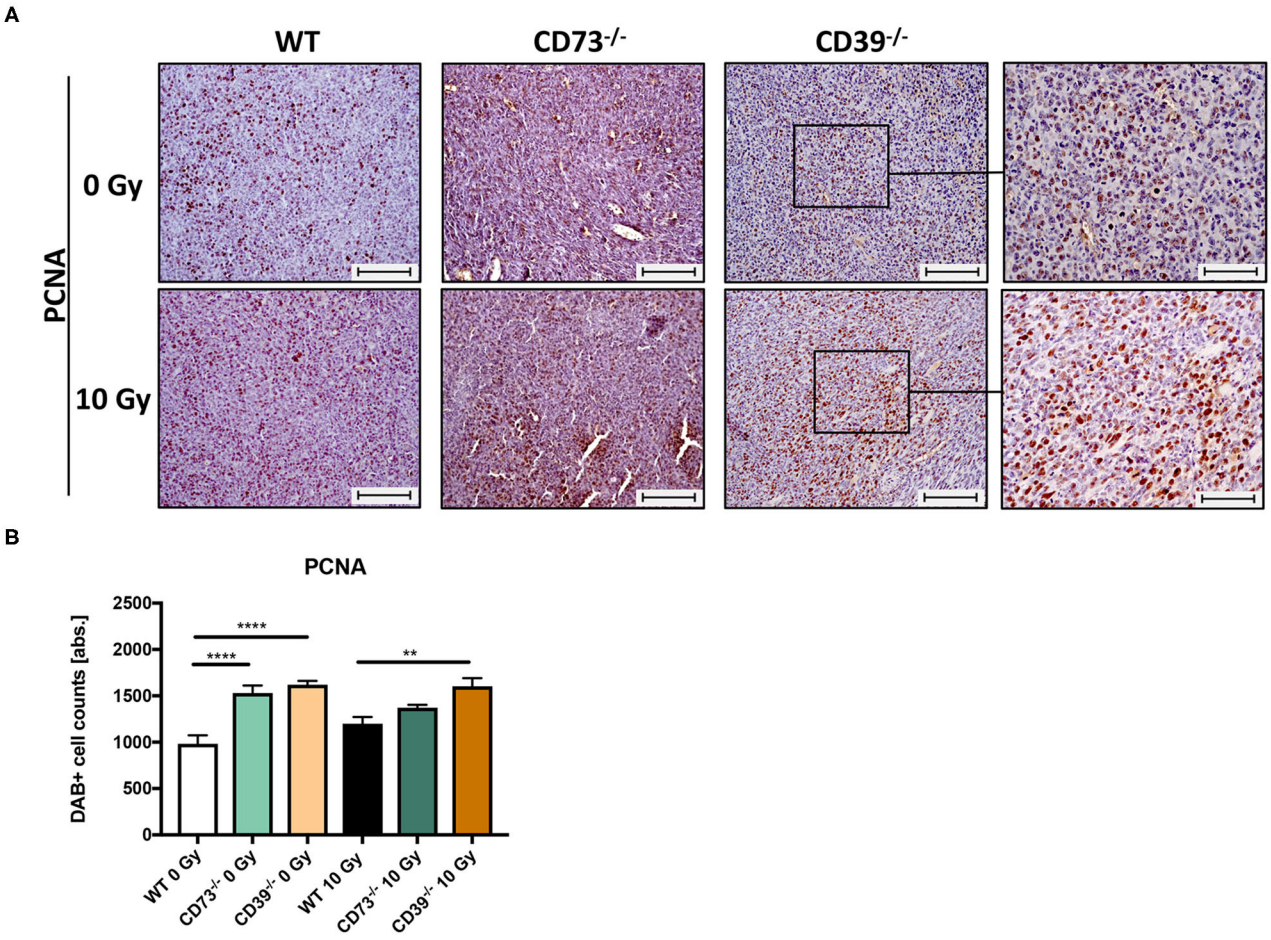

FIGURE 6 | LLC1 tumor grown on CD39$^{-/-}$ mice are not impaired in their proliferative activity after irradiation. LLC1 tumor cells (0.5 × 10^{6} cells each) were subcutaneously transplanted onto the hindlimb of C57BL/6 wild-type and CD39- and CD73-deficient [knockout ($^{-/-}$)] mice. Hind-leg single-dose irradiation with 0 or 10 Gy was conducted at the timepoint of tumor manifestation. Mice were sacrificed at the timepoint of maximal tumor volume (1,000 mm^{3}). IHC staining of proliferation cell nuclear antigen (PCNA) of paraffin-embedded LLC1 tumor tissue, magnification 200-fold, scale bar 100 μm **(A)**. Shown in bar diagrams are the absolute numbers of DAB^{+} cell counts per tissue section **(B)**. Magnified pictures (400-fold) highlight special structures. Shown are means ± SEM, $^{**}P \leq 0.01$, $^{****}P \leq 0.0001$, analyzed by one-way ANOVA followed by a *post hoc* Tukey test $n = 15/17$ (C57BL/6), $n = 17/13$ (CD39$^{-/-}$), $n = 7/13$ (CD73$^{-/-}$).

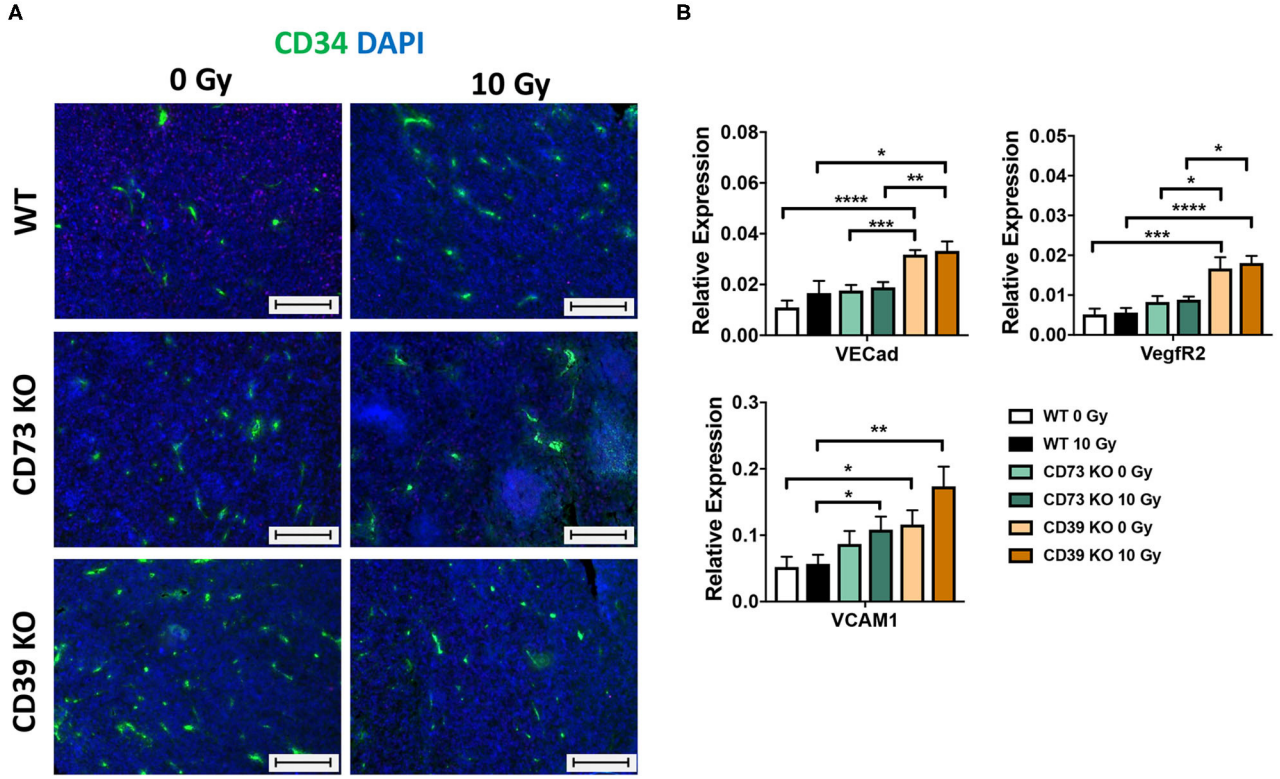

FIGURE 7 | LLC1 tumor grown on CD39$^{-/-}$ mice show an altered microvasculature. LLC1 tumor cells (0.5 × 10^6 cells each) were subcutaneously transplanted onto the hindlimb of C57BL/6 wild-type and CD39- and CD73-deficient [knockout ($^{-/-}$)] mice. Hind-leg single-dose irradiation with 0 or 10 Gy was conducted at the timepoint of tumor manifestation. Mice were sacrificed at the timepoint of maximal tumor volume (1,000 mm^3). **(A)** Immune fluorescent staining of CD34 (green) and DAPI (blue) of paraffin-embedded LLC1 tumor tissue, magnification 200-fold, scale bar 100 μm. 15/17 (C57BL/6), n = 17/13 (CD39$^{-/-}$), n = 7/13 (CD73$^{-/-}$). **(B)** RT qPCR analysis to reveal the relative expression of VE Cad, VegfR2, and VCAM1 to actin. The relative expression is shown in bar diagrams. Shown are means ± SEM, *$P \leq 0.05$, **$P \leq 0.01$, ***$P \leq 0.001$, ****$P \leq 0.0001$, analyzed by one-way ANOVA followed by a *post hoc* Tukey test n = 12/12 (C57BL/6), n = 12/12 (CD39$^{-/-}$), n = 12/12 (CD73$^{-/-}$).

Enhanced Growth and Resistance to Radiation-Induced Growth Delay of LLC1 Tumors Grown on CD39-Deficient Hosts Are Linked to Alterations in the Tumor Endothelial Compartment

Although not being directly obvious from the histological evaluation, we had the impression that the vasculature was altered in tumors growing on CD39-deficient hosts. We therefore performed immunofluorescence staining of tumor sections using the angiogenic endothelial cell marker CD34 (**Figure 7A**). As shown in **Figure 7A** (left panels), already unirradiated tumors grown on CD39$^{-/-}$ mice had more CD34$^+$ immunoreactive structures and increased microvascular densities as compared to tumors grown on WT or CD73$^{-/-}$ mice. Importantly, differences in microvascular density were still present after exposure of the tumors to a single high-dose irradiation with 10 Gy (**Figure 7A**, right panels). To further characterize the assumed differences in the vascular compartment, a qRT-PCR was performed using vascular endothelial cadherin (VE-Cad), the major angiogenic growth factor receptor VegfR2 and vascular cell adhesion protein 1 (VCAM1) as markers for tumor vascularization (**Figure 7B**). Indeed, tumors grown on CD39$^{-/-}$ mice displayed significantly enhanced expression levels of VE-Cad, VegfR2, and VCAM1 already under control conditions (0 Gy), and these differences persisted also upon irradiation as indicated by significantly increased levels of all three vascular markers, in tumors grown on CD39$^{-/-}$ mice compared to tumors grown on WT controls (**Figure 7B**). In contrast to CD39$^{-/-}$ mice, tumors grown on CD73$^{-/-}$ mice had similar expression level as tumors grown on WT mice. We could only detect a significantly increased expression of VCAM1 in irradiated tumors grown on CD73$^{-/-}$ mice compared to WT animals.

These data strongly suggest that loss of CD39 in the tumor host and the resulting changes in the TME enhance the proliferation capacity and growth of LLC1 tumors, and this was associated with alterations in the vascular compartment particularly with an increased microvascular density. The reduced sensitivity of CD39-deficient microvessels and the cytotoxic effects of RT observed in the present study particularly in CD39–/– mice may contribute to the reduced

radiation-induced tumor growth delay of LLC1 tumors and thus impact on radiation resistance.

Genetic Deficiency of CD39 Exacerbates Radiation-Induced Lung Fibrosis

A major challenge for novel strategies to improve RT outcome is to enhance tumor cell killing while limiting the risk for radiation-induced adverse effects in highly radiosensitive normal tissues such as the lung. The suggested dual role of ATP/CD39 in cancer and fibrosis and the adverse effects of CD39 deficiency in the tumor host on growth and radiation-response of LLC1 lung tumors prompted us to investigate in addition if genetic deficiency of CD39 would also alter radiation-induced adverse effects in normal lung tissue. Therefore, we examined the effects of a single high-dose WTI (15 Gy) on fibrosis development in CD39$^{-/-}$ mice compared to WT mice in our murine model of RT-induced lung disease (49). A detailed histological analysis of lungs isolated from CD39$^{-/-}$ mice and respective WT controls revealed a prominent thickening of alveolar septa, increased extracellular matrix deposition, and multiple fibrotic

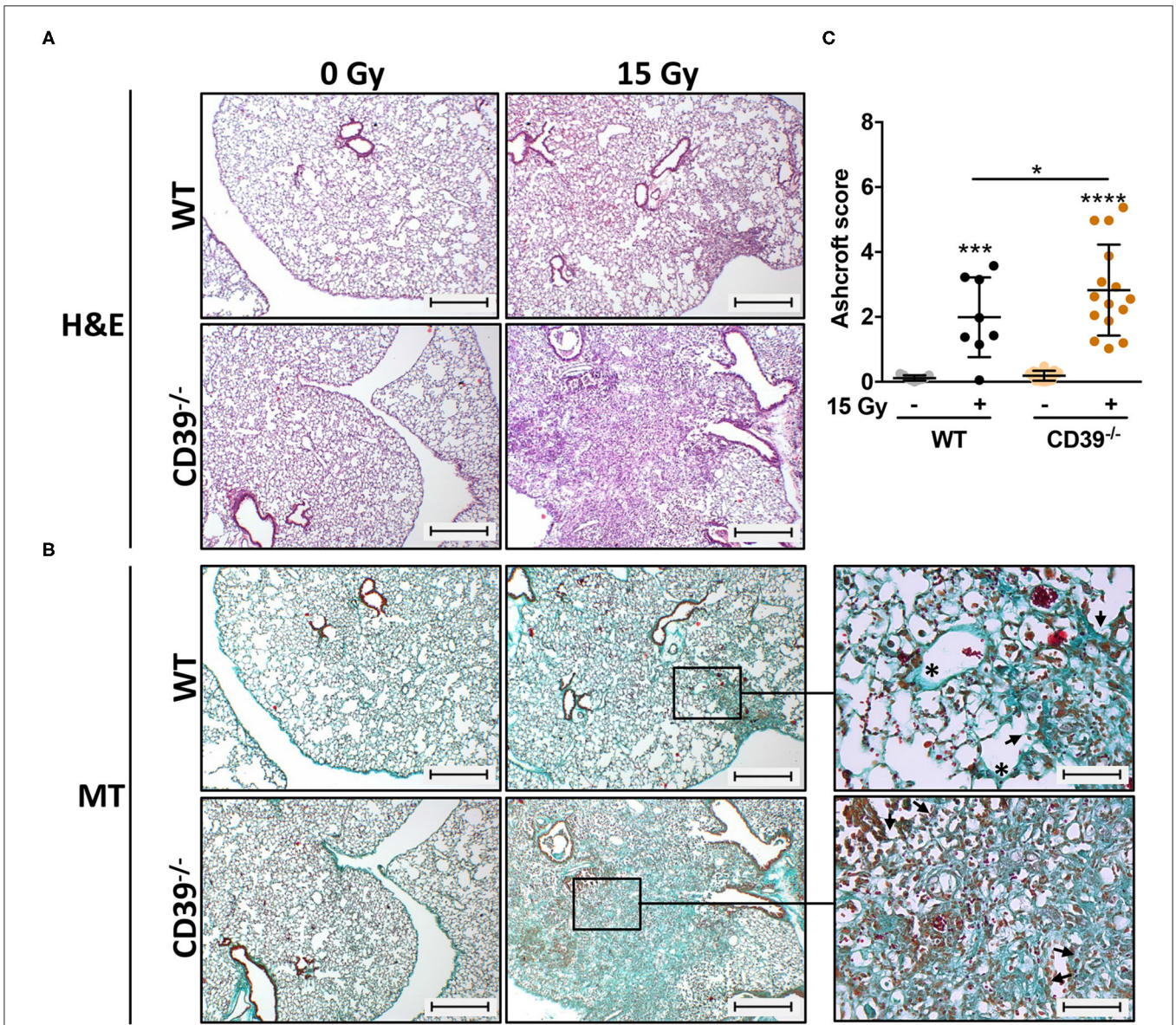

FIGURE 8 | CD39$^{-/-}$ mice develop enhanced pulmonary fibrosis 25 weeks after irradiation. C57BL/6 (WT) and CD39$^{-/-}$ mice received 0- or 15-Gy whole-thorax irradiation (WTI) and were sacrificed at 25 weeks after irradiation. **(A)** Hematoxylin-eosin (H&E) or **(B)** Masson Goldner trichrome (MT) stained lung sections at 25 weeks after irradiation. Lung sections were evaluated for fibrosis by using 10 non-overlapping randomized pictures (scale bar = 100 μm) per slide. Ashcroft scoring was done by three independent observers on slides blinded to the genotype and treatment condition. Magnified pictures (400-fold) highlight special structures. Asterisks emphasize thickening of alveolar wall structures and arrowheads fibrotic regions. **(C)** Quantification of fibrosis in WT ($n \geq 7$) and CD73$^{-/-}$ ($n = 7$) mice, horizontal lines represent mean values. *$P \leq 0.05$, ***$P \leq 0.001$, **** $P \leq 0.0001$ by one-way ANOVA followed by *post hoc* Newman–Keuls test, $n = 9/9/15/15$.

foci, characteristic for fibrosis development in irradiated WT mice as of 25 weeks after WTI (**Figures 8A,B**). Of note, a more severe fibrosis phenotype was prominent in lung sections of irradiated CD39$^{-/-}$ mice, as demonstrated by a further increase in extracellular matrix deposition and more severe fibrotic lesions yielding a significantly higher Ashcroft score (**Figure 8C**).

Because the observed results might not only be evoked by the canonical CD39/CD73/Ado pathway, we again addressed the non-canonical adenosinergic pathway in respective lung sections by using immunohistochemistry in combination with CD38 and CD203a/PC-1 antibodies. As shown in **Supplementary Figure 3**, our data revealed that both receptors CD38 and CD203a were not expressed in the alveolar and bronchial lung regions from untreated WT mice (**Supplementary Figure 3**, left panel). Even fibrotic alveolar and bronchial lung regions of irradiated WT mice did not express these receptors (**Supplementary Figure 3**, middle panels). CD38 and also CD203a expression was observed in only few numbers of small infiltrating immune cells, with a myeloid morphology, in the irradiated lungs (**Supplementary Figure 3**, magnification, right panel). The observed findings were true for WT, CD39$^{-/-}$, and CD73$^{-/-}$ mice, with no difference in the expression between all strains. Our results reveal that CD38/CD203a/CD73 ectoenzymatic signaling on infiltrating immune cells (monocytes/macrophages) might also impact irradiation-induced pneumopathy. However, expression of non-canonical ectoenzymes was similar in lungs from WT, CD39$^{-/-}$, and CD73$^{-/-}$ mice; thus, we conclude that the observed exacerbated fibrosis development in CD39$^{-/-}$ mice is independent from the non-canonical pathway.

Our previous work revealed that progressive activation of CD73 and chronic accumulation of Ado participated in shaping a profibrotic cross-talk between damaged resident cells, infiltrating immune cells, and other fibrosis mediators such as OPN, hyaluronic acid, and TGF-β (49, 50). To corroborate the induction of fibrosis and gain insight into potential underlying mechanisms, we additionally analyzed the expression levels of the profibrotic markers OPN and TGF-β, both known to be associated with fibrosis development, via immunohistochemistry (49, 77, 78). In line with the above observations, WTI induced clearly higher levels of OPN in the lungs of CD39$^{-/-}$ mice as compared to respective WT controls at 25 weeks after irradiation, particularly in the fibrotic areas (**Figures 9A,B**). Yet TGF-β was expressed to a similar extent in the lungs of both mouse strains (**Figures 9C,D**). Moreover, the time-dependent changes in infiltration of CD45^{+} leukocytes were rather similar in both mouse strains except for slightly more pronounced decrease in the fraction of CD45^{+} leukocytes in the lung tissue at 1 and 24 weeks after irradiation (data not shown).

Thus, genetic loss of CD39 did not only adversely affect the tumor response to RT but even correlated with an increased normal lung toxicity upon IR as revealed by the significantly enhanced progression of radiation-induced lung fibrosis.

DISCUSSION

Beyond CD73 and Ado, CD39 emerges as an attractive therapeutic target for cancer therapy. So far, the role of the purinergic pathway, particularly CD39-dependent signaling, in radiation responses of normal and tumor tissues remains largely

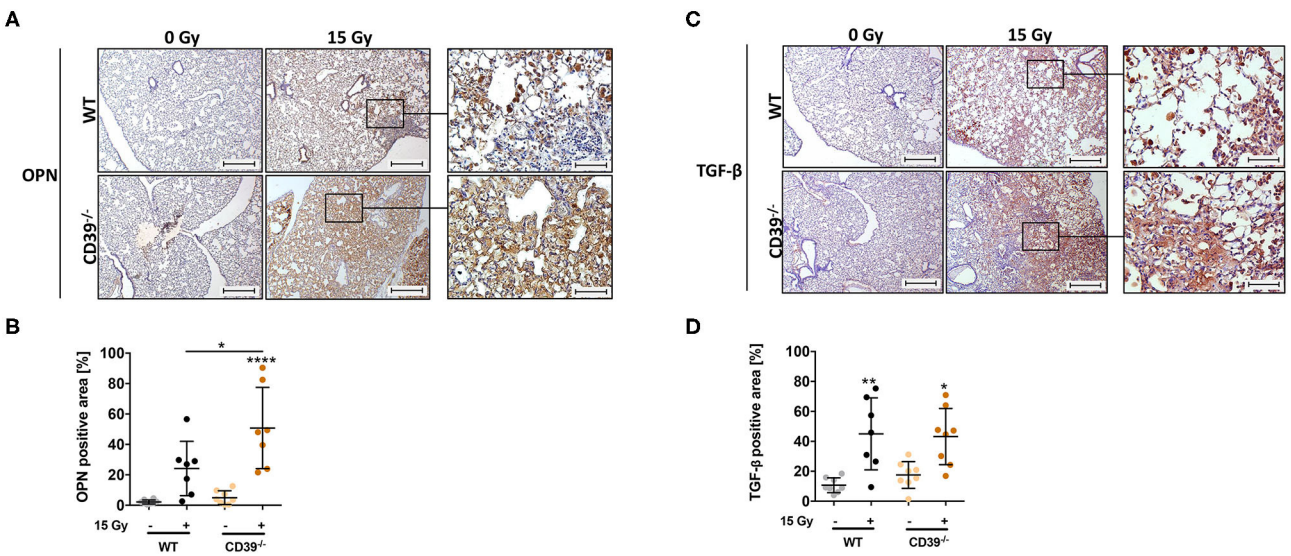

FIGURE 9 | A CD39 deficiency leads to an increased osteopontin expression and TGF-β accumulation after irradiation. C57BL/6 (WT) and CD39$^{-/-}$ mice received 0- or 15-Gy whole-thorax irradiation (WTI) and were sacrificed at 25 weeks after irradiation. Immunohistochemical staining of paraffin-embedded lung sections with a primary antibody for **(A,B)** osteopontin (OPN) and **(C,D)** transforming growth factor β (TGF-β). Shown in (**A,C** right panels) are representative overview pictures of each indicated group (scale bar = 100 μm, magnified pictures 400-fold). **(B,D)** Using the Software Orbit Image Analysis version 2.65, positive areas for OPN and TGF-β were analyzed and are shown in percentage of the whole lung section. *$P \leq 0.05$, **$P \leq 0.01$, ****$P \leq 0.0001$ by one-way ANOVA followed by *post hoc* Newman–Keuls test, $n = 8/7/8/8$.

unknown. Here, we demonstrated that host CD39 impacts both tumor growth and tumor and normal tissue responses to IR; murine LLC1 lung tumors grew faster on mice with genetic deficiency of CD39 and were more resistant to tumor growth delay induced by single high-dose irradiations, whereas genetic deficiency of CD73 in the tumor host did not significantly alter tumor growth and the response to RT. Radiation-induced lung fibrosis, however, was more severe in $CD39^{-/-}$ as compared to WT mice. The assumed defect of CD39-deficient host cells in degrading extracellular ATP did not foster tumor cell damage or increased immune cell infiltration upon irradiation, but increased tumor cell proliferation and survival. The increased tumor cell proliferation observed in LLC1 tumors of CD39-deficient mice (either or without RT treatment) was associated with increased angiogenesis. Thus, host CD39 supports the antineoplastic effects of RT in the murine LLC1 lung cancer model, while limiting radiation-induced fibrosis in respective mice.

The Role of CD39 Within Lung Tumors

In more detail, we used syngeneic LLC1 lung tumors xenografts grown on CD39- and CD73-deficient mice as compared to respective WT controls in combination with a single high-dose irradiation. LLC1 lung cancer cells do express neither CD39 nor CD73, thereby excluding potential confounding effects by tumor-associated CD39/CD73 signaling. Interestingly, LLC1 tumors grew faster on $CD39^{-/-}$ mice, whereas loss of CD73 had no significant effect on LLC1 tumor growth. Even more important, irradiation with 10 Gy was not sufficient to induce similar antitumor effects in tumors grown on $CD39^{-/-}$ mice as compared to WT mice, while radiation-induced growth retardation of tumors grown in $CD73^{-/-}$ mice was similar. Our initial idea was that genetic deficiency of CD39 in mice will inhibit degradation of extracellular ATP released into the microenvironment in response to radiation-induced tissue damage and that the resulting increase in ATP and reduced production of Ado might lead to increased activation of inflammatory responses. Regardless of the fact that unirradiated tumors grown on $CD39^{-/-}$ and $CD73^{-/-}$ mice already had higher percentages of tumor-infiltrating leukocytes, our flow cytometry data revealed that exposure to a single high-dose irradiation did not significantly increase the percentage of leukocytes and respective subsets infiltrating LLC1 tumors grown on $CD39^{-/-}$ mice after irradiation. Despite the fact that we found infiltrating leukocytes in all tumors (WT, $CD73^{-/-}$, and $CD39^{-/-}$), the poor overall immune cell infiltration observed at this time point corroborates the reported poor immunogenicity of LLC1 tumors (79).

Instead, LLC1 tumors grown on $CD73^{-/-}$ mice showed a higher percentage of cytotoxic T cells in the tumor tissue at day 3 after irradiation than LLC1 tumors growing on WT and $CD39^{-/-}$ mice. This is reminiscent of a recent study describing that a CD73-targeted therapy increased $CD8^+$ T-cell infiltration in a murine mammary carcinoma cell line TSA tumor hind-leg model only in combination with additional single high-dose tumor irradiation (20 Gy) (80). Yet, in our hands, the observed increased $CD8^+$ T-cell infiltration did not result in a significant effect on tumor growth delay. Thus, although deficiency of CD73 in the tumor host may reduce Ado levels in the tumor micromilieu and thereby facilitate radiation-induced antitumor immune responses as observed by others (24), the effects resulting from a single high-dose irradiation were not strong enough to induce net effects on LLC1 tumor growth retardation. Further work is required to define time-dependent changes in the micromilieu of irradiated tumors induced in response to IR in the different genetic backgrounds. Moreover, similar investigations should be performed using fractionated radiation schedules, tumor cells with higher immunogenicity, and CD39/CD73-positive tumor cells. In fact, CD73 overexpression has been described to be higher in tumors than in surrounding normal tissues and also to be tumor-specific (24).

In addition to its role in the regulation of inflammatory processes ATP has been described to modulate proliferation and death resistance of cancer cells. Human lung cancer cells were shown to use macropinocytosis or clathrin- and caveolae-mediated endocytotic processes to take up extracellular ATP and fuel extra energy for tumor growth, survival, and drug resistance (81). Moreover, while ATP inhibited proliferation or induced cell death via P2X7R in human cervix and breast cancer cells as well as in murine melanoma and colon cancer cells (76, 82–85), high levels of extracellular ATP promoted survival of A549 and H23 lung cancer cells as compared to normal cells (86); here, the authors attributed the differential effects on tumor and normal tissue cells to the decreased expression of P2X7R and an enhanced Bcl-2/Bax ratio in the cancer cells (86). Because our *in vitro* investigations revealed that LLC1 cells do not express P2X7R and did not undergo increased cell death in response to extracellular ATP alone or in combination with RT, we speculate that similar processes might contribute to the observed growth and resistance promoting effects of CD39 deficiency in the tumor host. Besides P2 receptor signaling, nucleotides can also act through intracellular uptake and compartmentalization with impact on cancer cell survival, proliferation, and metabolic function (75). In fact, with increasing concentration, extracellular Ado can enter the cell via equilibrative nucleoside transporters (ENTs) and subsequently induce cell death (87, 88). Herein, ATP degradation to Ado and subsequent uptake and conversion of Ado to AMP by ENT and Ado kinase, respectively, were shown to be the main drivers of growth inhibition and toxicity mediated by extracellular ATP (76, 89). High extracellular Ado levels could activate mitochondrial apoptosis through deregulation of the Bcl2 rheostat by decreasing antiapoptotic Bcl2 while increasing expression of proapoptotic Bax and Bak (90). Degradation of ATP to Ado induced growth inhibition and proapoptotic effects via activation of caspase-3 (91). Finally, depending on the concentration, AMP turned out to strongly inhibit cancer cell proliferation *in vitro* even more effective than Ado and ATP (92).

Ado signaling via the four ADORA receptors could alternatively impact tumor growth and survival in the LLC1 cells, because these cells express the ADORA receptors. The effect of Ado via both AdoRA1 and A3 has been described as proapoptotic in several cancer types, e.g., liver, lung, and colon (91, 93–96). The AdoRA1, for example, had an antiproliferative effect and promoted the differentiation of cancer stem cells, thereby inducing an increased sensitivity of these cells to

chemotherapeutic drugs (97). Furthermore, treatment with an agonist of AdoRA3 reduced the number of living colon cancer cells (98). Thus, alterations in extracellular nucleotides (ATP <-> Ado) due to the loss of host CD39 in our LLC1 tumor model could potentially affect tumor growth and the radiation response via ADORA signaling as well as through intracellular uptake and metabolic processing, independent of an immune response and P2 receptor signaling. Host CD39 expression seems to be important for maintaining a radiation-induced antitumor effect in CD39/CD73-negative LLC1 presumably by affecting the composition of extracellular nucleotides in the TME. Further work is needed to elucidate the effects of extracellular nucleotide uptake and subsequent intracellular nucleotide metabolism in LLC1 tumor development.

Because alternative nucleotide signaling might also contribute to our observed findings, we analyzed the role of the non-canonical adenosinergic CD38/CD203a/CD73 pathway. Although we could detect CD38 mRNA expression in LLC1 tumors, there was a lack of CD38 cell surface protein. By analyzing a panel of human lung cancer cell lines, Bu et al. (99) already described that most cell lines investigated had high copy numbers of CD38 mRNA, but not all cell lines expressed the respective protein. Moreover, we showed here that there was no CD203a mRNA and protein expression needed to produce Ado and fuel CD73. Therefore, we can exclude that non-canonical adenosinergic signaling in the LLC1 tumor tissue contributes to the observed tumoral behavior reported here. In addition to catalyzing the production of Ado, CD38 may promote tumor development by inducing other tumor-supporting processes, e.g., angiogenesis in the TME, thus exerting functions beyond the CD38/CD203a/CD73 signaling (100). We observed here that tumors grown on CD39-deficient background were characterized by an increased neovascularization and that this phenotype was even maintained after RT. Radiation usually induces phenotypic changes of the tumor vasculature (e.g., apoptosis or senescence), as well as a wide range of environmental changes, which in turn govern recruitment of immune cells (101–104). Herein, angiogenic and thus less mature blood vessels are characterized by an increased radiosensitivity (61, 73, 105). We speculate that the sustained angiogenesis observed in the context of CD39 deficiency might result from increased proangiogenic signaling induced by higher extracellular ATP levels due to the failure of extracellular ATP degradation and the increased ATP release from RT-damaged cells. At the same time, extracellular ATP has been reported to mediate antiapoptotic effects in endothelial cells, either via P2 or Ado receptors (106). Likewise, CD39-deficient endothelial cells might be less sensitive to the cytotoxic effects of RT, thereby contributing to the reduced sensitivity of LLC1 tumors to radiation. ATP was already shown being able to activate the VEGF receptor in the absence of VEGF, and the P2YR–VEGFR2 interaction and the resulting signal transduction are critical determinants of vascular homoeostasis and tumor-mediated angiogenesis (107). Moreover, CD38-dependent signaling can impact on (tumor) angiogenesis (55, 108). Herein, CD38 turned out to be an important regulator for the intrinsic expression of key angiogenic factors (100, 109, 110). Although non-canonical purinergic signaling seemed not to impact on non-canonical ADO generation because of the lack of CD203a expressions as reported here, increased tumor angiogenesis together with the well-known abnormal phenotype of the tumor vasculature may lead to factors contributing to radiation resistance (increased vascular permeability, vessel instability, increased interstitial fluid pressure, non-directed blood flow, endothelial anergy) (104, 111, 112).

The Role of CD39 Within Normal Lung Toxicity

Concerning normal tissue toxicity, we showed here that genetic loss of CD39 exacerbates radiation-induced lung disease. Since our earlier work revealed a pathogenic role of the CD73/Ado-dependent arm of purinergic signaling in radiation-induced lung fibrosis (49, 50), genetic loss of CD39 with assumed activation of the ATP-dependent proinflammatory arm of purinergic signaling and genetic loss of CD73 with assumed activation of the Ado-dependent anti-inflammatory, repair-promoting arm of purinergic signaling result in opposing outcomes in radiation-induced lung fibrosis. A pathology-promoting effect of low CD39 expression or high pulmonary ATP levels were already known for several lung pathologies, including pulmonary fibrosis (113–115). High extracellular ATP levels, for example, have been observed in the bronchoalveolar lavage fluid of patients with idiopathic pulmonary fibrosis, as well as in a murine model of bleomycin-induced lung fibrosis (116). In our hands, the more severe lung fibrosis observed in irradiated lungs from $CD39^{-/-}$ mice was associated with enhanced levels of the multifunctional and proinflammatory protein OPN in the irradiated lungs $CD39^{-/-}$ mice compared to WT mice. Based on the observation that extracellular ATP can induce OPN expression in response to mechanical stress at least *in vitro* (117), we speculate that genetic deficiency of CD39 may cause a disease-promoting increase in extracellular ATP concentrations in irradiated lungs, presumably in response to the initial radiation damage in irradiated murine lungs. CD39-dependent vascular effects may also play a major role in regulating severity of radiation-induced fibrosis. Increasing evidence suggests that vascular remodeling contributes to the pathogenesis of pulmonary fibrosis (66, 73, 118, 119). Of note, loss of CD39 induced vascular remodeling of pulmonary arteries and contributed to vascular dysfunction and arterial hypertension in patients suffering from idiopathic pulmonary arterial hypertension (120, 121). However, further work is needed to elucidate the contribution of vascular changes and also epithelial cell impairments to lung damage and fibrosis upon CD39 deficiency.

We further analyzed if the non-canonical adenosinergic CD38/CD203a pathway might contribute to radiation-induced lung fibrosis. The expression of both receptors was restricted to only a minor group of lungs infiltrating myeloid/ macrophage-like cells, whereas resident lung cells clearly showed no immunoreactivity. These findings were in line with recent reports investigating non-canonical adenosinergic CD38/CD203a signaling within immune cells. CD203a expression was found to

be restricted to plasma B cells (122). Accordingly, CD203a/PC-1 expression was found to be rather low on lymphocytes, monocytes, and granulocytes of the bone marrow (123). In contrast to CD203a, a high CD38 expression on circulating monocytes has been described (56, 124, 125). Resident lung macrophages can also express CD38 (126, 127). Both studies highlight that CD38 expression on macrophages was associated with an inflammatory M1 phenotype and chronic inflammation. Of note, in the study from Dewhurst et al., it is further described that only the small alveolar and interstitial macrophages express CD38 and that there was only a low expression on big foamy macrophages (126). We showed already that small macrophages can be distinguished from bigger foamy macrophages, which organize in clusters during fibrosis development (50). Here we revealed that only the smaller myeloid-like cells were positive for CD38. As CD38 is suggested to normal inflammatory responses in the lung toward hyperinflammation (55), we conclude that CD38 signaling on small monocytes/macrophages, with a potential M1 phenotype, is not linked to a profibrotic phenotype. However, non-canonical adenosinergic signaling might have an indirect impact on profibrotic signaling: NAD^+/CD38 signaling was shown to influence Treg survival, phenotype, and function. $CD38^{-/-}$-deficient mice studies revealed that extracellular NAD^+ can deplete and reduce Treg (128). In contrast, an increase in Tregs during the fibrotic phase of radiation-induced pneumopathy already highlighted that besides M2-like macrophages also Treg might contribute to the development of lung fibrosis (49, 129, 130). Herein, extracellular Ado positively alters Treg survival and functions (131). Thus, besides CD73/Ado signaling (Ado accumulation), even CD38/CD203a signaling (NAD^+ reduction) could led to the observed increase in Treg during the fibrotic phase (49).

CONCLUSION

Genetic deficiency of CD39 in the host may result in long-term adaptive processes, e.g., in the microvasculature or the immune system, respectively, with impact on tumor growth and radiation response in tumor and normal tissues. Such adverse effects are reminiscent of suggested risks of sustained CD39 inhibition (132). Thus, a careful testing of pharmacologic strategies interfering with CD39 activity is needed to exclude that such a therapeutic strategy exerts growth- and resistance-promoting effects in tumor tissues, adverse effects in normal tissues, or both, particularly when used in combination with a single dose or clinically more relevant fractionated radiation schedules. Loss of CD39 or activation of CD73 impacts on radiation-induced changes in the lung environment, e.g., ATP/Ado ratio, as well as phenotype and function of resident cells and recruited immune cells with impact on cell survival, vascular function, immune defense, matrix deposition, and fibrosis. Of note, both CD39 and CD73 are important regulators of the TME, particularly in hypoxic tumors, with the ability to suppress immune-mediated tumor cell killing and to promote tumor growth, angiogenesis, and progression (133). Thus, targeting pathologic aspects of CD39/CD73 signaling might be an attractive approach to enhance efficacy of therapies involving RT in malignant tumors without enhancing normal tissue toxicity or to protect normal tissues from the adverse effects of RT without protecting the tumor. Further work is highly needed to unravel the multifaceted roles of purinergic signaling in the complex interactions and signaling networks between the microenvironment in tumor and normal tissues by using orthotopic lung tumor models and/or genetically engineered mouse models as well as clinically relevant fractionated radiation schedules.

DATA AVAILABILITY STATEMENT

The raw data supporting the conclusions of this article will be made available by the authors, without undue reservation.

ETHICS STATEMENT

The animal study was reviewed and approved by Landesamt für Natur, Umwelt und Verbraucherschutz (LANUV), Regierungspräsidium Düsseldorf. Written informed consent was obtained from the owners for the participation of their animals in this study.

AUTHOR CONTRIBUTIONS

AM designed research, performed experiments and evaluated data, wrote, and critically reviewed manuscript. FW and DK designed research, performed experiments, analyzed data, wrote, critically reviewed, and revised the manuscript. SL and KS performed experiments and critically reviewed manuscript. MS discussed data and critically reviewed manuscript. SR provided unique reagents. VJ designed research, wrote, and critically reviewed manuscript. All authors approved the final version of the manuscript.

FUNDING

This study was supported by grants of the Doctoral Programs of the Deutsche Forschungsgemeinschaft (DFG) grant numbers GRK1739/2 and JE275/4-1 (VJ) and the Bundesministerium für Bildung und Forschung (BMBF) grant numbers 02NUK024D and 02NUK047D (VJ). We acknowledge support by the Open Access Publication Fund of the University of Duisburg-Essen.

ACKNOWLEDGMENTS

We thank Eva Gau and Mohamed Benchellal for excellent technical support.

SUPPLEMENTARY MATERIAL

The Supplementary Material for this article can be found online at: https://www.frontiersin.org/articles/10.3389/fonc.2020.554883/full#supplementary-material

REFERENCES

1. Curran WJ Jr, Paulus R, Langer CJ, Komaki R, Lee JS, Hauser S, et al. Sequential vs. concurrent chemoradiation for stage III non-small cell lung cancer: randomized phase III trial RTOG 9410. *J Natl Cancer Inst.* (2011) 103:1452–60. doi: 10.1093/jnci/djr325
2. Bradley JD, Paulus R, Komaki R, Masters G, Blumenschein G, Schild S, et al. Standard-dose versus high-dose conformal radiotherapy with concurrent and consolidation carboplatin plus paclitaxel with or without cetuximab for patients with stage IIIA or IIIB non-small-cell lung cancer (RTOG 0617): a randomised, two-by-two factorial phase 3 study. *Lancet Oncol.* (2015) 16:187–99. doi: 10.1016/S1470-2045(14)71207-0
3. Ohri N. Radiotherapy dosing for locally advanced non-small cell lung carcinoma: "MTD" or "ALARA" ? *Front Oncol.* (2017) 7:205. doi: 10.3389/fonc.2017.00205
4. Pfeifer GP. How the environment shapes cancer genomes. *Curr Opin Oncol.* (2015) 27:71–7. doi: 10.1097/CCO.0000000000000152
5. Morgan MA, Parsels LA, Maybaum J, Lawrence TS. Improving the efficacy of chemoradiation with targeted agents. *Cancer Discov.* (2014) 4:280–91. doi: 10.1158/2159-8290.CD-13-0337
6. Ganss R, Ryschich E, Klar E, Arnold B, Hammerling GJ. Combination of T-cell therapy and trigger of inflammation induces remodeling of the vasculature and tumor eradication. *Cancer Res.* (2002) 62:1462–70.
7. Formenti SC, Demaria S. Systemic effects of local radiotherapy. *Lancet Oncol.* (2009) 10:718–26. doi: 10.1016/S1470-2045(09)70082-8
8. Gupta A, Probst HC, Vuong V, Landshammer A, Muth S, Yagita H, et al. Radiotherapy promotes tumor-specific effector CD8+ T cells via dendritic cell activation. *J Immunol.* (2012) 189:558–66. doi: 10.4049/jimmunol.1200563
9. Liang H, Deng L, Chmura S, Burnette B, Liadis N, Darga T, et al. Radiation-induced equilibrium is a balance between tumor cell proliferation and T cell-mediated killing. *J Immunol.* (2013) 190:5874–81. doi: 10.4049/jimmunol.1202612
10. Nakad R, Schumacher B. DNA damage response and immune defense: links and mechanisms. *Front Genet.* (2016) 7:147. doi: 10.3389/fgene.2016.00147
11. Krombach J, Hennel R, Brix N, Orth M, Schoetz U, Ernst A, et al. Priming anti-tumor immunity by radiotherapy: dying tumor cell-derived DAMPs trigger endothelial cell activation and recruitment of myeloid cells. *Oncoimmunology.* (2019) 8:e1523097. doi: 10.1080/2162402X.2018.1523097
12. Antonia SJ, Villegas A, Daniel D, Vicente D, Murakami S, Hui R, et al. Durvalumab after chemoradiotherapy in stage III non-small-cell lung cancer. *N Engl J Med.* (2017) 377:1919–29. doi: 10.1056/NEJMoa1709937
13. Shaverdian N, Lisberg AE, Bornazyan K, Veruttipong D, Goldman JW, Formenti SC, et al. Previous radiotherapy and the clinical activity and toxicity of pembrolizumab in the treatment of non-small-cell lung cancer: a secondary analysis of the KEYNOTE-001 phase 1 trial. *Lancet Oncol.* (2017) 18:895–903. doi: 10.1016/S1470-2045(17)30380-7
14. Westermann W, Schobl R, Rieber EP, Frank KH. Th2 cells as effectors in postirradiation pulmonary damage preceding fibrosis in the rat. *Int J Radiat Biol.* (1999) 75:629–38. doi: 10.1080/095530099140276
15. Paun A, Kunwar A, Haston CK. Acute adaptive immune response correlates with late radiation-induced pulmonary fibrosis in mice. *Radiat Oncol.* (2015) 10:45. doi: 10.1186/s13014-015-0359-y
16. Wirsdorfer F, Jendrossek V. Modeling DNA damage-induced pneumopathy in mice: insight from danger signaling cascades. *Radiat Oncol.* (2017) 12:142. doi: 10.1186/s13014-017-0865-1
17. Wennerberg E, Lhuillier C, Vanpouille-Box C, Pilones KA, Garcia-Martinez E, Rudqvist NP, et al. Barriers to radiation-induced *in situ* tumor vaccination. *Front Immunol.* (2017) 8:229. doi: 10.3389/fimmu.2017.00229
18. De Ruysscher D. Combination of radiotherapy and immune treatment: first clinical data. *Cancer Radiother.* (2018) 22:564–6. doi: 10.1016/j.canrad.2018.07.128
19. Kordbacheh T, Honeychurch J, Blackhall F, Faivre-Finn C, Illidge T. Radiotherapy and anti-PD-1/PD-L1 combinations in lung cancer: building better translational research platforms. *Ann Oncol.* (2018) 29:301–10. doi: 10.1093/annonc/mdx790
20. Allard B, Beavis PA, Darcy PK, Stagg J. Immunosuppressive activities of adenosine in cancer. *Curr Opin Pharmacol.* (2016) 29:7–16. doi: 10.1016/j.coph.2016.04.001
21. Allard B, Longhi MS, Robson SC, Stagg J. The ectonucleotidases CD39 and CD73: novel checkpoint inhibitor targets. *Immunol Rev.* (2017) 276:121–44. doi: 10.1111/imr.12528
22. Inoue Y, Yoshimura K, Kurabe N, Kahyo T, Kawase A, Tanahashi M, et al. Prognostic impact of CD73 and A2A adenosine receptor expression in non-small-cell lung cancer. *Oncotarget.* (2017) 8:8738–51. doi: 10.18632/oncotarget.14434
23. Leone RD, Emens LA. Targeting adenosine for cancer immunotherapy. *J Immunother Cancer.* (2018) 6:57. doi: 10.1186/s40425-018-0360-8
24. Allard D, Chrobak P, Allard B, Messaoudi N, Stagg J. Targeting the CD73-adenosine axis in immuno-oncology. *Immunol Lett.* (2019) 205:31–9. doi: 10.1016/j.imlet.2018.05.001
25. Antonioli L, Blandizzi C, Pacher P, Hasko G. Immunity, inflammation and cancer: a leading role for adenosine. *Nat Rev Cancer.* (2013) 13:842–57. doi: 10.1038/nrc3613
26. Deaglio S, Dwyer KM, Gao W, Friedman D, Usheva A, Erat A, et al. Adenosine generation catalyzed by CD39 and CD73 expressed on regulatory T cells mediates immune suppression. *J Exp Med.* (2007) 204:1257–65. doi: 10.1084/jem.20062512
27. Kaku H, Cheng KF, Al-Abed Y, Rothstein TL. A novel mechanism of B cell-mediated immune suppression through CD73 expression and adenosine production. *J Immunol.* (2014) 193:5904–13. doi: 10.4049/jimmunol.1400336
28. Leibovich SJ, Chen JF, Pinhal-Enfield G, Belem PC, Elson G, Rosania A, et al. Synergistic up-regulation of vascular endothelial growth factor expression in murine macrophages by adenosine A(2A) receptor agonists and endotoxin. *Am J Pathol.* (2002) 160:2231–44. doi: 10.1016/S0002-9440(10)61170-4
29. Hasko G, Pacher P. Regulation of macrophage function by adenosine. *Arterioscler Thromb Vasc Biol.* (2012) 32:865–9. doi: 10.1161/ATVBAHA.111.226852
30. Thompson LF, Eltzschig HK, Ibla JC, Van De Wiele CJ, Resta R, Morote-Garcia JC, et al. Crucial role for ecto-5'-nucleotidase (CD73) in vascular leakage during hypoxia. *J Exp Med.* (2004) 200:1395–405. doi: 10.1084/jem.20040915
31. Thompson LF, Takedachi M, Ebisuno Y, Tanaka T, Miyasaka M, Mills JH, et al. Regulation of leukocyte migration across endothelial barriers by ECTO-5'-nucleotidase-generated adenosine. *Nucleosides Nucleotides Nucleic Acids.* (2008) 27:755–60. doi: 10.1080/15257770802145678
32. Ferrari D, Gambari R, Idzko M, Muller T, Albanesi C, Pastore S, et al. Purinergic signaling in scarring. *FASEB J.* (2016) 30:3–12. doi: 10.1096/fj.15-274563
33. Sitkovsky MV. T regulatory cells: hypoxia-adenosinergic suppression and re-direction of the immune response. *Trends Immunol.* (2009) 30:102–8. doi: 10.1016/j.it.2008.12.002
34. Stagg J, Divisekera U, Mclaughlin N, Sharkey J, Pommey S, Denoyer D, et al. Anti-CD73 antibody therapy inhibits breast tumor growth and metastasis. *Proc Natl Acad Sci USA.* (2010) 107:1547–52. doi: 10.1073/pnas.0908801107
35. Clayton A, Al-Taei S, Webber J, Mason MD, Tabi Z. Cancer exosomes express CD39 and CD73, which suppress T cells through adenosine production. *J Immunol.* (2011) 187:676–83. doi: 10.4049/jimmunol.1003884
36. Stagg J, Divisekera U, Duret H, Sparwasser T, Teng MW, Darcy PK, et al. CD73-deficient mice have increased antitumor immunity and are resistant to experimental metastasis. *Cancer Res.* (2011) 71:2892–900. doi: 10.1158/0008-5472.CAN-10-4246
37. Wang L, Fan J, Thompson LF, Zhang Y, Shin T, Curiel TJ, et al. CD73 has distinct roles in nonhematopoietic and hematopoietic cells to promote tumor growth in mice. *J Clin Invest.* (2011) 121:2371–82. doi: 10.1172/JCI45559
38. Young A, Ngiow SF, Barkauskas DS, Sult E, Hay C, Blake SJ, et al. Co-inhibition of CD73 and A2AR adenosine signaling improves anti-tumor immune responses. *Cancer Cell.* (2016) 30:391–403. doi: 10.1016/j.ccell.2016.06.025
39. Vaupel P, Multhoff G. Adenosine can thwart antitumor immune responses elicited by radiotherapy: therapeutic strategies alleviating

protumor ADO activities. *Strahlenther Onkol.* (2016) 192:279–87. doi: 10.1007/s00066-016-0948-1
40. Bastid J, Regairaz A, Bonnefoy N, Dejou C, Giustiniani J, Laheurte C, et al. Inhibition of CD39 enzymatic function at the surface of tumor cells alleviates their immunosuppressive activity. *Cancer Immunol Res.* (2015) 3:254–65. doi: 10.1158/2326-6066.CIR-14-0018
41. Canale FP, Ramello MC, Nunez N, Araujo Furlan CL, Bossio SN, Gorosito Serran M, et al. CD39 expression defines cell exhaustion in tumor-infiltrating $CD8^+$ T cells. *Cancer Res.* (2018) 78:115–28. doi: 10.1158/0008-5472.CAN-16-2684
42. Ampollini L, Madeddu D, Falco A, Frati C, Lorusso B, Graiani G, et al. Lung mesenchymal cells function as an inductive microenvironment for human lung cancer propagating cellsdagger. *Eur J Cardiothorac Surg.* (2014) 46:e103–12. doi: 10.1093/ejcts/ezu359
43. Bichsel CA, Wang L, Froment L, Berezowska S, Muller S, Dorn P, et al. Increased PD-L1 expression and IL-6 secretion characterize human lung tumor-derived perivascular-like cells that promote vascular leakage in a perfusable microvasculature model. *Sci Rep.* (2017) 7:10636. doi: 10.1038/s41598-017-09928-1
44. Li J, Wang L, Chen X, Li L, Li Y, Ping Y, et al. CD39/CD73 upregulation on myeloid-derived suppressor cells via TGF-beta-mTOR-HIF-1 signaling in patients with non-small cell lung cancer. *Oncoimmunology.* (2017) 6:e1320011. doi: 10.1080/2162402X.2017.1320011
45. Young A, Mittal D, Stagg J, Smyth MJ. Targeting cancer-derived adenosine: new therapeutic approaches. *Cancer Discov.* (2014) 4:879–88. doi: 10.1158/2159-8290.CD-14-0341
46. Kepp O, Loos F, Liu P, Kroemer G. Extracellular nucleosides and nucleotides as immunomodulators. *Immunol Rev.* (2017) 280:83–92. doi: 10.1111/imr.12571
47. Vijayan D, Young A, Teng MWL, Smyth MJ. Targeting immunosuppressive adenosine in cancer. *Nat Rev Cancer.* (2017) 17:709–24. doi: 10.1038/nrc.2017.86
48. Mandapathil M, Szczepanski MJ, Szajnik M, Ren J, Lenzner DE, Jackson EK, et al. Increased ectonucleotidase expression and activity in regulatory T cells of patients with head and neck cancer. *Clin Cancer Res.* (2009) 15:6348–57. doi: 10.1158/1078-0432.CCR-09-1143
49. Wirsdorfer F, De Leve S, Cappuccini F, Eldh T, Meyer AV, Gau E, et al. Extracellular adenosine production by ecto-5'-nucleotidase (CD73) enhances radiation-induced lung fibrosis. *Cancer Res.* (2016) 76:3045–56. doi: 10.1158/0008-5472.CAN-15-2310
50. De Leve S, Wirsdorfer F, Cappuccini F, Schutze A, Meyer AV, Rock K, et al. Loss of CD73 prevents accumulation of alternatively activated macrophages and the formation of prefibrotic macrophage clusters in irradiated lungs. *FASEB J.* (2017) 31:2869–80. doi: 10.1096/fj.201601228R
51. Haag F, Adriouch S, Brass A, Jung C, Moller S, Scheuplein F, et al. Extracellular NAD and ATP: partners in immune cell modulation. *Purinergic Signal.* (2007) 3:71–81. doi: 10.1007/s11302-006-9038-7
52. Lewis JE, Singh N, Holmila RJ, Sumer BD, Williams NS, Furdui CM, et al. Targeting NAD^+ metabolism to enhance radiation therapy responses. *Semin Radiat Oncol.* (2019) 29:6–15. doi: 10.1016/j.semradonc.2018.10.009
53. Horenstein AL, Chillemi A, Zaccarello G, Bruzzone S, Quarona V, Zito A, et al. A CD38/CD203a/CD73 ectoenzymatic pathway independent of CD39 drives a novel adenosinergic loop in human T lymphocytes. *Oncoimmunology.* (2013) 2:e26246. doi: 10.4161/onci.26246
54. Ferretti E, Horenstein AL, Canzonetta C, Costa F, Morandi F. Canonical and non-canonical adenosinergic pathways. *Immunol Lett.* (2019) 205:25–30. doi: 10.1016/j.imlet.2018.03.007
55. Konen JM, Fradette JJ, Gibbons DL. The good, the bad and the unknown of CD38 in the metabolic microenvironment and immune cell functionality of solid tumors. *Cells.* (2019) 9:52. doi: 10.3390/cells9010052
56. Vaisitti T, Arruga F, Guerra G, Deaglio S. Ectonucleotidases in blood malignancies: a tale of surface markers and therapeutic targets. *Front Immunol.* (2019) 10:2301. doi: 10.3389/fimmu.2019.02301
57. Grobben B, Anciaux K, Roymans D, Stefan C, Bollen M, Esmans EL, et al. An ecto-nucleotide pyrophosphatase is one of the main enzymes involved in the extracellular metabolism of ATP in rat C6 glioma. *J Neurochem.* (1999) 72:826–34. doi: 10.1046/j.1471-4159.1999.0720826.x
58. Zimmermann H, Zebisch M, Strater N. Cellular function and molecular structure of ecto-nucleotidases. *Purinergic Signal.* (2012) 8:437–502. doi: 10.1007/s11302-012-9309-4
59. Enjyoji K, Sevigny J, Lin Y, Frenette PS, Christie PD, Esch JS II, et al. Targeted disruption of cd39/ATP diphosphohydrolase results in disordered hemostasis and thromboregulation. *Nat Med.* (1999) 5:1010–7. doi: 10.1038/12447
60. Wirsdorfer F, Cappuccini F, Niazman M, De Leve S, Westendorf AM, Ludemann L, et al. Thorax irradiation triggers a local and systemic accumulation of immunosuppressive CD4+ FoxP3+ regulatory T cells. *Radiat Oncol.* (2014) 9:98. doi: 10.1186/1748-717X-9-98
61. Klein D, Schmitz T, Verhelst V, Panic A, Schenck M, Reis H, et al. Endothelial Caveolin-1 regulates the radiation response of epithelial prostate tumors. *Oncogenesis.* (2015) 4:e148. doi: 10.1038/oncsis.2015.9
62. Panic A, Ketteler J, Reis H, Sak A, Herskind C, Maier P, et al. Progression-related loss of stromal Caveolin 1 levels fosters the growth of human PC3 xenografts and mediates radiation resistance. *Sci Rep.* (2017) 7:41138. doi: 10.1038/srep41138
63. Kanagavelu S, Gupta S, Wu X, Philip S, Wattenberg MM, Hodge JW, et al. *In vivo* effects of lattice radiation therapy on local and distant lung cancer: potential role of immunomodulation. *Radiat Res.* (2014) 182:149–62. doi: 10.1667/RR3819.1
64. Chen JX, Chen M, Zheng YD, Wang SY, Shen ZP. Up-regulation of BRAF activated non-coding RNA is associated with radiation therapy for lung cancer. *Biomed Pharmacother.* (2015) 71:79–83. doi: 10.1016/j.biopha.2015.02.021
65. Moreau M, Yasmin-Karim S, Kunjachan S, Sinha N, Gremse F, Kumar R, et al. Priming the abscopal effect using multifunctional smart radiotherapy biomaterials loaded with immunoadjuvants. *Front Oncol.* (2018) 8:56. doi: 10.3389/fonc.2018.00056
66. Klein D, Steens J, Wiesemann A, Schulz F, Kaschani F, Rock K, et al. Mesenchymal stem cell therapy protects lungs from radiation-induced endothelial cell loss by restoring superoxide dismutase 1 expression. *Antioxid Redox Signal.* (2017) 26:563–82. doi: 10.1089/ars.2016.6748
67. Stritt M, Stalder AK, Vezzali E. Orbit image analysis: an open-source whole slide image analysis tool. *PLoS Comput Biol.* (2020) 16:e1007313. doi: 10.1371/journal.pcbi.1007313
68. Schindelin J, Arganda-Carreras I, Frise E, Kaynig V, Longair M, Pietzsch T, et al. Fiji: an open-source platform for biological-image analysis. *Nat Methods.* (2012) 9:676–82. doi: 10.1038/nmeth.2019
69. Ashcroft T, Simpson JM, Timbrell V. Simple method of estimating severity of pulmonary fibrosis on a numerical scale. *J Clin Pathol.* (1988) 41:467–70. doi: 10.1136/jcp.41.4.467
70. Feoktistova M, Geserick P, Leverkus M. Crystal violet assay for determining viability of cultured cells. *Cold Spring Harb Protoc.* (2016) 2016:pdb prot087379. doi: 10.1101/pdb.prot087379
71. Klein D, Demory A, Peyre F, Kroll J, Augustin HG, Helfrich W, et al. Wnt2 acts as a cell type-specific, autocrine growth factor in rat hepatic sinusoidal endothelial cells cross-stimulating the VEGF pathway. *Hepatology.* (2008) 47:1018–31. doi: 10.1002/hep.22084
72. Klein D, Schmetter A, Imsak R, Wirsdorfer F, Unger K, Jastrow H, et al. Therapy with multipotent mesenchymal stromal cells protects lungs from radiation-induced injury and reduces the risk of lung metastasis. *Antioxid Redox Signal.* (2016) 24:53–69. doi: 10.1089/ars.2014.6183
73. Wiesemann A, Ketteler J, Slama A, Wirsdorfer F, Hager T, Rock K, et al. Inhibition of radiation-induced Ccl2 signaling protects lungs from vascular dysfunction and endothelial cell loss. *Antioxid Redox Signal.* (2019) 30:213–31. doi: 10.1089/ars.2017.7458
74. Zheng LM, Zychlinsky A, Liu CC, Ojcius DM, Young JD. Extracellular ATP as a trigger for apoptosis or programmed cell death. *J Cell Biol.* (1991) 112:279–88. doi: 10.1083/jcb.112.2.279
75. Li S, Li X, Guo H, Liu S, Huang H, Liu N, et al. Intracellular ATP concentration contributes to the cytotoxic and cytoprotective effects of adenosine. *PLoS ONE.* (2013) 8:e76731. doi: 10.1371/journal.pone.0076731
76. Mello Pde A, Filippi-Chiela EC, Nascimento J, Beckenkamp A, Santana DB, Kipper F, et al. Adenosine uptake is the major effector of extracellular ATP

toxicity in human cervical cancer cells. *Mol Biol Cell.* (2014) 25:2905–18. doi: 10.1091/mbc.e14-01-0042
77. Khalil N, O'connor RN, Unruh HW, Warren PW, Flanders KC, Kemp A, et al. Increased production and immunohistochemical localization of transforming growth factor-beta in idiopathic pulmonary fibrosis. *Am J Respir Cell Mol Biol.* (1991) 5:155–62. doi: 10.1165/ajrcmb/5.2.155
78. Pardo A, Gibson K, Cisneros J, Richards TJ, Yang Y, Becerril C, et al. Up-regulation and profibrotic role of osteopontin in human idiopathic pulmonary fibrosis. *PLoS Med.* (2005) 2:e251. doi: 10.1371/journal.pmed.0020251
79. Lechner MG, Karimi SS, Barry-Holson K, Angell TE, Murphy KA, Church CH, et al. Immunogenicity of murine solid tumor models as a defining feature of *in vivo* behavior and response to immunotherapy. *J Immunother.* (2013) 36:477–89. doi: 10.1097/01.cji.0000436722.46675.4a
80. Wennerberg E, Spada S, Rudqvist NP, Lhuillier C, Gruber S, Chen Q, et al. CD73 blockade promotes dendritic cell infiltration of irradiated tumors and tumor rejection. *Cancer Immunol Res.* (2020) 8:465–78. doi: 10.1158/2326-6066.CIR-19-0449
81. Qian Y, Wang X, Li Y, Cao Y, Chen X. Extracellular ATP a new player in cancer metabolism: NSCLC cells internalize ATP *in vitro* and *in vivo* using multiple endocytic mechanisms. *Mol Cancer Res.* (2016) 14:1087–96. doi: 10.1158/1541-7786.MCR-16-0118
82. Zhou X, Zhi X, Zhou P, Chen S, Zhao F, Shao Z, et al. Effects of ecto-5'-nucleotidase on human breast cancer cell growth *in vitro* and *in vivo*. *Oncol Rep.* (2007) 17:1341–6. doi: 10.3892/or.17.6.1341
83. Feng L, Sun X, Csizmadia E, Han L, Bian S, Murakami T, et al. Vascular CD39/ENTPD1 directly promotes tumor cell growth by scavenging extracellular adenosine triphosphate. *Neoplasia.* (2011) 13:206–16. doi: 10.1593/neo.101332
84. Haanes KA, Schwab A, Novak I. The P2X7 receptor supports both life and death in fibrogenic pancreatic stellate cells. *PLoS ONE.* (2012) 7:e51164. doi: 10.1371/journal.pone.0051164
85. Zhou JZ, Riquelme MA, Gao X, Ellies LG, Sun LZ, Jiang JX. Differential impact of adenosine nucleotides released by osteocytes on breast cancer growth and bone metastasis. *Oncogene.* (2015) 34:1831–42. doi: 10.1038/onc.2014.113
86. Song S, Jacobson KN, Mcdermott KM, Reddy SP, Cress AE, Tang H, et al. ATP promotes cell survival via regulation of cytosolic [Ca2+] and Bcl-2/Bax ratio in lung cancer cells. *Am J Physiol Cell Physiol.* (2016) 310:C99–114. doi: 10.1152/ajpcell.00092.2015
87. Kamiya H, Kanno T, Fujita Y, Gotoh A, Nakano T, Nishizaki T. Apoptosis-related gene transcription in human A549 lung cancer cells via A(3) adenosine receptor. *Cell Physiol Biochem.* (2012) 29:687–96. doi: 10.1159/000312589
88. Tsuchiya A, Kanno T, Saito M, Miyoshi Y, Gotoh A, Nakano T, et al. Intracellularly transported adenosine induces apoptosis in [corrected] MCF-7 human breast cancer cells by accumulating AMID in the nucleus. *Cancer Lett.* (2012) 321:65–72. doi: 10.1016/j.canlet.2012.02.023
89. Ohkubo S, Nagata K, Nakahata N. Adenosine uptake-dependent C6 cell growth inhibition. *Eur J Pharmacol.* (2007) 577:35–43. doi: 10.1016/j.ejphar.2007.08.025
90. Gao ZW, Wang HP, Dong K, Lin F, Wang X, Zhang HZ. Adenosine inhibits migration, invasion and induces apoptosis of human cervical cancer cells. *Neoplasma.* (2016) 63:201–7. doi: 10.4149/204_150723N407
91. Wen LT, Knowles AF. Extracellular ATP and adenosine induce cell apoptosis of human hepatoma Li-7A cells via the A3 adenosine receptor. *Br J Pharmacol.* (2003) 140:1009–18. doi: 10.1038/sj.bjp.0705523
92. Hugo F, Mazurek S, Zander U, Eigenbrodt E. *In vitro* effect of extracellular AMP on MCF-7 breast cancer cells: inhibition of glycolysis and cell proliferation. *J Cell Physiol.* (1992) 153:539–49. doi: 10.1002/jcp.1041530315
93. Saito M, Yaguchi T, Yasuda Y, Nakano T, Nishizaki T. Adenosine suppresses CW2 human colonic cancer growth by inducing apoptosis via A(1) adenosine receptors. *Cancer Lett.* (2010) 290:211–5. doi: 10.1016/j.canlet.2009.09.011
94. Cohen S, Stemmer SM, Zozulya G, Ochaion A, Patoka R, Barer F, et al. CF102 an A3 adenosine receptor agonist mediates anti-tumor and anti-inflammatory effects in the liver. *J Cell Physiol.* (2011) 226:2438–47. doi: 10.1002/jcp.22593
95. Gessi S, Merighi S, Sacchetto V, Simioni C, Borea PA. Adenosine receptors and cancer. *Biochim Biophys Acta.* (2011) 1808:1400–12. doi: 10.1016/j.bbamem.2010.09.020
96. Kanno T, Nakano T, Fujita Y, Gotoh A, Nishizaki T. Adenosine induces apoptosis in SBC-3 human lung cancer cells through A(3) adenosine receptor-dependent AMID upregulation. *Cell Physiol Biochem.* (2012) 30:666–77. doi: 10.1159/000341447
97. Daniele S, Zappelli E, Natali L, Martini C, Trincavelli ML. Modulation of A1 and A2B adenosine receptor activity: a new strategy to sensitise glioblastoma stem cells to chemotherapy. *Cell Death Dis.* (2014) 5:e1539. doi: 10.1038/cddis.2014.487
98. Sakowicz-Burkiewicz M, Kitowska A, Grden M, Maciejewska I, Szutowicz A, Pawelczyk T. Differential effect of adenosine receptors on growth of human colon cancer HCT 116 and HT-29 cell lines. *Arch Biochem Biophys.* (2013) 533:47–54. doi: 10.1016/j.abb.2013.02.007
99. Bu X, Kato J, Hong JA, Merino MJ, Schrump DS, Lund FE, et al. CD38 knockout suppresses tumorigenesis in mice and clonogenic growth of human lung cancer cells. *Carcinogenesis.* (2018) 39:242–51. doi: 10.1093/carcin/bgx137
100. Ben Baruch B, Blacher E, Mantsur E, Schwartz H, Vaknine H, Erez N, et al. Stromal CD38 regulates outgrowth of primary melanoma and generation of spontaneous metastasis. *Oncotarget.* (2018) 9:31797–811. doi: 10.18632/oncotarget.25737
101. Oh ET, Park MT, Song MJ, Lee H, Cho YU, Kim SJ, et al. Radiation-induced angiogenic signaling pathway in endothelial cells obtained from normal and cancer tissue of human breast. *Oncogene.* (2014) 33:1229–38. doi: 10.1038/onc.2013.70
102. Wang Y, Boerma M, Zhou D. Ionizing radiation-induced endothelial cell senescence and cardiovascular diseases. *Radiat Res.* (2016) 186:153–61. doi: 10.1667/RR14445.1
103. Guipaud O, Jaillet C, Clement-Colmou K, Francois A, Supiot S, Milliat F. The importance of the vascular endothelial barrier in the immune-inflammatory response induced by radiotherapy. *Br J Radiol.* (2018) 91:20170762. doi: 10.1259/bjr.20170762
104. Klein D. The tumor vascular endothelium as decision maker in cancer therapy. *Front Oncol.* (2018) 8:367. doi: 10.3389/fonc.2018.00367
105. Venkatesulu BP, Mahadevan LS, Aliru ML, Yang X, Bodd MH, Singh PK, et al. Radiation-induced endothelial vascular injury: a review of possible mechanisms. *JACC Basic Transl Sci.* (2018) 3:563–72. doi: 10.1016/j.jacbts.2018.01.014
106. Feliu C, Peyret H, Poitevin G, Cazaubon Y, Oszust F, Nguyen P, et al. Complementary role of P2 and adenosine receptors in ATP induced-anti-apoptotic effects against hypoxic injury of HUVECs. *Int J Mol Sci.* (2019) 20:1446. doi: 10.3390/ijms20061446
107. Rumjahn SM, Yokdang N, Baldwin KA, Thai J, Buxton IL. Purinergic regulation of vascular endothelial growth factor signaling in angiogenesis. *Br J Cancer.* (2009) 100:1465–70. doi: 10.1038/sj.bjc.6604998
108. Wo YJ, Gan ASP, Lim X, Tay ISY, Lim S, Lim JCT, et al. The roles of CD38 and CD157 in the solid tumor microenvironment and cancer immunotherapy. *Cells.* (2019) 9:26. doi: 10.3390/cells9010026
109. Molica S, Cutrona G, Vitelli G, Mirabelli R, Molica M, Digiesi G, et al. Markers of increased angiogenesis and their correlation with biological parameters identifying high-risk patients in early B-cell chronic lymphocytic leukemia. *Leuk Res.* (2007) 31:1575–8. doi: 10.1016/j.leukres.2007.03.009
110. Ben Baruch B, Mantsur E, Franco-Barraza J, Blacher E, Cukierman E, Stein R. CD38 in cancer-associated fibroblasts promotes pro-tumoral activity. *Lab Invest.* (2020). doi: 10.1038/s41374-020-0458-8. [Epub ahead of print].
111. Wachsberger P, Burd R, Dicker AP. Tumor response to ionizing radiation combined with antiangiogenesis or vascular targeting agents: exploring mechanisms of interaction. *Clin Cancer Res.* (2003) 9:1957–71.
112. Kunjachan S, Detappe A, Kumar R, Ireland T, Cameron L, Biancur DE, et al. Nanoparticle mediated tumor vascular disruption: a novel strategy in radiation therapy. *Nano Lett.* (2015) 15:7488–96. doi: 10.1021/acs.nanolett.5b03073
113. Visovatti SH, Hyman MC, Bouis D, Neubig R, Mclaughlin VV, Pinsky DJ. Increased CD39 nucleotidase activity on microparticles from patients with idiopathic pulmonary arterial hypertension. *PLoS ONE.* (2012) 7:e40829. doi: 10.1371/journal.pone.0040829

114. Visovatti SH, Hyman MC, Goonewardena SN, Anyanwu AC, Kanthi Y, Robichaud P, et al. Purinergic dysregulation in pulmonary hypertension. *Am J Physiol Heart Circ Physiol.* (2016) 311:H286–98. doi: 10.1152/ajpheart.00572.2015
115. Aliagas E, Munoz-Esquerre M, Cuevas E, Careta O, Huertas D, Lopez-Sanchez M, et al. Is the purinergic pathway involved in the pathology of COPD? Decreased lung CD39 expression at initial stages of COPD. *Respir Res.* (2018) 19:103. doi: 10.1186/s12931-018-0793-0
116. Riteau N, Gasse P, Fauconnier L, Gombault A, Couegnat M, Fick L, et al. Extracellular ATP is a danger signal activating P2X7 receptor in lung inflammation and fibrosis. *Am J Respir Crit Care Med.* (2010) 182:774–83. doi: 10.1164/rccm.201003-0359OC
117. Wongkhantee S, Yongchaitrakul T, Pavasant P. Mechanical stress induces osteopontin via ATP/P2Y1 in periodontal cells. *J Dent Res.* (2008) 87:564–8. doi: 10.1177/154405910808700601
118. Barratt S, Millar A. Vascular remodelling in the pathogenesis of idiopathic pulmonary fibrosis. *QJM.* (2014) 107:515–9. doi: 10.1093/qjmed/hcu012
119. Murray LA, Habiel DM, Hohmann M, Camelo A, Shang H, Zhou Y, et al. Antifibrotic role of vascular endothelial growth factor in pulmonary fibrosis. *JCI Insight.* (2017) 2:e92192. doi: 10.1172/jci.insight.92192
120. Helenius MH, Vattulainen S, Orcholski M, Aho J, Komulainen A, Taimen P, et al. Suppression of endothelial CD39/ENTPD1 is associated with pulmonary vascular remodeling in pulmonary arterial hypertension. *Am J Physiol Lung Cell Mol Physiol.* (2015) 308:L1046–57. doi: 10.1152/ajplung.00340.2014
121. Pinsky DJ. Cd39 as a critical ectonucleotidase defense against pathological vascular remodeling. *Trans Am Clin Climatol Assoc.* (2018) 129:132–9.
122. Ferrero E, Faini AC, Malavasi F. A phylogenetic view of the leukocyte ectonucleotidases. *Immunol Lett.* (2019) 205:51–8. doi: 10.1016/j.imlet.2018.06.008
123. Morandi F, Marimpietri D, Horenstein AL, Corrias MV, Malavasi F. Microvesicles expressing adenosinergic ectoenzymes and their potential role in modulating bone marrow infiltration by neuroblastoma cells. *Oncoimmunology.* (2019) 8:e1574198. doi: 10.1080/2162402X.2019.1574198
124. Zilber MT, Gregory S, Mallone R, Deaglio S, Malavasi F, Charron D, et al. CD38 expressed on human monocytes: a coaccessory molecule in the superantigen-induced proliferation. *Proc Natl Acad Sci USA.* (2000) 97:2840–5. doi: 10.1073/pnas.050583197
125. Musso T, Deaglio S, Franco L, Calosso L, Badolato R, Garbarino G, et al. CD38 expression and functional activities are up-regulated by IFN-gamma on human monocytes and monocytic cell lines. *J Leukoc Biol.* (2001) 69:605–12. doi: 10.1189/jlb.69.4.605
126. Dewhurst JA, Lea S, Hardaker E, Dungwa JV, Ravi AK, Singh D. Characterisation of lung macrophage subpopulations in COPD patients and controls. *Sci Rep.* (2017) 7:7143. doi: 10.1038/s41598-017-07101-2
127. Lam JH, Ng HHM, Lim CJ, Sim XN, Malavasi F, Li H, et al. Expression of CD38 on macrophages predicts improved prognosis in hepatocellular carcinoma. *Front Immunol.* (2019) 10:2093. doi: 10.3389/fimmu.2019.02093
128. Hubert S, Rissiek B, Klages K, Huehn J, Sparwasser T, Haag F, et al. Extracellular NAD+ shapes the Foxp3+ regulatory T cell compartment through the ART2-P2X7 pathway. *J Exp Med.* (2010) 207:2561–8. doi: 10.1084/jem.20091154
129. Xiong S, Guo R, Yang Z, Xu L, Du L, Li R, et al. Treg depletion attenuates irradiation-induced pulmonary fibrosis by reducing fibrocyte accumulation, inducing Th17 response, and shifting IFN-gamma, IL-12/IL-4, IL-5 balance. *Immunobiology.* (2015) 220:1284–91. doi: 10.1016/j.imbio.2015.07.001
130. Chakraborty K, Chatterjee S, Bhattacharyya A. Impact of Treg on other T cell subsets in progression of fibrosis in experimental lung fibrosis. *Tissue Cell.* (2018) 53:87–92. doi: 10.1016/j.tice.2018.06.003
131. Ohta A, Sitkovsky M. Extracellular adenosine-mediated modulation of regulatory T cells. *Front Immunol.* (2014) 5:304. doi: 10.3389/fimmu.2014.00304
132. Allard D, Allard B, Stagg J. On the mechanism of anti-CD39 immune checkpoint therapy. *J Immunother Cancer.* (2020) 8:e000186. doi: 10.1136/jitc-2019-000186
133. Di Virgilio F, Adinolfi E. Extracellular purines, purinergic receptors and tumor growth. *Oncogene.* (2017) 36:293–303. doi: 10.1038/onc.2016.206

Conflict of Interest: The authors declare that the research was conducted in the absence of any commercial or financial relationships that could be construed as a potential conflict of interest.

frontiers in Oncology

ORIGINAL RESEARCH
published: 11 November 2020
doi: 10.3389/fonc.2020.536377

MTHFD2 Blockade Enhances the Efficacy of β-Lapachone Chemotherapy With Ionizing Radiation in Head and Neck Squamous Cell Cancer

Kirtikar Shukla[1], Naveen Singh[2], Joshua E. Lewis[3,4], Allen W. Tsang[1], David A. Boothman[2†], Melissa L. Kemp[3,4] and Cristina M. Furdui[1]*

[1] Department of Internal Medicine, Section on Molecular Medicine, Wake Forest School of Medicine, Winston-Salem, NC, United States, [2] Department of Biochemistry and Molecular Biology, Simon Cancer Center, Indiana University School of Medicine, Indianapolis, IN, United States, [3] The Parker H. Petit Institute of Bioengineering and Bioscience, Georgia Institute of Technology, Atlanta, GA, United States, [4] The Wallace H. Coulter Department of Biomedical Engineering, Georgia Institute of Technology and Emory School of Medicine, Atlanta, GA, United States

OPEN ACCESS

Edited by:
Mary Helen Barcellos-Hoff, University of California, San Francisco, United States

Reviewed by:
Michael Wayne Epperly, University of Pittsburgh, United States
Sunyoung Jang, Princeton Radiation Oncology Center, United States
Shisuo Du, Fudan University, China

***Correspondence:**
Cristina M. Furdui
cfurdui@wakehealth.edu

[†] In memoriam

Specialty section:
This article was submitted to Radiation Oncology, a section of the journal Frontiers in Oncology

Received: 19 February 2020
Accepted: 31 August 2020
Published: 11 November 2020

Citation:
Shukla K, Singh N, Lewis JE, Tsang AW, Boothman DA, Kemp ML and Furdui CM (2020) MTHFD2 Blockade Enhances the Efficacy of β-Lapachone Chemotherapy With Ionizing Radiation in Head and Neck Squamous Cell Cancer. Front. Oncol. 10:536377. doi: 10.3389/fonc.2020.536377

Head and Neck Squamous Cell Cancer (HNSCC) presents with multiple treatment challenges limiting overall survival rates and affecting patients' quality of life. Amongst these, resistance to radiation therapy constitutes a major clinical problem in HNSCC patients compounded by origin, location, and tumor grade that limit tumor control. While cisplatin is considered the standard radiosensitizing agent for definitive or adjuvant radiotherapy, in recurrent tumors or for palliative care other chemotherapeutics such as the antifolates methotrexate or pemetrexed are also being utilized as radiosensitizers. These drugs inhibit the enzyme dihydrofolate reductase, which is essential for DNA synthesis and connects the 1-C/folate metabolism to NAD(P)H and $NAD(P)^+$ balance in cells. In previous studies, we identified MTHFD2, a mitochondrial enzyme involved in folate metabolism, as a key contributor to NAD(P)H levels in the radiation-resistant cells and HNSCC tumors. In the study presented here, we investigated the role of MTHFD2 in the response to radiation alone and in combination with β-lapachone, a NQO1 bioactivatable drug, which generates reactive oxygen species concomitant with NAD(P)H oxidation to $NAD(P)^+$. These studies are performed in a matched HNSCC cell model of response to radiation: the radiation resistant rSCC-61 and radiation sensitive SCC-61 cells reported earlier by our group. Radiation resistant rSCC-61 cells had increased sensitivity to β-lapachone compared to SCC-61 and knockdown of MTHFD2 in rSCC-61 cells further potentiated the cytotoxicity of β-lapachone with radiation in a dose and time-dependent manner. rSCC-61 MTHFD2 knockdown cells irradiated and treated with β-lapachone showed increased PARP1 activation, inhibition of mitochondrial respiration, decreased respiration-linked ATP production, and increased mitochondrial superoxide and protein oxidation as compared to control rSCC-61 scrambled shRNA. Thus, these studies point to MTHFD2 as a potential target for development of radiosensitizing chemotherapeutics and potentiator of β-lapachone cytotoxicity.

Keywords: head and neck cancer, radiation resistance, NQO1, β-lapachone, MTHFD2

INTRODUCTION

Head and neck squamous cell cancer (HNSCC) is an aggressive disease with a high rate of mortality and morbidity in the United States. A recent statistical report from the National Cancer Institute estimated that more than 53,000 people will have oropharyngeal cancer in the United States in 2020 accounting for ∼4–5% of overall cancer types (1). Radiation therapy is a key component of standard of care treatment for HNSCC, but radioresistance and side effects of treatment limit patients' overall survival and long-term quality of life (2). There is a need for new molecular approaches to treat radiation resistant HNSCC tumors using combination therapies, and indeed, current efforts to enhance the efficacy of radiation therapy in HNSCC include combination treatment with targeted therapies (e.g., against Epidermal Growth Factor Receptor, EGFR), and immunomodulators, which are increasingly investigated in clinical studies (3).

Over the last decades, work pioneered by Boothman's group has established β-lapachone (β-lap), a NAD(P)H:quinone oxidoreductase 1 (NQO1) bioactivatable substrate, as a promising cancer therapeutic and radiation sensitizer targeting a broad spectrum of cancers including HNSCC (4–9). NQO1 metabolizes β-lap into an unstable hydroquinone, which is then oxidized back to the quinone state through a semiquinone intermediate releasing superoxide O_2^-. This futile redox cycle depletes the cells of NAD(P)H and generates toxic amounts of reactive oxygen species (ROS) leading to DNA damage and PARP1 hyperactivation (5, 6, 10, 11). PARP1 activity further consumes the NAD^+ produced in the NQO1/β-lap cycle instigating a specific mechanism of μ-Calpain-mediated cell death called Keresis (12). The cumulative body of evidence supports the tumor-selective efficacy of β-lap derivatives and a version of this, ARQ761, has already been investigated in phase I/II clinical trials for patients with metastatic solid tumors (13). However, not all patients responded to treatment and while there was an association of tumor response with NQO1 expression, clearly other factors limited the efficacy of β-lap/ARQ761 treatment in these studies. Logically, based on the known mechanism of action, the cytotoxicity of β-lap is expected to be driven by the expression and activity of NQO1, the expression and activity of ROS-metabolizing enzymes (e.g., catalase, SOD1, etc.) (11, 14), and the availability of NAD(P)H, which is needed to support both the NQO1-catalyzed generation of ROS and the activity of key ROS-suppressing redox regulatory enzymes [e.g., thioredoxin reductase (14)]. In this context, the localization of NAD(P)H may also become important considering the predominant cytoplasmic localization of NQO1. The expression of NQO1 is regulated in cells by KEAP1/Nrf2 pathways, and a series of studies have established prolonged induction of NQO1 expression by ionizing radiation in lung cancer cells and in FSall mice tumors (15, 16). These findings raised the possibility of improved chemotherapeutic and radiation sensitizing activity of β-lap, which have now been confirmed in numerous cancers, including HNSCC (9).

Recognizing the importance of NAD(P)H availability to sustain the NQO1-dependent activity of β-lap, we have started to investigate the metabolic contribution to intracellular NAD(P)H first by computational flux balance analysis taking advantage of HNSCC data available in online repositories (e.g., TCGA, Human Protein Atlas), and multi-omics data collected for a matched model of response to radiation (radiation sensitive SCC-61 and radiation resistant rSCC-61) developed by our group (17–21).

In the study presented here, we evaluated mitochondrial methylenetetrahydrofolate dehydrogenase 2 (MTHFD2), one of the metabolic enzymes identified by the computational studies as a major producer of NAD(P)H in radiation resistant HNSCC cells and patient tumors. We report a series of *in vitro* and *in vivo* studies assessing the role of MTHFD2 in enhancing the efficacy of response to ionizing radiation and β-lap using the radiation sensitive SCC-61 and radiation resistant rSCC-61 matched cell system highlighted above.

MATERIALS AND METHODS

Materials

The following materials were utilized for the studies included here: Dulbecco's Modified Eagle Medium/Nutrient Mixture F-12 (DMEM/F12), penicillin/streptomycin, fetal bovine serum (FBS) (Gibco, Thermo Fisher Scientific, USA); β-lap (Xoder Technologies, USA); Lipofectamine 2000 and oligomycin (Thermo Fisher Scientific, USA); carbonyl cyanide 4-(trifluoromethoxy) phenylhydrazone (FCCP) (Cayman Chemicals, USA); Antimycin A (Abcam, USA); Rotenone (Millipore-Sigma, USA); MitoSOX (Invitrogen, Thermo Fisher Scientific, USA); antibodies against NQO1, MTHFD2, catalase, PARP1, p-γH_2AX(S139), β-actin, and GAPDH (Cell Signaling Technology, USA); shRNA (MTHFD2 and scrambled control), PAR and α-tubulin antibodies (Santa Cruz Biotechnology, USA); Bicinchoninic acid (BCA) assay, CyQuant kit, and SuperSignal chemiluminescent HRP substrate (Thermo Fisher Scientific, USA). Matrigel Growth Factor Reduced (GFR) Basement Membrane Matrix, LDEV-free was obtained from Corning Inc., USA (LDEV-free: free of viruses, including lactose dehydrogenase elevating virus or LDEV). Modified RIPA buffer for cell lysis was prepared in the laboratory and contained: 50 mM Tris-HCl, pH 7.4; 1% NP40; 0.25% sodium deoxycholate; 15 mM NaCl; 1 mM EDTA; 1 mM NaF; and, Roche protease and phosphatase inhibitor tablets (Basel, Switzerland). Fluorescence-activated cell sorting (FACS) buffer and Western blot TBST buffer were similarly prepared in the laboratory (FACS: PBS (Ca^{2+}/Mg^{2+} free), 1% BSA, and 0.1% sodium azide; TBST: 20 mM Tris buffer, 0.1% Tween 20, pH 7.4).

HNSCC Cells and Cell Culture Conditions

The HNSCC radiation sensitive SCC-61, genetically matched radiation resistant rSCC-61 cells (17–21), MTHFD2 knockdown rSCC-61 cells (MTHFD2 KD rSCC-61), and the respective scramble shRNA control rSCC-61 cells (scRNA rSCC-61) were cultured in DMEM/F12 media containing 10% FBS and 1% penicillin/streptomycin at 37°C using a 5% CO_2 incubator. The cell culture media was replaced every other day and

before lysis when the cells reached 80–90% confluency. Stable MTHFD2 KD rSCC-61 and scRNA cells were generated by transfection of rSCC-61 cells with MTHFD2 shRNA and the scRNA, respectively. rSCC-61 cells were seeded in 6-well tissue culture plates at a density of 3,000 cells/cm^2 and allowed 24 h to attach to the culture plates. When the cells reached 70–75% confluency, the cells were transfected with 50 nM MTHFD2 shRNA or 50 nM scRNA using Lipofectamine 2000 as recommended by the manufacturer's protocol and incubated for 48 hrs. The cells were then incubated with complete cell culture media (DMEM/F12, 10% FBS) containing puromycin (1 μg/mL) to facilitate the selection of MTHFD2 KD cells. The cells were further maintained in selection medium for additional 48 h resulting in stably transfected MTHFD2 KD rSCC-61 cells and the respective scRNA rSCC-61cells.

Treatment With Ionizing Radiation and Formulation of β-Lapachone

HNSCC cells and tumors have received indicated doses of ionization radiation (IR) using a 444 TBq 12,000 Ci self-shielded ^{137}Cs (Cesium) irradiator (Mark 1, Model 68A, JL Shepherd and Associates, San Fernando, CA, USA). β-Lapachone stock solution (50 mM) was prepared in DMSO and kept in 10 μL aliquots at −80°C. For the *in vivo* studies, β-lap was complexed with cyclodextrin (HPβCD) to increase solubility and bioavailability, as described previously (22).

Cell Proliferation and Clonogenic Cell Survival Assays

Both cell proliferation and clonogenic survival assays were performed. Briefly, for proliferation assays the cells were trypsinized and ∼5,000 cells/well were seeded in 96-well plates. After 24 h, the cells were treated with 2, 4, 8, and 12 μM β-lap and incubated for 2 h at 37°C in a 5% CO_2 incubator. The culture media was then replaced with fresh complete media, and the cells were incubated for additional 24 h at 37°C/5% CO_2 incubator. Cell proliferation was quantified using the fluorescence based CyQuant assay following the manufacturer's protocol.

Clonogenic survival assays were performed to determine the synergy with β-lap and ionizing radiation following previously reported methods (23). HNSCC cells (SCC-61, rSCC-61, MTHFD2 KD rSCC-61, and scRNA rSCC-61) were seeded at a density of 300 cells/well into 6-well plates. Cells were kept overnight at 37°C in a 5% CO_2 incubator. The next day, the cells were irradiated (2 Gy, single dose or sham) followed by addition of the indicated concentration of β-lap or vehicle control and further incubated for 2 h. Upon completion of the incubation period, the culture media was replaced with fresh complete media and the cells were returned to the 37°C/5% CO_2 incubator for 6–7 days. The cells were then fixed with a solution of ice-cold acetic acid: methanol (3:7) and stained with 0.5% crystal violet for 2 h at room temperature. The plates were washed with running water to remove the residual stain. Colonies containing >50 cells were counted under a light microscope and the survival fraction was calculated as described (23).

Western Blot Analysis

HNSCC cells were lysed with modified RIPA buffer supplemented with Roche protease and phosphatase inhibitor tablets, and the protein concentration was measured using the BCA assay. An equal amount of protein (20 mg) was separated by SDS-PAGE and transferred to nitrocellulose membranes for Western blot analysis. Membranes were probed with indicated primary antibodies overnight at 4°C. Next day, the membranes were washed three times with TBST buffer and further incubated with corresponding secondary antibodies for 1 h at room temperature. The membranes were washed again three times with TBST buffer (in all cases, each TBST wash cycle was 15 min), incubated with the SuperSignal chemiluminescent HRP substrate, and the images were collected using an Amersham Imager 600 (GE Healthcare Life Sciences). Antibodies against actin, α-tubulin, or GAPDH were utilized as controls for equal loading.

Enzyme Activity Assays

NQO1 activity in cell extracts was assayed following published protocols (5). Briefly, NADH (200 μM) used as a reducing agent (electron donor) and menadione (10 μM) as the intermediate electron acceptor were mixed in 50 mM Tris-HCl buffer (pH 7.5) reaction mixture containing 77 μM cytochrome C (Sigma, USA) and 0.14% BSA. The cell lysate was then added into the reaction mixture and the absorbance was read at 550 nm. The enzymatic activity of NQO1 was calculated as nmol cytochrome c reduced/min/μg protein.

Cell Cycle

About 2 × 10^5 MTHFD2 KD and scRNA rSCC-61 cells were seeded into 6-well cell culture plates, allowed to attach, incubated overnight in serum-free medium, and then irradiated (2 Gy or sham) and treated with β-lap (3 μM) or vehicle control for 2 h. After completion of the incubation period, the culture media was replaced with fresh serum-free media and the cells were incubated for another 22 h. At the end of the incubation period, the cells were washed with PBS, trypsinized, and centrifuged at 200 × g for 5 min. The cells were again washed with PBS, fixed with ice-cold 70% ethanol for 30 min at 4°C, further washed with PBS (two times), and incubated with PBS containing 100 μg/mL RNase A and 50 μg/mL propidium iodide. The cells were washed three times with PBS and resuspended into 300 μL FACS buffer and subjected to flow cytometry using a BD Accuri 6 for analysis. Data analysis to quantify the cell cycle distribution was performed with FCS Express 6 Flow software (*De Novo* Software, Pasadena, CA, USA).

Mitochondrial Respirometry Analysis

The effects of β-lap on mitochondrial function were measured using the Seahorse Mito Stress Test following the manufacturer's protocol on a Seahorse XF24 (Agilent Technologies, Santa Clara, CA, USA). MTHFD2 KD and scRNA rSCC-61 cells (∼4,000 cells/well) were seeded on a 24-well Seahorse plate and allowed to attach for 24 h. Next day, the cells were exposed to β-lap (3 μM) or vehicle control for 2 h in complete growth media, washed, and transferred to the Seahorse instrument for

collection of oxygen consumption data. After baseline reading, the injections were performed as follows: (1) oligomycin (1 μM) at 27 min, FCCP (1 μM) at 51 min, and Antimycin A/Rotenone (1 μM) at 75 min. After the completion of data collection, the cells were lysed and quantified with CyQuant for data normalization. The data were analyzed with Wave software (Agilent Technologies).

Flow Cytometry Analysis of Mitochondrial ROS and Mitochondrial Protein Oxidation

Mitochondrial ROS was detected in live cells using MitoSOX and flow cytometry analysis. Briefly, MTHFD2 KD and scRNA rSCC-61 cells were irradiated (2 Gy or sham) and further treated with β-lap (3 μM) or vehicle control for 2 h After completion of the incubation period, the cells were washed with PBS and further incubated with 1 μM MitoSOX for 30 min at 37°C in a 5% CO_2 incubator. The cells were then washed three times with PBS, resuspended in FACS buffer and subjected to flow cytometry using a BD FACS Canto II Cell Analyzer (BD Biosciences, San Jose, CA, USA). Similarly, to determine the mitochondrial protein oxidation, the cells were treated with radiation and β-lap as described for MitoSOX analysis, and then stained with DCP-NEt_2C (for 30 min at 37°C). DCP-NEt_2C contains a protein sulfenic acid reacting group and coumarin to facilitate localization to mitochondria (24). After completion of the incubation period, cells were washed with PBS, fixed with ice-cold methanol for 5 min, further washed with PBS, resuspended in the FACS buffer and analyzed using a BD LSRFortessa Flow Cytometer. Data analysis was performed with FCS Express 6 Flow software (*De Novo* Software, Pasadena, CA, USA).

Tumor Xenograft Implant in Nude Mice

The effects of MTHFD2 KD on the anti-tumor efficacy of β-lap and ionizing radiation were investigated *in vivo* using 4–5 weeks old female nu/nu nude mice obtained from Charles River Laboratories, MA, USA. The animal studies were performed under a protocol approved by the Wake Forest University Institutional Animal Care and Use Committee and in accordance with the guidelines for ethical conduct in the care and use of animals in research. Mice were housed for 1 week after arrival at the animal facility before the start of the experiment. Mice were fed pellet diet and received water *ad libitum*. The xenograft tumor was generated subcutaneously by injecting 5 × 10^5 MTHFD2 KD and scRNA rSCC-61 cells suspended in growth factor reduced matrigel in a single flank on the dorsal surface of mice. Once the tumor size reached minimum 100 mm^3, the mice were randomly divided into subgroups (5 mice/group) and treated as follows: (1) HPβCD (intravenous administration); (2) ionizing radiation (2 Gy) targeted to the xenograft tumor; (3) β-lap/HPβCD complex (20 mg/kg body weight; intravenous administration); or (4) ionizing radiation (2 Gy) + β-lap/HPβCD complex (20 mg/kg; intravenous administration). Mice have received treatment every other day and tumor volume was measured using a digital caliper. Mice were euthanized after 10 days, the tumors were collected, washed with PBS, and weighted. A portion of the tumor was fixed in 10% formaldehyde and stained with hematoxylin and eosin.

Statistical Analyses

All experiments were performed in minimum three biological replicates and data are presented as mean ± standard deviation (SD). ANOVA or Students' *t*-test was utilized for statistical analysis using SPSS 7.0 and Excel software.

RESULTS

Radiation Resistant HNSCC rSCC-61 Cells Display Increased Sensitivity to β-Lapachone

The initial studies focused on the evaluation of previously reported biomarkers underlying the mechanisms of β-lap cytotoxicity (NQO1, catalase, PARP1) and MTHFD2 in the SCC-61 and rSCC-61 HNSCC cells (9). The Western blot analysis in **Figure 1A** show statistically significant increased expression of NQO1, MTHFD2, and PARP1, and slight but not statistically significant difference in the catalase levels ($p > 0.05$) in rSCC-61 relative to SCC-61 cells, suggesting potentially higher sensitivity to β-lap in rSCC-61 cells driven by increased NQO1 to catalase ratio. The activity of NQO1 was also significantly higher in rSCC-61 cells corroborating the Western blot analysis ($p < 0.001$, **Figure 1B**). To further investigate if the differences in the NQO1 and catalase profiles translated in increased sensitivity of rSCC-61 cells to β-lap, we performed *in vitro* cell proliferation assays. The data confirmed the anticipated increased sensitivity of rSCC-61 to β-lap (IC50 2.8 μM) compared with SCC-61 [IC50 5.7 μM) (**Figure 1C**). As radiation therapy is being used as first line treatment for HNSCC, and β-lap was shown previously to sensitize cells to radiation treatment (9)], we sought to quantify the impact of combined radiation and β-lap on clonogenic survival of SCC-61 and rSCC-61 cells. The cells were irradiated with 2 Gy and immediately treated with increasing doses of β-lap for 5 min to 2 h time intervals as noted in **Figure 1D**. As expected, in the absence of β-lap the extent of radiation-induced inhibition of clonogenic survival was greater in the radiation sensitive SCC-61 cells than in the radiation resistant rSCC-61 cells, constituting an important internal control for the assay. Addition of β-lap further decreased survival of SCC-61 in both time and dose-dependent manner ($p < 0.01$), but the cytotoxic efficacy in rSCC-61 cells was notably stronger across conditions ($p < 0001$).

MTHFD2 Knockdown Sensitizes rSCC-61 Cells to Radiation and β-Lapachone Treatment

Our previous computational analysis identified mitochondrial MTHFD2 as a major contributor to NAD(P)H production (20, 21). Indeed, the data in **Figure 1A** show higher level of MTHFD2 expression in the radiation resistant rSCC-61 cells compared to SCC-61 cells. To further investigate the role of MTHFD2 in the response of rSCC-61 cells to β-lap and ionizing radiation, we generated MTHFD2 KD and scRNA control rSCC-61 cells using shRNA technology (**Figure 2A**). Irradiated or sham-irradiated MTHFD2 KD and scRNA rSCC-61 cells were treated with increasing concentrations of β-lap (2–12 μM)

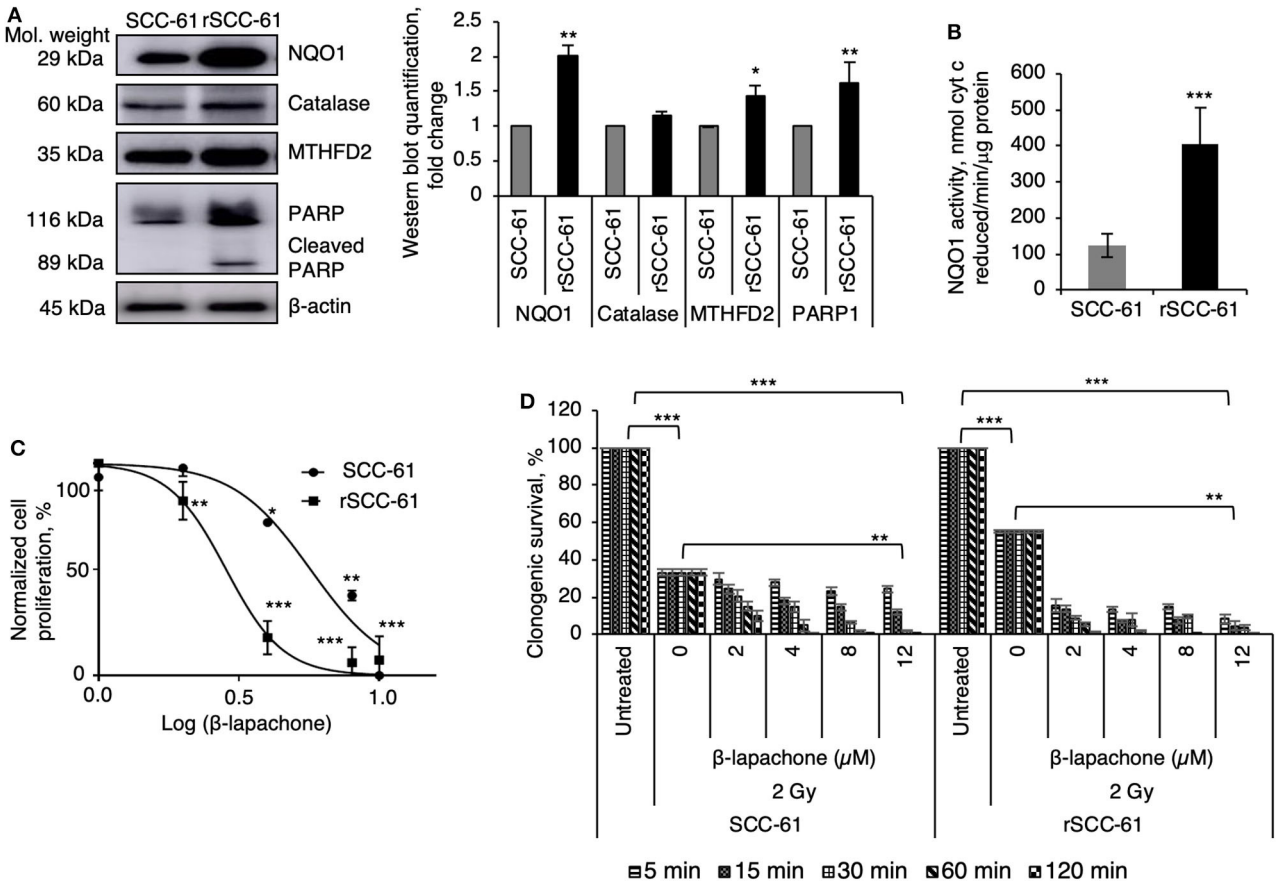

FIGURE 1 | Radiation resistant rSCC-61 cells have increased sensitivity to β-lapachone. **(A)** Western blot analysis of radiation sensitive SCC-61 and radiation resistant rSCC-61 cell lysates show approximately equal expression of catalase and increased levels of NQO1, MTHFD2, and cleaved PARP1 in rSCC-61 cells. The quantification of Western blots is presented in the right panel ($n = 3$; Student's *t*-test $^{*}p$ 0.01–0.05, $^{**}p$ 0.001–0.01 relative to SCC-61). **(B)** Measurement of NQO1 activity validate the findings from Western blot analysis showing ∼4-fold higher activity in rSCC-61 cells ($n = 3$; $^{***}p < 0.001$). **(C)** Cellular proliferation of SCC-61 and rSCC-61 cells treated with 0, 2, 4, 8, 12 μM β-lap demonstrate increased sensitivity of rSCC-61 cells to β-lap ($n = 3$, One-Way ANOVA with multiple comparisons $^{*}p$ 0.01–0.05, $^{**}p$ 0.001–0.01, and $^{***}p < 0.001$ relative to the respective untreated cells). **(D)** Clonogenic survival assays demonstrate the radiation sensitizing activity of β-lap, which is dependent on both the concentration of β-lap and the time of exposure to drug. *p*-values are indicated on the graph ($n = 3$, One-Way ANOVA with multiple comparisons).

or vehicle control for different time intervals (5 min−2 h) and the survival fraction was quantified for each treatment condition. As shown in **Figure 2B**, the clonogenic survival of MTHFD2 KD rSCC-61 cells was lower than scRNA rSCC-61 across treatment conditions. MTHFD2 KD rSCC-61 cells showed greater sensitivity to radiation treatment compared to scRNA rSCC-61 ($p < 0.05$), and treatment with β-lap resulted in more pronounced dose and time-dependent increases in cell death in MTHFD2 KD rSCC-61 as compared to scRNA rSCC-61 cells.

Combined β-Lapachone and Radiation Treatment Induces DNA Damage and Increases Mitochondrial ROS and Protein Oxidation in MTHFD2 Deficient rSCC-61 Cells

NQO1-dependent β-lap induced cell death has been reported to be the result of increased DNA damage initiated by the massive generation of ROS. To evaluate the consequence of MTHFD2 KD on the sensitivity of rSCC-61 cells to ionizing radiation and β-lap - induced DNA damage, MTHFD2 KD and scRNA rSCC-61 cells were irradiated followed by treatment with β-lap (3 μM, 1 h). Western blot analysis shown in **Figure 3A** indicates a significant amount of protein PARylation induced by combined radiation and β-lap treatment but only in MTHFD2 deficient rSCC-61 cells. Cleaved-PARP1 was also relatively increased upon treatment with radiation and β-lap in MTHFD2 KD rSCC-61 cells. Phosphorylation of γH_2AX was significantly higher in irradiated cells regardless of MTHFD2 status or β-lap treatment (p 0.001–0.01). The MTHFD2 KD rSCC-61 cells show slightly more DNA damage when treated with β-lap alone (p 0.074) or in combination with radiation (p 0.004) as reflected indirectly by the phosphorylation status of γH_2AX (**Figure 3A**).

Given the predominant mitochondrial localization of MTHFD2, we quantified next the effects of MTHFD2 depletion on mitochondrial ROS using MitoSOX and mitochondrial

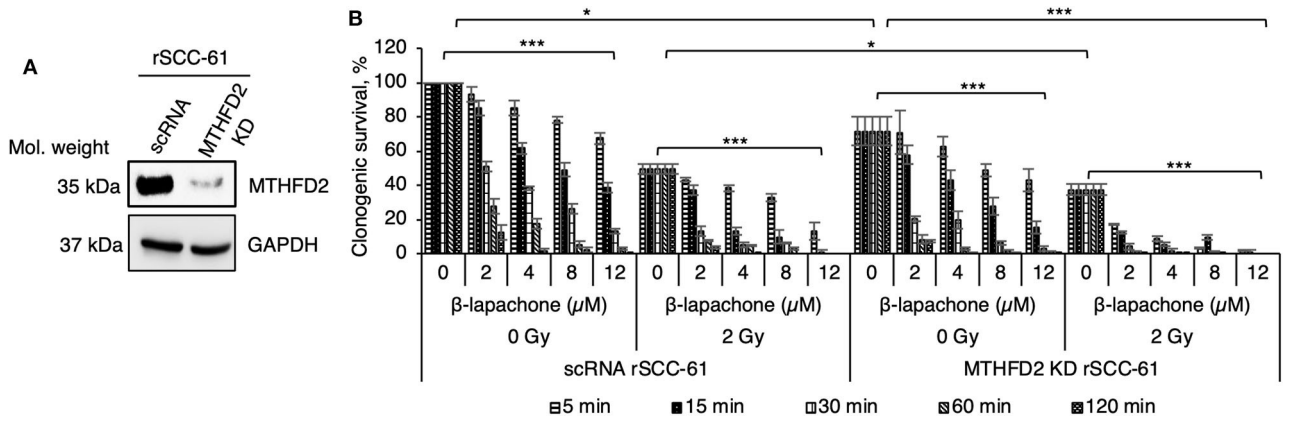

FIGURE 2 | MTHFD2 depletion in rSCC-61 increases β-lapachone cytotoxicity and sensitizes cells to radiation therapy. **(A)** Western blot analysis of scRNA control and MTHFD2 KD rSCC-61 confirms depletion of MTHFD2 in rSCC-61 cells transfected with MTHFD2 shRNA. **(B)** Clonogenic survival assays demonstrate increased sensitivity to both β-lap and ionizing radiation in MTHFD2 KD rSCC-61, which is dependent on both the concentration of β-lap and the time of exposure to drug. The maximum suppression of clonogenic survival was achieved in MTHFD2 KD rSCC-61 cells treated with combined ionizing radiation and β-lap. $n = 3$, One-Way ANOVA with multiple comparisons *p 0.01–0.05 and ***$p < 0.001$.

protein oxidation with DCP-NEt_2C, a selective fluorescent probe targeting protein sulfenylation (24). As shown in **Figure 3B**, MTHFD2 knockdown or radiation induced only minor changes in mitochondrial ROS or protein sulfenylation (either not significant or p 0.01–0.05). However, treatment with β-lap alone or in combination with radiation induced significantly higher levels of both mitochondrial ROS and protein sulfenylation, which was augmented by MTHFD2 depletion.

MTHFD2 Knockdown Enhances Mitochondrial Toxicity of β-Lapachone in rSCC-61

Earlier studies have established the effects of β-lap on mitochondrial respiration (7, 25) and the results in **Figure 3B** corroborate the findings in these publications. Given the function of MTHFD2 in mitochondrial NAD(P)H production, we hypothesized a more drastic collapse of mitochondrial respiration in MTHFD2 deficient cells. Therefore, we set up to determine the effects of β-lap on mitochondrial respiration by measuring the oxygen consumption rate in MTHFD2 KD and scRNA rSCC-61 cells using the standard Seahorse Mito Stress test (**Figure 4**). As anticipated, β-lap treatment decreased basal respiration in both MTHFD2 KD and scRNA rSCC-61 cells but achieved statistical significance only in MTHFD2 depleted cells. Similarly, the effect of β-lap treatment on all other parameters of mitochondrial respiration was augmented by MTHFD2 depletion with the exception of spare respiratory capacity, which was completely obliterated with β-lap treatment regardless of MTHFD2 status.

MTHFD2 Knockdown Does Not Significantly Impact Cell Cycle Distribution in rSCC-61 Cells

Both treatment with ionizing radiation and β-lap are known to induce cell cycle arrest at G1/S and G2/M checkpoints (18, 26, 27). In order to investigate the contribution of MTHFD2 to these effects, the cell cycle distribution was analyzed side-by-side in MTHFD2 KD and scRNA rSCC-61 cells treated with β-lap (3 μM, 2 h), ionizing radiation (2 Gy), and their respective vehicle and sham-irradiation controls. As shown in **Figure 5**, MTHFD2 depletion did not alter cell cycle distribution in rSCC-61 cells and as expected, ionizing radiation increased the proportion of cells in G2 phase in both scRNA control and MTHFD2 KD cells. This is consistent with well-established mechanisms of radiation resistance preventing cells with DNA damage from entering mitosis. Interestingly, while β-lap promoted cell cycle progression from G1 to S-phase, MTHFD2 knockdown prevented this activity, and the cell cycle distribution of MTHFD2 KD rSCC-61 cells treated with β-lap resembled the profile of radiation-treated rSCC-61 cells (scRNA or MTHFD2 KD). Overall, combined treatment with ionizing radiation and β-lap shows a statistically significant decreased distribution of cells in S-phase and increased G2-phase compared to untreated cells, regardless of MTHFD2 status.

MTHFD2 Knockdown Suppresses rSCC-61 Tumor Growth and Increases Sensitivity to Radiation

To further investigate the consequence of MTHFD2 knockdown on the response to ionizing radiation and β-lap, we performed *in vivo* studies using subcutaneous scRNA and MTHFD2 KD rSCC-61 xenograft tumors in nu/nu nude mice (**Figure 6A**). When the tumor reached minimum 100 mm^3, the mice were randomly divided into subgroups for treatment. The results summarized in **Figure 6B**, show significantly decreased tumor growth in MTHFD2 KD rSCC-61 tumors compared with scRNA rSCC-61 controls by ∼50%. As expected based on the results of the cell culture studies, the scRNA rSCC-61 tumors were more sensitive to β-lap than to ionizing radiation, and the combined ionizing radiation and β-lap treatment (2 Gy followed by β-lap 20

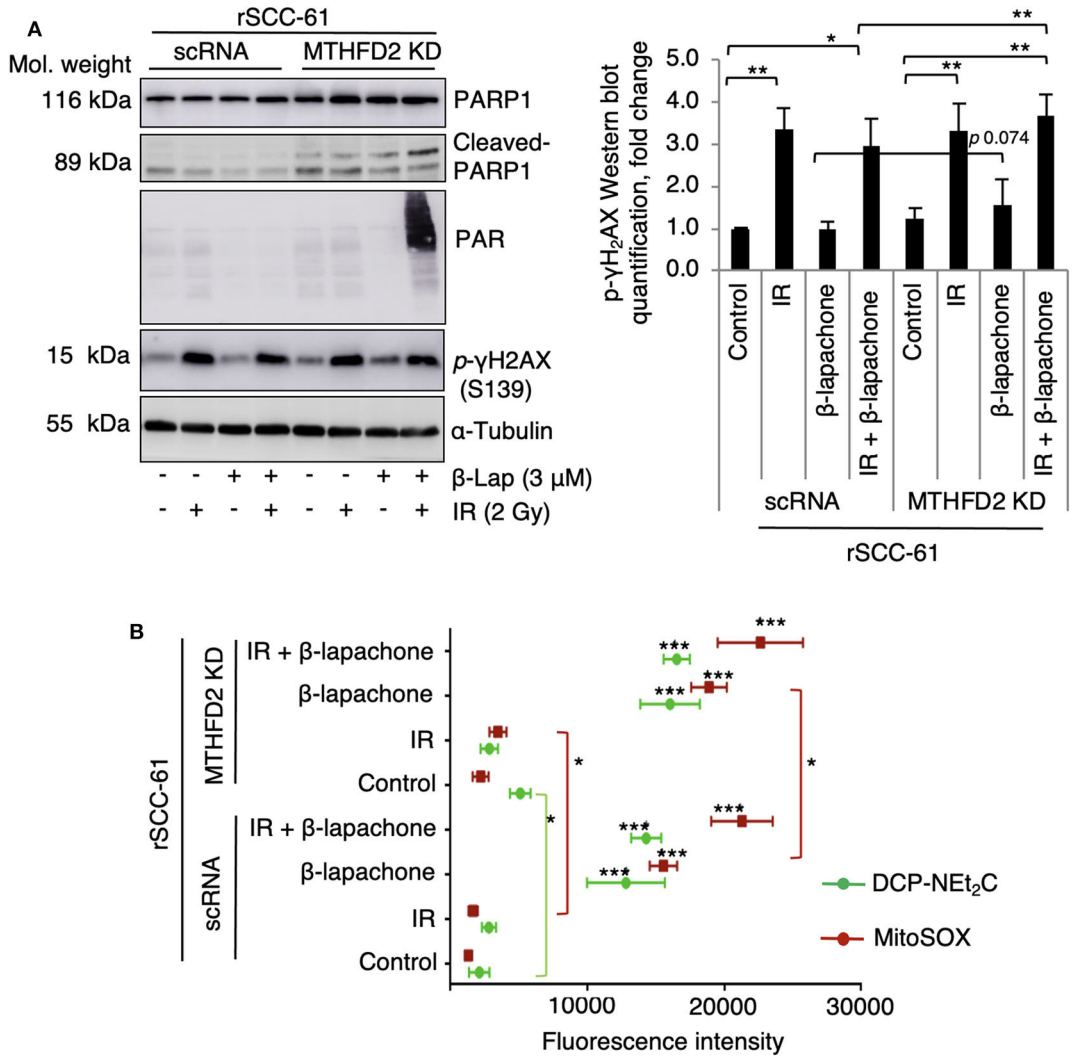

FIGURE 3 | Combination of radiation and β-lapachone treatment induces mitochondrial ROS and DNA damage in MTHFD2 KD rSCC-61. **(A)** Western blot analysis of biomarkers of DNA damage in control scRNA and MTHDF2 KD rSCC-61 cells exposed to radiation (IR, 2 Gy) and β-lap (3 μM, 1 h). The blots were probed with antibodies against phosphorylated γH_2AX (pS139), PARP1, cleaved PARP1, and protein PARylation. α-Tubulin antibodies were used as loading control. Quantification of phosphorylated γH_2AX Western blot data is shown on the right panel. $n = 3$, Student's *t*-test **p* 0.01–0.05, and ***p* 0.001–0.01. **(B)** Flow cytometry analysis of mitochondrial oxidative state in control scRNA and MTHFD2 KD rSCC-61 cells treated as in *Panel A* and further stained with MitoSOX and DCP-NEt_2C probes to detect mitochondrial superoxide and mitochondrial protein sulfenylation, respectively ($n = 3$; Student's *t*-test ****p* < 0.001 relative to untreated scRNA rSCC-61 cells, **p* 0.01–0.05 indicate statistically significant effects of MTHFD2 KD for control and treatment conditions).

mg/kg body weight) resulted in an almost complete suppression of tumor growth irrespective of MTHFD2 status. It is possible that the contribution of MTHFD2 noted in the cell culture studies (**Figure 2**) is masked in these experiments by the strong activity of combined β-lap and radiation treatment. However, depletion of MTHFD2 significantly sensitized the tumors to radiation treatment and slightly improved the efficacy of β-lap (**Figure 6C**). At the end of the experiment, the xenograft tumors were isolated, fixed and stained with hematoxylin and eosin (H&E, **Figure 6D**). While treatment with ionizing radiation did not significantly alter the morphology of either scRNA or MTHFD2 KD rSCC-61 tumors, treatment with β-lap caused suppression of tumor vascularization in both scRNA and MTHFD2 KD rSCC-61 tumors. Necrosis was noted in the core of both tumor types; however, necrosis was higher in the MTHFD2 knockdown tumors. In the groups receiving combined radiation and β-lap treatment, there was more extensive necrosis occurring in the central and peripheral areas of scRNA rSCC-61 tumors, and this was increased in MTHFD2 KD rSCC-61 tumors showing large centralized and peripheral necrosis in the entire tumor.

DISCUSSION

Clinical management of HNSCC presents with multiple treatment challenges limiting overall survival rates and patients'

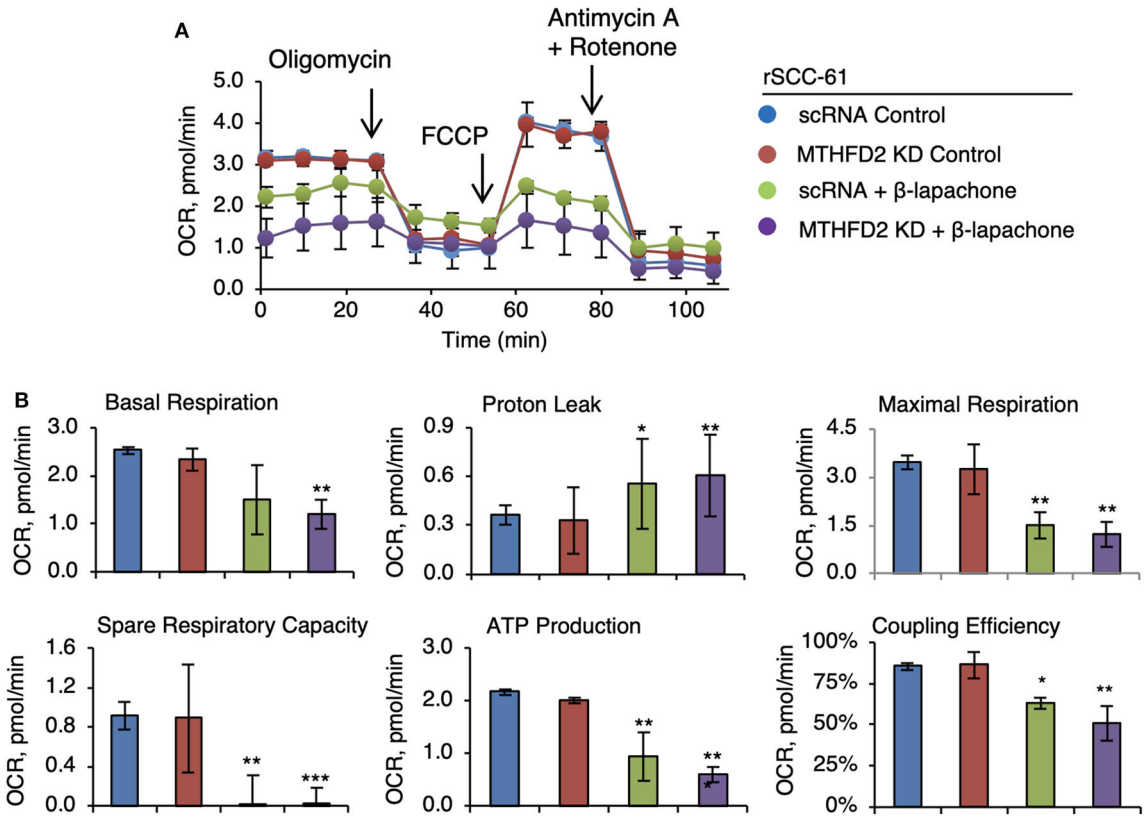

FIGURE 4 | MTHFD2 depletion does not significantly impact mitochondrial respiration but cooperates with β-lapachone to decrease ATP production. **(A)** Mitochondrial respirometry analysis in control scRNA and MTHFD2 KD rSCC-61 cells pre-treated with β-lap (3 μM, 2 h) or the respective vehicle control. **(B)** Analysis of mitochondrial respirometry parameters indicate significant effects of combined MTHFD2 knockdown and β-lap treatment on the basal respiration, coupling efficiency, ATP production and H^+-leak. Treatment with β-lap alone completely depleted the spare respiratory capacity ($n = 3$; Student's *t*-test **p* 0.01–0.05, ***p* 0.001–0.01, and ****p* <0.001 calculated relative to scRNA rSCC-61 cells).

quality of life. Amongst these, resistance to radiation or chemoradiation treatment constitutes a significant problem and new approaches are needed to improve the response to standard of care therapies and to prevent the associated damage to normal tissues. Currently, Federal Drug Administration approved the use of four chemotherapeutics (methotrexate, bleomycin, docetaxel, and hydroxyurea), one targeted therapy (Cetuximab, monoclonal antibody against EGFR), and one drug combination (docetaxel, cisplatin, and 5-fluorouracil) for treatment of HNSCC. Cetuximab received FDA approval in 2007 and is used as radiation sensitizer in patients with locally advanced HNSCC. However, despite the broad overexpression of EGFR in HNSCC, only 10–15% of patients respond to Cetuximab, emphasizing the need for new approaches to treat radiation resistant HNSCC (28).

β-Lapachone and its derivatives have emerged as a lead class of quinone-based NQO1 bioactivatable therapeutics and radiation sensitizers for numerous cancers (6, 7). Traditionally, the activity of β-lap has been linked to NQO1 expression and the NQO1 to catalase ratio, a higher ratio indicating increased capacity of ROS accumulation and cell death as ROS production outpaces degradation to non-toxic products (e.g., H_2O_2 dismutation by catalase to H_2O and O_2). Indeed, treatment with ionizing radiation was shown to induce expression of NQO1 and higher levels of NQO1 are found in radiation resistant tumors (16), emphasizing the concept of combined radiation and β-lap treatment as an approach for treatment of radiation resistant tumors. The data presented in **Figure 1** support this core principle and show increased sensitivity to β-lap in radiation resistant rSCC-61 cells expressing higher levels of NQO1 but comparable catalase relative to the matched radiation sensitive SCC-61 cells. These findings are also consistent with previously published data showing radiation sensitizing activity of β-lap in NQO1 overexpressing SqCC/Y1 HNSCC tumors (9, 21). However, despite these promising results, the translation to clinic has been challenging [e.g., ARQ761 phase I/II clinical trials (Gerber et al., 2018)] limited in part by the lack of knowledge of the molecular factors driving the efficacy of β-lap or ARQ761. As the chemotherapeutic activity of β-lap is intrinsically linked to the availability of NAD(P)H, and our prior dynamic flux balance analysis identified mitochondrial MTHFD2 as a key driver of NAD(P)H in HNSCC, including

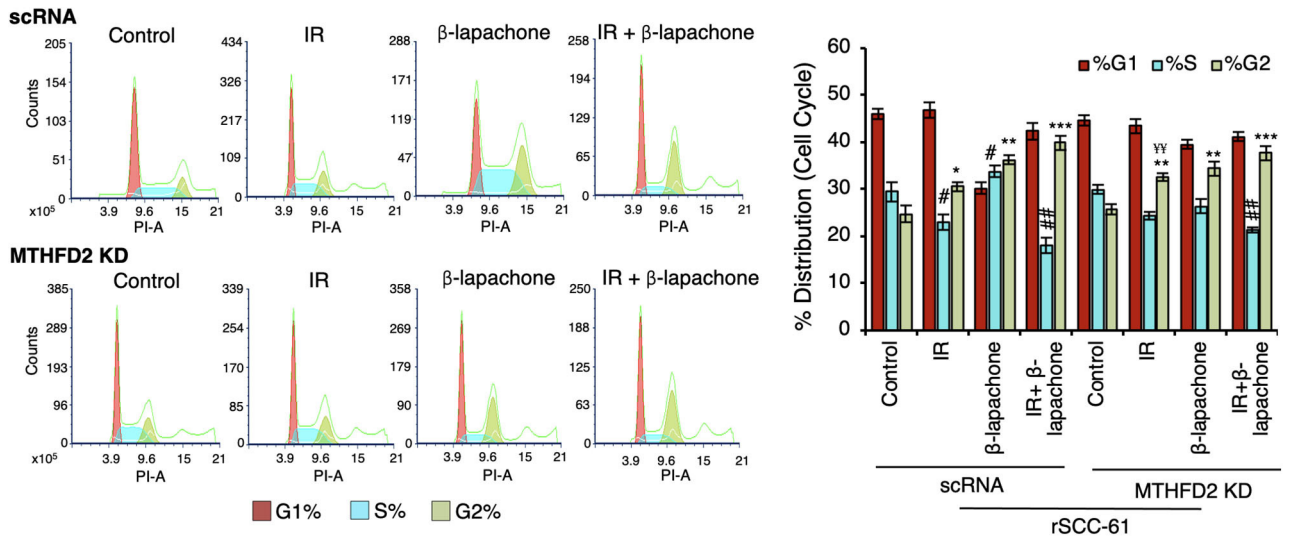

FIGURE 5 | MTHFD2 knockdown significantly alters the effects of β-lapachone on cell cycle progression. Flow cytometry analysis of control scRNA and MTHDF2 KD rSCC-61 cells exposed to radiation (IR, 2 Gy) and β-lap (3 μM, 2 h) and stained with propidium iodide for cell cycle analysis shows comparable shifts in cell cycle distribution in control and MTHFD2 depleted cells under all treatment conditions with the exception of β-lap alone (n=3; One-Way ANOVA with multiple comparisons $^{*}p$ 0.01–0.05, $^{**}p$ 0.001–0.01, and $^{***}p$ <0.001 calculated relative to %G2-phase of vehicle-treated scRNA rSCC-61 cells; $^{\#}p$ 0.01–0.05, $^{\#\#}p$ 0.001–0.01 calculated relative to %S-phase of vehicle-treated scRNA rSCC-61 cells; and, $^{¥¥}p$ 0.001–0.01 relative to radiation treated scRNA rSCC-61).

the SCC-61/rSCC-61 cells (20, 21), we sought to investigate here the contribution of MTHFD2 to the efficacy of response to β-lap when used alone or combined with ionizing radiation. The focus on MTHFD2 was also driven by the clinical precedent of folate inhibitors for treatment of HNSCC, and key publications showing increased MTHFD2 expression in rapidly proliferating solid tumors compared to normal tissue (29), MTHFD2-mediated folate metabolism playing a pivotal role in the progression and metastasis of several cancer types (30–32) with evidence that this might occur independent of its enzymatic activity (33), MTHFD2 function in purine and pyrimidine biosynthesis, critical metabolites for DNA synthesis and DNA damage repair (34), and evidence of additional nuclear localization of MTHFD2 at DNA synthesis sites (33). In the phenotypically matched HNSCC cells utilized here, the radiation resistant rSCC-61 cells showed significantly increased expression of both NQO1 and MTHFD2, thus enabling investigations of the crosstalk between these enzymes in determining the radiation sensitizing activity of β-lap.

Indeed, the *in vitro* and *in vivo* data (**Figures 2**, **6**) show statistically significant suppression of clonogenic survival and tumor growth for rSCC-61 cells depleted of MTHFD2, and radiation sensitizing effects of either MTHFD2 knockdown or β-lap treatment. MTHFD2 depletion significantly increased mitochondrial protein oxidation, augmented the mitochondrial ROS induced by either radiation or β-lap treatment, and increased the DNA damage (pS139 γH_2AX) when cells were treated with β-lap alone or in combination with radiation (**Figure 3**). Overall, treatment with β-lap drastically increased mitochondrial ROS and protein oxidation in both scRNA and MTHFD2 KD rSCC-61 cells, but induced a much lesser activation of DNA damage response (pS139 γH_2AX), completely opposite compared to radiation, which strongly induced DNA damage and had a lesser effect on mitochondrial ROS and protein oxidation. This activity pattern in itself may explain the enhanced anti-tumor effects of combined radiation and β-lap treatment.

Interestingly, MTHFD2 KD alone did not impact mitochondrial respiration likely due to its dominant effects being exerted on NADPH and/or due to replenishing of mitochondrial NADH by the malate-aspartate shuttle. On the other hand, β-lap significantly decreased mitochondrial basal respiration, ATP production, and completely obliterated the spare respiratory capacity in these cells (**Figure 4**), effects further increased by MTHFD2 depletion. MTHFD2 knockdown also increased cleaved PARP1, though interestingly significant protein PARylation is observed only with combined radiation and β-lap treatment in MTHFD2 KD rSCC-61 and not in the scRNA control cells (**Figure 3**). MTHFD2 depletion did not significantly impact the cell cycle progression in rSCC-61 cells, consistent with findings in HeLa cells (33) but contrary to reports showing cell cycle G1/S arrest in colorectal cancer cells (35). Combination of radiation with β-lap treatment enhanced G2/M arrest in rSCC-61 cells irrespective of MTHFD2 status, but MTHFD2 knockdown prevented the accumulation of cells in S-phase induced by β-lap treatment (**Figure 5**). Thus, MTHFD2 knockdown in rSCC-61 cells treated with β-lap display the G1/S arrest phenotype noted in colorectal cancer cells. Clearly, more studies are needed to follow-up on these intriguing findings and elucidate the function of MTHFD2 in regulation of cell cycle and the relationship with the response to β-lap and radiation treatment. The tumor-selective cytotoxic mechanism of β-lap was further confirmed *in vivo* using xenograft animal models

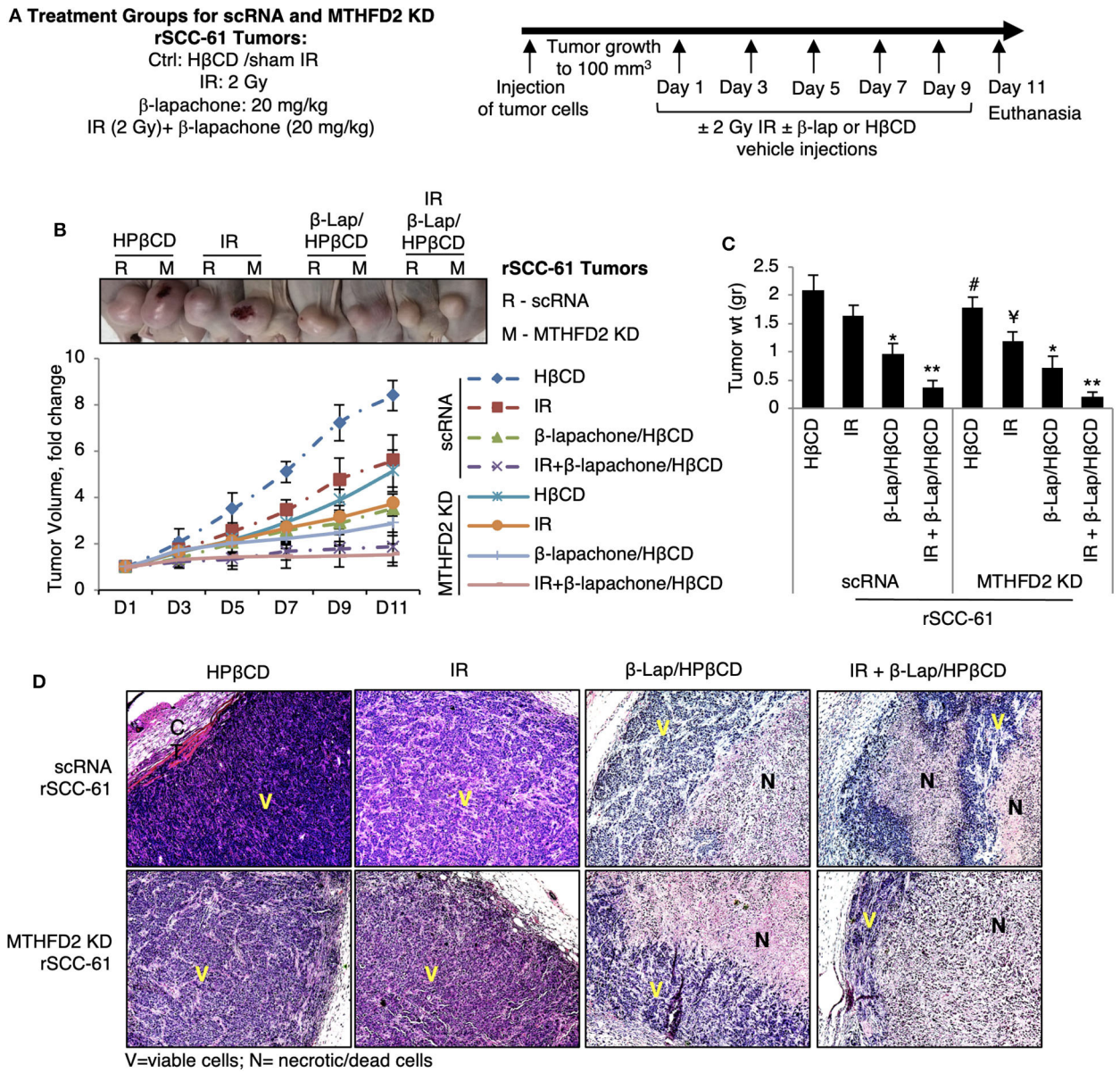

FIGURE 6 | *In vivo* study of combined antitumor activity of β-lapachone with radiation in HNSCC xenograft mice. **(A)** Description of treatment groups and experimental design. **(B)** Athymic mice (nu/nu) bearing 100 mm^3 scRNA or MTHFD2 KD rSCC-61 tumor xenografts were randomly divided into subgroups (5 mice/group) to receive treatment as described in Materials and Methods. Data represent the fold change in the mean value of tumor volume (mean ± SD). The images at the top represent the tumors at Day 11. **(C)** Comparison of tumor weight measured after euthanasia at Day 11 ($n = 5$; * represent comparisons with the respective untreated tumors in each group, scRNA and MTHFD2 KD rSCC-61, respectively; Student's *t*-test *p 0.01–0.05, **p 0.001–0.01; $^{\#}p$ 0.01–0.05 represents the comparison of untreated MTHFD2 KD and scRNA rSCC-61 tumors, and $^{¥}p$ 0.01–0.05 represents the comparison of radiation treated MTHFD2 KD and scRNA rSCC-61 tumors). **(D)** Representative H&E images of tumors isolated from the eight animal groups. IR, ionizing radiation; V, viable cells; N, necrotic/dead cells.

of radiation resistant HNSCC, which revealed cooperative mechanisms of tumor suppression and extensive necrosis in MTHFD2 knockdown tumors treated with combined β-lap and ionizing radiation (**Figure 6**).

In conclusion, the data presented here point to potential mechanisms of interorganelle communication connecting mitochondrial sources of NAD(P)H, cytosolic NQO1 activity, nuclear DNA damage, and cell cycle regulation. The findings are important given the increased interest in targeting mitochondrial metabolism for cancer therapies, and the ongoing efforts for both the development of MTHFD2 inhibitors and of more potent derivatives of β-lap. Considering the mitochondrial subcellular location of MTHFD2 and the cytosolic location of NQO1, an important direction for future studies is to investigate the contribution of physical and functional partitioning of NADH and NADPH between and within subcellular compartments,

in particular given the dual pro- and antioxidant function of NADPH (e.g., supporting ROS production by NADPH oxidases and NQO1/β-lap, and ROS suppressing activities of thioredoxin and glutathione reductases). Importantly, our computational analysis also identified other metabolic enzymes besides MTHFD2 as significant contributors to the NAD(P)H across HNSCC tumors. Thus, the understanding of tumor heterogeneity with respect to drivers of NAD(P)H in individual cells is critical to amplify the β-lap bystander cytotoxicity and advance the clinical success of β-lap therapeutics. These studies will require use of mixed tumor cells and patient-derived xenografts, which fortunately are becoming increasingly available. This research would also benefit from development of chemical tools and methods for selective imaging of ROS and/or their oxidation products to more robustly quantify the build-up and resolution of these species upon treatment with redox-altering chemotherapeutics like β-lap *in vivo*.

DATA AVAILABILITY STATEMENT

The datasets generated for this study are available on request to the corresponding author.

ETHICS STATEMENT

The animal study was reviewed and approved by Institutional Animal Care and Use Committee (IACUC) at Wake Forest School of Medicine.

AUTHOR CONTRIBUTIONS

KS performed the majority of studies presented here and was assisted by NS, who performed parallel assays of NQO1 activity to confirm the results. JEL and MLK guided the selection of MTHFD2 as target of NAD(P)H metabolism. DAB and CMF guided the experimental approach. KS prepared the initial draft of the manuscript, which was edited and finalized by AWT, MLK, and CMF. DAB reviewed the data before his passing in November 2019. All authors contributed to the article and approved the submitted version.

FUNDING

This project was supported by NIH/NCI U01 CA215848 (PIs MLK and CMF). The authors wish to acknowledge Wake Forest Baptist Comprehensive Cancer Center for use of Shared Resources (Flow Cytometry Shared Resource, Cellular Imaging Shared Resource) supported by the National Cancer Institute's Cancer Center Support Grant award number P30 CA012197. The content is solely the responsibility of the authors and does not necessarily represent the official views of the National Cancer Institute.

ACKNOWLEDGMENTS

The authors wish to thank members of CMF, MLK, and DAB's laboratories for helpful feedback on the project during individual laboratory and joint monthly Webex meetings.

REFERENCES

1. Howlader N, Noone AM, Krapcho M, Miller D, Brest A, Yu M, et al. *SEER Cancer Statistics Review,* 1975–2016 (2019).
2. Perri F, Pacelli R, Della Vittoria Scarpati G, Cella L, Giuliano M, Caponigro F, et al. Radioresistance in head and neck squamous cell carcinoma: biological bases and therapeutic implications. *Head Neck.* (2015) 37:763–70. doi: 10.1002/hed.23837
3. Chen X, Mims J, Huang X, Singh N, Motea E, Planchon SM, et al. Modulators of redox metabolism in head and neck cancer. *Antioxid Redox Signal.* (2018) 29:1660–90. doi: 10.1089/ars.2017.7423
4. Boothman DA, Trask DK, Pardee AB. Inhibition of potentially lethal DNA damage repair in human tumor cells by beta-lapachone, an activator of topoisomerase I. *Cancer Res.* (1989) 49:605–12.
5. Pink JJ, Planchon SM, Tagliarino C, Varnes ME, Siegel D, Boothman DA. NAD(P)H:Quinone oxidoreductase activity is the principal determinant of beta-lapachone cytotoxicity. *J Biol Chem.* (2000) 275:5416–24. doi: 10.1074/jbc.275.8.5416
6. Li LS, Bey EA, Dong Y, Meng J, Patra B, Yan J, et al. Modulating endogenous NQO1 levels identifies key regulatory mechanisms of action of beta-lapachone for pancreatic cancer therapy. *Clin Cancer Res.* (2011) 17:275–85. doi: 10.1158/1078-0432.CCR-10-1983
7. Huang X, Dong Y, Bey EA, Kilgore JA, Bair JS, Li LS, et al. An NQO1 substrate with potent antitumor activity that selectively kills by PARP1-induced programmed necrosis. *Cancer Res.* (2012) 72:3038–47. doi: 10.1158/0008-5472.CAN-11-3135
8. Huang X, Motea EA, Moore ZR, Yao J, Dong Y, Chakrabarti G, et al. Leveraging an NQO1 bioactivatable drug for tumor-selective use of poly(ADP-ribose) polymerase inhibitors. *Cancer Cell.* (2016) 30:940–52. doi: 10.1016/j.ccell.2016.11.006
9. Li LS, Reddy S, Lin ZH, Liu S, Park H, Chun SG, et al. NQO1-mediated tumor-selective lethality and radiosensitization for head and neck cancer. *Mol Cancer Ther.* (2016) 15:1757–67. doi: 10.1158/1535-7163.MCT-15-0765
10. Bey EA, Bentle MS, Reinicke KE, Dong Y, Yang CR, Girard L, et al. An NQO1- and PARP-1-mediated cell death pathway induced in non-small-cell lung cancer cells by beta-lapachone. *Proc Natl Acad Sci USA.* (2007) 104:11832–7. doi: 10.1073/pnas.0702176104
11. Bey EA, Reinicke KE, Srougi MC, Varnes M, Anderson VE, Pink JJ, et al. Catalase abrogates beta-lapachone-induced PARP1 hyperactivation-directed programmed necrosis in NQO1-positive breast cancers. *Mol Cancer Ther.* (2013) 12:2110–20. doi: 10.1158/1535-7163.MCT-12-0962
12. Tagliarino C, Pink JJ, Reinicke KE, Simmers SM, Wuerzberger-Davis SM, Boothman DA. Mu-calpain activation in beta-lapachone-mediated apoptosis. *Cancer Biol Ther.* (2003) 2:141–52. doi: 10.4161/cbt.2.2.237
13. Gerber DE, Beg MS, Fattah F, Frankel AE, Fatunde O, Arriaga Y, et al. Phase 1 study of ARQ 761, a beta-lapachone analogue that promotes NQO1-mediated programmed cancer cell necrosis. *Br J Cancer.* (2018) 119:928–36. doi: 10.1038/s41416-018-0278-4
14. Torrente L, Prieto-Farigua N, Falzone A, Elkins CM, Boothman DA, Haura EB, et al. Inhibition of TXNRD or SOD1 overcomes NRF2-mediated resistance to beta-lapachone. *Redox Biol.* (2020) 30:101440. doi: 10.1016/j.redox.2020.101440
15. Park HJ, Ahn KJ, Ahn SD, Choi E, Lee SW, Williams B, et al. Susceptibility of cancer cells to beta-lapachone is enhanced by ionizing radiation. *Int J Radiat Oncol Biol Phys.* (2005) 61:212–9. doi: 10.1016/j.ijrobp.2004.09.018
16. Choi EK, Terai K, Ji I-M, Kook YH, Park KH, Oh ET, et al. Upregulation of NAD(P)H:quinone oxidoreductase by radiation potentiates the effect of bioreductive beta-lapachone on cancer cells. *Neoplasia.* (2007) 9:634–42. doi: 10.1593/neo.07397

17. Chen X, Liu L, Mims J, Punska EC, Williams KE, Zhao W, et al. Analysis of DNA methylation and gene expression in radiation-resistant head and neck tumors. *Epigenetics.* (2015) 10:545–61. doi: 10.1080/15592294.2015.1048953
18. Bansal N, Mims J, Kuremsky JG, Olex AL, Zhao W, Yin L, et al. Broad phenotypic changes associated with gain of radiation resistance in head and neck squamous cell cancer. *Antioxid Redox Signal.* (2014) 21:221–36. doi: 10.1089/ars.2013.5690
19. Mims J, Bansal N, Bharadwaj MS, Chen X, Molina AJ, Tsang AW, et al. Energy metabolism in a matched model of radiation resistance for head and neck squamous cell cancer. *Radiat Res.* (2015) 183:291–304. doi: 10.1667/RR13828.1
20. Lewis JE, Costantini F, Mims J, Chen X, Furdui CM, Boothman DA, et al. Genome-scale modeling of NADPH-driven beta-lapachone sensitization in head and neck squamous cell carcinoma. *Antioxid Redox Signal.* (2018) 29:937–52. doi: 10.1089/ars.2017.7048
21. Lewis JE, Singh N, Holmila RJ, Sumer BD, Williams NS, Furdui CM, et al. Targeting NAD(+) metabolism to enhance radiation therapy responses. *Semin Radiat Oncol.* (2019) 29:6–15. doi: 10.1016/j.semradonc.2018.10.009
22. Nasongkla N, Wiedmann AF, Bruening A, Beman M, Ray D, Bornmann WG, et al. Enhancement of solubility and bioavailability of beta-lapachone using cyclodextrin inclusion complexes. *Pharm Res.* (2003) 20:1626–33. doi: 10.1023/A:1026143519395
23. Franken NA, Rodermond HM, Stap J, Haveman J, van Bree C. Clonogenic assay of cells *in vitro*. *Nat Protoc.* (2006) 1:2315–9. doi: 10.1038/nprot.2006.339
24. Holmila RJ, Vance SA, Chen X, Wu H, Shukla K, Bharadwaj MS, et al. Mitochondria-targeted probes for imaging protein sulfenylation. *Sci Rep.* (2018) 8:6635. doi: 10.1038/s41598-018-24493-x
25. Silvers MA, Deja S, Singh N, Egnatchik RA, Sudderth J, Luo X, et al. The NQO1 bioactivatable drug, beta-lapachone, alters the redox state of NQO1+ pancreatic cancer cells, causing perturbation in central carbon metabolism. *J Biol Chem.* (2017) 292:18203–16. doi: 10.1074/jbc.M117.813923
26. Santivasi WL, Xia F. Ionizing radiation-induced DNA damage, response, and repair. *Antioxid Redox Signal.* (2014) 21:251–9. doi: 10.1089/ars.2013.5668
27. Dias RB, de Araujo TBS, de Freitas RD, Rodrigues A, Sousa LP, Sales CBS, et al. beta-Lapachone and its iodine derivatives cause cell cycle arrest at G2/M phase and reactive oxygen species-mediated apoptosis in human oral squamous cell carcinoma cells. *Free Radic Biol Med.* (2018) 126:87–100. doi: 10.1016/j.freeradbiomed.2018.07.022
28. Bonner JA, Harari PM, Giralt J, Azarnia N, Shin DM, Cohen RB, et al. Radiotherapy plus cetuximab for squamous-cell carcinoma of the head and neck. *N Engl J Med.* (2006) 354:567–78. doi: 10.1056/NEJMoa053422
29. Nilsson R, Jain M, Madhusudhan N, Sheppard NG, Strittmatter L, Kampf C, et al. Metabolic enzyme expression highlights a key role for MTHFD2 and the mitochondrial folate pathway in cancer. *Nat Commun.* (2014) 5:3128. doi: 10.1038/ncomms4128
30. Tibbetts AS, Appling DR. Compartmentalization of mammalian folate-mediated one-carbon metabolism. *Ann Rev Nutr.* (2010) 30:57–81. doi: 10.1146/annurev.nutr.012809.104810
31. Tedeschi PM, Vazquez A, Kerrigan JE, Bertino JR. Mitochondrial Methylenetetrahydrofolate dehydrogenase (MTHFD2) overexpression is associated with tumor cell proliferation and is a novel target for drug development. *Mol Cancer Res.* (2015) 13:1361–6. doi: 10.1158/1541-7786.MCR-15-0117
32. Shin M, Momb J, Appling DR. Human mitochondrial MTHFD2 is a dual redox cofactor-specific methylenetetrahydrofolate dehydrogenase/methenyltetrahydrofolate cyclohydrolase. *Cancer Metab.* (2017) 5:11. doi: 10.1186/s40170-017-0173-0
33. Gustafsson Sheppard N, Jarl L, Mahadessian D, Strittmatter L, Schmidt A, Madhusudan N, et al. The folate-coupled enzyme MTHFD2 is a nuclear protein and promotes cell proliferation. *Sci Rep.* (2015) 5:15029. doi: 10.1038/srep15029
34. Locasale JW. Serine, glycine and one-carbon units: cancer metabolism in full circle. *Nat Rev Cancer.* (2013) 13:572–83. doi: 10.1038/nrc3557
35. Wei Y, Liu P, Li Q, Du J, Chen Y, Wang Y, et al. The effect of MTHFD2 on the proliferation and migration of colorectal cancer cell lines. *Onco Targets Ther.* (2019) 12:6361–70. doi: 10.2147/OTT.S210800

Conflict of Interest: CMF holds patents on detection of protein sulfenylation and is co-founder of Xoder Technologies, LLC, which provides consulting services and commercializes reagents for redox investigations.

The remaining authors declare that the research was conducted in the absence of any commercial or financial relationships that could be construed as a potential conflict of interest.

frontiers in Cell and Developmental Biology

ORIGINAL RESEARCH
published: 18 February 2021
doi: 10.3389/fcell.2021.539893

Gene Expression Profiles Reveal Extracellular Matrix and Inflammatory Signaling in Radiation-Induced Premature Differentiation of Human Fibroblast *in vitro*

Carsten Herskind[1], Carsten Sticht[2], Ahmad Sami[1], Frank A. Giordano[3†] and Frederik Wenz[3†]*

[1] Cellular and Molecular Radiation Oncology Laboratory, Department of Radiation Oncology, Universitaetsmedizin Mannheim, Medical Faculty Mannheim, Heidelberg University, Mannheim, Germany, [2] Centre for Medical Research, Medical Faculty Mannheim, Heidelberg University, Mannheim, Germany, [3] Department of Radiation Oncology, Universitaetsmedizin Mannheim, Medical Faculty Mannheim, Heidelberg University, Mannheim, Germany

Purpose: Fibroblasts are considered to play a major role in the development of fibrotic reaction after radiotherapy and premature radiation-induced differentiation has been proposed as a cellular basis. The purpose was to relate gene expression profiles to radiation-induced phenotypic changes of human skin fibroblasts relevant for radiogenic fibrosis.

Materials and Methods: Exponentially growing or confluent human skin fibroblast strains were irradiated *in vitro* with 1–3 fractions of 4 Gy X-rays. The differentiated phenotype was detected by cytomorphological scoring and immunofluorescence microscopy. Microarray analysis was performed on Human Genome U133 plus2.0 microarrays (Affymetrix) with JMP Genomics software, and pathway analysis with Reactome R-package. The expression levels and kinetics of selected genes were validated with quantitative real-time PCR (qPCR) and Western blotting.

Results: Irradiation of exponentially growing fibroblast with 1 × 4 Gy resulted in phenotypic differentiation over a 5-day period. This was accompanied by downregulation of cell cycle-related genes and upregulation of collagen and other extracellular matrix (ECM)-related genes. Pathway analysis confirmed inactivation of proliferation and upregulation of ECM- and glycosaminoglycan (GAG)-related pathways. Furthermore, pathways related to inflammatory reactions were upregulated, and potential induction and signaling mechanisms were identified. Fractionated irradiation (3 × 4 Gy) of confluent cultures according to a previously published protocol for predicting the risk of fibrosis after radiotherapy showed similar downregulation but differences in upregulated genes and pathways.

OPEN ACCESS

Edited by:
Bernd Kaina, Johannes Gutenberg University Mainz, Germany

Reviewed by:
Gerald Burgstaller, Helmholtz Zentrum München, Helmholtz-Gemeinschaft Deutscher Forschungszentren (HZ), Germany
Franz Rödel, University Hospital Frankfurt, Germany

***Correspondence:**
Carsten Herskind
carsten.herskind@medma.uni-heidelberg.de

†Present address:
Frank A. Giordano, Department of Radiation Oncology, Center for Integrated Oncology (CIO), University Hospital Bonn, University of Bonn, Bonn, Germany
Frederik Wenz, University Medical Center, Freiburg, Germany

Specialty section:
This article was submitted to Molecular and Cellular Oncology, a section of the journal Frontiers in Cell and Developmental Biology

Received: *02 March 2020*
Accepted: *27 January 2021*
Published: *18 February 2021*

Citation:
Herskind C, Sticht C, Sami A, Giordano FA and Wenz F (2021) Gene Expression Profiles Reveal Extracellular Matrix and Inflammatory Signaling in Radiation-Induced Premature Differentiation of Human Fibroblast in vitro. Front. Cell Dev. Biol. 9:539893. doi: 10.3389/fcell.2021.539893

Conclusion: Gene expression profiles after irradiation of exponentially growing cells were related to radiation-induced differentiation and inflammatory reactions, and potential signaling mechanisms. Upregulated pathways by different irradiation protocols may reflect different aspects of the fibrogenic process thus providing a model system for further hypothesis-based studies of radiation-induced fibrogenesis.

Keywords: fibroblast differentiation, extracellular matrix, radiation-induced fibrosis of the skin, inflammatory signaling, cell cycle-related genes

INTRODUCTION

Fibroblasts are the most abundant cells in connective tissue and are the major source of extracellular matrix (ECM) proteins. Thus fibroblasts are considered to play a major role in the development of fibrotic reaction after radiotherapy. Fibroblasts show a limited proliferation capacity *in vitro* (the socalled 'Hayflick limit') which was initially thought to correlate with the age of donors (Hayflick, 1965, 1980). However, no correlation was found in a large longitudinal study when only healthy patients were included in the analysis (Cristofalo et al., 1998). In fact, heterogeneity of cell populations is observed in fibroblast cultures from donors of all ages, representing a terminal differentiation lineage with a progenitor compartment with potentially mitotic fibroblasts and a functional compartment with postmitotic but metabolically active cells that can remain functional for many months, if not years (Bayreuther et al., 1988a,b; Bayreuther et al., 1992). In early-passage cultures established from human skin, three subtypes of progenitor fibroblasts can be distinguished which have been characterized at the morphological and biochemical level (Rodemann et al., 1989). Treatment with cytotoxic agents such as the alkylating agent Mitomycin C or ionizing radiation induces premature differentiation terminal to a postmitotic phenotype characterized by an increase in cell size with enlarged or multiple nuclei and increased synthesis of ECM proteins (Rodemann, 1989; Rodemann et al., 1991; Herskind et al., 2000). Thus radiation-induced differentiation of fibroblasts has been proposed as a cellular basis of radiation-induced fibrosis (Rodemann and Bamberg, 1995; Herskind et al., 1998).

Most studies on radiation-induced gene expression in fibroblasts have focused on the early time interval 1–24 h after irradiation, and identified genes involved in signaling, RNA and DNA synthesis, metabolism, DNA damage response and cell-cycle arrest (Khodarev et al., 2001; Ding et al., 2005; Kis et al., 2006; Zhou et al., 2006; Kalanxhi and Dahle, 2012). However, the differentiated phenotype is not expressed at such early time points. Rodningen et al. (2005) analyzed gene expression 2 and 24 h after irradiation of confluent cultures of skin fibroblasts with a single dose of 3.5 Gy or 2 h after a fractionated scheme of 3 × 3.5 Gy given at 24 h intervals (Rodningen et al., 2005). In addition to radiation-responsive genes, differentially regulated genes were involved in ECM remodeling, Wnt signaling, and IGF signaling (Rodningen et al., 2005), and a 13-gene signature for predicting radiotherapy patients individual risk of developing subcutaneous fibrosis was identified (Alsner et al., 2007; Andreassen et al., 2013). Tachiiri et al. (2006) studied gene expression at 1–72 h after doses in the range 0.5–50 Gy and found upregulation of two collagens (COL1A1 and COL5A1) in the late phase after giving a dose of 5 Gy (Tachiiri et al., 2006). A more recent study investigated radiation-induced senescence and found a strong increase in expression of SA-βGal positive cells 72–120 h after high single doses of 15–20 Gy with pathway analysis showing differential regulation of cell cycle-related genes (Marthandan et al., 2016). However, these studies did not consider other functional changes associated with radiation-induced differentiation of fibroblast.

The purpose of the present work was to study gene expression profiles in relation to radiation-induced phenotypic changes of human skin fibroblasts relevant for radiogenic fibrosis. Early-passage fibroblasts were irradiated in sparse cultures in order to allow expression of the differentiated phenotype, and differential gene expression was analyzed 2–5 days after irradiation. Furthermore, the expression profiles of the previously published irradiation protocol for predictive testing and the present protocol were compared.

MATERIALS AND METHODS

Cell Culture

Three strains of primary human skin fibroblasts, GS3, GS4, and GS5, were a gift from Dr. J. H. Peacock, Institute of Cancer Research, Sutton, United Kingdom. The completely anonymized strains were established prior to the Human Tissue Act 2004 by outgrowth of explants taken from surplus tissue obtained during surgical reduction mammoplasty [breast reduction (Carlomagno et al., 2000)] on healthy donors younger than 40 years of age (J. H. Peacock, personal communication). The GS ("gold standard") fibroblast strains (Kote-Jarai et al., 2004) were made available to the EU BIOMED 2 Concerted Action "The development of predictive tests of normal tissue response to radiotherapy" (European_Commission, 1999). For the present experiments, the cultures were grown in AmnioMax C-100 Medium supplemented with 7.5% AmnioMax supplement (Gibco/Invitrogen, Darmstadt, Germany) and 7.5% fetal bovine serum (FBS, South American origin; Biochrom, Berlin, Germany; HyClone, Fisher Scientific GmbH, Schwerte, Germany), 2 mM glutamine, penicillin, and streptomycin at 37°C under 7% CO_2. In the Mannheim (MA) protocol, early-passage cells were seeded in sparse mass culture in T75 flasks (0.5×10^6 cells/flask; Falcon) and irradiated in exponential growth phase with 4 Gy of 6 MV X-rays on the following day (day 0). For determining changes in cell densities after irradiation, the cells were seeded on microscope slides at the same density ($6.67 \times 10^3/cm^2$),

fixed at different time points and stained with Coomassie blue and Giemsa as previously described (Herskind et al., 1998). The cells were photographed and relative changes in cell numbers were determined by scoring the number of cells per area.

The design of the microarray experiments and quantitative real-time reverse transcription (RT-) PCR (qPCR) experiments is shown in **Table 1**. Two technical replicate experiments (#1 and #2) were performed with GS4 fibroblasts. RNA was isolated from T75 flasks on day 1 (0 Gy) and day 2, 3, and 5 (4 Gy), or day 5 (2 × 4 Gy), yielding approximately the same number of cells per unit area in unirradiated and irradiated flasks (MA protocol). Furthermore, the protocol used by Overgaard's group in Aarhus (AR protocol) was run in parallel in these experiments. In this protocol, confluent cultures were irradiated with three fractions of 4 Gy of 6 MV X-rays (equivalent to 3.5 Gy of orthovolt X-rays) given on day 0, 1, and 2, and RNA was isolated 2 h after the last fraction (Rodningen et al., 2008; Andreassen et al., 2013). To verify differentially regulated genes and pathways common to all three fibroblast strains, experiments using the MA protocol with RNA isolation on day 3 after irradiation were performed (experiments #3–#5). Additional, independent experiments to test the kinetics and validate the microarray data for selected genes were performed with RNA isolation at 24 h intervals on day 1–6 after irradiation and determined gene expression by qPCR. **Supplementary Experiments** for qPCR validation and protein detection were performed with isolation of RNA and protein at selected time points as indicated.

Fibroblast Phenotype

Sparse mass cultures were seeded in chamber slides and irradiated with 1 × 4 Gy as described above. On day 1–5, the cells were fixed using 3.7% paraformaldehyde in PBS followed by staining with Coomassie blue/Giemsa as described (Herskind et al., 1998). Cell morphology was visualized in bright-field microscopic images using 10–20× objectives. For quantification of the size distributions, the areas of 300–600 individual cells for each condition were determined in additional repeat experiments using Image J software (Schneider et al., 2012). For quantitative changes in cell numbers, 100 cells were seeded per well in six-well plates, irradiated and fixed on day 1, 3, and 6 as described above. Cell numbers were counted in six wells per plate under a microscope. The colony formation assay (CFA) was used to determine changes in fibroblast phenotype (differentiation state, surviving fraction). Cells were seeded in triplicate T75 flasks at 100 cells/flask for cytomorphological scoring, and at 300–4,000 cells/flask for scoring colonies. After 11 days incubation, the cells were fixed and stained, and the L:E ratio between colonies (min. 50 cells) in late (L) and early (E) differentiation state was determined by cytomorphological scoring as previously described (Herskind et al., 1998; Herskind and Rodemann, 2000). The yields of postmitotic differentiated fibrocytes (PMF) and clones with less than 50 cells (large clusters: 11–49 cells; small clusters: 2–10 cells) were determined by cytomorphological scoring of single cells with no nearest neighbors within 2.5 mm in CFA seeded at low cell density (100 cells per T75 flask) as described (Herskind et al., 2000).

Immunocytochemistry

Cells were seeded in chamber slides (BD Biosciences, Heidelberg, Germany) at a density of 6×10^3 cells/cm^2, the day before irradiation with 4 Gy. 1–5 days after irradiation, cells were fixed in methanol, washed and blocked with 1% bovine serum albumin in phosphate-buffered saline with 0.2% Triton-X100 (PBST). Incubation with 1:300 primary anti-α-smooth muscle actin (α-sma, ACTA2) mouse monoclonal antibody (sc-32251, Santa Cruz Inc., Heidelberg) in PBST was done for 1h. After washing three times with PBST, the slides were incubated with secondary FITC-conjugated goat anti-mouse IgG (1:20000) in PBST for 1h in the dark, washed three times and covered.

TABLE 1 | Experimental design of microarray and qPCR experiments.

Fib. strain	*Cult. seed.*	*Irrad. dose*	*Day (d) on which RNA was isolated*						*Protocol and type of experiment*
GS4	Expon.	0 Gy	**d1**						MA protocol
GS4	Expon.	4 Gy		**d2**	**d3**		**d5**		Microarrays; exp. #1–2
GS4	Expon.	2×4 Gy			4 Gy		**d5**		Microarrays; exp. #1–2
GS4	Confl.	0 Gy	0 Gy	0 Gy + **2h**					AR protocol
GS4	Confl.	4 Gy	4 Gy	4 Gy + **2 h**					Microarrays; exp. #1–2
GS3-5	Expon.	0 Gy	**d1**						MA protocol
GS3-5	Expon.	4 Gy			**d3**				Microarrays; exp. #3–5
GS3-5	Expon.	0 Gy	d1						MA protocol
GS3-5	Expon.	4 Gy	**d1**	**d2**	**d3**	**d4**	**d5**	**d6**	qPCR; kinetics/validation
GS3-5	Expon.	0 Gy	**d1**	**d2**	**d3**		**d5**		MA protocol suppl. exp.
GS3-5	Expon.	4 Gy		**d2**	**d3**		**d5**		qPCR; WB suppl. kinet./valid.
→→→→		|→→→	|→→→	|→→→	|→→→	|→→→	|→→→	|→→→|	Post-IR day (d) after first dose
−1		0	1	2	3	4	5	6	Post-IR day (d) after first dose

Columns: 'Fib. Strain,' individual strains: GS3, GS4, GS5; 'Cult. seed', culture seeded, expon.(exponential growth phase), confl. (confluent cultures); 'Irrad. dose', irradiation dose; 'Isolate RNA', post irradiation time d1–d6 (day 1–6). MA, Mannheim protocol; AR, Aarhus protocol. Cells were irradiated on day 0, and also on d1 and d2 for the AR protocol. The time line is shown at the bottom. WB: Western blots.

The cells were photographed at 400× magnification with an inverted fluorescence microscope (Axio Observer.Z1, Carl Zeiss Microscopy Deutschland GmbH, Oberkochen, Germany).

Immunoblotting

Protein lysates were prepared on the indicated days. Cells were lysed on ice by incubation with ice-cold RIPA lysis buffer, including the Complete Protease Inhibitor Cocktail (Roche, Mannheim, Germany). The lysates were centrifuged at 12,000 × *g* for 10 min at 4°C and the protein concentration was determined by the Bradford method. Cell lysates (20 μg of total protein) were mixed with equal volumes of 2 × Laemmli sample buffer with 5% β-mercaptoethanol and 1 mM dithiothreitol, denatured at 97°C for 5 min and separated by electrophoresis in 12% Bis–Tris acrylamide gels. The proteins were electroblotted onto Amersham Protran 0.2 μm nitrocellulose membranes (GE Healthcare, Freiburg, Germany) and probed with the following primary antibodies: anti-CCNB1 (ab32053) and anti-PTX3 (ab190838) from Abcam (Berlin, Germany), anti-RPA1 (#2267) and anti-NBN (#2267) from Cell Signaling Inc. (Frankfurt a.M., Germany), anti-α-smooth muscle actin (α-sma, ACTA2; sc-32251) from Santa Cruz Inc. (Heidelberg, Germany), and anti-ACTB (A5441) from Sigma-Aldrich/Merck (Darmstadt, Germany). After washing, the membranes were incubated with horseradish peroxidase-conjugated secondary antibody (P0447, P0448; Agilent/Dako, Hamburg, Germany) for 1 h at room temperature, washed, processed with a Western Lightning Plus ECL kit (PerkinElmer, Hamburg, Germany) and fluorescence detected with a Fusion FX7/SL Advance imaging system (Vilber Lourmat, Eberhardzell, Germany). Band intensities were quantified with Image J software (Schneider et al., 2012), corrected for the intensity of the loading control ACTB, and normalized to the values on day 1 of the unirradiated samples.

RNA

Total RNA was prepared using Trizol (Gibco) followed by additional purification using the RNeasy Mini Kit (Qiagen). RNA was tested by capillary electrophoresis on an Agilent 2100 bioanalyzer (Agilent) and high quality was confirmed. The RNA samples from exp. #1 and exp. #2 were stored and processed separately for each experiment but biostatistical analysis was performed together. RNA samples from exp. #3–#5 were stored, processed and analyzed together. Biotinylated antisense cRNA was prepared according to the Affymetrix standard labeling protocol with the GeneChip® WT Plus Reagent Kit and the GeneChip® Hybridization, Wash and Stain Kit (both from Affymetrix Inc., Santa Clara, CA, United States). RNA samples for qPCR were stored for each experimental series (15 genes in the main text, 9 and 3 genes in **Supplementary Experiment**) and the assays were performed over a short period of time.

Microarrays

Gene expression profiling was performed using Human Genome U133 Plus 2.0 microarrays (Affymetrix Inc., Santa Clara, CA, United States). Hybridization was performed in a GeneChip Hybridization oven 640, then dyed in the GeneChip Fluidics Station 450 and thereafter scanned with a GeneChip Scanner 3000. All of the equipment used was from Affymetrix UK Ltd. (High Wycombe, United Kingdom).

Irradiation and Dosimetry

Irradiation was performed with 6 MV X-rays from a clinical radiotherapy machine (Elekta Synergy, Elekta Oncology Systems, Crawley, United Kingdom) with a dose rate of 6 Gy/min. Dose build-up above the cells was equivalent to 15 mm water depth and 8 cm water-equivalent backscatter material was added below the flasks. Dosimetry was performed as part of the daily quality check for radiation therapy.

Bioinformatics

A Custom CDF Version 24 with ENTREZ based gene definitions was used to annotate the arrays (Dai et al., 2005). All samples assigned to a gene were summarized using the RMA method (Irizarry et al., 2003). The raw fluorescence intensity values were normalized by applying quantile normalization and RMA background correction for exp. #1 and #2 combined, and for exp. #3–#5 combined. In order to minimize variations between independent experiments, batch correction was performed using the batch normalization process of the JMP Genomics Software version 7 (SAS Institute, Cary, NC, United States). In brief, a *K*-Means clustering is applied to group batch profiles into clusters and the batch normalization is performed by correcting the within-cluster mean profile for each cluster. The resulting expression levels were used to determine the log2 values of fold change [log2(FC)], in each experiment by subtracting the expression level in unirradiated fibroblasts from that of irradiated cells at a given time point. The independent replicates for GS4 (exp. #1 and #2) showed a high degree of correlation (**Supplementary Figures 1A–E**). Therefore, data were filtered for mean log2(FC) > 2 or <-2 and 95% confidence intervals were determined from the variance of the difference of individual replicates and their mean value (within the filtered gene sets, which was 48 ± 11% larger than the variance for the complete gene set). Notably, all individual replicate data points in the filtered gene sets ($2n = 3670$) showed absolute log2(FC) values > 1.4 corresponding to larger than 2.6-fold changes. The differential expression in a completely independent experiment with GS4 (exp. #3) showed excellent correlation ($R^2 = 0.95$) with the mean values of the filtered genes from experiments #1 and #2 although, numerically, log2(FC) values were 15% smaller overall (**Supplementary Figure 1F**). Importantly, however, all of the filtered genes were regulated in the same direction in all three experiments with none of the genes showing changes in opposite directions. Out of 113 up- and 232 down-regulated genes identified in the first two experiments, 97% showed at least twofold changes. Only five genes in each group showed log2(FC) values in experiment #3 in the range 0.6–1.0 (corresponding to 1.5–2-fold changes), while a single uncharacterized LOC gene showed log2(FC) = 0.42 (corresponding to 1.34-fold up-regulation). The strong agreement between replicate experiments suggests that false discoveries of up- or down-regulated genes are extremely unlikely within the filtered gene sets.

The same method of filtering and determination of the variance of the filtered gene set around mean values for each gene was used to analyze experiments #3–#5, yielding mean values and confidence intervals for differentially expressed genes in fibroblast strains (GS4, GS3, and GS5) from three individual donors. In this case, absolute log2(FC) values were larger than 0.66 corresponding to larger than 1.5-fold changes for all individual data points (n = 966) within the filtered gene set (122 up- and 200 down-regulated genes). In this case, the variance between strains was 6.5-fold larger for the filtered genes than for the whole gene set, implying that quantitative variations between fibroblast strains from individual donors were larger than the technical variation between experiments. Nevertheless, the direction of the differential regulation was the same in all strains for all 322 filtered genes.

Gene Set Enrichment Analysis (GSEA) was used to determine whether defined lists (or sets) of genes exhibit a statistically significant bias in their distribution within a ranked gene list using *ReactomePA* and ClusterProfiler in the software package R (Yu and He, 2016). The gene list was ranked according to the log2(FC) values of each gene for irradiated versus unirradiated cultures. Curated pathways over- or under-represented in differentially expressed genes were identified by normalized enrichment scores (NES). Pathways with p-values < 0.05 after adjustment for multiple testing were considered significant.

The raw and normalized data are deposited in the Gene Expression Omnibus (GEO) database[1] (accession number GSE147733).

Quantitative Real-Time RT-PCR (qPCR)

Validation of selected genes was done by qPCR using RNA isolated from independent repeat experiments performed once for each strain 1 year after the original experiments. qPCR was performed with SYBR-green using Gene Globe primer and detection system according to the manufacturer's protocol (Qiagen, Hilden, Germany). The fold induction was calculated by the ΔΔCt method using *ACTB* as control gene. Mean values and standard errors for the three strains are shown. *ACTB* was chosen as control gene based on pilot experiments showing no significant change in *C*t values with time after irradiation (day 0–6, P = 0.77, n = 20; ANOVA) for the three fibroblast strains. This was corroborated when analyzing all *ACTB* expression data from the qPCR validation experiments for the 15 genes although minor but significant deviations ($P < 0.001$, n = 105; ANOVA) were observed for day 2 and day 3 (**Supplementary Figure 2**).

Statistics

Mean values and standard deviations, standard errors, or 95% confidence intervals are shown as indicated in the graphs. Statistical significance was tested by student's t-test or by ANOVA. JMP statistical discovery software v.14 (Böblingen, Germany) and Excel (MS Office 2016) were used.

[1] http://www.ncbi.nlm.nih.gov/geo/

RESULTS

Radiation-Induced Change of Fibroblast Phenotype

A marked change in fibroblast morphology was observed in micrographs after irradiation of fibroblasts in sparse cultures. On day one after irradiation, no change was visible. However, beginning on day 2, the cell size and morphology changed from typical spindle-like shape to large extended cells, representing radiation-induced premature differentiation (**Figure 1A**). Although the density of the cultures appeared to increase, this was largely due to the increase in cell size. Preliminary image analysis indicated that the major increase in cell size occurred between day 1 and 3 (not shown) and this was validated by analyzing the cell size distributions in three independent repeat experiments for day 1 and day 3 (**Supplementary Figure 3**). A shift in the frequency of cells with small areas toward larger areas (approximately >1,500 μm^2) was observed in irradiated cultures. Thus the median area increased significantly (p = 0.02; N = 3, paired t-test) from 934 ± 131 μm^2 (0 Gy, day 1) to 2,161 ± 46 μm^2 (4 Gy, day 3). Additional experiments with GS3, GS4 and GS5 in six-well plates were performed to count the number of cells fixed on day 1, 3, and 6. This confirmed that the number of cells per unit area did not change significantly after irradiation (P = 0.51, N = 12, n = 3 per group), indicating permanent cell-cycle arrest of most cells after this dose (**Figure 1B**).

Clonogenic survival showed surviving fractions (SF) in the range 1.21–6.7% after 4 Gy. This dose was used because it was equivalent to the fraction size applied in postmastectomy patients in which fibrosis after radiotherapy had previously been studied (Johansen et al., 1996; Herskind et al., 1998; Alsner et al., 2007). Microscopic scoring of clone sizes showed a radiation-induced decrease in the number of colonies and clones with 11–49 cells after irradiation (P = 0.018, N = 6) which was approximately balanced by a significant increase (P = 0.03, N = 6) in the number of small clones with 2–10 cells and single post-mitotic cells (**Figure 1C**). Thus inactivated clonogenic cells were either arrested permanently or able to undergo max. 1–3 cell divisions in the time that undamaged cells would form colonies. The surviving colonies showed an approximately twofold increase in the L:E ratio between the number of colonies in late and early different state (geometric mean 2.07, range 1.55–2.76; P = 0.04, N = 6) implicating a shift in fibroblast differentiation after irradiation (**Figure 1D**). Taken together, these results show the radiation-induced phenotype of premature terminal differentiation developing 2–5 days after irradiation of fibroblasts in sparse cultures *in vitro* (i.e., after DNA repair and cell recovery are assumed to have been completed).

Changes in Gene Expression Profile After Irradiation

Differential gene expression after the single-dose (MA) protocol (1 × 4 Gy, exponential growth) was studied for GS4 cells on day 2, 3, and 5 after irradiation. A parallel flask was given a second fraction of 4 Gy on day 3 after the first

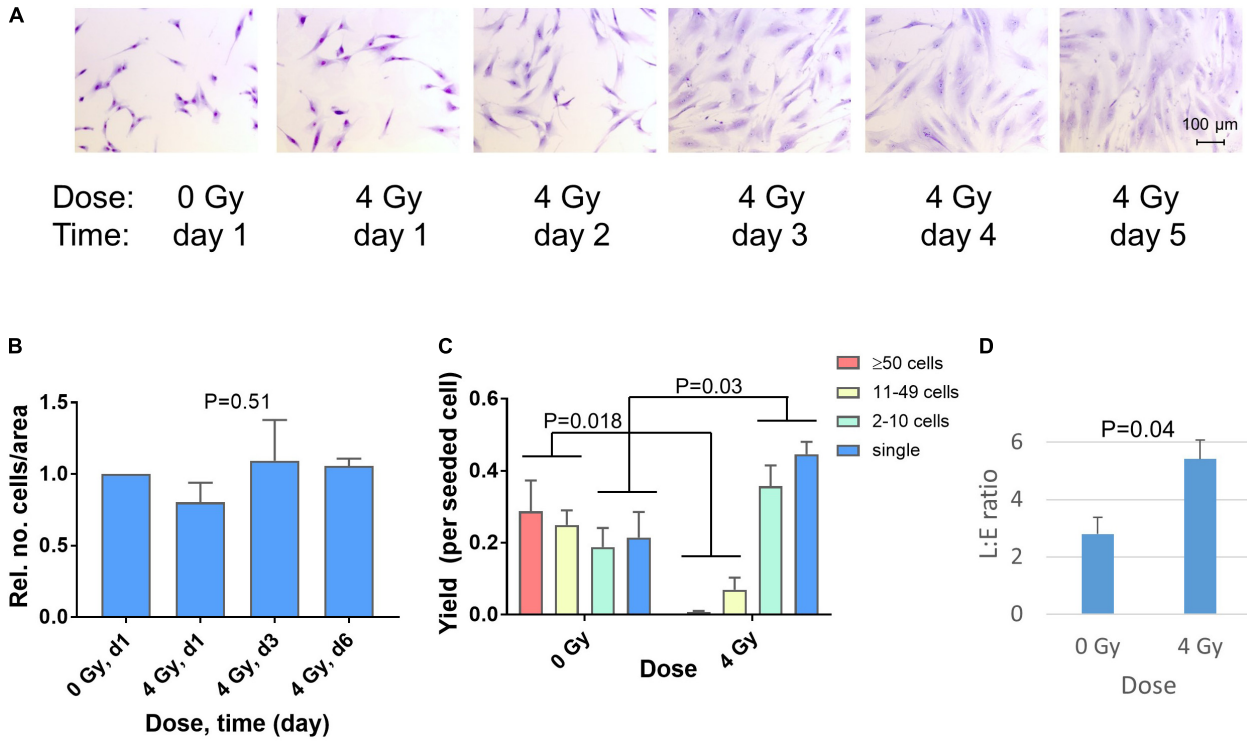

FIGURE 1 | Changes in cell morphology 1–5 days after irradiation of GS4 in microscope chamber slides with a dose of 4 Gy **(A)**. Relative numbers of cells on day 1, 3, and 6 after irradiation of GS3, GS4, and GS5 in six-well plates with 4 Gy. For each fibroblast strain, the total number of cells in all six wells of the plate was scored. $P = 0.51$ (ANOVA, $N = 12$, $n = 3$ per group) **(B)**. The yield of clones per seeded cell in the colony formation assay (T75 flasks) with GS3, GS4, and GS5, irradiated at low cell density after doses of 0 Gy (sham) and 4 Gy. Cytomorphological assay (clonal culture at low cell density), clones sizes: ≥50 cells (colonies), 11–49 cells (large clusters), 2–10 cells (small clusters), single cells (postmitotic). *P*-values for changes in colonies + large clusters and small clusters + single cells are shown (unpaired *t*-test, $N = 6$) **(C)**. Ratio of colony-forming fibroblasts in late (L) and early (E) differentiation state in the colony formation assay for GS3, GS4, and GS5 irradiated with 0 Gy (sham) or 4 Gy. *P*-value for unpaired *t*-test ($N = 6$) **(D)**. Mean values and standard errors ($n = 3$) for the three strains are shown in **(B–D)**.

irradiation and RNA was isolated on day 5 (i.e., 2 days after the second fraction). Two independent replicate experiments were performed showing a high degree of correlation (R^2 = 0.81–0.91; n = 20,422 genes; **Supplementary Figure 1**). Filtered genes with mean log2(FC) > 2 or <−2 (i.e., at least fourfold up- or down-regulation) are included with 95% confidence intervals in a **Supplementary Excel Table**. All filtered genes showed changes in the same directions in both replicate experiments and were significant at the 95% confidence level. Heat maps of the top 25 up- and down-regulated genes [mean log2(FC)] on day 2, 3, and 5 after irradiation are shown in **Figure 2A** and mean values and 95% confidence intervals for the top 25 up- and down-regulated genes are listed in **Supplementary Table 1**. The kinetics of selected genes showed differences in the upregulation of different collagen genes (**Figure 2B**), either a continuous increase (*COL11A1* and *COL12A1*), leveling off on day 3–5 (*COL4A1* and *COL8A1*), or a late increase (*COL15A1*). By contrast, proliferation- and cell division-related genes were down-regulated in a broadly similar way (**Figure 2B**). Other genes showing stronger up- or down-regulation on day 2 tended to change less on day 3–5 (**Figure 2C**). The differential expression after giving two fractions of 4 Gy was highly correlated with that observed 5 days after giving a single fraction (**Figure 2D**) and less so with the earlier time points (R^2 = 0.93 versus 0.88 and 0.76 for day 3 and 2, respectively; data not shown). Thus, the transcription signature for 2 × 4 Gy was more similar to the time after the first fraction (5 days) than the second (2 days). However, whereas upregulated genes showed little effect of the second fraction, some of the most down-regulated genes on day 5 seemed to be more strongly down-regulated after the second dose (**Figures 2B–D**).

GSEA was used to identify significant pathways with NES > 1.5 (over-represented, i.e., upregulated after irradiation) or <−1.5 (underrepresented, i.e., downregulated after irradiation). 268 pathways were downregulated at least at one of the time points d2, d3, or d5, with 216 (81%) downregulated at all three time points, while 106 pathways were upregulated at one or more of the three time points with 45 (42%) common to all three (**Supplementary Figure 4**). 40% of the 216 common down-regulated pathways were related to cell division, chromosome organization, or cell-cycle and replication/proliferation, with additional 18% related to gene expression and protein modification, and 19% to cell stress and DNA repair (**Figure 3A**). 49% of the 45 common up-regulated pathways were related to the ECM,

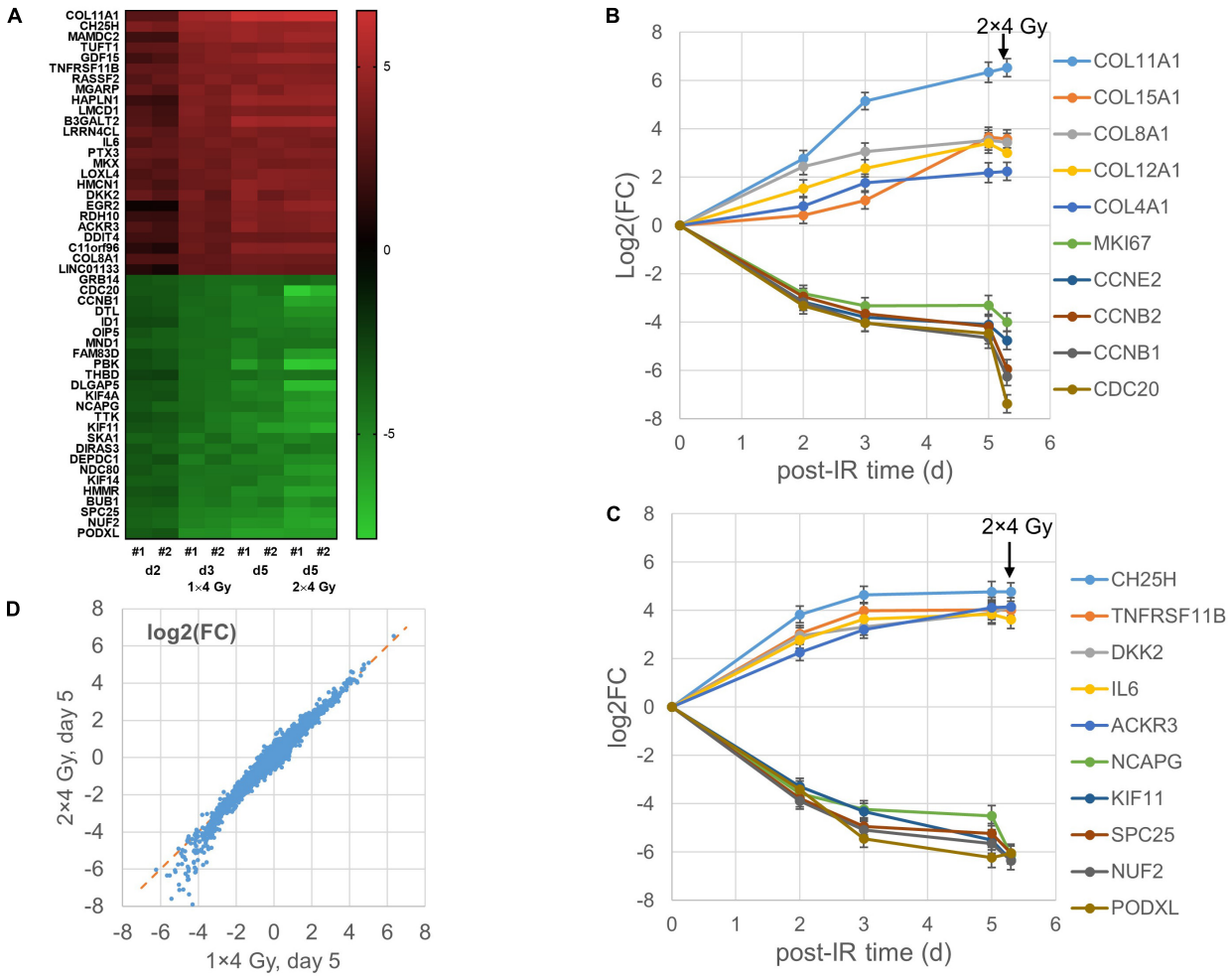

FIGURE 2 | Heat map of top 25 up- and down-regulated genes for the MA protocol in independent replicate microarray experiments #1–2 **(A)**. Examples of log2 fold changes [log2(FC)] in expression of differentially regulated genes 2–5 days after a single dose of 4 Gy or 5 days after the first of two fractions of 4 Gy; mean values and error bars (95% confidence intervals) from the two experiments are shown **(B,C)**. Correlation between mean log2(FC) values after 2 × 4 Gy and 1 × 4 Gy **(D)** with RNA isolation on day 5 after the first dose.

GAG, or cell–cell and cell–matrix interactions (**Figure 3B**) with an additional 13% related to inflammation and immune reactions. The complete list of pathways is included in a **Supplementary Excel Table**.

Influence of Irradiation Protocol on Gene Expression Pathways

Comparing the differential expression of the AR protocol showed the best correlation (R^2 = 0.52) with MA day 5 (**Figure 4A**). Downregulated genes showed a higher degree of correlation but strongly down-regulated gene seemed to be more down-regulated in the AR than in the MA protocol. Upregulated genes tended to be less up-regulated in the AR protocol but considerable divergence was observed and this was also the case for the 13-gene predictive signature (**Figure 4B**). The top 25 up- and down-regulated genes for the AR protocol are listed in **Supplementary Table 2** and shown as a heatmap together with day 5 for the MA protocol (**Figure 4C**). Downregulated genes, including several cell cycle- and cell division-related genes, showed overlap with the MA protocol (day 5) for nine genes. By contrast, only one of the top 25 up-regulated genes showed overlap (*GDF15*) although *COL15A1*, which was outside top 25 on day 5 of the MA protocol, was upregulated to a similar degree [log2(FC) = 3.65]. The complete list of differentially regulated genes is included in the **Supplementary Excel Table**. Pathway analysis showed 37 up-regulated pathways common to both protocol with 52% relating to the ECM or GAG, and 14% to inflammation and the immune system (**Figure 4D**). Additional 37 upregulated pathways were significant for MA d5 with 41% relating to GAG or cell–cell/cell–matrix interactions and only one pathway to ECM. By contrast, among the 27 pathways significantly upregulated for AR only, just 7% were related to GAG and none to ECM or cell–cell/cell–matrix interactions. Instead, 22% were related to cholesterol and bile acid/salts pathways, 15%

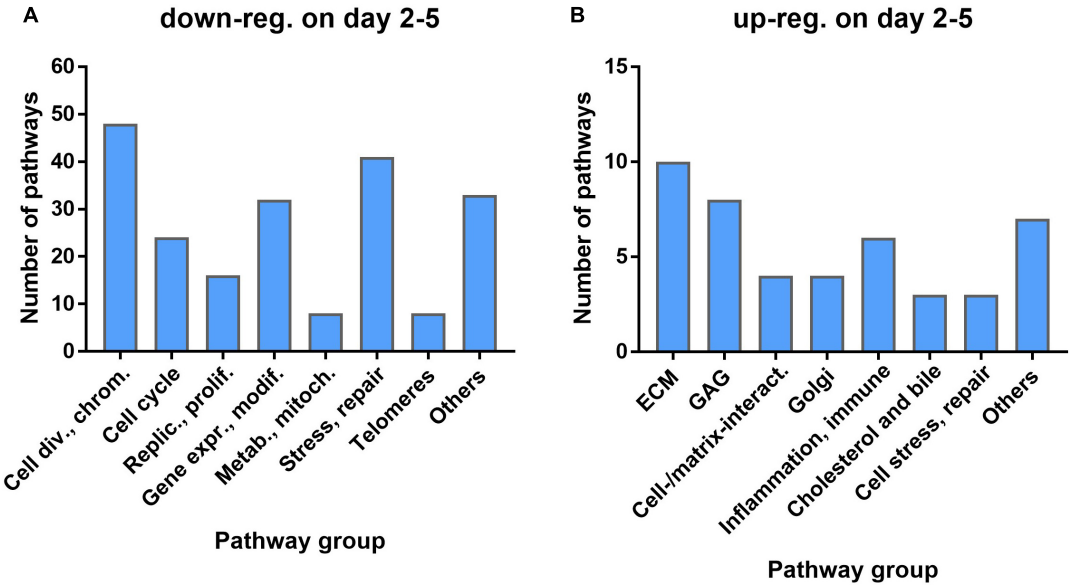

FIGURE 3 | Number of pathways by functional group for pathways commonly down-regulated **(A)** or up-regulated **(B)** at all three time points.

to translation, and 15% to metabolism. Both protocols also upregulated pathways related to inflammation and immune reactions that were significant for only the MA and not the AR protocol or vice versa.

Robustness of Radiation-Induced Pathways in Different Fibroblast Strains

The robustness of the gene expression profile obtained with GS4 for d3 (MA protocol) was tested in a second series of microarray experiments including two further fibroblast strains, GS3 and GS5. The top25 mean log2(FC) upregulated genes for all three strains are shown as a heatmap (**Figure 5A**) and mean log2(FC) values and 95% confidence intervals in **Supplementary Table 3**. The complete list of filtered genes is included in the **Supplementary Excel Table**. qPCR validation of 27 genes is described below. Pathway analysis showed 320 downregulated pathways, 243 of which were common to all three strains (**Figure 5B**). The major groups were similar to the previous results for GS4 on day 2–5. 125 pathways were upregulated with 59 being common to all three strains (**Figure 5C**). The top 25 common pathways (**Table 2**) ranked by the mean NES for the three fibroblast strains confirmed the high fraction of ECM-related pathways but also included four pathways related to inflammation and immune reaction: Interferon alpha/beta signaling (R-HSA-909733) and three pathways involving the complement system. Further six inflammatory pathways with NES values in the range from 1.59 to 1.94 were outside top 25, including Interferon gamma signaling (R-HSA-877300) and Interleukin-20 family signaling (R-HSA-8854691). Thus 10/59 pathways (17%) upregulated on day 3 in all three strains represented early aspects of inflammatory signaling. The complete list of differentially regulated pathways is included in the **Supplementary Excel Table**.

Expression Kinetics and qPCR Validation of 15 Selected Genes

To study the expression kinetics of selected genes and validate the microarray results by qPCR, additional independent experiments were performed with irradiation of the three strains isolating RNA each day from day 1 to day 6 (**Figures 6A–E**). Genes were selected based on the filtered lists and their potential relevance for the extracellular matrix, differentiation and fibrosis. Ten genes were part of the filtered gene list from exp. #1–2 as well as exp. #3–5. *MMP12* and *ACTA2* were in the filtered gene list for exp. #1–2 (GS4 only), and although *COL1A1*, *COL3A1*, and *COL5A1*, were in neither of the filtered gene lists, they were included because they are the major fibrillary collagen genes. Several collagen genes (*COL11A1, COL15A1, COL12A1, COL5A1, COL3A1*, and *COL1A1*) and *LOXL4*, the product of which is involved in trimerization of collagen fibers, were upregulated to different levels. Notably, of the three collagen genes which were upregulated >twofold on microarrays although they did not pass the stringent filtering ($|\log2(FC)| > 2$), *COL1A1* and *COL3A1* were continuously upregulated up to day 6 while *COL5A1* reached a lower plateau on day 4. Furthermore, the *FAP* gene coding for a serine protease was moderately upregulated while *MMP12* coding for matrix metalloproteinase 12 was downregulated.

GDF15 coding for a TGF-beta superfamily cytokine was strongly upregulated. *THBS1* coding for the signaling glycoprotein, thrombospondin 1, showed intermediate upregulation up to day 5 while *THBS2* showed a moderate response with a plateau on day 1–4. *CYP1B1* coding for the

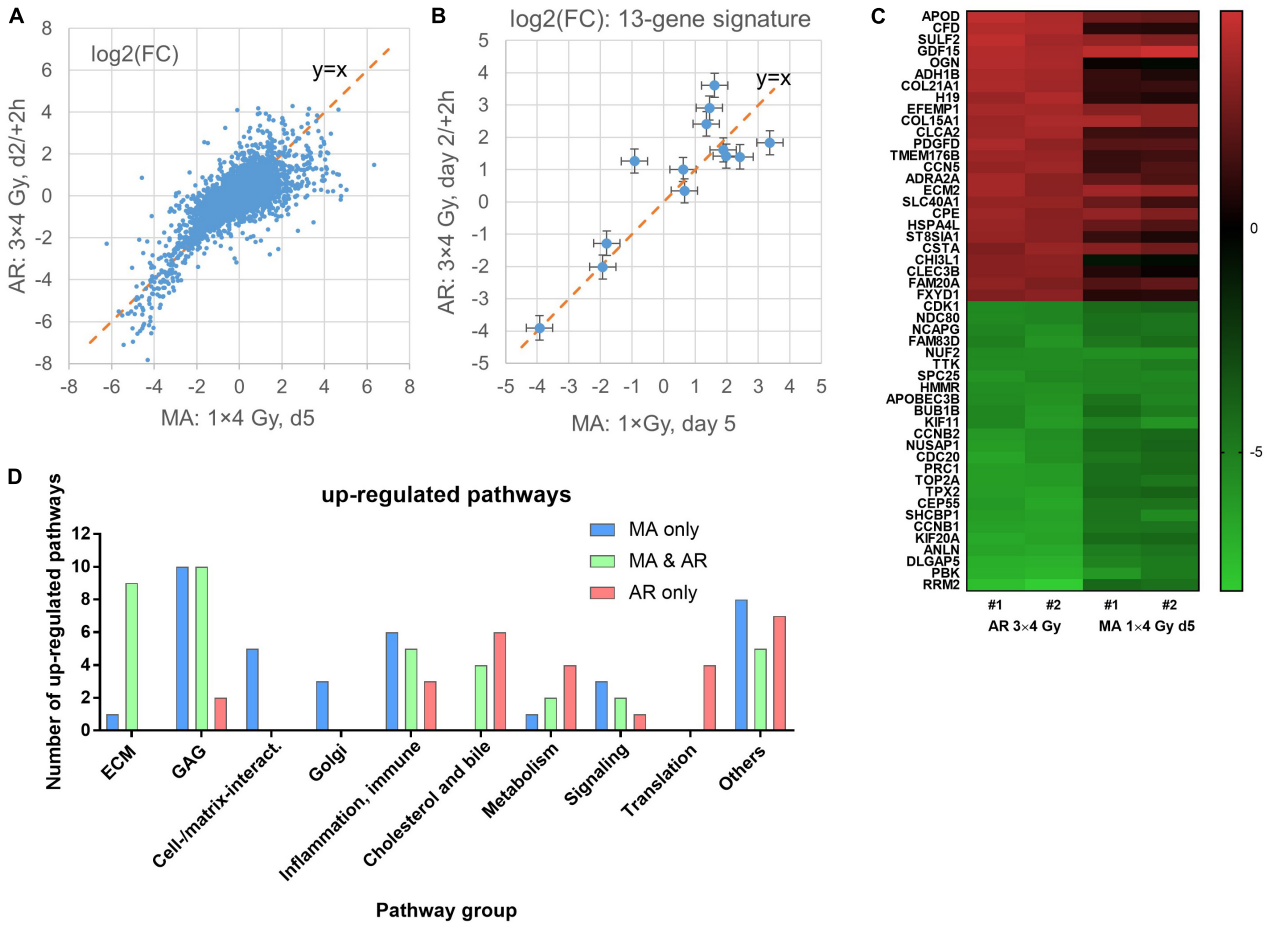

FIGURE 4 | Correlation of mean log2 fold changes [log2(FC)] after irradiation of confluent cultures with 3 × 4 Gy (AR protocol) and irradiation of exponentially growing cultures with 1 × 4 Gy (MA protocol) in microarray experiments #1–2 **(A)**. Same for the 13 genes in the predictive signature for subcutaneous fibrosis (Alsner et al., 2007). Mean values and 95% confidence intervals for data from experiments #1–2 are shown **(B)**. Heat map of the top25 up- and down-regulated genes for irradiation with the AR protocol and the same genes on day 5 for the MA protocol; data from independent replicate experiments #1–2 **(C)**. Number of pathways by functional group for pathways that were significant for only one of the two or common to both protocols **(D)**.

cytochrome P450 1B1 enzyme was strongly upregulated similar to the *PTX3* gene coding for a long pentraxin. Expression of *ACTA2* coding for the myofibroblast marker α-smooth muscle actin (α-sma) was only upregulated on day 5–6 after irradiation.

A comparison of the log2(FC) values for microarray and PCR analyses for the three strains on day 3 showed a reasonably good correlation, considering that the RNA was isolated from two individual series of experiments separated by approximately 9 months (**Figure 6F**). Some genes with moderate upregulation showed lower log2(FC) than for microarrays but only three were significant, two of which (THBS2, COL15A1) showed lower log2(FC) values ($P = 0.01$ and 0.02, respectively; unpaired t-test, $n = 2 \times 3$ per gene) and one (LOXL) a higher value ($P = 0.02$). Overall, the correlation for all three strains yielded $R^2 = 0.50$ which increased to $R^2 = 0.72$ when GS3 was excluded. More detailed analysis (not shown) suggested that the GS3 qPCR experiment underestimated the log2(FC) of some genes, possibly owing to experimental factors. Nevertheless, the full kinetics including other time points (**Figures 6A–E**) supported the radiation-induced differential expression obtained from the microarray experiments.

Additional Validation of Gene Expression at the RNA and Protein Levels

It may be argued that part of the time-dependent changes in gene expression may be related to culture conditions rather than irradiation. In order to test this, additional irradiation experiments were undertaken, including unirradiated controls at the time points on day 2, 3, and 5 in addition to day 1 used in the microarray experiments. Because unirradiated cultures would reach confluence and might undergo density arrest during the experiment, unirradiated cultures were seeded at lower densities to reach approximately the same cell density as the irradiated cultures at the time of RNA and protein isolation. mRNA expression of nine genes determined by qPCR are shown in **Supplementary Figure 4**. For some of the genes, notably the cyclins *CCNB1* and *CCNE2*, expression in unirradiated controls

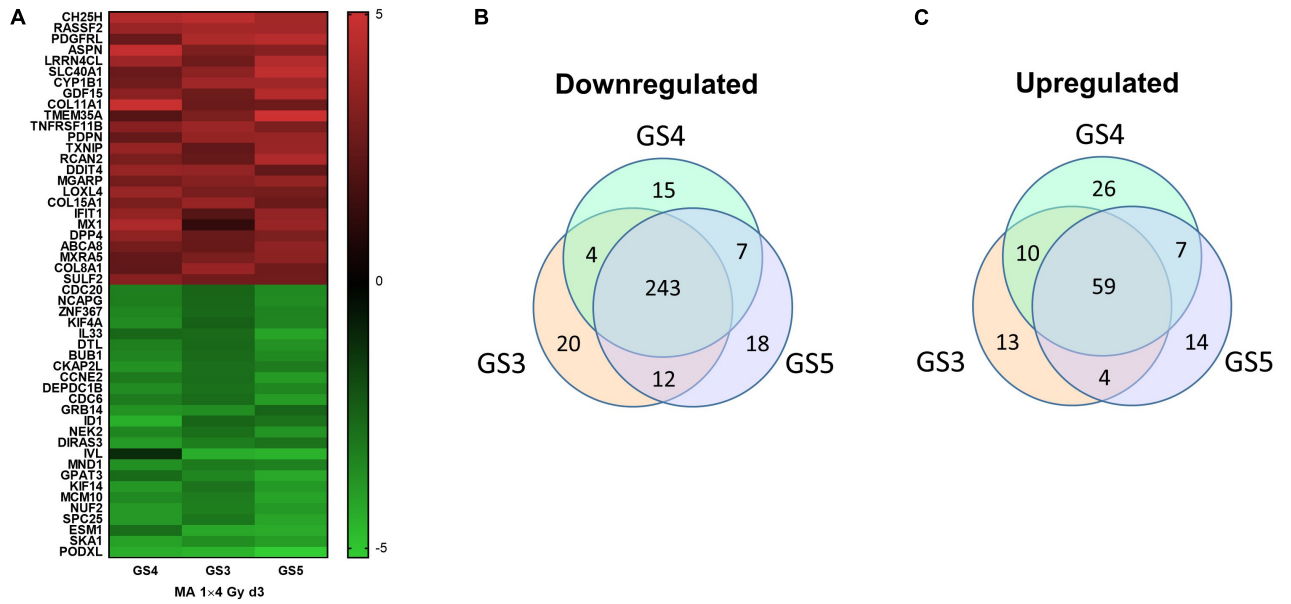

FIGURE 5 | Heat map of top25 up- and downregulated genes in the three fibroblast strains (GS3-5) on day 3 in microarray experiments #3–5 **(A)**. Venn diagrams for pathways upregulated **(B)** or downregulated **(C)** on day 3 after a single dose of 4 Gy to the three fibroblast strains GS3, GS4, and GS5.

actually showed some decrease with time. This may be explained by a slowing-down of proliferation, possible due to serum depletion, but from previous experience, these cultures do not lose the capacity to proliferate after reseeding into new flask. In spite of the changes with time in unirradiated cultures, the effect of irradiation was statistically significant at $P < 0.05$ in 6/9 genes on day 3 and in 7/9 genes on day 5, with strong trends ($P < 0.09$) in the remaining genes. The effect of irradiation was supported by *K*-means clustering analysis which separated day 3 and 5 of all irradiated samples from unirradiated samples and irradiated samples day 2 (not shown). Western blotting confirmed down-regulation of CCNB1 in unirradiated samples but downregulation was stronger after irradiation. Furthermore, PTX3 and α-sma were upregulated significantly on day 3–5 in irradiated compared to unirradiated cultures (**Supplementary Figures 5, 6A,B**). Immunofluorescence staining showed that upregulation of α-sma did not occur uniformly in all cells but showed contiguous stress fiber-like patterns covering small clusters of cells (**Supplementary Figure 6C**), suggesting the formation of small contractile cell clusters.

Pathway analysis showed downregulation of several stress and repair pathways after irradiation (MA protocol; **Figure 3A**). This may appear counter-intuitive if it is assumed that cells are arrested because of incomplete repair. However, permanent cell-cycle arrest may result from unrepaired or misrepaired DNA double-strand breaks (DSBs) leading to formation of micronuclei or dicentric chromosomes. In order to confirm downregulation of repair-related genes, we identified *RPA1*, *NBN*, and *POLD3* as the most frequent genes in the top 3 of leading core genes in 41 down-regulated stress and repair pathways. These genes are involved in different repair pathways such as translesion synthesis (*RPA1* and *POLD3*), and DNA damage response and telomere maintenance (*NBN*). Irradiation experiments were performed with isolation of RNA and protein from irradiated and unirradiated cultures for early and intermediate time points (4–72 h). qPCR showed significant down-regulation of these genes ($P = 0.0002–0.02$) at 24–72 h relative to unirradiated fibroblasts at the same time points, and this was further validated at the protein level for RPA1 and NBN in Western blots (**Supplementary Figure 7**).

DISCUSSION

In the present work, genes and pathways that are differentially expressed during phenotypic changes following irradiation of primary skin fibroblasts *in vitro* were identified. The radiation-induced phenotype was characterized by inactivation of clonogenicity accompanied by a gradual increase in cell size and change in morphology typical of radiation-induced differentiation of proliferating fibroblasts to postmitotic fibrocytes (Bayreuther et al., 1988b; Rodemann et al., 1991; Herskind et al., 2000). Furthermore, surviving colony-forming progenitor fibroblasts showed a two–threefold increase in the L:E ratio indicating a shift in the differentiation state after irradiation as previously described (Herskind and Rodemann, 2000).

The main result is the overall change in down-regulated genes and pathways related to proliferation and the up-regulation of genes and pathways related to the extracellular matrix and inflammation. A previous study on the IMR90 fibroblast strain identified 1,381 genes with more than twofold down-regulation genes after replicative senescence or radiation-induced arrest 5 days after a single dose of 5 Gy, while 660 genes were more than twofold up-regulated (Lackner et al., 2014). The overlap

TABLE 2 | Top25 upregulated pathways overrepresented with NES > 1.5 and adjusted *p*-value < 0.05 in each of the three fibroblast strains (GS3, GS4, and GS5) on day 3 after irradiation with 1 × 4 Gy (MA protocol).

ID	Description	Gene set size	Mean NES	Adjusted *p*
R-HSA-1650814	Collagen biosynthesis and modifying enzymes	67	2.43	<0.0016
R-HSA-909733	Interferon alpha/beta signaling	62	2.43	<0.0016
R-HSA-1474244	Extracellular matrix organization	297	2.40	<0.0016
R-HSA-8948216	Collagen chain trimerization	44	2.40	<0.0016
R-HSA-1474290	Collagen formation	90	2.31	<0.0016
R-HSA-3000178	ECM proteoglycans	75	2.27	<0.0016
R-HSA-1566948	Elastic fiber formation	44	2.27	<0.0016
R-HSA-2022090	Assembly of collagen fibrils and other multimeric structures	61	2.27	<0.0016
R-HSA-1442490	Collagen degradation	63	2.24	<0.0016
R-HSA-166658	Complement cascade	51	2.20	<0.0016
R-HSA-2129379	Molecules associated with elastic fibers	37	2.19	<0.0016
R-HSA-381426	Regulation of Insulin-like Growth Factor (IGF) transport and uptake by Insulin-like Growth Factor Binding Proteins (IGFBPs)	120	2.19	<0.0016
R-HSA-977606	Regulation of Complement cascade	40	2.17	<0.0016
R-HSA-8957275	Post-translational protein phosphorylation	104	2.16	<0.0016
R-HSA-1474228	Degradation of the extracellular matrix	137	2.15	<0.0016
R-HSA-186797	Signaling by PDGF	58	2.09	<0.0016
R-HSA-194068	Bile acid and bile salt metabolism	43	2.04	<0.0049
R-HSA-216083	Integrin cell surface interactions	84	2.04	<0.0016
R-HSA-211976	Endogenous sterols	27	2.03	<0.0016
R-HSA-2173782	Binding and Uptake of Ligands by Scavenger Receptors	39	2.03	<0.0063
R-HSA-192105	Synthesis of bile acids and bile salts	34	2.01	<0.0038
R-HSA-2243919	Crosslinking of collagen fibrils	18	1.99	<0.0099
R-HSA-3000171	Non-integrin membrane-ECM interactions	58	1.99	<0.0115
R-HSA-2022857	Keratan sulfate degradation	13	1.98	<0.0027
R-HSA-166663	Initial triggering of complement	20	1.96	<0.0063

Mean NES, mean value of normalized enrichments score for the three strains. 'Adjusted p' shows the largest adjusted p-values from separate pathway analyses for each of the three strains. NES values and adjusted p-values for each strain are given in the ***Supplementary Excel Table****.*

between the two types of arrest was smaller for up-regulated (93/660 = 14%) than for down-regulated genes (298/1381 = 22%). The ratio of the number of down- to up-regulated genes after irradiation was 1.77:1 (530:299 genes), compared with 3.5:1 for more than fourfold upregulated genes in GS4 on day 5 (256:74 genes) in the present study.

Functionally, the downregulated genes were dominated by genes related to cell-cycle progression and mitosis, consistent with the phenotypic loss of proliferation. Genes such as *MKI67*, *CCNB1/2* and *CCNE2*, and *CDC20*, showed similarly strong (approximately eightfold) downregulation on day 2 leveling off on day 3–5. The high mean fold downregulation (10–50-fold) is a clear indicator of efficient shut-down of cell-cycle progression in the vast majority of the cells. Among the most downregulated genes, *PODXL* (podocalyxin-like) and *ID1* (inhibitor of DNA binding 1) have been associated with migration and epithelial-mesenchymal transition (EMT) (Scharpfenecker et al., 2009; Frose et al., 2018; Wong et al., 2019). *ID1* was originally identified as being repressed in senescent fibroblasts where its expression represses the expression of the endogenous cyclin-dependent kinase inhibitor p16/CDKN2A (Hara et al., 1994; Zheng et al., 2004). A number of the genes down-regulated in the present study (e.g., *MKI67, CCNB1*, and *ID3*) were commonly down-regulated in replicative senescence and senescence induced by a single high dose of 20 Gy (Marthandan et al., 2016).

Pathway analysis showed 40% of all down-regulated pathway being related to cell division/chromosomes, cell cycle, and replication/proliferation, and almost 20% related to stress/repair. Pathways belonging to the former group were previously found for replicative senescence (Lackner et al., 2014), while another study found repair pathways to be down-regulated during senescence 5 days after a high single dose of 20 Gy (Marthandan et al., 2016). However, not all proliferation-related genes are down-regulated. Thus, early >2-fold up-regulation of the anti-proliferative BTG2 gene 1–24 h was shown in fibroblasts after a single dose of 5 Gy (Tachiiri et al., 2006). In the present study, 2.5–3.8-fold upregulation [log2(FC) = 1.34–1.97] of BTG2 was observed in GS4 in the MA protocol, increasing from day 2 to day 5 but, in the AR protocol, 5.9-fold upregulation [log2(FC) = 2.55 ± 0.34] occurred 2 h after the last fraction (early after the last fraction but 2 days after the first). In the MA protocol, upregulation in the three

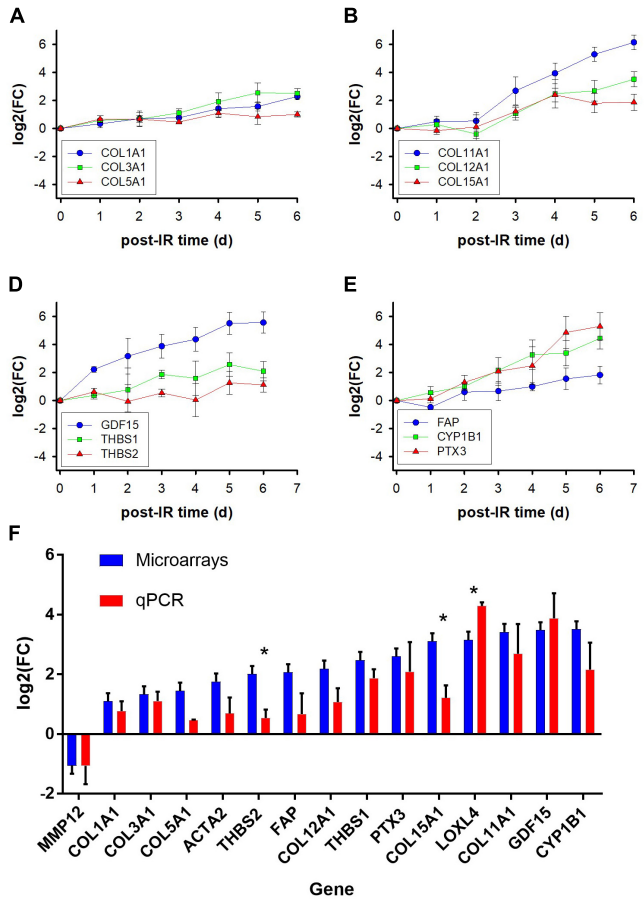

P-values	qPCR (day vs 0 Gy)		qPCR vs m.a.
Gene (time)	(d1-2)	(d3-6)	(d3)
COL1A1	0.14	6×10^{-5} *	0.40
COL3A1	0.004*	3×10^{-5} *	0.52
COL5A1	0.03*	3×10^{-4} *	0.06
COL11A1	0.18	6×10^{-6} *	0.59
COL12A1	0.92	1.2×10^{-4} *	0.08
COL15A1	0.96	6×10^{-5} *	0.02*
ACTA2	0.65	0.009 *	0.13
LOXL	0.04*	4×10^{-9} *	0.02*
MMP12	0.17	6×10^{-5} *	0.99
GDF15	0.007*	1.3×10^{-7} *	0.70
THBS1	0.47	2×10^{-4} *	0.43
THBS2	0.65	0.06	0.01*
FAP	0.87	0.0014 *	0.12
CYP1B1	0.03*	1.7×10^{-5} *	0.24
PTX3	0.11	1.3×10^{-4} *	0.67

FIGURE 6 | Kinetics of gene expression (fold induction determined with qPCR) of selected genes on day 1–6 after irradiation of GS3, GS4, and GS5 fibroblasts with a single dose of 4 Gy; mean values and standard errors of $n = 3$ independent experiments are shown **(A–E)**. Comparison of log2 fold changes [log2(FC)] for microarrays and qPCR on day 3 after a single dose of 4 Gy. The microarray and qPCR assays were performed on RNA from GS3, GS4, and GS5 irradiated in separate, independent experiments; Mean values and standard errors are shown **(F)**. The table shows *P*-values for log2(FC) of irradiated samples relative to unirradiated controls at early time points (day 1–2 together) and late time points (d3–d6 together) for the qPCR experiments (heteroscedastic *t*-test, $N = 9$ and 15, respectively) and for qPCR versus microarrays (m.a.) from experiments #3–5 for GS3, GS4, and GS5 (unpaired *t*-tests, $N = 6$). Asterisks indicates $P < 0.05$.

fibroblast strains was 2.6-fold [mean log2(FC) = 1.36 ± 0.92] on day 3, suggesting that upregulation is not restricted to early time points.

Several ECM related genes and pathways were upregulated after irradiation with the MA protocol. Tachiiri et al. (2006) found late upregulation of COL1A1, COL5A1, and IGFBP5 48–72 h after 5 Gy, which were also upregulated in the present study although at lower levels [log2(FC) = 1.10 – 1.45] than the filtering criteria [log2(FC) > 2]. By contrast, collagen and thrombospondin genes in ECM receptor pathways, which were upregulated in our study, were down-regulated after senescence observed five days after a dose of 20 Gy in the study by Marthandan et al. (2016). These previous findings support the view that the up-regulation of ECM-related genes and pathways 2–5 days after irradiation of exponentially growing fibroblasts in the present study (MA protocol) represent a transcriptional signature for progression of progenitor fibroblast to functional, prematurely differentiated cells which can be metabolically active for several months or even years (Bayreuther et al., 1988b) rather than senescence as a precursor to cell death.

Our aim was to test the hypothesis that radiation-induced differentiation can be related to changes in gene expression pathways after irradiation of fibroblast strains *in vitro* and to provide a framework for future studies on potential mechanisms. In the following, some individual genes that are potentially interesting for further studies are discussed and briefly reviewed. Complete lists for data mining are included as **Supplementary Material**.

Genes Related to the Extracellular Matrix

Several genes coding for collagens as a major component of the extracellular matrix (ECM) were upregulated after irradiation. Fibrillar collagens (Exposito et al., 2010) such as *COL1A1*, coding for the most abundant collagen (type I), and *COL3A1* coding for collagen type III which confers strength to the fibrils, showed five–sixfold upregulation over 5–6 days (qPCR) although they were not among the Top25 genes in microarrays. *COL5A1* coding

for type V which regulates fibril thickness (Sun et al., 2011), showed twofold upregulation but *COL11A1* coding for collagen type XI which is frequently found in cartilage (Blaschke et al., 2000) was in Top25 at all time points and reached 80-fold upregulation in qPCR. Furthermore, *COL12A1* and *COL15A1* coding for type XII and XV fibril-associated collagens with interrupted triple helices (FACIT) (Ivanova and Krivchenko, 2014) were upregulated 4–12-fold. *LOXL4* coding for lysyl oxidase homolog 4, which regulates collagen fibril organization (Herchenhan et al., 2015), was upregulated up to 20-fold in qPCR. The differential upregulation of these genes strongly suggests that irradiation not only increases the production but also leads to a change in the properties of collagen fibers. Thus it is tempting to speculate that increased expression of collagen types XI, XII, and XV, may contribute to tissue hardening and rigidity in subcutaneous fibrosis. In addition, microarray analysis showed eightfold upregulation of *COL8A1* coding for non-fibrillar short-chain collagen type VIII which promotes remodeling and fibrosis (Skrbic et al., 2015), and fourfold upregulation of *COL4A1* coding for type IV which is essential to the sheet-like structure of basement membranes (Jayadev and Sherwood, 2017), both of which appeared to reach a plateau 3–5 days after irradiation. Finally, expression of *ACTA2* was upregulated with delayed kinetics on day 5–6. Its product, α-smooth muscle actin (α-sma, ACTA2), is a marker for myofibroblast differentiation and was observed in single cells or small clusters of adjacent cells separated by non-expressing cells. We speculate if this may represent formation of contractile cell clusters. Thus the irradiated cultures showed essential hallmarks of radiation-induced, premature terminal differentiation of mitotic progenitor fibroblasts to post-mitotic functional cells distinct from the senescent state (Bayreuther et al., 1988b; Rodemann et al., 1989, 1991; Herskind and Rodemann, 2000; Herskind et al., 2000).

Although downregulation of matrix metalloproteinases (MMPs) might have been anticipated to contribute to enhanced ECM deposition, most MMPs showed little or only moderate modulation in the three strains on day 3. *MMP12*, coding for macrophage metalloelastase was downregulated twofold on day 3 but increased to eightfold downregulation on day 6 in qPCR, while *MMP10* coding for stromelysin 2 was downregulated fourfold on day 3–5 in microarray analysis of GS4 which was confirmed for day 3 in all three strains. By contrast, *FAP* coding for a prolyl endopeptidase associated with tissue remodeling and fibrosis (Hamson et al., 2014) was upregulated from day 2, reaching fourfold on day 5–6. The related gene, *DPP4*, coding for dipeptidylpeptidase-IV was upregulated 6–11-fold on day 3 in the three strains and has been associated with organ fibrosis and systemic sclerosis (Min et al., 2014; Soare et al., 2020). *MXRA5* coding for matrix-remodeling-associated protein 5 (adlican), was upregulated on day three in microarray analysis in all three strains and has been described as anti-inflammatory and anti-fibrotic (Poveda et al., 2017). Taken together, these findings strongly implicated increased ECM deposition and remodeling rather than reduced collagen degradation in the fibrogenic process after irradiation. This was supported by pathway analysis showing collagen degradation among the top-10 upregulated pathways common to the three strains on day 3. Thus the balance between pro-fibrotic deposition of structurally modified ECM molecules and degradation as part of ECM remodeling mechanisms may determine the development of clinical fibrosis.

Signals Leading to Phenotypic Changes

The signals initiating the gene expression program associated with radiation-induced differentiation and phenotypic changes are poorly understood. Transforming growth factor-β1 is considered a master switch in the development of fibrosis (Martin et al., 2000) but *TGFB1* was not among the radiation-induced upregulated genes in the present study. Latent TGF-β1 is stored in the ECM (and in blood platelet) and can be released by various agents such as including reactive oxygen species, reduced pH, and proteases such as plasmin and thrombospondin (Barcellos-Hoff and Dix, 1996; Ehrhart et al., 1997; Annes et al., 2003). However, in a previous study of fibroblasts *in vitro*, the total amount of active TGF-β1 released per flask released over a 24 h period from fibroblast cultures irradiated with 4 Gy was not significantly increased relative to unirradiated controls (Herskind and Rodemann, 2000). Nevertheless, the present study showed 3.5–6-fold upregulation of *THBS1* on day 2–6 and 1.5–3-fold for *THBS2*. Since the latter can antagonize TGF-β1 activation by THBS1 (Murphy-Ullrich, 2019) this provides a potential mechanism for a tightly regulated release of active TGF-β1 stored in the ECM or in blood platelets *in vivo*.

Perhaps a more important signal for the differentiation program leading to phenotypic changes is suggested by the early, strong upregulation of *GDF15* coding for the TGF-β1 family protein growth/differentiation factor 15 in the MA irradiation protocol and which was also upregulated in the AR protocol. GDF15 (also known as macrophage inhibitory cytokine-1, MIC-1) is upregulated by various stresses and has been associated with inflammation, cancer, and cardiovascular disease (Emmerson et al., 2018; Zhang et al., 2018; Kalli et al., 2019; Patel et al., 2019). Although it has been reported to signal via TGFβR2 and the downstream SMAD pathway, more recent studies implicated binding to a GFRAL/RET heterodimer with signaling to ERK and AKT pathways [reviewed in Emmerson et al. (2018)]. The GDF15 protein was recently proposed as a potential marker for radiation response and radiosensitivity in hTERT-immortalized human foreskin fibroblasts (Sandor et al., 2015). Furthermore, it has been reported to contribute to radiation-induced senescence in human aortic endothelial cells (Park et al., 2016) and has been associated with liver fibrosis (Koo et al., 2018).

Inflammatory Pathways

CH25H coding for cholesterol 25-hydroxylase was consistently one of the top3 upregulated genes at different time points and in different strains. The enzyme is important for the synthesis of oxysterol which together with cholesterol promote inflammatory reaction (Gold et al., 2014; Pandak and Kakiyama, 2019) and may contribute to intestinal fibrosis (Raselli et al., 2019). Consistent with this, *IL-6* showed 5-fold upregulation on day 2, increasing to 14-fold at later time points although not sufficient to include it in top25 on day 5 for GS4 or on day 3 for all three cell strains. Pathway analysis showed upregulation of interferon alpha/beta, interferon gamma, and IL-20 family,

signaling pathways corroborating that inflammatory signals were induced in the irradiated cultures.

In addition, platelet and neutrophil degranulation pathways and six pathways involving the complement system were upregulated. Notably, the *PTX3* gene coding for the long pentraxin 3 showed consistently strong upregulation in microarrays and qPCR. Pentraxins are important for complement activation (Bonavita et al., 2015; Ma and Garred, 2018). The complement system is an important component of the inflammatory reaction leading to recruitment of blood platelets and neutrophils in the early phases of wound healing (Sinno and Prakash, 2013; Rafail et al., 2015), thus providing a link between radiation-induced inflammation and wound healing (Cazander et al., 2012; Ellis et al., 2018) that may eventually result in fibrotic reaction, analogous to scarring in normal wound healing (Wynn and Ramalingam, 2012).

The *AKCR3* gene coding for atypical chemokine receptor 3 (formerly known as C-X-C chemoreceptor type 7, CXCR7) was among the early upregulated genes in GS4 and five—eightfold upregulated on day 3 in the three strains [mean log2(FC) = 2.8; rank 32]. ACKR3 is a scavenger for CXCL12 and modulates inflammatory signaling through the CXCL12/CXCR4 axis to effector kinases and other targets [reviewed in Giordano et al. (2019); Koenen et al. (2019)]. Interestingly, CXCL12 was part of the 13-gene discovery expression signature associated with the individual risk of subcutaneous fibrosis (Alsner et al., 2007).

Comparison of Pathways Activated in Different Irradiation Protocols

The MA protocol for studying differentiation showed a high proportion (∼80%) of pathways down-regulated at all three time points, with half of these pathways related to proliferation, cell cycle, cell division, and cell stress and DNA repair. Downregulation of cell stress and DNA repair pathways may appear counter-intuitive but can be explained if the early radiation response is completed by the time RNA was isolated. In contrast with down-regulated pathways, only ∼43% of the upregulated pathways were common to all three time points. These pathways were related to ECM proteins, glycosylation, and interactions of cells with neighboring cells and the ECM, corroborating the association with the radiation-induced phenotypic changes. The differential gene expression after irradiation with two fractions showed that the second fraction enhanced downregulation of most strongly downregulated genes while it had no effect on upregulated genes suggesting that incubation time after the first fraction was of major importance for the transcriptional response.

The expression profile for the fractionated irradiation protocol (AR) for confluent cultures previously used to identify the13-gene predictor of fibrosis risk (later reduced and confirmed for nine genes) (Alsner et al., 2007; Andreassen et al., 2013) was compared with the present protocol. The correlation of differentially expressed genes in the AR protocol applying three fractions to confluent cells was greater with day 5 in the single-dose MA protocol, and the strongest correlation was observed for downregulated genes including those related to the cell cycle. This supports the importance of the first fraction although subsequent fractions may enhance downregulation, whereas the 2 h-interval after the last fraction may not be critical for the radiation-induced expression profile. Upregulated pathways showed some overlap (37/101 significant pathways) between the two protocols, including pathways related to ECM, GAG, inflammation, and cholesterol and bile acid/salts. However, the pathways overrepresented only in the MA protocol (37/74) were dominated by GAG, cell–cell/cell–matrix interactions, and inflammation, whereas the pathways overrepresented only in the AR protocol (27/64) were associated with cholesterol and bile acid/salts, translation, metabolism, and different inflammatory pathways. Thus, although some pathways were common, the two protocols showed considerable differences in the functions of their activated pathways that may represent different aspects of the fibrogenic process.

Limitations and Conclusion

The main limitation of the present study is the small number of repeat experiments and fibroblast strains. However, the fold change in the expression of the filtered, strongly regulated genes (>4-fold) showed little variation between replicate experiments. A third, independent experiment confirmed the high reproducibility for the same fibroblast strain further supporting that the rate of false discoveries was very low. Differential gene expression in three different strains with additional qPCR experiments showed similar results, corroborating the robustness of the main findings. Pathway analysis grouped tens to hundreds of genes into individual pathways thus reducing the influence of stochastic variation of the expression of individual genes. Only genes and pathways that were upregulated on day three in all three fibroblast strains were considered, thus neglecting variation between individual strains. Pathway analysis is inherently biased toward the available curated pathways and in some cases may contain partially overlapping genes sets. However, the number of Reactome pathways was relatively large ($>10^3$) and a wide variety of different pathways categories were represented in the results so that the general expression profiles may be considered to reflect true changes with a high degree of certainty.

The results of this study demonstrate that gene expression profiles after irradiation of exponentially growing skin fibroblasts *in vitro* can be related to radiation-induced differentiation and inflammatory reactions. Furthermore, it suggests signaling mechanisms for phenotypic changes and inflammatory pathways that may be tested in future *in vitro* and *in vivo* studies. The irradiation protocol influences the expression profiles and upregulated pathways which seem to reflect different aspects of the fibrogenic process. Thus the present findings provide a model system and a framework for further hypothesis-based studies of radiation-induced fibrogenesis.

DATA AVAILABILITY STATEMENT

The raw and normalized data are deposited in the Gene Expression Omnibus (GEO) database (http://www.ncbi.nlm.nih.gov/geo/; accession number GSE147733).

AUTHOR CONTRIBUTIONS

CH: experimental design, data analysis, and manuscript writing. CS: microarray and pathway analysis. AS: qPCR, pathway analysis and manuscript writing and editing. FG: manuscript writing and editing and funding. FW: infrastructure and funding. All authors contributed to the article and approved the submitted version.

FUNDING

AS was supported by grant no. KTS-00.020.2019 from the Klaus Tschira Stiftung gGmbH.

ACKNOWLEDGMENTS

Ms. Anne Kirchner (née Schwegler), Ms. Maria Muciek, Ms. Miriam Bierbaum, and Ms. Adriana Gbrenicek are gratefully acknowledged for expert technical assistance.

SUPPLEMENTARY MATERIAL

The Supplementary Material for this article can be found online at: https://www.frontiersin.org/articles/10.3389/fcell.2021.539893/full#supplementary-material

REFERENCES

Alsner, J., Rodningen, O. K., and Overgaard, J. (2007). Differential gene expression before and after ionizing radiation of subcutaneous fibroblasts identifies breast cancer patients resistant to radiation-induced fibrosis. *Radiother. Oncol.* 83, 261–266. doi: 10.1016/j.radonc.2007.05.001

Andreassen, C. N., Overgaard, J., and Alsner, J. (2013). Independent prospective validation of a predictive test for risk of radiation induced fibrosis based on the gene expression pattern in fibroblasts irradiated in vitro. *Radiother. Oncol.* 108, 469–472. doi: 10.1016/j.radonc.2013.08.029

Annes, J. P., Munger, J. S., and Rifkin, D. B. (2003). Making sense of latent TGFbeta activation. *J. Cell Sci.* 116, 217–224. doi: 10.1242/jcs.00229

Barcellos-Hoff, M. H., and Dix, T. A. (1996). Redox-mediated activation of latent transforming growth factor-beta 1. *Mol. Endocrinol.* 10, 1077–1083. doi: 10.1210/me.10.9.1077

Bayreuther, K., Francz, P. I., and Rodemann, H. P. (1992). Fibroblasts in normal and pathological terminal differentiation, aging, apoptosis and transformation. *Arch. Gerontol. Geriatr.* 15(Suppl. 1), 47–74. doi: 10.1016/s0167-4943(05)80006-8

Bayreuther, K., Rodemann, H. P., Francz, P. I., and Maier, K. (1988a). Differentiation of fibroblast stem cells. *J. Cell Sci. Suppl.* 10, 115–130.

Bayreuther, K., Rodemann, H. P., Hommel, R., Dittmann, K., Albiez, M., and Francz, P. I. (1988b). Human skin fibroblasts in vitro differentiate along a terminal cell lineage. *Proc. Natl. Acad. Sci. U.S.A.* 85, 5112–5116. doi: 10.1073/pnas.85.14.5112

Blaschke, U. K., Eikenberry, E. F., Hulmes, D. J., Galla, H. J., and Bruckner, P. (2000). Collagen XI nucleates self-assembly and limits lateral growth of cartilage fibrils. *J. Biol. Chem.* 275, 10370–10378. doi: 10.1074/jbc.275.14.10370

Bonavita, E., Gentile, S., Rubino, M., Maina, V., Papait, R., Kunderfranco, P., et al. (2015). PTX3 is an extrinsic oncosuppressor regulating complement-dependent inflammation in cancer. *Cell* 160, 700–714. doi: 10.1016/j.cell.2015.01.004

Carlomagno, F., Burnet, N. G., Turesson, I., Nyman, J., Peacock, J. H., Dunning, A. M., et al. (2000). Comparison of DNA repair protein expression and activities between human fibroblast cell lines with different radiosensitivities. *Int. J. Cancer* 85, 845–849. doi: 10.1002/(sici)1097-0215(20000315)85:6<845::aid-ijc18>3.0.co;2-c

Cazander, G., Jukema, G. N., and Nibbering, P. H. (2012). Complement activation and inhibition in wound healing. *Clin. Dev. Immunol.* 2012:534291.

Cristofalo, V. J., Allen, R. G., Pignolo, R. J., Martin, B. G., and Beck, J. C. (1998). Relationship between donor age and the replicative lifespan of human cells in culture: a reevaluation. *Proc. Natl. Acad. Sci. U.S.A.* 95, 10614–10619. doi: 10.1073/pnas.95.18.10614

Dai, M., Wang, P., Boyd, A. D., Kostov, G., Athey, B., Jones, E. G., et al. (2005). Evolving gene/transcript definitions significantly alter the interpretation of GeneChip data. *Nucleic Acids Res.* 33:e175. doi: 10.1093/nar/gni179

Ding, L. H., Shingyoji, M., Chen, F., Hwang, J. J., Burma, S., Lee, C., et al. (2005). Gene expression profiles of normal human fibroblasts after exposure to ionizing radiation: a comparative study of low and high doses. *Radiat. Res.* 164, 17–26. doi: 10.1667/rr3354

Ehrhart, E. J., Segarini, P., Tsang, M. L., Carroll, A. G., and Barcellos-Hoff, M. H. (1997). Latent transforming growth factor beta1 activation in situ: quantitative and functional evidence after low-dose gamma-irradiation. *FASEB J.* 11, 991–1002. doi: 10.1096/fasebj.11.12.9337152

Ellis, S., Lin, E. J., and Tartar, D. (2018). Immunology of wound healing. *Curr. Dermatol. Rep.* 7, 350–358.

Emmerson, P. J., Duffin, K. L., Chintharlapalli, S., and Wu, X. (2018). GDF15 and growth control. *Front. Physiol.* 9:1712. doi: 10.3389/fphys.2018.01712

European_Commission. (1999). "Summaries of research projects supported under Biomed 2," in *Community Research, Biomedical and Health Research Programme 1994-1998*, (Brussels: Directorate-General for Research).

Exposito, J. Y., Valcourt, U., Cluzel, C., and Lethias, C. (2010). The fibrillar collagen family. *Int. J. Mol. Sci.* 11, 407–426. doi: 10.3390/ijms11020407

Frose, J., Chen, M. B., Hebron, K. E., Reinhardt, F., Hajal, C., Zijlstra, A., et al. (2018). Epithelial-Mesenchymal Transition induces podocalyxin to promote extravasation via ezrin signaling. *Cell Rep.* 24, 962–972. doi: 10.1016/j.celrep.2018.06.092

Giordano, F. A., Link, B., Glas, M., Herrlinger, U., Wenz, F., Umansky, V., et al. (2019). Targeting the post-irradiation tumor microenvironment in glioblastoma via inhibition of CXCL12. *Cancers (Basel.)* 11, 272. doi: 10.3390/cancers11030272

Gold, E. S., Diercks, A. H., Podolsky, I., Podyminogin, R. L., Askovich, P. S., Treuting, P. M., et al. (2014). 25-Hydroxycholesterol acts as an amplifier of inflammatory signaling. *Proc. Natl. Acad. Sci. U.S.A.* 111, 10666–10671. doi: 10.1073/pnas.1404271111

Hamson, E. J., Keane, F. M., Tholen, S., Schilling, O., and Gorrell, M. D. (2014). Understanding fibroblast activation protein (FAP): substrates, activities, expression and targeting for cancer therapy. *Proteom. Clin. Appl.* 8, 454–463. doi: 10.1002/prca.201300095

Hara, E., Yamaguchi, T., Nojima, H., Ide, T., Campisi, J., Okayama, H., et al. (1994). Id-related genes encoding helix-loop-helix proteins are required for G1 progression and are repressed in senescent human fibroblasts. *J. Biol. Chem.* 269, 2139–2145. doi: 10.1016/s0021-9258(17)42146-6

Hayflick, L. (1965). The limited in vitro lifetime of human diploid cell strains. *Exp. Cell Res.* 37, 614–636. doi: 10.1016/0014-4827(65)90211-9

Hayflick, L. (1980). Recent advances in the cell biology of aging. *Mech. Ageing Dev.* 14, 59–79.

Herchenhan, A., Uhlenbrock, F., Eliasson, P., Weis, M., Eyre, D., Kadler, K. E., et al. (2015). Lysyl oxidase activity is required for ordered collagen fibrillogenesis by tendon cells. *J. Biol. Chem.* 290, 16440–16450. doi: 10.1074/jbc.m115.641670

Herskind, C., Bentzen, S. M., Overgaard, J., Overgaard, M., Bamberg, M., and Rodemann, H. P. (1998). Differentiation state of skin fibroblast cultures versus risk of subcutaneous fibrosis after radiotherapy. *Radiother. Oncol.* 47, 263–269. doi: 10.1016/s0167-8140(98)00018-8

Herskind, C., Johansen, J., Bentzen, S. M., Overgaard, M., Overgaard, J., Bamberg, M., et al. (2000). Fibroblast differentiation in subcutaneous fibrosis

after postmastectomy radiotherapy. *Acta Oncol.* 39, 383–388. doi: 10.1080/028418600750013159

Herskind, C., and Rodemann, H. P. (2000). Spontaneous and radiation-induced differentiation of fibroblasts. *Exp. Gerontol.* 35, 747–755. doi: 10.1016/s0531-5565(00)00168-6

Ivanova, V. P., and Krivchenko, A. I. (2014). [A current viewpoint on structure and evolution of collagens. II. The fibril-associated collagens with interrupted triple helices]. *Zh. Evol. Biokhim. Fiziol.* 50, 245–254.

Irizarry, R. A., Hobbs, B., Collin, F., Beazer-Barclay, Y. D., Antonellis, K. J., Scherf, U., et al. (2003). Exploration, normalization, and summaries of high density oligonucleotide array probe level data. *Biostatistics* 4, 249–264. doi: 10.1093/biostatistics/4.2.249

Jayadev, R., and Sherwood, D. R. (2017). Basement membranes. *Curr. Biol.* 27, R207–R211.

Johansen, J., Bentzen, S. M., Overgaard, J., and Overgaard, M. (1996). Relationship between the in vitro radiosensitivity of skin fibroblasts and the expression of subcutaneous fibrosis, telangiectasia, and skin erythema after radiotherapy. *Radiother. Oncol.* 40, 101–109. doi: 10.1016/0167-8140(96)01777-x

Kalanxhi, E., and Dahle, J. (2012). Genome-wide microarray analysis of human fibroblasts in response to gamma radiation and the radiation-induced bystander effect. *Radiat. Res.* 177, 35–43. doi: 10.1667/rr2694.1

Kalli, M., Minia, A., Pliaka, V., Fotis, C., Alexopoulos, L. G., and Stylianopoulos, T. (2019). Solid stress-induced migration is mediated by GDF15 through Akt pathway activation in pancreatic cancer cells. *Sci. Rep.* 9:978.

Khodarev, N. N., Park, J. O., Yu, J., Gupta, N., Nodzenski, E., Roizman, B., et al. (2001). Dose-dependent and independent temporal patterns of gene responses to ionizing radiation in normal and tumor cells and tumor xenografts. *Proc. Natl. Acad. Sci. U.S.A.* 98, 12665–12670. doi: 10.1073/pnas.211443698

Kis, E., Szatmari, T., Keszei, M., Farkas, R., Esik, O., Lumniczky, K., et al. (2006). Microarray analysis of radiation response genes in primary human fibroblasts. *Int. J. Radiat. Oncol. Biol. Phys.* 66, 1506–1514. doi: 10.1016/j.ijrobp.2006.08.004

Koenen, J., Bachelerie, F., Balabanian, K., Schlecht-Louf, G., and Gallego, C. (2019). Atypical chemokine receptor 3 (ACKR3): a comprehensive overview of its expression and potential roles in the immune system. *Mol. Pharmacol.* 96, 809–818. doi: 10.1124/mol.118.115329

Koo, B. K., Um, S. H., Seo, D. S., Joo, S. K., Bae, J. M., Park, J. H., et al. (2018). Growth differentiation factor 15 predicts advanced fibrosis in biopsy-proven non-alcoholic fatty liver disease. *Liver Int.* 38, 695–705. doi: 10.1111/liv.13587

Kote-Jarai, Z., Williams, R. D., Cattini, N., Copeland, M., Giddings, I., Wooster, R., et al. (2004). Gene expression profiling after radiation-induced DNA damage is strongly predictive of BRCA1 mutation carrier status. *Clin. Cancer Res.* 10, 958–963. doi: 10.1158/1078-0432.ccr-1067-3

Lackner, D. H., Hayashi, M. T., Cesare, A. J., and Karlseder, J. (2014). A genomics approach identifies senescence-specific gene expression regulation. *Aging Cell* 13, 946–950. doi: 10.1111/acel.12234

Ma, Y. J., and Garred, P. (2018). Pentraxins in complement activation and regulation. *Front. Immunol.* 9:3046. doi: 10.3389/fimmu.2018.03046

Marthandan, S., Menzel, U., Priebe, S., Groth, M., Guthke, R., Platzer, M., et al. (2016). Conserved genes and pathways in primary human fibroblast strains undergoing replicative and radiation induced senescence. *Biol. Res.* 49:34.

Martin, M., Lefaix, J., and Delanian, S. (2000). TGF-beta1 and radiation fibrosis: a master switch and a specific therapeutic target? *Int. J. Radiat. Oncol. Biol. Phys.* 47, 277–290. doi: 10.1016/s0360-3016(00)00435-1

Min, H. S., Kim, J. E., Lee, M. H., Song, H. K., Kang, Y. S., Lee, M. J., et al. (2014). Dipeptidyl peptidase IV inhibitor protects against renal interstitial fibrosis in a mouse model of ureteral obstruction. *Lab. Invest.* 94, 598–607. doi: 10.1038/labinvest.2014.50

Murphy-Ullrich, J. E. (2019). Thrombospondin 1 and Its diverse roles as a regulator of extracellular matrix in fibrotic disease. *J. Histochem. Cytochem.* 67, 683–699. doi: 10.1369/0022155419851103

Pandak, W. M., and Kakiyama, G. (2019). The acidic pathway of bile acid synthesis: not just an alternative pathway(). *Liver Res.* 3, 88–98. doi: 10.1016/j.livres.2019.05.001

Park, H., Kim, C. H., Jeong, J. H., Park, M., and Kim, K. S. (2016). GDF15 contributes to radiation-induced senescence through the ROS-mediated p16 pathway in human endothelial cells. *Oncotarget* 7, 9634–9644. doi: 10.18632/oncotarget.7457

Patel, S., Alvarez-Guaita, A., Melvin, A., Rimmington, D., Dattilo, A., Miedzybrodzka, E. L., et al. (2019). GDF15 Provides an endocrine signal of nutritional stress in mice and humans. *Cell Metab.* 29, 707–718e8.

Poveda, J., Sanz, A. B., Fernandez-Fernandez, B., Carrasco, S., Ruiz-Ortega, M., Cannata-Ortiz, P., et al. (2017). MXRA5 is a TGF-beta1-regulated human protein with anti-inflammatory and anti-fibrotic properties. *J. Cell Mol. Med.* 21, 154–164. doi: 10.1111/jcmm.12953

Rafail, S., Kourtzelis, I., Foukas, P. G., Markiewski, M. M., Deangelis, R. A., Guariento, M., et al. (2015). Complement deficiency promotes cutaneous wound healing in mice. *J. Immunol.* 194, 1285–1291. doi: 10.4049/jimmunol.1402354

Raselli, T., Wyss, A., Gonzalez Alvarado, M. N., Weder, B., Mamie, C., Spalinger, M. R., et al. (2019). The oxysterol synthesising enzyme CH25H contributes to the development of intestinal fibrosis. *J. Crohns Colitis* 13, 1186–1200. doi: 10.1093/ecco-jcc/jjz039

Rodemann, H. P. (1989). Differential degradation of intracellular proteins in human skin fibroblasts of mitotic and mitomycin-C (MMC)-induced postmitotic differentiation states in vitro. *Differentiation* 42, 37–43. doi: 10.1111/j.1432-0436.1989.tb00605.x

Rodemann, H. P., and Bamberg, M. (1995). Cellular basis of radiation-induced fibrosis. *Radiother. Oncol.* 35, 83–90. doi: 10.1016/0167-8140(95)01540-w

Rodemann, H. P., Bayreuther, K., Francz, P. I., Dittmann, K., and Albiez, M. (1989). Selective enrichment and biochemical characterization of seven human skin fibroblasts cell types in vitro. *Exp. Cell Res.* 180, 84–93. doi: 10.1016/0014-4827(89)90214-0

Rodemann, H. P., Peterson, H. P., Schwenke, K., and Von Wangenheim, K. H. (1991). Terminal differentiation of human fibroblasts is induced by radiation. *Scanning Microsc.* 5, 1135–1142.

Rodningen, O. K., Borresen-Dale, A. L., Alsner, J., Hastie, T., and Overgaard, J. (2008). Radiation-induced gene expression in human subcutaneous fibroblasts is predictive of radiation-induced fibrosis. *Radiother. Oncol.* 86, 314–320. doi: 10.1016/j.radonc.2007.09.013

Rodningen, O. K., Overgaard, J., Alsner, J., Hastie, T., and Borresen-Dale, A. L. (2005). Microarray analysis of the transcriptional response to single or multiple doses of ionizing radiation in human subcutaneous fibroblasts. *Radiother. Oncol.* 77, 231–240. doi: 10.1016/j.radonc.2005.09.020

Sandor, N., Schilling-Toth, B., Kis, E., Benedek, A., Lumniczky, K., Safrany, G., et al. (2015). Growth Differentiation Factor-15 (GDF-15) is a potential marker of radiation response and radiation sensitivity. *Mutat. Res. Genet. Toxicol. Environ. Mutagen.* 793, 142–149. doi: 10.1016/j.mrgentox.2015.06.009

Scharpfenecker, M., Kruse, J. J., Sprong, D., Russell, N. S., Ten Dijke, P., and Stewart, F. A. (2009). Ionizing radiation shifts the PAI-1/ID-1 balance and activates notch signaling in endothelial cells. *Int. J. Radiat. Oncol. Biol. Phys.* 73, 506–513. doi: 10.1016/j.ijrobp.2008.09.052

Schneider, C. A., Rasband, W. S., and Eliceiri, K. W. (2012). NIH Image to ImageJ: 25 years of image analysis. *Nat. Methods* 9, 671–675. doi: 10.1038/nmeth.2089

Sinno, H., and Prakash, S. (2013). Complements and the wound healing cascade: an updated review. *Plast. Surg. Int.* 2013, 146764.

Skrbic, B., Engebretsen, K. V., Strand, M. E., Lunde, I. G., Herum, K. M., Marstein, H. S., et al. (2015). Lack of collagen VIII reduces fibrosis and promotes early mortality and cardiac dilatation in pressure overload in mice. *Cardiovasc. Res.* 106, 32–42. doi: 10.1093/cvr/cvv041

Soare, A., Gyorfi, H. A., Matei, A. E., Dees, C., Rauber, S., Wohlfahrt, T., et al. (2020). Dipeptidylpeptidase 4 as a marker of activated fibroblasts and a potential target for the treatment of fibrosis in systemic sclerosis. *Arthritis Rheumatol.* 72, 137–149. doi: 10.1002/art.41058

Sun, M., Chen, S., Adams, S. M., Florer, J. B., Liu, H., Kao, W. W., et al. (2011). Collagen V is a dominant regulator of collagen fibrillogenesis: dysfunctional regulation of structure and function in a corneal-stroma-specific Col5a1-null mouse model. *J. Cell Sci.* 124, 4096–4105. doi: 10.1242/jcs.091363

Tachiiri, S., Katagiri, T., Tsunoda, T., Oya, N., Hiraoka, M., and Nakamura, Y. (2006). Analysis of gene-expression profiles after gamma irradiation of normal human fibroblasts. *Int. J. Radiat. Oncol. Biol. Phys.* 64, 272–279. doi: 10.1016/j.ijrobp.2005.08.030

Wong, B. S., Shea, D. J., Mistriotis, P., Tuntithavornwat, S., Law, R. A., Bieber, J. M., et al. (2019). A direct podocalyxin-dynamin-2 interaction regulates cytoskeletal

dynamics to promote migration and metastasis in pancreatic cancer cells. *Cancer Res.* 79, 2878–2891. doi: 10.1158/0008-5472.can-18-3369

Wynn, T. A., and Ramalingam, T. R. (2012). Mechanisms of fibrosis: therapeutic translation for fibrotic disease. *Nat. Med.* 18, 1028–1040. doi: 10.1038/nm.2807

Yu, G., and He, Q. Y. (2016). ReactomePA: an R/Bioconductor package for reactome pathway analysis and visualization. *Mol. Biosyst.* 12, 477–479. doi: 10.1039/c5mb00663e

Zhang, Y., Zhang, G., Liu, Y., Chen, R., Zhao, D., Mcalister, V., et al. (2018). GDF15 regulates Malat-1 Circular RNA and inactivates NFkappaB signaling leading to immune tolerogenic DCs for preventing alloimmune rejection in heart transplantation. *Front. Immunol.* 9:2407. doi: 10.3389/fimmu.2018.02407

Zheng, W., Wang, H., Xue, L., Zhang, Z., and Tong, T. (2004). Regulation of cellular senescence and p16(INK4a) expression by Id1 and E47 proteins in human diploid fibroblast. *J. Biol. Chem.* 279, 31524–31532. doi: 10.1074/jbc.m400365200

Zhou, T., Chou, J. W., Simpson, D. A., Zhou, Y., Mullen, T. E., Medeiros, M., et al. (2006). Profiles of global gene expression in ionizing-radiation-damaged human diploid fibroblasts reveal synchronization behind the G1 checkpoint in a G0-like state of quiescence. *Environ. Health Perspect.* 114, 553–559. doi: 10.1289/ehp.8026

Conflict of Interest: The authors declare that the research was conducted in the absence of any commercial or financial relationships that could be construed as a potential conflict of interest.

Advantages of publishing in Frontiers

OPEN ACCESS
Articles are free to read for greatest visibility and readership

FAST PUBLICATION
Around 90 days from submission to decision

HIGH QUALITY PEER-REVIEW
Rigorous, collaborative, and constructive peer-review

TRANSPARENT PEER-REVIEW
Editors and reviewers acknowledged by name on published articles

Frontiers
Avenue du Tribunal-Fédéral 34
1005 Lausanne | Switzerland

Visit us: www.frontiersin.org
Contact us: frontiersin.org/about/contact

REPRODUCIBILITY OF RESEARCH
Support open data and methods to enhance research reproducibility

DIGITAL PUBLISHING
Articles designed for optimal readership across devices

FOLLOW US
@frontiersin

IMPACT METRICS
Advanced article metrics track visibility across digital media

EXTENSIVE PROMOTION
Marketing and promotion of impactful research

LOOP RESEARCH NETWORK
Our network increases your article's readership